

## Editor's preface

Physical Organic Chemistry is a mature discipline that is blessed with a rich history and a bright future. It is therefore fitting that the chapters in this 37th volume of *Advances in Physical Organic Chemistry* deal with investigations that can be traced back to the birth of the field, but which are continuing to produce results critical to our understanding of the stability of organic molecules and the mechanisms for their reactions.

Three chapters in this volume deal with various aspects of the stability of carbocations, and their role as putative intermediates in chemical and enzymatic reactions.

Aboud, Alkorta, Dávalos and Müller summarize the results of recent experimental work to determine the thermodynamic gas phase stabilities of carbocations relative to neutral precursors, the results of high level calculations of these stabilities and additional structural information that can only be easily obtained through such calculations. The chapter concludes with a description of the effect of solvent on the condensed-phase stability of carbocations, and the role of solvent in determining whether carbocations form as intermediates of solution reactions. This chapter is richly referenced and can be read with interest by anyone wishing to remain abreast of modern developments in a historically important subject.

The generation and characterization of vinyl carbocations remains a challenging problem because of the great instability of positive charge at  $sp$  hybridized carbon. Physical organic chemists have classically produced unstable carbocations through heterolytic cleavage of bonds to weakly basic atoms or molecules. The past success of this approach has prompted the experimental studies of vinyl(aryl)iodonium salts described in the chapter by Okuyama and Lodder. Although these salts are good electrophiles that carry an excellent iodoarene nucleofuge, photoexcitation to the excited state is required to drive heterolytic cleavage to form simple primary vinyl carbocations. This chapter describes the great diversity in the products obtained from the thermal and photochemical chemical reactions of vinyl(aryl)iodonium salts and the reasoning used in moving from these product yields to detailed conclusions about the mechanisms for their formation.

Oxocarbenium ions are commonly written as intermediates of organic reactions. However, the lifetimes of oxocarbenium ions in water approach the vibrational limit and their formation as reaction intermediates in this medium is sometimes avoided through a concerted mechanism. The determination of whether oxocarbenium ions form as intermediates in related enzymatic processes is a particularly challenging problem, because the protein catalyst will shield these ions from interactions with solvent and solutes which might provide evidence for their formation. Deuterium, tritium, and heavy atom kinetic isotope effects provide a wealth of information about reaction mechanism, but these are sometimes masked for enzymatic reactions by the high efficiency for turnover of enzyme-bound substrates. However, it is often possible for creative enzymologists to develop substrates or reaction conditions under which the rate constants for enzymatic reactions are limited by chemical bond cleavage, and are therefore subject to significant kinetic isotope effects. The design and interpretation of such multiple kinetic isotope effect studies to probe the changes in chemical bonding at sugar substrates that occur on proceeding to the transition states for enzyme-catalyzed cleavage of glycosides is described in a chapter by Berti and Tanaka.

Organometallic chemistry has largely been the domain of synthetic organic and inorganic chemists, and the mechanisms for organometallic transformations have not generally been subject to the same type of detailed experimental analyses developed in studies on the mechanism of multistep organic reactions. Claude Bernasconi, a leading figure in the study of organic reaction mechanisms, summarizes here the results of studies on the reactions of organometallic Fischer carbene complexes in aqueous solution. Finally, Drechsler and Rotello describe how the redox properties of flavins, quinones and related molecules can be varied through the rational design of molecules in which a given oxidation state is stabilized by electrostatic, hydrogen-bonding,  $\pi$ -stacking and other noncovalent interactions. The design and physical characterization of these finely tuned redox systems has potential applications in the development of a variety of molecular “devices”.

We are pleased to note that the masthead lists a revamped and expanded Editorial Advisory Board. This board is assisting the coeditors in the planning of future volumes in order to ensure that *Advances in Physical Organic Chemistry* continues to highlight the most important applications of physical and theoretical methods to the characterization of the structure and stability of organic molecules and the mechanisms for their reactions.

**J. P. Richard**  
**T. T. Tidwell**

# Contents

**Editor's preface** **vii**

**Contributors to Volume 37** **ix**

**Nucleophilic Vinylic Substitution and Vinyl Cation Intermediates in the Reactions of Vinyl Iodonium Salts** **1**

TADASHI OKUYAMA and GERRIT LODDER

- 1 Introduction 1
- 2 Vinylic  $S_N2$  reactions 3
- 3 Vinyl cations as  $S_NV1$  intermediates 23
- 4 Borderline mechanisms 43
- 5 Photochemical reactions 48
- 6 Summary 52
  - Acknowledgments 53
  - References 53

**Thermodynamic Stabilities of Carbocations** **57**

JOSÉ-LUIS M. ABBOUD, IBON ALKORTA, JUAN Z. DÁVALOS, PAUL MÜLLER and ESTHER QUINTANILLA

- 1 Introduction 57
- 2 Quantitative thermodynamic criteria of stability in the gas phase 58
- 3 Theoretical calculations 64
- 4 Uncertainties 65
- 5 Thermodynamics and structure of selected species 67
- 6 Solution reactivity 116
- 7 Conclusion 126
  - Acknowledgments 127
  - References 127

**The Physical Organic Chemistry of Fischer Carbene Complexes** **137**

CLAUDE F. BERNASCONI

- 1 Introduction 137
- 2 Reactions at the metal 143

3 Reactions at the carbene carbon	158
4 Acid–base reactions at the $\alpha$ -carbon	207
Acknowledgments	232
References	233

**Transition State Analysis Using Multiple Kinetic Isotope Effects:  
Mechanisms of Enzymatic and Non-enzymatic Glycoside Hydrolysis  
and Transfer** **239**

PAUL J. BERTI and KELLY S.E. TANAKA

1 Introduction	240
2 TS analysis: principles and procedures	247
3 TS analysis: results and recent developments	255
4 Specific reactions	283
5 Conclusions and future directions	306
Acknowledgments	308
References	308

**The Interplay between Redox and Recognition Processes:  
Models and Devices** **315**

ULF DRECHSLER and VINCENT M. ROTELLO

1 Introduction	315
2 Non-covalent interactions and redox potentials	316
3 Redox modulation through hydrogen bonding	323
4 Redox modulation through $\pi$ -stacking and donor atom– $\pi$ interactions	326
5 Redox modulation and specific binding applied to the design of molecular devices	328
6 Conclusion and outlook	334
References	335

**Author Index** **339**

**Cummulative Index of Authors** **355**

**Cummulative Index of Titles** **357**

## Contributors to Volume 37

**José-Luis M. Abboud** Instituto de Química Física “Rocasolano”, CSIC, Madrid, Spain

**Ibon Alkorta** Instituto de Química Médica, CSIC, Madrid, Spain

**Claude F. Bernasconi** Department of Chemistry and Biochemistry, University of California, Santa Cruz, California, USA

**Paul J. Berti** Departments of Chemistry and Biochemistry and the Antimicrobial Research Centre, McMaster University, 1280 Main Street W., Hamilton, Ontario, Canada

**Juan Z. Dávalos** Instituto de Química Física “Rocasolano”, CSIC, Madrid, Spain

**Ulf Drechsler** Department of Chemistry, University of Massachusetts, Amherst, Massachusetts, USA

**Gerrit Lodder** Gorlaeus Laboratories, Leiden Institute of Chemistry, Leiden University, Leiden, The Netherlands

**Paul Müller** Department of Organic Chemistry, University of Geneva, Geneva, Switzerland

**Tadashi Okuyama** Faculty of Science, Himeji Institute of Technology, Kamigori, Hyogo, Japan

**Esther Quintanilla** Instituto de Química Física “Rocasolano”, CSIC, Madrid, Spain

**Vincent M. Rotello** Department of Chemistry, University of Massachusetts, Amherst, Massachusetts, USA

**Kelly S.E. Tanaka** Department of Biochemistry, Albert Einstein College of Medicine, 1300 Morris Park Avenue, Bronx, New York, USA

## Cumulative Index of Authors

- Abboud, J.-L.M., **37**, 57  
 Ahlberg, P., **19**, 223  
 Alberty, W.J., **16**, 87; **28**, 139  
 Alden, J.A., **32**, 1  
 Alkorta, I., **37**, 57  
 Allinger, N.I., **13**, 1  
 Amyes, T.L., **35**, 67  
 Anbar, M., 7, 115  
 Arnett, E.M., **13**, 83; **28**, 45  
 Ballester, M., **25**, 267  
 Bard, A.J., **13**, 155  
 Baumgarten, M., **28**, 1  
 Beer, P.D., **31**, 1  
 Bell, R.P., **4**, 1  
 Bennett, J.E., **8**, 1  
 Bentley, T.W., **8**, 151; **14**, 1  
 Berg, U., **25**, 1  
 Bcrger, S., **16**, 239  
 Bernasconi, C.F., **27**, 119;  
**37**, 137  
 Berti, P.J., **37**, 239  
 Bethell, D., 7, 153; **10**, 53  
 Blackburn, G.M., **31**, 249  
 Blandamer, M.J., **14**, 203  
 Bond, A.M., **32**, 1  
 Bowden, K., **28**, 171  
 Brand, J.C.D., **1**, 36S  
 Brändström, A., **15**, 267  
 Brinkman, M.R., **10**, 53  
 Brown, H.C., **1**, 3S  
 Buncel, E., **14**, 133  
 Bunton, C.A., **21**, 213  
 Cabell-Whiting, P.W., **10**, 129  
 Cacace, F., **8**, 79  
 Capon, B., **21**, 37  
 Carter, R.E., **10**, 1  
 Chen, Z., **31**, 1  
 Collins, C.J., **2**, 1  
 Compton, R.G., **32**, 1  
 Cornelisse, J., **11**, 225  
 Cox, R.A., **35**, 1  
 Crampton, M.R., 7, 211  
 Datta, A., **31**, 249  
 Dávalos, J.Z., **37**, 57  
 Davidson, R.S., **19**, 1; **20**, 191  
 de Gunst, G.P., **11**, 225  
 de Jong, F., **17**, 279  
 Denham, H., **31**, 249  
 Desvergne, J.P., **15**, 63  
 Dosunmu, M.I., **21**, 37  
 Drechsler, U., **37**, 315  
 Ebersson, K., **11**, 1; **18**, 79;  
**31**, 91  
 Ebersson, L., **36**, 59  
 Ekland, J.C., **32**, 1  
 Emsley, J., **26**, 255  
 Engdahl, C., **19**, 223  
 Farnum, D.G., **11**, 123  
 Fendler, E.J., **8**, 271  
 Fendler, J.H., **8**, 271; **13**, 279  
 Ferguson, G., **1**, 203  
 Fields, E.K., **6**, 1  
 Fife, T.H., **11**, 1  
 Fleischmann, M., **10**, 155  
 Frey, H.M., **4**, 147  
 Fujio, M., **32**, 267  
 Gale, P.A., **31**, 1  
 Gilbert, B.C., **5**, 53  
 Gillespie, R.J., **9**, 1  
 Gold, V., 7, 259  
 Goodin, J.W., **20**, 191  
 Gould, I.R., **20**, 1  
 Greenwood, H.H., **4**, 73  
 Gritsan, N.P., **36**, 255  
 Hammerich, O., **20**, 55  
 Harvey, N.G., **28**, 45  
 Hasegawa, M., **30**, 117  
 Havinga, E., **11**, 225  
 Henderson, R.A., **23**, 1  
 Henderson, S., **23**, 1  
 Hibbert, F., **21**, 113; **26**, 255  
 Hine, J., **15**, 1  
 Hogen-Esch, T.E., **15**, 153  
 Hogeveen, H., **10**, 29, 129  
 Huber, W., **28**, 1  
 Ireland, J.F., **12**, 131  
 Iwamura, H., **26**, 179  
 Johnson, S.L., **5**, 237  
 Johnstone, R.A.W., **8**, 151  
 Jonsäll, G., **19**, 223  
 José, S.M., **21**, 197  
 Kemp, G., **20**, 191  
 Kia, J.L., **17**, 65  
 Kirby, A.J., **17**, 183; **19**, 87  
 Kitagawa, T., **30**, 173  
 Kluger, R.H., **25**, 99  
 Kochi, J.K., **29**, 185; **35**, 193  
 Kohnstam, G., **5**, 121  
 Korolev, V.A., **30**, 1  
 Korth, H.-G., **26**, 131  
 Kramer, G.M., **11**, 177  
 Kreevoy, M.M., **6**, 63;  
**16**, 87  
 Kunitake, T., **17**, 435  
 Kurtz, H.A., **29**, 273  
 Le Fèvre, R.J.W., **3**, 1  
 Ledwith, A., **13**, 155  
 Lee, I., **27**, 57  
 Liler, M., **11**, 267  
 Lin, S.-S., **35**, 67  
 Lodder, G., **37**, 1  
 Long, F.A., **1**, 1  
 Lüning, U., **30**, 63  
 Maccoll, A., **3**, 91  
 McWeeny, R., **4**, 73  
 Mandolini, L., **12**, 1  
 Maran, F., **36**, 85  
 Matsson, O., **31**, 143  
 Melder, L., **10**, 1  
 Mile, B., **8**, 1  
 Miller, S.I., **6**, 185  
 Modena, G., **9**, 185  
 More O'Ferrall, R.A., **5**, 331  
 Morsi, S.E., **15**, 63  
 Müllen, K., **28**, 1  
 Müller, P., **37**, 57  
 Nefedov, O.M., **30**, 1  
 Neta, P., **12**, 223  
 Nibbering, N.M.M., **24**, 1  
 Norman, R.O.C., **5**, 33  
 Novak, M., **36**, 167  
 Nyberg, K., **12**, 1  
 O'Donoghue, A.M.C., **35**, 67  
 Okamoto, K., **30**, 173  
 Okuyama, T., **37**, 1  
 Olah, G.A., **4**, 305  
 Page, M.I., **23**, 165  
 Parker, A.J., **5**, 173  
 Parker, V.D., **19**, 131;  
**20**, 55  
 Peel, T.E., **9**, 1  
 Perkampus, H.H., **4**, 195  
 Perkins, M.J., **17**, 1  
 Pittman, C.U, Jr., **4**, 305  
 Platz, M.S., **36**, 255  
 Pletcher, D., **10**, 155  
 Pross, A., **14**, 69; **21**, 99  
 Quintanilla, E., **37**, 57  
 Rajagopal, S., **36**, 167  
 Ramirez, F., **9**, 25

- Rappoport, Z., **7**, 1; **17**, 239  
 Rathore, R., **35**, 193  
 Reeves, L.W., **3**, 187  
 Reinhoudt, D.N., **17**, 279  
 Richard, J.P., **35**, 67  
 Ridd, J.H., **16**, 1  
 Riveros, J.M., **21**, 197  
 Robertson, J.M., **1**, 203  
 Rose, P.L., **28**, 45  
 Rosenthal, S.N., **13**, 279  
 Rotello, V.M., **37**, 315  
 Ruasse, M.-F., **28**, 207  
 Russell, G.A., **23**, 271  
 Samuel, D., **3**, 123  
 Sanchez, M, de N, de M.,  
**21**, 37  
 Sandström, J., **25**, 1  
 Savéant, J.-M., **26**, 1; **35**, 117  
 Savelli, G., **22**, 213  
 Schaleger, L.L., **1**, 1  
 Scheraga, H.A., **6**, 103  
 Schleyer, P., von R., **14**, 1  
 Schmidt, S.P., **18**, 187  
 Schuster, G.B., **18**, 187;  
**22**, 311  
 Scorrano, G., **13**, 83  
 Shatenshtein, A.I., **1**, 156  
 Shine, H.J., **13**, 155  
 Shinkai, S., **17**, 435  
 Siehl, H.-U., **23**, 63  
 Silver, B.L., **3**, 123  
 Simonyi, M., **9**, 127  
 Sinnott, M.L., **24**, 113  
 Stock, L.M., **1**, 35  
 Sugawara, T., **32**, 219  
 Sustmann, R., **26**, 131  
 Symons, M.C.R., **1**, 284  
 Takashima, K., **21**, 197  
 Takasu, I., **32**, 219  
 Takeuchi, K., **30**, 173  
 Tanaka, K.S.E., **37**, 239  
 Ta-Shma, R., **27**, 239  
 Tedder, J.M., **16**, 51  
 Tee, O.S., **29**, 1  
 Thatcher, G.R.J., **25**, 99  
 Thomas, A., **8**, 1  
 Thomas, J.M., **15**, 63  
 Tidwell, T.T., **36**, 1  
 Tonellato, U., **9**, 185  
 Toteva, M.M., **35**, 67  
 Toullec, J., **18**, 1  
 Tsuji, Y., **35**, 67  
 Tsuno, Y., **32**, 267  
 Tüdös, F., **9**, 127  
 Turner, D.W., **4**, 31  
 Turro, N.J., **20**, 1  
 Ugi, I., **9**, 25  
 Walton, J.C., **16**, 51  
 Ward, B., **8**, 1  
 Watt, C.I.F., **24**, 57  
 Wayner, D.D.M., **36**, 85  
 Wentworth, P., **31**, 249  
 Westaway, K.C., **31**, 143  
 Westheimer, F.H., **21**, 1  
 Whalley, E., **2**, 93  
 Williams, A., **27**, 1  
 Williams, D.L.H., **19**, 381  
 Williams, J.M., Jr., **6**, 63  
 Williams, J.O., **16**, 159  
 Williams, K.B., **35**, 67  
 Williams, R.V., **29**, 273  
 Williamson, D.G., **1**, 365  
 Wilson, H., **14**, 133  
 Wolf, A.P., **2**, 201  
 Wolff, J.J., **32**, 121  
 Workentin, M.S., **36**, 85  
 Wortmann, R., **32**, 121  
 Wyatt, P.A.H., **12**, 131  
 Zimmt, M.B., **20**, 1  
 Zollinger, H., **2**, 163  
 Zuman, P., **5**, 1

# Cumulative Index of Titles

- Abstraction, hydrogen atom, from O—H bonds, **9**, 127
- Acid–base behaviour macrocycles and other concave structures, **30**, 63
- Acid–base properties of electronically excited states of organic molecules, **12**, 131
- Acid solutions, strong, spectroscopic observation of alkylcarbonium ions in, **4**, 305
- Acids, reactions of aliphatic diazo compounds with, **5**, 331
- Acids, strong aqueous, protonation and solvation in, **13**, 83
- Acids and bases, oxygen and nitrogen in aqueous solution, mechanisms of proton transfer between, **22**, 113
- Activation, entropies of, and mechanisms of reactions in solution, **1**, 1
- Activation, heat capacities of, and their uses in mechanistic studies, **5**, 121
- Activation, volumes of, use for determining reaction mechanisms, **2**, 93
- Addition reactions, gas-phase radical directive effects in, **16**, 51
- Aliphatic diazo compounds, reactions with acids, **5**, 331
- Alkyl and analogous groups, static and dynamic stereochemistry of, **25**, 1
- Alkylcarbonium ions, spectroscopic observation in strong acid solutions, **4**, 305
- Ambident conjugated systems, alternative protonation sites in, **11**, 267
- Ammonia liquid, isotope exchange reactions of organic compounds in, **1**, 156
- Anions, organic, gas-phase reactions of, **24**, 1
- Antibiotics,  $\beta$ -lactam, the mechanisms of reactions of, **23**, 165
- Aqueous mixtures, kinetics of organic reactions in water and, **14**, 203
- Aromatic photosubstitution, nucleophilic, **11**, 225
- Aromatic substitution, a quantitative treatment of directive effects in, **1**, 35
- Aromatic substitution reactions, hydrogen isotope effects in, **2**, 163
- Aromatic systems, planar and non-planar, **1**, 203
- N-Arylnitrenium ions, **36**, 167
- Aryl halides and related compounds, photochemistry of, **20**, 191
- Arynes, mechanisms of formation and reactions at high temperatures, **6**, 1
- A-S<sub>E</sub>2 reactions, developments in the study of, **6**, 63
- Base catalysis, general, of ester hydrolysis and related reactions, **5**, 237
- Basicity of unsaturated compounds, **4**, 195
- Bimolecular substitution reactions in protic and dipolar aprotic solvents, **5**, 173
- Bond breaking, **35**, 117
- Bond formation, **35**, 117
- Bromination, electrophilic, of carbon–carbon double bonds: structure, solvent and mechanisms, **28**, 207
- <sup>13</sup>C NMR spectroscopy in macromolecular systems of biochemical interest, **13**, 279
- Captodative effect, the, **26**, 131
- Carbanion reactions, ion-pairing effects in, **15**, 153
- Carbene chemistry, structure and mechanism in, **7**, 163
- Carbenes having aryl substituents, structure and reactivity of, **22**, 311
- Carbocation rearrangements, degenerate, **19**, 223
- Carbocationic systems, the Yukawa-Tsuno relationship in, **32**, 267
- Carbocations, partitioning between addition of nucleophiles and deprotonation, **35**, 67
- Carbon atoms, energetic, reactions with organic compounds, **3**, 201
- Carbon monoxide, reactivity of carbonium ions towards, **10**, 29
- Carbonium ions, gaseous, from the decay of tritiated molecules, **8**, 79
- Carbonium ions, photochemistry of, **10**, 129
- Carbonium ions, reactivity towards carbon monoxide, **10**, 29



- Carbonium ions (alkyl), spectroscopic observation in strong acid solutions, **4**, 305
- Carbonyl compounds, reversible hydration of, **4**, 1
- Carbonyl compounds, simple, enolisation and related reactions of, **18**, 1
- Carboxylic acids, tetrahedral intermediates derived from, spectroscopic detection and investigation of their properties, **21**, 37
- Catalysis, by micelles, membranes and other aqueous aggregates as models of enzyme action, **17**, 435
- Catalysis, enzymatic, physical organic model systems and the problem of, **11**, 1
- Catalysis, general base and nucleophilic, of ester hydrolysis and related reactions, **5**, 237
- Catalysis, micellar, in organic reactions; kinetic and mechanistic implications, **8**, 271
- Catalysis, phase-transfer by quaternary ammonium salts, **15**, 267
- Catalytic antibodies, **31**, 249
- Cation radicals, in solution, formation, properties and reactions of, **13**, 155
- Cation radicals, organic, in solution, and mechanisms of reactions of, **20**, 55
- Cations, vinyl, **9**, 135
- Chain molecules, intramolecular reactions of, **22**, 1
- Chain processes, free radical, in aliphatic systems involving an electron transfer reaction, **23**, 271
- Charge density-NMR chemical shift correlation in organic ions, **11**, 125
- Chemically induced dynamic nuclear spin polarization and its applications, **10**, 53
- Chemiluminescence of organic compounds, **18**, 187
- Chirality and molecular recognition in monolayers at the air–water interface, **28**, 45
- CIDNP and its applications, **10**, 53
- Conduction, electrical, in organic solids, **16**, 159
- Configuration mixing model: a general approach to organic reactivity, **21**, 99
- Conformations of polypeptides, calculations of, **6**, 103
- Conjugated molecules, reactivity indices, in, **4**, 73
- Cross-interaction constants and transition-state structure in solution, **27**, 57
- Crown-ether complexes, stability and reactivity of, **17**, 279
- Crystallographic approaches to transition state structures, **29**, 87
- Cyclodextrins and other catalysts, the stabilization of transition states by, **29**, 1
- D<sub>2</sub>O—H<sub>2</sub>O mixtures, protolytic processes in, **7**, 259
- Degenerate carbocation rearrangements, **19**, 223
- Deuterium kinetic isotope effects, secondary, and transition state structure, **31**, 143
- Diazo compounds, aliphatic, reactions with acids, **5**, 331
- Diffusion control and pre-association in nitrosation, nitration, and halogenation, **16**, 1
- Dimethyl sulphoxide, physical organic chemistry of reactions, in, **14**, 133
- Diolefin crystals, photodimerization and photopolymerization of, **30**, 117
- Dipolar aprotic and protic solvents, rates of bimolecular substitution reactions in, **5**, 173
- Directive effects, in aromatic substitution, a quantitative treatment of, **1**, 35
- Directive effects, in gas-phase radical addition reactions, **16**, 51
- Discovery of mechanisms of enzyme action 1947–1963, **21**, 1
- Displacement reactions, gas-phase nucleophilic, **21**, 197
- Donor/acceptor organizations, **35**, 193
- Double bonds, carbon–carbon, electrophilic bromination of: structure, solvent and mechanism, **28**, 171
- Effective charge and transition-state structure in solution, **27**, 1
- Effective molarities of intramolecular reactions, **17**, 183
- Electrical conduction in organic solids, **16**, 159
- Electrochemical methods, study of reactive intermediates by, **19**, 131
- Electrochemical recognition of charged and neutral guest species by redox-active receptor molecules, **31**, 1
- Electrochemistry, organic, structure and mechanism in, **12**, 1
- Electrode processes, physical parameters for the control of, **10**, 155
- Electron donor–acceptor complexes, electron transfer in the thermal and photochemical activation of, in organic and organometallic reactions, **29**, 185
- Electron spin resonance, identification of organic free radicals, **1**, 284

- Electron spin resonance, studies of short-lived organic radicals, **5**, 23
- Electron storage and transfer in organic redox systems with multiple electrophores, **28**, 1
- Electron transfer, **35**, 117
- Electron transfer, in thermal and photochemical activation of electron donor-acceptor complexes in organic and organometallic reactions, **29**, 185
- Electron-transfer, single, and nucleophilic substitution, **26**, 1
- Electron-transfer, spin trapping and, **31**, 91
- Electron-transfer paradigm for organic reactivity, **35**, 193
- Electron-transfer reaction, free radical chain processes in aliphatic systems involving an, **23**, 271
- Electron-transfer reactions, in organic chemistry, **18**, 79
- Electronically excited molecules, structure of, **1**, 365
- Electronically excited states of organic molecules, acid-base properties of, **12**, 131
- Energetic tritium and carbon atoms, reactions of, with organic compounds, **2**, 201
- Enolisation of simple carbonyl compounds and related reactions, **18**, 1
- Entropies of activation and mechanisms of reactions in solution, **1**, 1
- Enzymatic catalysis, physical organic model systems and the problem of, **11**, 1
- Enzyme action, catalysis of micelles, membranes and other aqueous aggregates as models of, **17**, 435
- Enzyme action, discovery of the mechanisms of, 1947–1963, **21**, 1
- Equilibrating systems, isotope effects in NMR spectra of, **23**, 63
- Equilibrium constants, NMR measurements of, as a function of temperature, **3**, 187
- Ester hydrolysis, general base and nucleophilic catalysis, **5**, 237
- Ester hydrolysis, neighbouring group participation by carbonyl groups in, **28**, 171
- Excess acidities, **35**, 1
- Exchange reactions, hydrogen isotope, of organic compounds in liquid ammonia, **1**, 156
- Exchange reactions, oxygen isotope, of organic compounds, **2**, 123
- Excited complexes, chemistry of, **19**, 1
- Excited molecular, structure of electronically, **3**, 365
- Force-field methods, calculation of molecular structure and energy by, **13**, 1
- Free radical chain processes in aliphatic systems involving an electron-transfer reaction, **23**, 271
- Free Radicals 1900–2000, The Gomberg Century, **36**, 1
- Free radicals, and their reactions at low temperature using a rotating cryostat, study of, **8**, 1
- Free radicals, identification by electron spin resonance, **1**, 284
- Gas-phase heterolysis, **3**, 91
- Gas-phase nucleophilic displacement reactions, **21**, 197
- Gas-phase pyrolysis of small-ring hydrocarbons, **4**, 147
- Gas-phase reactions of organic anions, **24**, 1
- Gaseous carbonium ions from the decay of tritiated molecules, **8**, 79
- General base and nucleophilic catalysis of ester hydrolysis and related reactions, **5**, 237
- The Gomberg Century: Free Radicals 1900–2000, **36**, 1
- Gomberg and the Nobel Prize, **36**, 59
- H<sub>2</sub>O–D<sub>2</sub>O mixtures, protolytic processes in, **7**, 259
- Halides, aryl, and related compounds, photochemistry of, **20**, 191
- Halogenation, nitrosation, and nitration, diffusion control and pre-association in, **16**, 1
- Heat capacities of activation and their uses in mechanistic studies, **5**, 121
- Heterolysis, gas-phase, **3**, 91
- High-spin organic molecules and spin alignment in organic molecular assemblies, **26**, 179
- Homoaromaticity, **29**, 273
- How does structure determine organic reactivity, **35**, 67
- Hydrated electrons, reactions of, with organic compounds, **7**, 115
- Hydration, reversible, of carbonyl compounds, **4**, 1
- Hydride shifts and transfers, **24**, 57
- Hydrocarbons, small-ring, gas-phase pyrolysis of, **4**, 147
- Hydrogen atom abstraction from O–H bonds, **9**, 127
- Hydrogen bonding and chemical reactivity, **26**, 255

- Hydrogen isotope effects in aromatic substitution reactions, **2**, 163  
Hydrogen isotope exchange reactions of organic compounds in liquid ammonia, **1**, 156  
Hydrolysis, ester, and related reactions, general base and nucleophilic catalysis of, **5**, 237
- Interface, the air-water, chirality and molecular recognition in monolayers at, **28**, 45  
Intermediates, reactive, study of, by electrochemical methods, **19**, 131  
Intermediates, tetrahedral, derived from carboxylic acids, spectroscopic detection and investigation of their properties, **21**, 37  
The interplay between redox and recognition processes: models and devices, **37**, 315  
Intramolecular reactions, effective molarities for, **17**, 183  
Intramolecular reactions, of chain molecules, **22**, 1  
Ionic dissociation of carbon-carbon  $\alpha$ -bonds in hydrocarbons and the formation of authentic hydrocarbon salts, **30**, 173  
Ionization potentials, **4**, 31  
Ion-pairing effects in carbanion reactions, **15**, 153  
Ions, organic, charge density-NMR chemical shift correlations, **11**, 125  
Isomerization, permutational, of pentavalent phosphorus compounds, **9**, 25  
Isotope effects, hydrogen, in aromatic substitution reactions, **2**, 163  
Isotope effects, magnetic, magnetic field effects and, on the products of organic reactions, **20**, 1  
Isotope effects, on NMR spectra of equilibrating systems, **23**, 63  
Isotope effects, steric, experiments on the nature of, **10**, 1  
Isotope exchange reactions, hydrogen, of organic compounds in liquid ammonia, **1**, 150  
Isotope exchange reactions, oxygen, of organic compounds, **3**, 123  
Isotopes and organic reaction mechanisms, **2**, 1
- Kinetics, and mechanisms of reactions of organic cation radicals in solution, **20**, 55  
Kinetics and mechanism of the dissociative reduction of C–X and X–X bonds (X=O, S), **36**, 85  
Kinetics and spectroscopy of substituted phenylnitrenes, **36**, 255  
Kinetics, of organic reactions in water and aqueous mixtures, **14**, 203  
Kinetics, reaction, polarography and, **5**, 1
- $\beta$ -Lactam antibiotics, mechanisms of reactions, **23**, 165  
Least nuclear motion, principle of, **15**, 1
- Macrocycles and other concave structures, acid-base behaviour in, **30**, 63  
Macromolecular systems of biochemical interest,  $^{13}\text{C}$  NMR spectroscopy in, **13**, 279  
Magnetic field and magnetic isotope effects on the products of organic reactions, **20**, 1  
Mass spectrometry, mechanisms and structure in: a comparison with other chemical processes, **8**, 152  
Matrix infrared spectroscopy of intermediates with low coordinated carbon silicon and germanium atoms, **30**, 1  
Mechanism and reactivity in reactions of organic oxyacids of sulphur and their anhydrides, **17**, 65  
Mechanism and structure, in carbene chemistry, **7**, 153  
Mechanism and structure, in mass spectrometry: a comparison with other chemical processes, **8**, 152  
Mechanism and structure, in organic electrochemistry, **12**, 1  
Mechanism of the dissociative reduction of C–X and X–X bonds (X=O, S), kinetics and, **36**, 85  
Mechanisms, nitrosation, **19**, 381  
Mechanisms, of proton transfer between oxygen and nitrogen acids and bases in aqueous solutions, **22**, 113  
Mechanisms, organic reaction, isotopes and, **2**, 1  
Mechanisms of reaction, in solution, entropies of activation and, **1**, 1  
Mechanisms of reaction, of  $\beta$ -lactam antibiotics, **23**, 165  
Mechanisms of solvolytic reactions, medium effects on the rates and, **14**, 10  
Mechanistic analysis, perspectives in modern voltammeter: basic concepts and, **32**, 1  
Mechanistic applications of the reactivity–selectivity principle, **14**, 69  
Mechanistic studies, heat capacities of activation and their use, **5**, 121  
Medium effects on the rates and mechanisms of solvolytic reactions, **14**, 1

- Meisenheimer complexes, **7**, 211
- Metal complexes, the nucleophilicity of towards organic molecules, **23**, 1
- Methyl transfer reactions, **16**, 87
- Micellar catalysis in organic reactions: kinetic and mechanistic implications, **8**, 271
- Micelles, aqueous, and similar assemblies, organic reactivity in, **22**, 213
- Micelles, membranes and other aqueous aggregates, catalysis by, as models of enzyme action, **17**, 435
- Molecular recognition, chirality and, in monolayers at the air-water interface, **28**, 45
- Molecular structure and energy, calculation of, by force-field methods, **13**, 1
- N*-Arylnitrenium ions, **36**, 167
- Neighbouring group participation by carbonyl groups in ester hydrolysis, **28**, 171
- Nitration, nitrosation, and halogenation, diffusion control and pre-association in, **16**, 1
- Nitrosation, mechanisms, **19**, 381
- Nitrosation, nitration, and halogenation, diffusion control and pre-association in, **16**, 1
- NMR chemical shift-charge density correlations, **11**, 125
- NMR measurements of reaction velocities and equilibrium constants as a function of temperature, **3**, 187
- NMR spectra of equilibrating systems, isotope effects on, **23**, 63
- NMR spectroscopy, <sup>13</sup>C, in macromolecular systems of biochemical interest, **13**, 279
- Nobel Prize, Gomberg and the, **36**, 59
- Non-linear optics, organic materials for second-order, **32**, 121
- Non-planar and planar aromatic systems, **1**, 203
- Norbornyl cation: reappraisal of structure, **11**, 179
- Nuclear magnetic relaxation, recent problems and progress, **16**, 239
- Nuclear magnetic resonance see NMR
- Nuclear motion, principle of least, **15**, 1
- Nuclear motion, the principle of least, and the theory of stereoelectronic control, **24**, 113
- Nucleophiles, partitioning of carbocations between addition and deprotonation, **35**, 67
- Nucleophilic aromatic photosubstitution, **11**, 225
- Nucleophilic catalysis of ester hydrolysis and related reactions, **5**, 237
- Nucleophilic displacement reactions, gas-phase, **21**, 197
- Nucleophilic substitution, in phosphate esters, mechanism and catalysis of, **25**, 99
- Nucleophilic substitution, single electron transfer and, **26**, 1
- Nucleophilic vinylic substitution, **7**, 1
- Nucleophilic vinylic substitution and vinyl cation intermediates in the reactions of vinyl iodonium salts, **37**, 1
- Nucleophilicity of metal complexes towards organic molecules, **23**, 1
- O—H bonds, hydrogen atom abstraction from, **9**, 127
- Organic materials for second-order non-linear optics, **32**, 121
- Organic reactivity, electron-transfer paradigm for, **35**, 193
- Organic reactivity, structure determination of, **35**, 67
- Oxyacids of sulphur and their anhydrides, mechanisms and reactivity in reactions of organic, **17**, 65
- Oxygen isotope exchange reactions of organic compounds, **3**, 123
- Partitioning of carbocations between addition of nucleophiles and deprotonation, **35**, 67
- Perchloro-organic chemistry: structure, spectroscopy and reaction pathways, **25**, 267
- Permutational isomerization of pentavalent phosphorus compounds, **9**, 25
- Phase-transfer catalysis by quaternary ammonium salts, **15**, 267
- Phenylitrenes, Kinetics and spectroscopy of substituted, **36**, 255
- Phosphate esters, mechanism and catalysis of nucleophilic substitution in, **25**, 99
- Phosphorus compounds, pentavalent, turnstile rearrangement and pseudoration in permutational isomerization, **9**, 25
- Photochemistry, of aryl halides and related compounds, **20**, 191
- Photochemistry, of carbonium ions, **9**, 129
- Photodimerization and photopolymerization of diolefin crystals, **30**, 117
- Photosubstitution, nucleophilic aromatic, **11**, 225

- The physical organic chemistry of Fischer carbene complexes, **37**, 137
- Planar and non-planar aromatic systems, **1**, 203
- Polarizability, molecular refractivity and, **3**, 1
- Polarography and reaction kinetics, **5**, 1
- Polypeptides, calculations of conformations of, **6**, 103
- Pre-association, diffusion control and, in nitrosation, nitration, and halogenation, **16**, 1
- Principle of non-perfect synchronization, **27**, 119
- Products of organic reactions, magnetic field and magnetic isotope effects on, **30**, 1
- Protic and dipolar aprotic solvents, rates of bimolecular substitution reactions in, **5**, 173
- Protolytic processes in H<sub>2</sub>O–D<sub>2</sub>O mixtures, **7**, 259
- Proton transfer between oxygen and nitrogen acids and bases in aqueous solution, mechanisms of, **22**, 113
- Protonation and solvation in strong aqueous acids, **13**, 83
- Protonation sites in ambident conjugated systems, **11**, 267
- Pseudorotation in isomerization of pentavalent phosphorus compounds, **9**, 25
- Pyrolysis, gas-phase, of small-ring hydrocarbons, **4**, 147
- Radiation techniques, application to the study of organic radicals, **12**, 223
- Radical addition reactions, gas-phase, directive effects in, **16**, 51
- Radicals, cation in solution, formation, properties and reactions of, **13**, 155
- Radicals, organic application of radiation techniques, **12**, 223
- Radicals, organic cation, in solution kinetics and mechanisms of reaction of, **20**, 55
- Radicals, organic free, identification by electron spin resonance, **1**, 284
- Radicals, short-lived organic, electron spin resonance studies of, **5**, 53
- Rates and mechanisms of solvolytic reactions, medium effects on, **14**, 1
- Reaction kinetics, polarography and, **5**, 1
- Reaction mechanisms, in solution, entropies of activation and, **1**, 1
- Reaction mechanisms, use of volumes of activation for determining, **2**, 93
- Reaction velocities and equilibrium constants, NMR measurements of, as a function of temperature, **3**, 187
- Reactions, in dimethyl sulphoxide, physical organic chemistry of, **14**, 133
- Reactions, of hydrated electrons with organic compounds, **7**, 115
- Reactive intermediates, study of, by electrochemical methods, **19**, 131
- Reactivity, organic, a general approach to: the configuration mixing model, **21**, 99
- Reactivity indices in conjugated molecules, **4**, 73
- Reactivity-selectivity principle and its mechanistic applications, **14**, 69
- Rearrangements, degenerate carbocation, **19**, 223
- Receptor molecules, redox-active, electrochemical recognition of charged and neutral guest species by, **31**, 1
- Redox systems, organic, with multiple electrophores, electron storage and transfer in, **28**, 1
- Reduction of C–X and X–X bonds (X=O, S), kinetics and mechanism of the dissociative, **36**, 85
- Refractivity, molecular, and polarizability, **3**, 1
- Relaxation, nuclear magnetic, recent problems and progress, **16**, 239
- Selectivity of solvolyses and aqueous alcohols and related mixtures, solvent-induced changes in, **27**, 239
- Short-lived organic radicals, electron spin resonance studies of, **5**, 53
- Small-ring hydrocarbons, gas-phase pyrolysis of, **4**, 147
- Solid state, tautomerism in the, **32**, 129
- Solid-state chemistry, topochemical phenomena in, **15**, 63
- Solids, organic, electrical conduction in, **16**, 159
- Solutions, reactions in, entropies of activation and mechanisms, **1**, 1
- Solvation and protonation in strong aqueous acids, **13**, 83
- Solvent, protic and dipolar aprotic, rates of bimolecular substitution-reactions in, **5**, 173
- Solvent-induced changes in the selectivity of solvolyses in aqueous alcohols and related mixtures, **27**, 239
- Solvolytic reactions, medium effects on the rates and mechanisms of, **14**, 1

- Spectroscopic detection of tetrahedral intermediates derived from carboxylic acids and the investigation of their properties, **21**, 37
- Spectroscopic observations of alkylcarbonium ions in strong acid solutions, **4**, 305
- Spectroscopy,  $^{13}\text{C}$  NMR, in macromolecular systems of biochemical interest, **13**, 279
- Spectroscopy of substituted phenylnitrenes, kinetics and, **36**, 255
- Spin alignment, in organic molecular assemblies, high-spin organic molecules and, **26**, 179
- Spin trapping, **17**, 1
- Spin trapping, and electron transfer, **31**, 91
- Stability and reactivity of crown-ether complexes, **17**, 279
- Stereochemistry, static and dynamic, of alkyl and analogous groups, **25**, 1
- Stereoelectronic control, the principle of least nuclear motion and the theory of, **24**, 113
- Stereoselection in elementary steps of organic reactions, **6**, 185
- Steric isotope effects, experiments on the nature of, **10**, 1
- Structure, determination of organic reactivity, **35**, 67
- Structure and mechanism, in carbene chemistry, **7**, 153
- Structure and mechanism, in organic electrochemistry, **12**, 1
- Structure and reactivity of carbenes having aryl substituents, **22**, 311
- Structure of electronically excited molecules, **1**, 365
- Substitution, aromatic, a quantitative treatment of directive effects in, **1**, 35
- Substitution, nucleophilic vinylic, **7**, 1
- Substitution reactions, aromatic, hydrogen isotope effects in, **2**, 163
- Substitution reactions, bimolecular, in protic and dipolar aprotic solvents, **5**, 173
- Sulphur, organic oxyacids of, and their anhydrides, mechanisms and reactivity in reactions of, **17**, 65
- Superacid systems, **9**, 1
- Tautomerism in the solid state, **32**, 219
- Temperature, NMR measurements of reaction velocities and equilibrium constants as a function of, **3**, 187
- Tetrahedral intermediates, derived from carboxylic acids, spectroscopic detection and the investigation of their properties, **21**, 37
- Thermodynamic stabilities of carbocations, **37**, 57
- Topochemical phenomena in solid-state chemistry, **15**, 63
- Transition state analysis using multiple kinetic isotope effects: mechanisms of enzymatic and non-enzymatic glycoside hydrolysis and transfer, **37**, 239
- Transition state structure, crystallographic approaches to, **29**, 87
- Transition state structure, in solution, effective charge and, **27**, 1
- Transition state structure, secondary deuterium isotope effects and, **31**, 143
- Transition states, structure in solution, cross-interaction constants and, **27**, 57
- Transition states, the stabilization of by cyclodextrins and other catalysts, **29**, 1
- Transition states, theory revisited, **28**, 139
- Tritiated molecules, gaseous carbonium ions from the decay of, **8**, 79
- Tritium atoms, energetic reactions with organic compounds, **2**, 201
- Turnstile rearrangements in isomerization of pentavalent phosphorus compounds, **9**, 25
- Unsaturated compounds, basicity of, **4**, 195
- Vinyl cations, **9**, 185
- Vinylic substitution, nucleophilic, **7**, 1
- Voltammetry, perspectives in modern: basic concepts and mechanistic analysis, **32**, 1
- Volumes of activation, use of, for determining reaction mechanisms, **2**, 93
- Water and aqueous mixtures, kinetics of organic reactions in, **14**, 203
- Yukawa–Tsuno relationship in carboranic systems, the, **32**, 267

# Author Index

*Numbers in italics refer to the pages on which references are listed at the end of each chapter*

- Abbound, J.-L.M., 57, 128, 129, 131, 132, 135  
Abdulah, D.R., 312  
Abel, E.W., 233, 336  
Ackermann, K., 234  
Adamczak, O., 128  
Adamo, C., 314  
Adams, N.G., 132  
Afeefy, H.Y., 128  
Agawa, T., 54  
Ahlrichs, R., 130  
Ahrens, M.-L., 235  
Alem, K.V., 336  
Ali, M., 236, 237  
Alkorta, I., 57, 131, 132  
Al-Laham, M.A., 314  
Allara, D.L., 337  
Almo, S.C., 309, 310  
Alper, H., 233  
Altenbach, H.-J., 233  
Alves, S., 335  
Amin, S.R., 237  
Amyes, T.L., 135, 237, 311  
Anderson, B.A., 233  
Anderson, R.L., 207, 233, 234, 237  
Anderson, S.W., 55  
Anderson, V.E., 308, 311  
Andraos, J., 236  
Andres, R.P., 337  
Andres, J.L., 314  
Andrews, C.W., 310  
Andrews, M.N., 55  
Andrews, T., 310  
Anelli, P.L., 335  
Anet, F.A., 132  
Angeletti, R.H., 309  
Angelici, R.J., 235  
Anicich, V.G., 127  
Anthony, C., 335  
Antoine, R., 312  
Aoyagi, Y., 310  
Apeloig, Y., 55, 133  
Apitz-Castro, R., 312  
Araki, K., 335  
Arima, K., 129  
Armstrong, G.D., 312  
Arnett, E.M., 72, 120, 123, 126, 130, 135  
Arnold, J.J., 337  
Arvagli, M., 132  
Asano, T., 53  
Asao, T., 135  
Asensi, M.A., 127  
Asher, R.L., 129  
Ashton, P.R., 337  
Atreya, S.K., 127  
Atwood, J.L., 336  
Aubry, C., 97, 132  
Aue, D.H., 55, 128, 131  
Aumann, R., 180, 182, 194, 195, 233, 235, 236  
Ausloos, P., 62, 129, 130, 133  
Avendaño, C., 134  
Axelsson, S., 308  
Ayala, P.Y., 314  
Baboul, A.G., 53  
Bach, R.D., 53, 133  
Badenhoop, J., 134  
Badia, A., 337  
Baer, T., 59, 128, 130  
Baeyer, A.v., 134  
Bagdassarian, C.K., 309, 313  
Bagno, A., 55, 133  
Bahn, C.A., 55  
Bahnon, B.J., 308, 311  
Baines, S., 310  
Baker, E.B., 134  
Ballardini, R., 335  
Balle, T., 129  
Ballesteros, E., 129  
Ballou, D.P., 312  
Balzani, V., 335, 336, 337  
Banait, N.S., 134, 236  
Banaszkiewicz, M., 127  
Banks, G.A., 310  
Barbour, L., 336  
Barker, C., 310  
Barnes, J.A., 311  
Barone, V., 314  
Bartlett, R.J., 130, 132  
Bartmess, J.E., 59, 60, 128  
Bartolotti, L.J., 237  
Bassi, P., 54  
Bau, R., 134  
Beak, P., 308  
Beauchamp, J.L., 97, 101, 129, 130, 132, 133

- Bebout, D.C., 130  
 Becalski, A., 310  
 Bechara, J.N., 234  
 Becher, J., 337  
 Becke, A.D., 257, 313  
 Bein, T., 337  
 Bell, A.F., 311  
 Bell, C.E., 310, 312  
 Bell, R.A., 235  
 Bell, S.E.J., 234  
 Belohradski, M., 337  
 BeMiller, J.N., 308  
 Benet-Buchholz, J., 335  
 Benkovic, S.J., 335  
 Bennet, A.J., 240, 283, 286, 308, 309, 311, 312  
 Bennett, M.J., 312  
 Bentley, T.W., 54, 55, 135  
 Bentz, H., 55  
 Bergman, R.G., 53  
 Berkowitz, J., 99, 130, 133  
 Berner, M., 131  
 Bernasconi, C.F., 137, 235, 236, 237, 263, 266, 310, 311  
 Berti, P.J., 239, 308, 309, 310  
 Bese, R., 55  
 Bezard, B., 127  
 Bien, J.T., 337  
 Bierbaum, V.M., 133  
 Bigler, P., 134  
 Bingham, C.R., 135  
 Bisell, R.A., 336  
 Bittner, E.W., 130  
 Black, K.A., 309  
 Blackburn, G.M., 311, 312  
 Blair, L., 131  
 Blakley, R.L., 335  
 Blanc, J., 135  
 Blanchard, J.S., 312, 313  
 Blanchard, P., 337  
 Blanke, S.R., 308, 312  
 Blush, J.A., 129  
 Boal, A.K., 337  
 Boche, G., 54  
 Bocher, S., 55  
 Bodley, J.W., 312  
 Boese, R., 128, 335  
 Bogey, M., 133  
 Boggs, J.E., 133  
 Böhme, D.K., 59, 128, 130  
 Bols, M., 310  
 Bolvin, H., 133  
 Bommuswamy, J., 312  
 Boodhoo, A., 312  
 Bordwell, F.G., 224, 236, 237  
 Boronat, M., 128  
 Boschke, F.L., 335  
 Botschwina, P., 129, 133  
 Bott, K., 56  
 Boutellier, M., 313  
 Bowen, J.P., 310  
 Bowers, M.T., 128  
 Boyer, G., 129  
 Boyle, W.J., Jr., 236  
 Brant, S.R., 236  
 Braun, M., 233  
 Braunheim, B.B., 313  
 Breinlinger, E., 336, 337  
 Bremer, M., 133  
 Breuckmann, R., 128  
 Brookhart, M., 133, 233  
 Brouard, M., 130  
 Brown, H.C., 132, 134, 135  
 Brown, S.D., 236  
 Bruce, J.M., 336  
 Bruce, P.Y., 237  
 Bruner, M., 309, 310  
 Bruner, S.D., 272, 313  
 Bruno, J.W., 237  
 Brunsvold, W.P., 235  
 Brunsvold, W.R., 237  
 Bug, T., 135  
 Bühl, M., 133  
 Bull, H.G., 308, 311, 312  
 Bülow, A., 310  
 Bumm, L.A., 337  
 Buncel, E., 308  
 Bunnell, C.A., 235  
 Burant, J.C., 313  
 Burgin, T.P., 337  
 Burkert, U., 335  
 Burkhardt, T.I., 234, 235  
 Burrichter, A., 134  
 Burton, G.W., 308, 309  
 Bushick, R.D., 135  
 Buss, V., 132  
 Buzek, P., 130  
 Cahill, S.M., 310  
 Cai, R., 234  
 Calabrese, J.C., 235  
 Caldwell, W.S., 311  
 Callender, R.H., 311, 313  
 Cammi, R., 314  
 Capon, B., 308  
 Capozzi, G., 54  
 Capozzi, G., 54  
 Carey, F.A., 131  
 Carey, P.R., 311, 312  
 Carnahan, E.J., 55  
 Carter, E.A., 233  
 Casamassina, T.E., 309  
 Casey, C.P., 154, 207, 233, 234, 235, 237  
 Castaño, O., 129, 132  
 Castro, R., 336  
 Cenci di Bello, I., 310



- Cesa, M.C., 234  
 Challacombe, M., 314  
 Chan, A.W.-Y., 313  
 Chan, C., 134  
 Chan, Y.L., 311  
 Chang, J.C., 313  
 Chang, L.W.K., 135  
 Chantooni, M.K., 237  
 Chapman, S.K., 335  
 Charton, B.I., 129  
 Charton, M., 55, 129  
 Chase, M.W., 68  
 Cheeseman, J.R., 313  
 Chelsky, D., 313  
 Chen, D.-W., 54  
 Chen, P., 129, 133  
 Chen, W., 127, 130, 314  
 Chen, X.-Y., 236, 309, 313  
 Chen, Y., 336  
 Chen, Z.-C., 54  
 Cheng, H., 311  
 Cherian, X.M., 312  
 Chesnut, D.B., 237  
 Chickos, J.S., 128  
 Childs, R.F., 131  
 Chisholm, M.H., 235  
 Choe, J.C., 134  
 Choe, S., 312  
 Choi, H.S., 235  
 Chuchani, G., 129  
 Cioslowski, J., 314  
 Claramunt, R., 129  
 Clark, D.T., 132  
 Clark, T., 131  
 Clarke, T.C., 53  
 Cleland, W.W., 309  
 Clifford, S., 314  
 Cockle, S.A., 312  
 Cohen, P., 313  
 Collier, C.P., 337  
 Collier, R.J., 312  
 Collman, J.P., 234  
 Comisarow, M.B., 132, 134  
 Comte, P., 134  
 Connor, J.A., 234  
 Connor, T.M., 134  
 Cook, P.F., 308, 309, 312  
 Cook, W.J., 309  
 Cooke, G., 336  
 Corbin, D.R., 134  
 Cordes, E.H., 294, 308, 311, 312  
 Cordonnier, M., 133  
 Cordova, E., 336  
 Corma, A., 127, 128  
 Correll, C.C., 311  
 Cossi, M., 314  
 Costopoulos, M.G., 131  
 Couch, D.A., 235  
 Cox, R.A., 119, 135  
 Cozens, F., 134  
 Cozens, F.L., 134  
 Crabtree, R.H., 139, 233  
 Craig, N.C., 133  
 Craig, S.P., III, 313  
 Credi, A., 336, 337  
 Cremer, D., 133  
 Crofton, M.W., 129, 133  
 Crooks, R.M., 335  
 Cseh, G., 55  
 Cuccia, L., 337  
 Cuello, A.O., 336, 337  
 Cui, Q., 314  
 Cukier, R., 336  
 Curmi, P.M., 312  
 Curtiss, L.A., 129, 130  
 Cygan, M.T., 337  
 Cyrański, M.K., 133  
 Czarnick, A.W., 312  
 Czarnocki, Z., 133  
 Dahlgren, R.M., 234  
 Daniels, A.D., 314  
 Dapprich, S., 313  
 Dávalos, J., 131, 132  
 Dávalos, J.Z., 57, 129, 131, 132  
 Davico, G.E., 133  
 Davies, G., 312  
 Davis, R.D., 56  
 Deans, R., 336, 337  
 de Diego, C., 134  
 Dedieu, A., 236  
 DeFrees, D.J., 131, 132  
 Degano, M., 310, 313  
 de Konig, L.J., 130  
 Della, E.W., 129, 135  
 de M. Carneiro, J.W., 130, 131  
 de Meijere, A., 131, 142, 233  
 Demers, L., 337  
 Demuyne, C., 133  
 Deng, H., 311, 313  
 Deng, L., 313  
 Deno, N.C., 131, 135  
 DePuy, C.H., 133  
 de Rege, P.J., 336  
 De Silva, A.P., 335  
 Deslongchamps, P., 312  
 Destombes, J.L., 133  
 Destro, R., 54  
 de Weck, G., 233  
 Diaz, A., 133  
 Diederich, F., 335, 336  
 Dinner, A.R., 311  
 Disch, R.L., 133  
 Divisia-Blohorn, B., 336  
 Dixon, D.A., 129  
 Djordjevic, S., 312

- Doering, W.v.E., 109, 134  
 Domalski, E.S., 128  
 Dong, J., 312  
 Dong, W., 310  
 Donkai, N., 54  
 Donovan, D.J., 130  
 D'Ordine, R.L., 311  
 Dorling, P., 310  
 Dorofeeva, O.V., 128  
 Dorogi, M., 337  
 Doron, A., 337  
 Dörwald, F.Z., 233  
 Dötz, K.H., 137, 143, 202, 233, 234, 236  
 Dougherty, D.A., 336  
 Doyle, M.P., 233  
 Drechsler, U., 315  
 Drohat, A.C., 311, 312  
 Drossart, P., 127  
 Dueber, T.E., 54  
 Duetsch, M., 233  
 Dunathan, H.C., 312  
 Dunbar, T.D., 337  
 Dunkin, D.B., 130  
 Duraisamy, M., 54  
 Duran, M., 234  
 Dutler, R., 132  
 Dwek, R.A., 308  
 Dyke, J., 72, 129, 130  
  
 Eakin, A.E., 313  
 Ealick, S.E., 277, 309  
 East, A.L.L., 128  
 Echegoyen, L., 335  
 Edmondson, D., 336  
 Edwards, B.H., 234  
 Eichinger, D., 312  
 Eiden, G.C., 134  
 Eigen, M., 235  
 Eisenberg, D., 310, 312  
 Elder, F.A., 134  
 Elguero, J., 129, 134  
 Ellis, A., 130  
 Ellison, G.B., 99, 133  
 Encrenaz, T.H., 127  
 Endo, Y., 313  
 Engel, P., 134  
 Eren, M., 336  
 Eriks, H., 134  
 Ervin, K.M., 59, 128  
 Escribano, R., 133  
 Estupinan, B., 310, 312, 313  
 Evans, G.B., 311  
 Evans, S.V., 310  
 Evantova, I., 235  
  
 Faggiani, R., 131  
 Fahey, R.C., 312  
 Fairchild, C., 309  
  
 Fairley, D.A., 127  
 Falkenberg-Andersen, C., 131  
 Fang, Y.R., 311  
 Farcasiu, D., 127, 128, 135  
 Farkas, O., 314  
 Farnum, D.G., 134  
 Fassberg, J., 235, 236  
 Federov, A.A., 309  
 Fedorov, A., 309  
 Fedorov, E., 309  
 Feher, G., 336  
 Fehsenfeld, F.C., 130  
 Feller, D., 129  
 Fellows, L., 310  
 Fellows, L.E., 310  
 Fendrich, G., 236  
 Feng, S., 337  
 Feng, W.Q., 135  
 Feng, Y., 311  
 Ferguson, E.E., 132  
 Ferguson, L.N., 134  
 Feringa, B.L., 336  
 Fermin, M.C., 237  
 Ferraz, J.P., 312  
 Fersht, A.R., 309  
 Feuchtgruber, H., 127  
 Fickling, M.M., 237  
 Field, F.H., 129, 130, 131  
 Finet, J.-P., 55  
 Finke, R.G., 234  
 Fischer, A., 237  
 Fischer, E.O., 147, 153, 154, 167, 171, 179,  
     195, 233, 234, 235, 236  
 Fischer, H., 147, 152, 153, 154, 167, 168, 202,  
     203, 233, 234, 235, 236, 237  
 Fischer, I., 133  
 Fleet, G., 310  
 Fleet, G.W.J., 310  
 Fleischer, U., 133  
 Fleming, I., 233  
 Flores, F.X., 235, 236, 237  
 Flores, H., 129  
 Flügge, J., 133  
 Focia, P.J., 313  
 Foley, H.C., 234  
 Foote, C.S., 135  
 Foresman, J.B., 314  
 Fornarini, S., 24, 55  
 Forsyth, D.A., 130  
 Fort, R.C., Jr., 132  
 Fouchet, T., 127  
 Fox, D.J., 314  
 Frank, A., 235  
 Frank, R.M., 135  
 Fraser-Reid, B., 310  
 Frenking, G., 133  
 Frere, P., 337  
 Frisch, M.J., 313

- Fry, A., 309  
Fujii, G., 312  
Fujio, M., 129  
Fujisaki, N., 134  
Fujita, E., 54  
Fujita, M., 54, 55  
Fukuyama, K., 336  
Fukuzumi, S., 336  
Furieux, R.H., 309, 310, 311, 313  
Furutani, M., 54  
Fyfe, M.C.T., 337
- Gabrys, C.M., 133  
Gainsford, G.J., 309  
Gallop, M.A., 233  
Galow, T.H., 336, 337  
Gandler, J.R., 235, 236, 237  
Ganem, B., 313  
García, H., 127  
García-Río, L., 236, 237  
Garrat, P.J., 134  
Gaúman, T., 134  
Gauss, J., 133  
Gaw, J.F., 133  
Gawlita, E., 308, 311  
Gawronska, K., 54  
Gawronski, J., 54  
Geoffroy, G.L., 234  
Ghisla, S., 335  
Giblin, D., 131  
Gilat, S.L., 337  
Gilbert, T., 133  
Gill, P.M.W., 314  
Gilliland, G.L., 313  
Girvin, M.E., 310  
Glad, S.S., 309, 311  
Glassgold, A.E., 127  
Gluck, A., 313  
Glukhovtsev, M.N., 53, 79, 131, 133  
Gobbi, A., 133  
Gobbi, L., 336  
Goddard, R., 236  
Goddard, W.A., III, 233  
Goedken, V., 54  
Goitein, R.K., 313  
Gokel, G.W., 336  
Gold, V., 135  
Gomberg, M., 134  
Gomes da Mesquita, A.H., 134  
Gómez, P.C., 133  
Gomez-Lopez, M., 335  
Gomperts, R., 129, 132, 314  
Gonzalez, C., 314  
Goodman, A., 337  
Gopaul, D.N., 313  
Gordley, R.G., 313  
Gordon, K.C., 234  
Goren, A., 130
- Goto, S., 54  
Gotta, M.F., 135  
Gottlieb, C.A., 127  
Graige, M.S., 336  
Grammer, J.C., 311  
Greaves, M.D., 336  
Greenberg, A., 128  
Gresser, M.J., 235  
Grob, C.A., 55, 132  
Gronheid, R., 54, 55, 56  
Gross, M.L., 131  
Grubmeyer, C., 310, 313  
Grunwald, E., 55, 236  
Guelin, M., 127  
Guerchais, V., 233  
Gunaratne, H.Q.N., 335  
Gund, T.M., 132  
Gurvich, L.V., 128  
Gustafson, S.M., 309  
Gut, H.-P., 234  
Gutfreund, H., 309  
Guthrie, J.P., 182, 236  
Guthrie, R.D., 309  
Gutman, D., 99
- Haber, M.T., 236  
Haddon, R.C., 133  
Häfelinger, G., 133  
Hafner, A., 233  
Hagen, E.L., 130  
Hagen, L., 130  
Halcomb, R.L., 312  
Hall, M.B., 233  
Hall, N.E., 134  
Haller, K.J., 234  
Haltner, G., 235  
Hammond, B.L., 131  
Hanack, M., 41, 53, 55  
Hancu, D., 127, 128  
Handy, N.C., 133  
Hansch, C., 236  
Hansch, S.C., 236  
Hanson, J.C., 309  
Hantzsch, A., 134  
Harch, P., 135  
Harding, C.E., 55  
Hargrove, R.J., 55  
Hariharan, P.C., 130  
Harkless, J.A.W., 133  
Harms, K., 54  
Harris, J.M., 135  
Harvey, D.F., 233  
Hasako, T., 55  
Hasford, J.J., 335  
Hawes, B.W.V., 135  
Hawkins, B., 233  
Hayashi, Y., 54  
Hazell, R.G., 310

- Hazzard, J., 335  
 Head-Gordon, M., 314  
 Hearing, E.D., 128  
 Heath, J.R., 337  
 Hecht, S.M., 308  
 Heck, A.J.R., 130  
 Heckl, B., 234, 235  
 Hegedus, L.S., 233, 234  
 Hehre, E.J., 312  
 Hehre, W.J., 131, 311  
 Heilbronner, E., 131  
 Heinen, A., 233  
 Held, W., 235  
 Hemsworth, R.S., 130  
 Henderson, J.I., 337  
 Hepp, W., 234  
 Herchlag, D., 236  
 Hering, N., 135  
 Herreros, M., 129  
 Hershberger, S.A., 235  
 Heus, H.A., 311  
 Hiebert, T., 309  
 Himmelreich, D., 234  
 Hine, J., 135, 236  
 Hinkle, R.J., 36, 39, 54, 55  
 Hinterding, P., 236  
 Hiraoka, K., 129, 131, 132  
 Hodge, J.D., 131  
 Hofelich, T.C., 135  
 Hoffmann, R., 131  
 Hofmann, P., 233, 234  
 Hogeveen, H., 55  
 Hol, W.G.J., 336  
 Holan, G., 310  
 Hollenstein, S., 130  
 Holman, R.W., 131  
 Holmes, J.L., 132  
 Honegger, M., 131  
 Hoos, R., 310  
 Horenstein, B.A., 272, 309, 310, 312, 313  
 Hori, Y., 55  
 Horig, H., 309  
 Horn, M., 129, 133  
 Hosie, L., 286, 309  
 Houk, K.N., 309  
 Houle, F.A., 101, 130, 133  
 Houriet, R., 132, 135  
 Houser, J.J., 131  
 Huang, X., 309  
 Huang, X.C., 286, 311  
 Hückel, E.Z., 109, 134  
 Hudgens, J.W., 129  
 Hughes, A.B., 310  
 Huixin, J., 310  
 Hummel, K., 55  
 Hunter, C.A., 336  
 Hunter, E.P.L., 128  
 Hupe, D.J., 236  
 Hurley, J., 335  
 Huskey, W.P., 308, 309  
 Hussenius, A., 308  
 Hyun, K.H., 53  
 Ichikawa, M., 310  
 Ichikawa, Y., 310, 312, 313  
 Igarashi, Y., 310  
 Iizaki, T., 335  
 Ilhan, F., 336  
 Imamura, S., 53, 56  
 Imbriglio, J., 336  
 Indurugalla, D., 312  
 Inoue, H., 129  
 Inouye, S., 310  
 Irikura, K.K., 129  
 Irrgang, B., 135  
 Ishida, Y., 55, 56  
 Ito, S., 135  
 Ito, T., 310  
 Itoh, S., 336  
 Jablonowski, J.A., 312  
 Jacob, G.S., 310  
 Jacox, M.E., 129  
 Jagadeesh, G.J., 313  
 Jagerovic, N., 129  
 Jagod, J.F., 129  
 Jagod, M.-F., 133  
 Jagow, R.H., 312  
 Janker, B., 135  
 Jarret, R.M., 132  
 Jaruzelski, J.J., 131  
 Jarvis, G.K., 130  
 Jayaprakash, K.N., 237  
 Jencks, W.P., 235, 236, 292, 309, 312  
 Jensen, F., 309, 311  
 Jeong, J.H., 310  
 Jespersen, T.M., 310  
 Jestin, I., 337  
 Jeuell, G.L., 131  
 Jiang, Y.L., 313  
 Jiménez, P., 129, 132  
 Johnson, B.G., 314  
 Johnson, K.E., 134  
 Johnson, R.A., 235  
 Johnson, R.D., 129  
 Johnson, R.W., 311  
 Johnson, S.A., 132  
 Johnston, H.S., 309  
 Jonathan, N., 129, 130  
 Jones, G.D., 312  
 Jones, L., 337  
 Jones, M., Jr., 237  
 Jorgensen, W.L., 131  
 Jorish, S.V., 128  
 Jovine, L., 312  
 Jucker, F.M., 311

- Julich, E., 310  
 Jursic, B.S., 130  
  
 Kabakoff, D.S., 131  
 Kafafi, S.A., 129  
 Kaifer, A.E., 335, 336, 337  
 Kajimoto, T., 310, 312  
 Kalbfus, W., 235  
 Kaljurand, I., 129  
 Kalk, K.H., 336  
 Kamieth, M., 335  
 Kampf, J.W., 336  
 Kanagasabapathy, V.M., 134, 236  
 Kantardjieff, K.A., 312  
 Karplus, M., 311  
 Karsten, W.E., 312  
 Kates, M.R., 131  
 Kati, W.M., 313  
 Katritzky, A.R., 133  
 Katz, E., 337  
 Kaufman, H.L., 309  
 Kawai, S.H., 337  
 Kawakami, H., 336  
 Kazunari, T., 313  
 Kebarle, P., 59, 65, 128, 129, 131, 132, 134  
 Keenan, C., 336  
 Kehrmann, F., 134  
 Keister, J.W., 130  
 Keith, T., 314  
 Keller, U.M., 134  
 Kelly, D.P., 131  
 Kelsey, D.R., 53  
 Kemnitzer, W., 335  
 Kempf, B., 135  
 Kendrick, R.D., 130  
 Kern, J.M., 336  
 Kessinger, R., 335  
 Ketner, R.J., 236  
 Kevill, D.N., 55  
 Kicska, G., 309  
 Kicska, G.A., 309  
 Kida, M., 54  
 Killion, R.B., 235, 236  
 Kim, B.J., 308  
 Kim, C.K., 9, 53  
 Kim, M.S., 134  
 Kim, S.-J., 130  
 Kinoshita, T., 129  
 Kin-Yan, , 237  
 Kirby, A.J., 236  
 Kirby, S.P., 128  
 Kirkpatrick, C.M., 233  
 Kirsch, J.F., 308  
 Kitagawa, T., 127  
 Kitamura, T., 56  
 Kittredge, K., 237  
 Kittredge, K.W., 236, 237  
  
 Klabunde, U., 234  
 Klarner, F.G., 335  
 Klein, M.H., 312  
 Kleine, W., 234  
 Kline, P.C., 308, 309  
 Klinman, J., 336  
 Klopper, W., 130  
 Klug, D.D., 133  
 Knauss, L., 235  
 Knox, L.H., 109, 134  
 Kobayashi, S., 55, 56  
 Koch, W., 130, 131, 132, 133  
 Kochi, J.K., 134  
 Koenig, T., 129  
 Koerner, T., 311  
 Koga, K., 55  
 Kohen, A., 336  
 Kohno, T., 313  
 Kollmeier, H.-J., 234  
 Koltthoff, I.M., 237  
 Kolthoff, I.M., 237  
 Komaromi, I., 314  
 Komatsu, K., 127  
 Komatsu, M., 54  
 Koshland, D.E., Jr., 312  
 Kouno, T., 310  
 Kovacevic, B., 133  
 Kramer, G.M., 130  
 Kreiner, W.A., 129  
 Kreis, G., 235  
 Kreiss, G., 236  
 Kreissl, F.R., 233, 235, 236  
 Kreiter, C.G., 171, 207, 234, 235, 237  
 Kresge, A.J., 236, 237, 263, 264, 311  
 Krey, G.D., 336  
 Krishnamurty, V.V., 132  
 Kristjánsdóttir, S.S., 236  
 Krohn, K., 233  
 Krokan, H.E., 312  
 Kropp, P.J., 56  
 Krowczyniski, A., 55  
 Krüger, C., 236  
 Kruger, J.D., 131  
 Kruizinga, W., 336  
 Kruppa, G.H., 97, 132  
 Krygowski, T.M., 133  
 Ku, A.T., 132  
 Kubiak, C.P., 337  
 Kudin, K.N., 314  
 Kuekes, P.J., 337  
 Kunishima, M., 54  
 Kutzelnigg, W., 130, 133  
  
 Laasonen, K., 133  
 Ladner, J.E., 313  
 Lai, C.-J., 312  
 Laidig, K.E., 131  
 Laiter, S., 131

- Lakshminarasimhan, P.H., 134  
 Lam, C.T., 235  
 Lammerstma, K., 133  
 Lamzin, V.S., 335  
 Langford, S.J., 336  
 Lantz, M., 311  
 Lara, L.M., 127  
 LaReau, R.D., 311  
 Larese, J.Z., 309  
 Lathan, W.A., 130  
 Lattuada, L., 233  
 Laube, T., 130, 133, 134  
 Lawton, R.G., 336  
 Ledlie, D.B., 131  
 Lee, E., 129  
 Lee, E.P.F., 134  
 Lee, I., 53  
 Lee, J.K., 308  
 Lee, T.A., 308  
 Lee, T.J., 133  
 Leeds, C.C., 308  
 Leffler, J.E., 236  
 Legler, G., 310  
 Lehn, J.-M., 335, 337  
 Leito, I., 129  
 Lellouch, E., 127  
 Lennartz, H.-W., 128  
 Lennox, R.B., 337  
 Lenoir, D., 135  
 Leo, A., 236  
 Lesar, A., 133  
 Lesser, M., 313  
 Lester, A.W., Jr., 133  
 Leung, H.B., 311  
 Leupold, M., 234, 235  
 Levy, S.B., 309  
 Lewis, B.E., 268, 311  
 Lewis, D.E., 242, 308  
 Lewis, S.D., 312  
 Leyes, A.E., 235, 237  
 Leyh, T.S., 311  
 Li, C.M., 310  
 Li, W.S., 335  
 Liang, G., 131, 132, 133  
 Liang, X., 310  
 Lias, S.G., 59, 62, 128, 129, 130, 133  
 Liashenko, A., 314  
 Licandro, E., 233  
 Liebeskind, L.S., 233  
 Liebman, J.F., 127, 128  
 Liebman, J.L., 128  
 Lifshitz, C., 134  
 Lightfoot, P.D., 130  
 Limbach, H.H., 131  
 Lin, S.-S., 135  
 Lin, Z., 133  
 Link, T.M., 313  
 Link, U., 234  
 Linstrom, P.J., 128, 129  
 Litorja, M., 129  
 Liu, B., 130, 131, 132  
 Liu, G., 314  
 Liu, H., 310  
 Liu, J., 130, 337  
 Liu, J.D., 131  
 Liu, K.K.C., 310  
 Llewellyn, G., 55  
 Loch, C., 312  
 Lock, C.J.L., 131  
 Lodder, G., 1, 54, 55, 56  
 Lok, S.M., 131  
 Lomas, J.S., 129  
 Long, L., 309  
 Loos, R., 135  
 López-Moreno, J., 127  
 Lossing, F.P., 130, 133  
 Lozynski, M., 336  
 Lu, F., 236  
 Lu, K.-T., 134  
 Lu, X., 313  
 Lucchini, V., 24, 53, 54, 55  
 Lukinskas, P., 127  
 Lundt, I., 310  
 Lustgarten, R.K., 133  
  
 Ma, M., 134  
 Maasböl, A., 195, 233  
 Maass, G., 235  
 MacGillvary, C.H., 134  
 Macho, V., 131, 132  
 Maciel, G.E., 134  
 Mack, H.-G., 336  
 Maestri, M., 335  
 Mahendran, M., 131  
 Mahoney, W., 337  
 Maiorana, S., 233  
 Maksic, Z.B., 133  
 Malick, D.K., 314  
 Mallard, W.G., 128, 129  
 Malow, M., 130  
 Mandolini, L., 236  
 Mann, B.R., 237  
 Mao, C., 309  
 Marcus, R.A., 210, 236  
 Mareda, J., 129, 132, 135  
 Märkl, R., 55, 234, 237  
 Marsch, M., 54  
 Marschner, T.M., 311  
 Marshall, A.G., 59, 113, 128  
 Martin, R.L., 314  
 Martínez, A., 127  
 Martínez, A.G., 55  
 Martínez, C., 127  
 Martinho Simões, J.A., 128  
 Marx, D., 130, 133  
 Marynick, D.S., 233

- Masaki, Y., 54  
 Massböl, A., 233  
 Massey, V., 335  
 Mataga, N., 337  
 Mateescu, G.D., 132, 133  
 Matsson, O., 267, 308, 311  
 Matsubara, H., 336  
 Matsuo, M., 336  
 Mattei, P., 335  
 Mattersteig, G., 337  
 Mattevi, A., 336  
 Mayhew, C.A., 133  
 Mayr, H., 127, 135  
 Mazzella, L.J., 310  
 McCarter, J.D., 310  
 McCarthy, M.C., 127  
 McClelland, R.A., 134, 236  
 McCoy, C.P., 335  
 McEwan, M.J., 127  
 McGarvey, G.J., 312  
 McGarvey, J.J., 156, 234  
 McIntosh, C.M., 336  
 McIver, R.T., Jr., 131  
 McKormick, D., 336  
 McMahan, T.B., 130  
 McNeely, S.A., 56  
 McNeil, A.J., 55  
 McNicholl, R.-A., 234  
 McRobbie, I.M., 336  
 Mecozzi, S., 336  
 Melander, L., 309  
 Mennucci, B., 314  
 Mentch, F., 310  
 Menzer, S., 337  
 Meot-Ner, M., 129, 130, 131  
 Merling, G., 134  
 Merrigan, S.R., 308  
 Mesić, M., 132  
 Meyer, S.L., 313  
 Meyer, T., 335  
 Miles, R.W., 309, 311, 313  
 Milin, D., 135  
 Millam, J.M., 314  
 Miller, J.R., 234  
 Miller, S.I., 53  
 Milligan, D.B., 127  
 Millot, F., 236  
 Mills, O.S., 237  
 Minas da Piedade, M.E., 128  
 Minkin, V.I., 133  
 Mishima, M., 110, 129, 311  
 Mitsui, Y., 313  
 Mó, O., 129  
 Mo, Y., 133  
 Modena, G., 24, 53, 54, 55, 133  
 Modro, A., 134  
 Molina-Cuberos, G.J., 127  
 Moloney, M.G., 41, 56  
 Monahan, C., 337  
 Montgomery, J.A., 313  
 Moodie, R.B., 134  
 Moodie, S.L., 311  
 Moon, J.H., 134  
 Moore, E.J., 237  
 Moore, P.B., 312  
 Moors, E.H., 311  
 Morel, G., 236  
 Mori, S., 54  
 Morin, F., 337  
 Morita, N., 135  
 Morokuma, K., 314  
 Morris, A., 129, 130  
 Motsch, A., 234  
 Muchall, H.M., 132  
 Mueller, F., 335  
 Mühlemeier, J., 234  
 Müller, A., 54  
 Müller, H., 130  
 Muller, H.M., 311  
 Müller, J., 235  
 Müller, P., 57, 127, 129, 131, 132, 135  
 Müller, T., 55, 133  
 Mulzer, J., 233  
 Munishkin, A., 311  
 Munson, B., 130  
 Murai, H., 310  
 Murray, B.W., 310  
 Mustanir, ., 311  
 Myhre, P.C., 130, 132  
 Myrhe, P.C., 131  
  
 Nagao, Y., 54  
 Nagaoka, T., 54  
 Nakamura, C., 236  
 Nakamura, E., 54  
 Namanworth, E.J., 131  
 Namchuk, M.N., 310  
 Namgoong, S.K., 310  
 Nanayakkara, A., 314  
 Nandi, M., 237  
 Narasaka, K., 54  
 Naylor, R.D., 128  
 Nazaretian, K.L., 236  
 Neunschwander, M., 134  
 Ng, C.Y., 59, 128, 130  
 Ng, Y., 130  
 Nibbering, N.M.M., 130  
 Nicolaidis, A., 109, 134  
 Nielsen, M.B., 337  
 Niemz, A., 336, 337  
 Nienaber, H., 233  
 Nieves, E., 309  
 Niida, T., 310  
 Nishikawa, F., 313  
 Nishikawa, S., 313  
 Nocera, D., 336

- Norris, F.F., 134  
 Northrop, D.B., 309  
 Norton, C., 133  
 Norton, J.P., 236  
 Norton, J.R., 234, 237  
 Norton, S.H., 128  
 Notario, R., 128, 129  
 Novak, M., 135  
 Nussenzweig, V., 312  
  
 Oae, S., 54  
 Ober, M., 337  
 Obmolova, G., 336  
 Ochiai, M., 14, 53, 54, 55  
 Ochterski, J., 314  
 O'Donoghue, A., 135  
 Offial, A.R., 135  
 Ohga, Y., 134  
 Ohshiro, Y., 54  
 Ohwada, T., 133  
 Oka, H., 54  
 Oka, T., 129, 130, 133  
 Okada, T., 337  
 Okamoto, K., 127  
 Okamoto, Y., 134  
 Okamura, M.Y., 336  
 Okazaki, T., 129, 134  
 Okuyama, T., 1, 53, 54, 55, 56  
 Olah, G.A., 105, 130, 131, 132, 133, 134  
 Oleary, M.H., 311  
 Olsnes, S., 313  
 Olson, S.T., 312  
 Olvera, C., 133  
 Omont, A., 127  
 Oppenheimer, N.J., 311, 312  
 Ordronneau, C., 133  
 Orita, M., 305, 313  
 Orłowski, M., 313  
 Orłowski, R., 313  
 Ortiz, J.V., 314  
 Oshima, K., 53, 54  
 Osifchin, R.G., 337  
 Oskam, A., 234  
 Osuka, A., 337  
 Oswald, R., 133  
 Otsuki, J., 335  
 Otto, A.H., 133  
 Ozturk, D.H., 313  
  
 Packer, J., 237  
 Paddock, M.L., 336  
 Paneth, P., 308, 311  
 Pankiewicz, K.W., 312, 313  
 Papagni, A., 233  
 Paquette, L.A., 233  
 Pardi, A., 311  
 Parikh, S.S., 312  
 Parker, A.J., 237  
  
 Parker, W., 135  
 Parkin, D.W., 308, 310, 311, 312, 313  
 Parr, A.C., 134  
 Parrinello, M., 130, 133  
 Parsons, S.M., 313  
 Pasquato, L., 53, 54  
 Patai, S., 56  
 Patz, M., 135  
 Pauling, L., 309  
 Pearson, R.G., 236  
 Pederson, R.L., 310  
 Pedley, J.B., 128  
 Peng, C.Y., 314  
 Percac, K., 132  
 Perdew, J.P., 258, 313  
 Pereira, M.E.A., 312  
 Perera, S.A., 130, 132  
 Perez, G.S., 236  
 Perlberger, J.C., 135  
 Peterson, B.L., 130  
 Peterson, K.A., 129  
 Petersson, G.A., 314  
 Petro, C., 130  
 Pfab, R., 133  
 Pfeifer, W.D., 55  
 Phillips, L.M., 308  
 Pickering, R.A., 235  
 Pienta, N.J., 135  
 Pihl, A., 313  
 Pilhaja, K., 128  
 Pilling, M.J., 130  
 Pina, F., 335  
 Pinhey, J.T., 56  
 Piskorz, P., 314  
 Pitchumani, K., 134  
 Pittman, C.U., Jr., 132  
 Plabst, W., 233  
 Plocica, J., 131  
 Pohl, S., 310  
 Poirier, R.A., 311  
 Pomelli, C., 314  
 Pople, J.A., 128, 129, 130, 131, 314  
 Popov, V., 335  
 Porco, J.A., Jr., 310  
 Porter, R.D., 131  
 Poulter, G.T., 54  
 Powell, W.H., 127  
 Prakash, G.K.S., 132  
 Prakash, R.V., 132  
 Pranata, J., 133  
 Prevost, N., 134  
 Pross, A., 53, 131  
 Pulay, P., 133  
  
 Quintanilla, E., 57, 131  
  
 Rabuck, A.D., 314  
 Rachon, J., 54



- Radom, L., 53, 68, 109, 128, 130, 131, 134, 309  
 Radzicka, A., 309  
 Raehm, L., 336  
 Ragains, M.L., 237  
 Raghavachari, K., 128, 129, 131, 314  
 Rakowski, K., 311  
 Ramamurthy, V., 134  
 Ramsey, B., 131  
 Ranganayakulu, K., 131  
 Rankel, L.A., 235  
 Rappoport, Z., 1, 3, 53, 54, 55, 56, 131, 133, 235, 236  
 Rascher, H., 234  
 Rasul, G., 132, 134  
 Rauk, A., 132  
 Rausch, M.D., 234  
 Raymo, F.M., 336, 337  
 Read, R.J., 312  
 Redhouse, A.D., 237  
 Rehfuss, B.D., 133  
 Rehfuss, G.D., 129  
 Rei, M.-H., 135  
 Reich, K.A., 312  
 Reichel, F., 133  
 Reid, G.A., 335  
 Reifenberger, R., 337  
 Reindl, B., 131  
 Reinganum, S.J., 133  
 Reissig, H.-U., 233  
 Remennikov, G., 135  
 Ren, Z., 311  
 Renfrow, R.A., 236  
 Replogle, E.S., 314  
 Rezaee, M., 308  
 Rhodes, D., 312  
 Ribbi, A., 312  
 Ricco, A., 335  
 Richard, J.P., 135, 236, 237, 311  
 Richey, H.G., Jr., 133  
 Richey, J.S., 131  
 Riedmuller, S., 235  
 Riemenschneider, J.L., 133  
 Riley, J.S., 130  
 Rising, K.A., 310  
 Ritchie, C.D., 312  
 Rizzo, C.J., 335  
 Robb, M.A., 313  
 Roberts, D.D., 312  
 Roberts, K., 135  
 Robles, E.S.J., 129  
 Robyt, J.F., 308  
 Rodrigo, R., 127  
 Rogers, L.J., 336  
 Romero, R., 311  
 Roncali, J., 337  
 Roobeek, C.F., 55  
 Rooney, A.D., 234  
 Rooney, J.J., 234  
 Roper, W.R., 233  
 Roque, A., 335  
 Rose, I.W., 248, 309  
 Rosenberg, S., 308  
 Rosenfeld, J., 130  
 Rossi, R.H., 235  
 Rossier, J.-C., 127, 129, 131, 132, 135  
 Rotello, V.M., 315, 336, 337  
 Roth, W.R., 128  
 Rouse, E.A., 55  
 Roux, M.V., 129, 132  
 Rowe, P.M., 308  
 Rudge, A.J., 310  
 Rundle, H.W., 130  
 Rušćic, B., 129, 130, 133  
 Rusinska-Roszak, D., 336  
 Ryberg, P., 308  
 Sacchetti, J.C., 310, 313  
 Saenger, W., 313  
 Sak, K., 129  
 Sakanishi, Y., 54, 55  
 Salcedo, R., 133  
 Salem, L., 131  
 Sander, E.G., 236  
 Sanders, W.W., 134  
 Sankararaman, S., 134  
 Sarkar, A., 237  
 Sathe, K.M., 237  
 Sato, K., 53, 54, 55  
 Sato, H., 55  
 Satterthwait, A.C., 235  
 Saunders, M., 130, 131, 132  
 Saunders, W.H., Jr., 309  
 Sauvage, J.-P., 336  
 Sayre, L.M., 335  
 Scapin, G., 313  
 Schadt, F.L., 54  
 Schaefer, H.F., III, 130  
 Scharer, O.D., 313  
 Scheck, D.M., 234  
 Scheiner, S., 336  
 Schenkman, S., 312  
 Scheuring, J., 288, 309, 310  
 Schiff, H.I., 130  
 Schimmel, H., 135  
 Schindler, M., 132, 133  
 Schirmer, H., 233  
 Schlegel, H.B., 53, 313  
 Schlemper, H., 237  
 Schleyer, P.v.R., 53, 54, 55, 75, 105, 128, 130, 131, 132, 133, 135  
 Schmid, P., 235  
 Schmidt, G., 135  
 Schmidt, M.A., 234  
 Schmitz, L.R., 131  
 Schneider, H.J., 135

- Schneider, W.G., 134  
 Schoberth, W., 55  
 Schoevaars, A.M., 336  
 Schötz, K., 133  
 Schowen, R.L., 309  
 Schramm, V., 308  
 Schramm, V.L., 268, 288, 308, 309, 310, 311, 312, 313  
 Schreiner, P.R., 130  
 Schriesheim, A., 131, 135  
 Schröder, J., 180, 182, 235  
 Schuber, F., 311, 312  
 Schubert, U., 171, 233, 234, 235  
 Schuck, D.F., 236  
 Schulman, J.M., 133  
 Schultz, J.C., 72, 130  
 Schwartz, S.D., 313  
 Schwarz, H., 132  
 Schwenger, A., 131  
 Schwesinger, R., 237  
 Scott, A.P., 309  
 Scrimin, P., 54  
 Scuseria, G.E., 313  
 Sears, P., 312  
 Seiler, P., 336  
 Sekino, Y., 313  
 Semeluk, G.P., 130  
 Semenyaka, A., 313  
 Senda, T., 313  
 Seno, M., 335  
 Senoff, C.V., 235  
 Sen Sharma, D.K., 129, 131, 132, 134  
 Servaas, P.C., 234  
 Shafer, J.A., 312  
 Shainyan, B.A., 54  
 Shamma, T., 134  
 Sharma, R.B., 129, 131, 132  
 Sharp, D.W.A., 134  
 Sharp, R.E., 335  
 Shatavsky, M., 133  
 Sheppard, N., 134  
 Shi, H., 312  
 Shi, W., 309, 310  
 Shi, Y., 237  
 Shiba, E., 129  
 Shih, J.G., 132  
 Shing, T.K.M., 310  
 Shiratori, H., 337  
 Shiro, M., 54  
 Shoel, H., 310  
 Shold, D.M., 130  
 Shusterman, A.J., 234  
 Sieber, S., 130, 132, 133  
 Siehl, H.U., 131  
 Sierks, M.R., 310  
 Sigano, D.M., 233  
 Simanek, E.E., 312  
 Simkin, B.Ya., 133  
 Sims, L.B., 242, 308, 309  
 Singleton, D.A., 242, 308  
 Sinnott, M., 312  
 Sinnott, M.L., 283, 286, 308, 309, 312  
 Sipos, G., 132  
 Skrydstrup, T., 310  
 Slupphaug, G., 312  
 Smith, B.D., 337  
 Smith, B.J., 128, 130, 134, 310  
 Smith, D., 132  
 Smith, M.R., 135  
 Snell, W., 129  
 Solà, M., 234  
 Solomon, J.J., 129, 130, 131  
 Song, Y., 130  
 Songstad, J., 236  
 Sonoda, T., 56  
 Sorensen, T.S., 131, 132  
 Spear, R.J., 133  
 Spek, A.L., 336  
 Spencer, N., 335  
 Speranza, M., 24, 55  
 Spiesecke, H., 134  
 Sprague, J.R., 133  
 Staley, R.H., 129  
 Stang, P.J., 53, 54, 55, 56, 131, 133  
 Stanger, A., 55  
 Staral, J.S., 133  
 Steenken, S., 134, 236  
 Stefanov, B.B., 314  
 Stein, P.E., 312  
 Stein, R.L., 311  
 Stein, S.E., 128  
 Steiner, U.E., 234  
 Steinmetz, A.L., 235  
 Steitz, T.A., 311  
 Stern, M.J., 311  
 Stevens, P.S., 133  
 Stewart, R., 134  
 Stivers, J.T., 301, 308, 311, 312, 313  
 Stoddart, J.F., 335, 336, 337  
 Stoermer, M.J., 56  
 Stone, F.G.A., 233  
 Strain, M.C., 314  
 Stratmann, R.E., 313  
 Streitwieser, A., Jr., 312  
 Stronach, M.W., 235  
 Strubinger, L.M., 234  
 Studabaker, W.B., 233  
 Stufkens, D.J., 156, 234  
 Sturtevant, J.M., 309  
 Subramanian, K., 55  
 Subramanian, L.R., 53, 55  
 Sudholter, E.J.R., 336  
 Sueda, T., 54, 55  
 Sugden, T.M., 131  
 Sugimura, T., 55  
 Suhnel, J., 309

- Sukal, S., 311  
Sullivan, J.M., 237  
Sumi, K., 54  
Summerville, R.H., 53  
Sun, W., 237  
Sundberg, R.J., 131  
Sunko, D.E., 132, 311  
Surry, C., 309  
Surya Prakash, G.K., 132, 134  
Suzuki, S., 312  
Suzuki, T., 56  
Svoboda, J.J., 132  
Swager, T.M., 335, 337  
Sweigart, D.A., 235  
Swenson, R., 336  
Swenson, R.P., 336  
Szele, I., 56, 311  
Szulejko, J.E., 130  
  
Taft, R.W., 113, 115, 119, 130, 135, 236  
Tainer, J.A., 312  
Takahashi, M., 336  
Takahashi, Y., 134  
Takaoka, Y., 54  
Takasuka, M., 129, 134  
Takatera, K., 335  
Takayama, S., 310  
Takeuchi, K., 126, 127, 129, 134  
Takino, T., 53, 54  
Tanaka, K.S.E., 239, 311, 313  
Tanaka, T., 127  
Tanaka, Y., 312  
Tang, J., 130  
Taniguchi, H., 56  
Taniguchi, S., 337  
Tao, G.L., 337  
Tao, T., 134  
Tao, W., 312, 313  
Targos, T.S., 234  
Tarnus, C., 311, 312  
Tashma, R., 312  
Taylor, C.A., 131  
Taylor, T.E., 233  
Tencer, M., 56  
Terrier, F., 235, 236  
Thaddeus, P., 127  
Therien, M., 336  
Thiyagarajan, B., 237  
Thomas, A.A., 308  
Thomas, D.B., 55  
Thomas, F., 135  
Thomas, Q.A., 55  
Thomsen, I.B., 310  
Thornton, J.M., 311  
Thrush, B.A., 134  
Tollin, G., 335  
Tomasi, J., 314  
Tomuschat, P., 234  
  
Tonellato, U., 54  
Toney, M.D., 308  
Tonge, P.J., 311  
Toole, A.J., 233  
Topolski, M., 54  
Tordova, M., 313  
Torrent, M., 150, 234  
Toteva, M.M., 135  
Tour, J.M., 337  
Toyonari, M., 54  
Traeger, J.C., 130  
Trauter, R.L., 135  
Travers, M.J., 132  
Trifan, D.S., 127  
Trost, R.H., 233  
Trucks, G.W., 313  
Tsai, B.P., 129  
Tsang, W., 128  
Tse, J.S., 133  
Tsuji, Y., 135  
Tsuji, Y., 135  
Tsuji, Y., 135  
Tsuno, Y., 129  
Tsurugi, K., 313  
Tsuruoka, T., 310  
Tulinski, A., 336  
Turi, L., 336  
Tyler, P.C., 309, 310, 311, 313  
  
Uchiyama, K., 54  
Udagawa, Y., 336  
Unger, S.H., 236  
Usui, S., 129  
Uy, D., 133  
  
Vale, G., 54  
van Alem, K., 55  
Van Arman, S.A., 312  
Vančik, H., 132  
van den Berkel, W.J.H., 336  
van Heyningeneds, S., 313  
VanPham, T., 311  
Vasella, A., 310  
Vaughan, J., 237  
Veldman, N., 336  
Venner, H., 313  
Venturi, M., 336, 337  
Verdine, G.L., 313  
Vidal, P.L., 336  
Vieth, H.M., 131  
Viruela, P., 128  
Vogel, P., 130, 131, 134  
Vogel, P.C., 311  
Vollendorf, N.W., 234  
  
Wade, D., 268, 311  
Walborsky, H.M., 54  
Walcher, G., 312  
Walsh, A.D., 131

- Walsh, R., 93  
 Walton, C.W., 132  
 Wan, W., 311  
 Wang, F., 309  
 Wang, H., 237  
 Wang, J.H., 311  
 Wang, Y., 258, 311, 313  
 Ward, J.E.H., 235  
 Warshel, A., 308  
 Watanabe, K.A., 313  
 Watanabe, T., 335  
 Watt, C.I.F., 135  
 Watt, W., 336  
 Wattenpugh, K., 336  
 Watts, W.E., 132  
 Weinhold, F., 134  
 Weinstein, B.R., 312  
 Weiss, K., 233, 235  
 Weiss, M.S., 312  
 Weiss, P., 310  
 Weiss, P.M., 308  
 Weiss, P.S., 337  
 Weisshaar, J.C., 134  
 Weitzel, K.-M., 130  
 Welk, N., 234  
 Wells, J.M., 93  
 Welte, N., 234  
 Wentzel, F., 134  
 Wenzel, P.J., 263, 311  
 Werner, H., 145, 159, 234, 235  
 Werner, R.M., 301, 311, 313  
 Werstiuk, N.H., 132  
 West, A.P., 336  
 Westaway, K.C., 267, 311  
 White, A.M., 131  
 White, E.T., 130  
 White, M.G., 129  
 Whitesell, C., 235  
 Whiteside, R.A., 128  
 Whitworth, S.M., 132  
 Wiberg, K.B., 131  
 Wiedmann, R.T., 129  
 Wieting, R.D., 129  
 Wilk, E., 313  
 Wilkie, J., 309  
 Wilkinson, G., 233  
 Willetts, A., 133  
 Williams, D.J., 337  
 Williams, I.H., 309, 311  
 Williams, K.B., 135, 311  
 Williams, R.S., 337  
 Williams, S., 336  
 Willner, I., 337  
 Wilson, B.A., 312  
 Wilson, J.C., 309  
 Winchester, B., 310  
 Winkler, D.A., 310  
 Winstein, S., 55, 105, 132, 133  
 Wisotsky, M.J., 131  
 Withers, S.G., 308, 310, 312  
 Wolf, J.F., 135  
 Wolfenden, R., 309, 313  
 Wong, C.-H., 310, 312  
 Wong, E.W., 337  
 Wong, M.W., 309, 314  
 Woodward, R.B., 105, 131, 133  
 Wool, I.G., 311, 313  
 Wright, T.G., 134  
 Wu, J., 311  
 Wu, W., 133  
 Wu, X., 308  
 Wulff, W.D., 233, 237  
  
 Xiao, G., 313  
 Xie, Y., 133  
 Xu, R., 337  
 Xu, Y.-C., 233, 237  
 Xue, H., 308  
  
 Yaeta, E., 313  
 Yagi, M., 310  
 Yamamoto, A., 55  
 Yamamoto, Y., 54  
 Yamataka, H., 53, 55, 311  
 Yan, J., 54  
 Yan, K., 237  
 Yáñez, M., 129  
 Yang, C.C., 235  
 Yang, D.C., 237  
 Yang, J., 312  
 Yannoni, C.S., 130, 131, 132  
 Yano, Y., 335  
 Yip, P.F., 311  
 Yonan, P.K., 53  
 Yoneshima, R., 337  
 Yoshida, Y., 54  
 Young, G., 313  
 Yount, R.G., 311  
 Yungman, V.S., 129  
  
 Zabinski, R.F., 313  
 Zakrzewski, V.G., 313  
 Zaupa, T., 54  
 Zechel, D.L., 308  
 Zerner, M.C., 131  
 Zeuner, S., 237  
 Zhang, Q., 133  
 Zhang, Y., 312  
 Zhdankin, V.V., 54  
 Zhong, Z., 310  
 Zhou, M., 309  
 Zhou, Q., 335  
 Zhou, X.Z., 308  
 Zhou, Z., 336  
 Zhu, J., 309  
 Zijlstra, R.W.J., 336

Zink, J.I., 234  
Zollinger, H., 56  
Zuilhof, H., 55, 336  
Zurawski, B., 130  
Zweep, S.D., 131  
Zwonenik, J.J., 134

# Nucleophilic Vinylic Substitution and Vinyl Cation Intermediates in the Reactions of Vinyl Iodonium Salts

TADASHI OKUYAMA<sup>†</sup> and GERRIT LODDER<sup>‡</sup>

<sup>†</sup>*Faculty of Science, Himeji Institute of Technology, Kamigori, Hyogo, Japan*

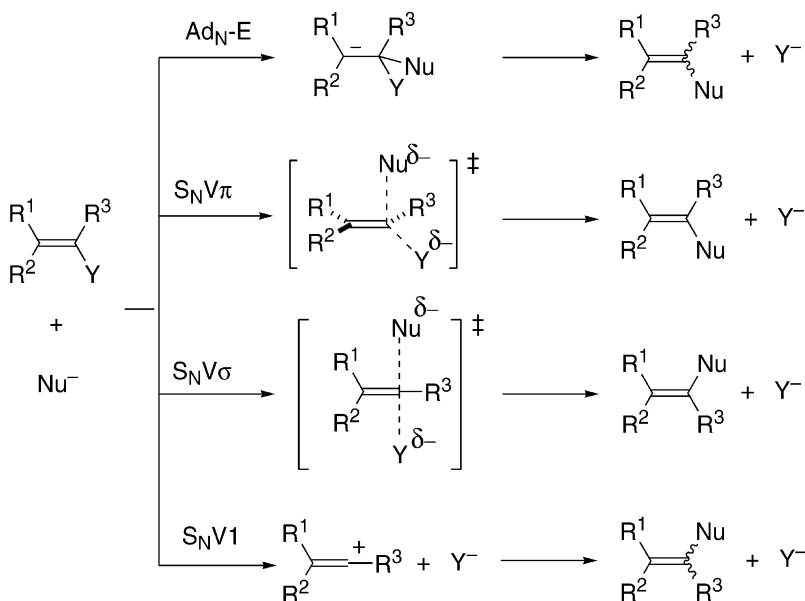
<sup>‡</sup>*Gorlaeus Laboratories, Leiden Institute of Chemistry, Leiden University, Leiden, The Netherlands*

1	Introduction	1
2	Vinylic S <sub>N</sub> 2 reactions	3
	S <sub>N</sub> V reactions with inversion	3
	Theoretical considerations	6
	In-plane substitution (S <sub>N</sub> Vσ) of vinyl iodonium salts	13
	Out-of-plane substitution (S <sub>N</sub> Vπ) of vinyl iodonium salts	22
3	Vinyl cations as S <sub>N</sub> V1 intermediates	23
	Stability of vinyl cations	24
	Leaving ability of the iodonio group	27
	Vinylenebenzenium ion intermediates	30
	β-Alkyl group participation	34
	Chirality probe approach	37
	Other attempts to generate primary vinyl cations	41
4	Borderline mechanisms	43
	Solvolysis of β-alkylvinyl iodonium salts	44
	Reactions of β,β-dialkylvinyl iodonium salts with halide ions	45
	Reactions of β-phenylvinyl iodonium salts with halide ions	47
5	Photochemical reactions	48
6	Summary	52
	Acknowledgments	53
	References	53

## 1 Introduction

Nucleophilic vinylic substitution (S<sub>N</sub>V) has a wide variety of mechanistic possibilities, including more than 10 main routes which can be further sub-divided into over 30 variants, as reviewed by Rappoport.<sup>1</sup> Four main straightforward mechanisms are illustrated in [Scheme 1](#).

Nucleophilic attack at the alkene carbon can in principle occur either toward the π\* or σ\* orbitals since the sp<sup>2</sup>-hybridized carbon has two types of vacant orbitals. That is, both out-of-plane (perpendicular) and in-plane attack are possible. The out-of-plane mode of attack is part of the addition–elimination pathway (Ad<sub>N</sub>–E) with a



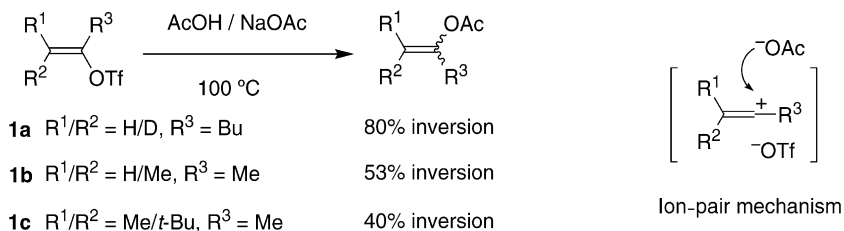
**Scheme 1** Mechanisms of nucleophilic vinylic substitution.

carbanion as an intermediate. This associative mechanism is generally observed for activated unsaturated systems<sup>1-3</sup> and gives rise to products with stereochemistry ranging from retention to stereoconvergence depending on the (in)stability of the intermediate carbanions.

As the leaving group ability of  $\text{Y}^-$  increases, it ultimately departs concurrently with the nucleophilic attack and the reaction occurs via a “concerted addition–elimination” mechanism.<sup>1-3</sup> This type of mechanism should result in retention of configuration and may be designated as  $\text{S}_{\text{N}}\text{V}\pi$ . In contrast, the in-plane  $\sigma^*$  attack of a nucleophile should lead to substitution with inversion of configuration and may be referred to as  $\text{S}_{\text{N}}\text{V}\sigma$ .

With further increasing leaving ability of  $\text{Y}^-$ , the reaction becomes dissociative and becomes a vinylic  $\text{S}_{\text{N}}1$  ( $\text{S}_{\text{N}}\text{V1}$ ) reaction involving a vinyl cation as intermediate.  $\text{S}_{\text{N}}\text{V1}$  reactions have been extensively studied, both with substrates giving stabilized vinyl cations and/or with substrates with a good nucleofuge such as triflate (trifluoromethanesulfonate,  $\text{TfO}^-$ ) and are the subjects of several reviews.<sup>4-6</sup> Their stereochemical consequences are discussed in Section 2.

The  $\text{S}_{\text{N}}\text{V}\sigma$  mechanism is a logical analogue of the  $\text{S}_{\text{N}}2$  reaction at saturated carbon that occurs via backside attack of the nucleophile, but it has long been rejected as a feasible pathway on the basis of steric considerations<sup>7,8</sup> and of early theoretical calculations on a rather crude model system.<sup>9</sup> However, quite recently definite examples of  $\text{S}_{\text{N}}\text{V}\sigma$  reactions have been found,<sup>10,11</sup> and recent theoretical studies<sup>12-16</sup> show that the  $\text{S}_{\text{N}}\text{V}\sigma$  as well as the  $\text{S}_{\text{N}}\text{V}\pi$  mechanism is feasible. If imbalance of bond formation and bond cleavage occurs, the dissociative extreme of



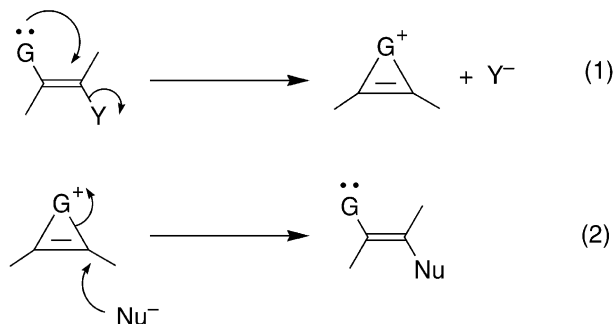
Scheme 2

the in-plane  $S_NV\sigma$  mechanism is formation of a vinyl cation ( $S_NV1$  mechanism) and the associative extreme of the out-of-plane  $S_NV\pi$  mechanism is the  $Ad_N-E$  route. The reviews of Rappoport<sup>1-3</sup> mainly concern the associative to concerted part,  $Ad_N-E/S_NV\pi$ , of the mechanistic spectrum of nucleophilic vinylic substitution. In this chapter we discuss the concerted-dissociative part ( $S_NV\sigma/S_NV1$  dichotomy) of the mechanistic spectrum, mainly on the basis of our recent results obtained in the study of reactions of vinyl iodonium salts. Also, photochemical dissociative reactions generating vinyl cations are discussed and compared with the corresponding thermal reactions.

## 2 Vinylic $S_N2$ reactions

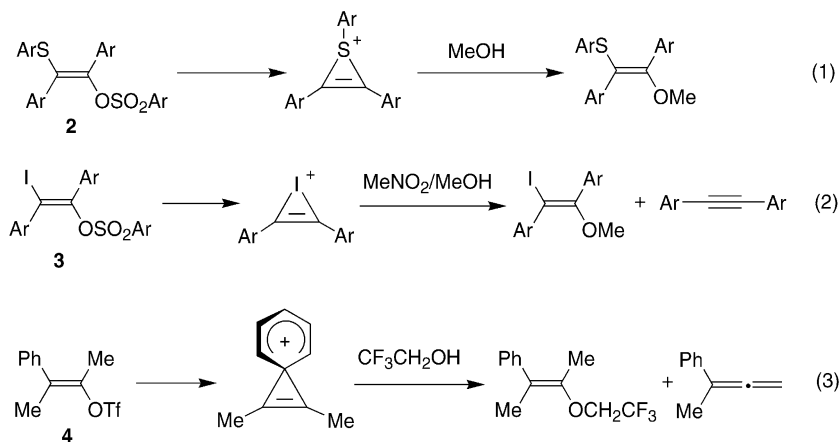
### $S_NV$ REACTIONS WITH INVERSION

The stereochemistry of nucleophilic vinylic substitution via the  $Ad_N-E$  mechanism ranges from retention of configuration to stereoconvergence. For  $S_NV1$ -type reactions, often partial inversion has been observed. The inversion has been attributed to nucleophilic attack on an ion pair intermediate.<sup>17-20</sup> As illustrative examples, results of the acetolysis of the vinyl triflates **1a-c** in the presence of sodium acetate are given in Scheme 2.<sup>19,20</sup> The fraction of inversion ranges from 40 to 80%, and is smaller the more stable the intermediate cation;  $\beta$ -alkyl substitution



Scheme 3



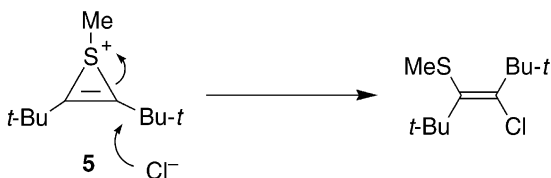


Scheme 4

stabilizes vinyl cations, as discussed below. In less nucleophilic solvents such as trifluoroethanol and trifluoroacetic acid the fractions of inversion are also much smaller (< 10%).<sup>18,20</sup> More stabilized vinyl cations, with e.g., an  $\alpha$ -aryl substituent, lead to products of stereoconvergence. These trends are consistent with a change of mechanism from ion pair to free ion with increasing stabilization of the cations.

The intramolecular processes outlined in Scheme 3 occur formally with inversion of configuration at the electrophilic carbon. Example (1) is participation of a nucleophilic neighboring group, where the nucleophile is constrained to attack in-plane, while example (2) is the microscopic reverse of the first one, and the preferred path must again be in-plane attack. These reactions are postulated to occur via the  $S_NV\sigma$  pathway to give the inverted product.<sup>21–23</sup> Their consecutive occurrence results in an anchimerically assisted reaction, and the net stereochemical outcome is retention of configuration due to double inversion. The overall mechanism of this type of reaction can be classified as  $S_NV1$ , since the corresponding process in the solvolysis of saturated aliphatic derivatives is classified as an  $S_N1$  reaction with neighboring group participation.

Participation of  $\beta$ -sulfur,<sup>24</sup>  $\beta$ -iodine,<sup>25</sup> and  $\beta$ -aryl groups<sup>26</sup> has been reported for the solvolysis of the vinylic substrates 2–4 (Scheme 4). Each of the reaction steps occurs with inversion, and the overall process results in retention of configuration. The cyclic 3-membered thiirenium ion 5 also gave exclusively inverted



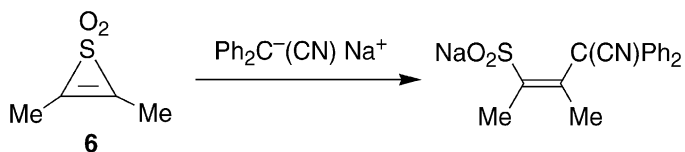
Scheme 5

nucleophilic substitution product (Scheme 5).<sup>27–29</sup> However, retention of configuration was observed for the reaction of the neutral cyclic substrate, thiirene 1,1-dioxide **6** (Scheme 6).<sup>30</sup>

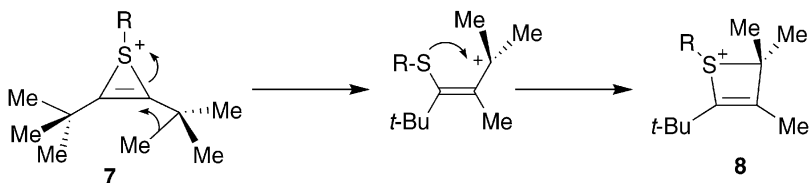
The intramolecular transfer of the nucleophilic group in Scheme 7 is also claimed to be an  $S_NV\sigma$  reaction.<sup>22,23</sup> The anionotropic rearrangement of the di-*tert*-butylthiirenium ion **7** into the thietium ion **8** involves the stereospecific backside attack of the internal methide at the unsaturated carbon.

Examples of acyclic vinylic systems that undergo nucleophilic substitution with complete inversion of configuration are very rare. The reaction of 1,2-dibromo-1,2-difluoroethene (**9**) with *p*-toluenethiolate affords products of apparently inverted structure without loss of stereochemical purity (Scheme 8).<sup>31</sup> However, the authors are not sure whether this is due to the stereospecificity of the reaction or to the thermodynamic stabilities of the products.

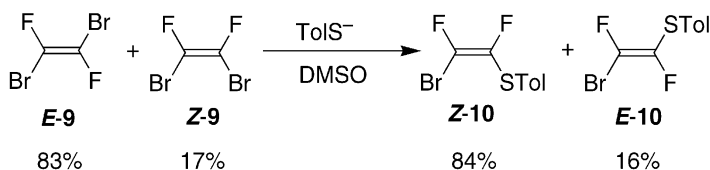
An unambiguous example is the nucleophilic substitution of 1-alkenyl(aryl)iodonium salts with halide ions (Scheme 9).<sup>32</sup> 1-Decenyl(phenyl)iodonium tetra-



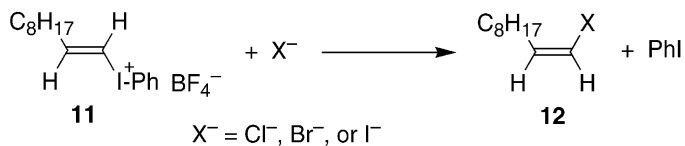
Scheme 6



Scheme 7



Scheme 8



Scheme 9

fluoroborate (**11**) gave the completely inverted haloalkene **12** when it reacted with chloride, bromide, or iodide ions. Details of this reaction are discussed in a section below (see Scheme 14).

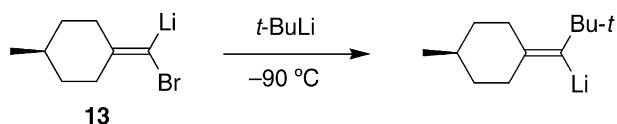
The nucleophilic substitution of the alkylidene carbenoid 1-bromo-1-lithioethene **13** with *tert*-butyllithium stereospecifically gives the inverted product (Scheme 10).<sup>33–35</sup> This could be an  $S_NV\sigma$  reaction.

An  $S_N2$ -type substitution at the  $sp^2$ -hybridized nitrogen atom of a C=N bond has recently been reported for the acid-catalyzed intramolecular reaction of oxime **14** (Scheme 11).<sup>36</sup> The results have been rationalized by theoretical calculations.

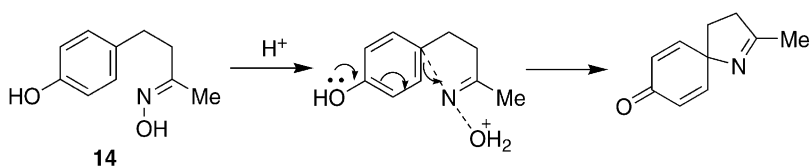
#### THEORETICAL CONSIDERATIONS

It has long been believed that in-plane nucleophilic substitution at vinylic carbon ( $S_NV\sigma$ ) is an unfavorable process, partly due to steric reasons.<sup>7,8</sup> The nucleophilic attack occurs at the vacant orbital of the electrophilic substrate, and the LUMO of alkenes was generally thought to have  $\pi$  symmetry and not  $\sigma$  symmetry ( $\sigma^*$  orbitals are in general higher in energy than  $\pi^*$  orbitals). This would make perpendicular attack at the vinylic carbon ( $\pi^*$ ) by a nucleophile more favorable than in-plane attack ( $\sigma^*$ ). Early theoretical calculations for the system  $H_2C=CH_2 + H^-$ , using the extended Hückel method, in fact showed a very high energy barrier ( $326 \text{ kJ mol}^{-1}$ ) for the in-plane  $S_NV\sigma$  reaction and a low barrier ( $75 \text{ kJ mol}^{-1}$ ) for the perpendicular  $\pi$  attack.<sup>9</sup> Later theoretical studies undertaken in the 1970s and 1980s focused on the perpendicular and not on the in-plane reactions. Inspired by experimental indications that the in-plane  $S_NV$  process is feasible, more sophisticated MO calculations on such reactions were undertaken in the 1990s. The results thereof are at variance with the conclusions of the early calculations.

First, it was shown that the LUMO of vinylic substrates is not necessarily of  $\pi$  symmetry. For some classes of vinylic compounds the LUMO is a  $\sigma^*$  orbital (Table 1).<sup>13</sup> While simple vinylic compounds such as vinyl chloride and triflate (entries 4 and 5) have an anticipated  $\pi^*$  orbital as LUMO, charged substrates (entries

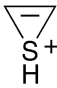

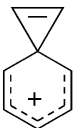
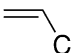
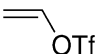
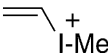
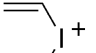
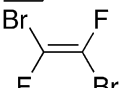
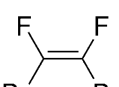
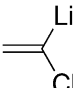


Scheme 10



Scheme 11

**Table 1** Energies of the lowest vacant orbitals (in hartree) with  $\pi$  and  $\sigma$  symmetry for the vinylic portion of some model substrates

No.		LUMO (symmetry)	LUMO + 1 (symmetry)
1		-0.1046 ( $\sigma$ )	-0.0954 ( $\pi$ )
2		0.0819 ( $\pi$ )	0.1878 ( $\sigma$ )
3		-0.1395 ( $\sigma$ )	-0.0713 ( $\pi$ )
4		0.1454 ( $\pi$ )	0.1824 ( $\sigma$ )
5		0.1328 ( $\pi$ )	0.1811 ( $\sigma$ )
6		-0.065 ( $\sigma$ ) <sup>a</sup>	-0.029 ( $\pi$ ) <sup>a</sup>
7		-0.106 ( $\sigma$ ) <sup>a</sup>	-0.035 ( $\pi$ ) <sup>a</sup>
8		0.1226 ( $\sigma$ ) <sup>b</sup>	0.1421 ( $\pi$ ) <sup>b</sup>
9		0.1355 ( $\sigma$ ) <sup>b</sup>	0.1391 ( $\pi$ ) <sup>b</sup>
10		0.0476 ( $\sigma$ )	0.1195 ( $\pi$ )

Calculated at 6-311G\*\*//3-21G\* (Ref. 13) unless noted otherwise.

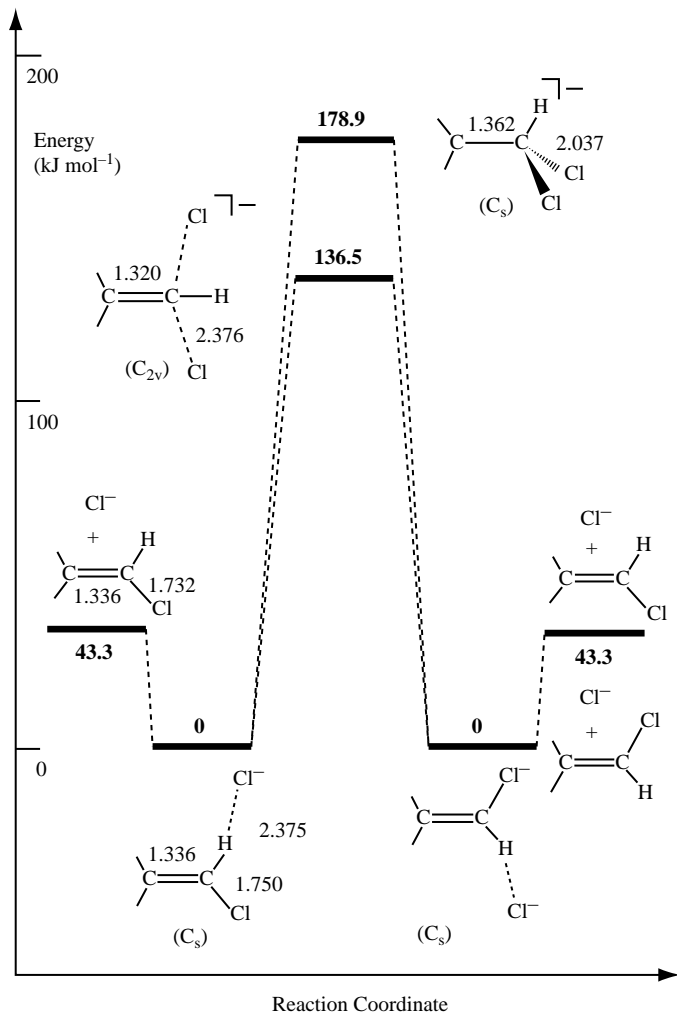
<sup>a</sup>Calculated at 6-31G\* (MP2).<sup>14</sup>

<sup>b</sup>Calculated at 3-21G\*\*//3-21G\*.<sup>13</sup>

1, 3, 6, and 7) have a  $\sigma^*$  orbital as LUMO. Thus, frontier orbital considerations rationalize the observed inversion in the  $S_NV$  reactions of the charged substrates in Schemes 5, 7 and 9. In accordance with the experimental observation of substitution with retention in Scheme 6, the cyclic sulfone (entry 2) has a LUMO with  $\pi$  symmetry. Polyhaloethenes have lowest  $\sigma^*$  and  $\pi^*$  orbitals which are very close in energy to

each other, and the bromo analogues (**8** and **9**) have  $\sigma$  LUMO in accordance with the observed inversion in the nucleophilic substitution of this kind of substrate (Scheme 8). The carbenoid (entry 10) has a long and very weak C–Cl bond,<sup>34</sup> and this may be why it has a  $\sigma$  LUMO and in turn why it gives an  $S_NV\sigma$  reaction (Scheme 10).

*Ab initio* MO calculations at the G2(+) level of theory in the gas phase have shown that even the prototypical  $S_NV$  reaction of vinyl chloride with chloride ion can favorably take place via backside in-plane  $\sigma$  attack, in spite of its LUMO with  $\pi$  symmetry.<sup>12</sup> The energy profiles calculated for the in-plane and the out-of-plane attack are shown in Fig. 1. Attack by  $Cl^-$  on  $CH_2=CHCl$  first forms a hydrogen-



**Fig. 1** Energy profile for the identity  $S_N2$  reaction of  $CH_2=CHCl$  with  $Cl^-$ , calculated at the G2(+) level. Bond lengths are in angstroms. Taken from Ref. 12.

bonded complex in which the incoming  $\text{Cl}^-$  is located in the plane of the alkene. The reaction then proceeds via the in-plane  $\sigma$  ( $\text{S}_{\text{N}}\text{V}\sigma$ ) pathway with a barrier of  $137 \text{ kJ mol}^{-1}$  or via the out-of-plane  $\pi$  pathway ( $\text{S}_{\text{N}}\text{V}\pi$ ) with a barrier of  $179 \text{ kJ mol}^{-1}$ . Thus, the  $\text{S}_{\text{N}}\text{V}\sigma$  process is  $42 \text{ kJ mol}^{-1}$  more favorable than the  $\text{S}_{\text{N}}\text{V}\pi$  pathway in the gas phase. This conclusion has recently been confirmed at higher levels of theory.<sup>16</sup> The negative charge in the transition state (TS) of the former pathway is less delocalized than that in the latter TS, and solvent effects stabilizing the TSs are expected to be larger for the former route. This simplistic consideration suggests that the gas-phase preference for the  $\text{S}_{\text{N}}\text{V}\sigma$  pathway will be maintained in solution. No two-step pathway via a carbanion intermediate ( $\text{Ad}_{\text{N}}\text{-E}$ ) was found for this unactivated vinyl substrate. The  $\beta,\beta$ -dichloroethyl anion, the potential intermediate in the  $\text{Ad}_{\text{N}}\text{-E}$  process, is unstable and collapses to the starting complex.

Quite recently, Lee and co-workers<sup>15</sup> have theoretically examined the reactions of vinyl chloride with various nucleophiles in quest of the driving force of the unexpected preference for the  $\text{S}_{\text{N}}\text{V}\sigma$  process. Calculations were carried out at three levels, RHF/6-311 + G\*\* (RHF), MP2/6-311 + G\*\* (MP2), and G2(+)(MP2), with MP2/6-311 + G\*\* geometries for the latter two levels. The preference for  $\sigma$  or  $\pi$  attack is dependent on the level of calculation and the nature of the nucleophile. The highest level results are summarized in Table 2 and typical structures of TSs for the  $\text{S}_{\text{N}}\text{V}\sigma$  and  $\text{S}_{\text{N}}\text{V}\pi$  pathways are shown in Fig. 2. The data show that the  $\text{S}_{\text{N}}\text{V}\sigma$  route is energetically favored over the  $\text{S}_{\text{N}}\text{V}\pi$  route for  $\text{Cl}^-$  and  $\text{Br}^-$  as nucleophile, while the reverse is the case for  $\text{OH}^-$  and  $\text{SH}^-$ .

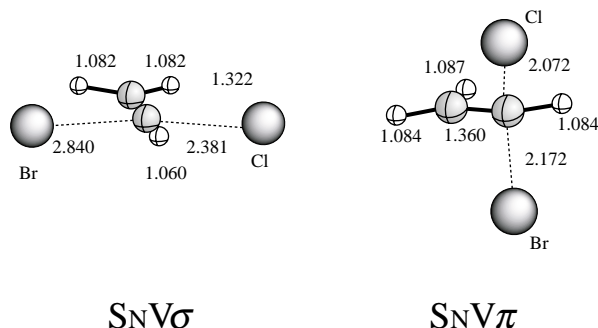
The substitution reactions of  $\text{CH}_2=\text{CHCl}$  with  $\text{OH}^-$  and  $\text{SH}^-$  are exergic, whereas that with  $\text{Br}^-$  is endergic ( $\Delta G^0$ ). The  $\text{S}_{\text{N}}\text{V}\sigma$  route is not feasible with the strong base  $\text{OH}^-$  in the gas phase; the TS for the  $\sigma$  attack by  $\text{OH}^-$  could not be located, and the barrier for the  $\text{S}_{\text{N}}\text{V}\pi$  route is very low ( $\Delta G^\ddagger = 9.0 \text{ kJ mol}^{-1}$ ). The barriers for the  $\sigma$  and  $\pi$  route of  $\text{Br}^-$  ( $\Delta G^\ddagger = 134$  and  $165 \text{ kJ mol}^{-1}$ ) are both higher than those for  $\text{Cl}^-$  ( $125$  and  $144 \text{ kJ mol}^{-1}$ ), largely due to the endergicity of the

**Table 2** Energies ( $\text{kJ mol}^{-1}$ ) for the reactions of vinyl chloride with various nucleophiles  $\text{Nu}^-$ , in the gas phase and in acetonitrile, calculated at the G2(+)(MP2) level<sup>15</sup>

Mechanism	$\text{Nu}^-$	$\Delta G_{\text{g}}^\ddagger$	$\Delta G_{\text{g}}^0$	$\Delta G_{\text{AN}}^\ddagger$ <sup>a</sup>
$\text{S}_{\text{N}}\text{V}\sigma$	$\text{Cl}^-$	124.5	0.0	192.9
	$\text{Br}^-$	134.3	38.2	194.8
	$\text{OH}^-$ <sup>b</sup>	–	–	–
	$\text{SH}^-$	110.7	–79.7	171.6
$\text{S}_{\text{N}}\text{V}\pi$	$\text{Cl}^-$	144.5	0.0	210.1
	$\text{Br}^-$	165.3	38.2	222.2
	$\text{OH}^-$	9.0	–222.6	72.6
	$\text{SH}^-$	101.9	–79.7	160.8

<sup>a</sup>Values in acetonitrile calculated by the isodensity polarizable continuum model.

<sup>b</sup>The transition state could not be located for the  $\text{S}_{\text{N}}\text{V}\sigma$ -route.



**Fig. 2** Transition states for the  $S_N2$  reaction of vinyl chloride with  $Br^-$ . Bond lengths are in angstroms. Adopted from Ref. 15.

reaction of  $Br^-$  ( $\Delta G^0 = 38 \text{ kJ mol}^{-1}$ ). The reverse reaction,  $Cl^- + CH_2=CHBr$ , should be exergic and the barriers should be lower. The halide exchange reactions proceed preferably via the  $S_NV\sigma$  rather than the  $S_NV\pi$  pathway.

The TSs for the  $S_NV\sigma$  route are quite loose with a small degree of bond formation and a large degree of bond cleavage. On the other hand, the TSs for the  $S_NV\pi$  pathway are relatively tight with a large extent of bond formation and a small degree of bond cleavage. This contrast is clearly demonstrated by the calculated percentages of bond-order changes in going from the initial state to the TS,  $\% \Delta n^\ddagger$ , given in Table 3. The bond formation and cleavage percentages are 30–35 and 55–65 for the  $S_NV\sigma$  route and 55–60 and 25–40 for the  $S_NV\pi$  route. In the  $S_NV\pi$  TS the  $\pi$  bond is partially broken (to a single bond in the limit), while in the  $S_NV\sigma$  transition state a second  $\pi$  bond is partially formed (toward a triple bond). That is, triple-bond character has developed in the  $S_NV\sigma$  TS.

The loose TS on the  $S_NV\sigma$  path is associated with a large energy of deformation ( $\Delta E_{\text{def}}$ , which is the energy required to deform the reactant, vinyl chloride, to its geometry in the TS without interaction with the nucleophile). This should lead to a high activation barrier. The difference in the  $\Delta E_{\text{def}}$  values for the two routes (Table 3, last column) must be closely related to the relative ease of the  $\sigma$  and  $\pi$  attack. The

**Table 3** Percentage changes in bond order,  $\% \Delta n^\ddagger$ , and deformation energies ( $\Delta E_{\text{def}}$ ) on going from reactants to the transition state<sup>15</sup>

Mechanism	Nu <sup>-</sup>	C–Nu	C–Cl	C=C	$\Delta E_{\text{def}}$ (kJ mol <sup>-1</sup> )
$S_NV\sigma$	$Cl^-$	34.5	65.5	14.2	247.4
	$Br^-$	37.3	66.2	9.1	258.0
	$SH^-$	30.8	57.4	2.1	204.3
$S_NV\pi$	$Cl^-$	62.3	37.7	20.5	164.9
	$Br^-$	62.3	43.5	16.7	195.6
	$OH^-$	22.5	3.5	13.5	11.9
	$SH^-$	56.3	24.0	32.0	108.4

larger energies of deformation for the  $S_NV\sigma$  than for the  $S_NV\pi$  pathway were considered to be responsible for the unfavorability of the in-plane  $\sigma$  attack compared with the out-of-plane  $\pi$  attack, as has long been accepted by organic chemists. What factors cause the reverse of this trend in  $\Delta E_{\text{def}}$  values to overall preference for the  $S_NV\sigma$  over the  $S_NV\pi$  pathway?

As already pointed out the frontier MO levels do not always predict correctly the ease of the reaction pathways. The ground state LUMO symmetry at the  $\alpha$ -carbon of the vinylic substrate is therefore not the dominant factor determining the mechanistic preference in the  $S_NV$  reactions. Another factor considered, intramolecular *geminal* and *vicinal*  $\sigma-\sigma^*$  type charge-transfer interactions in the TS, is also not responsible for the energetic preference of the  $S_NV\sigma$  pathway in the substitution of unactivated vinylic substrate by halide ions. Examination of  $\sigma-\sigma^*$  proximate delocalization in the TSs showed that such TS stabilizing interactions are larger in the  $S_NV\pi$  than in the  $S_NV\sigma$  pathway.

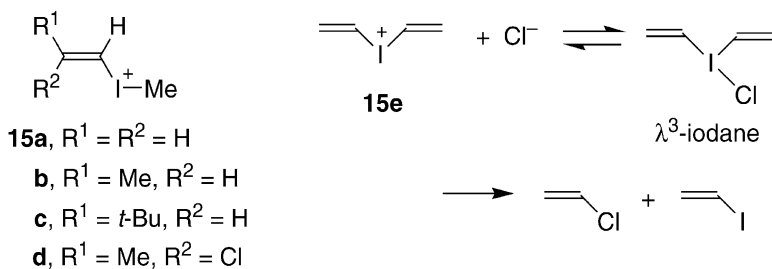
Another important energy term in TS interactions is the electrostatic one. In the loose TS of the  $S_NV\sigma$  process, a considerable positive charge is developed at the  $\alpha$ -carbon, which gives a strong electrostatic (Coulombic) interaction with the anionic nucleophile. The electrostatic interaction energies  $\Delta E_{\text{es}}$  are quite large for the  $S_NV\sigma$  reactions involving  $\text{Cl}^-$  and  $\text{Br}^-$  (Table 4). The stabilization due to  $\Delta E_{\text{es}}$  exceeds the larger destabilization due to  $\Delta E_{\text{def}}$  for the  $S_NV\sigma$  routes and more than compensates for the large deformation energies in favor of the  $S_NV\sigma$  over the  $S_NV\pi$  process. Also solvent effects have been studied, using a continuum model, but the relative preference of the two pathways is barely affected by the solvent, acetonitrile (Table 2,  $\Delta G_{\text{AN}}^\ddagger$ ).

In conclusion, in the substitution reaction of unactivated vinylic substrates the out-of-plane  $S_N2$  pathway with retention ( $S_NV\pi$ ) is favored with chalcogenides,  $\text{OH}^-$  and  $\text{SH}^-$ , while the in-plane  $S_N2$  pathway with inversion ( $S_NV\sigma$ ) is energetically preferred with halides,  $\text{Cl}^-$  and  $\text{Br}^-$ . The  $S_NV\pi$  TS is relatively tight and predominantly stabilized by proximate  $\sigma-\sigma^*$  charge-transfer interactions. In contrast, the  $S_NV\sigma$  TS is relatively loose and stabilized mainly by electrostatic interactions.

**Table 4** Calculated energies ( $\Delta E_{\text{es}}$ ,  $\text{kJ mol}^{-1}$ ) for the major electrostatic interactions of  $\text{C}_\alpha$  and  $\text{H}_\alpha$  with Nu and leaving  $\text{Cl}^{15}$

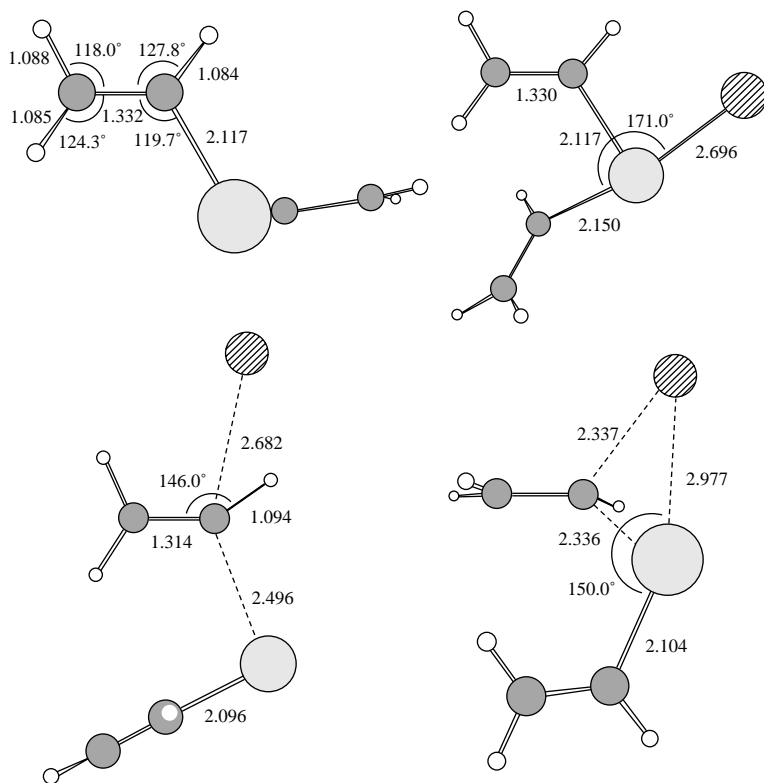
Mechanism	Nu <sup>-</sup>	$\text{C}_\alpha\text{-Nu}$	$\text{C}_\alpha\text{-Cl}$	$\text{H}_\alpha\text{-Nu}$	$\text{H}_\alpha\text{-Cl}$	Total
$S_NV\sigma$	$\text{Cl}^-$	-74.1	-74.1	-118.0	-118.0	-384.1
	$\text{Br}^-$	46.4	-51.0	-98.3	-109.6	-305.4
	$\text{SH}^-$	-20.5	-18.8	-106.3	-90.0	-235.6
$S_NV\pi$	$\text{Cl}^-$	0.4	0.4	-34.7	-34.7	-68.6
	$\text{Br}^-$	7.1	9.6	-29.3	-40.2	-52.7
	$\text{OH}^-$	-10.0	-0.8	-165.3	-10.0	-186.2
	$\text{SH}^-$	30.1	22.2	-33.5	-23.0	-4.2





Scheme 12

The reactions of the vinyl iodonium ions **15a–e** with chloride ion (Scheme 12) have been theoretically examined at the MP2/DZ + d level.<sup>14</sup> The transition structures calculated for the reaction of divynyliodonium ion **15e** with chloride are shown in Fig. 3. The  $\text{Cl}^-$  first coordinates to the positive iodine to form a  $\lambda^3$ -iodane intermediate; next, the TSs for the in-plane ( $\text{S}_{\text{N}}\text{V}\sigma$ ) and out-of-plane attack ( $\text{S}_{\text{N}}\text{V}\pi$ )



**Fig. 3** Calculated structures of  $(\text{CH}_2=\text{CH})_2\text{I}^+$  (**15e**) and its  $\lambda^3$ -chloriodane and transition states for the  $\text{S}_{\text{N}}\text{V}\sigma$  and  $\text{S}_{\text{N}}\text{V}\pi$  reactions. Bond lengths are in angstroms. Adopted from Ref. 14.

**Table 5** Energy barriers,  $\Delta G^\ddagger$  (in  $\text{kJ mol}^{-1}$ ) calculated for the reactions of vinylic iodonium ion (**15**) with  $\text{Cl}^-$  in the gas phase and in acetonitrile<sup>14</sup>

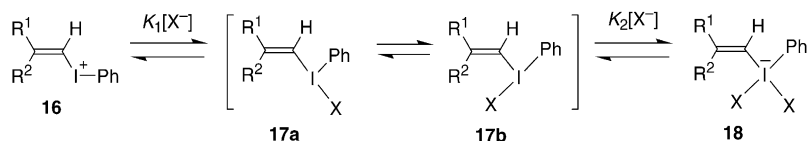
Substrate	$S_NV\sigma$		$S_NV\pi$	
	Gas phase	Solution	Gas phase	Solution
<b>15a</b>	105.0	84.5	95.4	101.7
<b>15b</b>	106.3	111.3	102.1	117.6
<b>15c</b>	115.1	138.9	94.6	112.5
<b>15d</b>	130.5	136.8	98.7	107.5
<b>15e</b>	111.7	55.6	95.0	97.9

of chloride are reached. In the TS of the latter route chlorine interacts with iodine. Thus, this reaction is a quasi-intramolecular process within the  $\lambda^3$ -iodane intermediate, and is called the ligand coupling reaction. The gas-phase activation energies summarized in Table 5 show that the  $S_NV\sigma$  TS is higher than the  $S_NV\pi$  TS in spite of the  $\sigma$  symmetry of the LUMO of all vinyl iodonium ions calculated. In the reaction of these charged substrates with an anionic nucleophile, the TSs are neutralized and the loose  $S_NV\sigma$  TSs have a larger dipole moment than the  $S_NV\pi$  TSs. Hence, solvent effects on the two reaction routes are different, as demonstrated by using a dielectric continuum model calculation (Table 5). This is contrary to the finding for the neutral substrates examined above. For the unsubstituted vinyl derivatives **15a** and **15e**, the solvent effects reverse the mechanistic preference in solution. However, the  $S_NV\sigma$  pathways of the  $\beta$ -*tert*-butyl- and  $\beta$ -chlorovinyl iodonium ions **15c** and **15d** have considerably higher energy barriers than the  $S_NV\pi$  or ligand coupling routes both in the gas phase and in solution. These trends are consistent with the experimental observations, presented in the next section.

#### IN-PLANE SUBSTITUTION ( $S_NV\sigma$ ) OF VINYL IODONIUM SALTS

Vinyl iodonium salts are good substrates for vinylic nucleophilic substitution owing to the excellent nucleofugality of the iodonio leaving group, which is evaluated to be about  $10^{12}$  times a better leaving group than iodide itself and  $10^6$  times better than triflate.<sup>37</sup> General methods of preparation of this class of iodonium salts were developed only in the 1980s,<sup>38–43</sup> and it was found that their  $S_NV$  reactions give products with stereochemistry ranging from exclusive inversion to complete retention, depending on their structure and on the reaction conditions.<sup>44,45</sup>

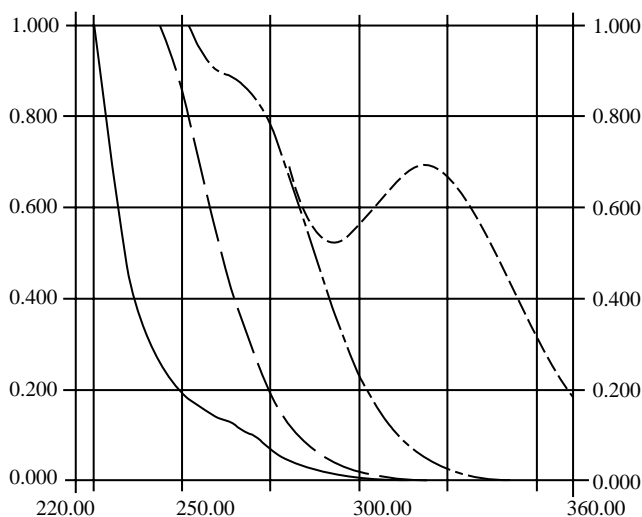
Before discussing the  $S_NV$  reactions of vinyl iodonium salts, it is worthwhile mentioning their structures. The tetrafluoroborate salts are essentially dissociated or exist as an ion pair in solution. In the crystalline state the counterion  $\text{BF}_4^-$  is located in the apical position of a pseudo-trigonal bipyramidal structure with the iodine at the center.<sup>39</sup> However, the long atomic distance of  $\text{I}-\text{F}(\text{BF}_3)$  suggests that the apical bonding is ionic rather than hypervalent, even in the solid state.<sup>44</sup> In contrast, the halide salts of vinyl iodonium compounds in solution are in equilibrium with hypervalent  $\lambda^3$ -haloiodanes (**17**), and also with dihaloiodates (**18**) at higher



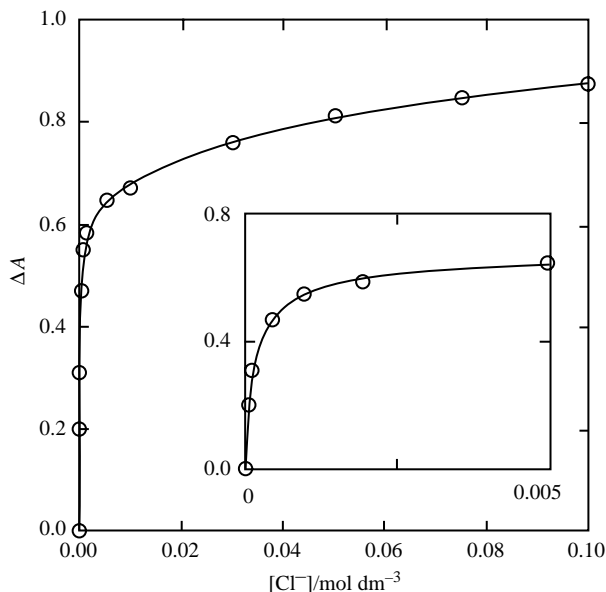
Scheme 13

concentration of halide ions (Scheme 13).<sup>10,11,46–49</sup> The solution of a tetrafluoroborate salt of a vinyl iodonium ion usually shows only a strong UV–Vis absorption band below 250 nm, but upon addition of halide ions a strong new band develops at longer wavelengths (Fig. 4). The new absorption is ascribed to λ<sup>3</sup>-haloiodane 17, and the association constants can be evaluated from the dependence of the absorbance on halide concentrations (Fig. 5). Their values are listed in Table 6 for the iodonium salts 11 and 20–22, given in Scheme 14. The associated forms, however, are less reactive than the free iodonium ions.<sup>10,11,47,19</sup> Furthermore, there is little information about the association with most other anions. For these reasons, the substrates are simply designated as iodonium rather than iodane, although at higher concentrations of halide ions in solution the reactive species can actually be the λ<sup>3</sup>-haloiodane.

Ochiai and co-workers<sup>32</sup> first discovered that the nucleophilic substitution of (*E*)-1-alkenyl(phenyl)iodonium tetrafluoroborates (e.g., 11) with tetrabutylammonium halides (except with fluoride) in various solvents at room temperature occurs with complete inversion of configuration to give (*Z*)-1-haloalkenes (e.g., *Z*-12) (Scheme



**Fig. 4** UV absorption spectra of vinyl iodonium tetrafluoroborate 11 in acetonitrile solution containing no additional salt (—) and 0.01 mol dm<sup>-3</sup> of Bu<sub>4</sub>NCl (---), Bu<sub>4</sub>NBr (- · - ·), and Bu<sub>4</sub>NI (· · ·) measured at 25°C. Taken from Ref. 11.



**Fig. 5** The initial absorbance of **20** at 250 nm in  $\text{Bu}_4\text{NCl}$  solution in acetonitrile at  $\mu = 0.10$  and  $25^\circ\text{C}$ . The solid curves are the theoretical ones calculated with data given in [Table 6](#). Taken from [Ref. 10](#).

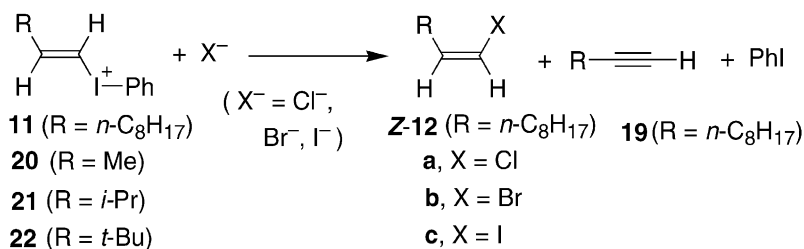
14; also see [Scheme 9](#)). Various mechanistic examinations established that the reaction occurs via the  $\text{S}_{\text{N}}\text{V}\sigma$  mechanism,<sup>10,11</sup> a conclusion supported by theoretical calculations.<sup>14</sup> The side reaction is elimination, yielding a 1-alkyne (e.g., **19**). The product distributions of the reactions of (*E*)-1-decenyl(phenyl)iodonium tetrafluoroborate (**11**) with halide ions ( $\text{X}^-$ ) at  $[\text{Bu}_4\text{NX}] = 0.1 \text{ mol dm}^{-3}$  and  $25^\circ\text{C}$  are summarized in [Table 7](#).<sup>11</sup> The fraction of elimination product **19** decreases with concentration of halide and in the order,  $\text{Cl}^- > \text{Br}^- > \text{I}^-$ . Deuterium labeling of

**Table 6** Product ratios and kinetic parameters for the reactions of 1-alkenyl(phenyl)iodonium salts **11** and **20–22** with chloride ion

	<b>20</b> (R = Me)	<b>11</b> (R = $\text{C}_8\text{H}_{17}$ )	<b>21</b> (R = <i>i</i> -Pr)	<b>22</b> (R = <i>t</i> -Bu)
$s/e^a$	72/28	54/46	41/59	0/100
$K_1$ ( $\text{mol}^{-1} \text{ dm}^3$ )	5900	7200	7600	5600
$K_2$ ( $\text{mol}^{-1} \text{ dm}^3$ )	16	15	25	11
$k_1 + k_2K_1$ ( $\text{mol}^{-1} \text{ dm}^3 \text{ s}^{-1}$ )	0.82	2.30	2.91	4.65
$k_2K_1 + k_3K_1K_2$ ( $\text{mol}^{-2} \text{ dm}^6 \text{ s}^{-1}$ )	95.7	203	239	0.93

Equilibrium and rate constants are defined in [Schemes 13 and 16](#). Values were determined at  $25^\circ\text{C}$  and the ionic strength of 0.1 in acetonitrile.<sup>10</sup>

<sup>a</sup>Product ratio of substitution/elimination obtained at  $[\text{Bu}_4\text{NCl}] = 0.01 \text{ mol dm}^{-3}$  without adjusting the ionic strength.



Scheme 14

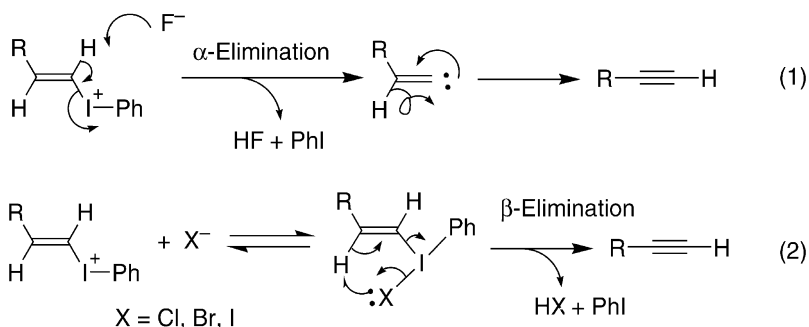
substrate **11** showed that these halides gave **19** with loss of the  $\beta$ -hydrogen (via  $\beta$ -elimination).<sup>11,32</sup> In contrast, fluoride ion induces exclusively elimination affording **19** in all solvents. In this case, deuterium labeling experiments showed that product **19** was formed with loss of the  $\alpha$ -hydrogen (via  $\alpha$ -elimination). The kinetic isotope effects are also consistent with this mechanistic variation:  $\alpha$ - or  $\beta$ -deuterium exhibits a primary kinetic isotope effect depending on the mechanism. This contrasting behavior of halides is due to the basicity of fluoride ( $\text{p}K_{\text{a}}$  3.17), which induces abstraction of the highly acidic  $\alpha$ -hydrogen, while the much less basic chloride through iodide abstract the  $\beta$ -hydrogen within the  $\lambda^3$ -haloiodane intermediate (Scheme 15).

Solvent effects on the product distribution of the reactions of **11** at 50°C and  $[\text{Bu}_4\text{NX}] = 0.05 \text{ mol dm}^{-3}$  including protic solvents are presented in Table 8.<sup>11</sup> The fraction of substitution tends to increase with increasing polarity of the solvent. The substitution products are exclusively in the *Z* form (inversion) in aprotic solvents and in methanol, trifluoroethanol (TFE), and acetic acid. In more highly ionizing solvents such as hexafluoro-2-propanol (HFIP), formic acid, and trifluoroacetic acid (TFA) a small amount of the *E* isomer (*E*-**12**) is also formed. The partial formation of retained product in the highly ionizing solvents at first seemed to be due to ionization of the substrate, i.e. the ion pair mechanism. However, at a lower concentration of chloride ( $[\text{Cl}^-] = 0.01 \text{ mol dm}^{-3}$ ) the fraction of *E*-**12a** was as high as 85%, and as by-product (*E*)-iodoalkene **12c** was formed. From these

**Table 7** Product distributions in the reactions of 1-deceny(phenyl)iodonium salt **11** with various halide ions

Halide	Solvent	Z-12	19
$\text{Cl}^-$	$\text{CHCl}_3$	85	15
$\text{Cl}^-$	MeCN	90	10
$\text{Cl}^-$	THF	95	5
$\text{Br}^-$	$\text{CHCl}_3$	92	8
$\text{Br}^-$	MeCN	96	4
$\text{I}^-$	$\text{CHCl}_3$	91	9
$\text{I}^-$	MeCN	99.6	0.4
$\text{F}^-$	MeCN	0	100

Obtained with tetrabutylammonium halide at  $[\text{Bu}_4\text{NX}] = 0.1 \text{ mol dm}^{-3}$  and 25°C.<sup>11</sup>



Scheme 15

observations, the retained product is concluded to be produced via the perpendicular attack ( $S_NV\pi$ ), as discussed below in terms of the ligand coupling mechanism.

Kinetic results are also consistent with a mechanism involving mainly the  $S_NV\sigma$  pathway. Solvent effects on the rate of the reaction of **11** with bromide at  $[\text{Bu}_4\text{NBr}] = 0.05 \text{ mol dm}^{-3}$  are rather small and tend to decrease with increasing polarity of the solvents. The effect of substituents at the leaving phenyliodonio group is also small:  $\rho$  is about 0.75, which should be compared to the substituent effect with  $\rho = 1.8$  on the solvolysis of 4-*t*-butyl-1-cyclohexenyl(aryl)iodonium tetrafluoroborates,<sup>37</sup> where a vinyl cation is produced in the rate-determining step (see [Scheme](#)

**Table 8** Product distributions in the reactions of 1-decenyl(phenyl)iodonium salt **11** with halide ions in various solvents

Halide	Solvent <sup>a</sup> ( $Y_{\text{OTs}}^b$ )	<b>12</b> ( <i>Z/E</i> )	<b>19</b>	Remarks
$\text{Cl}^-$	$\text{CHCl}_3$	61 (100/0)	39	
$\text{Cl}^-$	MeCN	76 (100/0)	24	
$\text{Cl}^-$	MeOH (-0.92)	80 (100/0)	20	Solvolysis products
$\text{Cl}^-$	TFE (1.80)	94 (100/0)	6	Solvolysis products
$\text{Cl}^-$	97HFIP (3.61)	92 (98.4/1.6)	8	
$\text{Cl}^-$	AcOH (-0.61)	87 (100/0)	13	
$\text{Cl}^-$	$\text{HCO}_2\text{H}$ (3.04)	98 (96.9/3.1)	2	Solvolysis products
$\text{Cl}^-$	TFA (4.57)	100 (85/15)	0	0.7% <b>12c</b>
$\text{Cl}^{-c}$	TFA (4.57)	100 (15/85)	0	3.5% <b>12c</b>
$\text{Br}^-$	MeOH (-0.92)	84 (100/0)	16	
$\text{Br}^-$	TFE (1.80)	97 (100/0)	3	
$\text{Br}^-$	AcOH (-0.61)	86 (100/0)	14	
$\text{Br}^{-d}$	$\text{HCO}_2\text{H}$ (3.04)	98 (98.4/1.6)	2	
$\text{Br}^-$	TFA (4.57)	100 (98.6/1.4)	0	
$\text{Br}^{-c}$	TFA (4.57)	100 (85/15)	0	0.6% <b>12c</b>

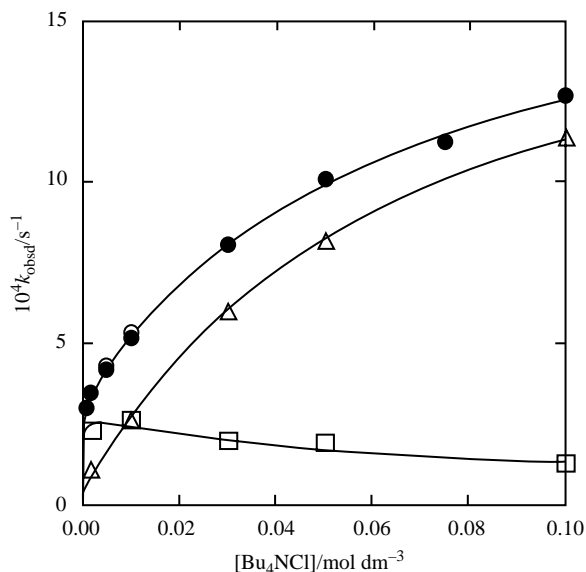
Obtained with tetrabutylammonium halide at  $[\text{Bu}_4\text{NX}] = 0.05 \text{ mol dm}^{-3}$  and  $50^\circ\text{C}$ .<sup>11</sup>

<sup>a</sup>TFE = 2,2,2-trifluoroethanol, HFIP = 1,1,1,3,3,3-hexafluoro-2-propanol, TFA = trifluoroacetic acid.

<sup>b</sup>Solvent ionizing power.<sup>50</sup>

<sup>c</sup>Obtained at  $[\text{X}^-] = 0.01 \text{ mol dm}^{-3}$ .

<sup>d</sup>NaBr was used as a salt.

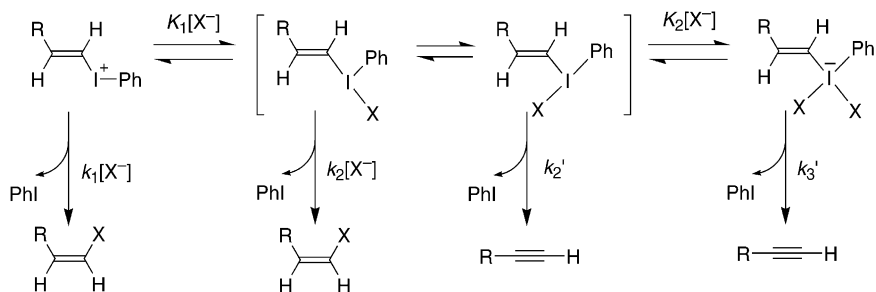


**Fig. 6** Rate constants for the reaction of **11** with chloride ion in acetonitrile at  $\mu = 0.10$  and  $25^\circ\text{C}$ : (●)  $k_{\text{obsd}}$ ; (△)  $k_s$  (for substitution); (□)  $k_e$  (for elimination). The solid curves are calculated with data given in Table 6. Taken from Ref. 10.

25). The secondary kinetic deuterium isotope effects at the  $\alpha$ - and  $\beta$ -position of **11** of about 1.1 and 1.1–1.2, respectively, on the rate of substitution are also consistent with the  $\text{S}_{\text{N}}\text{V}\sigma$  mechanism. Furthermore, the small positive apparent volume of activation obtained at  $[\text{Bu}_4\text{NBr}] = 0.05 \text{ mol dm}^{-3}$  and  $20^\circ\text{C}$ ,  $\Delta V^\ddagger = 4.6 \text{ cm}^3 \text{ mol}^{-1}$ , is not incompatible with this mechanism.<sup>11</sup>

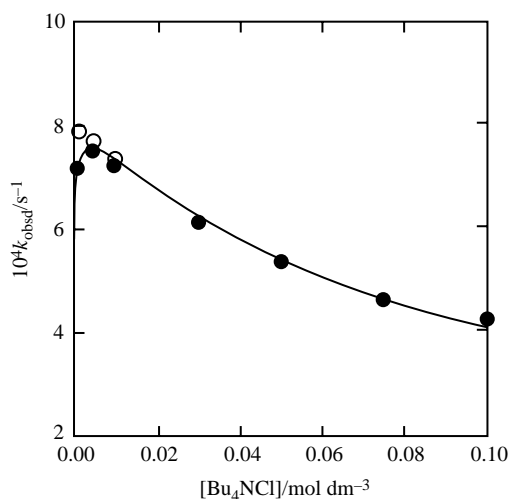
The dependence of the observed rate constants on the concentration of halide ion  $[\text{X}^-]$  is complicated due to formation of the iodane adduct in a pre-equilibrium. Kinetic analysis shows that the nucleophilic substitution is bimolecular. A typical rate dependence is shown in Fig. 6 for the reaction of **11** with chloride ion in acetonitrile at  $25^\circ\text{C}$ .<sup>10</sup> The curvatures are theoretically simulated according to the reaction scheme given in Scheme 16 and parameters are given in Table 6. Because of the pre-equilibrium formation of the two adducts, iodane and iodate, the intramolecular nature of the  $\beta$ -elimination, and the lower reactivity of iodate, the curvature for the elimination reaction decreases after its initial increase with increasing  $[\text{Cl}^-]$ . In contrast, the curvature for the substitution reaction shows saturation with increasing  $[\text{Cl}^-]$ , in agreement with the bimolecular reactions of **11**, and of the iodane with chloride, and the accompanying formation of the unreactive adduct, iodate. The equilibrium constants for the formation of iodane and iodate from the kinetic analysis agree with those obtained from the changes in UV absorbance (Fig. 5).

The effects of the  $\beta$ -alkyl groups of the 1-alkenylidonium salts **11** and **20–22** on the product ratios and rate constants in their reaction with chloride ion are



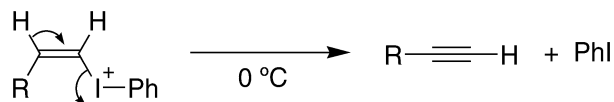
summarized in Table 6.<sup>10</sup> The results are consistent with the proposed mechanisms involving in-plane substitution ( $S_NV\sigma$ ) and  $\beta$ -elimination (Scheme 16). The fraction of substitution decreases in the order  $R = \text{Me} > n\text{-C}_8\text{H}_{17} > i\text{-Pr} \gg t\text{-Bu}$ , suggesting steric hindrance against the in-plane nucleophilic attack. The *t*-butyl derivative **22** only gives the elimination product and the kinetic curve is typical of the intramolecular reaction of the iodane adduct (Fig. 7).

A stereochemical investigation using substrates of opposite configuration (e.g., *Z*-**11** next to *E*-**11**) is desirable to establish that the substitution reaction is stereospecifically inversion. However, *Z*-**11** does not undergo nucleophilic substitution with halides but yields quantitatively the elimination product, **19**. (*Z*)-1-Alkenyliodonium salts are known to be too labile to be isolated due to their facile *anti*- $\beta$ -elimination (Scheme 17).<sup>51</sup>



**Fig. 7** Observed rate constants for the reaction of **22** with chloride ion in acetonitrile at 25°C. The solid curve is calculated with data given in Table 6. Taken from Ref. 10.



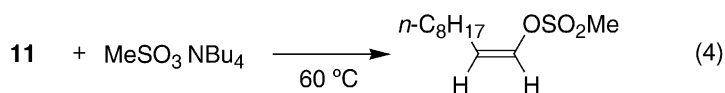
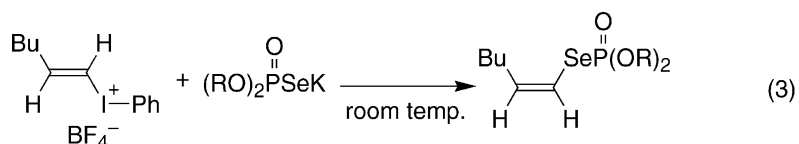
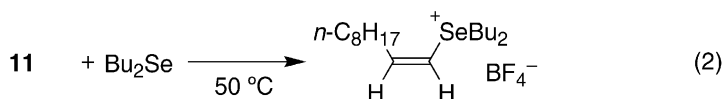
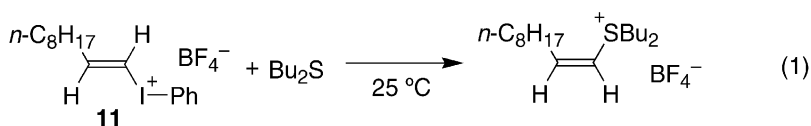


Scheme 17

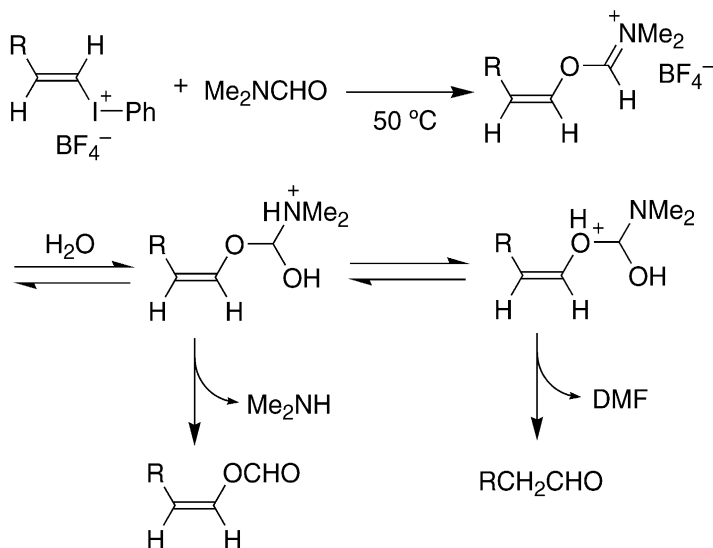
Therefore, the reactions of geometrically isomeric iodonium salts of  $\beta,\beta$ -dialkylvinyl derivatives with halide ions have been investigated.<sup>49</sup> However, the reactions are not stereospecific and give significant amounts of rearranged products. The results are discussed in Section 4 as a borderline case. The mechanism is obviously different from that of the monoalkylvinyl derivatives.

Other nucleophiles, which give substitution with inversion in their reaction with (*E*)-1-alkenylidonium salts, include dialkyl sulfide and selenide,<sup>45</sup> phosphoroselenoates,<sup>52</sup> and sulfonates<sup>53</sup> (Scheme 18). Amides also react with (*E*)-1-alkenylidonium salts and give a *Z* enol formate (Scheme 19).<sup>54</sup> The mechanism of these reactions, involving very weakly basic or non-basic nucleophiles, may well be in-plane  $S_NV\sigma$  attack. Moderately basic nucleophiles such as amines and carboxylates, even dichloroacetate, give  $\alpha$ -elimination.

It was found that the tetrafluoroborate anion itself can act as nucleophile: inverted (*Z*)-1-fluoroalkenes were obtained upon thermolysis of (*E*)-1-alkenyl(phenyl)iodo-



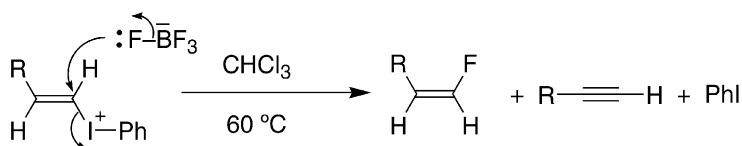
Scheme 18



Scheme 19

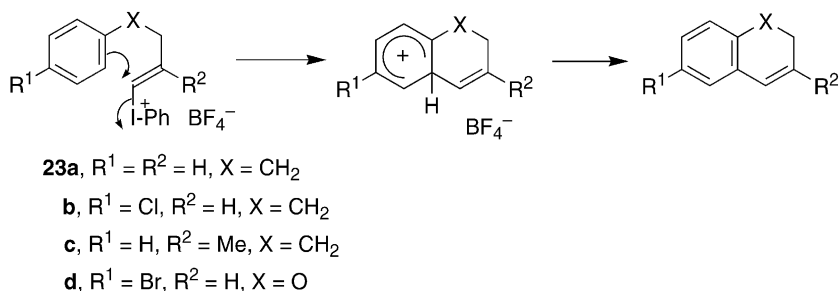
anium tetrafluoroborates at 60°C in chloroform (Scheme 20).<sup>55</sup> In this reaction, tetrafluoroborate and not fluoride is the nucleophile. If free fluoride ion  $\text{F}^-$  were formed by dissociation of  $\text{BF}_4^-$ ,  $\alpha$ -elimination would have occurred. It should be noted that even the *t*-butyl derivative **22** gives some inverted product.

The intramolecular Friedel–Crafts-type reaction of alkenyliodonium salts **23** proceeds efficiently at 40–60°C in various solvents including methanol, acetonitrile, and chloroform (Scheme 21).<sup>56</sup> The *Z* isomer of **23c** does not undergo ring closure, thus the reaction does not involve the formation of a vinyl cation. The mechanism of the reaction may well be in-plane  $\text{S}_{\text{N}}\text{V}\sigma$  attack by the intramolecular aromatic nucleophile.



<b>20</b> (R = Me)	93	7
<b>11</b> (R = <i>n</i> -C <sub>8</sub> H <sub>17</sub> )	95	5
<b>22</b> (R = <i>t</i> -Bu)	22	78

Scheme 20

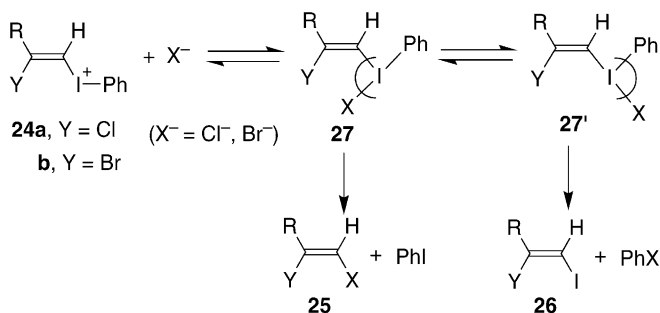


Scheme 21

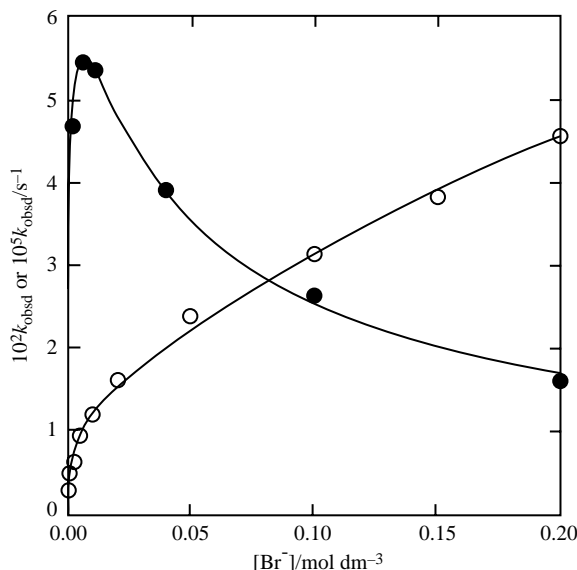
OUT-OF-PLANE SUBSTITUTION ( $S_NV\pi$ ) OF VINYL IODONIUM SALTS

The reactions of the  $\beta$ -halogenovinylidonium salts **24a,b** with halide ions are quite slow, but proceed at 60°C to give a substitution product, (*Z*)-1,2-dihaloalkene **25**, with complete retention of configuration (Scheme 22).<sup>46,57</sup> No inverted products were detected. As shown in Fig. 8 the rate of the reaction changes with halide concentration in the same way as for the  $\beta$ -elimination. That is, the reaction must occur as an intramolecular process of the  $\lambda^3$ -haloiodane intermediate as does the  $\beta$ -elimination. Another characteristic of the reaction is the formation of the retained iodoalkene **26**. The results are best accounted for by the ligand coupling mechanism within the hypervalent iodine intermediate **27**.<sup>58-60</sup> The trends have been explained using theoretical calculations on compound **15d** (Scheme 12, Table 5).<sup>14</sup> The  $\beta$ -chloro substituent considerably raises the barrier for the  $S_NV\sigma$  reaction, but does not significantly influence the  $S_NV\pi$  barrier.

The iodane **27** is in equilibrium with its conformational isomer **27'**. Coupling between the apical and equatorial ligand should result in **25** from **27** and **26** from **27'**. The ligand coupling mechanism can be regarded as a pseudo-intramolecular (unimolecular) variant of the (bimolecular)  $S_NV\pi$  pathway, as discussed in the theoretical section (Fig. 3).



Scheme 22

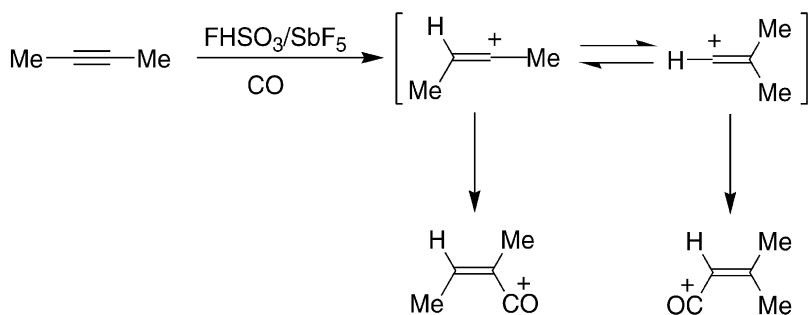


**Fig. 8** Observed rate constants for the reactions of **11** (○,  $10^2 k_{\text{obsd}}$ , 50°C) and **24b** (●,  $10^5 k_{\text{obsd}}$ , 60°C) with bromide ion in acetonitrile. Solid curves are theoretical ones. Taken from Ref. 46.

The reaction of 1-decenyliodonium salt **11** with halide ions in acidic solvents such as trifluoroacetic acid, formic acid, and HFIP, yields significant amounts of the retained products *E*-**12** (Table 8).<sup>11</sup> The reactions in these solvents were quite slow and product *E*-**12** was always accompanied by a small amount of iodoalkene *E*-**12c**. The retained substitution products must be produced via ligand coupling in the intermediate iodane. When the facile  $S_NV\sigma$  reaction becomes sluggish, due to the reduced reactivity of the nucleophile (by hydrogen-bond solvation), a second possible  $S_NV\pi$  reaction shows up. So, all substitution reactions of 1-alkenyliodonium salts can be interpreted solely in terms of  $S_NV2$  mechanisms, mostly  $S_NV\sigma$ , but accompanied by ligand coupling ( $S_NV\pi$ ) if the nucleophilicity of the halide is reduced by hydrogen-bond solvation.

### 3 Vinyl cations as $S_NV1$ intermediates

Vinyl cations are admittedly unstable species in both thermodynamic and kinetic terms, and were recognized as reactive intermediates only in the mid-1960s.<sup>61</sup> Early progress in this field of chemistry was made in the 1970s through studies of solvolysis of vinylic substrates, especially by using the “super” leaving group triflate.<sup>4,62</sup> This progress has been summarized in the monograph *Vinyl Cations* in 1979.<sup>5</sup> In the next two decades, modern techniques of chemistry, such as NMR, laser

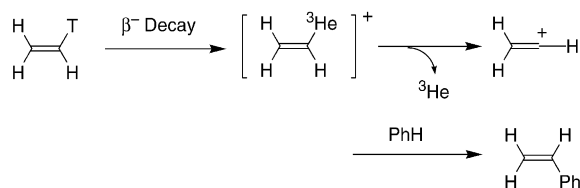


Scheme 23

photolysis, and sophisticated computational methods, extended the scope of vinyl cation chemistry, as reviewed in the book *Dicoordinated Carbocations* in 1997.<sup>6</sup> Most recently, a new family of compounds, vinyl iodonium salts, allowed the study of simpler, less stabilized vinylic cations thanks to the enormous nucleofugality of the iodonio group.

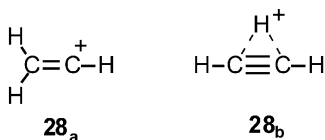
#### STABILITY OF VINYL CATIONS

The parent vinyl cation,  $\text{H}_2\text{C}=\text{C}^+\text{H}$ , and the primary vinyl cations  $\text{RHC}=\text{C}^+\text{H}$ , are very unstable both thermodynamically and kinetically and can only be generated under forced conditions in solution. Lucchini and Modena<sup>63</sup> suggested the formation of the parent vinyl cation as an intermediate in the acid-catalyzed hydration of ethyne in strong sulfuric acid ( $> 15 \text{ mol dm}^{-3}$ ). Formation of a primary vinyl cation from 2-butyne was proposed on the basis of trapping a rearranged cation with carbon monoxide in the superacid  $\text{FHSO}_3/\text{SbF}_5$  (Scheme 23).<sup>64</sup> Fornarini and Speranza<sup>65,66</sup> used the nuclear decay of tritiated ethene to generate the parent vinyl cation (Scheme 24). Radioactive tritium ( $^3\text{H}$ , half-life, 12.26 years) spontaneously decays to  $^3\text{He}$  with emission of a  $\beta^-$  particle to give vibrationally excited  $[\text{H}_2\text{C}=\text{CH}-^3\text{He}]^+$ , which converts to the free vinyl cation by heterolysis of the very weak  $\text{C}-^3\text{He}$  bond. In benzene as solvent, the Friedel–Crafts product, styrene, is detected after 10–14 months. Photoexcitation of appropriate precursors also generates primary vinyl cations as discussed in the last part of Section 3 and in Section 5.



Scheme 24

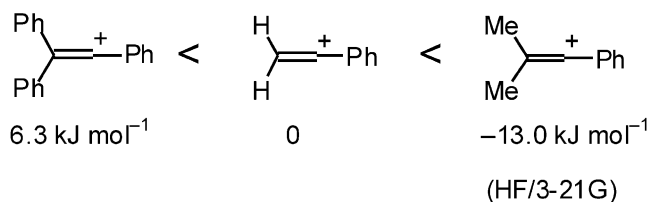
In the gas phase, vinyl cations are easily produced by mass spectrometric techniques, which also allow measurement of their heats of formation.<sup>67</sup> Gas-phase spectroscopic studies show that the smallest vinylic cation,  $C_2H_3^+$ , has a structure of protonated acetylene (**28<sub>b</sub>**) and not that of the classical vinyl cation (**28<sub>a</sub>**).<sup>67-69</sup>



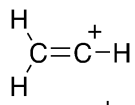
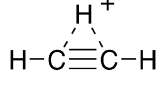
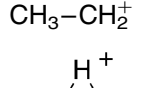
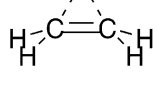
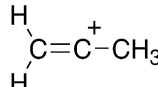
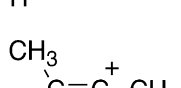
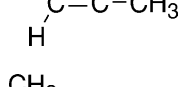
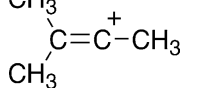
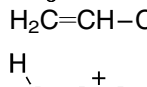
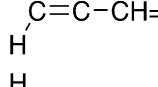
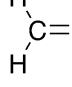
The results of recent *ab initio* MO studies are consistent with the experimental data and show that the bridged form (**28<sub>b</sub>**) is  $19 \text{ kJ mol}^{-1}$  more stable than the classical one (**28<sub>a</sub>**).<sup>68</sup> Thus, primary vinyl cations generated in solution may well also be bridged, though no solution-phase structural information is available. Theoretical calculations using dielectric continuum models showed that solvation has only a minor effect on the relative stability of the two forms of the vinylic cation **28**.<sup>70</sup> The RISM SCF calculations also suggested similar stabilization of both forms of the cation by solvent.<sup>71</sup> These results indicate that the hydrogen-bridged form of the vinyl cation is also in solution more stable than the open ion.

Table 9 summarizes the relative stabilities of related cations obtained from theoretical calculations and/or gas-phase thermochemical data. The values are based on the isodesmic reaction  $\text{RH} + C_2H_3^+ \rightarrow R^+ + CH_2=CH_2$ , and give an idea how unstable simple vinyl cations are. The stability of the parent vinyl cation is in between that of the methyl and ethyl cation.  $\alpha$ -Alkyl substitution markedly stabilizes the cation, and stabilization by an  $\alpha$ -phenyl group is still much larger. Such stabilized secondary vinyl cations are common intermediates in vinylic solvolysis and in electrophilic addition to alkynes. A substituent at the  $\beta$ -position also significantly affects the stability of the vinyl cation. A  $\beta$ -alkyl group stabilizes the classical vinyl cation while a  $\beta$ -phenyl group destabilizes it.<sup>72</sup> 1,2-Participation by the  $\beta$ -substituent stabilizes the cation. The phenyl-bridged vinylenebenzenium ion **29** is quite stable,<sup>73,74</sup> and is an intermediate in the solvolysis of  $\beta$ -aryl-substituted vinyl derivatives.<sup>26,75-77</sup>

Relative stability<sup>72</sup>

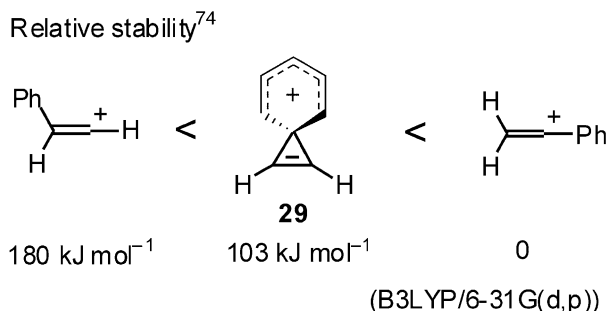


**Table 9** Relative stabilities of vinylic cations

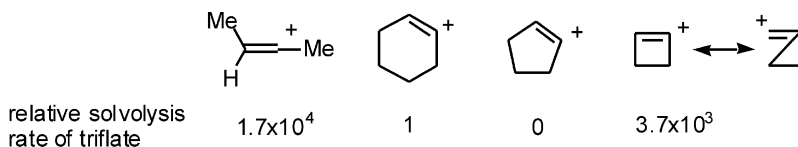
$R^+$	$\Delta E^a$ (kJ mol <sup>-1</sup> )	$-\Delta HIA^b$ (kJ mol <sup>-1</sup> )
$CH_3^+$	97	108
	19	-
	0	0
$CH_3-CH_2^+$	-47	-
	-47	-
	-74	-73
	-97	-96
	-122	
	-151	
$CH_3$ $H_2C=CH-CH_2^+$	-167	-134
	-138	
	-202	
	-185	
		-155

<sup>a</sup>The energy of the isodesmic reaction of  $RH + C_2H_3^+ \rightarrow R^+ + CH_2=CH_2$  calculated by the *ab initio* MO method at MP2(fu)/6-31G\* (taken from compilations in Ref. 68).

<sup>b</sup>The hydride ion affinity of the cation ( $R^+ + H^- \rightarrow RH$ ) relative to that of the vinyl cation (taken from a list in Ref. 67).



Because of the preferred linearity of vinyl cations, the stability of cyclic vinyl cations depends on the ring strain or the ring size. Rates of solvolysis of triflates show that the 1-cyclohexenyl cation is  $6 \times 10^{-5}$ -fold less readily generated than the 1-methyl-1-propenyl cation.<sup>78,79</sup> The 1-cyclopentenyl cation is not formed at all.<sup>80</sup> On the other hand, 1-cyclobutenyl triflate is 3700 times more reactive than 1-cyclohexenyl triflate.<sup>81</sup> The stability of the cyclobutenyl cation is due to resonance involving cyclopropyl-stabilization of the positive charge.<sup>68</sup>



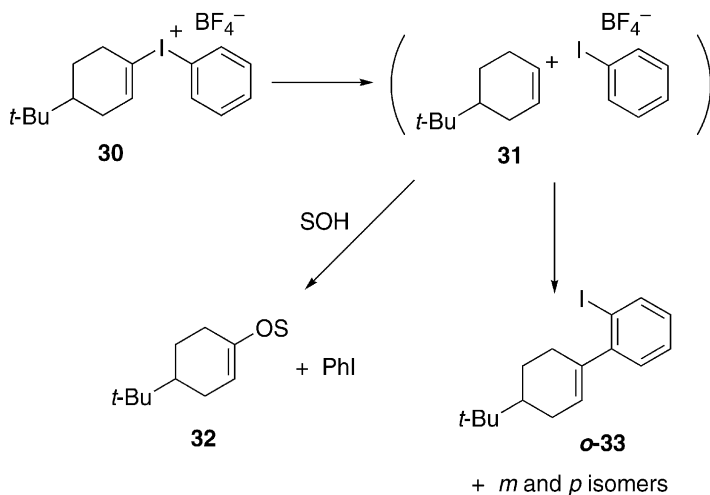
#### LEAVING ABILITY OF THE IODONIO GROUP

The kinetic stability of vinyl(phenyl)iodonium salts is largely due to the instability of the corresponding vinyl cations formed on departure of the iodobenzene nucleofuge. Thus,  $\alpha$ -phenyl- or  $\alpha$ -alkyl-substituted (secondary) vinyl iodonium ions so far could not be prepared as stable salts.<sup>43</sup>

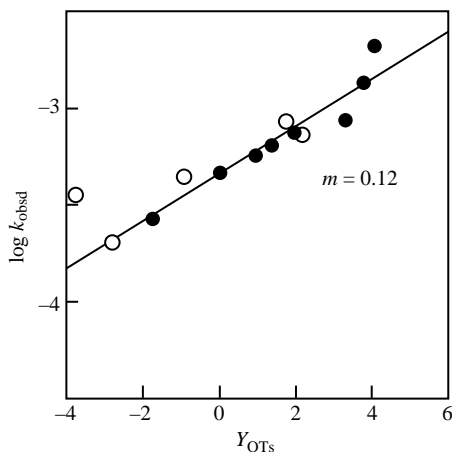
1-Cyclohexenylidonium salts are moderately stable due to a compromise between the stability of the secondary vinyl cation and the ring strain of the cyclic structure. Solvolysis of 4-*t*-butyl-1-cyclohexenyl(phenyl)iodonium tetrafluoroborate (**30**) was investigated in various alcoholic and aqueous solutions.<sup>37</sup> The main products are those expected for a cyclohexenyl cation intermediate (**31**), the enol ether (**32**) and/or cyclohexanone as well as iodobenzene (Scheme 25).

In addition to these expected solvolysis products, (4-*t*-butyl-1-cyclohexenyl)iodobenzenes (**33**) were obtained in yields of 13–15% in methanol and aqueous solutions and of 30–40% in TFE. The *ortho* derivative *o*-**33** is the predominant isomer of these products, and evidently is formed via the internal return of the contact ion–molecule pair of cyclohexenyl cation (**31**) and iodobenzene. The rates

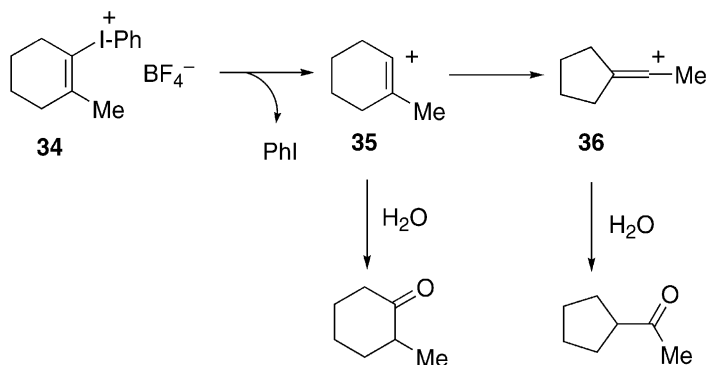




of solvolysis are only slightly (the Winstein–Grunwald  $m = 0.12$ )<sup>82</sup> affected by the solvents employed as shown in Fig. 9. This is compatible with a reaction of an ionic substrate giving an ionic intermediate in the rate-determining step. From comparison of the rate constant of **30** with that of 1-cyclohexenyl triflate,<sup>78,79</sup> the phenyliodonio group was evaluated to be about  $10^6$  times more effective as a nucleofuge than the triflate leaving group. Introduction of an electron-withdrawing substituent in the iodonio group further enhances the leaving ability. These values show that the iodonio group is the most efficient leaving group ever determined quantitatively.



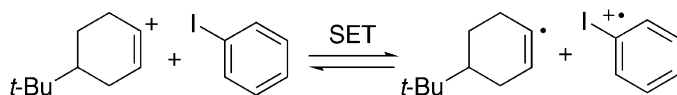
**Fig. 9** Solvent effects on the solvolysis rates of **30** at 50°C. Closed circles show data obtained in ethanol–water solvents. Taken from Ref. 37.



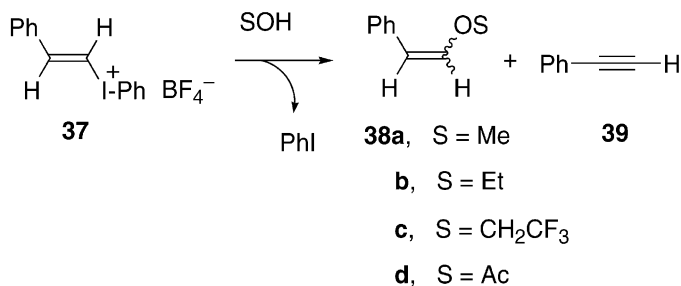
Scheme 26

Intermediacy of the cyclohexenyl cation was further supported by the observation of carbocationic rearrangement during the solvolysis of 2-methyl-1-cyclohexenyl-(phenyl)iodonium tetrafluoroborate (**34**). The strained bent 2-methyl-1-cyclohexenyl cation (**35**) formed rearranges to the more stable linear secondary vinyl cation **36** (Scheme 26). Solvolysis of **34** in 60% aqueous ethanol at  $-20^{\circ}\text{C}$  gave both a rearranged and an unrearranged ketone in the ratio of 14/86. Such a 1,2-rearrangement is characteristic of electron-deficient carbon species. The 2-methyl iodonium salt **34** decomposes quite readily and its rate of solvolysis in 60% aqueous ethanol shows that the 2-methyl group enhances the reactivity of **30** about 250-fold (provided the influence of the 4-alkyl group is small). This is in accordance with the prediction that a  $\beta$ -methyl group stabilizes vinyl cations.

Although no free-radical products were detected under the usual solvolysis conditions, careful examination of the products of **30** in the presence of a good hydrogen atom donor, 1,4-cyclohexadiene, or in 2-propanol, showed formation of about 1% of 4-*t*-butyl-1-cyclohexene. In principle, apparent heterolysis can occur via initial homolysis followed by single electron transfer (SET). However, this possibility is inconsistent with the rate effects of substituents at the leaving iodobenzene. Electron-withdrawing groups, which would destabilize the iodobenzene cation radical, accelerate the solvolysis with  $\rho = +1.7$ . The major reaction pathway must be rate-determining heterolysis yielding vinyl cation **31** (S<sub>N</sub>V1). The free radical product may be formed via reverse SET (Scheme 27), since the ionization potentials of the cyclohexenyl radical and iodobenzene are quite similar.



Scheme 27



Scheme 28

## VINYLENEBENZONIUM ION INTERMEDIATES

$\beta$ -Phenylvinylidonium salts are not expected to afford the primary classical  $\beta$ -phenylvinyl cation since this species is thermodynamically less stable than the parent vinyl cation (p. 27). Solvolysis of (*E*)-styryl(phenyl)iodonium tetrafluoroborate (**37**), however, takes place at a reasonable rate at 50–70°C.<sup>75,76</sup> Substitution as well as elimination products, **38** and **39**, are formed (Scheme 28). The ratios of substitution/elimination (**38/39**) and the *Z/E* isomeric ratios of **38** depend on the solvent used (Table 10). The only product of trifluoroethanolysis is the (*E*)-styryl ether *E*-**38c**, formed via exclusive substitution with retention. With increasing nucleophilicity/basicity of the solvent, the percentage of inversion in the substitution products increases and so does the percentage of elimination: in methanol and ethanol more than 90% is elimination and one-third of the substitution occurs with inversion. The elimination product **39** is formed via  $\alpha$ -elimination due to the basicity of the solvent. But what is the mechanism of the substitution?

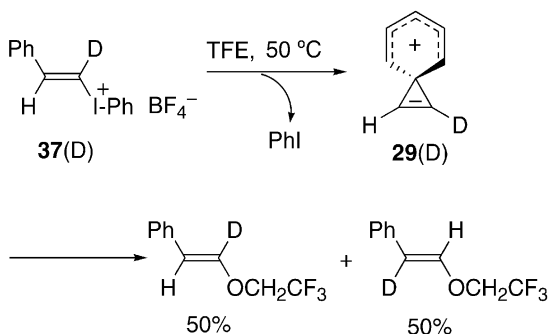
In TFE, the  $\alpha$ -deuterated substrate **37(D)** gives a 1:1 mixture of  $\alpha$ - and  $\beta$ -deuterated *E*-**38c** (Scheme 29). These stereochemical and *H/D* scrambling results are best explained by a symmetric 1,1-vinylenebenzenium ion intermediate **29(D)**.

In acetic acid and methanol, **37(D)** affords both stereoisomers of **38**, and the deuterium distributions are different in the two isomers: complete scrambling of deuterium between the  $\alpha$ - and  $\beta$ -positions in *E*-**38** as was the case in TFE, and complete retention of the isotope at the original position in *Z*-**38** (Scheme 30, results in methanol). Obviously *E*-**38** and *Z*-**38** are formed via different mechanisms. The inverted products *Z*-**38** are formed presumably via the in-plane  $S_NV\sigma$  pathway. If

Table 10 Product distribution in the solvolysis of **37** in some solvents<sup>76</sup>

Solvent	Temperature (°C)	<b>38</b> ( <i>Z/E</i> )	<b>39</b>
TFE	50	100 (0/100)	0
AcOH	70	85 (14/86)	15
MeOH <sup>a</sup>	60	6 (34/66)	94
EtOH <sup>a</sup>	60	7 (30/70)	93

<sup>a</sup>Contained trifluoroacetic acid (1 mmol dm<sup>-3</sup>).



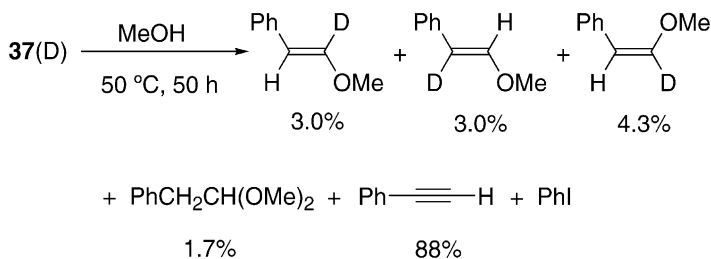
Scheme 29

they were formed via a primary vinyl cation intermediate, the deuterium distribution between the  $\alpha$  and  $\beta$  position of *E*-**38** would not have been equal.

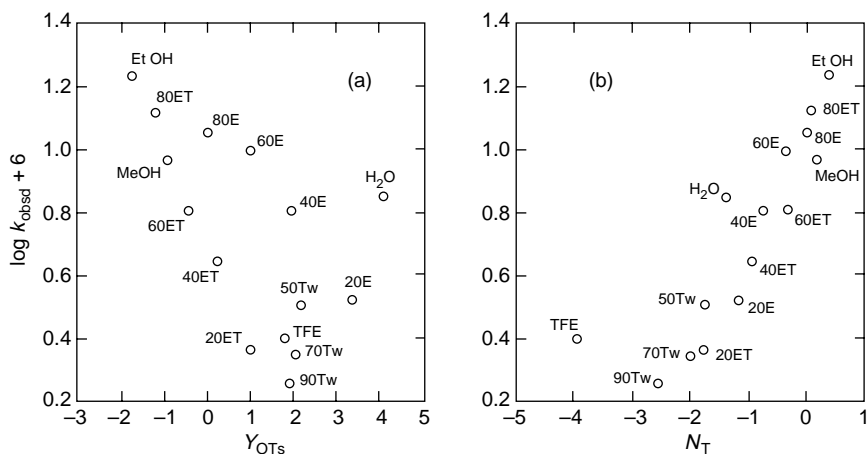
Solvent effects on the rate of solvolysis of **37** are also consistent with these conclusions. As Fig. 10 shows, a large scattering is obvious in the plot against the solvent ionizing power parameter,  $Y_{\text{OTs}}$ ,<sup>50,83</sup> but the rates correlate with the solvent nucleophilicity parameter,  $N_{\text{T}}$ .<sup>84,85</sup> The solvolysis of the ionic substrate via a benzenium ion should not be very dependent on the solvent polarity or nucleophilicity, but the competing pathways of bimolecular substitution ( $\text{S}_{\text{N}}\text{V}\sigma$ ) and  $\alpha$ -elimination will be very dependent on the solvent nucleophilicity/basicity. Large amounts of the latter products were formed in the more nucleophilic solvents, consistent with the kinetic results.

The benzenium ion intermediate **29** is formed by participation of the  $\beta$ -phenyl group of **37**. For stereoelectronic reasons the participation should occur from the *trans* position with respect to the nucleofuge. This can be confirmed by comparing the product distributions of the *E* and *Z* isomers of the substrate.

The *Z* isomer of **37** is too unstable to be isolated as a salt due to its facile  $\beta$ -elimination.<sup>51</sup> Therefore, the solvolysis of (*E*)- and (*Z*)-2-phenyl-1-propenyl(phenyl)iodonium tetrafluoroborate (**40**) was examined.<sup>77</sup> As anticipated, the solvolysis of the *E* isomer *E*-**40** is much faster than that of *Z*-**40**, e.g., 4000 times in TFE at 60°C. The distributions of the products from *E*-**40** and *Z*-**40** are quite different (Table 11).

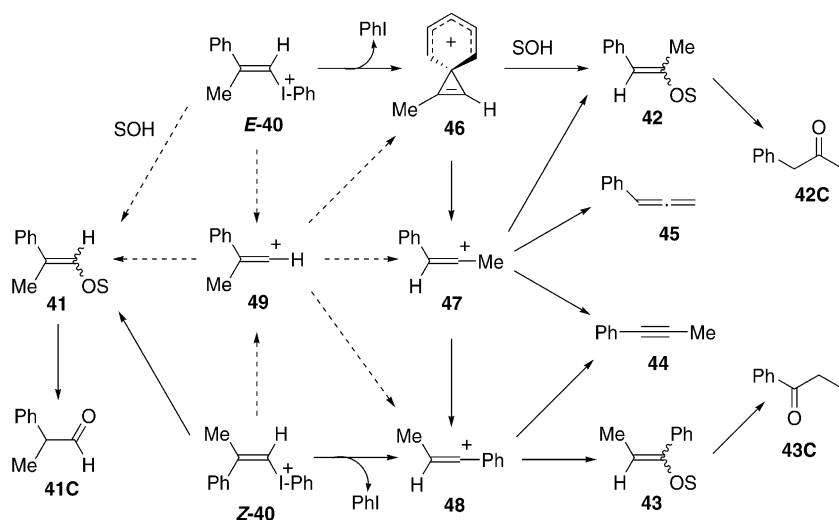


Scheme 30



**Fig. 10** Solvent effects on the solvolysis rates of **37** obtained at 50°C as plotted against solvent ionizing power  $Y_{\text{OTs}}$  (a) and nucleophilicity  $N_T$  (b). Taken from Ref. 76.

The *E* substrate *E*-**40** gives mainly the phenyl-migrated substitution product **42** and two elimination products, **44** and **45**, which are derived from the phenyl-migrated cation **47** (and/or **46**) (Scheme 31). In the less nucleophilic solvents the methyl-migrated product **43** is also formed. In contrast, *Z*-**40** gives unrearranged **41** and the methyl-migrated products, **43** and **44**. *Z*-**40** does not yield any phenyl-migrated products. The results are consistent with participation of the *trans*



**Scheme 31**

**Table 11** Product distributions (in percent yields) in the solvolysis of **40** at 60°C<sup>77</sup>

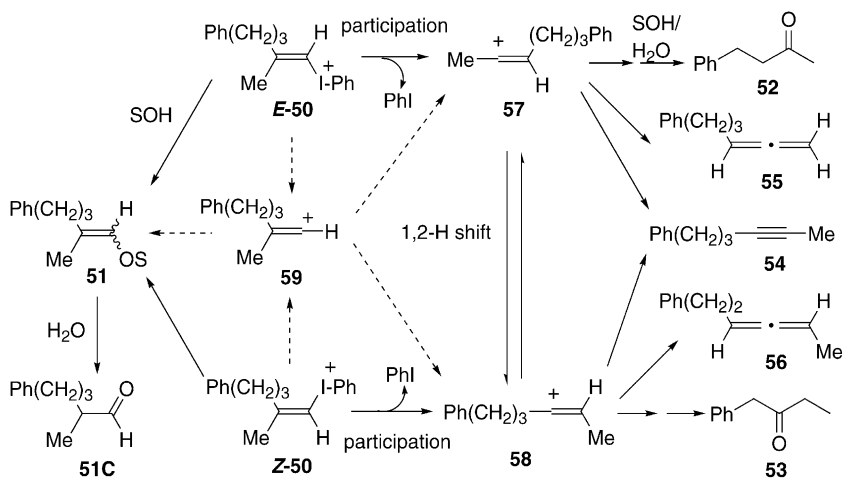
Substrate	Solvent	Reaction time (h)	<b>41</b> ( <i>E/Z</i> ) <sup>a</sup>	<b>42</b> ( <i>E/Z</i> ) <sup>b</sup>	<b>43</b> ( <i>E/Z</i> ) <sup>c</sup>	<b>44</b>	<b>45</b>	PhI
<i>E-40</i>	MeOH	1	0	29 (15/0)	0	28	30	97
<i>Z-40</i>	MeOH	95	5.8 (5.8/0)	0	4.9	81	0	87
<i>E-40</i>	AcOH	1	0	42 (35/7.1)	8.1 (3.1/5.0)	35	7.3	97
<i>Z-40</i>	AcOH	122	12.8 (5.2/7.6)	0	56 (20/36)	30	0	92
<i>E-40</i>	TFE	0.5	0	20	11	17	6.4	85
<i>Z-40</i>	TFE	170	0	0	14	6.7	0	22

For structures of the products, see [Scheme 31](#).

<sup>a</sup>Total yields of **41** and **41C** with the isomer yields of *E-41/Z-41* in parentheses.

<sup>b</sup>Total yields of **42** and **42C** with the isomer yields of *E-42/Z-42* in parentheses.

<sup>c</sup>Total yields of **43** and **43C** with the isomer yields of *E-43/Z-43* in parentheses.



Scheme 32

$\beta$ -substituent (phenyl or methyl) in the departure of the iodobenzene nucleofuge. In the less nucleophilic solvents a further 1,2-hydride shift across the double bond of vinyl cation **47**, formed from  $E$ -**40**, occurs to give the more stable cation **48**, but the reverse rearrangement does not take place. The phenyl group has a higher migratory aptitude than the methyl group. This may be the reason why  $Z$ -**40** affords the unrearranged product **41**, and  $E$ -**40** only gives rearranged products. The results indicate that the primary vinyl cation **49** is not formed during the thermal solvolysis of  $E$ -**40** or  $Z$ -**40**.

Photosolvolysis of **40** gives quite different results, which suggest formation of the primary cation **49**, as discussed in Section 5.

#### $\beta$ -ALKYL GROUP PARTICIPATION

$\beta,\beta$ -Dialkylvinylidonium salts have a better chance to afford primary vinyl cations than their  $\beta$ -phenyl counterparts due to the stabilizing effect of  $\beta$ -alkyl substituents discussed above. Solvolysis of ( $E$ )- and ( $Z$ )-2-methyl-5-phenyl-1-pentenyl(phenyl)-iodonium tetrafluoroborate (**50**) gave a variety of extensively rearranged products, as illustrated in Scheme 32 and summarized in Table 12.<sup>86,87</sup>

The unsymmetrically substituted substrate gave preferentially the products derived from migration of the *trans*-alkyl group, but the products of the *cis*-alkyl migrations were also observed (last column in Table 12). The amount of the latter products was very small in methanol, but substantial in less nucleophilic solvents. If the migration of the alkyl group was solely due to participation in the heterolysis reaction, only the *trans* group could have migrated, and the formation of products from the migration of the *cis*- $\beta$ -alkyl group could be considered as evidence for the formation of the classical primary vinyl cation **59**. However, the *cis*-alkyl-migrated

**Table 12** Product distribution in the solvolysis of **50** at 60°C<sup>87</sup>

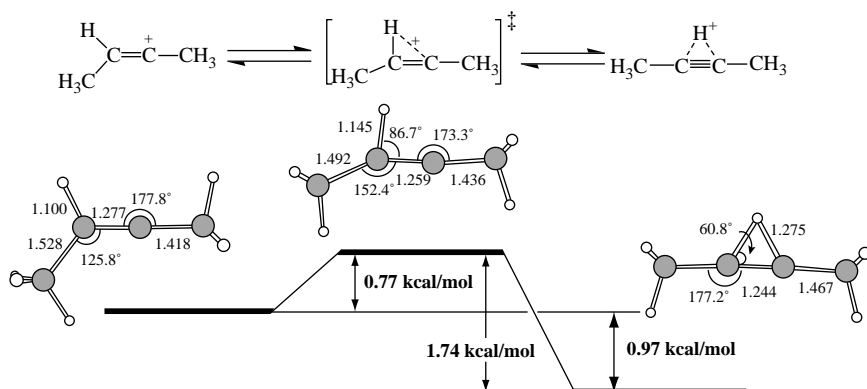
Structure of <b>50</b>	Solvent	Time (h)	PhI	Yield (%)							% Rearr.	Ratio <sup>c</sup>
				<b>51</b> ( <i>Z/E</i> ) <sup>a</sup>	<b>52</b>	<b>53</b>	<b>54</b>	<b>55</b>	<b>56</b>	<b>57</b>		
<i>E</i>	TFE	30	85	0.9 (nd)	15	8.9	30	0.54	0.17	0	98	63/37
<i>Z</i>	TFE	80	62	2.9 (nd)	11	17	34	0.34	0.39	0	96	39/61
<i>E</i>	AcOH	40	63	2.0 (trace/0.4)	21	3.4	50	2.7	(1) <sup>b</sup>	0	98	84/16
<i>Z</i>	AcOH	80	70	9.0 (1.0/3.9)	7.7	22	47	0.5	(3) <sup>b</sup>	0	90	25/75
<i>E</i>	EtOH	14	98	27 (5.8/12)	16	0.8	38	12	0.9	4.6	73	94/6
<i>Z</i>	EtOH	40	89	62 (13/38)	0.8	5.6	15	Trace	3.9	11	37	8/92
<i>E</i>	MeOH	16	80	26 (6.2/16)	12	Trace	25	7.0	0.3	2.8	63	Large
<i>Z</i>	MeOH	46	68	61 (10.3/31)	Trace	3.7	12	Trace	2.7	5.4	23	Small
<i>E(Z)</i>	MeOH	1	79	80 (17/47)	0	0	1.7	0	0	9.3		

<sup>a</sup>Combined yields of **51** and the aldehyde **51C** obtained after acid treatments are given with percent yields of the *Z* and *E* isomers of **51** in parentheses before acid hydrolysis.

<sup>b</sup>Partially overlapped with another peak.

<sup>c</sup>Ratio of **52** + **55** to **53** + **56**





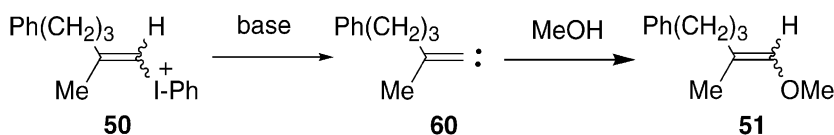
**Fig. 11** Energy barrier for the degenerate hydride transfer of 1,2-dimethylvinyl cation calculated at MP2/6-31G\*. Data are taken from Ref. 87.

products can also be formed via the very facile interconversion of the secondary vinyl cations, **57** and **58**, by 1,2-hydride shift.

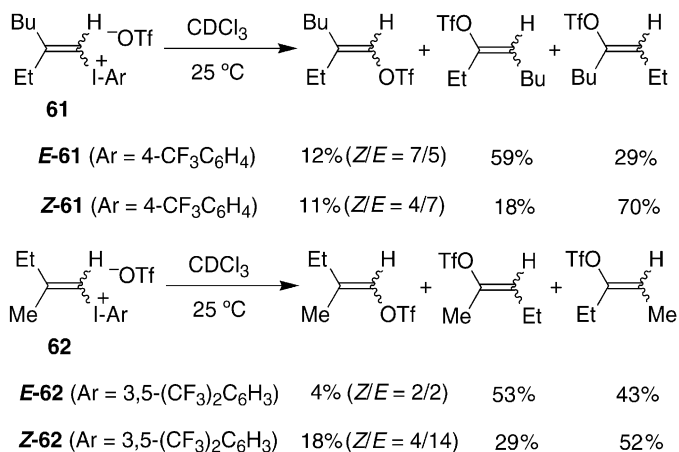
Model calculations of the dimethylvinyl cation system at the MP2/6-31G\* level show that the hydrogen-bridged cation is more stable than the secondary cation and that the barrier for the degenerate hydride transfer is very low ( $< 1 \text{ kcal mol}^{-1}$ , Fig. 11).<sup>87</sup> The isomeric allylic cation, which could be generated by a 1,2-hydride shift across the single bond of the secondary vinyl cation, is much more stable than the vinyl cation, but the barrier for this 1,2-hydride shift is very high since allylic conjugation cannot contribute to the stabilization of the transition state for the hydride shift.

Also, the unrearranged enol ether products **51** were obtained, without stereoselectivity. This seems to suggest the intermediacy of the primary cation **59**. However, products **51** in methanol and ethanol were concluded to be derived mostly from the alkylidencarbene **60** formed by  $\alpha$ -elimination (Scheme 33). Products **51** in more polar solvents amount to only a few percent and we now think that their formation is no definite support for the intermediacy of **59**. Alternative direct routes ( $S_NV\sigma$  and  $S_NV\pi$ ) to give these products seem to be more reasonable in view of the results obtained with other systems (see the next section and Section 4).

Hinkle and co-workers<sup>88-90</sup> have studied the thermal decomposition of a number of  $\beta,\beta$ -dialkylvinyl iodonium triflates, using an iodobenzene leaving group of enhanced nucleofugality, i.e. 4-trifluoromethyl and 3,5-bis(trifluoromethyl) deriva-



**Scheme 33**

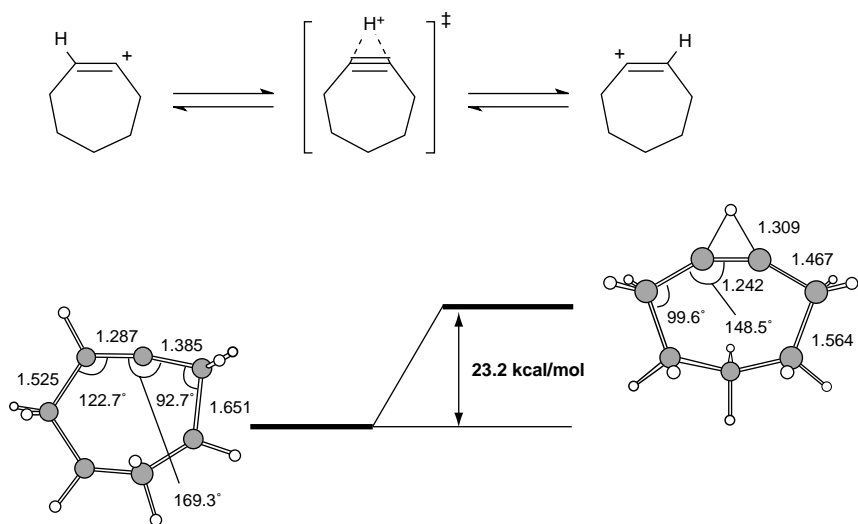


Scheme 34

tives. The 3,5-bis(trifluoromethyl)phenyl iodonium salts are 28 times more reactive than the phenyl salts, and were expected to generate primary vinyl cations. Typical results of the thermolysis of the *E/Z* isomeric triflate salts **61** and **62** in chloroform are given in Scheme 34. As in the solvolysis of **50**, extensive rearrangements and formation of both isomers of the unrearranged substitution products were observed. The results were initially regarded as evidence for the involvement of primary vinyl cation intermediates,<sup>89</sup> but are now concluded to indicate participation of the *trans*  $\beta$ -alkyl group in the C–I bond heterolysis, followed by a 1,2-hydride shift to give the isomeric rearranged product.<sup>90</sup> The S<sub>N</sub>2 and ligand coupling pathways afford the unrearranged *E* and *Z* products. These conclusions are in full agreement with our views summarized above.

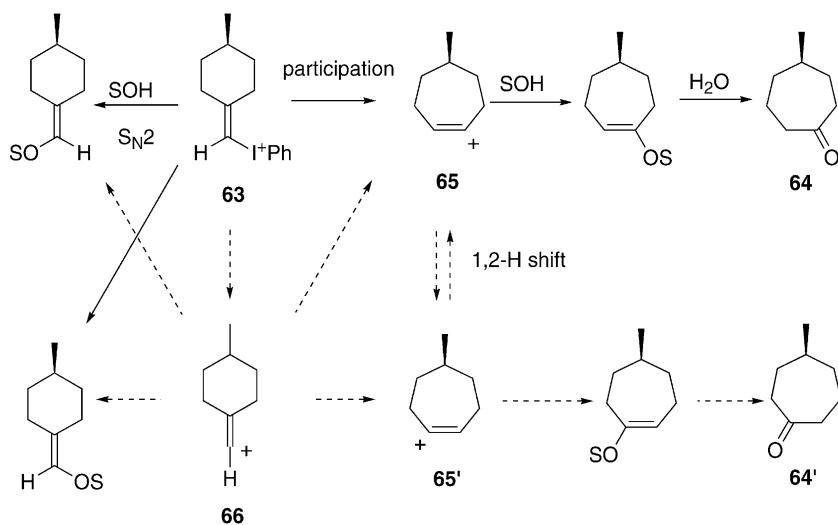
## CHIRALITY PROBE APPROACH

The product analysis of solvolysis of unsymmetrically substituted  $\beta,\beta$ -dialkylvinyl substrates does not provide definitive information about the intermediacy of primary vinyl cations, mainly due to the facile 1,2-hydride shift of the secondary vinyl cations involved. Cyclic vinyl cations are expected to have a high barrier for this rearrangement, since hydrogen-bridged vinylic cations have a structure similar to that of a protonated acetylene and small-ring acetylenes are very strained. In fact, *ab initio* MO calculations (MP2/6-31G\*) of the cycloheptenyl cationic system show the barrier for the 1,2-hydride shift to be quite high (23 kcal mol<sup>-1</sup>) (Fig. 12).<sup>91</sup> So, solvolysis of optically active (*R*)-4-methylcyclohexylidene-methyl(phenyl)iodonium tetrafluoroborate (**63**) should give the optically active (*R*)-4-methylcycloheptanone (**64**) with complete retention of enantiomeric purity if the rearrangement occurs with  $\beta$ -C–C bond participation, producing the chiral secondary cation **65** (Scheme 35).<sup>91</sup> On the other hand, if the primary vinyl cation **66** was generated

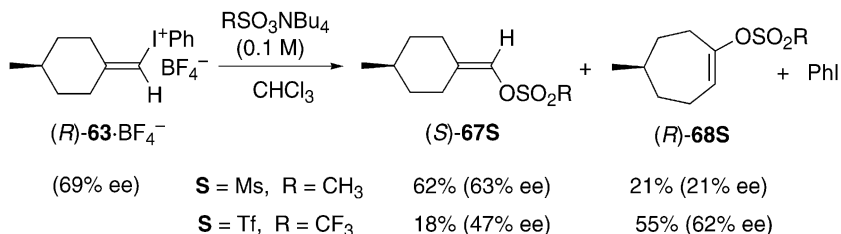


**Fig. 12** Energy barrier for the hydride transfer of cycloheptenyl cation calculated at MP2/6-31G\*. Taken from Ref. 91.

during the reaction, extensive racemization should occur due to the loss of chirality: the linear vinyl cation is achiral. A further advantage of the chiral system **63** is that the two  $\beta$ -substituent groups are identical and the complications arising from different migratory aptitudes of the  $\beta$ -alkyl groups of unsymmetrical substrates such as **50**, **61**, and **62** are avoided.



**Scheme 35**

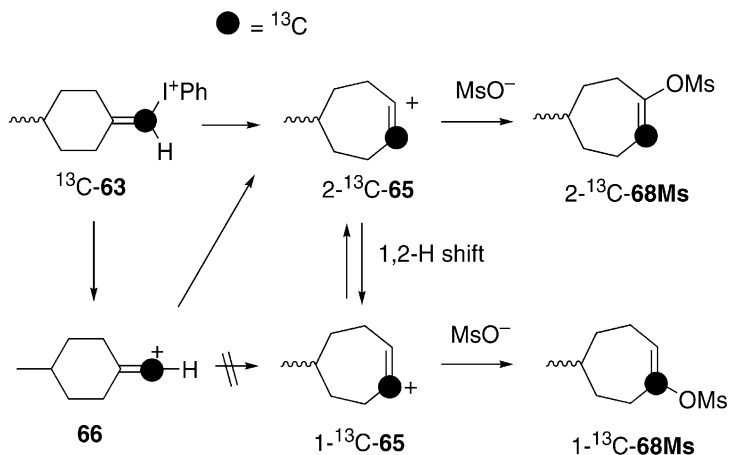


Scheme 36

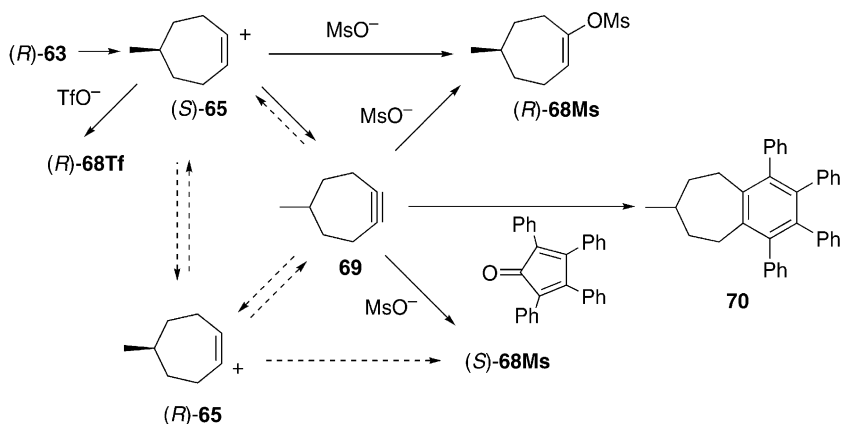
Cycloheptanone **64** produced in the solvolysis of  $(R)\text{-63}$  of 69% ee (enantiomeric excess) in methanol, aqueous methanol, TFE, and HFIP (1,1,1,3,3,3-hexafluoro-2-propanol) in all cases was the *R* isomer of **68**—69% ee, the ee being unchanged within experimental error. So, the primary vinyl cation **66** is not formed under the reaction conditions, not even in a highly ionizing non-nucleophilic solvent. Ion **66** is also not produced upon using a better leaving group: the 3-trifluoromethyl derivative of **63** provided the same stereochemical results.

In view of the results reported by Hinkle and co-workers for the reactions of vinyl iodonium triflates in chloroform,<sup>88–90</sup> the reactions of **63** with weakly nucleophilic sulfonates in chloroform have also been examined.<sup>92</sup> Reaction of **63** with triflate and mesylate in chloroform gave both unrearranged and rearranged sulfonates, **67S** and **68S** (Scheme 36). Unexpectedly, the products are racemized to various extents: the 7-membered-ring mesylate, **68Ms**, is largely racemized, but the triflate products only moderately. In the framework of a mechanism similar to that given in Scheme 35, there are two possibilities for racemization of **68Ms**. One is formation of the primary cation **66** and the other is a 1,2-hydride shift of the rearranged cation **65**.

The two possibilities can be distinguished by using substrate **63** labeled with <sup>13</sup>C at the exocyclic position (<sup>13</sup>C-**63**, Scheme 37). The label will be at the 2-position of



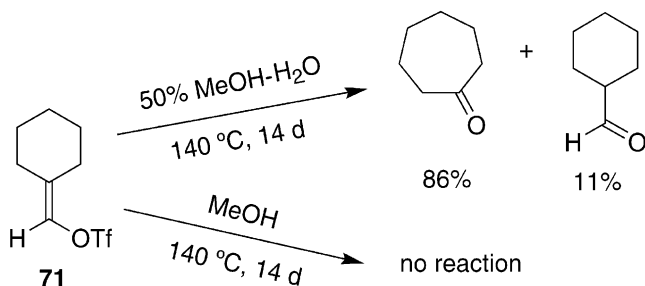
Scheme 37



Scheme 38

product **68Ms**, irrespective of intervention of **66**, but at the 1- and 2-position if interconversion between the enantiomeric ions **65** occurs. NMR analysis of the reaction products shows extensive scrambling of the  $^{13}\text{C}$  between the 1- and 2-position of **68Ms**. The extent of the scrambling agrees well with the degree of racemization of the product obtained from optically active (*R*)-**63**. That is, the primary cation **66** is obviously not involved in the reaction, and the racemization occurs due to scrambling of the exocyclic carbon atom of the substrate. What is the cause of this scrambling? Can the 1,2-hydride shift in **65**, which was not observed during the solvolysis reaction, be facilitated by added mesylate ion?

In the presence of a small amount of  $\text{CH}_3\text{OD}$ , the reaction of **63** with mesylate afforded **68Ms** containing a considerable amount of deuterium at the 2-position. This deuterium incorporation suggests an elimination–addition mechanism of interconversion of the isomeric cations **65** via cycloheptyne **69** as intermediate. Cycloalkyne **69** could in fact be trapped by tetraphenylcyclopentadienone giving **70** during the reaction (Scheme 38). In this trapping experiment, some adduct **68Ms** was still isolated, now with the same optical purity as substrate (*R*)-**63**. These results are best accommodated within the mechanism outlined in Scheme 38. Mesylate ion acts on **65** both as a base and a nucleophile to give **69** and (*R*)-**68Ms**, respectively. The highly strained cycloalkyne then undergoes nucleophilic attack by the mesylate ion affording racemic **68Ms**. In contrast, triflate reacts with **65** mostly as a nucleophile to give (*R*)-**68Tf**, and **69** is essentially not involved. This was confirmed by performing the reaction of **63** in the presence of both nucleophiles. The stereochemical purity of each of the products was not affected by the presence of the other sulfonate. Triflate cannot react with **69**. The cycloalkyne **69** is captured by the nucleophile mesylate, but not reprotonated to give back **65**: this would lead to interconversion of (*S*)- and (*R*)-**65**, which does not occur.

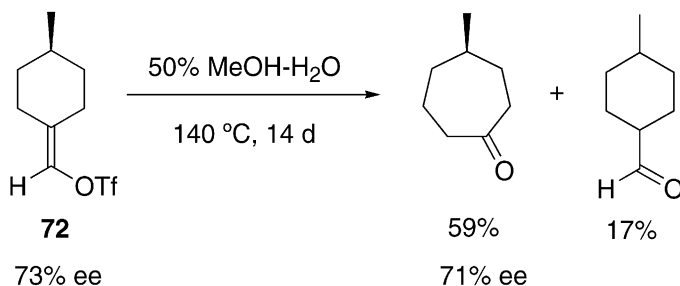


Scheme 39

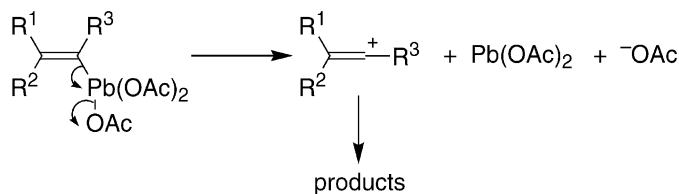
## OTHER ATTEMPTS TO GENERATE PRIMARY VINYL CATIONS

Hanack and co-workers<sup>93</sup> have suggested the formation of a primary vinyl cation during the solvolysis of cyclohexylidenemethyl triflate (**71**) in 50% aqueous methanol at 140 °C. This was based on their observation that the solvolysis gave the rearranged ketone, cycloheptanone as well as cyclohexanecarboxaldehyde in spite of the lack of reactivity of **71** in less polar pure methanol (Scheme 39). A chirality probe approach has now also been applied to this system. Solvolysis of the optically active (*R*)-4-methylcyclohexylidenemethyl triflate (**72**, 73% ee)<sup>94</sup> was carried out under the same conditions as employed by Hanack *et al.*<sup>93</sup> The main product is (*R*)-4-methylcycloheptanone with 71% ee (Scheme 40). That is, the rearranged product retains the optical purity of the substrate, which is definitive evidence against involvement of the primary vinyl cation **66**. The rearrangement occurs via  $\beta$ -C-C bond participation, as in the solvolysis of the iodonium salt **63**. The aldehyde product may be formed via a nucleophilic reaction at the sulfonic sulfur yielding an enol.

Moloney and co-workers<sup>95</sup> have studied the decomposition of vinyllead triacetates prepared by the reactions of vinylmercury or vinyltin compounds with lead tetraacetate. Vinyllead triacetates generated in chloroform undergo reductive elimination of lead(II) acetate to afford vinyl cations (Scheme 41). The products are those of substitution (acetates) or elimination (alkynes), depending on the reaction



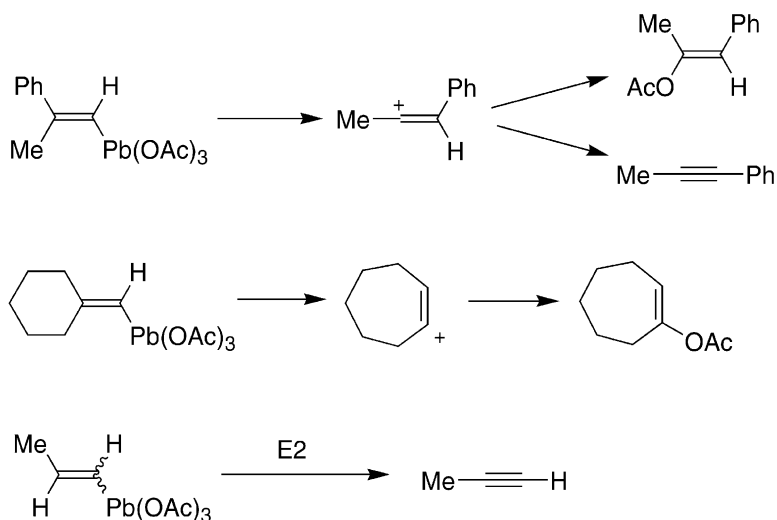
Scheme 40



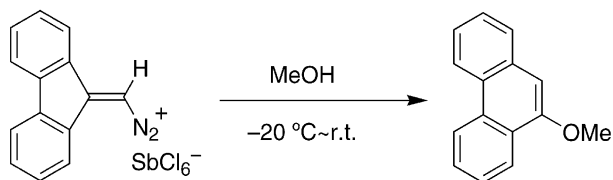
Scheme 41

conditions. However, the  $\alpha$ -hydrogen-bearing vinylic derivatives only gave rearranged products or products of  $\beta$ -elimination (Scheme 42). No indication of the formation of primary vinyl cations was found.

The extreme leaving group He generated by nuclear decay of tritium has been demonstrated to give a vinyl cation from tritioethene<sup>65,66</sup> (see Scheme 24). However, the super leaving groups of triflate and iodonio do not afford primary vinyl cations as described above. Diazonium salts with  $N_2$  as leaving group, which has a leaving ability in between that of He and the super leaving groups, are promising precursors to unstable carbocations. The phenyl cation has been generated from its diazonium precursor.<sup>96</sup> Several attempts to generate primary vinyl cations by dediazonation of alkenediazonium salts have been reported, and usually rearranged products were obtained.<sup>97</sup> One example is given in Scheme 43.<sup>98</sup> Rearranged products are expected if primary cations are formed, but the possibility of their direct formation via neighboring group participation has never been excluded. More detailed studies of alkenediazonium salts are required to reach a conclusion about the involvement of primary vinyl cations in their chemistry.



Scheme 42



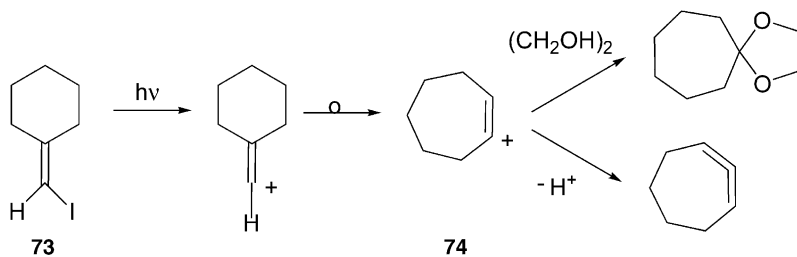
Scheme 43

The leaving group ability of halides in electronically excited vinyl halides is greatly enhanced compared to the ground state molecules. This makes photolysis of vinyl halides an excellent entry to vinyl cations.<sup>99</sup> For a dozen compounds the method has been used to produce cations from  $\alpha$ -hydrogen-bearing vinylic bromides and iodides. In all cases studied but one, rearrangement of the initially formed primary vinyl cations to more stable secondary species is much faster than reaction with nucleophiles or bases. For example, iodomethylenecyclohexane (**73**) exclusively yields a nucleophilic photosubstitution and a photoelimination product derived from the ring-expanded, cycloheptenyl, cation **74** (Scheme 44).<sup>100</sup>

In the exceptional case, the reaction of the cation with the nucleophile occurs intramolecularly. Irradiation of the  $\beta,\beta$ -bis(*o*-methoxyphenyl)vinyl bromide **75** yields a benzofuran derived from **76**, next to a benzofuran and an acetylene derived from **77** (Scheme 45).<sup>101</sup> Here, the reaction of the primary vinyl cation **76** with the internal nucleophile can compete with the 1,2-shift across the C=C double bond, yielding the  $\alpha$ -aryl-substituted vinyl cation **77**.

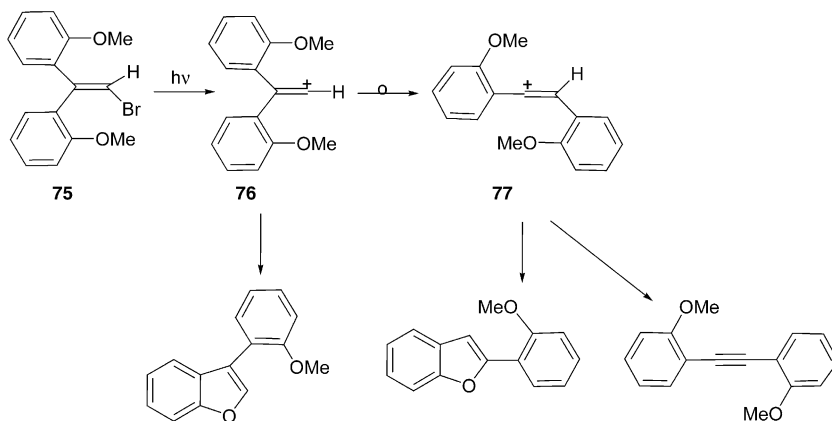
#### 4 Borderline mechanisms

Thus far, we have discussed typical vinylic  $S_N2$  and  $S_N1$  reactions. The former involve reactions of good nucleophiles with simple 1-alkenylidonium salts ( $S_NV\sigma$ ) and unactivated  $\beta$ -halo derivatives ( $S_NV\pi$ ), while the latter reactions occur under poor nucleophilic conditions (solvolysis) if the substrates can give stabilized vinylic cations of secondary or bridged structure. In this section, reactions which have characteristics of both categories are presented.



Scheme 44



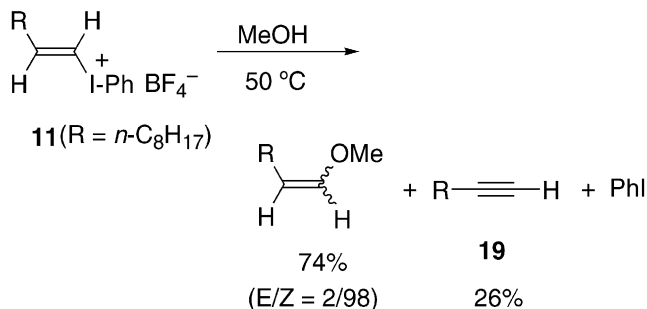


Scheme 45

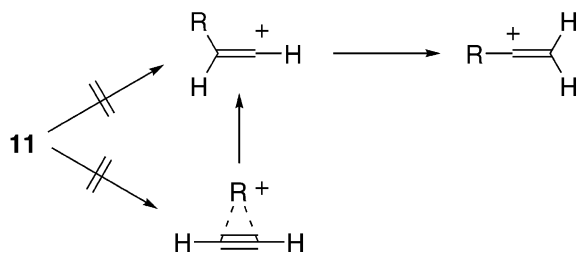
SOLVOLYSIS OF  $\beta$ -ALKYLVINYL IODONIUM SALTS

The typical primary vinylic substrate (*E*)-1-deceny(phenyl)iodonium tetrafluoroborate (**11**) displays unexpected reactivity under solvolytic conditions.<sup>102</sup> Its solvolysis was expected to be sluggish due to the instability of the possible primary vinyl cation intermediate, but it proceeded smoothly and as rapidly as that of the cyclohexenyl derivative **30** in alcoholic and aqueous solvents. However, the rates of solvolysis of **11** depend on the nucleophilicity of the solvent and not on the ionizing power. Both substitution (enol ether or aldehyde) and elimination products (**19**) are formed, in ratios which depend on the basicity of the medium (Scheme 46).

The enol ether products are essentially only formed with inversion of configuration and are concluded to be produced via an  $S_NV2$  reaction, and not via an intermediate primary vinyl cation. Both the in-plane  $S_NV\sigma$  and the out-of-plane  $S_NV\pi$  route are theoretically feasible as  $S_NV2$  pathways, leading to inversion and retention of configuration, respectively (see Scheme 1), and the major substitution reaction of **11** follows the first route, and the minor reaction the second route.



Scheme 46



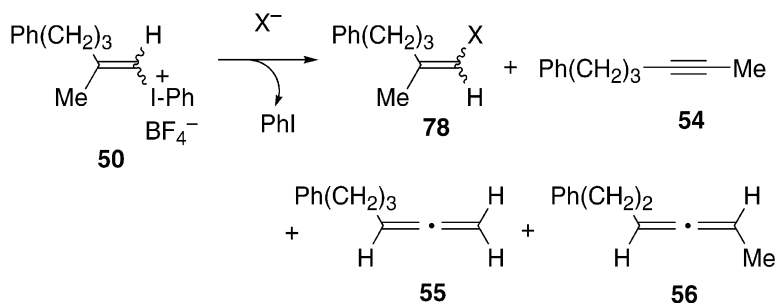
Scheme 47

No indications for the formation of the primary 1-alkenyl cation were detected. If it were formed, its rearrangement via a facile 1,2-hydride shift to the more stable secondary cation should have been observed (Scheme 47). Furthermore, the possibility of the formation of an alkyl-bridged cation and the alkyl-participation mechanism were ruled out on the basis of the lack of isotope scrambling in the product from the deuterium-labeled substrate.<sup>75</sup>

The elimination product **19** in Scheme 46 is formed via  $\alpha$ - or  $\beta$ -elimination, depending on the reaction conditions. Fluoride ion induces the  $\alpha$ -elimination pathway, while chloride and bromide ions induce  $\beta$ -elimination (see Scheme 15). In neutral methanol, the ratio of  $\alpha$ - to  $\beta$ -elimination is about 3:1, but in the presence of weakly basic additives such as dichloroacetate ( $pK_a$  1.35) and dihydrogen phosphate ( $pK_a$  2.12) in methanol the main route is  $\alpha$ -elimination.<sup>102</sup>

#### REACTIONS OF $\beta,\beta$ -DIALKYLVINYL IODONIUM SALTS WITH HALIDE IONS

Comparative investigations of geometrically isomeric  $\beta$ -monoalkylvinyl iodonium salts such as **11** are not possible due to the unavailability of the *Z* isomer of 1-alkenyl-iodonium salts.<sup>51</sup> Therefore, the reactions of the *E*- and *Z*-isomer of  $\beta,\beta$ -dialkylvinyl-iodonium salt **50** with halide ions were studied.<sup>49</sup> Although the main products are those of substitution with inversion, significant amounts of retained products are also formed, as well as small amounts of rearranged products (Scheme 48, Table 13). These results seem to suggest formation of a primary vinyl cation,

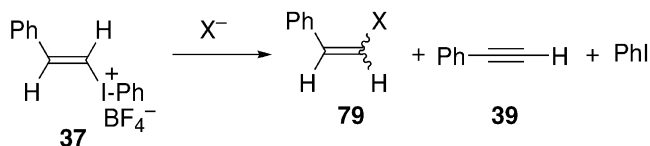


Scheme 48

**Table 13** Product distribution in the reactions of **50** with halide ions<sup>49</sup>

Structure of <b>50</b>	$X^{-a}$ (conc./mol dm <sup>-3</sup> )	Solvent ( $\mu^b$ )	Temperature, °C (time, h)	Product yield (%)			
				<b>78</b> ( <i>Z/E</i> )	<b>54</b>	<b>55</b>	<b>56</b>
<i>E</i>	Cl <sup>-</sup> (0.04)	MeCN (0.2)	50 (40)	70 (75/25)	11	0.5	0
<i>Z</i>	Cl <sup>-</sup> (0.04)	MeCN (0.2)	50 (30)	87 (9/91)	2.9	0	Trace
<i>E</i>	Cl <sup>-</sup> (0.001)	MeCN (0.2)	50 (40)	25 (75/25)	30	0.8	0
<i>E</i>	Cl <sup>-</sup> (0.001)	MeCN (0.001)	50 (40)	47 (72/28)	18	0.3	0
<i>Z</i>	Cl <sup>-</sup> (0.001)	MeCN (0.2)	50 (45)	65 (10/90)	11	0	0.7
<i>Z</i>	Cl <sup>-</sup> (0.001)	MeCN (0.001)	50 (40)	72 (13/87)	4.0	0	Trace
<i>E</i>	Cl <sup>-</sup> (0.04)	CHCl <sub>3</sub> (0.2)	50 (20)	72 (77/23)	5	Trace	0
<i>Z</i>	Cl <sup>-</sup> (0.04)	CHCl <sub>3</sub> (0.04)	50 (24)	61 (77/23)	0	0	0
<i>E</i>	Br <sup>-</sup> (0.04)	MeCN (0.1)	50 (20)	84 (77/23)	5.2	0.3	0.1
<i>Z</i>	Br <sup>-</sup> (0.04)	MeCN (0.1)	50 (20)	98 (8/92)	0.9	Trace	0
<i>E</i>	I <sup>-</sup> (0.04)	MeCN (0.04)	50 (17)	90 (71/29)	1.2	0	0
<i>Z</i>	I <sup>-</sup> (0.04)	MeCN (0.04)	50 (16)	98 (8/92)	0	0	0
<i>E</i> <sup>c</sup>	Br <sup>-</sup> (0.05)	MeOH (0.05)	60 (25)	18 (80/20)	17	4.2	0.2
<i>Z</i> <sup>c</sup>	Br <sup>-</sup> (0.05)	MeOH (0.05)	60 (25)	45 (4.4/95.6)	8.5	0	2.1
<i>E</i> <sup>c</sup>	Br <sup>-</sup> (0.05)	TFE (0.05)	60 (25)	11 (86/14)	39	2.4	0.5
<i>Z</i> <sup>c</sup>	Br <sup>-</sup> (0.05)	TFE (0.05)	60 (25)	37 (2.6/97.4)	15	Trace	0.6

<sup>a</sup>Added as Bu<sub>4</sub>NX.<sup>b</sup>Ionic strength adjusted with Bu<sub>4</sub>NClO<sub>4</sub>.<sup>c</sup>Significant amounts of solvolysis products were also obtained.



Scheme 49

which would give mainly inversion product via nucleophilic trapping in the ion pair intermediate (ion pair mechanism, Scheme 2), and would afford the rearranged products via 1,2-alkyl shift. However, various lines of evidence are incompatible with this suggestion. The stereoselectivity for inversion is larger with the *Z* isomer than with the *E* isomer, and it tends to be larger in more polar media, that is, at higher ionic strength and in polar protic solvents. The halide reactions of **50** were concluded to be mainly  $S_NV\sigma$  accompanied by minor pathways of  $S_NV\pi$  and ligand coupling (intramolecular  $S_NV\pi$ ) as well as heterolysis with  $\beta$ -alkyl participation leading to the rearranged secondary vinyl cations (see Scheme 32). Formation of 1-iodoalkene **78** with retained configuration is considered evidence for the ligand coupling mechanism. However, the very small dependence of the stereoselectivity on the halide concentration indicates similarity in molecularity of the reactions which give the inverted and the retained products. As the inverted product is formed by the bimolecular  $S_NV\sigma$  reaction, the bimolecular  $S_NV\pi$  pathway to give the retained product must also be involved.

#### REACTIONS OF $\beta$ -PHENYLVINYL IODONIUM SALTS WITH HALIDE IONS

The reactions of (*E*)-styryl(phenyl)iodonium salt **37** with halide ions give results similar to those obtained with **50** (Scheme 49, Table 14).<sup>47</sup> In this case the main product is that of elimination. In aprotic solvents the substitution products (**79**) are predominantly inverted but in TFE a significant amount of retained **79** was also

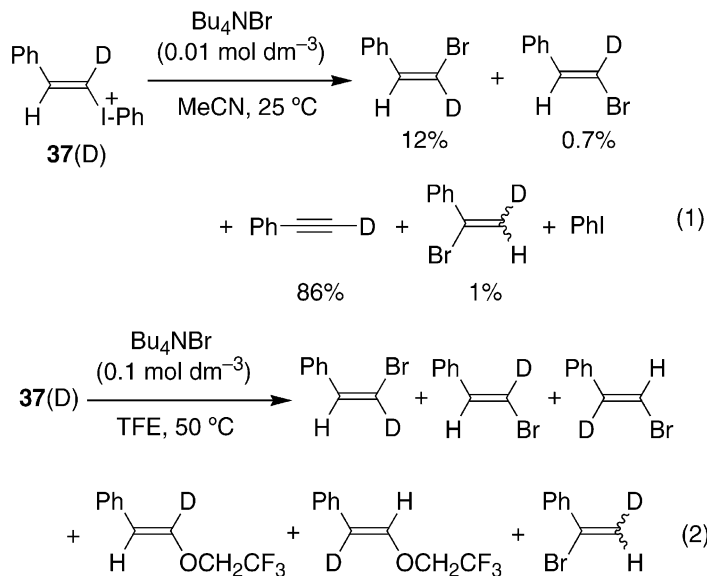
**Table 14** Product yields in the reactions of **37** with halide ions

$X^{-a}$	Solvent	Time (h)	<b>79</b> ( <i>Z/E</i> )	<b>39</b>	<b>79/39</b>
$Cl^{-}$	MeCN	8	14 (99.8/0.2)	71	16/84
$Cl^{-}$	$CHCl_3$	5	6.7 (98.5/1.5)	73	8.4/91.6
$Br^{-}$	MeCN	3	48 (99.4/0.6)	43	53/47
$Br^{-}$	$CHCl_3$	3	26 (98.3/1.7)	72	27/73
$Br^{-}$	Dioxane	1.5	45 (99.6/0.4)	40	53/47
$Br^{-}$	THF	0.25	57 (99.8/0.2)	49	59/41
$Br^{-}$	DMSO	5	19 (98.6/1.4)	17	53/47
$Br^{-}$	TFE	120	17 (70/30)	12	<sup>b</sup>
$I^{-}$	MeCN	2	77 (98.8/1.2)	10	88/12

Obtained at  $[Bu_4NX^{-}] = 0.1 \text{ mol dm}^{-3}$  and  $50^\circ\text{C}$ .<sup>47</sup>

<sup>a</sup>Tetrabutyl ammonium halide,  $Bu_4NX$ .

<sup>b</sup>Solvolysis products were also obtained.

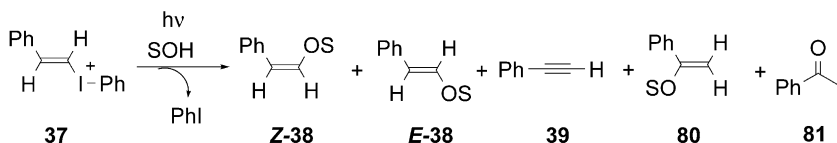


Scheme 50

obtained. Products from the reaction of the  $\alpha$ -deuterated substrate with bromide nucleophile in acetonitrile and TFE were examined by  $^1\text{H}$  NMR (Scheme 50). In acetonitrile, no scrambling or loss of deuterium was observed. However, in TFE, the stereochemically retained product showed scrambling of the deuterium between the  $\alpha$ - and  $\beta$ -positions while the inverted product did not. These results show that substitution with retention of configuration takes place via different mechanisms in aprotic solvent and in TFE: the  $\text{S}_{\text{N}}\text{V}\pi$  mechanism gives the normal product of retention but the D/H scrambled product is formed by trapping of the vinylenebenzenium ion intermediate in TFE as observed for trifluoroethanolysis (see Scheme 29).

## 5 Photochemical reactions

As discussed in the previous sections, the thermal solvolysis reactions of alkenyl iodonium salts usually occur via *trans*  $\beta$ -phenyl- or *trans*  $\beta$ -alkyl-assisted departure of the iodobenzene leaving group, by in-plane vinylic  $\text{S}_{\text{N}}2$  substitution or by ligand



Scheme 51

**Table 15** Quantum yields of formation of products in the photosolvolysis of **37** in MeOH and TFE at 20°C<sup>103</sup>

Solvent	<i>Z</i> - <b>38</b>	<i>E</i> - <b>38</b>	<b>39</b>	<b>80</b>	<b>81</b>	PhI
MeOH	0.12	0.39	0.32	0.04	0.01	0.75
TFE	0.007	0.007	<0.02		0.23	0.46

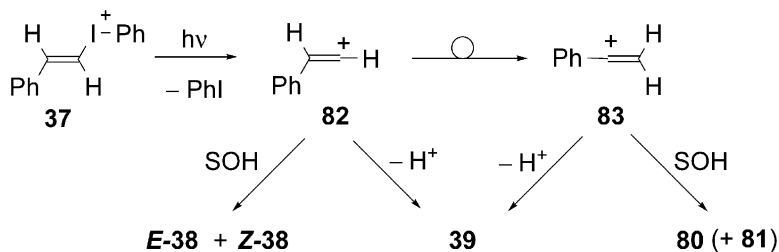
coupling. The only unambiguous examples of spontaneous dissociative formation of vinyl cations (vinyl  $S_N1$  reactions) seem to be the generation of secondary cations **31** from **30** (Scheme 25) and **35** from **34** (see Scheme 26).

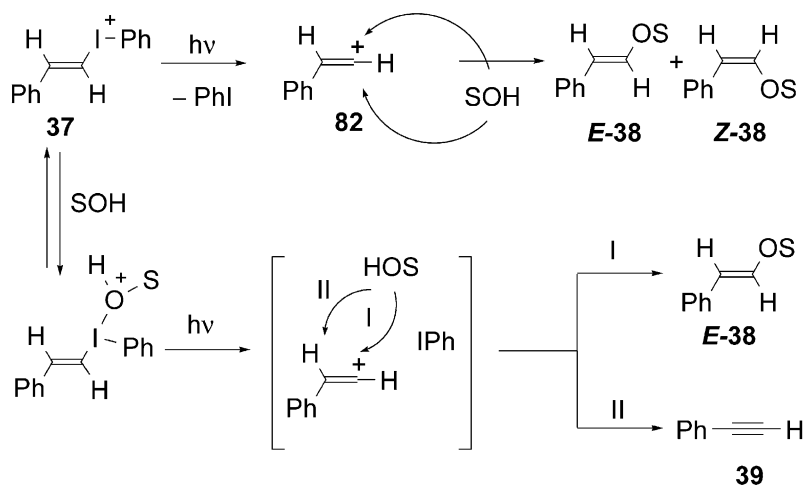
The situation is quite different for the photochemical solvolysis reactions of vinyl iodonium salts. In all cases studied thus far these reactions involve direct, unassisted heterolytic cleavage of the vinylic C–I bond, yielding primary and endocyclic secondary vinyl cations. For example, photosolvolysis of (*E*)-styryl(phenyl)iodonium tetrafluoroborate (**37**) very efficiently yields the products resulting from heterolytic cleavage of the vinylic C–I bond, depicted in Scheme 51.<sup>103</sup> (Also smaller amounts of products resulting from heterolytic cleavage of the phenylic C–I bond and homolytic cleavage of the vinylic C–I bond are formed, but they are not discussed here.)

As in the corresponding thermal solvolysis (see Scheme 28) two unrearranged enol ethers, *E*- and *Z*-**38**, are formed but, in marked contrast, also a rearranged enol ether **80** (and its hydrolysis product **81**). The ratios of formation of unrearranged/rearranged substitution product (**38/80 + 81**) of *E/Z* isomeric substitution product (*E*-**38/Z**-**38**), and of substitution/elimination (**38 + 80 + 81/39**) depend on the solvent used (Table 15).

The photochemical results are best accounted for by heterolytic cleavage of the vinylic C–I bond, yielding iodobenzene and the open primary styryl cation **82** (Scheme 52). This species can undergo nucleophilic attack by the solvent yielding *E/Z*-**38**, or loss of a  $\beta$ -hydrogen yielding **39**. Alternatively, **82** can rearrange by a 1,2-hydrogen shift to the  $\alpha$ -phenylvinyl cation **83**, which upon nucleophilic reaction with the solvent gives **80**, and upon  $\beta$ -proton loss **39**.

In methanol, the main enol ether products are the unrearranged **38**; in TFE by far the major product is the rearranged enol ether **80**. This difference is due to the difference in lifetime of the primary styryl cation (**82**) in the two solvents. Its

**Scheme 52** Mechanism of formation of photoproducts from **37**.



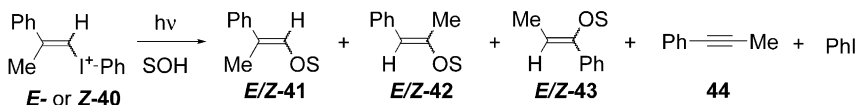
Scheme 53

lifetime will be longer in the good cation-stabilizing TFE than in the nucleophilic methanol. This gives **82** more time to rearrange to the more stable **83**.

In methanol the *E/Z* ratio of the unrearranged enol ethers (**38**) is 3.3 (i.e. mainly retention of configuration), while in TFE the *E/Z* ratio is 1. This difference is ascribed to the coordination of the nucleophilic solvent methanol with the hypervalent iodine (8-I-2) compound **37** to give the corresponding tricoordinated 10-I-3 ( $\lambda^3$ -iodane) species. This coordination is less important for the less nucleophilic TFE. Excitation of the free iodonium yields **82** in an  $\text{S}_{\text{N}}1$  mechanism, which gives substitution products **38** in  $\sim 1:1$  *E/Z* ratio (Scheme 53). Excitation of the  $\lambda^3$ -iodane results in the formation of **82**, iodobenzene and a solvent molecule within a solvent cage. Nucleophilic attack of the solvent molecule within the cage will give preferentially *E*-**38**, in an  $\text{S}_{\text{N}}i$  mechanism.

In methanol the efficiency of formation of elimination product **39** is higher than in TFE. In the cation–molecule pair formed upon photolysis of **37** in methanol (Scheme 53), the methanol not only acts as a nucleophile but also as a base. In TFE the proton has to be abstracted by the less basic agents iodobenzene, the leaving group, or external TFE.

The photochemical solvolysis of (*E*)- and (*Z*)-2-phenyl-1-propenyl(phenyl)iodonium tetrafluoroborate (**40**) in methanol and TFE yields the heterolytic vinylic C–I bond cleavage products shown in Scheme 54 and summarized in Table 16.<sup>77</sup>



Scheme 54

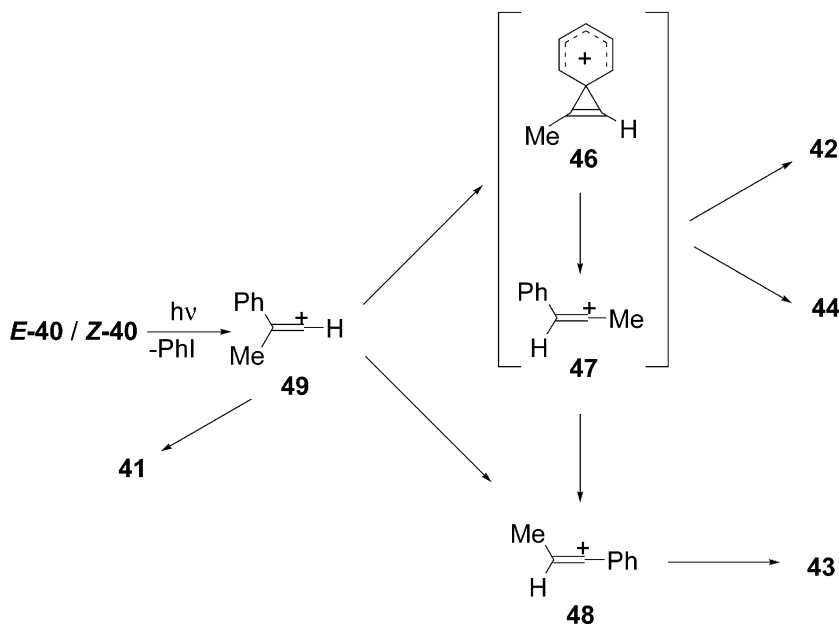
**Table 16** Product distributions (in percentages) in the photosolvolytic of *E*- and *Z*-**40** in MeOH and TFE at 20°C<sup>77</sup>

Substrate	Solvent	<i>E</i> - <b>41</b>	<i>Z</i> - <b>41</b>	<i>E</i> - <b>42</b>	<i>Z</i> - <b>42</b>	<i>E</i> - <b>43</b>	<i>Z</i> - <b>43</b>	<b>44</b>	PhI
<i>E</i> - <b>40</b>	MeOH	34.1	13.4	6.5	0	8.2	8.6	15.3	66.3
<i>Z</i> - <b>40</b>	MeOH	14.8	38.5	7.5	0	10.8	11.5	16.7	71.5
<i>E</i> - <b>40</b>	TFE	0	0	32.6 <sup>a</sup>	4.4 <sup>a</sup>	36.6 <sup>b</sup>		<2	81
<i>Z</i> - <b>40</b>	TFE	0	0	11.0 <sup>c</sup>	2.2 <sup>c</sup>	54.1 <sup>d</sup>		<2	70

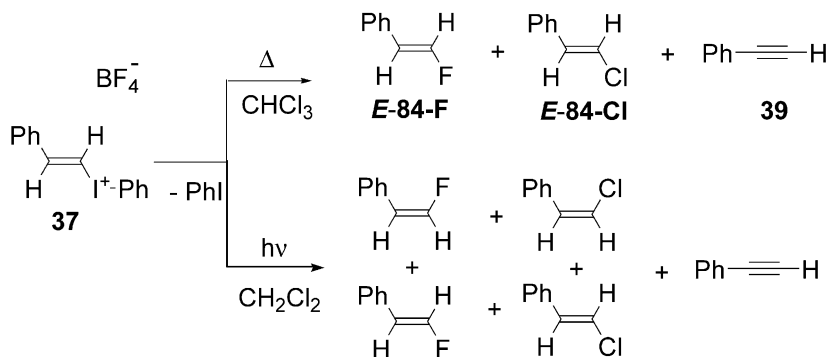
<sup>a</sup>In addition 9.9% of ketone **42C** is formed.<sup>b</sup>In addition 10.2% ketone **43C**.<sup>c</sup>In addition 2% **42C**.<sup>d</sup>In addition 10.4% **43C**.

Five enol ethers are produced, two unrearranged (**41**), one 1,2-phenyl-shifted (**42**) and two 1,2-methyl-shifted (**43**). Unlike the corresponding thermal reaction (see [Scheme 31](#) and [Table 11](#)), the product patterns are barely affected by the geometrical structure of **40**: the ratio **41/42** + **43** = 2.0 for *E*-**40** and 1.8 for *Z*-**40**. This indicates formation of a common intermediate, the primary vinyl cation **49**, from both stereoisomers ([Scheme 55](#)). This cation gives **41** and rearranges to the more stable vinylic cations **46–48**, which in turn give **42** and **43**.

As in the case of **37**, the amount of rearranged product is much smaller in methanol than in TFE. Also, preferential retention of configuration in the unrearranged enol ethers **41** was observed in methanol but not in TFE, and

**Scheme 55**





Scheme 56

elimination was found to be far more important in methanol than in TFE. As discussed for **37**, lifetime differences of the initially formed vinyl cation, ion nucleophile reaction inside or outside a solvent cage, and ion base reaction inside or outside a solvent cage (see Scheme 53), account for the solvent effects.

The product mixtures of the photochemical reactions of both **37** and *E*- and *Z*-**40** are strikingly different from those of the corresponding thermal reactions (Scheme 51/Table 15 versus Scheme 28/Table 10; and Scheme 54/Table 16 versus Scheme 31/Table 11). Photolysis of **37** gives a rearranged substitution product, while its thermolysis does not. Photolysis of *E*- and *Z*-**40** gives quite similar product mixtures, while their thermolysis gives quite different mixtures. These marked contrasts mean that the thermal and photochemical reactions of **37** and **40** do proceed through different product-forming reactive intermediates. Whereas primary vinyl cations are involved in the photolysis, they are not in the thermolysis.

A dichotomy in the thermal versus photochemical behavior of vinyl iodonium salts has also been observed in the reactions of **37** in chlorinated alkanes (Scheme 56).<sup>55,103</sup>

In the thermolysis the *E* isomers of fluoro- and chlorostyrene (*E*-**84-F** and *E*-**84-Cl**) are formed exclusively, which indicates the intermediacy of the vinylenebenzenium ion **29** (see Scheme 29) as the species abstracting a fluoride from the counterion  $\text{BF}_4^-$ , or a chloride from the solvent. Photochemically both *E*- and *Z*-**84** are formed, indicating the intermediacy of the primary styryl cation **82** (see Scheme 52). Preferentially the *Z*-isomer of **84-F** is formed. The fluoride-abstrating species must not be **82** itself, but a tight ion–molecule pair of **82** and iodobenzene (see Scheme 53), which hampers the approach of the fluoride donor to the side of **82** where this group leaves.

## 6 Summary

Vinyl(aryl)iodonium salts are good electrophiles carrying an excellent nucleofuge, an iodoarene, which makes them good substrates for nucleophilic substitution ( $\text{S}_{\text{N}}2$ )

as well as versatile precursors for vinyl cations ( $S_N1$ ). For the vinylic  $S_N2$  reactions, two pathways are possible:  $S_NV\sigma$  and  $S_NV\pi$  leading to inversion and retention of configuration, respectively. Primary vinyl cations are unstable both thermodynamically and kinetically, and their thermal generation from vinyl iodonium salts is avoided by participation of the *trans*  $\beta$ -phenyl or  $\beta$ -alkyl groups or an external nucleophile. In contrast, photoexcited vinyl iodonium ions readily undergo heterolysis to give primary cations.

## Acknowledgments

The authors are grateful to Professor Masahito Ochiai (Tokushima University) for the fruitful collaboration on the topics summarized in this chapter. They also appreciate the support of their cooperative research by the Yamada Science Foundation.

## References

1. Rappoport, Z. (1985). *Rec. Chim. Pays-Bas* **104**, 309–349
2. Rappoport, Z. (1981). *Acc. Chem. Res.* **14**, 7–15
3. Rappoport, Z. (1992). *Acc. Chem. Res.* **25**, 474–479
4. Stang, P.J. (1978). *Acc. Chem. Res.* **11**, 107–114
5. Stang, P.J., Rappoport, Z., Hanack, M. and Subramanian, L.R. (1979). *Vinyl Cations*. Academic Press, New York
6. Rappoport, Z. and Stang, P.J. (eds) (1997). *Dicoordinated Carbocations*. Wiley, Chichester
7. Miller, S.I. and Yonan, P.K. (1957). *J. Am. Chem. Soc.* **79**, 5931–5937
8. Miller, S.I. (1968). *Adv. Phys. Org. Chem.* **6**, 185–332
9. Kelsey, D.R. and Bergman, R.G. (1971). *J. Am. Chem. Soc.* **93**, 1953–1961
10. Okuyama, T., Takino, T., Sato, K. and Ochiai, M. (1998). *J. Am. Chem. Soc.* **120**, 2275–2282
11. Okuyama, T., Takino, T., Sato, K., Oshima, K., Imamura, S., Yamataka, H., Asano, T. and Ochiai, M. (1998). *Bull. Chem. Soc. Jpn* **71**, 243–257
12. Glukhovtsev, M.N., Pross, A. and Radom, L. (1994). *J. Am. Chem. Soc.* **116**, 5961–5962
13. Lucchini, V., Modena, G. and Pasquato, L. (1995). *J. Am. Chem. Soc.* **117**, 2297–2300
14. Okuyama, T. and Yamataka, H. (1999). *Can. J. Chem.* **77**, 577–583
15. Kim, C.K., Hyun, K.H., Kim, C.K. and Lee, I. (2000). *J. Am. Chem. Soc.* **122**, 2294–2299
16. Bach, R.D., Baboul, A.G. and Schlegel, H.B. (2001). *J. Am. Chem. Soc.* **123**, 5787–5793
17. Clarke, T.C., Kelsey, D.R. and Bergman, R.G. (1972). *J. Am. Chem. Soc.* **94**, 3626–3627
18. Clarke, T.C. and Bergman, R.G. (1974). *J. Am. Chem. Soc.* **96**, 7934–7944
19. Summerville, R.H. and Schleyer, P.v.R. (1972). *J. Am. Chem. Soc.* **94**, 3629–3631
20. Summerville, R.H. and Schleyer, P.v.R. (1974). *J. Am. Chem. Soc.* **96**, 1110–1120
21. Rappoport, Z. (1978). *Tetrahedron Lett.* 1073–1076
22. Lucchini, V., Modena, G. and Pasquato, L. (1993). *J. Am. Chem. Soc.* **115**, 4527–4531

23. Destro, R., Lucchini, V., Modena, G. and Pasquato, L. (2000). *J. Org. Chem.* **65**, 3367–3370
24. Modena, G. and Tonellato, U. (1971). *J. Chem. Soc. (B)* 374
25. Bassi, P. and Tonellato, U. (1974). *J. Chem. Soc. Perkin Trans. 2* 1283
26. Stang, P.J. and Dueber, T.E. (1977). *J. Am. Chem. Soc.* **99**, 2602–2610
27. Capozzi, G., Lucchini, V., Modena, G. and Scrimin, P. (1977). *Tetrahedron Lett.* 911–912
28. Lucchini, V., Modena, G. and Zaupa, T. (1982). *J. Org. Chem.* **47**, 590–592
29. Lucchini, V., Modena, G., Vale, G. and Capozzi, G. (1981). *J. Org. Chem.* **46**, 4720–4724
30. Yoshida, Y., Komatsu, M., Ohshiro, Y. and Agawa, T. (1979). *J. Org. Chem.* **44**, 830
31. Shainyan, B.A. and Rappoport, Z. (1993). *J. Org. Chem.* **58**, 3421–3428
32. Ochiai, M., Oshima, K. and Masaki, Y. (1991). *J. Am. Chem. Soc.* **113**, 7059–7061
33. Duraisamy, M. and Walborsky, H.M. (1984). *J. Am. Chem. Soc.* **106**, 5035–5037
34. Boche, G., Marsch, M., Müller, A. and Harms, K. (1993). *Angew. Chem. Int. Ed. Engl.* **32**, 1032–1033
35. Topolski, M., Duraisamy, M., Rachon, J., Gawronski, J., Gawronska, K., Goedken, V. and Walborsky, H.M. (1993). *J. Org. Chem.* **58**, 546
36. Mori, S., Uchiyama, K., Hayashi, Y., Narasaka, K. and Nakamura, E. (1998). *Chem. Lett.* 111–112
37. Okuyama, T., Takino, T., Sueda, T. and Ochiai, M. (1995). *J. Am. Chem. Soc.* **117**, 3360–3367
38. Ochiai, M., Sumi, K., Nagao, Y. and Fujita, E. (1985). *Tetrahedron Lett.* **26**, 2351–2354
39. Ochiai, M., Sumi, K., Takaoka, Y., Kunishima, M., Nagao, Y., Shiro, M. and Fujita, E. (1988). *Tetrahedron* **44**, 4095–4112
40. Ochiai, M., Toyonari, M., Nagaoka, T., Chen, D.-W. and Kida, M. (1997). *Tetrahedron Lett.* **38**, 6709–6712
41. Hinkle, R.J., Poulter, G.T. and Stang, P.J. (1993). *J. Am. Chem. Soc.* **115**, 11626–11627
42. Hinkle, R.J. and Stang, P.J. (1994). *Synthesis* 313–316
43. Stang, P.J. and Zhdankin, V.V. (1996). *Chem. Rev.* **96**, 1123–1178
44. Okuyama, T. (1999). *Rev. Heteroatom Chem.* **21**, 257–275
45. Ochiai, M. (2000). *J. Organomet. Chem.* **611**, 494–508
46. Okuyama, T., Takino, T., Sato, K. and Ochiai, M. (1997). *Chem. Lett.* 955–956
47. Okuyama, T., Oka, H. and Ochiai, M. (1998). *Bull. Chem. Soc. Jpn* **71**, 1915–1921
48. Ochiai, M., Kida, M., Sato, K., Takino, T., Goto, S., Donkai, N. and Okuyama, T. (1999). *Tetrahedron Lett.* **40**, 1559–1562
49. Okuyama, T., Sato, K. and Ochiai, M. (2000). *Bull. Chem. Soc. Jpn* **73**, 2341–2349
50. Schadt, F.L., Bentley, T.W. and Schleyer, P.v.R. (1976). *J. Am. Chem. Soc.* **98**, 7667–7674
51. Ochiai, M., Oshima, K. and Masaki, Y. (1991). *J. Chem. Soc. Chem. Commun.* 869–870
52. Yan, J. and Chen, Z.-C. (1999). *Tetrahedron Lett.* **40**, 5757–5758
53. Fujita, M., Sakanishi, Y., Furutani, M. and Okuyama, T. (2001). Unpublished results
54. Ochiai, M., Yamamoto, Y. and Sato, K. (1999). *J. Chem. Soc. Chem. Commun.* 1363–1364
55. Okuyama, T., Fujita, M., Gronheid, R. and Lodder, G. (2000). *Tetrahedron Lett.* **41**, 5125–5129
56. Ochiai, M., Takaoka, Y., Sumi, K. and Nagao, Y. (1986). *J. Chem. Soc. Chem. Commun.* 1382–1384
57. Ochiai, M., Oshima, K. and Masaki, Y. (1994). *Chem. Lett.* 871–872
58. Oae, S. (1986). *Croatia Chem. Acta* **59**, 129–151
59. Oae, S. (1996). *Pure Appl. Chem.* **68**, 805–812

60. Finet, J.-P. (1998). *Ligand Coupling Reactions with Heteroatomic Compounds*, pp. 122–129. Pergamon, Oxford
61. Grob, C.A. and Cseh, G. (1964). *Helv. Chim. Acta* **47**, 194
62. Stang, P.J., Hanack, M. and Subramanian, L.R. (1982). *Synthesis* 85–126
63. Lucchini, V. and Modena, G. (1990). *J. Am. Chem. Soc.* **112**, 6291–6296
64. Hogeveen, H. and Roobeek, C.F. (1971). *Tetrahedron Lett.* 3343–3346
65. Fornarini, S. and Speranza, M. (1984). *Tetrahedron Lett.* **25**, 869–872
66. Fornarini, S. and Speranza, M. (1989). *J. Am. Chem. Soc.* **111**, 7402–7407
67. Aue, D.H. (1997). In *Dicoordinated Carbocations*, Rappoport, Z. and Stang, P.J. (eds), pp. 105–156. Wiley, Chichester
68. Apeloig, Y. and Müller, T. (1997). In *Dicoordinated Carbocations*, Rappoport, Z. and Stang, P.J. (eds), pp. 9–104. Wiley, Chichester
69. van Alem, K., Lodder, G. and Zuilhof, H. (2000). *J. Phys. Chem. A* **104**, 2780–2787
70. Bagno, A. and Modena, G. (1999). *Eur. J. Org. Chem.* 2893–2897
71. Sato, H. (2001). Unpublished results
72. Kobayashi, S., Hori, Y., Hasako, T., Koga, K. and Yamataka, H. (1996). *J. Org. Chem.* **61**, 5274–5279
73. Rappoport, Z., Kobayashi, S., Stanger, A. and Bese, R. (1999). *J. Org. Chem.* **64**, 4370–4375
74. Gronheid, R. (2001). PhD Thesis, Leiden University, The Netherlands
75. Okuyama, T. and Ochiai, M. (1997). *J. Am. Chem. Soc.* **119**, 4785–4786
76. Okuyama, T., Ishida, Y. and Ochiai, M. (1999). *Bull. Chem. Soc. Jpn* **72**, 163–170
77. Gronheid, R., Lodder, G., Ochiai, M., Sueda, T. and Okuyama, T. (2001). *J. Am. Chem. Soc.* **123**, 8760–8765
78. Pfeifer, W.D., Bahn, C.A., Schleyer, P.v.R., Bocher, S., Harding, C.E., Hummel, K., Hanack, M. and Stang, P.J. (1971). *J. Am. Chem. Soc.* **93**, 1513–1515
79. Hargrove, R.J. and Stang, P.J. (1976). *Tetrahedron* **32**, 37–41
80. Hanack, M., Bentz, H., Märkl, R. and Subramanian, L.R. (1978). *Ann. Chem.* 1894
81. Hanack, M., Carnahan, E.J., Krowczyniski, A., Schoberth, W., Subramanian, L.R. and Subramanian, K. (1979). *J. Am. Chem. Soc.* **101**, 100–108
82. Grunwald, E. and Winstein, S. (1948). *J. Am. Chem. Soc.* **70**, 846–858
83. Bentley, T.W. and Llewellyn, G. (1990). *Prog. Phys. Org. Chem.* **17**, 121–158
84. Kevill, D.N. and Anderson, S.W. (1991). *J. Org. Chem.* **56**, 1845–1850
85. Kevill, D.N. (1996). In *Advances in Quantitative Structure–Property Relationship*, Charton, M. (ed.), **vol. 1**, pp. 61–115. JAI Press, Greenwich, CT
86. Okuyama, T., Sato, K. and Ochiai, M. (1998). *Chem. Lett.* 1177–1178
87. Okuyama, T., Yamataka, H. and Ochiai, M. (1999). *Bull. Chem. Soc. Jpn* **72**, 2761–2769
88. Hinkle, R.J. and Thomas, D.B. (1997). *J. Org. Chem.* **72**, 7534–7535
89. Hinkle, R.J., McNeil, A.J., Thomas, Q.A. and Andrews, M.N. (1999). *J. Am. Chem. Soc.* **121**, 7437–7438
90. McNeil, A.J., Hinkle, R.J., Rouse, E.A., Thomas, Q.A. and Thomas, D.B. (2001). *J. Org. Chem.* **66**, 5556–5565
91. (a) Fujita, M., Sakanishi, Y. and Okuyama, T. (2000). *J. Am. Chem. Soc.* **122**, 8787–8788; (b) Fujita, M., Sakanishi, Y., Nishii, M., Yamataka, H. and Okumaya, T. (2002). *J. Org. Chem.* (in press)
92. (a) Fujita, M., Sakanishi, Y. and Okuyama, T. (2001). *J. Am. Chem. Soc.* **123**, 9190–9191; (b) Fujita, M., Sakanishi, Y., Nishii, M. and Okumaya, T. (2002). *J. Org. Chem.* (in press)
93. Hanack, M., Märkl, R. and Martinez, A.G. (1982). *Chem. Ber.* **115**, 772–782
94. Fujita, M., Yamamoto, A., Sugimura, T. and Okuyama, T. (2001). *Chem. Lett.* 806–807

95. Moloney, M.G., Pinhey, J.T. and Stoermer, M.J. (1990). *J. Chem. Soc. Perkin Trans. I* 2645–2655
96. Zollinger, H. (1994). *Diazo Chemistry. I. Aromatic Heteroaromatic Compounds*, pp. 162–177. VCH, Weinheim
97. Bott, K. (1983). In *The Chemistry of Functional Groups, Supplement C. The Chemistry of Triple-Bonded Functional Groups*, Patai, S. and Rappoport, Z. (eds), pp. 671–697. Wiley, Chichester
98. Szele, I., Tencer, M. and Zollinger, H. (1983). *Helv. Chim. Acta* **66**, 1704–1709
99. Lodder, G. (1997). In *Dicoordinated Carbocations*, Rappoport, Z. and Stang, P.J. (eds), pp. 377–431. Wiley, Chichester
100. Kropp, P.J., McNeely, S.A. and Davis, R.D. (1983). *J. Am. Chem. Soc.* **105**, 6907–6915
101. Suzuki, T., Kitamura, T., Sonoda, T., Kobayashi, S. and Taniguchi, H. (1981). *J. Org. Chem.* **46**, 5324–5328
102. Okuyama, T., Imamura, S. and Ishida, Y. (2001). *Bull. Chem. Soc. Jpn* **74**, 543–548
103. Gronheid, R., Lodder, G. and Okuyama, T. (2002). *J. Org. Chem.* **67**, 693–702

# The Interplay between Redox and Recognition Processes: Models and Devices

ULF DRECHSLER and VINCENT M. ROTELLO

*Department of Chemistry, University of Massachusetts, Amherst, Massachusetts, USA*

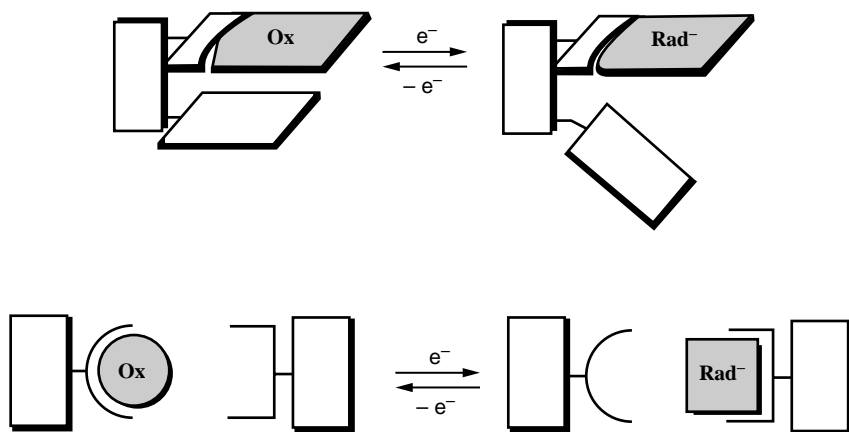
- 1 Introduction 315
- 2 Non-covalent interactions and redox potentials 316
- 3 Redox modulation through hydrogen bonding 323
- 4 Redox modulation through  $\pi$ -stacking and donor atom– $\pi$  interactions 326
- 5 Redox modulation and specific binding applied to the design of molecular devices 328
- 6 Conclusion and outlook 334
- References 335

## 1 Introduction

Understanding the fundamental principles controlling the interdependence of molecular recognition and redox processes is of crucial importance both in the context of biochemistry as well as in the field of materials science,<sup>1</sup> where biological systems can be used as models for pragmatic devices.<sup>2–5</sup> Potential applications include, among others, molecular shuttles,<sup>6</sup> switches,<sup>7</sup> wires,<sup>8</sup> logical gates,<sup>9</sup> and biosensors<sup>10</sup> (Fig. 1).

In biological systems, the interdependence between electron-transfer processes and specific non-covalent interactions is a common phenomenon. Enzymes containing redox-active cofactors, such as flavins,<sup>11</sup> quinones,<sup>12</sup> nicotinamides,<sup>13</sup> or pterins<sup>14</sup> use specific interactions between these small molecules and the enzyme to regulate the reactivity of the cofactor. Through hydrogen bonding, aromatic stacking, donor atom– $\pi$  interaction, and other electrostatic interactions, these systems selectively stabilize oxidation and protonation states by controlling the redox behavior of the cofactor. In addition, enzyme–cofactor interactions provide control over the molecular orbital distribution, and finally, the protein matrix plays a crucial role in both intra- and interprotein electron-transfer processes.<sup>15,16</sup> In consequence, redox enzymes can be seen as powerful molecular devices that utilize molecular recognition to control all aspects of electron-transfer processes.

In biological systems, the effects of the various electrostatic interactions are difficult to isolate and quantify individually, weak interactions may even go unnoticed. In order to acquire insight into these processes and to apply them to



**Fig. 1** Schematic illustration of redox-based recognition-mediated molecular switches discussed within this chapter.

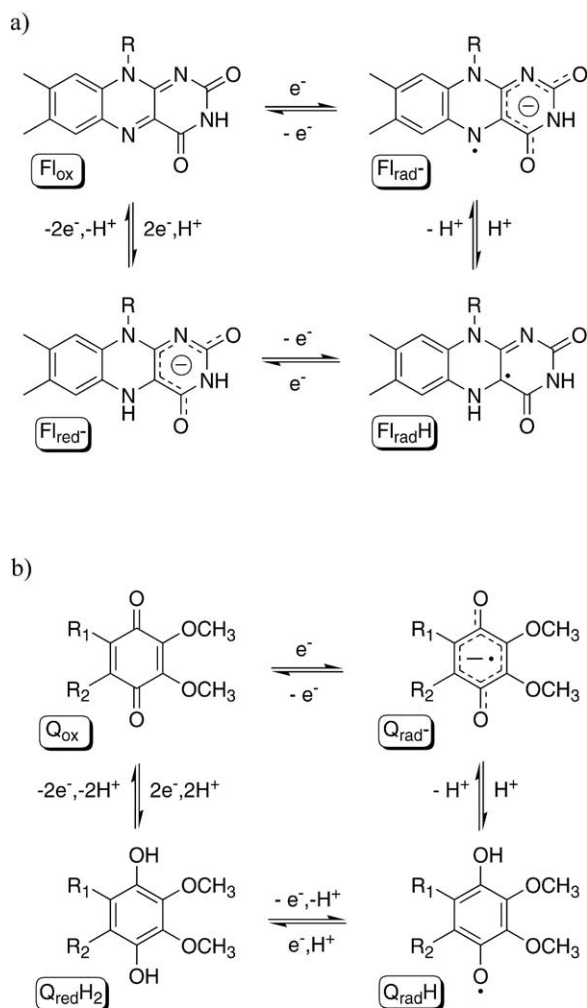
the design of practical devices, model systems utilizing individual effects have to be developed.

This chapter will discuss our investigations into the fundamental non-covalent enzyme–cofactor interactions controlling the redox behavior and physical properties of bio-organic cofactors, as well as studies on supramolecular model systems designed to decouple the effects of the different electrostatic and other interactions. Research towards the design and fabrication of molecular devices based on these same principles will be presented.

## 2 Non-covalent interactions and redox potentials

Redox-active cofactors are important species in biological systems, playing vital roles in redox and electron-transfer processes. Among the structurally and functionally diverse redox enzymes, flavoproteins containing the flavin cofactors flavin adenine dinucleotide (FAD) or flavin mononucleotide (FMN) are involved in many different biochemical processes serving as a highly versatile redox system.<sup>11,17–20</sup> These enzymes display considerable variations in their redox behavior using a single electrochemically active unit.<sup>21</sup> The oxidized flavin ( $\text{Fl}_{\text{ox}}$ ) can undergo either one- or two-electron reduction to a flavosemiquinone in an anionic ( $\text{Fl}_{\text{rad}^-}$ ) or neutral ( $\text{Fl}_{\text{rad}}\text{H}$ ) form, or the fully reduced flavohydroquinone anion ( $\text{Fl}_{\text{red}}\text{H}^-$ ), respectively (Fig. 2a). Similar one- or two-electron reductions are observed in quinone-based systems (Fig. 2b).

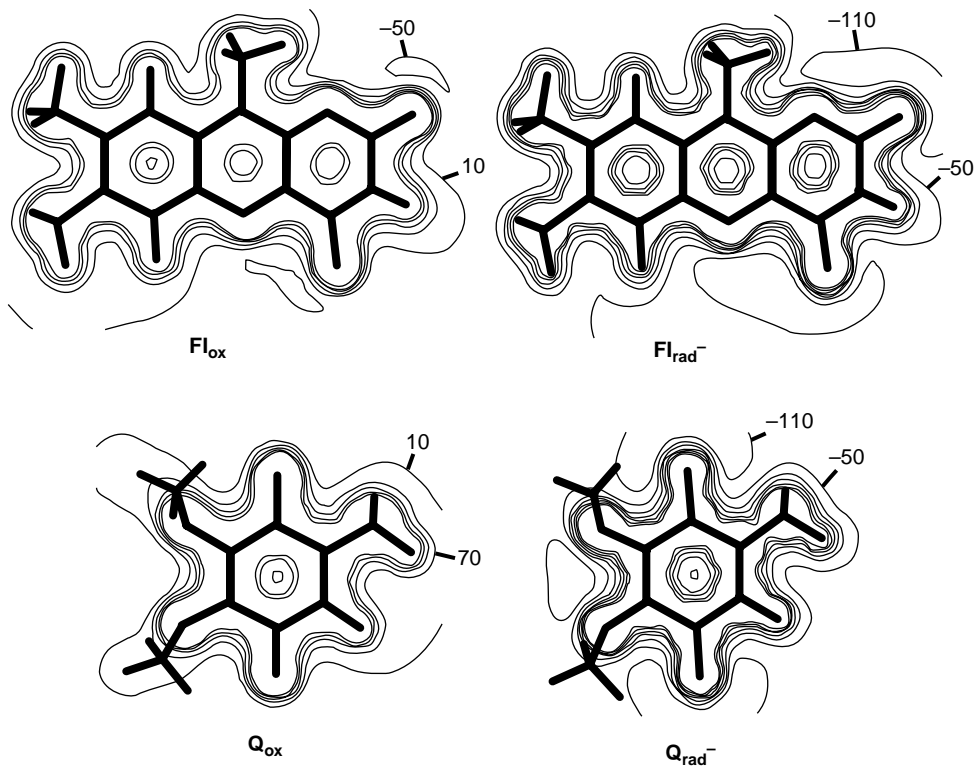
The one-electron reduction potential of flavin in flavoproteins varies over a wide (>500 mV) potential range, corresponding to a free energy difference of  $\Delta\Delta G > 10$  kcal/mol.<sup>17</sup> Since the redox-active isoalloxazine nucleus is the same in all systems, these extensive variations must arise from apoenzyme–cofactor non-



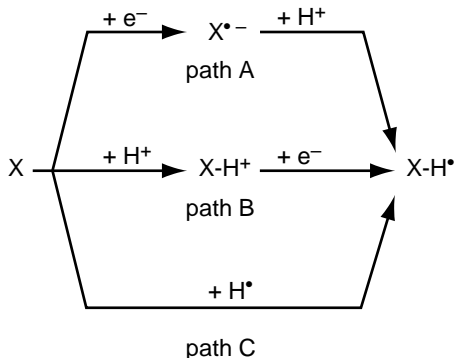
**Fig. 2** Common oxidation and protonation states of (a) flavin and (b) quinone cofactors.

covalent interactions. These interactions include charge attraction and repulsion, dipolar interactions such as hydrogen bonding, aromatic stacking, as well as less prominent donor atom- $\pi$  interactions. As will be demonstrated within this chapter, all these interactions modulate the redox potentials of the cofactor. Given the essentially electrostatic nature of recognition events,<sup>22,23</sup> they should be particularly sensitive to changes in the charge density distribution within the host-guest complex. Obviously, significant changes occur upon changing the oxidation state in redox-active molecules. Using well-established B3LYP-DFT calculations, which have been shown to reproduce experimentally available data accurately,<sup>24,25</sup> these





**Fig. 3** Electrostatic potential maps derived from B3LYP-DFT calculations for lumiflavin and ubiquinone in the respective oxidized ( $Fl_{ox}$  and  $Q_{ox}$ ) and radical anion forms ( $Fl_{rad^-}$  and  $Q_{rad^-}$ ). Contour lines are at 60 kcal/mol intervals.



**Scheme 1** Proton- and electron-transfer pathways.

changes can be visualized in electrostatic potential maps for both the oxidized and reduced forms. Figure 3 shows the electrostatic potentials for the flavin and ubiquinone systems. As can be seen from the calculations for flavin, the one-electron reduction substantially increases the negative potentials of the carbonyl oxygens O(2) and O(4): the O(2) potential rises from  $-45$  kcal/mol ( $Fl_{ox}$ ) to  $-116$  kcal/mol ( $Fl_{rad-}$ ) at the van der Waals radius, making these oxygens more basic, and thus stronger hydrogen bond acceptors.

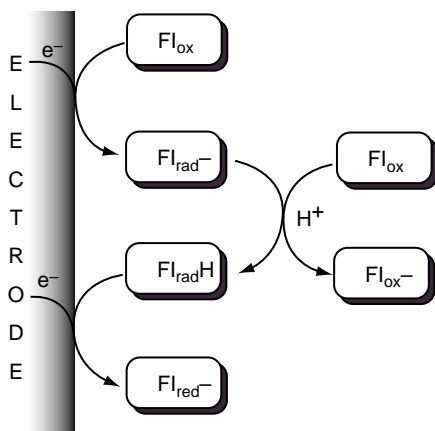
This reduction also converts the electron-deficient aromatic framework of  $Fl_{ox}$  into the highly electron-rich  $Fl_{rad-}$ . In the oxidized form the flavin nucleus, particularly the central ring, is capable of forming favorable  $\pi$ -stacking interactions with electron-rich aromatic systems, as well as interacting with electron-rich functional groups. The reduced  $Fl_{rad-}$  on the other hand, exhibits mostly negative electrostatic potentials over the entire framework, hence making interactions with neighboring electron-rich moieties highly unfavorable. The relationship between selective binding and redox potentials can be quantified by the equation

$$\frac{K_a(\text{red})}{K_a(\text{ox})} = e^{nF/RT(E_{1/2}(\text{bound}) - E_{1/2}(\text{unbound}))} \quad (1)$$

where  $K_a(\text{red})$  and  $K_a(\text{ox})$  are the respective association constants in the reduced and oxidized form, and  $E_{1/2}(\text{bound})$  and  $E_{1/2}(\text{unbound})$  the standard reduction potentials in the host-guest complex and the free ligand. According to this equation, increased binding in the reduced form ( $K_a(\text{red}) > K_a(\text{ox})$ ) inherently renders the reduction potential in the bound form more positive ( $E_{1/2}(\text{bound}) - E_{1/2}(\text{unbound}) > 1$ ).<sup>26</sup>

Another important feature in redox processes is electron transfer, including proton-coupled electron transfer, a prevalently observed phenomenon. These events follow three basic mechanisms (Scheme 1): proton transfer can occur after (path A), prior to (path B), or simultaneous with (path C) electron transfer.

The first mechanism is often found in the electrochemical reduction and oxidation of quinones and flavins in aprotic media.<sup>27</sup> Using cyclic voltammetry (CV) and simultaneous electrochemistry and electron paramagnetic resonance (SEEP),



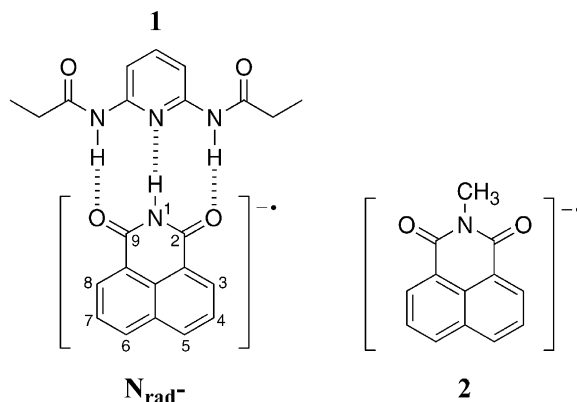
**Scheme 2** Schematic representation of the ECE pathway for the two-electron reduction of flavin in aprotic media.

studies on flavin in solvents of low dielectric constants, which effectively mimic the hydrophobic environment inside a protein, were carried out. These investigations have established that intermolecular transfer of the acidic imide proton of  $\text{Fl}_{\text{ox}}$  to an already reduced  $\text{Fl}_{\text{rad}^-}$  causes the cascade of reactions shown in [Scheme 2](#). Proton transfer occurs as the second step in an electrochemical/chemical/electrochemical (ECE) two-electron reduction to the fully reduced state. Since electron transfer is the initial step, proton transfer does not affect redox potentials or electron-transfer rates.

A similar ECE two-electron reduction was also observed for a ubiquinone–thiourea model system, where the complexing component not only serves as a proton source, but also enables specific recognition, which in turn provides direct control of the switching between one- and two-electron reactions. In these host–guest complexes, hydrogen bonding to the quinone allows direct two-electron reduction to occur via a facilitated proton transfer.<sup>28</sup> In this system, however, it appears to be difficult to determine whether proton transfer follows or precedes the second electron transfer. Preliminary studies suggest a pathway between a pre- or post-reduction proton transfer.

In contrast to protonation of the already reduced species, transfer of the proton prior to electron transfer causes significant changes in both the electron-transfer rates and the redox potentials. Simplified, the process can be seen as “acid-catalyzed” electron transfer.<sup>29</sup> Upon protonation of the redox-active unit, the reduction potential becomes substantially less negative, an effect analogous to hydrogen bonding. Although the conditions required for pre-protonation of the cofactor are highly acidic ( $\text{pH} < 0$ ), and therefore it would seem unlikely to occur in biological systems, there are systems where kinetic data indicate proton transfer occurs prior to or at least simultaneous with electron transfer.<sup>30</sup>

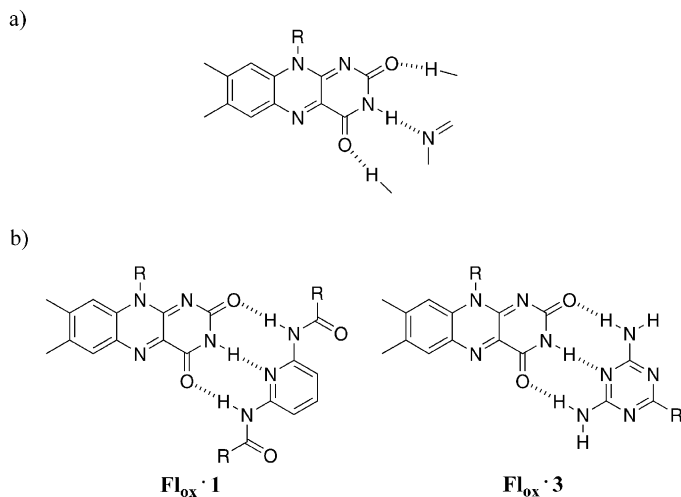
The third pathway (see [Scheme 1](#), path C), consisting of a directly coupled electron and proton transfer (i.e., formal hydrogen atom transfer), requires both



**Fig. 4** Hydrogen-bonded complex between naphthylimide radical anion ( $N_{\text{rad}}^-$ ) and a diacyl diaminopyridine receptor (**1**), and the negative control *N*-methyl naphthylimide (**2**), in which the methyl group blocks the binding site.

electron and proton tunneling.<sup>31</sup> While electron tunneling is an accepted and well-understood process, proton tunneling is far less common. However, proton tunneling can be readily understood considering the following: since the de Broglie wavelength of a proton possessing an energy of 2 kcal/mol is  $\sim 0.5$  Å, and the distance required to transfer a proton from a hydrogen bond donor to an acceptor is 0.7 Å, proton tunneling coupled to protein–cofactor motion is a reasonable possibility. As can be seen from these considerations, donor and acceptor must be in the close proximity provided by, e.g., hydrogen bonding, in order to enable efficient proton tunneling. This close spatial alignment is a natural feature in enzyme–cofactor complexes and has been replicated in hydrogen-bonding-based model systems.<sup>28</sup> In biomolecular systems, evidence for proton tunneling has been obtained from kinetic isotope effect experiments.<sup>32</sup> In a study on photoinduced electron transfer in metalloporphyrin model systems, it has been determined that the electron-transfer rate in a hydrogen-bound structure was twice that of a covalently linked analogue.<sup>33</sup>

Non-covalent interactions not only modulate the reduction potentials, but also have a significant effect on the orbital geometries of redox-active cofactors.<sup>34,35</sup> Changing the shape of the highest occupied molecular orbital (HOMO) will affect the oxidation behavior of a reduced species, while altering the geometry of the lowest unoccupied molecular orbital (LUMO) will have an impact on the reduction of an oxidized cofactor. While correlations between orbital geometries and redox behavior could provide further insight into redox processes, direct observations of the structures of HOMO and LUMO are not experimentally feasible. The singly occupied molecular orbital (SOMO) of a radical, on the other hand, can be monitored by EPR spectroscopy, where experimentally accessible hyperfine coupling constants (HFCs) are correlated to theoretical values. As a consequence,



**Fig. 5** (a) Acceptor–donor–acceptor three-point hydrogen bonding in flavin. (b) Hydrogen-bond complexes between oxidized flavin (Fl<sub>ox</sub>) and 2,6-diacyl diaminopyridine (**1**) and 2,6-diaminotriazine (**3**).

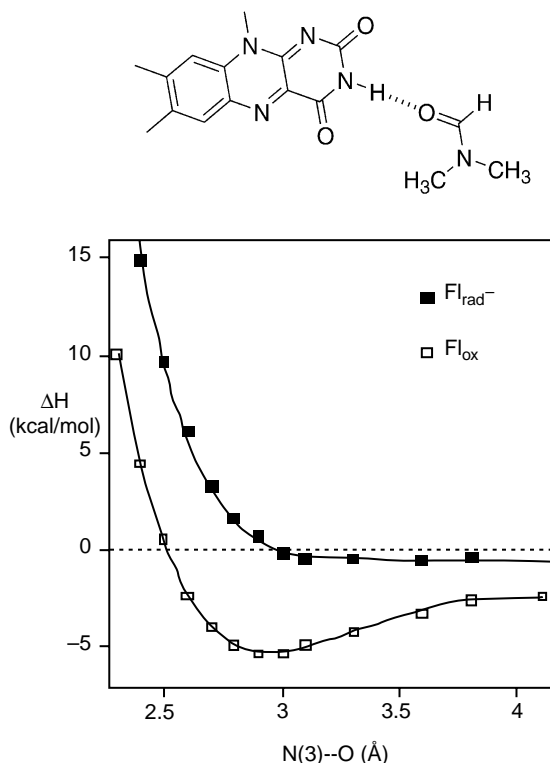
cofactors possessing stable radical forms are excellent tools for studying recognition-modulated effects on molecular orbitals.

In a recent study, the effects of hydrogen bonding on the spin density and thus the shape of the SOMO of a radical anion were examined.<sup>36</sup> The system studied consists of a complex between the naphthylimide radical anion (N<sub>rad</sub><sup>-</sup>) and a diacylated 2,6-diaminopyridine (**1** in Fig. 4). This system was chosen because of its resemblance to natural host–cofactor complexes and its relative structural simplicity, which provides readily interpretable EPR spectra and also allows application of complex computational methods. The SEEPR spectrum of N<sub>rad</sub><sup>-</sup> is significantly altered upon addition of receptor **1**. Control experiments with the non-binding *N*-methyl-N<sub>rad</sub><sup>-</sup> (**2**) confirmed that the change in the spectra is indeed a result of specific recognition. Spectrum simulation and curve fitting finally provided experimental HFCs.

Using UHF and DFT-B3LYP calculations, theoretical isotropic HFCs were calculated according to the equation

$$a(\text{N}) = \frac{8\pi}{3} g_e \beta_e g_N \beta_N \rho(r_N) \quad (2)$$

where the HFC of nucleus N,  $a(\text{N})$  is directly proportional to the corresponding Fermi contact integral (i.e., spin density) at the nucleus;  $g_e$  and  $g_N$  denote the respective electronic and nuclear  $g$ -factors, while  $\beta_e$  and  $\beta_N$  represent the Bohr and nuclear magneton, respectively. Theoretically obtained HFCs were in good overall quantitative agreement with the experimental results, and can therefore be used to predict properties not experimentally accessible, such as electrostatic potential, electron density, and spin-density distribution. According to the calculations,



**Fig. 6** Plot of the binding enthalpy for the flavin–DMF complex as a function of N(3)–O distance in the oxidized and radical anion form, based on B3LYP calculations.

complexation by the receptor shifts spin density away from the carbonyl oxygens involved in the recognition process, and towards carbons 3 and 8 within the naphthalene framework. Considering that hydrogen bonding is a two-electron process, lower, filled orbitals are distorted towards the binding site, which leads to an increase in charge density at the carbonyl oxygens. To maintain orthogonality between wavefunctions, the SOMO is distorted away from the binding site.

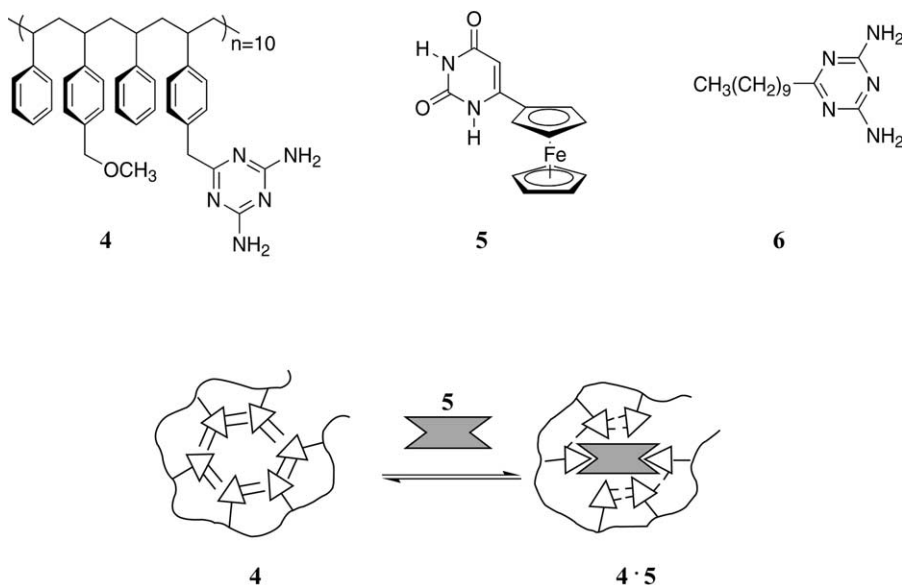
### 3 Redox modulation through hydrogen bonding

Since hydrogen bonding is a directed interaction,<sup>37</sup> a distinct array of hydrogen bond donor–acceptor functionalities provides greatly increased specificity to a recognition event. Single-, or even more efficiently, multiple-point hydrogen-bonding interactions can selectively stabilize or destabilize individual oxidation states, thereby modulating the redox potential between these states. An example for three-point hydrogen bonding between enzyme and cofactor can be seen in many flavoproteins, where the two carbonyl oxygens O(2) and O(4) serve as hydrogen

bond acceptors, and the imide N(3)–H function provides a donor site (Fig. 5a).<sup>38</sup> As pointed out in the previous section, reduction of the flavin cofactor to  $\text{Fl}_{\text{rad}^-}$  is expected to increase charge density on the carbonyl oxygens, making them stronger acceptors. Consequently, hydrogen bonding to O(2) and O(4) selectively stabilizes the  $\text{Fl}_{\text{rad}^-}$  oxidation state, thereby facilitating the reduction from  $\text{Fl}_{\text{ox}}$  to  $\text{Fl}_{\text{rad}^-}$ . To quantify this prediction, a number of studies have been carried out employing diaminopyridine model receptors mimicking the three-point hydrogen bonding. Using nuclear magnetic resonance (NMR) and CV measurements, it has been determined that complexation of flavin to diacyl diaminopyridine renders the reduction potential of  $\text{Fl}_{\text{ox}} \rightarrow \text{Fl}_{\text{rad}^-}$  155 mV (3.6 kcal/mol) less negative.<sup>39</sup>

Binding involving the imide N(3)–H function, however, is expected to show the opposite effect on the redox behavior. Reduction of  $\text{Fl}_{\text{ox}}$  to  $\text{Fl}_{\text{rad}^-}$  increases the charge density at this position, which in turn makes it a weaker donor compared to the oxidized form. Therefore, interactions at this position will make the reduction of  $\text{Fl}_{\text{ox}}$  to  $\text{Fl}_{\text{rad}^-}$  more unfavorable. In a recent study the role of N(3)–H has been investigated. Insight into recognition at this site was obtained through calculations on the lumiflavin–dimethylformamide (lumiflavin–DMF) complex providing a model for an isolated imide–carbonyl interaction. Based on B3LYP calculations, the binding enthalpy for  $\text{Fl}_{\text{ox}}$  and  $\text{Fl}_{\text{rad}^-}$  as a function of N(3)–O distance was examined. As can be seen in Fig. 6, the  $\text{Fl}_{\text{ox}}$ –DMF complex shows a behavior expected for a normal hydrogen bond: an optimal N(3)–O distance of 2.87 Å with a maximum binding energy of –5.3 kcal/mol. In contrast, no defined optimum was found for the  $\text{Fl}_{\text{rad}^-}$ –DMF interaction. In a series of experiments the redox potential of flavin in solvents with and without hydrogen-bond-accepting functionality were determined, demonstrating that hydrogen bonding at N(3)–H makes the reduction from  $\text{Fl}_{\text{ox}}$  to  $\text{Fl}_{\text{rad}^-}$  up to 80 mV (1.8 kcal/mol) more difficult. Through the separation of the N(3)–H interaction from the competing set of the two hydrogen-bond-accepting interactions, it is possible to make quantitative predictions on the effect of binding to the carbonyl oxygens: subtraction of the effect of N(3)–H from the potential shifts observed with the diacyl diaminopyridine receptor indicates that hydrogen bonding to O(2) and O(4) makes the reduction potential 227 mV (5.2 kcal/mol) less negative.<sup>40</sup>

Simplified, it can be deduced that each individual hydrogen bond donated to the redox-active unit contributes more than 100 mV to the facilitation of the reduction. In contrast, ligands that accept hydrogen bonds from the redox-active unit make the reduction substantially more difficult. Since the number of experimental studies available is very limited, this quantification is obviously quite preliminary. Changing the receptor from diacyl diaminopyridine (**1**) to a corresponding 2,6-diaminotriazine system (**3** in Fig. 5b) leads to a similar binding ( $K_{\text{a}}(\text{pyridine}) = 537 \text{ M}^{-1}$  versus  $K_{\text{a}}(\text{triazine}) = 480 \text{ M}^{-1}$ ), with the impact on the reduction potential, however, being much weaker ( $\Delta E_{1/2}(\text{pyridine}) = 155 \text{ mV}$  versus  $\Delta E_{1/2}(\text{triazine}) = 18 \text{ mV}$ ).<sup>41</sup> From these results, it becomes clear that the structure–function relationship in these systems is not yet fully understood, and careful parametric studies are required to shed more light on this aspect.

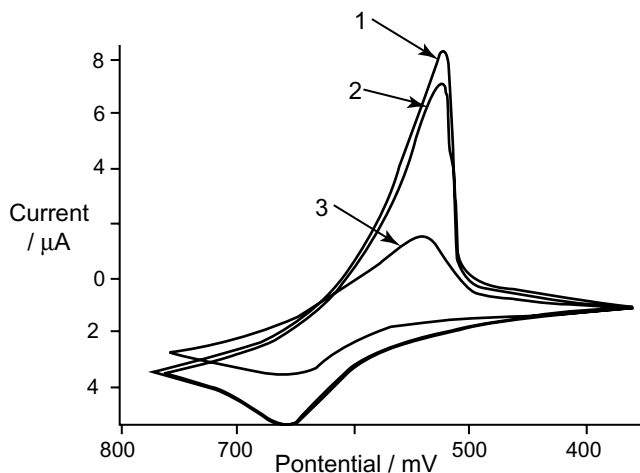


**Fig. 7** Structures of polymeric host (**4**), electroactive guest (**5**), and control receptor (**6**); and schematic representation of encapsulation of guest (**5**) by host (**4**).

With respect to the applicability of the hydrogen bonding–redox modulation interplay to functional devices, it is equally, if not more important to examine the inverse effect, i.e., the modulation of the specific binding induced by an oxidation/reduction event. In the previously discussed electrochemical studies on the flavin–diaminopyridine system, we observed that near-maximal shifts of the redox potentials occurred at receptor concentrations at which only 22% of the Fl<sub>ox</sub> would be bound. This indicates that binding to the receptor is dramatically increased upon reduction of Fl<sub>ox</sub> to Fl<sub>rad-</sub>. As already pointed out, this reduction leads to an increased hydrogen-bond-accepting ability of the carbonyl oxygens. The resulting recognition enhancement can be quantified using experimentally accessible thermodynamic variables to determine the free energy  $\Delta G$  and the association constant  $K_a$  for the binding of complex Fl<sub>rad-</sub>–receptor. Using these considerations, a 500-fold increase in binding ( $K_a(\text{red}) = 250,000 \text{ M}^{-1}$  versus  $K_a(\text{ox}) = 537 \text{ M}^{-1}$ )<sup>39</sup> was observed, corresponding to a free energy of  $\Delta G = -7.3$  versus  $-3.7 \text{ kcal/mol}$  in the oxidized form. This dramatic increase in binding makes the system particularly attractive as a potential molecular device, as will be discussed later in this chapter.

The above examples clearly demonstrate the profound effect of specific recognition on the redox potentials and vice versa. Specific recognition via hydrogen bonding can also be used to provide site-isolation of an electroactive center, preventing unwanted interactions between individual electroactive molecules. In a recent set of experiments, the effect of recognition-driven encapsulation



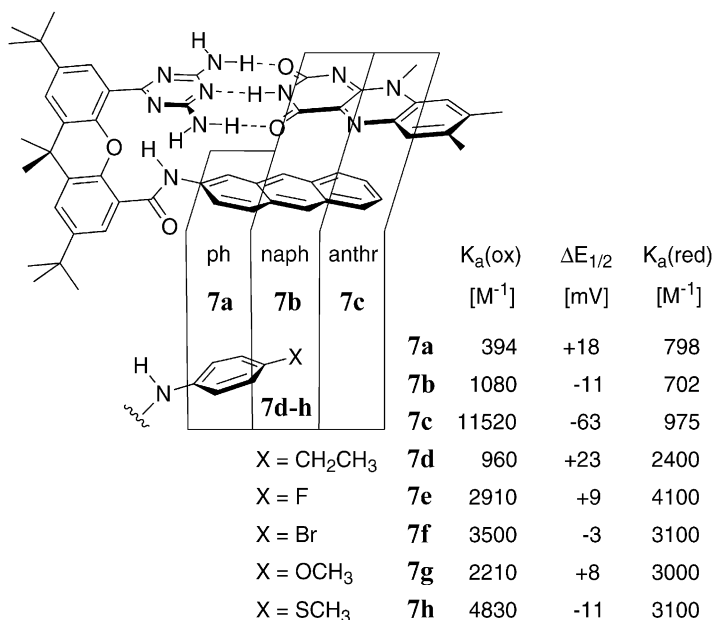


**Fig. 8** Cyclic voltammograms for guest (**5**) alone (trace 1), complex between **5** and control receptor (**6**) (trace 2), and complex between polymer (**4**) and **5** (trace 3).

of a redox-active guest (**5**) within a globular polymer (**4**) bearing complementary diaminotriazine functionalities was examined (Fig. 7).<sup>42</sup> Using NMR measurements, it was established that the flexible polymer “wraps around” an individual receptor molecule, thereby providing efficient encapsulation. This isolation has a significant effect on the redox behavior of the ferrocene, as can be seen from CV experiments (Fig. 8). The CV of a solution of **5** exhibits a sharp reduction wave that arises from precipitation of the oxidized ferrocenium species. Addition of the monomeric control receptor (**6**) had only a small effect on the electrochemical behavior (Fig. 8, trace 2), whereas addition of an equimolar amount of the polymer led to almost complete reversibility of the redox couple (Fig. 8, trace 3). These results clearly demonstrate that encapsulation of **5** within the polymeric host effectively prevents aggregation of the oxidized species.

#### 4 Redox modulation through $\pi$ -stacking and donor atom- $\pi$ interactions

In addition to hydrogen bonding, aromatic stacking<sup>43,44</sup> and interactions of the cofactor  $\pi$  system with electron-rich donor atoms such as oxygen<sup>45,46</sup> or sulfur<sup>38</sup> are among the fundamental forces in molecular recognition. In biological systems, it has been shown that interactions of the electron-deficient  $\pi$  systems of cofactors such as flavins or quinones with electron-rich sidechain residues and substrates have a considerable influence on the redox behavior of the cofactor.<sup>45</sup> In a study on the *Desulfovibrio vulgaris* flavodoxin, an electron-transfer protein,<sup>47,48</sup> selective mutations of aromatic residues near the flavin binding site were induced. It was



**Fig. 9** Molecular modeling structure (AMBER) of the flavin–host (**7**) complex and thermodynamic constants at 298 K.

found that the replacement of Tyr98 by Ala made the reduction potential of the  $\text{Fl}_{\text{rad}}\text{H}/\text{Fl}_{\text{red}}\text{H}^-$  couple (i.e., the second reduction) 140 mV less negative,<sup>49</sup> a range comparable to the effect of hydrogen bonding.

To determine directly the effects of interactions involving the  $\pi$  system on the redox behavior of flavin and related compounds, we developed a series of bidentate model receptors. These receptors contain a xanthene-based scaffold that provides for the arrangement of recognition elements in a well-defined geometry (Fig. 9). Using three-point hydrogen bonding, the diaminotriazine moiety at the top orients the flavin over the bottom aromatic surface. The phenyl receptor (**7a**) is expected to show no other interactions besides hydrogen bonding, and can therefore be used as a reference in order to isolate any other effects. In a first set of experiments,<sup>50</sup> the aromatic-stacking interactions between receptors **7a–c** and flavin were verified independently by fluorescence quenching and NMR titration studies. It was shown that with increasing  $\pi$ -overlap the fluorescence decreased progressively, to an almost complete quenching in the presence of the anthracene system (**7c**). Through NMR titration experiments, an enhanced association energy with receptors **7b** and **7c** relative to **7a** could be quantified. Due to the additional  $\pi$ - $\pi$  interaction in system  $\text{Fl}_{\text{ox}}-\text{7c}$  the association constant shows a 44-fold increase, corresponding to an increase in the free energy of 2.1 kcal/mol over the phenyl control system. Insight into the modulation of the redox potentials upon aromatic stacking was gained using CV experiments. While complexation of flavin with phenyl receptor **7a** resulted in

an 18 mV less negative reduction potential compared to the free flavin due to stabilization of  $\text{Fl}_{\text{rad}}^-$  by hydrogen bonding, increased aromatic-stacking interactions resulted in a shift to more negative values making the reduction more difficult. Using the phenyl receptor (**7a**) as a control, it was shown that the stacking interactions shift the reduction potential 81 mV more negative. This shift is indicative of unfavorable interactions between the electron-rich  $\text{Fl}_{\text{rad}}^-$  and the likewise electron-rich anthracene unit, resulting in a more-or-less prominent electrostatic repulsion.

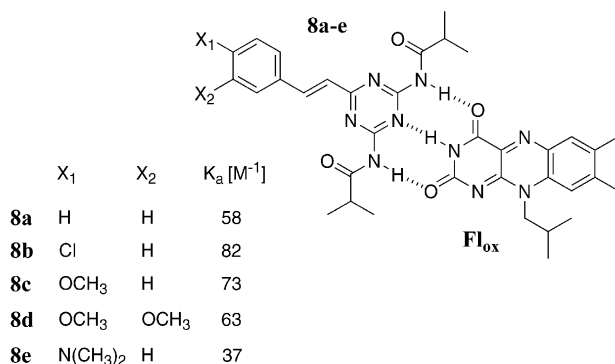
Due to its modular architecture, the same xanthene-based receptor type can be used to study the less obvious interactions between a  $\pi$ -electron-containing redox-active moiety and electron-rich groups or atoms in close proximity.<sup>51</sup> The rigid scaffold places donor atoms in direct contact with the electron-deficient region of the flavin nucleus, analogous to their flavoenzyme counterparts (Fig. 9). Again, parametric quantification of interactions can be achieved through reference to an electrostatically neutral control receptor. NMR titration and fluorescence quenching studies revealed up to fivefold increases in flavin binding upon incorporation of a donor atom, corresponding to a free energy change of  $-0.95$  kcal/mol relative to the control receptor (**7d**). In these studies, it has been observed that the increase of association can be correlated with the size and polarizability of the donor atom. However, it is not yet clear which of these factors, size or polarizability contributes more to the interaction.<sup>52</sup> As expected, CV experiments showed that donor atom- $\pi$  interactions shift the reduction potential to more negative values, indicating unfavorable interactions between two electron-rich systems upon reduction.<sup>51</sup>

In addition to these effects, other electrostatic interactions will affect the redox behavior of redox-active species. A study on flavodoxins for instance, has shown that anionic residues as far away as 13 Å have a measurable influence on the FMN cofactor.<sup>53</sup> A different study considering the influence of metal cations on the redox modulation established that  $\text{Ca}^{2+}$  binding to a pyrroloquinolinequinone (PQQ) cofactor made the reduction of the oxidized cofactor 570 mV (13 kcal/mol) less negative.<sup>54</sup>

## 5 Redox modulation and specific binding applied to the design of molecular devices

As pointed out in the previous sections, biological systems use the interplay of redox events and specific molecular recognition to regulate a wide variety of processes and transformations. We have also shown that the effects of hydrogen bonding, aromatic stacking and other electrostatic interactions on the redox potentials of electroactive molecules can be probed individually, opening the possibility of utilizing biochemical systems as prototypes for pragmatic molecular devices providing the ultimate goal in the miniaturization of mechanical systems.

One common requirement for the functioning and thus utilization of molecular devices is the ability to access them. Hence, the development of suitable interfaces

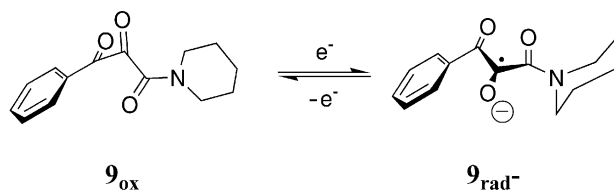


**Fig. 10** Structure of the flavin–receptor (**8**) complex and association constants at 298 K.

will be crucial. In recent studies, chemical and photochemical stimuli have been used to control the operation of a variety of devices.<sup>55–59</sup> Application of these devices, however, is complicated by the need to convert electronic input from a computer to either photonic or, even less feasible, chemical stimuli and vice versa. The use of electrochemical activation, on the other hand, provides an opportunity to greatly simplify the application of molecular devices.<sup>60</sup> Such systems allow direct interfacing to computer systems through the use of electronic input.<sup>61</sup> This simplicity makes redox-controlled systems very attractive candidates as the basis for molecular devices. The implementation of molecular recognition into the control of redox processes should enhance even further the viability of these systems.

Another equally important consideration is the communication of stimuli arising from molecular recognition events as well as the modification of molecular recognition over extended distances. This communication of information is central to the regulation of biological processes and the creation of functional devices. Based on a study of a series of diaminotriazine receptors for flavins which demonstrated that spatially remote substituents alter the hydrogen bond properties,<sup>41</sup> a more recent study extended this approach to even greater distances.<sup>62</sup> Using a family of chemosensors (**8a–e**) for flavins featuring extended conjugation (Fig. 10), the effects of variation of spatially remote (~11 Å away) substituents on the efficiency of the hydrogen-bonding-based recognition process were examined.

NMR titration experiments revealed that the strength of the receptor–flavin recognition is highly dependent upon the nature of the substituents present. Binding constants  $K_a$  varied from 37 M<sup>-1</sup> for the dimethylamino group to 82 M<sup>-1</sup> for the chloro substituent, resulting from alterations in the electrostatic potential and the polarizability of the hydrogen-bonding surface. Receptors carrying a donor substituent display a diminished acidity of the amide protons, and thus a weaker hydrogen-bonding capacity. Although this effect is in part compensated by an increased basicity of the triazine ring nitrogen, which would improve its hydrogen bond acceptor strength, the overall effect is a weakened recognition.



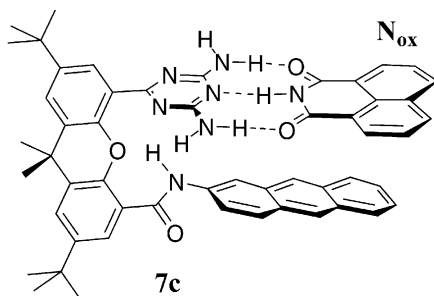
**Fig. 11** Reversible conformational rearrangement upon reduction of vicinal tricarbonyl (**9**).

Electron-accepting remote substituents cause the opposite effect and thus result in stronger binding.

To gain insight into the converse effect of binding events on the electronics of the receptor system, effects that are not experimentally accessible, a series of B3LYP-DFT calculations has been carried out. From these calculations, it can be seen that, upon binding, dramatic increases in electron density in the distal ring occur for the chloro receptor. This effect arises from an electron release in the amide protons upon binding. In strong contrast, for the dimethylamino-substituted receptor practically no change in the atomic charges upon binding to flavin is observed, an effect due to the electron-releasing nature of this group, which compensates for the changes in the electron-deficient triazine nucleus. From these results, it can be seen that information is communicated over a nanometer distance, a feature that makes these systems prototypes for molecular wires.<sup>8,63–65</sup> Another completely different approach to enable communication over extended distances is the utilization of molecular shuttles,<sup>55,57</sup> where a molecular probe “commutes” between two distinct locations.

A fundamental requirement for the creation of devices is the ability to switch between individual states; considerable interest has been devoted to the design and fabrication of organic-based systems possessing the potential to function as information storage or switching devices. Switching action can be provided, for example, by a conformational change in a molecule<sup>66</sup> or a considerable alteration of the binding behavior of a host–guest system upon external stimulation, as well as combinations of both. As shown in a recent study, vicinal tricarbonyls can undergo an electrochemically induced conformational switch.<sup>67</sup> SEEPR and CV experiments demonstrated that vicinal tricarbonyl (**9** in Fig. 11) can readily be reduced to the corresponding radical anion. This reduction was also shown to possess a very large peak potential difference ( $\Delta E_p \approx 400$  mV), a diagnostic of dramatic structural reorganization upon reduction.

To understand the nature of this reorganization, a series of B3LYP-DFT calculations was performed. Geometry optimization for  $\mathbf{9}_{\text{ox}}$  showed that the carbonyl groups are arranged in a helical fashion, due to electrostatic repulsion between the oxygen atoms. Upon reduction, however, the central O(2) carbonyl unit rearranges into an antiperiplanar position (Fig. 11). The calculations suggest that this particular conformation of  $\mathbf{9}_{\text{rad}^-}$  is stabilized by 20 kcal/mol over the helical conformation observed in  $\mathbf{9}_{\text{ox}}$ . This effect is due to an enhanced electron delocalization, as

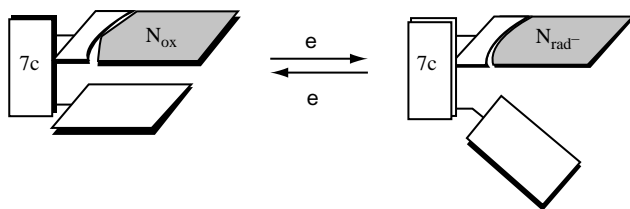


**Fig. 12** Structure of the naphthylimide–anthracyl receptor (**7c**) complex.

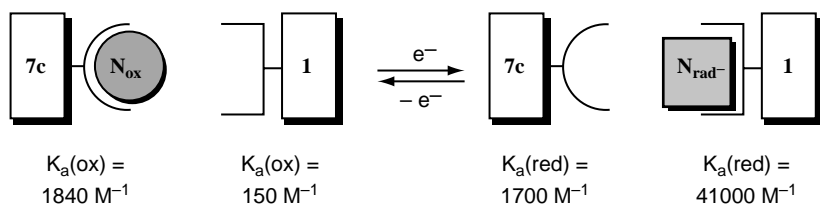
supported by the SEEPR spectrum, where greatly increased spin density in the phenyl ring is observed.

In the previous section, we have demonstrated that reduction of one component in a  $\pi$ -stacked system causes dramatic changes in the stacking behavior; two aromatic systems being attracted to each other in the oxidized form will repel each other upon reduction. This behavior can be utilized in the design of a conformational switch. In order to examine the feasibility of such a system, a series of experiments on a xanthene–naphthylimide system was carried out (Fig. 12).<sup>50</sup> Similar to the analogous flavin system, binding of the oxidized naphthylimide to the anthracene receptor (**7c**) was greatly increased relative to the phenyl control (**7a**), which proves a strong aromatic-stacking interaction.

SEEPR experiments were used to gain insight into the binding behavior of the reduced naphthylimide radical anion. Practically no change in the EPR spectra of both the anthracene and the phenyl system was observed, indicating a total lack of interaction between the anthracene moiety and  $N_{\text{rad}^-}$ . This behavior supports a structure for the complex with divergent aromatic surfaces; repulsion of the aromatic moieties causes a conformational change, where one aromatic system is “flipped away” (Fig. 13). Since reduction of the naphthylimide, on the other hand, enhances hydrogen bonding, the loss of aromatic-stacking interactions is in part compensated: the binding constant, as determined through NMR titrations, drops from  $1840 \text{ M}^{-1}$  in the oxidized form to  $1700 \text{ M}^{-1}$  upon reduction.

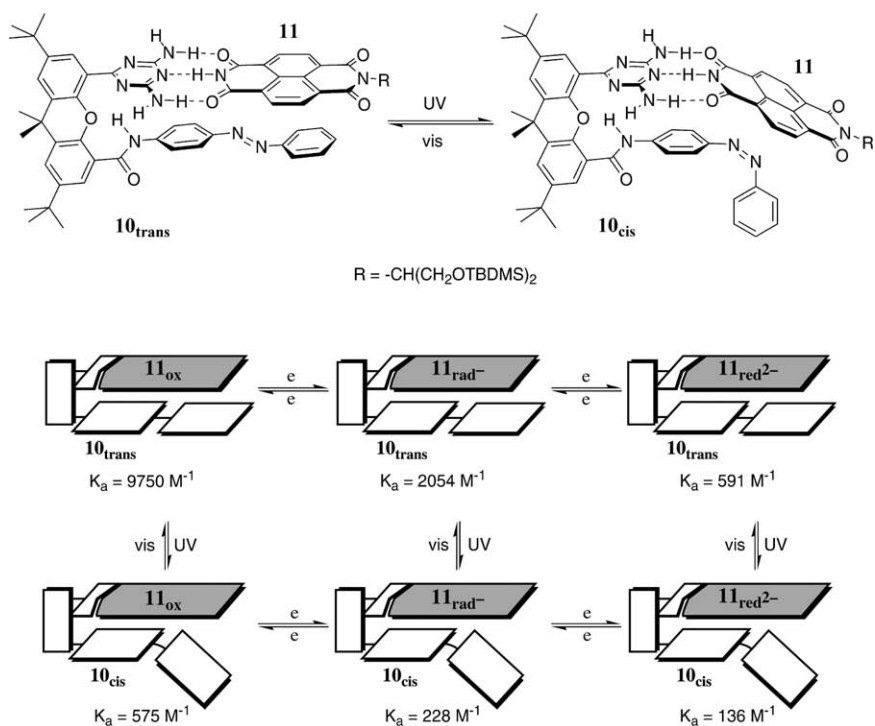


**Fig. 13** Schematic illustration of the redox-based conformational switching in the naphthylimide–**7c** complex.



**Fig. 14** Schematic representation of two-pole, three-component switching based on redox-modulated recognition.

In essence, it can be seen that hydrogen bonding and aromatic stacking show complementary modulation of the redox potentials, which in turn leads to redox-state-dependent molecular recognition. This selective recognition behavior can be employed to enhance the efficiency of a molecular switch, where the binding preference of a redox-active guest to each of the two competing hosts is regulated by the oxidation state of the guest. Using the bidentate receptor (**7c**) and a diacyl diaminopyridine (**1**), capable of only hydrogen binding, as the two hosts and naphthylimide as a redox-active guest, oxidation-state-mediated binding prefer-



**Fig. 15** Predicted structures (AMBER) of the azobenzene receptor (**10**)-naphthylimide (**11**) complexes and schematic illustration of redox ( $11_{\text{ox}}$ ,  $11_{\text{rad}^-}$ ,  $11_{\text{red}^{2-}}$ , left to right) and photochemical switching.

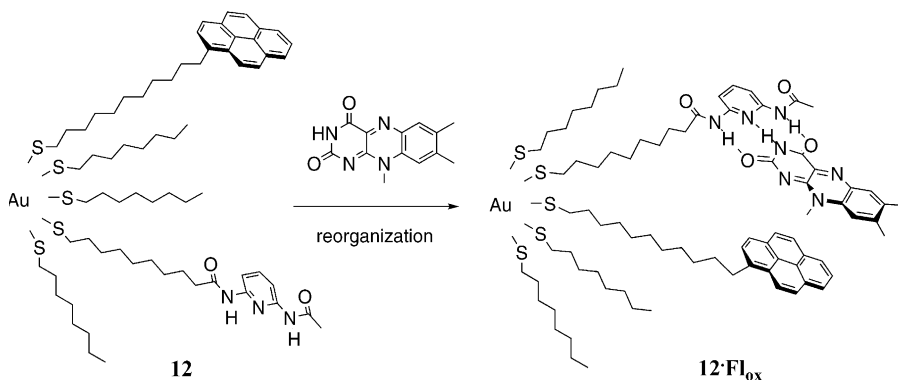
ences, and thus switching capabilities, were examined.<sup>68</sup> As already discussed, binding of the naphthylimide to the bidentate receptor (**7c**) decreases slightly upon reduction to  $N_{\text{rad}^-}$ . Binding of the naphthylimide to diaminopyridine, on the other hand, increases drastically upon reduction to  $N_{\text{rad}^-}$ . NMR titration experiments on a mixture of the hosts and the oxidized guest showed a clear preference of the guest for **7c**, due to favorable aromatic stacking. The opposite binding preference in the radical anion state has been demonstrated using SEEPR experiments. Using experimentally obtained association constants and  $E_{1/2}$  values, these preferences can be quantified. From thermodynamic considerations, it is shown that  $N_{\text{ox}}$  has a preference of 1.5 kcal/mol for the  $\pi$ -stacking receptor, whereas  $N_{\text{rad}^-}$  binds 1.9 kcal/mol more strongly to the hydrogen-bonding receptor (Fig. 14). This change in binding preference caused by a change of the oxidation state makes the system an efficient three-component, two-pole molecular switch.

As seen from the previous examples, molecular switches generally rely on two-state (off–on) switching. One way to further enhance the versatility of such devices is to incorporate multi-state switching. A recent study, for instance, used TTF in its three stable oxidation states to achieve three-pole switching.<sup>69</sup> Diversity of function can be even further increased through a set of orthogonal input stimuli.<sup>70,71</sup> In a recent study, a system capable of processing orthogonal inputs has been developed.<sup>72</sup> As shown in Fig. 15, a host–guest complex in which the host (**10**) possesses two discrete states that can be switched photochemically (*trans*–*cis*), together with a guest (**11**) featuring three stable oxidation states (ox,  $\text{rad}^-$ ,  $\text{red}^{2-}$ )<sup>73</sup> provides six possible discrete states.

Again, the system utilizes the complementarity of hydrogen bonding and aromatic-stacking effects. Initial studies using UV–Vis and NMR spectroscopy demonstrated the rapid and efficient reversible photoisomerization as well as an overall enhanced binding of the guest in the *trans* form, due to aromatic-stacking interactions. Stepwise reduction of the guest, on the other hand, resulted in a gradual decrease of binding strength, due to unfavorable electrostatic interactions between the electron-rich azobenzene moiety and the increasingly charged guest. Using electrochemically determined changes in free energy, the association constants of the receptor in both the *trans*- and *cis*-forms with the guest in all three oxidation states could be quantified. As can be seen in Fig. 15, the six possible binding states possess five distinct affinities, since the  $10_{\text{cis}} \cdot 11_{\text{ox}}$  and  $10_{\text{trans}} \cdot 11_{\text{red}^{2-}}$  complexes exhibit virtually identical binding constants. These five affinities are almost equally spaced exponentially over a 70-fold range, a feature extremely useful to fine-tune recognition properties.

So far, we have shown that redox-modulated recognition, a prevalent feature in biological systems, can be employed in the design of functional devices. As mentioned earlier, one challenge to the efficient application of such systems is the ability to immobilize, order and thus individually address them. One way to provide the desired anisotropy is through the use of colloids functionalized with self-assembled monolayers (SAMs).<sup>74,75</sup> In a recent model study, a diacyl diaminopyridine-functionalized gold colloid (DAP-Au), capable of binding flavin, has been





**Fig. 16** Self-assembly of the hydrogen bonding–aromatic stacking binding site on a colloid (**12**).

prepared.<sup>76</sup> Using NMR titration experiments, the association constant for the DAP-Au·Fl<sub>ox</sub> complex was found to be  $196 \text{ M}^{-1}$ , consistent with previously observed values ( $K_a = 193 - 537 \text{ M}^{-1}$ ). CV measurements showed a 81 mV (1.85 kcal/mol) stabilization of the bound Fl<sub>rad</sub><sup>-</sup>. Using equation (1), it has been established that the binding of flavin increases by greater than 20-fold upon reduction of Fl<sub>ox</sub> to Fl<sub>rad</sub><sup>-</sup>. An additional feature of these SAM-functionalized colloids, the mobility of thiols on the SAM surface,<sup>77</sup> led to an extension of this approach to create multivalent receptors providing templated guest recognition.<sup>78</sup> To provide a suitable system, thiol-functionalized diacyl diaminopyridine moieties were place-exchanged onto a colloid functionalized with pyrene units capable of aromatic stacking, to provide the bifunctional colloid (**12**). NMR titration experiments demonstrated the expected enhanced binding of this system to Fl<sub>ox</sub> due to a multivalent interaction. An association constant of  $K_a = 323 \text{ M}^{-1}$  was obtained, nearly twice that observed for the DAP-Au·Fl<sub>ox</sub> system, where only hydrogen bonding can occur.

To explore the use of colloid–flavin binding to self-assemble pre-organized binding sites on the nanoparticle surface, a trifunctional system with dilute hydrogen bonding and aromatic-stacking elements has been employed (Fig. 16). The templation of colloid binding sites was demonstrated by time-course NMR experiments. Enhanced binding over the course of 70 h was observed by monitoring the gradual downfield shift of the flavin N(3)–H proton. The association constant calculated from this shift increased from 168 to  $235 \text{ M}^{-1}$ , demonstrating the capability of this colloid–SAM system to reorganize to an imprinted system through the use of binding enthalpy.

## 6 Conclusion and outlook

The interplay between redox and recognition events is of crucial importance in biochemical regulation processes. Specific recognition controls various aspects of

the redox process such as redox potentials, electron-transfer pathways, protonation states, and orbital geometries. Series of parametric studies using synthetic model receptors have provided considerable insight into the nature of these regulation processes, probing the individual effects of hydrogen bonding, aromatic stacking, donor atom- $\pi$  and other interactions on the redox properties of electroactive cofactors.

The results obtained from our model studies were found to correlate with effects observed in naturally occurring enzymes, and are furthermore directly applicable to the creation of redox-based pragmatic molecular devices. However, many aspects remain to be explored in both biomolecular and synthetic model systems; one particular challenge will be the understanding of how the individual processes are linked together in biological systems. This understanding will ultimately provide a comprehensive model for the design of highly complex pragmatic devices on the molecular level.

## References

1. Kaifer, A.E. (1999). *Acc. Chem. Res.* **32**, 62–71
2. Roque, A., Pina, F., Alves, S., Ballardini, R., Maestri, M. and Balzani, V. (1999). *J. Mater. Chem.* **9**, 2265–2269
3. Diederich, F., Echegoyen, L., Gomez-Lopez, M., Kessinger, R. and Stoddart, J.F. (1999). *J. Chem. Soc., Perkin Trans. 2* 1577–1586
4. Mattei, P. and Diederich, F. (1997). *Helv. Chim. Acta* **80**, 1555–1588
5. Lehn, J.-M. (1995). *Supramolecular Chemistry: Concepts and Perspectives*. VCH, Weinheim
6. Anelli, P.L., Spencer, N. and Stoddart, J.F. (1991). *J. Am. Chem. Soc.* **113**, 5131–5133
7. Otsuki, J., Tsujino, M., Iizaki, T., Araki, K., Seno, M., Takatera, K. and Watanabe, T. (1997). *J. Am. Chem. Soc.* **119**, 7895–7896
8. Zhou, Q. and Swager, T.M. (1995). *J. Am. Chem. Soc.* **117**, 12593–12602
9. De Silva, A.P., Gunaratne, H.Q.N. and McCoy, C.P. (1997). *J. Am. Chem. Soc.* **119**, 7891–7892
10. Crooks, R.M. and Ricco, A. (1998). *J. Acc. Chem. Res.* **31**, 219–227
11. Ghisla, S. and Massey, V. (1989). *Eur. J. Biochem.* **181**, 1–17
12. Anthony, C. (1996). *Biochem. J.* **320**, 697–711
13. Popov, V. and Lamzin, V.S. (1994). *Biochem. J.* **301**, 625–643
14. Blakley, R.L. and Benkovic, S.J. (1985). *Chemistry and Biochemistry of Pterins*. Wiley, New York
15. Sharp, R.E., Chapman, S.K. and Reid, G.A. (1996). *Biochemistry* **35**, 891–899
16. Tollin, G., Hurley, J., Hazzard, J. and Meyer, T. (1993). *Biophys. Chem.* **48**, 259–279
17. For a comprehensive review, see Mueller, F. (ed.) (1990). *Chemistry and Biochemistry of Flavoenzymes*, vols. 1–3. CRC Press, Boca Raton
18. Yano, Y. (2000). *Rev. Heteroatom Chem.* **22**, 151–179
19. Hasford, J.J., Kemnitzer, W. and Rizzo, C.J. (1997). *J. Org. Chem.* **62**, 5244–5245
20. Li, W.S. and Sayre, L.M. (2001). *Tetrahedron* **57**, 4523–4536
21. Mueller, F. (1983). In *Topics in Current Chemistry*, Boschke, F.L. (ed.), vol. 108, pp. 71–108. Springer, Berlin
22. Klarner, F.G., Burkert, U., Kamieth, M., Boese, R. and Benet-Buchholz, J. (1999). *Chem. Eur. J.* **5**, 1700–1707

23. Mecozzi, S., West, A.P. and Dougherty, D.A. (1996). *Proc. Natl Acad. Sci., USA* **93**, 10566–10571
24. Lozynski, M., Rusinska-Roszak, D. and Mack, H.-G. (1998). *J. Phys. Chem. A* **102**(17), 2899–2903
25. Alem, K.V., Sudholter, E.J.R. and Zuilhof, H. (1998). *J. Phys. Chem. A* **102**(52), 10860–10868
26. Niemz, A. and Rotello, V.M. (1999). *Acc. Chem. Res.* **32**, 44–52
27. Niemz, A., Imbriglio, J. and Rotello, V.M. (1997). *J. Am. Chem. Soc.* **119**, 887–892
28. Greaves, M.D., Niemz, A. and Rotello, V.M. (1999). *J. Am. Chem. Soc.* **121**, 266–267
29. Fukuzumi, S. (1997). *Bull. Chem. Soc. Jpn* **70**, 1–28
30. Graige, M.S., Paddock, M.L., Bruce, J.M., Feher, G. and Okamura, M.Y. (1996). *J. Am. Chem. Soc.* **118**, 9005–9016
31. Cukier, R. and Nocera, D. (1999). *Annu. Rev. Phys. Chem.* **49**, 337–369
32. Kohen, A. and Klinman, J. (1998). *Acc. Chem. Res.* **31**, 397–404
33. de Rege, P.J., Williams, S. and Therien, M. (1995). *Science* **269**, 1409–1413
34. Takahashi, M., Matsuo, M. and Udagawa, Y. (1999). *Chem. Phys. Lett.* **308**, 195–198
35. Turi, L. (1999). *Chem. Phys.* **110**, 10364–10369
36. Niemz, A. and Rotello, V.M. (1997). *J. Am. Chem. Soc.* **119**, 6833–6836
37. Scheiner, S. (1997). *Hydrogen Bonding*. Oxford University Press, Oxford
38. Mattevi, A., Obmolova, G., Kalk, K.H., van den Berkel, W.J.H. and Hol, W.G.J. (1993). *J. Mol. Biol.* **230**, 1200–1215
39. Breinlinger, E., Niemz, A. and Rotello, V.M. (1995). *J. Am. Chem. Soc.* **117**, 5379–5380
40. Cuello, A.O., McIntosh, C.M. and Rotello, V.M. (2000). *J. Am. Chem. Soc.* **122**, 3517–3521
41. Deans, R., Cooke, G. and Rotello, V.M. (1997). *J. Org. Chem.* **62**, 836–839
42. Galow, T.H., Ilhan, F., Cooke, G. and Rotello, V.M. (2000). *J. Am. Chem. Soc.* **122**, 3595–3598
43. Hunter, C.A. (1994). *Chem. Soc. Rev.* **23**(2), 101–109
44. Chen, Y., Kampf, J.W. and Lawton, R.G. (1997). *Tetrahedron Lett.* **38**, 5781–5784
45. Watt, W., Tulinski, A., Swenson, R. and Wattenpugh, K. (1991). *J. Mol. Biol.* **218**, 195–208
46. Fukuyama, K., Matsubara, H. and Rogers, L.J. (1992). *J. Mol. Biol.* **225**, 775–789
47. Swenson, R.P., Krey, G.D. and Eren, M. (1987). In *Flavins and Flavoproteins*, Edmondson, D. and McKormick, D. (eds), pp. 98–107. de Gruyter, Berlin
48. Zhou, Z. and Swenson, R.P. (1996). *Biochemistry* **35**, 15980–15988
49. Swenson, R.P. and Krey, G.D. (1994). *Biochemistry* **33**, 8505–8514
50. Breinlinger, E. and Rotello, V.M. (1997). *J. Am. Chem. Soc.* **119**, 1165–1166
51. Breinlinger, E., Keenan, C. and Rotello, V.M. (1998). *J. Am. Chem. Soc.* **120**, 8606–8609
52. Rotello, V.M. (1998). *Heteroatom Chem.* 605–606
53. Zhou, Z. and Swenson, R.P. (1996). *Biochemistry* **35**, 12443–12454
54. Itoh, S., Kawakami, H. and Fukuzumi, S. (1998). *J. Am. Chem. Soc.* **120**, 7271–7277
55. Bisell, R.A., Cordova, E., Kaifer, A.E. and Stoddart, J.F. (1994). *Nature* **369**, 133–137
56. Schoevaars, A.M., Kruizinga, W., Zijlstra, R.W.J., Veldman, N., Spek, A.L. and Feringa, B.L. (1997). *J. Org. Chem.* **62**, 4943–4948
57. Balzani, V., Credi, A., Langford, S.J., Raymo, F.M., Stoddart, J.F. and Venturi, M. (2000). *J. Am. Chem. Soc.* **122**, 3542–3543
58. Gobbi, L., Seiler, P. and Diederich, F. (1999). *Angew. Chem., Int. Ed. Engl.* **38**, 674–678
59. Kern, J.M., Raehm, L., Sauvage, J.-P., Divisia-Blohorn, B. and Vidal, P.L. (2000). *Inorg. Chem.* **39**, 1555–1560
60. Abel, E., Castro, R., McRobbie, I.M., Barbour, L., Atwood, J.L., Kaifer, A.E. and Gokel, G.W. (1998). *Supramol. Chem.* **9**, 199–202

61. Collier, C.P., Wong, E.W., Belohradski, M., Raymo, F.M., Stoddart, J.F., Kuekes, P.J., Williams, R.S. and Heath, J.R. (1999). *Science* **285**, 391–394
62. Deans, R., Cuello, A.O., Galow, T.H., Ober, M. and Rotello, V.M. (2000). *J. Chem. Soc., Perkin Trans. 2* 1309–1313
63. Swager, T.M. (1998). *Acc. Chem. Res.* **31**, 201–207
64. Jestin, I., Frere, P., Blanchard, P. and Roncali, J. (1998). *Angew. Chem., Int. Ed. Engl.* **37**, 942–945
65. Bumm, L.A., Arnold, J.J., Cygan, M.T., Dunbar, T.D., Burgin, T.P., Jones, L., Allara, D.L., Tour, J.M. and Weiss, P.S. (1996). *Science* **271**, 1705–1707
66. Monahan, C., Bien, J.T. and Smith, B.D. (1998). *J. Chem. Soc., Chem. Commun.* 431–432
67. Galow, T.H., Cuello, A.O. and Rotello, V.M. (2000). *Tetrahedron Lett.* **41**, 9489–9492
68. Deans, R., Niemz, A., Breinlinger, E. and Rotello, V.M. (1997). *J. Am. Chem. Soc.* **119**, 10863–10864
69. Ashton, P.R., Balzani, V., Becher, J., Credi, A., Fyfe, M.C.T., Mattersteig, G., Menzer, S., Nielsen, M.B., Raymo, F.M., Stoddart, J.F., Venturi, M. and Williams, D.J. (1999). *J. Am. Chem. Soc.* **121**, 3951–3957
70. Doron, A., Katz, E., Tao, G.L. and Willner, I. (1997). *Langmuir* **13**, 1783–1790
71. Gilat, S.L., Kawai, S.H. and Lehn, J.-M. (1995). *Chem. Eur. J.* **1**, 275–284
72. Goodman, A., Breinlinger, E., Ober, M. and Rotello, V.M. (2001). *J. Am. Chem. Soc.* **123**, 6213–6214
73. Osuka, A., Yoneshima, R., Shiratori, H., Okada, T., Taniguchi, S. and Mataga, N. (1998). *J. Chem. Soc., Chem. Commun.* 1567–1568
74. Andres, R.P., Bein, T., Dorigi, M., Feng, S., Henderson, J.I., Kubiak, C.P., Mahoney, W., Osifchin, R.G. and Reifengerger, R. (1996). *Science* **272**, 1323–1325
75. Liu, J., Xu, R. and Kaifer, A.E. (1998). *Langmuir* **14**, 7337–7339
76. Boal, A.K. and Rotello, V.M. (1999). *J. Am. Chem. Soc.* **121**, 4914–4915
77. Badia, A., Cuccia, L., Demers, L., Morin, F. and Lennox, R.B. (1997). *J. Am. Chem. Soc.* **117**, 2682–2692
78. Boal, A.K. and Rotello, V.M. (2000). *J. Am. Chem. Soc.* **122**, 734–735

# The Physical Organic Chemistry of Fischer Carbene Complexes

CLAUDE F. BERNASCONI

*Department of Chemistry and Biochemistry, University of California, Santa Cruz, California, USA*

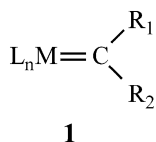
- 1 Introduction 137
  - What are Fischer carbene complexes? 137
  - Scope of this chapter 142
- 2 Reactions at the metal 143
  - Thermolysis 144
  - Substitution of CO by phosphines 145
  - The Dötz reaction 149
  - Rearrangement reactions with loss of CO 151
  - Photochemical reactions 153
- 3 Reactions at the carbene carbon 158
  - General features 158
  - Amine nucleophiles 159
  - Phospine and phosphite nucleophiles 167
  - Alcohols and alkoxide ion nucleophiles 171
  - Thiol and thiolate ion nucleophiles 179
  - Intramolecular nucleophilic reactions 191
  - Hydroxide ion and water as nucleophiles 194
  - Insertion reactions initiated by nucleophilic attack 201
- 4 Acid–base reactions at the  $\alpha$ -carbon 207
  - General features and methods 207
  - Kinetic and thermodynamic acidities 209
  - Effect of structure on  $pK_a$  values 210
  - Intrinsic rate constants for proton transfer 219
  - Thermodynamic acidities in organic solvents 223
  - Hydrolysis of ionizable carbene complexes 228
- Acknowledgments 232
- References 233

## 1 Introduction

### WHAT ARE FISCHER CARBENE COMPLEXES?

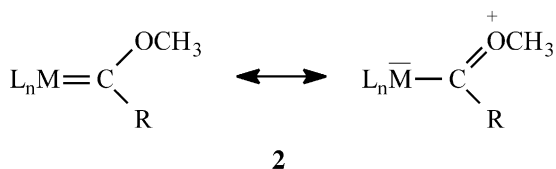
Fischer carbene complexes belong to a class of compounds commonly referred to as transition metal carbene complexes. The 1983 book by Dötz *et al.*<sup>1</sup> provides an excellent introduction to many of the most important general aspects of these

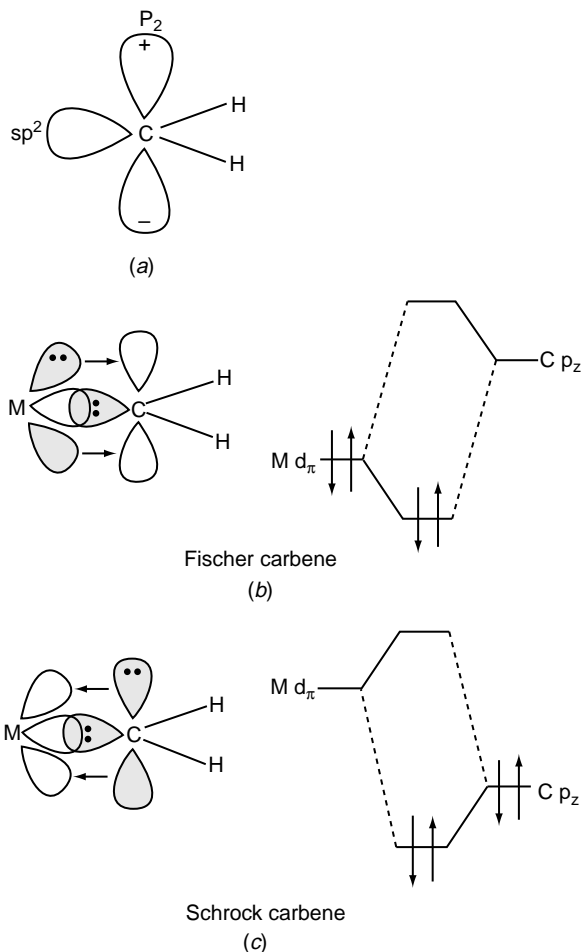
complexes. A common feature of transition metal carbene complexes is that they contain a formal carbon-to-metal double bond as schematically represented below:



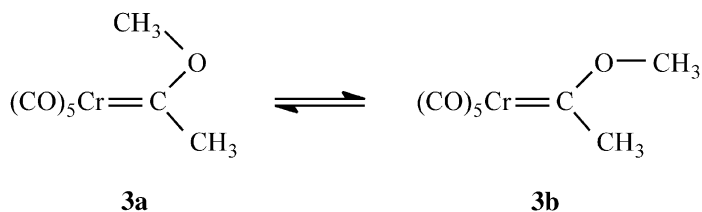
The electronic structure of these complexes can be visualized as arising from a coupling of the carbene fragment,  $\text{CR}_1\text{R}_2$ , to the metal fragment,  $\text{L}_n\text{M}$ , in the following way.<sup>2-4</sup> The carbon of the carbene fragment is  $\text{sp}^2$  hybridized. The two electrons that are not involved in the C–R bonds are assumed to be in the lower-lying  $\text{sp}^2$  orbital, leaving the p orbital unoccupied (Fig. 1a). Depending on the identity and the oxidation state of the metal, the ligands and the R-groups attached to the carbene carbon, two kinds of bonding situations arise. One leads to Fischer-type complexes, the other to Schrock-type complexes.

The Fischer carbene complexes are characterized by late-transition metals of low oxidation state, e.g., Cr(0), W(0), Fe(0), Re(0), etc.; they have  $\pi$ -acceptor ligands such as CO or NO at the metal and at least one  $\pi$ -donor group such as OMe, SMe, or  $\text{NMe}_2$ , etc. at the carbene carbon. The bonding situation is shown in Fig. 1b. The  $\sigma$ -bond is formed by donation of the lone pair on the carbene fragment to the metal. The  $\pi$ -bond may be understood as the result of back donation from a metal  $d_\pi$  orbital to the carbon p orbital. Because the energy level of the metal  $d_\pi$  orbital is lower than that of the carbene p orbital, the  $\pi$ -electrons remain largely on the metal fragment (Fig. 1b). As a consequence, the carbene carbon becomes highly electron deficient; this explains the requirement for a  $\pi$ -donor group that can partially compensate for this electron deficiency, as shown in **2** for a methoxy carbene complex. That the zwitterionic structure contributes extensively to the resonance hybrid is evidenced by the fact that, at low temperature, the complex **3** shows two separate  $^1\text{H}$  NMR signals for the methoxy protons.<sup>1,5</sup>





**Fig. 1** The relative energies of the  $\text{M}(d_{\pi})$  and the  $\text{C}(p_z)$  orbitals control the electrophilic or nucleophilic character of the carbene. (a) The orbitals of free  $\text{CH}_2$ . (b) If the  $\text{M}(d_{\pi})$  levels are lower in energy, a Fischer carbene will result. (c) If the  $\text{M}(d_{\pi})$  levels are higher in energy, a Schrock carbene will result. Shading represents occupied orbitals. (Figure taken from Crabtree, Ref. 4, by permission from Wiley & Sons.)



This situation is due to the relatively high barrier to rotation of the C–O bond, making the interconversion between the two isomers (**3a** and **3b**) slow on the NMR time scale. Additional evidence for the  $\pi$ -donor effect of alkoxy as well as other groups (mainly alkyl amino) comes from  $^{53}\text{Cr}$  NMR studies<sup>6</sup> and theoretical calculations.<sup>7</sup> Nevertheless, the carbene carbon remains electrophilic, a central feature of Fischer carbenes.

Schrock carbene complexes are characterized by early transition metals of higher oxidation state, e.g., Ta(V), W(VI); they have non- $\pi$ -acceptor ligands such as alkyl,  $\eta\text{-C}_5\text{H}_5$ , Cl, etc. and mainly alkyl groups or hydrogen but no  $\pi$ -donors attached to the carbene carbon. Just as for the Fischer carbenes, the  $\sigma$ -bond is the result of donation of the carbene lone pair to the metal. However, the polarization of the  $\pi$ -bond is such that most of the electron density is on the carbene carbon because here the metal  $d_\pi$  orbital is higher in energy than the carbene p orbital (Fig. 1c). Crabtree's<sup>4</sup> description is particularly illuminating: "One way of looking at this is to say that the two electrons originally in  $\text{M}(d_\pi)$  transfer to the more stable  $\text{C}(p_z)$  orbital, oxidizing the metal by two units and giving a  $\text{CR}_1\text{R}_2^-$  ligand. The system can, therefore, be seen as a metal-stabilized carbanion acting as a  $\sigma$  and  $\pi$  donor to the metal, not unlike the phosphorous ylides such as  $\text{Ph}_3\text{P}^+-\text{CH}_2^-$ . This oxidation of the metal translates into the Schrock carbene carbon acting as an  $\text{X}_2$  ligand, just as the oxo group acts as  $\text{O}^{2-}$  in a complex such as  $\text{Re}(=\text{O})\text{Cl}_3(\text{PPh}_3)_2$  or  $\text{Re}(=\text{O})\text{Me}_4$ ." This makes the carbene carbon nucleophilic.

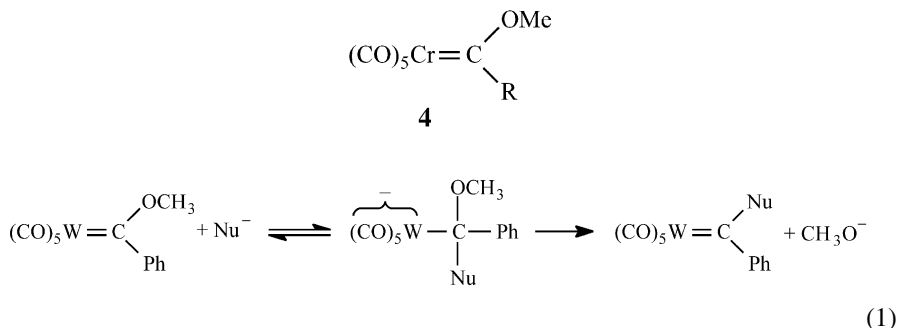
The extensive and ever increasing activity in the area of transition metal carbene complexes has been mainly driven by their usefulness in synthesis. To this date, the chemistry of the Fischer-type complexes has enjoyed the most extensive development and the present chapter will deal exclusively with this type. The key to the rich chemistry of the Fischer carbene complexes is that they can undergo reactions at several sites; they include modification of the carbene fragment, reaction on the side chain (R-group) or the metal (ligand exchange or change in the oxidation state), insertion of unsaturated organic molecules into the metal–carbon bond, etc. After such elaborations of the carbene complex, removal of the metal to complete the synthesis of the target organic molecule is usually a simple task.

The present chapter cannot possibly do justice to this rich chemistry and no such attempt will be made. Instead the reader is being referred to some of the main reviews that have been published on this subject over the last 20 years. References 8, 11–15, 18, 22 and 23 are reviews of broad scope, while Refs. 9, 10, 16, 17, 19–21,

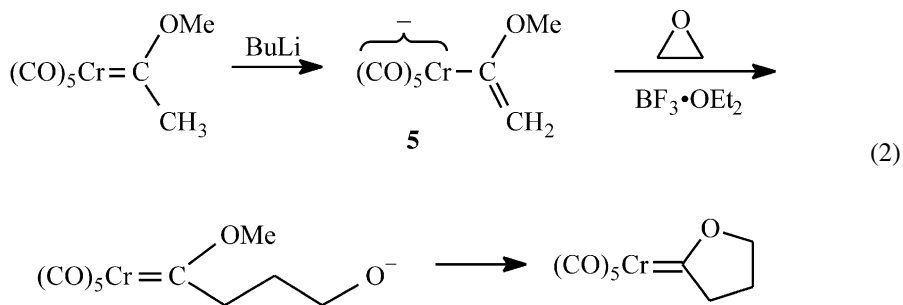


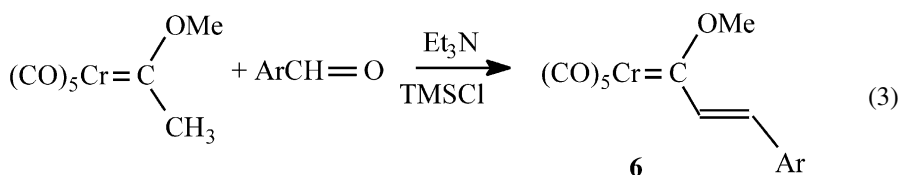
24 and 25 cover many specialized topics such as carbene and carbyne complexes of ruthenium, osmium, and iridium,<sup>9</sup> cyclopropanation reactions with olefins,<sup>10</sup> mono- and dinuclear (pentamethylcyclopentadienyl)iron carbene complexes,<sup>16</sup> applications of carbene complexes to amino acid synthesis,<sup>17</sup> carbene–alkyne–alkene cyclizations,<sup>19</sup>  $\beta$ -amino substituted  $\alpha,\beta$ -unsaturated Fischer carbene complexes,<sup>20</sup> 1-(alkynyl)carbene complexes,<sup>21</sup> 1-metal-1,3,5-hexatrienes and related compounds<sup>24</sup> and the great range of products that can be obtained from  $\alpha,\beta$ -unsaturated carbene-pentacarbonylchromium complexes.<sup>25</sup>

The most prominent systems studied thus far are the Fischer carbene complexes of the Group 6 metals, i.e., Cr, Mo and W, e.g., **4**. One important process that will be discussed at some length in this chapter is nucleophilic substitution, e.g., the replacement of the MeO group by a group with a different heteroatom such as an amino or thioalkyl group.<sup>1</sup> This reaction proceeds via a tetrahedral intermediate (equation 1) and is similar to nucleophilic substitutions on carboxylic esters.

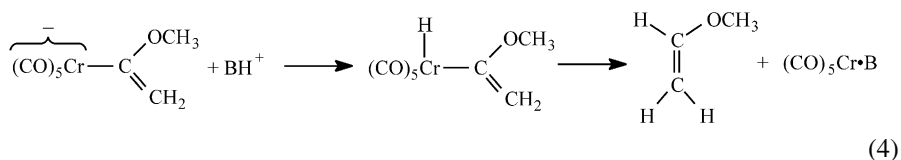


Another common reaction is based on the acidity of the  $\alpha$ -carbon proton, i.e., the carbon attached to the carbene carbon, a topic that will be discussed in detail in this chapter. The carbanion that results from the deprotonation of the  $\alpha$ -carbon can act as a nucleophile<sup>26</sup> and react with a variety of electrophiles, especially in the presence of Lewis acid catalysis, to form many different products (see, e.g., equations 2 or 3<sup>27,28</sup>). The basicity and nucleophilicity of the carbanion can be enhanced by substituting the MeO group by a  $\text{Me}_2\text{N}$  group<sup>29</sup> or replacing a CO ligand with an electron donating one, e.g.,  $\text{R}_3\text{P}$ .<sup>30</sup>





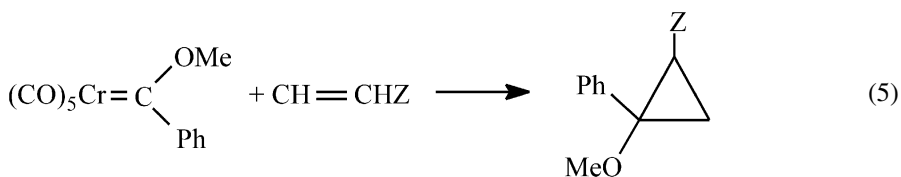
In the presence of weak bases such as pyridine and others the reaction of the carbanion with  $\text{BH}^+$  may lead to enol ether formation.<sup>23,31-33</sup> The mechanism of this reaction is usually assumed to involve protonation of the carbanion on the metal followed by a reductive-elimination (equation 4)<sup>23</sup> but evidence discussed at the end of this chapter suggests a different mechanism.

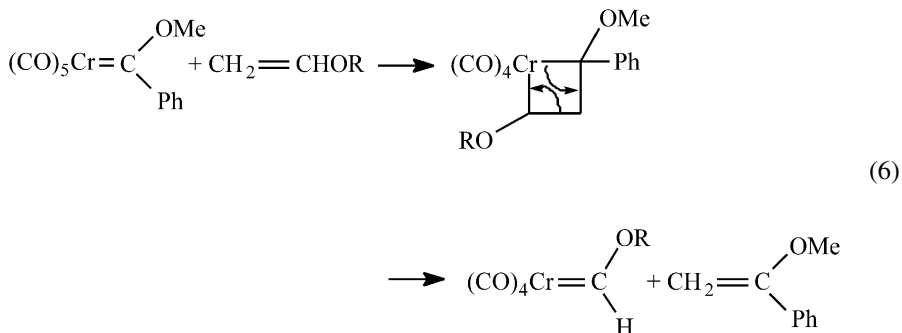


#### SCOPE OF THIS CHAPTER

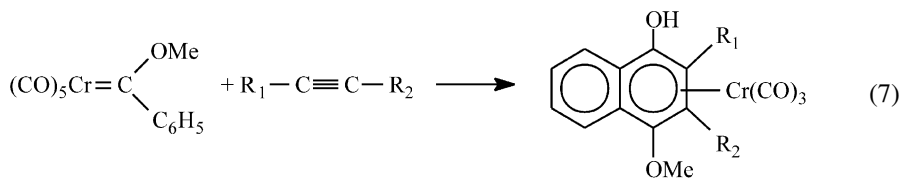
The thrust of this chapter deals with reactions of Fischer carbene complexes that have been the subject of kinetic and/or thermodynamic studies. The number of these is relatively limited. They include the reactions of equations (1) and (4), proton transfers that generate carbanions such as **5** (see equation 2), reactions at the metal center such as the loss or exchange of ligands as well as rearrangement reactions.

On the other hand, there have been hardly any kinetic investigations of the many reactions that have proven to be among the most useful or unique applications of Fischer carbene complex chemistry. Hence they are not part of this chapter although a few of the most prominent ones need to be mentioned. They include cyclopropanation of electrophilic olefins<sup>8,10,23,34</sup> (e.g., equation 5), metathesis (e.g., equation 6)<sup>1,23,35-37</sup> and reactions of  $\alpha,\beta$ -unsaturated carbene complexes such as **6** (see equation 3) that lead to what de Meijere *et al.*<sup>25</sup> have called an

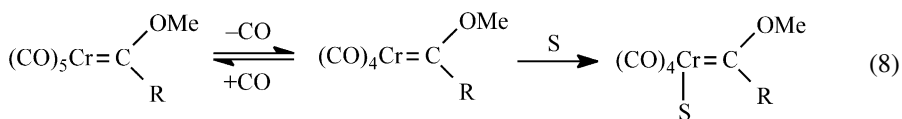




“incredible range of products,” including [4 + 2], [3 + 2] and [2 + 2] cycloadditions, Michael additions, aldol reactions, intramolecular cyclizations and, most prominently, the Dötz reaction.<sup>8,18,23,25,38</sup> This latter reaction, whose mechanism is quite complex, involves the combination of unsaturated alkoxy carbene complexes with alkynes to yield hydroquinone derivatives (e.g., equation 7).



It should be noted that a key element in most of these reactions is that they are initiated by the coordination of the substrate to the metal.<sup>39</sup> Since Fischer carbene complexes are coordinatively saturated, the coordination of the substrate needs to be preceded by the loss of a ligand (see, e.g., equation 8, S = substrate). This ligand loss can be initiated thermally as well as photochemically. This loss of CO is usually the rate-limiting step which is a major reason why kinetic experiments give little information about the complex steps that follow the initial ligand loss.

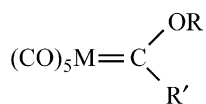


Last, but not least, the rich photochemistry<sup>17,40–43</sup> of Fischer carbene complexes that has found important synthetic applications needs to be mentioned.

## 2 Reactions at the metal

The generation of reactive, coordinatively unsaturated intermediates by loss of a CO ligand from carbene complexes such as **7** is a crucial step in numerous reactions of such complexes, the most prominent one being the Dötz reaction.<sup>8,18,23,25,38</sup> Other

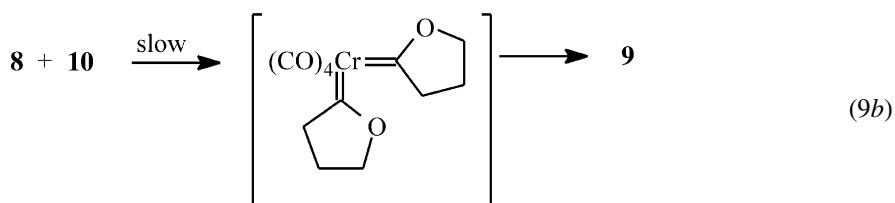
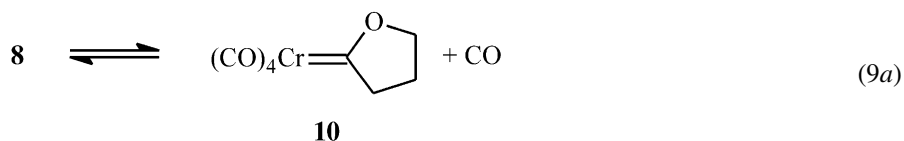
examples include thermal decomposition, substitution of CO by phosphines, reactions with alkenes and others.



7

## THERMOLYSIS

Reversible loss of CO was demonstrated in the thermolysis of the cyclic complex **8** which leads to the dimeric product **9** by the mechanism of equations (9).<sup>44</sup>



Reversibility of the first step was indicated by a large reduction of the rate of decomposition of **8** in the presence of added CO. For example, at 139.4°C in decalin, the second-order rate constant for the decomposition of **8** is reduced 27-fold under 1480 mm Hg CO pressure. Furthermore, exchange of <sup>13</sup>CO with **8** was found to be first order in the concentration of **8** and approximately 40-fold faster than thermal decomposition.

Additional evidence for reversible CO loss from several carbene complexes such as **11–15** was obtained from kinetic measurements of <sup>13</sup>CO exchange rates determined by <sup>13</sup>C NMR.<sup>45</sup> The results are summarized in Table 1. For the phenylmethoxycarbene complexes (**11–13**), CO dissociation from the tungsten complex is seen to be much slower than for the chromium and molybdenum derivatives. Changing the methoxy to a phenyl group (**14** versus **13**) increases the exchange rate which can be understood in terms of the reduced π-donor ability of

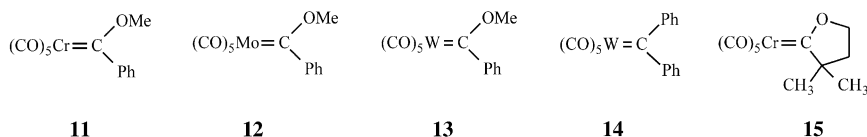
**Table 1** Rate constants and  $\Delta G^\ddagger$  values for CO dissociation from carbene complexes

Carbene complex	$T$ ( $^\circ\text{C}$ )	$k$ ( $\times 10^5 \text{ s}^{-1}$ )	$\Delta G^\ddagger$ ( $\text{kcal mol}^{-1}$ )
$(\text{CO})_5\text{Cr}=\text{C}(\text{OMe})\text{Ph}$ ( <b>11</b> )	44 <sup>a</sup>	18.0	24.0
$(\text{CO})_5\text{Mo}=\text{C}(\text{OMe})\text{Ph}$ ( <b>12</b> )	27 <sup>a</sup>	4.9	23.4
$(\text{CO})_5\text{W}=\text{C}(\text{OMe})\text{Ph}$ ( <b>13</b> )	77 <sup>b</sup>	2.3	28.0
$(\text{CO})_5\text{W}=\text{C}(\text{Ph})_2$ ( <b>14</b> )	40 <sup>a</sup>	4.9	24.5
$(\text{CO})_5\text{Cr}=\text{C}(\text{O})\text{CH}_2\text{CH}_2\text{CMe}_2$ ( <b>15</b> )	77 <sup>b</sup>	1.1	28.5

Reference 45.

<sup>a</sup>In hexane.<sup>b</sup>In toluene.

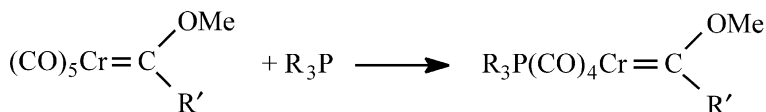
the phenyl group relative to the methoxy group.<sup>45</sup> This reduced  $\pi$ -donor effect is partially offset by stronger  $\pi$ -donation to the carbene carbon from the metal, which reduces the  $\pi$ -donation from the metal to the CO ligands and leads to weaker bonding to CO. The faster CO dissociation from **11** compared to **15** has a similar origin, i.e., the alkyl group in **15** is a better electron donor than the phenyl groups in **11**.



An important conclusion from this work is that the measured CO dissociation rates are fast compared to the overall rates of those reactions that are believed to be initiated by CO loss from the corresponding carbene complex, lending strong support to the notion that CO loss is the crucial first step. Those processes include the above-mentioned hydrogenolysis, reaction with alkenes and vinyl esters, substitution of CO by phosphines, the Dötz reactions, and others.

#### SUBSTITUTION OF CO BY PHOSPHINES

With respect to CO substitution by phosphines, it is noteworthy that there is very good agreement between the kinetic results obtained by Werner *et al.*<sup>46</sup> and the rate constant of  $1.8 \times 10^{-4} \text{ s}^{-1}$  listed in Table 1 for CO dissociation from **11**. Werner *et al.*<sup>46</sup> investigated the reaction of **16** with a series of tertiary phosphines in *n*-decane and some other solvents.



**16a:** R' = CH<sub>3</sub>

**16b:** R' = Ph ≡ **11**

**17a:** R' = CH<sub>3</sub>

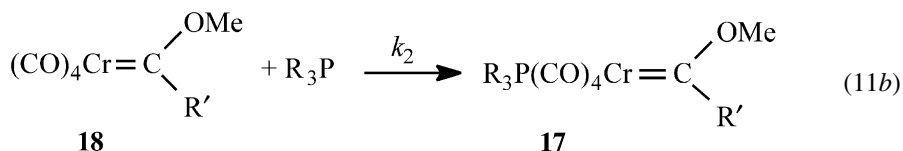
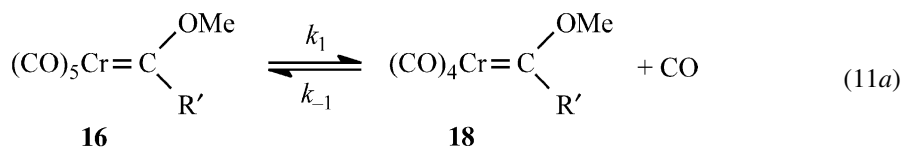
**17b:** R' = Ph

They found that the reaction followed mixed first- and second-order kinetics according to equation (10). With

$$-\frac{d[\mathbf{16}]}{dt} = k_I[\mathbf{16}] + k_{II}[\mathbf{16}][\text{R}_3\text{P}] \quad (10)$$

(C<sub>6</sub>H<sub>11</sub>)<sub>3</sub>P, (*p*-CH<sub>3</sub>C<sub>6</sub>H<sub>4</sub>)<sub>3</sub>P, (C<sub>6</sub>H<sub>5</sub>)<sub>3</sub>P, (C<sub>6</sub>H<sub>5</sub>)<sub>2</sub>(C<sub>2</sub>H<sub>5</sub>)P and (C<sub>6</sub>H<sub>5</sub>)(C<sub>2</sub>H<sub>5</sub>)<sub>2</sub>P the *k<sub>I</sub>* term is dominant while with the more basic (C<sub>2</sub>H<sub>5</sub>)<sub>3</sub>P and (*n*-C<sub>4</sub>H<sub>9</sub>)<sub>3</sub>P the *k<sub>II</sub>* term becomes significant at high phosphine concentrations.

The *k<sub>I</sub>* term was attributed to the S<sub>N</sub>1-type mechanism of equations (11a) and (11b)

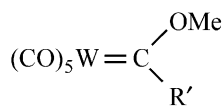
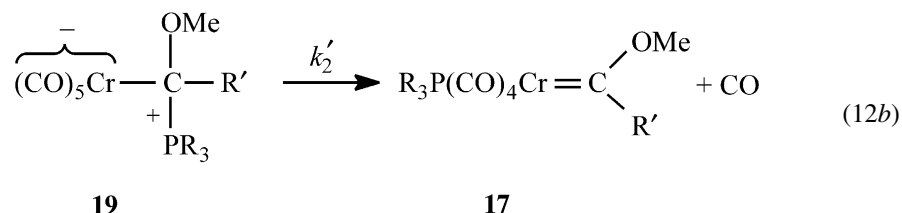
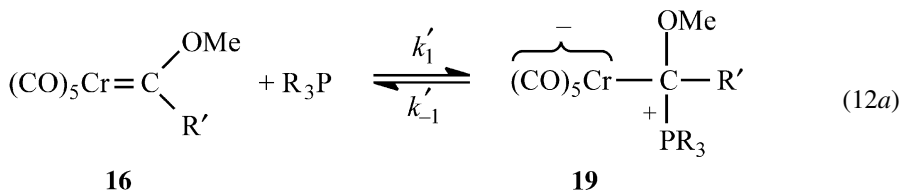


with  $k_2[\text{R}_3\text{P}] > (\gg) k_{-1}[\text{CO}]$  which renders the dissociation step ( $k_1 = k_{-1}$ ) rate limiting. Based on the structure of the reaction product (**17**), the CO being lost is likely to come from a *cis* position.

Some representative *k<sub>I</sub>* values are  $2.8 \times 10^{-4} \text{ s}^{-1}$  for **16a** at 68.2°C ( $\Delta H^\ddagger = 27.5 \text{ kcal mol}^{-1}$ ,  $\Delta S^\ddagger = 3.6 \text{ cal mol}^{-1} \text{ deg}^{-1}$ ) and  $2.5 \times 10^{-4} \text{ s}^{-1}$  for **16b** at 44.5°C ( $\Delta H^\ddagger = 27.0 \text{ kcal mol}^{-1}$ ,  $\Delta S^\ddagger = 10.8 \text{ cal mol}^{-1} \text{ deg}^{-1}$ ).

The mechanism of the second-order term could not be established with any degree of certainty. One possibility discussed by the authors is an S<sub>N</sub>2-type mechanism although this would require an unusual seven coordinate metal complex at the transition state. Alternatively, the phosphine could first attack the carbene carbon to form **19** followed by loss of CO and migration of R<sub>3</sub>P to the metal as shown in equations (12). This latter mechanism found support in a subsequent study by

Fischer *et al.*<sup>47</sup> in which rapid reversible  $R_3P$  addition to **16** (equation 12a) as well as to the tungsten analog **20** could be demonstrated.



**20a:**  $R' = \text{CH}_3$

**20b:**  $R' = \text{Ph}$

Equilibrium constants,  $K'_1 = k'_1/k'_{-1}$ , for equation (12a) were determined in toluene for the reactions of **16a** with  $\text{C}_6\text{H}_5(\text{C}_2\text{H}_5)_2\text{P}$  and  $(\text{C}_4\text{H}_9)_3\text{P}$  as well as for the reaction of **20a** with  $(\text{C}_4\text{H}_9)_3\text{P}$ . Some of the results are summarized in Table 2. They show a strong temperature dependence. For the reaction of **16a**,  $K'_1$  is quite small at the temperatures used in the kinetic study (58.8–68.8°C for the reaction of **16a** with  $(n\text{-C}_4\text{H}_9)_3\text{P}$ ).<sup>46</sup> This means  $K'_1[\text{R}_3\text{P}] < (\ll) 1$  and hence the rate law for the mechanism of equations (12a) and (12b) is given by equation (13), implying that  $k_{\text{II}}$  in

$$-\frac{d[\mathbf{16a}]}{dt} = K'_1 k'_2 [\mathbf{16a}] [\text{R}_3\text{P}] \quad (13)$$

Equation (10) is equal to  $K'_1 k'_2$ . The fact that  $K'_1[\text{R}_3\text{P}] < (\ll) 1$  is also consistent with the first term in equation (10) being independent of  $[\text{R}_3\text{P}]$ ; if  $K'_1[\text{R}_3\text{P}] \approx 1$ , the first term would be given by  $k_1[\mathbf{16}]/(1 + K'_1[\text{R}_3\text{P}])$  and show a decrease with increasing  $[\text{R}_3\text{P}]$ .

As to the details of reaction (12b), the most likely mechanisms involve either loss of CO from **19** (equation 14) and subsequent migration of  $\text{Ph}_3\text{P}$  from the carbene

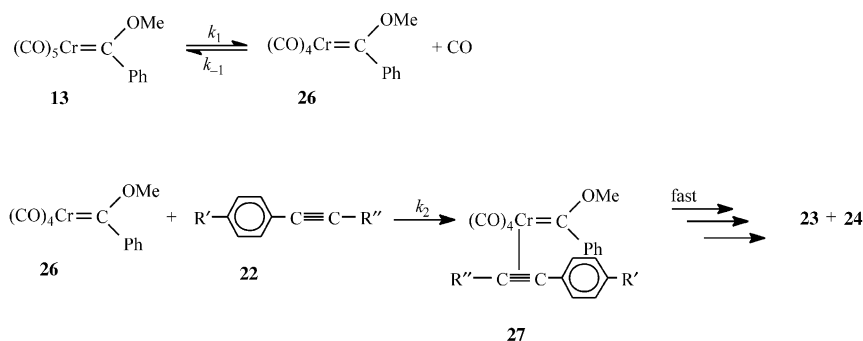
**Table 2** Equilibrium constants for  $(C_4H_9)_3P$  addition to  $(CO)_5M=C(OMe)CH_3$  in toluene

Carbene complex	$T$ ( $^{\circ}C$ )	$K'_1$ ( $M^{-1}$ )	$\Delta H^{\circ}$ ( $kcal\ mol^{-1}$ )	$\Delta S^{\circ}$ ( $cal\ mol^{-1}\ deg^{-1}$ )
$(CO)_5Cr=C(OMe)CH_3$ ; ( <b>20a</b> : $R' = CH_3$ )	10	30.2		
	17	19.4		
	25	6.22		
	30	3.69		
	38	1.98		
	45	0.68		
	52	0.46		
	60	0.15	-20.0	-63.8
$(CO)_5W=C(OMe)CH_3$ ; ( <b>20b</b> : $R' = CH_3$ )	4	$8.93 \times 10^4$		
	14	$5.25 \times 10^3$		
	30	$1.35 \times 10^3$		
	42	$5.00 \times 10^2$		
	45	$4.51 \times 10^3$	-15.1	-35.6

Ref. 47.







rate law is given by equation (17). The kinetic parameters

$$-\frac{d[\mathbf{13}]}{dt} = \frac{k_1 k_2 [\mathbf{22}]}{k_{-1} [\text{CO}] + k_2 [\mathbf{22}]} [\mathbf{13}] \quad (17)$$

are summarized in Table 3. The positive  $\Delta S^\ddagger$  value for the  $k_1$  step is consistent with rate-limiting CO dissociation; it contrasts with the strongly negative  $\Delta S^\ddagger$  values obtained for reactions where nucleophilic attack of the carbene complex is rate limiting, as discussed in a section titled “Insertion reactions initiated by nucleophilic attack.” The trend in the  $k_2/k_{-1}$  ratios is also consistent with the proposed mechanism; since  $k_{-1}$  is independent of the alkyne, these ratios mirror changes in  $k_2$  whose increase with the increasing electron donating effect of  $R''$  reflect enhanced nucleophilicity of the alkyne.

Based on a density functional theory (DFT) study of the model reaction of  $(\text{CO})_5\text{Cr}=\text{C}(\text{OH})\text{CH}=\text{CH}_2$  with  $\text{HC}\equiv\text{CH}$ , Torrent *et al.*<sup>50</sup> recently proposed that an association type mechanism according to which insertion of the alkyne into the  $\text{Cr}=\text{C}$  bond followed by CO dissociation may be energetically more favorable than the mechanism of Scheme 1. However, their claims have been rejected because they are contradicted by the above described kinetic results.<sup>51</sup>

**Table 3** Kinetic parameters for the benzannulation reaction (15) of  $(\text{CO})_5\text{Cr}=\text{C}(\text{OMe})\text{Ph}$  (**11**) with **22** ( $R' = \text{H}$ ) in dibutyl ether at 56.8°C

$R''$	$k_1^a (\times 10^{-3} \text{ s}^{-1})$	$k_2/k_{-1}$
4- $\text{CF}_3\text{C}_6\text{H}_4$	1.07	0.0043
$\text{C}_6\text{H}_5$	1.07	0.0050
4- $\text{MeC}_6\text{H}_4$	1.07	0.0055
$\text{CH}_3$	1.07	0.0260

Reference 49.

<sup>a</sup> $\Delta H^\ddagger = 25.8 \text{ kcal mol}^{-1}$ ,  $\Delta S^\ddagger = 6.22 \text{ cal mol}^{-1} \text{ deg}^{-1}$ .

**Table 4** Rate constants and activation parameters for the reaction of  $(\text{CO})_5\text{M}=\text{C}(\text{X})\text{NR}_2$  in 1,1,2-trichloroethane (equation 18)

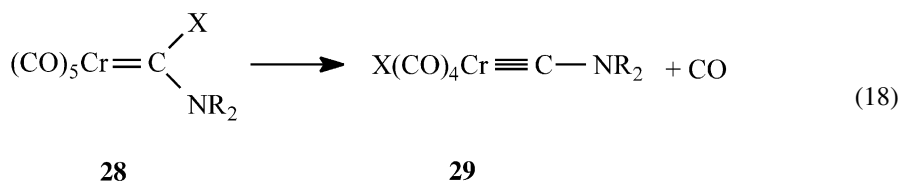
X	NR <sub>2</sub>	$k$ ( $\times 10^3 \text{ s}^{-1}$ )	$\Delta H^\ddagger$ (kcal mol <sup>-1</sup> )	$\Delta S^\ddagger$ (cal mol <sup>-1</sup> deg <sup>-1</sup> )
Cl	NMe <sub>2</sub>	0.109	26.2	7.0
Cl	NC <sub>5</sub> H <sub>10</sub>	0.394	23.9	2.0
Cl	NEt <sub>2</sub>	1.80	23.7	4.4
Cl	NPh <sub>2</sub>	11.3	19.3	-6.1
Br <sup>a</sup>	NEt <sub>2</sub>	905 <sup>b</sup>	18.0	-1.0

Reference 53. At 40°C.

<sup>a</sup>Reference 52 in CH<sub>2</sub>Cl<sub>2</sub>.<sup>b</sup>Calculated based on  $\Delta H^\ddagger$  and  $\Delta S^\ddagger$ .

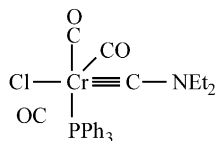
## REARRANGEMENT REACTIONS WITH LOSS OF CO

Carbene complexes of the type **28** with X being a halogen spontaneously rearrange to the dialkylaminocarbyne complex **29** under elimination of CO.<sup>52,53</sup>



In an initial kinetic study (R = Et; X = Cl and Br)<sup>52</sup> the reaction was found to follow a first-order rate law and yield rate constants that are much higher for X = Br than for X = Cl. An extension of the work to include different R<sub>2</sub>N groups (Me<sub>2</sub>N, C<sub>5</sub>H<sub>10</sub>N and Ph<sub>2</sub>N) was reported in 1985.<sup>53</sup> Some of the results are summarized in Table 4. They show that increasing the bulk of the dialkylamino group enhances the rate; for example, the change from NMe<sub>2</sub> to NPh<sub>2</sub> increases the  $k$  value 100-fold and, based on low temperature experiments, it was estimated that at 40°C the N(*i*-Pr)<sub>2</sub> derivative may be *ca.* 10<sup>7</sup>-fold more reactive than the NMe<sub>2</sub> derivative. There is also a dramatic increase in the rate upon changing X = Cl to X = Br. Furthermore, the rate increases with increasing solvent polarity although the effect is quite modest.

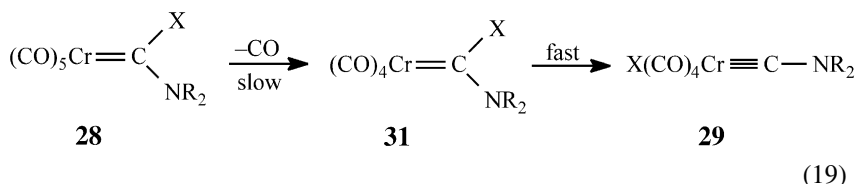
Other mechanistically relevant observations are the absence of any rate effect by added chloride ions, by running the reactions under CO pressures up to 78 atm, or by added radical initiators such as azobis(isobutyronitrile) or radical inhibitors such as hydroquinone. Furthermore, addition of high concentrations of PPh<sub>3</sub> in the reaction of **28** (R<sub>2</sub>N = Et<sub>2</sub>N, X = Cl) does not effect the rates either but it leads to a different product **30**.

**30**

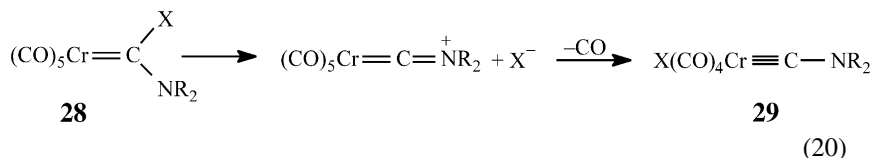
However, CO/PPh<sub>3</sub> exchange in **29** had been shown to be much faster than formation of **30** from **28**,<sup>54</sup> hence one concludes that **30** must have been formed from **29** rather than from **28**. Similar results have been reported for the rearrangement of other aminocarbene complexes such as **28** (R<sub>2</sub>N = Et<sub>2</sub>N) with X = SeR,<sup>55</sup> TePh,<sup>56</sup> SnPh<sub>3</sub><sup>57</sup> and PbPh<sub>3</sub>.<sup>58</sup>

In proposing a mechanism that would be consistent with all experimental observations, Fischer *et al.*<sup>53</sup> discussed the following possibilities.

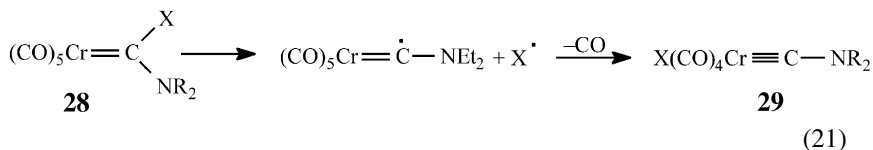
- (1) Rate-limiting loss of CO followed by rapid migration of X to the metal, equation (19).



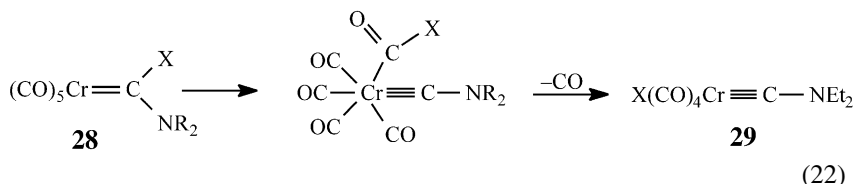
- (2) Heterolytic C–X bond cleavage followed by loss of CO and addition of X<sup>−</sup> to the metal, equation (20).



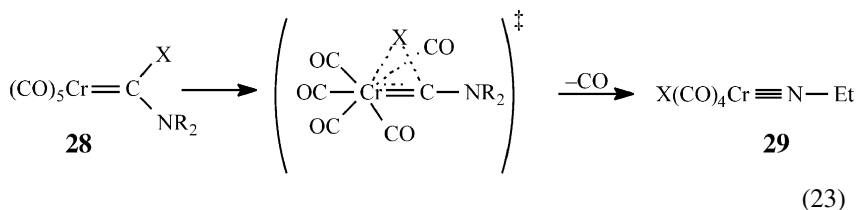
- (3) Homolytic C–X bond cleavage followed by loss of CO and addition of X<sup>·</sup> to the metal, equation (21).



- (4) Intramolecular nucleophilic attack of one of the *cis*-CO ligands by X, followed by loss of CO and rearrangement, equation (22).



- (5) Intramolecular attack by X on the metal that is concerted with the loss of CO, equation (23).



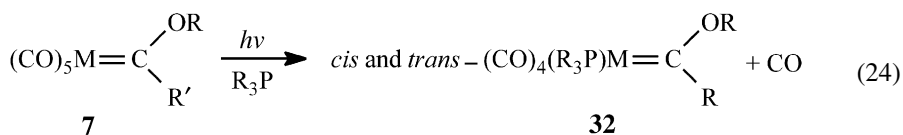
Mechanism (1) was excluded because the rate remains unaffected when the reaction is conducted under high CO pressure and the  $\Delta S^\ddagger$  values are much lower than is typical for reactions that are initiated by CO loss (see the section on Substitution of CO by phosphines). Mechanism (2) was excluded based on the rather small solvent dependence. Mechanism (3) was rejected because neither radical initiators nor radical scavengers have any influence on the reaction, and there is no correlation between  $\Delta H^\ddagger$  and the homolytic C–X bond energies. Intramolecular attack by X on one of the CO ligands (mechanism 4) is conceivable when X contains lone pairs (Cl, Br, SePh and TePh) but not with X = SnPh<sub>3</sub> or PbPh<sub>3</sub> and was also excluded.

In contrast, all observations are consistent with the concerted mechanism (5), including the small  $\Delta S^\ddagger$  values typical for intramolecular processes.

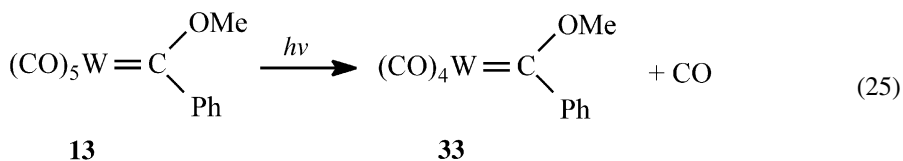
#### PHOTOCHEMICAL REACTIONS

The early work of Fischer *et al.*<sup>59</sup> showed that irradiation of several complexes of the type 7 (M = Cr or W) in the presence of phosphines led to tetracarbonyl phosphine

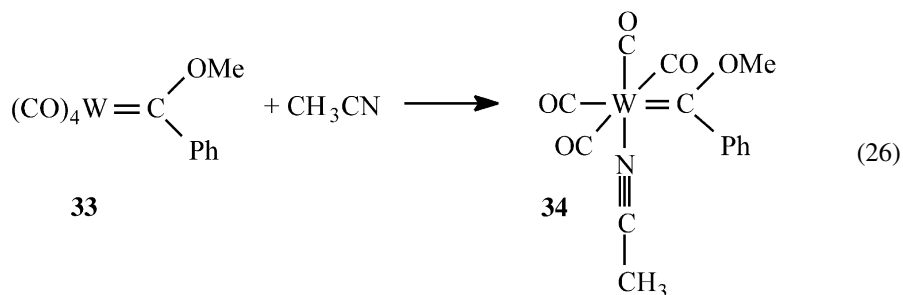
complexes, presumably the result of photoinduced loss of CO (equation 24) and subsequent trapping of  $(\text{CO})_4\text{M}=\text{C}(\text{OR})\text{R}'$  by the phosphine.



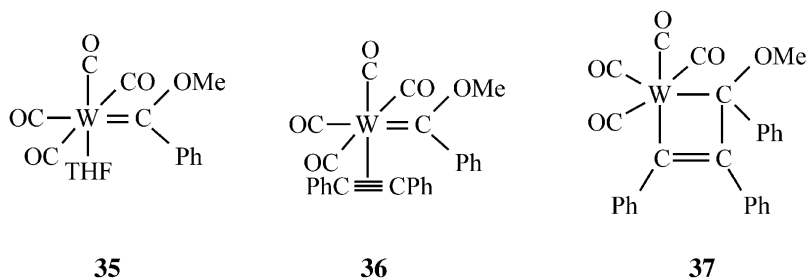
Even though work by Casey *et al.*<sup>60-62</sup> appeared to be consistent with Fischer *et al.*'s results, other reports did not.<sup>63,64</sup> A thorough study of the photolysis of **13** confirmed that UV radiation of this carbene complex induces CO loss (equation 25) to form **33**.<sup>65</sup>



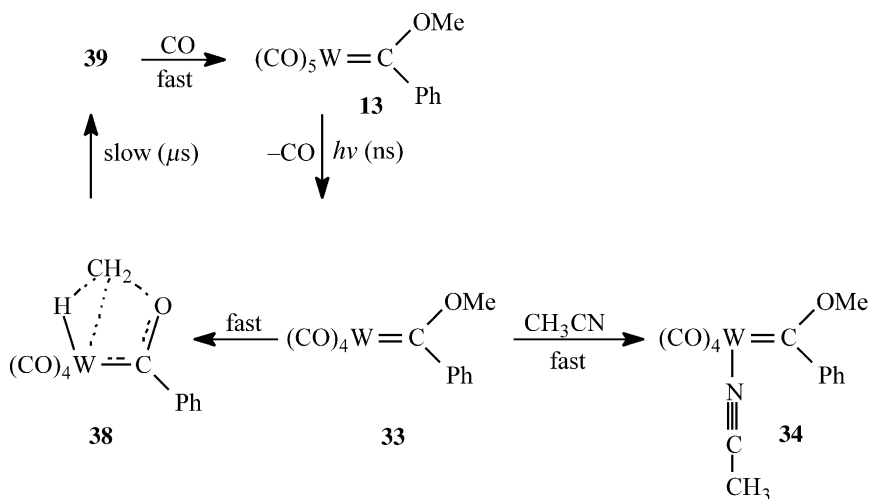
When the reaction is carried out in  $\text{CH}_3\text{CN}$  solution, **33** gets trapped immediately to form **34**, which is the observed product and can be isolated. The reaction is very clean as indicated by sharp isosbestic points in the UV and IR. Furthermore, **13** can be regenerated by reacting **34** with CO.



In THF solution, the photoproduct is the corresponding THF complex **35** while photolysis of **13** in the presence of  $\text{PhC}\equiv\text{CPh}$  in hexane solution leads to an insoluble complex whose structure could either be that of **36** or **37**.



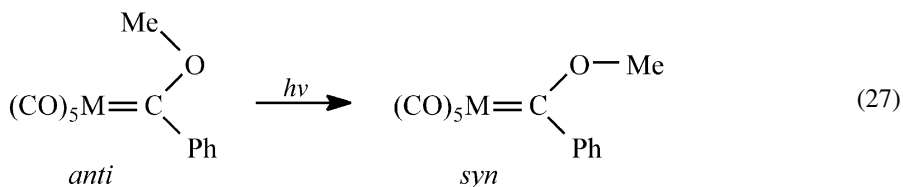
Additional detail about the photodissociation of CO from **13** has come from time-resolved Raman spectroscopy.<sup>66,67</sup> It was shown that the loss of CO occurs within the duration of a nanosecond laser pulse into the LF band and leads to a transient species that decays on a microsecond time scale to regenerate **13**; in solvents such as CH<sub>2</sub>Cl<sub>2</sub>, benzene or *n*-hexane formation and decay of this transient species are the only observable processes while in acetonitrile there is also rapid formation of **34**. The suggested sequence of reactions is shown in [Scheme 2](#).



**Scheme 2**

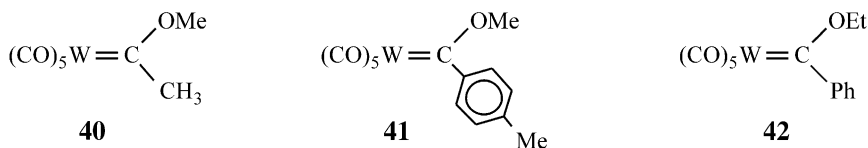
The proposed structure of the transient species **38** implies “self-solvation” by an agostic interaction of the hydrogen of the methoxy group with the metal which competes with the coordination of CH<sub>3</sub>CN to the metal; formation of both **34** and **38** occur on the same time scales. An additional species of unknown structure (**39**) has been postulated in order to explain why the rate of regeneration of **13** is independent of [CO].

The photochemistry of **11** and **13** in inert gas matrices at 10 K has also been reported.<sup>68</sup> Irradiation with visible light into the low-energy metal-to-ligand charge transfer (MLCT) band ( $\sim 370$  nm) was shown to induce complete conversion of the *anti* to the *syn* configurations (equation 27).



Irradiation into the LF band at  $\sim 350$  nm leads to the same *anti*  $\rightarrow$  *syn* conversion but there is subsequent loss of CO which, for the tungsten complex, is followed by a third process. It was suggested that this third process leads to **38**, the transient species that had been reported by McGarvey's group.<sup>66,67</sup>

Applying time-resolved Raman spectroscopy coupled with matrix isolation techniques to additional carbene complexes such as **40**–**42**, McGarvey and co-workers<sup>69</sup> were able to confirm the findings (equation 27) reported by Stufkens and co-workers<sup>68</sup> They showed that the *anti*  $\rightarrow$  *syn* conversion occurs in less than 10 ns. The lifetime of the *syn* isomer which spontaneously reverts back to the *anti* isomer is strongly dependent on the structure of the carbene complex and solvent polarity. The reported lifetimes are summarized in Table 5. The lifetimes are substantially longer for the methyl compared to the aryl carbene complexes and also increase with increasing solvent polarity. One factor that may contribute to the shorter lifetimes of the aryl derivatives is steric crowding in the *syn* isomers although “conventional” steric crowding cannot be the whole story<sup>69</sup> since the lifetime of the even more crowded *syn* isomer of  $(\text{CO})_5\text{W}=\text{C}(\text{OEt})(\text{SiPh}_3)$  is similar to that for **41** and **42**.<sup>70</sup> However, for the aryl carbene complexes the crowding may force the aryl group to rotate out of the plane of the carbene which reduces the  $\pi$ -overlap with the carbene carbon and hence leads to destabilization.<sup>69</sup>



The solvent dependence suggests stabilization of the *syn* isomers and/or a destabilization of the transition state by more polar solvents but the origin of these stabilizing/destabilizing effects was not discussed.<sup>69</sup>

A recent laser flash photolysis study of **13** using time-resolved IR and UV–Vis spectroscopy<sup>71</sup> has confirmed basic conclusions derived from the previous

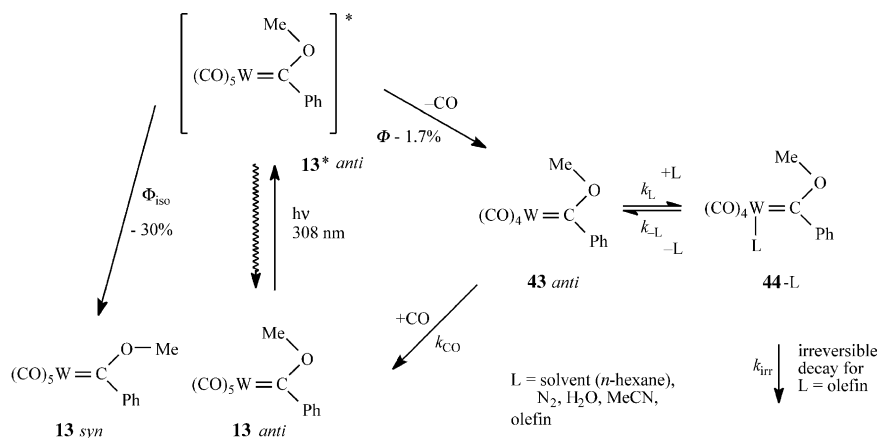


**Table 5** Lifetimes (in  $\mu\text{s}$ ) of *syn* isomers of tungsten carbene complexes at 20°C

Solvent	$(\text{CO})_5\text{W}=\text{C}(\text{OMe})\text{CH}_3$	$(\text{CO})_5\text{W}=\text{C}(\text{OMe})\text{C}_6\text{H}_4\text{-4-Me}$	$(\text{CO})_5\text{W}=\text{C}(\text{OEt})\text{Ph}$	$(\text{CO})_5\text{W}=\text{C}(\text{OMe})\text{Ph}^a$
<i>n</i> -Hexane	126	1.10	4.65	2.9
Cyclohexane	294	1.62	5.0	4.6
$\text{CH}_2\text{Cl}_2$	1200	3.70	14.3	11.1
Methanol	2642	6.6	20.7	
Acetonitrile	3356	7.1	23	

Reference 69.

<sup>a</sup>Reference 66.



investigations mentioned above and also provided additional quantitative kinetic information. Scheme 3<sup>71</sup> provides an overview of the various processes that occur upon excitation of the *anti* isomer of **13** with a laser flash at 308 nm. The initially formed upper ligand field excited state,  $[13^*]_{anti}$ , can undergo three processes: a radiationless decay back to the groundstate, isomerization to the *syn* isomer (quantum yield  $\approx 30\%$ ), and loss of CO to form the penta-coordinated tetracarbonyl carbene complex  $[43]_{anti}$  (quantum yield  $\approx 1.7\%$ ). This latter intermediate may revert back to  $[13]_{anti}$  upon irreversible addition of CO or reversibly add a ligand (L) such as the solvent (L = S) or other species such as  $N_2$ ,  $H_2O$ ,  $CH_3CN$  or an olefin.

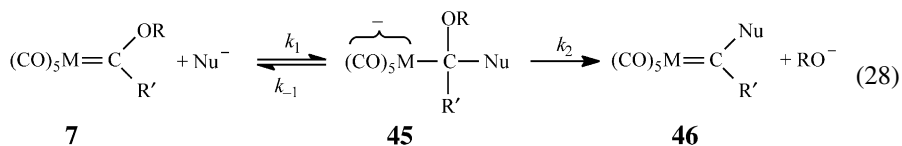
On the microsecond time scale of the reported experiments, **43** cannot be observed; hence the first detectable tetracarbonyl species was attributed to **44** with (L = S). A conversion of **44-S** into **44-N<sub>2</sub>** could be observed during the first 10  $\mu s$  in nitrogen-purged solutions, or into **44-H<sub>2</sub>O** in solutions purged with wet argon; these conversions are assumed to occur via **43** as the intermediate. The data also provided a rate constant of  $3.5 \times 10^8 \text{ M}^{-1} \text{ s}^{-1}$  for the exchange of the solvent or  $N_2$  ligands by CO.

### 3 Reactions at the carbene carbon

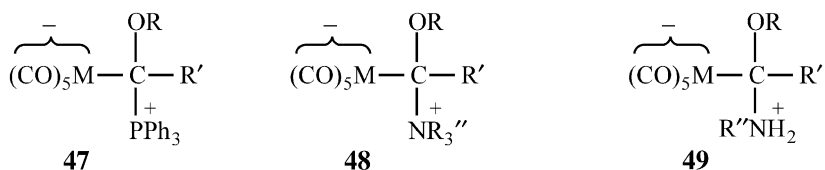
#### GENERAL FEATURES

Nucleophilic substitution of an alkoxy group of carbene complexes such as **7** is one of the prototypical reactions of Fischer carbene complexes. It has generally been

assumed to proceed via a tetrahedral intermediate (**45**) in analogy to the reaction of carboxylic esters with nucleophiles.



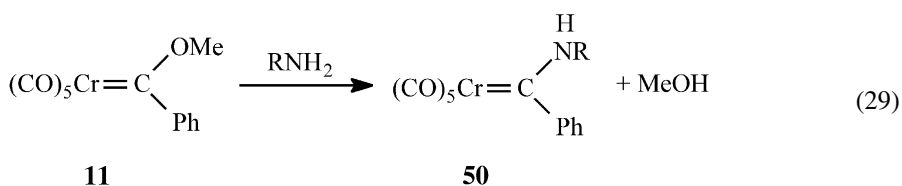
With neutral nucleophiles such as phosphines and amines, the nucleophilic attack on the carbene complex leads to zwitterionic intermediates such as **47–49**; if there is an acidic proton on the intermediate as in the case of **49**, the reaction can proceed to products by elimination of ROH, otherwise the reaction stops at the adduct stage.



Most synthetic applications have involved common nucleophiles such as amines,<sup>1,72–76</sup> hydrazine,<sup>1,77</sup> oximes,<sup>1,78</sup> alkoxide ions,<sup>1,79</sup> thiolate ions,<sup>1,80–82</sup> carbanions<sup>1,83–87</sup> as well as others.<sup>88–90</sup>

#### AMINE NUCLEOPHILES

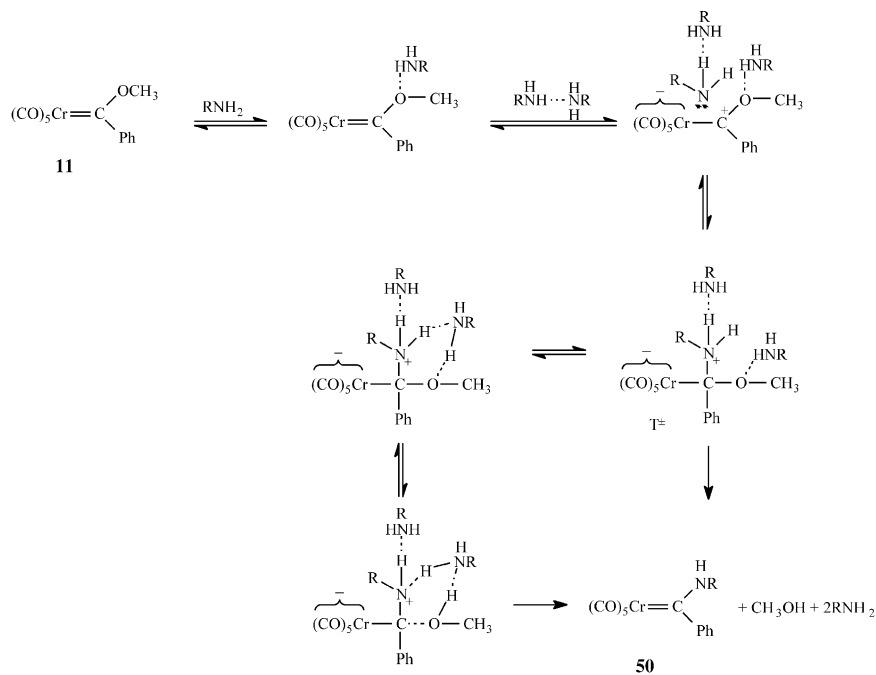
The first kinetic investigation of a nucleophilic substitution reaction was that of Werner *et al.*<sup>91,92</sup> who studied the reaction of **11** with several primary aliphatic amines (*n*-BuNH<sub>2</sub>, C<sub>6</sub>H<sub>11</sub>NH<sub>2</sub>, C<sub>6</sub>H<sub>5</sub>CH<sub>2</sub>NH<sub>2</sub>) in *n*-decane, dioxane, methanol and dioxane–methanol (1/1) mixtures.



In *n*-decane the rate was found to be third order with respect to amine concentration (equation 30), in dioxane second order (equation 31),

$$-\frac{d[\mathbf{11}]}{dt} = \frac{d[\mathbf{50}]}{dt} = k''[\mathbf{11}][\text{RNH}_2]^3 \quad (30)$$

$$-\frac{d[\mathbf{11}]}{dt} = \frac{d[\mathbf{50}]}{dt} = k''[\mathbf{11}][\text{RNH}_2]^2 \quad (31)$$



Scheme 4

while in dioxane–methanol mixtures or pure methanol a mixed first- and second-order dependence on amine was reported (equation 32).

$$-\frac{d[\mathbf{11}]}{dt} = \frac{d[\mathbf{50}]}{dt} = k'[\mathbf{11}][\text{RNH}_2] + k''[\mathbf{11}][\text{RNH}_2]^2 \quad (32)$$

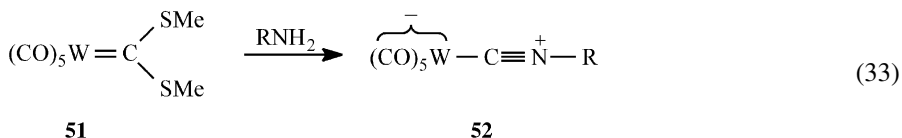
These rate laws indicate that up to three amine molecules may be present in the rate-limiting transition state but an unambiguous mechanistic interpretation is difficult because the sequence by which these amine molecules assemble cannot be ascertained. For the reactions in *n*-decane the authors proposed the mechanism shown in Scheme 4.

The function of the first amine molecule is to activate the substrate by hydrogen bonding to the methoxy group and possibly also to provide acid catalysis to  $\text{MeO}^-$  departure in the product forming step. The nucleophilic attack occurs with an amine molecule that is hydrogen bonded to a third amine which presumably helps stabilize the positive charge that develops on the nitrogen. In dioxane and methanol the  $\text{RNH}^{\text{H}} \cdots \text{N}^{\text{H}}\text{R}$  complex may be replaced by an amine–solvent complex, e.g.,  $\text{RNH}^{\text{H}} \cdots \text{OCH}_3$ . Furthermore, in methanol the solvent presumably takes on the role of the amine that hydrogen bonds to the methoxy group.

Support for this mechanism whose last step is probably rate limiting comes from  $^1\text{H}$  NMR studies that indicate the presence of association equilibria such as between

the carbene complex and the amine (first step in [Scheme 4](#)) and between two amine molecules. The negative  $\Delta H^\ddagger$  and strongly negative  $\Delta S^\ddagger$  values are also consistent with the proposed scheme.

Another aminolysis reaction of a Fischer carbene complex that has been studied kinetically is shown in equation (33).<sup>93</sup>



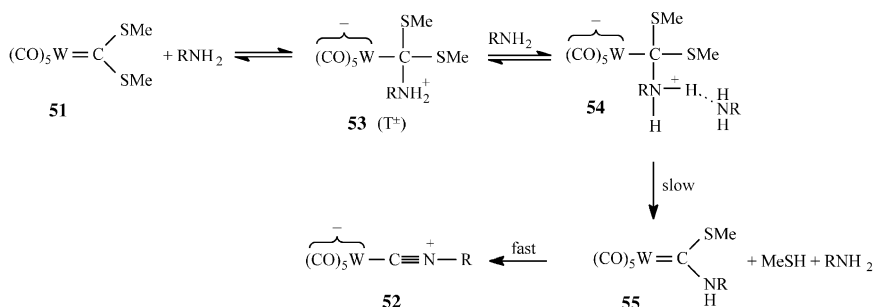
Rates were measured with monoamines such as *n*-PrNH<sub>2</sub>, *n*-BuNH<sub>2</sub>, C<sub>6</sub>H<sub>11</sub>NH<sub>2</sub> and PhCH<sub>2</sub>NH<sub>2</sub> as well as diamines such as H<sub>2</sub>N(CH<sub>2</sub>)<sub>2</sub>NH<sub>2</sub>, H<sub>2</sub>N(CH<sub>2</sub>)<sub>3</sub>NH<sub>2</sub>, H<sub>2</sub>N(CH<sub>2</sub>)<sub>4</sub>NH<sub>2</sub>, H<sub>2</sub>N(CH<sub>2</sub>)<sub>2</sub>NMe<sub>2</sub> and H<sub>2</sub>N(CH<sub>2</sub>)<sub>3</sub>NMe<sub>2</sub>; the majority of experiments was performed in THF but some data were also obtained in cyclohexane, pyridine, methanol, cyclohexane–THF and cyclohexane–pyridine mixtures. For the reactions of monoamines in THF the rate law was second-order in amine (equation 34), for the short chain diamines the rate law was first order in amine (equation 35) while for the longer chain diamines the rate law was that of equation (36). For the reactions with the primary amines the reaction was catalyzed by relatively high concentrations of DABCO and 4-picoline.

$$-\frac{d[\mathbf{51}]}{dt} = k_2[\mathbf{51}][\text{RNH}_2]^2 \quad (34)$$

$$-\frac{d[\mathbf{51}]}{dt} = k_1[\mathbf{51}][\text{RNH}_2] \quad (35)$$

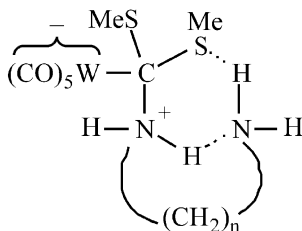
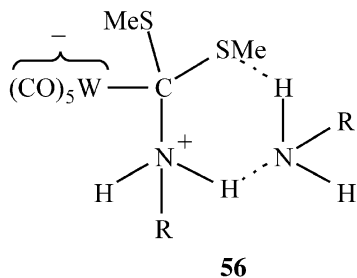
$$-\frac{d[\mathbf{51}]}{dt} = k_1[\mathbf{51}][\text{RNH}_2] + k_2[\mathbf{51}][\text{RNH}_2]^2 \quad (36)$$

The results with the monoamines were interpreted in terms of the mechanism outlined in [Scheme 5](#) with the conversion of **54** to **55** being the rate-limiting step; the



Scheme 5

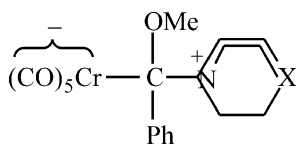
intermediacy of **55** which does not accumulate to detectable levels is supported by the fact that reaction of **51** with secondary amines leads to  $(\text{CO})_5\text{W}=\text{C}(\text{SMe})\text{NR}_2$ <sup>94</sup> which is stable. It was noted that the intermediate **54** may have the cyclic structure **56** which would allow direct proton transfer to the leaving group.



The mechanism of [Scheme 5](#) is quite similar to that of [Scheme 4](#) except that there is no association of an amine molecule with the leaving group. Not even methanol appears to hydrogen bond to the sulfur group which is consistent with the much weaker hydrogen bond acceptor ability of sulfur compared to oxygen.

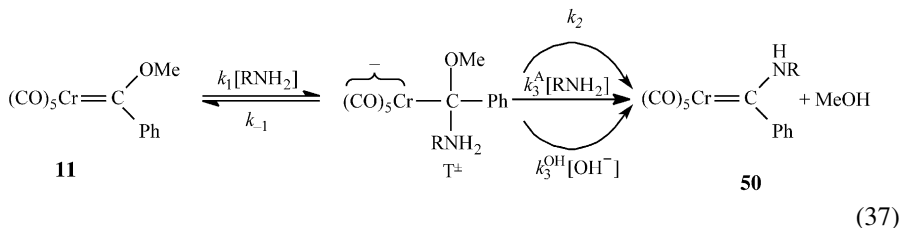
The reduced reaction order and the higher rate constants with diamines was explained in terms of intramolecular catalysis involving an intermediate like **57**.

The postulate of tetrahedral intermediates generated by nucleophilic attack on the carbene carbon (see  $\text{T}^\ddagger$  in [Schemes 4 and 5](#)) is reasonable even though the studies discussed above provide no direct evidence for them. However, support for such intermediates, at least in the reaction of **11** with amines, comes from reports that **11** forms isolable tetrahedral adducts such as **58** by reaction with DABCO or quinuclidine in ether.<sup>95,96</sup>



A more detailed study has provided additional strong evidence for the presence of tetrahedral intermediates in the reaction of **11** with primary amines ( $n\text{-BuNH}_2$ ,  $\text{MeOCH}_2\text{CH}_2\text{NH}_2$ ,  $\text{ClCH}_2\text{CH}_2\text{NH}_2$ ,  $\text{H}_2\text{NCOCH}_2\text{NH}_2$  and  $\text{EtO}_2\text{CCH}_2\text{NH}_2$ ) in 20%  $\text{MeCN}$ –80% water (v/v).<sup>97,98</sup> Furthermore, because in this highly polar solvent

there are no hydrogen bonding associations of the types observed in non-polar solvents which unduly complicate the situation, more clear cut conclusions could be drawn about mechanistic details. The proposed mechanism is outlined in equation (37).



The  $k_3^{\text{A}}$  and  $k_3^{\text{OH}}$  steps refer to base catalysis by the amine and by  $\text{OH}^-$ , respectively; the  $k_2$  step represents spontaneous, possibly intramolecularly catalyzed conversion of  $\text{T}^\pm$  to the product although its contribution to the overall reaction is negligible and is not included in the following kinetic analysis.

Applying the steady-state approximation to  $\text{T}^\pm$  leads to the rate law of equation (38)

$$-\frac{d[\mathbf{11}]}{dt} = \frac{d[\mathbf{50}]}{dt} = k_{\text{obsd}}[\mathbf{11}] \quad (38)$$

with the pseudo-first-order rate constant  $k_{\text{obsd}}$  given by equation (39), or the second-order rate constant,

$$k_{\text{obsd}} = \frac{k_1(k_3^{\text{A}}[\text{RNH}_2] + k_3^{\text{OH}}[\text{OH}^-])}{k_{-1} + k_3^{\text{A}}[\text{RNH}_2] + k_3^{\text{OH}}[\text{OH}^-]} [\text{R}_2\text{NH}] \quad (39)$$

$k_{\text{A}}$ , given by equation (40). The results are completely consistent with equation (40).

$$\begin{aligned}
 k_{\text{A}} &= \frac{k_{\text{obsd}}}{[\text{RNH}_2]} = \frac{k_1(k_3^{\text{A}}[\text{RNH}_2] + k_3^{\text{OH}}[\text{OH}^-])}{k_{-1} + k_3^{\text{A}}[\text{RNH}_2] + k_3^{\text{OH}}[\text{OH}^-]} \\
 &= \frac{k_1((k_3^{\text{A}}/k_{-1})[\text{RNH}_2] + (k_3^{\text{OH}}/k_{-1})[\text{OH}^-])}{1 + (k_3^{\text{A}}/k_{-1})[\text{RNH}_2] + (k_3^{\text{OH}}/k_{-1})[\text{OH}^-]} \quad (40)
 \end{aligned}$$

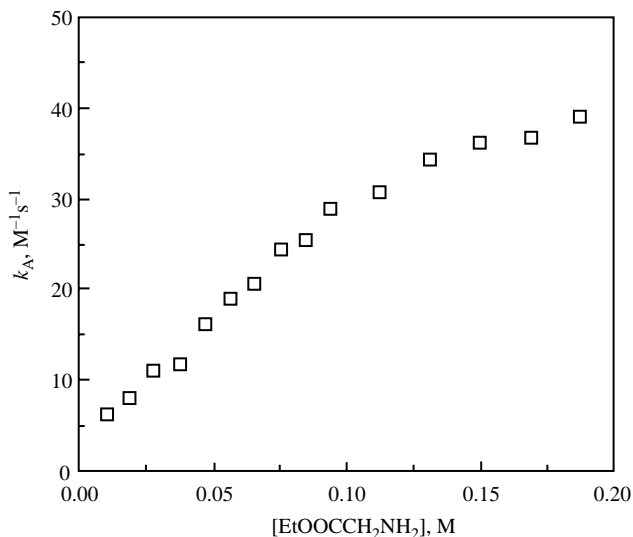
Representative plots of  $k_{\text{A}}$  versus  $[\text{RNH}_2]$  and  $[\text{OH}^-]$  are shown in Figs. 2 and 3, respectively. At low  $[\text{RNH}_2]$  and low  $[\text{OH}^-]$  equation (40) simplifies to equation (41), because  $(k_3^{\text{A}}/k_{-1})[\text{RNH}_2] + (k_3^{\text{OH}}/k_{-1})[\text{OH}^-] \ll 1$ ,

$$k_{\text{A}} = k_1 \frac{k_3^{\text{A}}}{k_{-1}} [\text{RNH}_2] + k_1 \frac{k_3^{\text{OH}}}{k_{-1}} [\text{OH}^-] \quad (41)$$

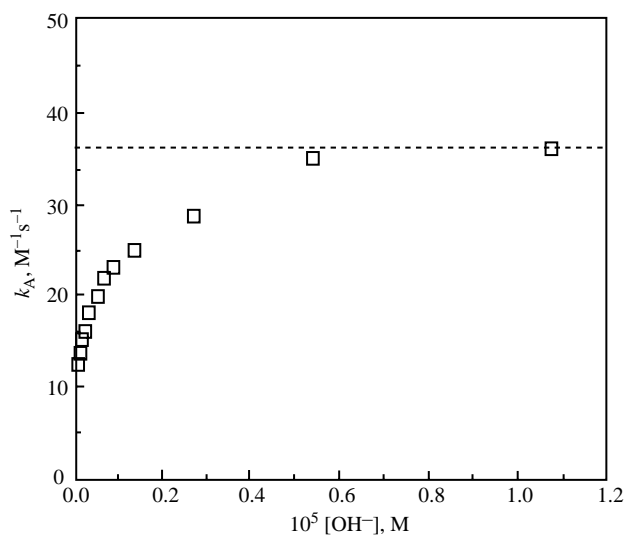
i.e.,  $k_{\text{A}}$  increases linearly with increasing  $[\text{RNH}_2]$  or  $[\text{OH}^-]$ .

At high  $[\text{RNH}_2]$  and/or high  $[\text{OH}^-]$  equation (40) is reduced to equation (42).

$$k_{\text{A}} = k_1 \quad (42)$$



**Fig. 2** Reaction of  $(CO)_5Cr=C(OMe)Ph$  (**11**) with glycine ethyl ester in 20% MeCN–80% water at 25°C. Second-order rate constants as a function of amine concentration. (Figure taken from Ref. 97, by permission from the American Chemical Society.)

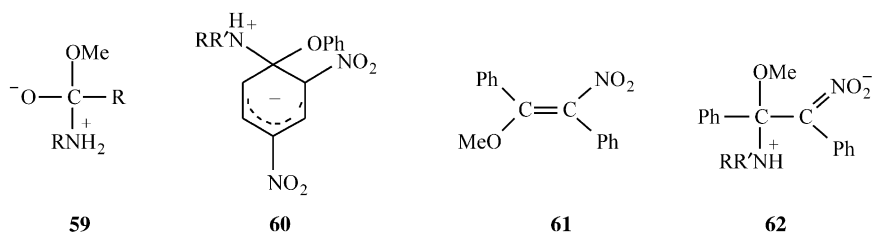


**Fig. 3** Reaction of  $(CO)_5Cr=C(OMe)Ph$  (**11**) with glycine ethyl ester in 20% MeCN–80% water at 25°C. Second-order rate constants as function of  $[OH^-]$ . (Figure taken from Ref. 97, by permission from the American Chemical Society.)

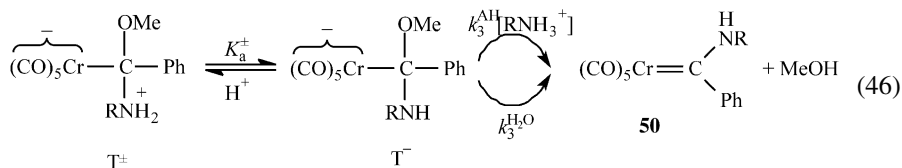




limiting.<sup>102–104</sup>



The second mechanism is shown in equation (46).



Here the proton transfer is a fast equilibrium and general acid-catalyzed loss of the methoxide ion by  $\text{RNH}_3^+$  and water, respectively, is rate limiting. For this mechanism  $k_3^{\text{A}}$  and  $k_3^{\text{OH}}$  are given by equations (47) and (48), respectively,

$$k_3^{\text{A}} = k_3^{\text{AH}} K_a^\pm / K_a^{\text{AH}} \quad (47)$$

$$k_3^{\text{OH}} = k_3^{\text{H}_2\text{O}} K_a^\pm / K_w \quad (48)$$

with  $K_a^{\text{AH}}$  being the acidity constant of  $\text{RNH}_3^+$  and  $K_w$  the ionic product of the solvent. An example where this second mechanism prevails is the aminolysis of strongly activated vinylic compounds such as  $\beta$ -methoxy- $\alpha$ -nitrostilbene (**61**), i.e., deprotonation of the corresponding zwitterionic intermediate (**62**) is fast and methoxide ion departure is rate limiting.<sup>105,106</sup>

For the aminolysis of **11**, rate-limiting deprotonation of  $\text{T}^\pm$  can be excluded on the basis of the  $k_3^{\text{OH}}/k_3^{\text{A}}$  ratios. These ratios increase from 240 for the *n*-BuNH<sub>2</sub> reaction to  $1.54 \times 10^5$  for the glycine ethyl ester reaction (Table 6). If proton transfer were rate limiting, these ratios should, according to equations (44) and (45), be given by equation (49).

$$k_3^{\text{OH}}/k_3^{\text{A}} = k_{3\text{p}}^{\text{OH}}/k_{3\text{p}}^{\text{A}} \quad (49)$$

The rate constant  $k_{3\text{p}}^{\text{OH}}$  refers to an essentially diffusion controlled proton transfer; it should be independent of the amine and have a value around  $10^{10} \text{ M}^{-1} \text{ s}^{-1}$ .<sup>107</sup> The rate constant  $k_{3\text{p}}^{\text{A}}$  should also be independent of the amine since an increase in the acidity of  $\text{RNH}_3^+$  should have a similar effect on the  $\text{p}K_a$  of  $\text{T}_A^\pm$ ; hence the  $\text{p}K_a$  difference between  $\text{T}_A^\pm$  and the respective  $\text{RNH}_3^+$  is expected to be constant. Furthermore, the  $\text{p}K_a^\pm$  of  $\text{T}^\pm$  is likely to be somewhat lower than the  $\text{p}K_a$  of the respective  $\text{RNH}_3^+$ ,<sup>97</sup> which would make the proton transfer from  $\text{T}_A^\pm$  to  $\text{RNH}_2$

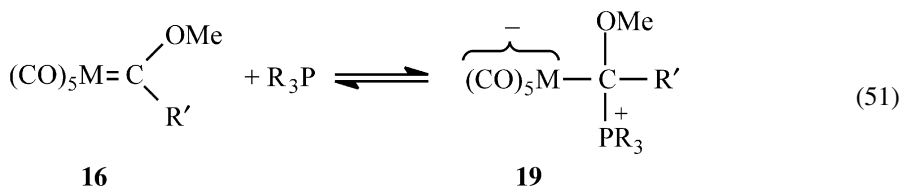
thermodynamically favorable, with a rate constant close to diffusion control,<sup>107</sup> probably of the order of  $4 \times 10^8 - 2 \times 10^9 \text{ M}^{-1} \text{ s}^{-1}$ .<sup>108</sup> Hence the  $k_3^{\text{OH}}/k_3^{\text{A}}$  ratios should be independent of the amine and have values of the order of 5–25. This contrasts with the experimental observation of a 640-fold change between *n*-butylamine and glycine ethyl ester.

On the other hand, the strong increase in the  $k_3^{\text{OH}}/k_3^{\text{A}}$  ratio with decreasing basicity of the amine is easily accounted for in terms of the mechanism of equation (46). According to equations (47) and (48), the  $k_3^{\text{OH}}/k_3^{\text{A}}$  ratio is given by equation (50). The  $K_{\text{a}}^{\text{AH}}/K_{\text{w}}$  ratio is proportional to  $K_{\text{a}}^{\text{AH}}$  while the  $k_3^{\text{H}_2\text{O}}/k_3^{\text{AH}}$  decreases somewhat with decreasing amine basicity because  $\text{RNH}_3^+$  becomes a better acid catalyst but overall  $k_3^{\text{OH}}/k_3^{\text{A}}$  increases with decreasing amine basicity.

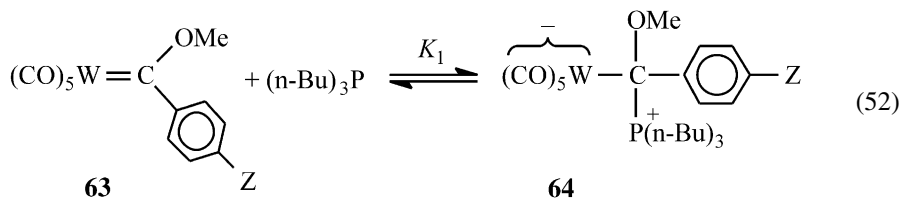
$$\frac{k_3^{\text{OH}}}{k_3^{\text{A}}} = \frac{k_3^{\text{H}_2\text{O}} K_{\text{a}}^{\text{AH}}}{k_3^{\text{AH}} K_{\text{w}}} \quad (50)$$

#### PHOSPHINE AND PHOSPHITE NUCLEOPHILES

With respect to nucleophilic attack on the carbene carbon, there are strong similarities between the reactions of phosphines or phosphites and those of amines. The reactions are exemplified by equation (51).<sup>1,47,109–111</sup> However, as discussed previously, **19** tends to rearrange to **17** (equation 12b), a process not observed with amine nucleophiles.



As discussed earlier, equilibrium constants for the addition of several tertiary phosphines (*n*-Bu)<sub>3</sub>P, Ph(C<sub>2</sub>H<sub>5</sub>)<sub>2</sub>P and (*i*-Pr)<sub>3</sub>P to (CO)<sub>5</sub>Cr=C(OMe)CH<sub>3</sub> and (CO)<sub>5</sub>W=C(OMe)CH<sub>3</sub> in toluene-*d*<sub>8</sub> have been reported by Fischer *et al.*<sup>47</sup> (Table 2). In a follow-up study, Fischer<sup>112</sup> investigated the temperature and substituent effect on the equilibrium constant for the reaction (52) in toluene (Z = MeO, Me, H, Br and CF<sub>3</sub>).



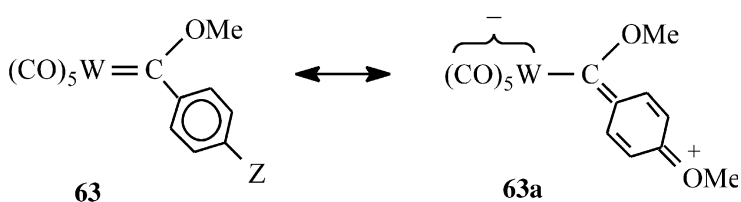
**Table 7** Thermodynamic parameters for the reaction of  $(\text{CO})_5\text{W}=\text{C}(\text{OMe})\text{C}_6\text{H}_4\text{Z}$  (**63**) with  $(n\text{-Bu})_3\text{P}$  (equation 52) in toluene at  $-48^\circ\text{C}$ 

Z	$\Delta G^\circ$ (kcal mol <sup>-1</sup> )	$\Delta H^\circ$ (kcal mol <sup>-1</sup> )	$\Delta S^\circ$ (cal mol <sup>-1</sup> deg <sup>-1</sup> )	log $K_1$
MeO	-1.20	-12.1	-43.5	1.04
Me	-2.44	-12.3	-39.5	2.13
H	-2.99	-12.7	-38.7	2.61
Br	-3.44	-13.4	-39.7	3.02
CF <sub>3</sub>	-4.26	-14.1	-39.2	3.72

Reference 112.

$\Delta G^\circ$ ,  $\Delta H^\circ$ ,  $\Delta S^\circ$  and log  $K_1$  values are summarized in Table 7. The  $K_1$  values show a strong dependence on Z. The log  $K_1$  values for Z = Me, H, Br and CF<sub>3</sub> correlate well with the Hammett  $\sigma$  constants from which one calculates  $\rho = 2.2$ ; the point for Z = MeO deviates negatively by about 0.9 log units from the Hammett line defined by the other substituents.

The negative deviation for the methoxy derivative is also seen in a correlation of log  $K_1$  with the vibrational CO force constants obtained from IR measurements; the more negative  $\Delta S^\circ$  values are further testimony to the deviant behavior of the methoxy derivative. Even though not stated in these terms by Fischer,<sup>112</sup> the most plausible source of the deviations with Z = MeO is the strong  $\pi$ -donor effect of the methoxy group (**63a**) which leads to a substantial stabilization of the carbene complex. The reduced CO vibrational force constants for the methoxy derivative are consistent with this explanation.



Also not discussed by the author are the possible reasons for the rather strong substituent dependence of  $K_1$  as reflected in the  $\rho$  value of 2.2. We offer the following interpretation. The positive  $\rho$  value implies that electron withdrawing substituents stabilize the adduct (**64**) and/or destabilize the carbene complex. Since in the adduct there is both a positive and a negative charge, the net substituent effect on this species cannot be very large; in view of the fact that the negative charge is more dispersed than the positive charge, an argument could be made that there should actually be a slight net *destabilization* of **64**. Hence the main factor that can account for the positive  $\rho$  value is a destabilization of the carbene complex, which is best understood in terms of an increased electron deficiency of the carbene carbon. A

**Table 8** Rate and equilibrium constants for the reaction of  $\text{PR}_3$  with  $(\text{CO})_5\text{M}=\text{C}(\text{OMe})\text{R}'$  in acetone at  $25^\circ\text{C}$  (equation 51)

M	R'	PR <sub>3</sub>	$k_1$ ( $\text{M}^{-1} \text{s}^{-1}$ )	$k_{-1}$ ( $\text{s}^{-1}$ )	$K_1^a$ ( $\text{M}^{-1}$ )
Cr	Me	P( <i>n</i> -Bu) <sub>3</sub>	34.7	0.70	50
Mo	Me	P( <i>n</i> -Bu) <sub>3</sub>	263	<sup>b</sup>	> 250
W	Me	P( <i>n</i> -Bu) <sub>3</sub>	225	1.2	200
Cr	Me	P( <i>n</i> -OBu) <sub>3</sub>	1.15	0.24	4.8
Mo	Me	P( <i>n</i> -OBu) <sub>3</sub>	10.4	0.26	40
W	Me	P( <i>n</i> -OBu) <sub>3</sub>	7.27	0.35	21
Cr	Ph	P( <i>n</i> -Bu) <sub>3</sub>	111	20.9	5.3
Mo	Ph	P( <i>n</i> -Bu) <sub>3</sub>	830	8.0	100
W	Ph	P( <i>n</i> -Bu) <sub>3</sub>	560	10.5	53
Cr	Ph	P( <i>n</i> -OBu) <sub>3</sub>	3.00	0.095	32
Mo	Ph	P( <i>n</i> -OBu) <sub>3</sub>	28.5	<sup>b</sup>	> 140
W	Ph	P( <i>n</i> -OBu) <sub>3</sub>	13.4	0.32	42

Reference 113.

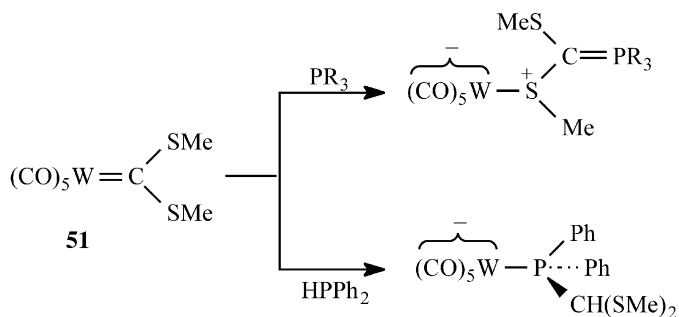
<sup>a</sup>Calculated as  $k_1/k_{-1}$ .<sup>b</sup>Too small for an accurate determination.

similar conclusion has recently been reached regarding the substituent effect on the reaction of **63** with *n*-BuNH<sub>2</sub> in 50% MeCN–50% water.<sup>98</sup>

Reactions of the type of equation (51) have also been the subject of a kinetic investigation.<sup>113</sup> Rate constants in the forward ( $k_1$ ) and reverse direction ( $k_{-1}$ ) were determined for a number of combinations of R, R', M in acetone at  $25^\circ\text{C}$ . The results are summarized in Table 8. A major conclusion drawn from these results is that steric effects are important. In the absence of steric effects one would expect  $K_1$  to show the following patterns: (i) It should be larger for P(*n*-Bu)<sub>3</sub> than for P(*n*-OBu)<sub>3</sub> because the former is more basic. (2) It should be larger for R' = Ph than R' = Me because the former is more electron withdrawing. For the methyl carbene complex (R' = Me)  $K_1$  is indeed larger with P(*n*-Bu)<sub>3</sub> than with P(*n*-OBu)<sub>3</sub> but for the bulkier phenylcarbene complex (R' = Ph) the  $K_1$  values for the two nucleophiles are comparable or even smaller with P(*n*-Bu)<sub>3</sub> in the case of the chromium complex. This reversal reflects the larger size of P(*n*-Bu)<sub>3</sub> relative to P(*n*-OBu)<sub>3</sub>.<sup>113</sup>

Interestingly, most of the steric effect that affects the equilibrium constants is expressed in  $k_{-1}$  while  $k_1$  is relatively unaffected. This is clearly seen in the large increase in  $k_{-1}$  for the change from R' = Me to R' = Ph with P(*n*-Bu)<sub>3</sub> as the nucleophile. These results suggest a transition state with little P–C bond formation in the  $k_1$  direction.

Phosphine and phosphite addition to dithiocarbene complexes such as **51** has also been reported.<sup>113,114</sup> Different products are obtained depending on whether the reaction is with a tertiary or a secondary phosphine (Scheme 6). The rate law for the

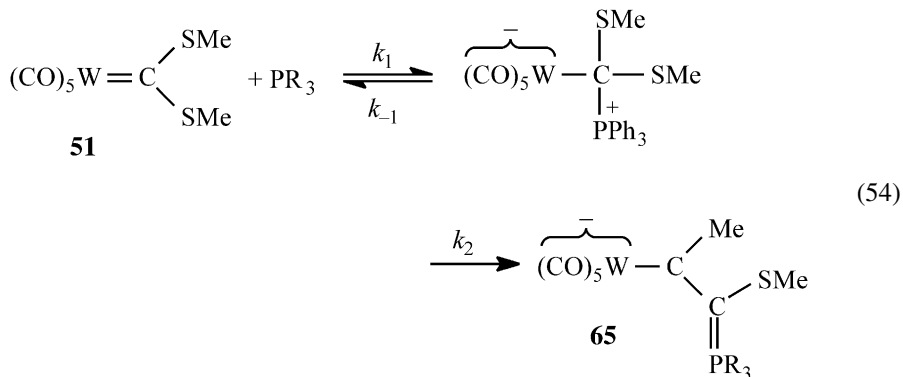


Scheme 6

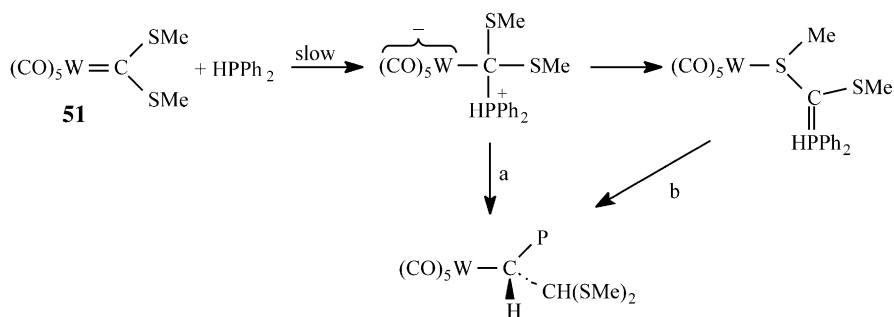
reactions of **51** with  $\text{PEt}_3$ ,  $\text{HPMe}_2$ ,  $\text{P(Ph)}_2\text{Me}$ ,  $\text{HPPH}_2$  and  $\text{P(OMe)}_3$  is given by equation (53).<sup>114</sup>

$$-\frac{d[\mathbf{51}]}{dt} = k[\mathbf{51}][\text{phosphine}] \quad (53)$$

The mechanism proposed for the reaction with tertiary phosphines is shown in equation (54).



Two possibilities were discussed: rate-limiting nucleophilic attack ( $k_2 \gg k_{-1}$ ;  $k_2 \gg k_1$ ) and rate-limiting rearrangement of the tetrahedral intermediate to the product ( $k_{-1} \gg k_2$ ;  $k_{-1} \gg k_1$ ). The authors favored the first based on the trend in the experimental  $k$  values that follow the basicities of the phosphines, i.e.,  $\text{PEt}_3 > \text{HPMe}_2 \approx \text{PPh}_2(\text{Me}) > \text{HPPH}_2 > \text{P(OMe)}_3$ . This interpretation is supported by the fact that  $\text{HPPH}_2$  fits into this order even though the reaction leads to a different product but apparently also involves rate-limiting nucleophilic attack on the carbene carbon. The proposed mechanism for this latter reaction is shown in Scheme 7. The rate-limiting nucleophilic addition of the phosphine is followed either by a direct rapid rearrangement involving H atom migration to

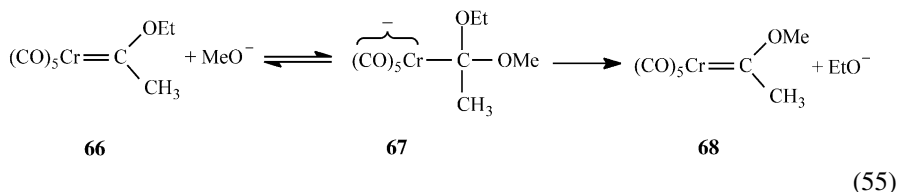


Scheme 7

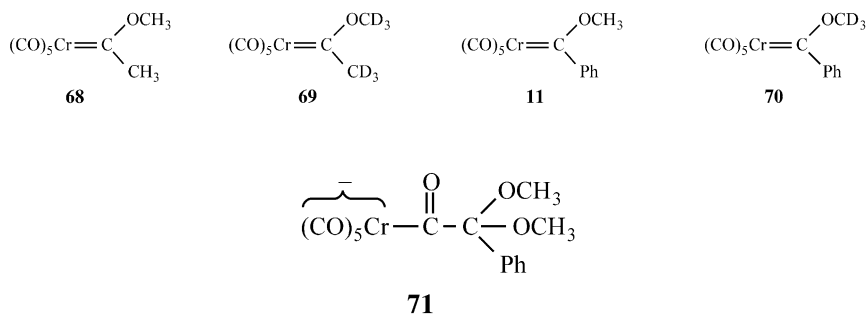
the carbon and P migration to the metal (path a) or by step-wise rearrangement according to path b.

## ALCOHOLS AND ALKOXIDE ION NUCLEOPHILES

In 1968, Kreiter<sup>115</sup> reported that the ethoxymethylcarbene complex **66** reacts with excess of methanol in the presence of catalytic amounts of NaOMe at room temperature to yield the corresponding methoxymethyl carbene complex. This reaction implies a process such as shown in equation (55).



Similar conclusions were reached by Schubert and Fischer<sup>116</sup> who showed that **68** in CD<sub>3</sub>OD in the presence of catalytic amounts of NaOCD<sub>3</sub> is rapidly converted to **69**, and **11** is converted to **70**. No direct evidence for the tetrahedral intermediate was obtained, though, because it reacts further to form products such as **71**.<sup>116,117</sup>



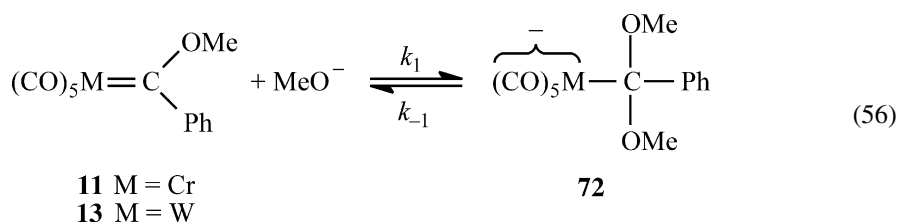
**Table 9** Rate and equilibrium constants for the reaction of  $(\text{CO})_5\text{Cr}=\text{C}(\text{OMe})\text{Ph}$  (**11**) and  $(\text{CO})_5\text{W}=\text{C}(\text{OMe})\text{Ph}$  (**13**) with  $\text{MeO}^-$  in methanol at  $25^\circ\text{C}$  (equation 56)

Parameter	<b>11</b>	<b>13</b>
$k_1$ ( $\text{M}^{-1} \text{s}^{-1}$ )	77.1	186
$k_{-1}$ ( $\text{s}^{-1}$ )	1.10	1.68
$K_1^a$ ( $\text{M}^{-1}$ )	70.1	111
$k_{-1}^{\text{BH}}$ ( $\text{M}^{-1} \text{s}^{-1}$ ) ( $\text{C}_6\text{H}_5\text{OH}$ ) <sup>b</sup>	9.43	16.8
$k_{-1}^{\text{BH}}$ ( $\text{M}^{-1} \text{s}^{-1}$ ) ( $3,5\text{-Cl}_2\text{C}_6\text{H}_3\text{OH}$ ) <sup>b</sup>	772	1500
$\log k_0^c$	$\sim 0.96$	$\sim 1.25$

Reference 118.

<sup>a</sup> $K_1$  obtained as  $k_1/k_{-1}$ .<sup>b</sup>General acid-catalyzed conversion of **72** to **11** and **13** by  $\text{C}_6\text{H}_5\text{OH}$  and  $3,5\text{-Cl}_2\text{C}_6\text{H}_3\text{OH}$ , respectively.<sup>c</sup> $k_0$  is the intrinsic rate constant, see text.

Direct evidence for the symmetrical dimethoxy adducts **72** ( $\text{M} = \text{Cr}$  and  $\text{W}$ ) was obtained by recording time-resolved UV-Vis spectra of its formation during a period of about 1 s starting 10 ms after mixing **11** or **13** with a *ca.* 0.2 M NaOMe solution in methanol.<sup>118</sup>



Acidification of the solution within 1–2 s after formation of **72** leads to almost quantitative recovery of **11** or **13**, respectively, but when acidification was delayed significantly little or no  $(\text{CO})_5\text{M}=\text{C}(\text{OMe})\text{Ph}$  could be recovered. NMR and low temperature IR experiments provided additional evidence for formation of **72**.

A stopped-flow kinetic study of this reaction<sup>118</sup> yielded the results summarized in Table 9. The  $k_{-1}^{\text{BH}}$  values refer to general acid catalyzed  $\text{MeO}^-$  expulsion, most probably by a concerted process with a transition state such as **73**; in the forward direction this would correspond to general base catalyzed addition of methanol.

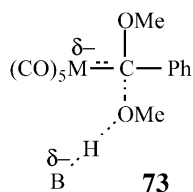
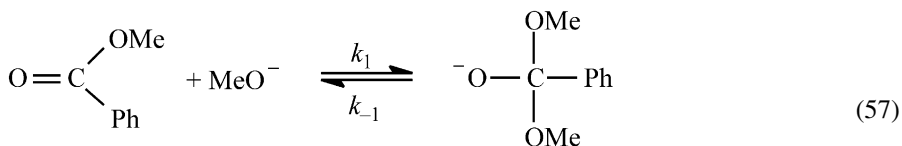




Table 9 includes an entry for  $\log k_0$ , with  $k_0$  being the *intrinsic* rate constant of the reaction which refers to the hypothetical situation where  $k_1 = k_{-1}$  and  $K_1 = 1$  or  $\Delta G^\circ = 0$ . The significance of  $k_0$  will be discussed below.

We note that the rate and equilibrium constants depend very little on the metal. This finding is reminiscent of the situation with phosphine addition (equation 51) where the kinetic and thermodynamic parameters are very similar for the Cr and W carbene complexes (Table 8).

As pointed out earlier, nucleophilic addition to Fischer carbene complexes is closely related to addition to carboxylic acid esters. The ester analog of reaction (56) is equation (57).



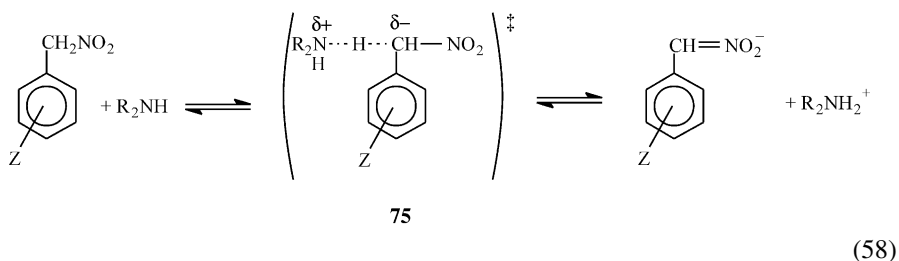
#### 74

However, the tetrahedral adduct (**74**) cannot be observed in methanol solution because the equilibrium of equation (57) is very unfavorable. An approximate  $K_1$  value between  $10^{-7}$  and  $5 \times 10^{-7} \text{ M}^{-1}$  may be estimated for equation (57), based on a combination of sources discussed in Ref. 118. This estimate suggests that formation of **72** is  $(2 \times 10^8)$ – $10^9$ -fold more favorable than formation of **74**, i.e., the  $(\text{CO})_5\text{M}$  moiety is much more effective in stabilizing negative charge than oxygen. This enhanced stabilization is in large measure attributable to a resonance effect brought about by delocalization of the negative charge into the CO ligands of **72**. Independent evidence for such charge delocalization comes from IR data. The CO stretching frequency shifts of the order of  $80$ – $90 \text{ cm}^{-1}$  observed upon conversion of **11** to **72**<sup>118</sup> indicate a reduction in the C=O double bond character of the CO ligands.

Additional insights into the resonance effect on the stabilization of **72** comes from a consideration of the rate constants  $k_1$  and  $k_{-1}$ , or, more precisely, the *intrinsic* rate constants. The general definition of the intrinsic rate constant,  $k_0$ , of a reaction with forward and reverse rate constants  $k_1$  and  $k_{-1}$ , respectively, is  $k_0 = k_1 = k_{-1}$  when  $K_1 = 1$ ; if dealing with free energies, one can define an intrinsic barrier,  $\Delta G_0^\ddagger$ , as  $\Delta G_0^\ddagger = \Delta G_1^\ddagger = \Delta G_{-1}^\ddagger$  when  $\Delta G^\circ = 0$ .<sup>119,120</sup> The significance of  $k_0$  or  $\Delta G_0^\ddagger$  is that they are purely kinetic measures of chemical reactivity because they separate out thermodynamic effects from kinetic effects and hence they allow meaningful comparisons of reactivity between different reactions.

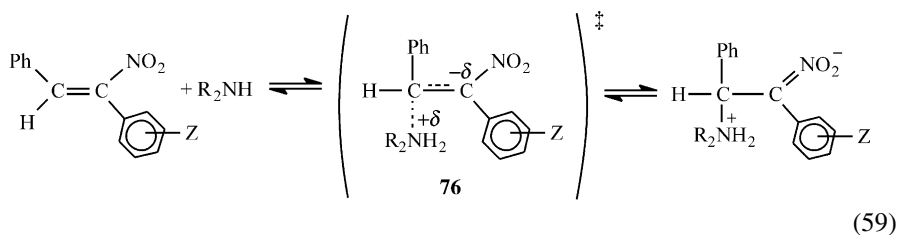
An extensive body of research has shown that reactions that lead to resonance stabilized products or involve resonance stabilized reactants that lose their resonance during the reaction invariably have higher intrinsic barriers or lower intrinsic rate constants than comparable reactions that do not involve resonance effects.<sup>121–123</sup> The underlying reason for the higher  $\Delta G_0^\ddagger$  or lower  $k_0$  values is that

the transition state is imbalanced in the sense that resonance development in the product lags behind, or the loss of resonance in the reactant is more advanced than bond changes. Such transition state imbalances have typically been inferred from Brønsted type structure reactivity coefficients. Most documented examples are from the field of proton transfers from carbon acids to a buffer base not subject to resonance effects (more on this in Section 4). In these reactions the imbalance manifests itself in the Brønsted  $\alpha$ -value (change in the rate constant for deprotonation of the carbon acid arising from the change in a remote substituent of the acid) being substantially greater than the Brønsted  $\beta$ -value (change in the rate constant for deprotonation of the carbon acid arising from a change in the buffer base basicity).<sup>121–123</sup> The best-known example is the deprotonation of substituted phenylnitromethanes by amines (equation 58) where  $\alpha = 1.29$  and  $\beta = 0.53$ .<sup>124</sup>



The reason why  $\alpha$  exceeds  $\beta$  ( $\beta$  is commonly assumed to be an approximate measure of the degree of proton transfer at the transition state<sup>125–127</sup>) is that at the transition state (75) the partial negative charge is mainly localized on the carbon and hence closer to the Z substituent than in the product ion where the charge is delocalized into the nitro group.

In nucleophilic addition reactions, the imbalance results in  $\alpha_{\text{nuc}}^{\text{n}}$  exceeding  $\beta_{\text{nuc}}^{\text{n}}$ ;  $\alpha_{\text{nuc}}^{\text{n}}$  and  $\beta_{\text{nuc}}^{\text{n}}$  are normalized structure–reactivity coefficients that are the analogs of  $\alpha$  and  $\beta$ , respectively, in proton transfers.<sup>128</sup> Note that since  $\alpha_{\text{nuc}}^{\text{n}}$  is usually obtained from the variation of a phenyl substituent, it is equal to the normalized Hammett  $\rho$  value. A representative example is shown in equation (59) where  $\alpha_{\text{nuc}}^{\text{n}} = 0.67$  and  $\beta_{\text{nuc}}^{\text{n}} = 0.37$ .<sup>129</sup> Again, the exalted  $\alpha_{\text{nuc}}^{\text{n}}$  coefficient is the result of the negative charge at the transition state 76 being closer to the Z substituent than it is in the adduct.



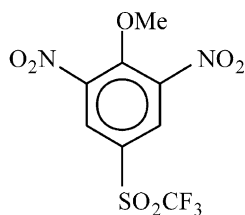
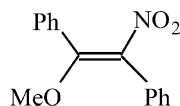
The connection between enhanced intrinsic barriers and the lack of synchrony between resonance effects and bond changes is a manifestation of a more general phenomenon called the principle of non-perfect synchronization (PNS). This principle applies to other types of transition state imbalances as well and states that any product stabilizing factor whose development at the transition state lags behind bond changes, or any reactant stabilizing factor that is lost ahead of bond changes, increases the intrinsic barrier or lowers the intrinsic rate constant.<sup>121–123</sup> Besides resonance, the kinds of stabilizing factors referred to here include solvation, hydrogen bonding effects and electrostatic effects. For factors that are *destabilizing*, e.g., steric effects, the changes in  $\Delta G_0^\ddagger$  or  $k_0$  are in the opposite direction and the same is true for stabilizing factors that develop ahead of bond formation, e.g., soft–soft, hard–hard acid–base interactions.

Intrinsic rate constants may be calculated based on the Marcus equation<sup>120</sup> although we prefer, when sufficient data are available, to obtain  $k_0$  from interpolated and extrapolated Brønsted plots.<sup>121–123</sup> For reactions (56) and (57) there were not enough data available for the construction of Brønsted plots and hence  $k_0$  was estimated based on the simplest version of the Marcus formalism (equation 60). The  $\log k_0$  values are approximately 0.96 and 1.25 for the reaction of **11** and **13** (equation 56), respectively (Table 9).

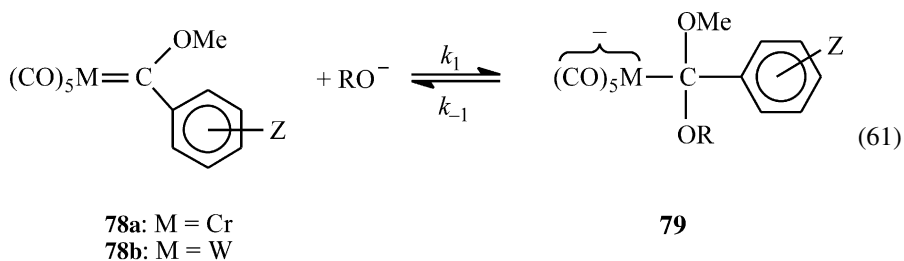
$$\log k_0 = \log k_1 - 0.5 \log K_1 \quad (60)$$

In comparison, the estimated  $\log k_0$  value for reaction (57) is 3.1,<sup>118</sup> i.e.,  $k_0$  for the Fischer carbenes is two orders of magnitude lower than for the ester. This is consistent with the fact that **72** derives a significant part of its stabilization from resonance while **74** does not.

The lowering of  $\log k_0$  for the reactions of **11** relative to the reaction of methylbenzoate, although substantial, is not as dramatic as that for the reaction of  $\text{MeO}^-$  or  $\text{OH}^-$  with nitro activated electrophiles such as **77**<sup>130</sup> ( $\log k_0 \approx -0.76$ ) or **61** ( $\log k_0 \approx -3.9$ ).<sup>131</sup> These latter  $\log k_0$  values show that the  $\pi$ -acceptor effect of nitro groups is significantly stronger than that of the  $(\text{CO})_5\text{M}$  moiety, a point to which we shall return in Section 4.

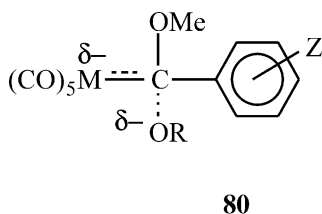
**77****61**

In an effort to examine whether reaction (56) or similar reactions in fact have an imbalanced transition state, substituent effects on the rate and equilibrium constants of the reaction of **78** with alkoxide ions (equation 61) were determined.<sup>132</sup>

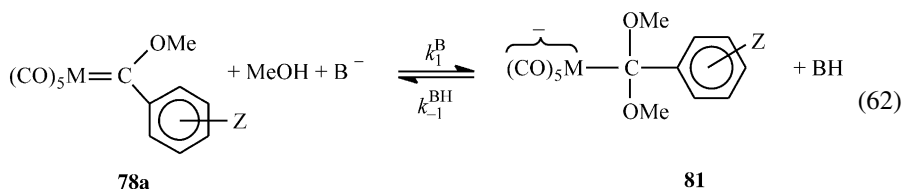


For **78a** the investigation included Z = 4-Me<sub>2</sub>N, 4-MeO, 4-Me, H, 4-F, 3-Cl and 4-CF<sub>3</sub>, for **78b** Z = 4-MeO, 4-Me, H, 4-F and 4-Cl; the nucleophile/solvent combinations used were MeO<sup>-</sup> in methanol and in 90% MeCN–10% methanol (v/v), and OH<sup>-</sup>, HC≡CCH<sub>2</sub>O<sup>-</sup> and CF<sub>3</sub>CH<sub>2</sub>O<sup>-</sup> in 50% MeCN–50% water (v/v). All reactions were at 25°C.

Some of the Hammett  $\rho$  values obtained in this study are summarized in Table 10 while  $\beta_{\text{nuc}}$ ,  $\beta_{\text{nuc}}^{\text{n}}$ , etc. for the reactions with HC≡CCH<sub>2</sub>O<sup>-</sup> and CF<sub>3</sub>CH<sub>2</sub>O<sup>-</sup> are reported in Table 11. With respect to the question of imbalance, the  $\alpha_{\text{nuc}}^{\text{n}}$  values average around  $0.56 \pm 0.05$  while for  $\beta_{\text{nuc}}^{\text{n}}$  the average is  $\leq 0.44$ , i.e.,  $\alpha_{\text{nuc}}^{\text{n}} > \beta_{\text{nuc}}^{\text{n}}$ , which suggests a transition state (**80**) with the partial negative charge residing mainly on the metal rather than dispersed into the CO ligands. The size of the imbalance is relatively modest, which is consistent with the fact that the intrinsic rate constants are only reduced by about two orders of magnitude relative to  $k_0$  for the ester reaction (equation 57).



Another type of transition state imbalance was noted by determining substituent effects on the rate and equilibrium constants for buffer-catalyzed MeOH addition to **78a** (equation 62).



**Table 10** Hammett  $\rho$  values for the reactions of alkoxide ions with  $(\text{CO})_5\text{Cr}=\text{C}(\text{OMe})\text{C}_6\text{H}_4\text{Z}$  (**78a**) and  $(\text{CO})_5\text{W}=\text{C}(\text{OMe})\text{C}_6\text{H}_4\text{Z}$  (**78b**) at 25°C (equation 61)

Reaction	$\rho(k_1)$	$\rho(k_{-1})$	$\rho(K_1)$	$\rho_n(k_1) = \alpha_{\text{nuc}}^n$	$\rho_n(k_{-1})$
<b>78a</b> + $\text{MeO}^-$ <sup>a</sup>	$2.67 \pm 0.10$	$-2.24 \pm 0.15$	$4.92 \pm 0.12$	$0.54 \pm 0.02$	$-0.46 \pm 0.2$
<b>78b</b> + $\text{MeO}^-$ <sup>a</sup>	$2.37 \pm 0.22$	$-1.67 \pm 0.17$	$4.04 \pm 0.08$	$0.59 \pm 0.05$	$-0.41 \pm 0.05$
<b>78a</b> + $\text{HC}\equiv\text{CCH}_2\text{O}^-$ <sup>b</sup>	$1.39 \pm 0.14$	$-1.06 \pm 0.11$	$2.45 \pm 0.24$	$0.57 \pm 0.01$	$-0.43 \pm 0.01$
<b>78b</b> + $\text{HC}\equiv\text{CCH}_2\text{O}^-$ <sup>b</sup>	$1.68 \pm 0.17$	$-1.39 \pm 0.16$	$3.07 \pm 0.01$	$0.55 \pm 0.05$	$-0.45 \pm 0.05$

Reference 132.

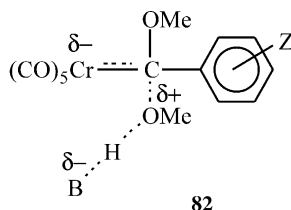
<sup>a</sup>In MeOH.<sup>b</sup>In 50% MeCN–50% water (v/v).

**Table 11** Brønsted coefficients for the reactions of  $\text{HC}\equiv\text{CCH}_2\text{O}^-$  and  $\text{CF}_3\text{CH}_2\text{O}^-$  with **78a** ( $Z = 4\text{-Cl}$ ) and **78b** ( $Z = 4\text{-Cl}$ ) in 50% MeCN–50% water at 25°C (equation 61)

	<b>78a</b> ( $Z = 4\text{-Cl}$ )	<b>78b</b> ( $Z = 4\text{-Cl}$ )
$\beta_{\text{nuc}} = d \log k_1 / d \text{p}K_{\text{a}}^{\text{ROH}}$	0.42	0.54
$\beta_{\text{lg}} = d \log k_{-1} / d \text{p}K_{\text{a}}^{\text{ROH}}$	$\leq -0.49$	$\leq -0.57$
$\beta_{\text{eq}} = d \log k_1 / d \text{p}K_{\text{a}}^{\text{ROH}}$	$\geq 0.91$	$\geq 1.11$
$\beta_{\text{nuc}}^{\text{n}} = d \log k_1 / d \log K_1$	$\leq 0.46$	$\leq 0.42$
$\beta_{\text{lg}}^{\text{n}} = d \log k_{-1} / d \log K_1$	$\leq -0.54$	$\leq -0.51$

Reference 132.

Normalized  $\rho$  values for this reaction catalyzed by three different aryloxy ions are reported in Table 12 while Brønsted coefficients for this type of catalysis are summarized in Table 13. The rather low  $\beta(k_1^{\text{B}})$  values (high  $\alpha(k_{-1}^{\text{BH}})$ ) suggest that the proton transfer from the attacking methanol nucleophile to the buffer base has made much less progress than the C–O bond formation at the transition state (or that in the reverse direction protonation of the departing  $\text{MeO}^-$  by the buffer acid is ahead of C–O bond cleavage), as shown in **82** ( $\delta^+$  on MeO group).



Finally, although not relevant with respect to the question of imbalance, some comments regarding the actual (non-normalized)  $\rho$  values for reaction (61) summarized in Table 10 are in order. The  $\rho(K_1)$  and  $\rho(k_1)$  values are seen to be significantly smaller and the  $\rho(k_{-1})$  significantly less negative for the reactions of  $\text{HC}\equiv\text{CCH}_2\text{O}^-$  in 50% MeCN–50% water than for the reactions of  $\text{MeO}^-$  in methanol. A combination of two factors appears to be responsible for this result. One

**Table 12** Normalized Hammett  $\rho$  values for buffer-catalyzed MeOH addition to  $(\text{CO})_5\text{Cr}=\text{C}(\text{OMe})\text{C}_6\text{H}_4\text{Z}$  (**78a**) in MeOH (equation 62)

$\text{B}^-$	$\rho_{\text{n}}(k_1^{\text{B}})$	$\rho_{\text{n}}(k_{-1}^{\text{BH}})$
$\text{C}_6\text{H}_5\text{O}^-$	$0.62 \pm 0.07$	$-0.38 \pm 0.07$
$4\text{-BrC}_6\text{H}_4\text{O}^-$	$0.58 \pm 0.07$	$-0.42 \pm 0.07$
$3,5\text{-Cl}_2\text{C}_6\text{H}_3\text{O}^-$	$0.59 \pm 0.06$	$-0.41 \pm 0.06$

Reference 132.

**Table 13** Brønsted coefficients for buffer catalysis of MeOH addition to  $(\text{CO})_5\text{-Cr}=\text{C}(\text{OMe})\text{C}_6\text{H}_4\text{Z}$  (**78a**) in MeOH (equation 62)

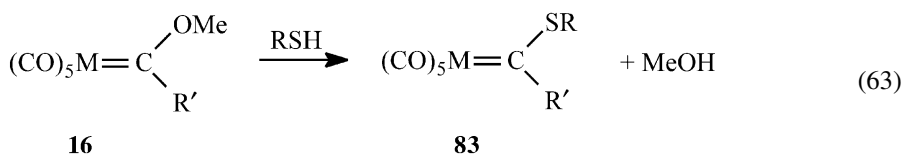
Z	$\beta(k_1^{\text{B}})$	$\alpha(k_{-1}^{\text{BH}})$
4-MeO	$0.17 \pm 0.02$	$0.83 \pm 0.02$
4-Me	$0.16 \pm 0.02$	$0.84 \pm 0.02$
H	$0.17 \pm 0.04$	$0.83 \pm 0.04$
4-F	$0.12 \pm 0.02$	$0.88 \pm 0.02$
4-Cl	$0.10 \pm 0.04$	$0.90 \pm 0.04$

Reference 132.

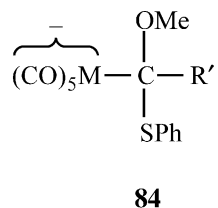
is the higher polarity of the aqueous acetonitrile ( $\epsilon = 58.8$ ) compared to that of methanol ( $\epsilon = 32.6$ ). The other is the change in the nucleophile; since the  $\text{HC}\equiv\text{CCH}_2\text{O}$  group in **79** or **80** is more electron withdrawing than the MeO group, it contributes more to the stabilization of the negative charge than the MeO group. This, just as is the case with a more polar solvent, reduces the requirement for stabilization of the charge by the Z substituent.

## THIOL AND THIOLATE ION NUCLEOPHILES

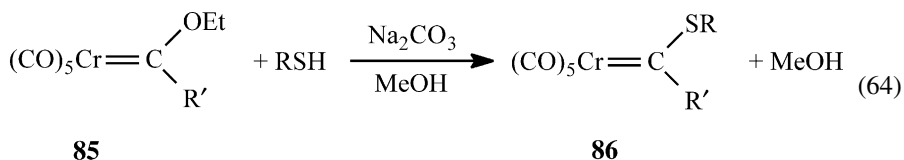
In 1972, Fischer *et al.*<sup>80</sup> reported the successful conversion of methoxy carbene complexes of the type **16** ( $\text{M} = \text{Cr}$  and  $\text{W}$ ;  $\text{R}' = \text{Me}$  and  $\text{Ph}$ ) into the thioalkyl carbene



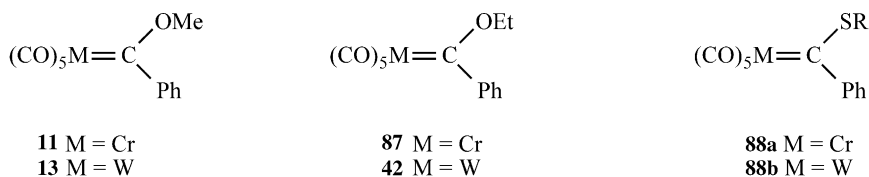
complexes **83** by treatment of the solid **16** with RSH ( $\text{R}' = \text{Me}$ , Et and Ph) in the absence of any solvent. In fact no reaction could be observed either in polar or non-polar solvents.<sup>80</sup> However, **83** ( $\text{R} = \text{Ph}$ ) was obtained in benzene–methanol mixtures when NaSPh was used as the nucleophile<sup>81</sup> in the reaction with **16** ( $\text{M} = \text{Cr}$ , Mo and W;  $\text{R}' = \text{Me}$ ). In this case there is an initial rapid formation of a stable intermediate that was assumed to be the tetrahedral adduct **84**. Subsequent addition of HCl to **84** led to conversion to products.



Using  $\text{Na}_2\text{CO}_3$  as a base catalyst in methanol, Aumann and Schröder<sup>82</sup> reacted **85** ( $\text{R}' = \text{Me}$  and  $\text{Ph}$ ) with several thiols ( $\text{R} = \text{C}_6\text{H}_{11}$ ,  $\text{Et}$ ,  $\text{Ph}$  and alkyl) to obtain the corresponding alkylthio carbene complexes, again assuming that the reaction involved a tetrahedral intermediate.



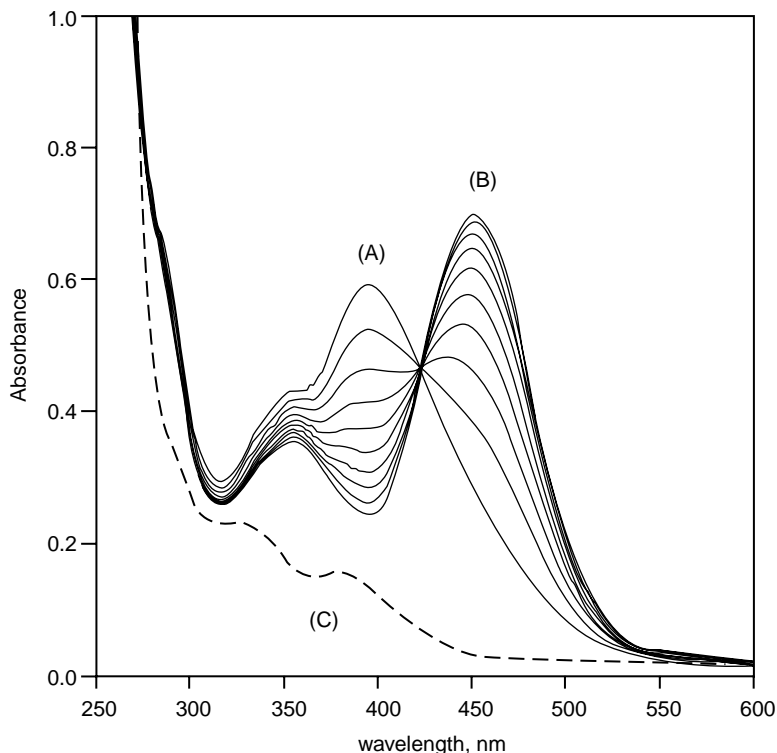
Direct evidence for the tetrahedral intermediate and its spectroscopic characterization along with a detailed kinetic study of the reactions of **11**, **13**, **42** and **87** with a series of alkane thiolate ions ( $n\text{-PrS}^-$ ,  $\text{HOCH}_2\text{CH}_2\text{S}^-$ ,  $\text{MeO}_2\text{CCH}_2\text{CH}_2\text{S}^-$  and  $\text{MeO}_2\text{CCH}_2\text{S}^-$ ) in 50%  $\text{MeCN}$ –50% water (v/v) were reported by Bernasconi *et al.*<sup>133,134</sup> Some of the salient features of these reactions can be summarized as follows.



In the presence of low thiolate ion concentrations at a pH below the  $\text{pK}_a^{\text{RSH}}$  of the thiol, a clean conversion of **11**, **13**, **42** or **87** to **88** was observed. This is shown in Fig. 4 for a representative example. The figure shows a sharp isosbestic point at 422 nm, indicating that there is no accumulation of an intermediate to detectable levels. A different situation arises at relatively high thiolate ion concentrations at a pH close to or higher than  $\text{pK}_a^{\text{RS}}$ . Here the carbene complex is rapidly converted into a new species whose UV spectrum (dashed line in Fig. 4) resembles neither that of the starting material nor that of the product. This species is stable for several minutes, but upon acidification of the solution yields the substitution product. This species is the tetrahedral intermediate, a conclusion that is not only consistent with the UV spectrum but also with IR,  $^1\text{H}$  NMR and  $^{13}\text{C}$  NMR spectra.<sup>134</sup>

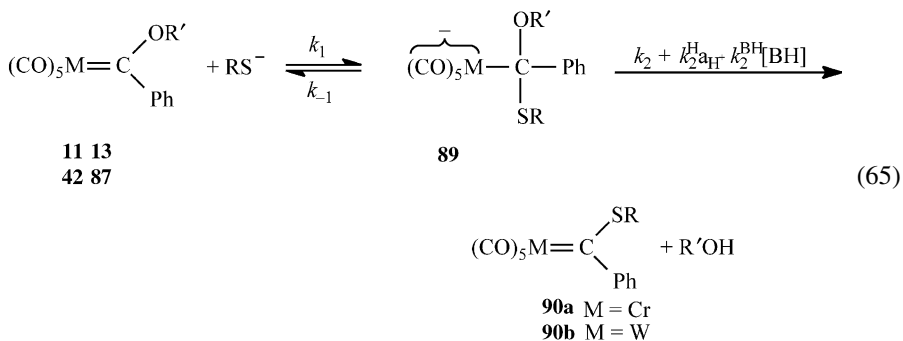
The above observations were interpreted in terms of equation (65). At high pH and high  $[\text{RS}^-]$  the first step is fast and the equilibrium favors the intermediate while





**Fig. 4** Conversion of  $5 \times 10^{-5}$  M  $(\text{CO})_5\text{W}=\text{C}(\text{OMe})\text{Ph}$  (**13**) (spectrum A) to  $(\text{CO})_5\text{W}=\text{C}(\text{SR})\text{Ph}$  (**90b**) ( $\text{R} = \text{MeOCOCH}_2\text{CH}_2$ , spectrum B) in the presence of  $7.94 \times 10^{-5}$  M  $\text{MeOCOCH}_2\text{CH}_2\text{S}^-$  and  $10^{-3}$  M  $\text{MeOCOCH}_2\text{CH}_2\text{SH}$  in an *N*-methylmorpholine buffer at pH 7.56 in 50% MeCN–50% water (v/v) at 20°C. Spectra taken every 10 s for 150 s. Spectrum C corresponds to intermediate (**89**) (equation 65) generated in the presence of  $10^{-3}$  M  $\text{MeOCOCH}_2\text{CH}_2\text{S}^-$  at pH 10.69. (Figure taken from Ref. 134, by permission from the American Chemical Society.)

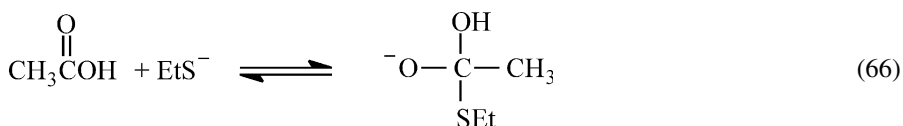
product formation is slow.



In fact spontaneous conversion of **89** to products ( $k_2$  step) is so slow that product formation only occurs after addition of acid, indicating  $H^+$  and/or buffer and catalyzed ( $k_2^H a_{H^+}$  and  $k_2^{BH}[BH]$ , respectively) alkoxide ion departure; this is reminiscent of the observations with NaSPh in benzene–methanol mixtures where product formation only occurs after addition of HCl.<sup>81</sup> At low pH, **89** turns into a steady-state intermediate because the equilibrium of the first step is no longer favorable and  $a_{H^+}$  and/or  $[BH]$  are high enough to ensure rapid product formation via the  $k_2^H a_{H^+}$  and/or  $k_2^{BH}[BH]$  pathways; this essentially corresponds to the situation in methanol in the presence of  $Na_2CO_3$  as reported by Aumann and Schröder.<sup>82</sup>

Kinetic analysis confirmed the above picture and allowed a determination of  $k_1$ ,  $k_{-1}$ ,  $k_2^H$  and  $k_2^{BH}$  ( $B = N$ -methylmorpholinium ion). A summary of the various rate and equilibrium constants is provided in Table 14. Several conclusions of general interest emerge from these data.

(1) As pointed out earlier, the reactivity of pentacarbonyl-type Fischer carbene complexes towards nucleophiles is much higher than that of carboxylic esters. For example,  $K_1$  for  $MeO^-$  addition to **11** (equation 56) is approximately  $2 \times 10^8$ – $10^9$  higher than for  $MeO^-$  addition to methylbenzoate. A comparison of  $K_1$  for  $n$ -PrS<sup>-</sup> addition to **11** ( $1.06 \times 10^4 M^{-1}$ ) with Guthrie's<sup>135</sup> estimate of  $K_1 \approx 7.9 \times 10^{-14} M^{-1}$  for EtS<sup>-</sup> addition to acetic acid in water (equation 66) suggests an even greater reactivity difference ( $\approx 1.3 \times 10^{17}$ -fold) between the Fischer carbene complex and the acryl analog.



This enhanced reactivity difference for thiolate addition has been attributed to the combination of two factors.<sup>134</sup> The first is the favorable soft acid–soft base<sup>136,137</sup> interaction for the reaction of the soft carbene complex with the soft thiolate ion which contrasts with the unfavorable hard acid ( $CH_3COH$ )–soft base ( $EtS^-$ ) interaction in reaction (66). The second is the favorable hard acid–hard base interaction between the hard  $MeO^-$  with the hard methylbenzoate which contrasts with the unfavorable soft acid–hard base interaction in the reaction of the carbene complex with  $MeO^-$ .

(2) Relative to their proton basicities, the thiolate ions are much more reactive towards Fischer carbene complexes than alkoxide ions. For example, for the reaction of  $n$ -PrS<sup>-</sup> ( $pK_a^{RSH} = 11.94$ ) with **11**,  $K_1 = 1.06 \times 10^4 M^{-1}$  and  $k_1 = 1.34 \times 10^4 M^{-1} s^{-1}$  (Table 14), while for the reaction of  $HC \equiv CCH_2O^-$  ( $pK_a^{ROH} = 13.68$ ) with **11**,  $K_1 = 1.67 \times 10^2 M^{-1}$  and  $k_1 = 47 M^{-1} s^{-1}$ .<sup>132</sup> These comparisons demonstrate the well-known high carbon basicity and high nucleophilicity of sulfur bases which have been mainly attributed to their strong polarizability<sup>138,139</sup> or softness.<sup>136,137</sup> As pointed out above, the softness of the carbene complex enhances the effect of the soft nucleophile. An additional factor,

**Table 14** Rate and equilibrium constants for the reactions of **11**, **13**, **47** and **87** with various thiolate ions in 50% MeCN–50% water, v/v) at 25°C (equation 65)

	CH <sub>3</sub> CH <sub>2</sub> CH <sub>2</sub> S <sup>-</sup> (pK <sub>a</sub> <sup>RSH</sup> = 11.94)	HOCH <sub>2</sub> CH <sub>2</sub> S <sup>-</sup> (pK <sub>a</sub> <sup>RSH</sup> = 10.79)	MeO <sub>2</sub> CCH <sub>2</sub> CH <sub>2</sub> S <sup>-</sup> (pK <sub>a</sub> <sup>RSH</sup> = 10.69)	MeO <sub>2</sub> CCH <sub>2</sub> S <sup>-</sup> (pK <sub>a</sub> <sup>RSH</sup> = 9.45)
(CO) <sub>5</sub> Cr=C(OMe)Ph ( <b>11</b> )				
<i>k</i> <sub>1</sub> (M <sup>-1</sup> s <sup>-1</sup> )	1.34 × 10 <sup>4</sup>	2.25 × 10 <sup>4</sup>	2.30 × 10 <sup>4</sup>	6.76 × 10 <sup>4</sup>
<i>k</i> <sub>2</sub> <sup>H</sup> (M <sup>-1</sup> s <sup>-1</sup> )	5.39 × 10 <sup>8</sup>	3.50 × 10 <sup>8</sup>	1.99 × 10 <sup>8</sup>	
<i>k</i> <sub>-1</sub> (s <sup>-1</sup> )	1.26	5.01	6.55	
<i>K</i> <sub>1</sub> = <i>k</i> <sub>1</sub> / <i>k</i> <sub>-1</sub> (M <sup>-1</sup> )	1.06 × 10 <sup>4</sup>	4.49 × 10 <sup>3</sup>	3.51 × 10 <sup>3</sup>	
<i>k</i> <sub>2</sub> <sup>BH</sup> (M <sup>-1</sup> s <sup>-1</sup> ) <sup>a</sup>		1.39 × 10 <sup>2</sup>	6.88 × 10 <sup>1</sup>	
(CO) <sub>5</sub> W=C(OMe)Ph ( <b>13</b> )				
<i>k</i> <sub>1</sub> (M <sup>-1</sup> s <sup>-1</sup> )	4.21 × 10 <sup>4</sup>	6.52 × 10 <sup>4</sup>	7.26 × 10 <sup>4</sup>	1.73 × 10 <sup>5</sup>
<i>k</i> <sub>2</sub> <sup>H</sup> (M <sup>-1</sup> s <sup>-1</sup> )	5.69 × 10 <sup>8</sup>	3.76 × 10 <sup>8</sup>	2.05 × 10 <sup>8</sup>	
<i>k</i> <sub>-1</sub> (s <sup>-1</sup> )	3.11	14.0	16.3	
<i>K</i> <sub>1</sub> = <i>k</i> <sub>1</sub> / <i>k</i> <sub>-1</sub> (M <sup>-1</sup> )	1.35 × 10 <sup>4</sup>	4.66 × 10 <sup>3</sup>	4.45 × 10 <sup>3</sup>	
<i>k</i> <sub>2</sub> <sup>BH</sup> (M <sup>-1</sup> s <sup>-1</sup> ) <sup>a</sup>		2.17 × 10 <sup>2</sup>	1.46 × 10 <sup>2</sup>	
(CO) <sub>5</sub> Cr=C(OEt)Ph ( <b>42</b> )				
<i>k</i> <sub>1</sub> (M <sup>-1</sup> s <sup>-1</sup> )	7.05 × 10 <sup>3</sup>	1.20 × 10 <sup>4</sup>	1.20 × 10 <sup>4</sup>	3.43 × 10 <sup>4</sup>
<i>k</i> <sub>2</sub> <sup>H</sup> (M <sup>-1</sup> s <sup>-1</sup> )	4.23 × 10 <sup>8</sup>	2.67 × 10 <sup>8</sup>	1.68 × 10 <sup>8</sup>	
<i>k</i> <sub>-1</sub> (s <sup>-1</sup> )	1.38	9.08	9.88	
<i>K</i> <sub>1</sub> = <i>k</i> <sub>1</sub> / <i>k</i> <sub>-1</sub> (M <sup>-1</sup> )	5.11 × 10 <sup>3</sup>	1.32 × 10 <sup>3</sup>	1.21 × 10 <sup>3</sup>	
<i>k</i> <sub>2</sub> <sup>BH</sup> (M <sup>-1</sup> s <sup>-1</sup> ) <sup>a</sup>		8.40 × 10 <sup>1</sup>	4.33 × 10 <sup>1</sup>	
(CO) <sub>5</sub> W=C(OEt)Ph ( <b>87</b> )				
<i>k</i> <sub>1</sub> (M <sup>-1</sup> s <sup>-1</sup> ) <sup>a</sup>	2.33 × 10 <sup>4</sup>	4.04 × 10 <sup>4</sup>	4.25 × 10 <sup>4</sup>	1.05 × 10 <sup>5</sup>
<i>k</i> <sub>2</sub> <sup>H</sup> (M <sup>-1</sup> s <sup>-1</sup> )	5.12 × 10 <sup>8</sup>	2.65 × 10 <sup>8</sup>	1.84 × 10 <sup>8</sup>	
<i>k</i> <sub>-1</sub> (s <sup>-1</sup> )	2.98 ± 0.33	20.7	26.4	
<i>K</i> <sub>1</sub> = <i>k</i> <sub>1</sub> / <i>k</i> <sub>-1</sub> (M <sup>-1</sup> )	7.82 × 10 <sup>3</sup>	1.95 × 10 <sup>3</sup>	1.61 × 10 <sup>3</sup>	
<i>k</i> <sub>2</sub> <sup>BH</sup> (M <sup>-1</sup> s <sup>-1</sup> ) <sup>a</sup>		9.23 × 10 <sup>1</sup>	6.47 × 10 <sup>1</sup>	

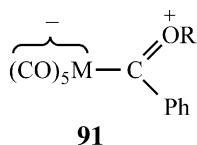
Reference 134.

<sup>a</sup>BH = *N*-methylmorpholinium ion.

particularly important in hydroxylic solvents, is the weaker solvation of thiolate ions compared to that of alkoxide ions.

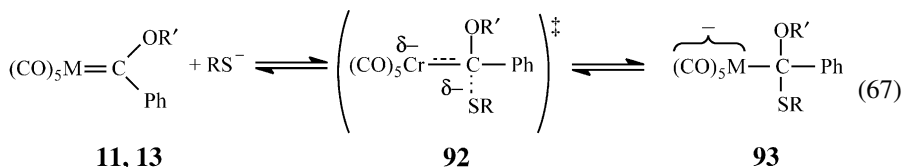
(3) Using equation (60), one can calculate approximate intrinsic rate constants for thiolate ion addition. For the reaction of  $n\text{-PrS}^-$  with **11** and **13** one obtains  $\log k_0 \approx 2.11$  and  $\approx 2.56$ , respectively. This compares with  $\log k_0 \approx 0.96$  and  $\approx 1.25$  for the reaction of  $\text{MeO}^-$  in methanol with **11** and **13**, respectively, or  $\log k_0 \approx 0.74$  and  $\approx 0.94$  for the reactions of  $\text{HC}\equiv\text{CCH}_2\text{O}^-$  in 50% MeCN–50% water with **11** and **13**, respectively.<sup>132</sup> The differences in the intrinsic rate constants between the thiolate and alkoxide ion reactions are believed to be the result of transition states that are imbalanced with respect to the factors that are responsible for the differences in the equilibrium constants, i.e., the strong solvation of the alkoxide ions<sup>134</sup> and the soft–soft interactions in the thiolate ion reactions. Specifically, following generally observed behavior,<sup>140,141</sup> the partial desolvation of the nucleophile that occurs as it enters the transition state should be more advanced than bond formation according to the rules of the PNS.<sup>121,122</sup> This has the effect of reducing  $k_0$  and more so for the reactions with the more strongly solvated alkoxide ions. Regarding the soft–soft interactions, it is not unreasonable to assume that they are more advanced than bond formation at the transition state,<sup>142</sup> which has the effect of enhancing  $k_0$  for the thiolate ion reactions. Hence both factors reinforce each other in increasing the difference in the intrinsic rate constants of these reactions.

(4) Nucleophilic addition to the tungsten carbene complexes is slightly favored over addition to chromium complexes. The effect on  $K_1$  is minimal but somewhat larger on  $k_1$ . The  $K_1(\text{W})/K_1(\text{Cr})$  ratios vary between 1.27 and 1.53, the  $k_1(\text{W})/k_1(\text{Cr})$  ratios between 2.56 and 3.54 (Table 14). Similar results were found for  $\text{MeO}^-$  addition to **11** and **13**:  $K_1(\text{W})/K_1(\text{Cr}) = 1.58$ ,  $k_1(\text{W})/k_1(\text{Cr}) = 2.41$  (Table 9). The rather small dependence of  $K_1$  on the metal may be the result of the extensive dispersion of the negative charge into the CO ligands of the adducts. Since this leaves little charge on the metal, the identity of the metal has only a small influence on the stability of the adduct. An additional factor is related to the strong contribution of **91** to the structure of **11** or **13**. Because **91** leads to substantial negative charge on the  $(\text{CO})_5\text{M}$  moiety of the carbene complex, the presumably greater stabilization of the negative charge by the  $(\text{CO})_5\text{W}$  moiety in the adduct is partially offset by a similar effect on the carbene complex, a point to which we shall return in Section 4.

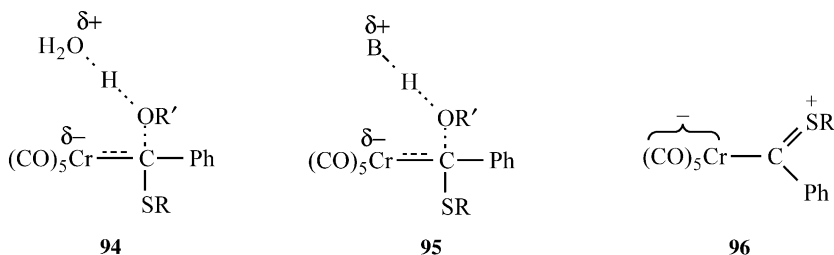


The fact that the  $k_1$  values show a somewhat greater dependence on the metal than  $K_1$  and that not only  $k_1$  but also  $k_{-1}$  is larger for the tungsten complexes is noteworthy; it means that the *intrinsic* rate constant is somewhat higher for the tungsten complexes than for the chromium complexes. This can be understood with

reference to equation (67). If, due to the typical imbalance, the fractional charge on the *metal* is greater at the transition state **92** than in the adduct **93** and tungsten is better able to support negative charge than chromium, the greater stabilization resulting from the change from chromium to tungsten will affect the transition state more than the adduct and increase  $k_1$  more than  $K_1$ .



(5) The mechanism of the acid-catalyzed leaving group departure is probably concerted, with transition states **94** for the  $k_2^{\text{H}}$  and **95** for the  $k_2^{\text{BH}}$  step, respectively. There is an increase in  $k_2^{\text{H}}$  and  $k_2^{\text{BH}}$  with increasing basicity of the thiolate ion. This indicates the operation of an electronic push by the RS group, presumably because of developing resonance (**96**) in the transition state. From the slopes of plots of  $\log k_2^{\text{H}}$  versus  $\text{p}K_{\text{a}}^{\text{RSH}}$ ,  $\beta_{\text{push}}$  values in the order of 0.3 were obtained.



With respect to the dependence on the leaving group, the  $k_2^{\text{H}}$  and  $k_2^{\text{BH}}$  values are slightly larger for the methoxy compared to the ethoxy derivative. In acid-catalyzed alkoxide ion departure the relative progress of C–O bond cleavage versus oxygen protonation determines which leaving group leaves faster. If C–O bond cleavage is ahead of proton transfer, the energetics of the reaction should be more reflective of

**Table 15** Brønsted-type coefficients for the dependence of  $K_1$ ,  $k_1$  and  $k_{-1}$  on  $\text{p}K_{\text{a}}^{\text{RSH}}$  in the reactions of (equation 65)

	11	13	42	87
$\beta_{\text{nuc}} = \text{d} \log k_1 / \text{d} \text{p}K_{\text{a}}^{\text{RS}}$	-0.28	-0.25	-0.28	-0.26
$\beta_{\text{lg}} = \text{d} \log k_{-1} / \text{d} \text{p}K_{\text{a}}^{\text{RSH}}$	-0.55	-0.57	-0.70	-0.75
$\beta_{\text{eq}} = \text{d} \log K_1 / \text{d} \text{p}K_{\text{a}}^{\text{RSH}}$	0.36	0.39	0.50	0.54

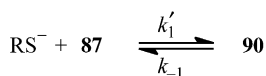
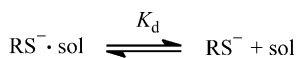
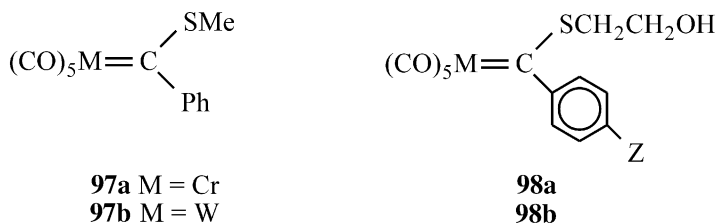
Reference 134.

C–O bond cleavage than of the proton transfer and hence the less basic leaving group  $\text{MeO}^-$  should leave faster. On the other hand, if proton transfer is ahead of C–O bond cleavage the opposite holds and the ethoxy derivative should react faster. The results suggest that the former situation applies.

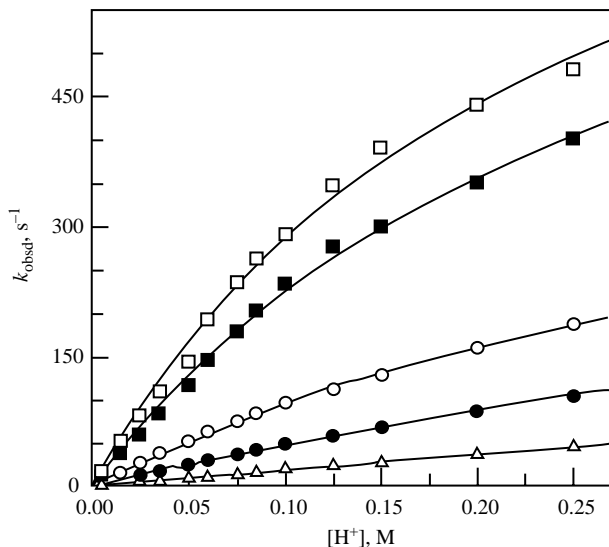
The dependence of  $K_1$ ,  $k_1$  and  $k_{-1}$  on  $\text{p}K_a^{\text{RSH}}$  yielded the Brønsted type coefficients summarized in Table 15. The most interesting feature is that  $\beta_{\text{nuc}}$  is negative, i.e., nucleophilic reactivity of the thiolate ions *decreases* with increasing basicity. Negative  $\beta_{\text{nuc}}$  values are unusual but not without precedent.<sup>143–146</sup> According to Jencks et al.,<sup>143</sup> they may result from the requirement of partial desolvation of the nucleophile prior to reaction, as shown in Scheme 8. In terms of Scheme 8, the experimental  $k_1$  values correspond to  $K_d k_1'$  with  $K_d$  being the equilibrium constant for partial desolvation of the nucleophile. In the simplest approach,  $\beta_{\text{nuc}}$  may be approximated by equation (68). Since desolvation becomes more difficult as the basicity of  $\text{RS}^-$  increases,  $\beta_d < 0$ . If  $\beta'_{\text{nuc}}$  is small because of an early transition state,  $\beta_{\text{nuc}}$  may be dominated by  $\beta_d$  and become negative. A more elaborate discussion which also takes into account the desolvation effect on  $\text{p}K_a^{\text{RSH}}$  is presented in Ref. 134.

$$\beta_{\text{nuc}} = \frac{d \log k_1}{d \text{p}K_a^{\text{RSH}}} = \frac{d \log K_d k_1'}{d \text{p}K_a^{\text{RSH}}} = \frac{d \log K_d}{d \text{p}K_a^{\text{RSH}}} + \frac{d \log k_1'}{d \text{p}K_a^{\text{RSH}}} = \beta_d + \beta'_{\text{nuc}} \quad (68)$$

A recent study of thiol/thiolate ion addition to alkylthio Fischer carbene complexes has led to additional insights into the structure–reactivity relationships of these nucleophilic addition reactions and also provides evidence for metal protonation of tetrahedral adducts.<sup>147</sup> Two reaction series were investigated in 50% MeCN–50% water (v/v) at 25°C. One is the reaction of **97** with a series of  $\text{RS}^-/\text{RSH}$  ( $\text{R} = n\text{-Pr}$ , Me,  $\text{HOCH}_2\text{CH}_2$ ,  $\text{MeO}_2\text{CCH}_2\text{CH}_2$  and  $\text{MeO}_2\text{CCH}_2$ ), the other is the reaction of **98** with  $\text{HOCH}_2\text{CH}_2\text{S}^-/\text{HOCH}_2\text{CH}_2\text{SH}$ ; in this case the phenyl substituent in the tungsten complexes was varied ( $\text{Z} = \text{CF}_3$ , Cl, F, H, Me, MeO and  $\text{Me}_2\text{N}$ ).

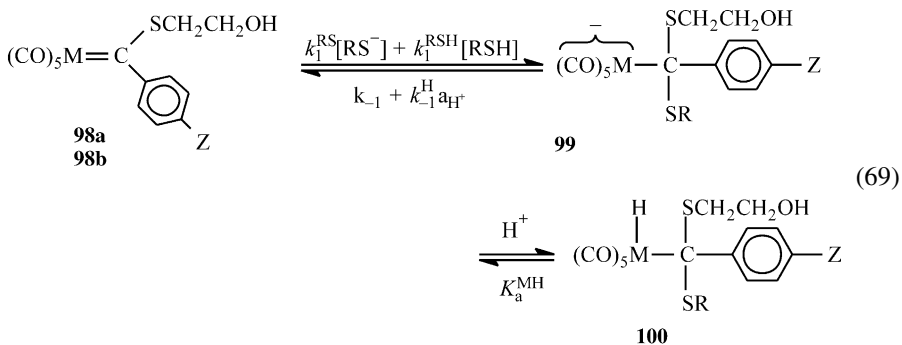


Scheme 8



**Fig. 5** Plots of  $k_{\text{obsd}}$  versus  $[\text{H}^+]$  according to equation (70) for the reaction of **99** ( $M = \text{W}$ ) with  $\text{HCl}$  in 50%  $\text{MeCN}$ –50% water (v/v) at  $25^\circ\text{C}$ .  $\square$ ,  $Z = \text{MeO}$ ;  $\blacksquare$ ,  $Z = \text{Me}$ ;  $\circ$ ,  $Z = \text{H}$ ;  $\bullet$ ,  $Z = \text{F}$ ;  $\triangle$ ,  $Z = \text{Cl}$ . (Figure taken from Ref. 147, by permission from the American Chemical Society.)

The reactions can be described by equation (69) which includes a rapid protonation equilibrium that becomes significant in highly acidic solutions.



The metal protonated adducts (**100**) could not be detected directly because they are very acidic ( $\text{p}K_a^{\text{MH}} < 1$ ). This means they cannot be generated at the required pH because the thiolate ions are protonated under these conditions and the corresponding thiols are not reactive enough to add to the carbene complex. However there is kinetic evidence for **100**. When **99** that has been generated at high pH is reacted with  $\text{HCl}$ , the pseudo-first-order rate constant for the conversion of **99** back to **98** shows a non-linear dependence on  $a_{\text{H}^+}$ , as shown in Fig. 5 for some representative examples. This dependence is consistent with  $\text{H}^+$ -catalyzed

**Table 16**  $pK_a^{MH}$  and  $k_{-1}^H$  values for the reactions of various alkylthio carbene complexes with  $\text{HOCH}_2\text{CH}_2\text{S}^-$  in 50% MeCN–50% water (v/v) at 25°C (equation 69)

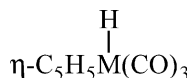
Carbene complex	$pK_a^{MH}$	$k_{-1}^H$ ( $\text{M}^{-1} \text{s}^{-1}$ )	Carbene complex	$pK_a^{MH}$	$k_{-1}^H$ ( $\text{M}^{-1} \text{s}^{-1}$ )
<b>98a</b> (Z = H)	0.74	15.2	<b>98b</b> (Z = H)	0.37	11.7
<b>98b</b> (Z = MeO)	0.62	40.4	<b>98b</b> (Z = F)	0.06	5.31
<b>98b</b> (Z = Me)	0.54	30.0	<b>98b</b> (Z = Cl)	-0.47	1.91

Reference 147.

expulsion of  $\text{RS}^-$  from **99** preceded by fast equilibrium protonation on the metal and can be described by equation (70).

$$k_{\text{obsd}} = \frac{K_a^{MH} k_{-1}^H a_{\text{H}^+}}{K_a^{MH} + a_{\text{H}^+}} \quad (70)$$

The  $pK_a^{MH}$  values obtained from this analysis are summarized in Table 16. This study was the first to provide such  $pK_a^{MH}$  values. The protonated adducts (**100**) bear some resemblance to hydrido transition metal complexes such as **101** whose  $pK_a^{MH}$  values have been determined in water, methanol and acetonitrile;<sup>148</sup> in water  $pK_a^{MH} = 5.4$  (Cr) and 8.0 (W); in methanol  $pK_a^{MH} = 6.4$  (Cr) and 9.0 (W), respectively. In 50% MeCN–50% water, the  $pK_a^{MH}$  values would be expected to be somewhat higher than in water, perhaps similar to the values in methanol. The fact that the  $pK_a^{MH}$  values for **100** are several units lower than those for **101** is consistent with the effect of replacing the electron donating cyclopentadienyl ligand with two electron withdrawing CO ligands and the  $\text{C}(\text{SR})_2\text{C}_6\text{H}_4\text{Z}$  moiety. What is more difficult to understand is why there is such a small metal dependence of the  $pK_a^{MH}$  values of **100** but a strong dependence for **101**.

**101**

Structure–reactivity comparisons of the reactions of thioalkyl carbene complexes with those of the alkoxy analogs reveal interesting differences as well as similarities. Table 17 provides a comparison of rate and equilibrium constants between the reactions of  $n\text{-PrS}^-$  with **97** and **11** or **13**. The following points are noteworthy.

- (1) The equilibrium constants for the MeS carbene complexes are over a 100-fold larger than for the MeO carbene complexes. This must be the result of the weaker  $\pi$ -donor effect of the MeS (**96**) group compared to that of the MeO (**91**) group. ( $\sigma_{\text{R}} = 0.43$  and 0.15 for MeO and MeS, respectively),<sup>149</sup> i.e., the MeS carbene complex is not as strongly stabilized as the MeO analog. The stronger steric hindrance in the adduct of the MeS derivative ( $E_{\text{S}} = -0.55$  and  $-1.07$  for MeO



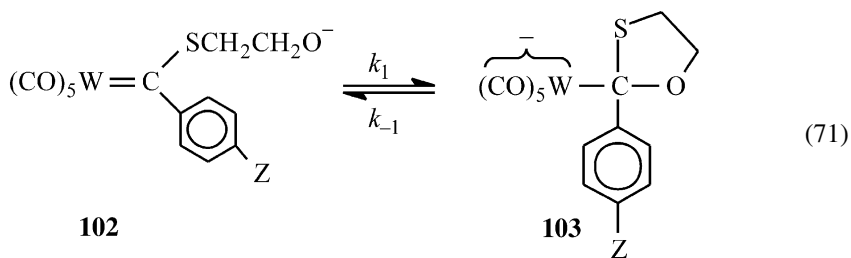
**Table 17** Rate and equilibrium constants for the reaction of  $n\text{-PrS}^-$  with **97a**, **97b**, **11** and **13** in 50% MeCN–50% water (v/v) at 25°C (equation 65)

	(CO) <sub>5</sub> Cr=C(SMe)Ph <b>97a</b>	(CO) <sub>5</sub> Cr=C(OMe)Ph <b>11</b>	(CO) <sub>5</sub> Cr=C(SMe)Ph <b>97b</b>	(CO) <sub>5</sub> W=C(OMe)Ph <b>13</b>
$k_1^{\text{RS}}$ (M <sup>-1</sup> s <sup>-1</sup> )	$5.33 \times 10^2$	$1.34 \times 10^4$	$1.58 \times 10^3$	$4.21 \times 10^4$
$k_{-1}$ (s <sup>-1</sup> )	$4.85 \times 10^{-4}$	1.26	$3.33 \times 10^{-4}$	3.11
$K_1^{\text{RS}}$ (M <sup>-1</sup> )	$1.10 \times 10^6$	$1.06 \times 10^4$	$4.75 \times 10^6$	$1.35 \times 10^4$
$k_{-1}^{\text{H}^+ a}$ (M <sup>-1</sup> s <sup>-1</sup> )	$5.09 \times 10^3$		$3.86 \times 10^3$	
$k_2^{\text{H}^+ b}$ (M <sup>-1</sup> s <sup>-1</sup> )		$5.39 \times 10^8$		$5.69 \times 10^8$

Reference 147.

<sup>a</sup>Refers to H<sup>+</sup>-catalyzed loss of MeS<sup>-</sup> from the respective adduct.<sup>b</sup>Refers to H<sup>+</sup>-catalyzed loss of MeO<sup>-</sup> from the respective adduct.

- and MeS, respectively)<sup>150</sup> and the weaker inductive effect of MeS ( $\sigma_F = 0.30$  and 0.20 for MeO and MeS, respectively),<sup>149</sup> both of which would make adduct formation less favorable for the MeS compared to the MeO carbene complexes are not nearly important enough to offset the influence of  $\pi$ -donor effects.
- (2) In contrast to the equilibrium constants, the  $k_1$  values for the MeS carbene complexes are about 25-fold *lower* than those for the MeO analogs. This reversal indicates that the *intrinsic* rate constants,  $k_0$ , for the MeO complexes are substantially larger than for the MeS complexes. These differences in the intrinsic rate constants are, once again, indicative of transition state imbalances where one or several of the factors – inductive, steric and  $\pi$ -donor effects – either lag behind or are ahead of bond formation. As a result of the imbalances the relative importance of these factors in how they affect the rate constants is different from how they affect the equilibrium constants and this is the reason why the intrinsic rate constants differ. A detailed analysis led to the conclusion that the steric effect whose development runs ahead of C–S bond formation and the lag in the charge delocalization into the  $(CO)_5M$  moiety which leads to a stronger transition state stabilization by the inductive effects of the MeX group when X = O than when X = S are mainly responsible for the differences in the intrinsic rate constants.<sup>147</sup> A potential third contribution is an imbalance involving the  $\pi$ -donor effects of the MeO and MeS groups.
- (3) The determination of the substituent effect on the reaction of **98b** with  $HOCH_2CH_2S^-/HOCH_2CH_2SH$  yielded the Hammett  $\rho$  values summarized in Table 18. The  $\rho$  values for the  $k_1^{RS} - k_{-1}$  pathway are strikingly smaller than the corresponding  $\rho$  values for alkoxide ion addition to **78c** or **78b** (equation 61). For example, for the reaction of  $HC\equiv CCH_2O^-$  with **78b**,  $\rho(k_1) = 1.68$ ,  $\rho(k_{-1}) = -1.39$  and  $\rho(K_1) = 3.07$  (Table 10) while the corresponding values for the reaction of  $HOCH_2CH_2S^-$  with **98b** are 0.78,  $-0.67$  and 1.45, respectively. Since one reaction involves an alkoxy carbene complex with an oxyanion nucleophile while the other is between an alkylthio carbene complex and a thiolate ion, it is not clear which of these two changes is responsible for large difference in the  $\rho$  values. The results of a substituent effect study on the intramolecular reaction (71)<sup>151</sup> (note that other aspects of reaction (71) will be discussed below) shed some light on this question.



The reported  $\rho$  values ( $\rho(k_1) \approx 0.96$ ,  $\rho(k_{-1}) = -1.65$  and  $\rho(K_1) \approx 2.67$ ) are much closer to those for the reaction of  $HC\equiv CCH_2O^-$  with the alkylthio

**Table 18** Hammett  $\rho$  values for the reaction of  $\text{HOCH}_2\text{CH}_2\text{S}^-/\text{HOCH}_2\text{CH}_2\text{SH}$  with **98b** ( $Z = \text{CF}_3, \text{Cl}, \text{F}, \text{H}, \text{Me}, \text{MeO}$  and  $\text{Me}_2\text{N}$ ) in 50% MeCN–50% water (v/v) at 25°C (equation 65)

Parameter	$\rho$	Parameter	$\rho$
$k_1^{\text{RS}}$	0.78	$k_1^{\text{RSH}}$	-1.04
$k_{-1}$	-0.67	$k_{-1}^{\text{H}}$	-2.65
$K_1^{\text{RS}} = k_1^{\text{RS}}/k_{-1}$	1.45	$K_1^{\text{MH}}$	2.08

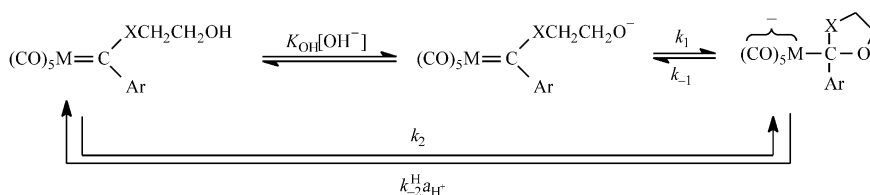
Reference 147.

complex (Table 18). This implies that it is the nature of the nucleophile rather than the identity of the group attached to the carbene carbon that dramatically changes the response to substituent effects. In other words,  $\rho(K_1)$  is only modestly affected by the change from a methoxy to an alkylthio group in the reactions with oxyanions, but  $\rho(K_1)$  is much smaller in the reaction with a thiolate ion than in the reaction of an oxyanion with the same carbene complex.

These results may be understood in the context of soft–hard acid–base theory.<sup>136,137</sup> As mentioned earlier, the Fischer carbene complexes can be regarded as soft electrophiles, especially the alkylthio complexes. Hence, the adducts **99** formed by the reaction of **98b** with a thiolate ion nucleophile enjoy enhanced stability due to the symbiotic effect<sup>136</sup> of adding a soft nucleophile. This stabilization apparently reduces the need for additional stabilization by the phenyl substituent, which translates to a reduced  $\rho(K_1)$  value.

## INTRAMOLECULAR NUCLEOPHILIC REACTIONS

Fischer carbene complexes of the type **104** and **105** undergo a cyclization reaction according to the general Scheme 9 ( $X = \text{O}$  or  $\text{S}$ );<sup>151,152</sup> some aspects of this process ( $M = \text{W}$ ,  $X = \text{S}$ , equation 71) have already been discussed above. The rate and equilibrium constants for the cyclization step via the  $k_1$ – $k_{-1}$  pathway are summarized in Table 19. As had been observed when comparing the relative reactivities of the MeS and MeO complexes **97** versus **11** and **13**, respectively, towards  $n\text{-PrS}^-$  (Table 17), we note again that the equilibrium constants are higher

**Scheme 9**

**Table 19** Rate and equilibrium constants for the cyclization step through the  $k_1$ - $k_{-1}$  pathway of [Scheme 9](#), intrinsic rate constants and effective molarities

Reactants	$K_1$	$k_1$ ( $s^{-1}$ )	$k_{-1}$ ( $s^{-1}$ )	$\log k_0^a$	EM( $K_1$ ) (M)	EM( $k_1$ ) (M)
(CO) <sub>5</sub> Cr=C(OCH <sub>2</sub> CH <sub>2</sub> OH)Ph ( <b>104a</b> )	$\approx 2.12 \times 10^5$	$\approx 7.21 \times 10^3$	$3.40 \times 10^{-2}$	$\approx 1.19$	$2.7 \times 10^4$	$7.0 \times 10^2$
(CO) <sub>5</sub> W=C(OCH <sub>2</sub> CH <sub>2</sub> OH)Ph ( <b>104b</b> )	$9.03 \times 10^4$	$1.81 \times 10^3$	$2.00 \times 10^{-2}$	$\approx 0.78$	$1.1 \times 10^4$	$9.9 \times 10^1$
(CO) <sub>5</sub> Cr=C(SCH <sub>2</sub> CH <sub>2</sub> OH)Ph ( <b>105a</b> )	$\approx 1.06 \times 10^6$	$\approx 30.5$	$2.88 \times 10^{-5}$	$\approx -1.53$		
(CO) <sub>5</sub> W=C(SCH <sub>2</sub> CH <sub>2</sub> OH)Ph ( <b>105b</b> )	$\approx 3.01 \times 10^5$	$\approx 55.3$	$1.83 \times 10^{-5}$	$\approx -1.50$		
(CO) <sub>5</sub> Cr=C(OMe)Ph + HC≡CCH <sub>2</sub> O <sup>b</sup>	167 <sup>c</sup>	47.0 <sup>d</sup>	0.281	0.56		
(CO) <sub>5</sub> W=C(OMe)Ph + HC≡CCH <sub>2</sub> O <sup>b</sup>	167 <sup>c</sup>	84.0 <sup>d</sup>	0.504	0.81		

In 50%MeCN–50% water (v/v) at 25°C, Ref. [152](#).

<sup>a</sup>log  $k_0$  obtained as  $\log k_1 - 0.5 \log K_1$ .

<sup>b</sup>Reference [132](#).

<sup>c</sup>In units of M<sup>-1</sup>.

<sup>d</sup>In units of M<sup>-1</sup> s<sup>-1</sup>.

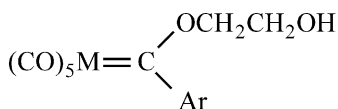
**Table 20** Rate and equilibrium constants for the cyclization steps through the  $k_2$ - $k_{-2}$  pathway of Scheme 9; intrinsic rate constants

Carbene complex	$K_2$ (M)	$k_2$ ( $\text{s}^{-1}$ )	$k_{-2}^{\text{H}}$ ( $\text{M}^{-1} \text{s}^{-1}$ )	$\log k_0^a$
$(\text{CO})_5\text{Cr}=\text{C}(\text{OCH}_2\text{CH}_2\text{OH})\text{Ph}$ ( <b>104a</b> )	$1.36 \times 10^{-8}$	1.50	$1.10 \times 10^5$	$\approx 5.11$
$(\text{CO})_5\text{W}=\text{C}(\text{OCH}_2\text{CH}_2\text{OH})\text{Ph}$ ( <b>104b</b> )	$4.59 \times 10^{-9}$	5.03	$1.12 \times 10^9$	$\approx 4.88$
$(\text{CO})_5\text{Cr}=\text{C}(\text{SCH}_2\text{CH}_2\text{OH})\text{Ph}$ ( <b>105a</b> )	$5.26 \times 10^{-9}$	$2.56 \times 10^{-2}$	$5.04 \times 10^6$	$\approx 2.56$
$(\text{CO})_5\text{W}=\text{C}(\text{SCH}_2\text{CH}_2\text{OH})\text{Ph}$ ( <b>105b</b> )	$1.50 \times 10^{-8}$	$7.11 \times 10^{-2}$	$4.74 \times 10^6$	$\approx 2.76$

In 50%MeCN–50% water (v/v) at 25°C, Ref. 152.

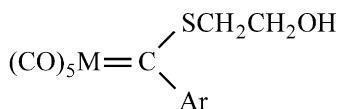
<sup>a</sup> $\log k_0$  obtained as  $\log k_2 - 0.5 \log K_2$ .

for the thia carbene compared with oxa complexes but the opposite is true when the  $k_1$  values are being compared. The implication is again that the intrinsic rate constants (included in Table 19) are lower for the alkylthio derivatives. This state of affairs can be explained as before, i.e., the higher  $K_1$  values for the alkylthio complexes result from the weaker  $\pi$ -donor effect of the sulfur group while the lower intrinsic rate constants arise from several transition state imbalances. One is early development of the steric effect (lowers  $k_0$  for the thia complexes more than for the oxa complexes); another is the delayed delocalization of the negative charge into the  $(\text{CO})_5\text{M}$  moieties that allows enhanced transition state stabilization by an inductive effect which is stronger for the oxa than the thia complexes.



**104a** M = Cr

**104b** M = W



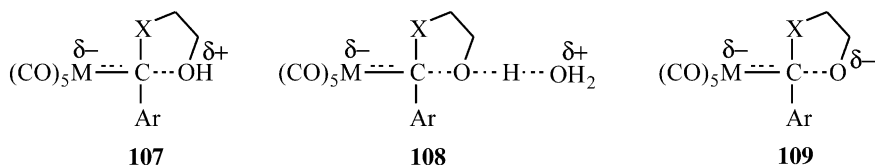
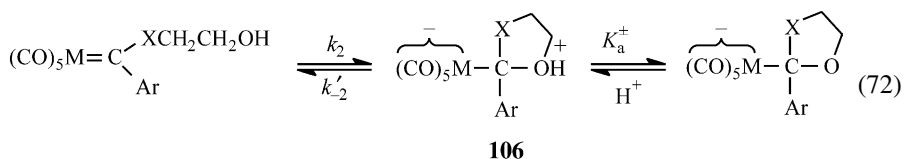
**105a** M = Cr

**105b** M = W

Table 19 includes the results for the *intermolecular* reactions of  $\text{HC}\equiv\text{CCH}_2\text{O}^-$  with  $(\text{CO})_5\text{M}=\text{C}(\text{OMe})\text{Ph}$  discussed earlier. Comparison with the intramolecular reactions of **102** yields the effective molarities (EMs)<sup>153,154</sup> given in the table. The EM values in Table 19 have been corrected for the difference in the  $\text{p}K_{\text{a}}$  values of the oxyanion nucleophiles.<sup>152</sup> These EM values are at the low end of the range which is common for the formation of 5-membered rings in conformationally flexible systems ( $10^4$ – $10^8$  M).<sup>153,154</sup>

The results for the  $k_2$ - $k_{-2}^{\text{H}}$  pathway are reported in Table 20. One possibility is that this pathway proceeds in two steps as shown in equation (72),<sup>152</sup> with a transition state for the rate-limiting step such as **107**. According to equation (72),  $k_{-2}^{\text{H}}$  in Scheme 9 takes on the meaning of  $k'_{-2}/K_{\text{a}}^{\pm}$ ; another possibility is that the reaction is concerted with a transition state such as **108**. Since no buffer catalysis could be

observed, the two-step mechanism seems more likely.



The most noteworthy feature of the results for the  $k_2-k_{-2}^{\text{H}}$  pathway is that, while the *relative* log  $k_0$  values for the oxa versus the thia complexes are close to those for the  $k_1-k_{-1}$  pathway, the *absolute* values are about 2.5 log units higher for the  $k_2-k_{-2}^{\text{H}}$  pathway.

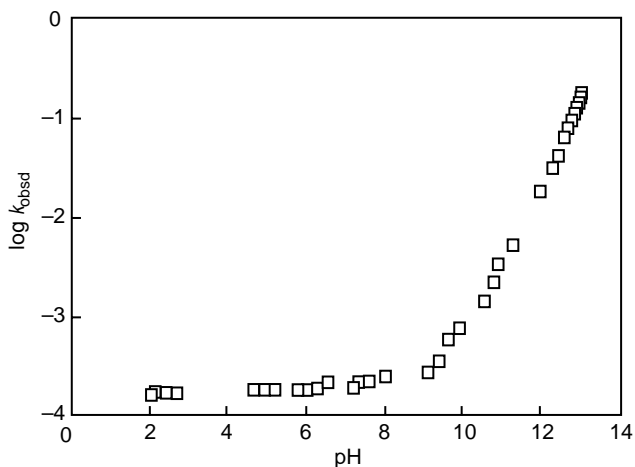
There are at least two factors that are likely to contribute to this difference in the intrinsic rate constants for the two pathways. One is that in the  $k_1-k_{-1}$  pathway the nucleophile is a strongly basic alkoxide ion. The strong solvation of such oxyanions is known to reduce their kinetic activity.<sup>140,141</sup> This reduction is a classic PNS<sup>121-123</sup> effect and the result of a transition state where the loss of solvation is ahead of bond formation. As discussed earlier, the lower intrinsic reactivity of alkoxide ions relative to thiolate ions was interpreted along similar lines.

The second factor is an electrostatic effect at the transition state. The transition state for the  $k_1-k_{-1}$  pathway is shown as **109**; the most likely transition state for the  $k_2-k_{-2}^{\text{H}}$  pathway is **107**. In **109** there is a destabilizing effect resulting from the two partial negative charges, while in **107** there is a stabilizing interaction between the positive and negative charge.

#### HYDROXIDE ION AND WATER AS NUCLEOPHILES

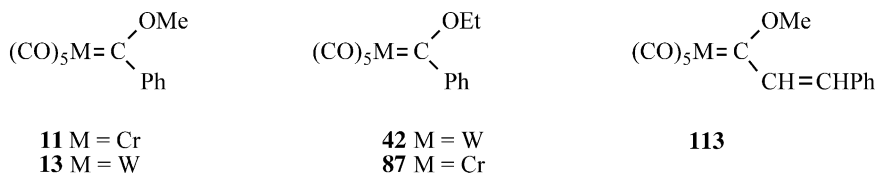
The hydrolysis of Fischer carbene complexes has received little attention in the early literature, probably because the major interest in these compounds has been their potential utility in synthesis. The first hydrolysis study was reported in 1993 by Aumann *et al.*<sup>155</sup> who investigated the reaction of several carbene complexes of the type **110** (R = Ph, CH=CHPh, C<sub>4</sub>H<sub>3</sub>S, CH=CHC<sub>6</sub>H<sub>3</sub>S and C≡CPh) in THF





**Fig. 6** Rate–pH profile of the hydrolysis of  $(\text{CO})_5\text{Cr}=\text{C}(\text{OMe})\text{CH}=\text{CHPh}$  (**113**) in 50% MeCN–50% water (v/v) at 25°C. (Figure taken from Ref. 157, by permission from the American Chemical Society.)

conversion of  $(\text{CO})_5\text{M}=\text{C}(\text{OH})\text{R}$  to the corresponding aldehyde ( $\text{RCH}=\text{O}$ ) and  $(\text{CO})_5\text{MOH}$ .



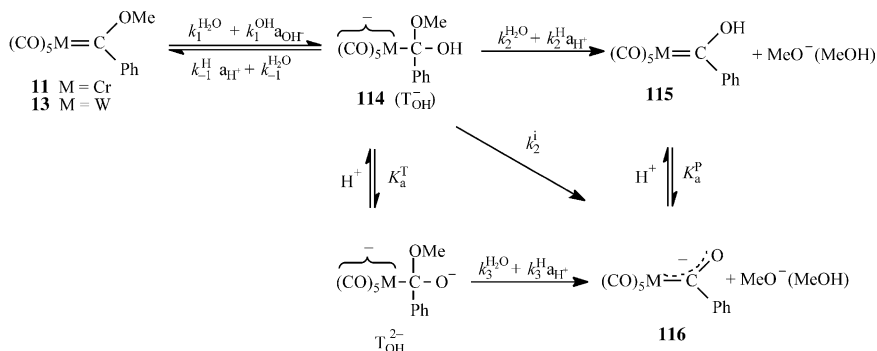
The kinetic study focused on the first process. A representative rate–pH profile is shown in Fig. 6 from which a  $k_{\text{H}_2\text{O}}$  for the water reaction (plateau) and a  $k_{\text{OH}}$  for the  $\text{OH}^-$  reaction were extracted. The  $k_{\text{H}_2\text{O}}$  and  $k_{\text{OH}}$  values are reported in Table 21. Not included in the table are  $k_{\text{B}}$  values that represent general base catalysis of the water reaction.

**Table 21** Summary of  $k_{\text{H}_2\text{O}}$  and  $k_{\text{OH}}$  values for the hydrolysis of several carbene complexes in 50% MeCN–50% water (v/v) at 25°C (Scheme 11)

Carbene complex	$k_{\text{H}_2\text{O}}$ ( $\text{s}^{-1}$ )	$k_{\text{OH}}$ ( $\text{M}^{-1} \text{s}^{-1}$ )
$(\text{CO})_5\text{Cr}=\text{C}(\text{OMe})\text{Ph}$ ( <b>11</b> )	$2.9 \times 10^{-3}$	26.6
$(\text{CO})_5\text{W}=\text{C}(\text{OMe})\text{Ph}$ ( <b>13</b> )	$2.8 \times 10^{-3}$	26.3
$(\text{CO})_5\text{Cr}=\text{C}(\text{OEt})\text{Ph}$ ( <b>42</b> )	$4.5 \times 10^{-4}$	10.5
$(\text{CO})_5\text{Cr}=\text{C}(\text{OEt})\text{Ph}$ ( <b>112</b> )	$2.8 \times 10^{-3}$	17.6
$(\text{CO})_5\text{Cr}=\text{C}(\text{OMe})\text{CH}=\text{CHPh}$ ( <b>113</b> )	$1.8 \times 10^{-4}$	14.6

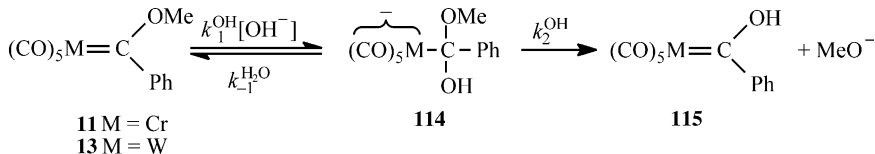
Reference 157.





Scheme 11

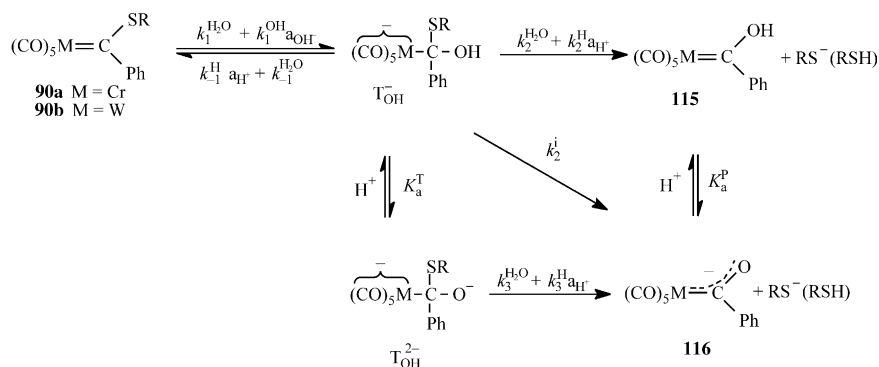
A central question that was addressed in this study is why no tetrahedral intermediates could be detected; based on the reactions of alkoxide ions with carbene complexes such as **11** or **13** (equation 61) one might have expected that, at high pH, these intermediates would accumulate to detectable levels. Two requirements must be met for an intermediate to become detectable in any two-step reaction. The first is that the equilibrium of the first step favors the intermediate, the second is that the rate of intermediate formation is faster than its conversion to products. Applied to equation (74), this would translate into  $K_1^{\text{OH}^-}[\text{OH}^-] > 1$  and  $k_1^{\text{OH}^-}[\text{OH}^-]/k_2^{\text{OH}^-} > 1$ .



(74)

Since  $K_1^{\text{OH}^-}$  can reasonably be expected to be at least as large and probably larger than the equilibrium constant for addition of the much less basic  $\text{HC}\equiv\text{CCH}_2\text{O}^-$  to  $(\text{CO})_5\text{Cr}=\text{C}(\text{OMe})\text{Ph}$  ( $K_1^{\text{RO}} = 167 \text{ M}^{-1}$ ),<sup>132</sup> the condition that  $K_1^{\text{OH}^-}[\text{OH}^-] > 1$  should easily be met at high pH. Furthermore, since the  $k_1^{\text{OH}^-}$  values ( $26 \text{ M}^{-1} \text{ s}^{-1}$ ) are comparable to  $k_1^{\text{RO}} = 47 \text{ M}^{-1} \text{ s}^{-1}$  for  $\text{HC}\equiv\text{CCH}_2\text{O}^-$ <sup>132</sup> and expulsion of  $\text{MeO}^-$  from **113** should proceed at a similar rate as expulsion of  $\text{MeO}^-$  from the corresponding  $\text{HC}\equiv\text{CCH}_2\text{O}^-$  adduct, one expects  $k_1^{\text{OH}^-}[\text{OH}^-]/k_2^{\text{OH}^-} > 1$  at high pH. Thus, even though both requirements for detectability of **114** appear to be met, the intermediate is not observable.

The reason for this apparent contradiction is that for **114** there are two additional pathways available for its conversion to products which result from the acidic nature of the OH group. These pathways are shown in the expanded Scheme 11 which also includes the various pathways in acidic solution, i.e., nucleophilic attack by water ( $k_1^{\text{H}_2\text{O}}$ ) and  $\text{H}^+$ -catalyzed expulsion of  $\text{OH}^-$  ( $k_{-1}^{\text{H}}$ ) and  $\text{RO}^-$  ( $k_2^{\text{H}}$ ) from  $\text{T}_{\text{OH}}^-$  as well as  $\text{H}^+$ -catalyzed expulsion of  $\text{RO}^-$  from  $\text{T}_{\text{OH}}^{2-}$  ( $k_3^{\text{H}}$ );  $k_2^{\text{I}}$  represents  $\text{RO}^-$  departure that is

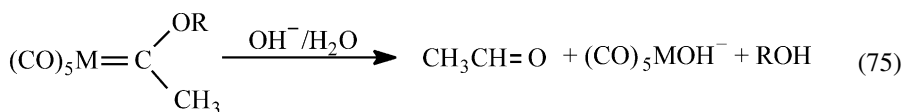


Scheme 12

intramolecularly acid catalyzed by the OH group. It is this  $k_2^i$  and/or the pathways through  $\text{T}_{\text{OH}}^{2-}$  that lead to a more rapid collapse of  $\text{T}_{\text{OH}}^-$  to products than via  $k_2^{\text{H}_2\text{O}}$  and prevent  $\text{T}_{\text{OH}}^-$  from becoming detectable. As a result, nucleophilic attack is rate limiting, i.e.,  $k_{\text{OH}} = k_1^{\text{OH}^-}$  and  $k_{\text{H}_2\text{O}} = k_1^{\text{H}_2\text{O}}$ .

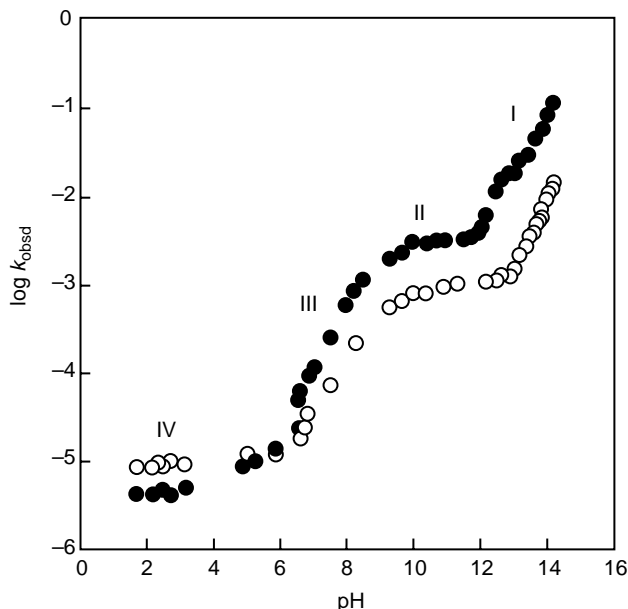
The driving force that makes the  $k_2^i$  step a potentially more favorable pathway than the  $k_2^{\text{H}_2\text{O}}$  step is that the acidity of the OH group increases strongly along the reaction coordinate which renders proton transfer to the departing  $\text{RO}^-$  thermodynamically favorable at the transition state, a pre-condition for effective acid catalysis.<sup>158</sup> In the pathway through  $\text{T}_{\text{OH}}^{2-}$ , the negative charge on the oxygen provides an extra electronic “push” in the form of transition state stabilization ( $k_3^{\text{H}_2\text{O}}$ -step) by the developing resonance of **116**. For this reason the collapse of  $\text{T}_{\text{OH}}^{2-}$  should be much faster than the collapse of  $\text{T}_{\text{OH}}^-$ .

Another interesting issue in the hydrolysis of alkoxy carbene complexes is the finding that replacement of the phenyl group with an alkyl group changes the mechanism even though the final products are the same (e.g., equation 75). The mechanism involves deprotonation of the alkyl group and hydrolytic breakdown of the anion, as discussed in Section 4.



Replacing the alkoxy group by an alkylthio group does not change the mechanism (Scheme 12) but it leads to a much more complex situation regarding the nature of the rate-limiting steps of the hydrolysis process.<sup>159</sup> This can be seen by inspection of the rate–pH profiles in Fig. 7 which suggest multiple changes in the rate-limiting step as the pH changes. The following interpretation of the rate–pH profiles was proposed.<sup>159</sup>

*Region I* (pH  $\geq 12.5$  for  $(\text{CO})_5\text{Cr}=\text{C}(\text{SMe})\text{Ph}$  and  $\geq 11.5$  for  $(\text{CO})_5\text{W}=\text{C}(\text{SMe})\text{Ph}$ ). Nucleophilic attack by  $\text{OH}^-$  is rate limiting, i.e., the observed pseudo-first-order rate constant is given by equation (76). This means that the



**Fig. 7** Rate-pH profiles of hydrolysis of  $(\text{CO})_5\text{M}=\text{C}(\text{SMe})\text{Ph}$  (**90a**, O; **90b**, •; in 50% MeCN-50% water (v/v) at 25°C. (Figure taken from Ref. 159, by permission from the American Chemical Society.)

relationships of equations (77) and (78) apply. Note that in equation (78) the  $k_2^{\text{H}}a_{\text{H}^+}$  term has been omitted because it is negligible down to pH 6 (see below).

$$k_{\text{obsd}} = k_1^{\text{OH}}[\text{OH}^-] \quad (76)$$

$$k_1^{\text{OH}}[\text{OH}^-] \gg k_1^{\text{H}_2\text{O}} \quad \text{and} \quad k_{-1}^{\text{H}_2\text{O}} \gg k_{-1}^{\text{H}}a_{\text{H}^+} \quad (77)$$

$$k_2^{\text{H}_2\text{O}} + k_2^{\text{i}} + k_a^{\text{T}}k_3^{\text{H}_2\text{O}}/a_{\text{H}^+} + k_a^{\text{T}}k_3^{\text{H}} \gg k_{-1}^{\text{H}_2\text{O}} \quad (78)$$

*Region II* (pH ~ 10 to ~ 12.5 for  $(\text{CO})_5\text{Cr}=\text{C}(\text{SMe})\text{Ph}$ , pH ~ 10 to ~ 11.5 for  $(\text{CO})_5\text{W}=\text{C}(\text{SMe})\text{Ph}$ ). Nucleophilic attack by water is rate limiting. Just as is the case for the hydrolysis of alkoxy carbene complexes, there is also general base catalysis of water attack, hence  $k_{\text{obsd}}$  is given by equation (79) ( $k_1^{\text{B}}[\text{B}]$  term not shown in Schemes 11 and 12). This rate law implies that the relationships of equations (80) and (81) hold; the  $k_2^{\text{H}}a_{\text{H}^+}$  term is again negligible and omitted from equation (81).

$$k_{\text{obsd}} = k_1^{\text{H}_2\text{O}} + k_1^{\text{B}}[\text{B}] \quad (79)$$

$$k_2^{\text{H}_2\text{O}} \gg k_1^{\text{OH}}[\text{OH}^-] \quad \text{and} \quad k_{-1}^{\text{H}}a_{\text{H}^+} \gg k_{-1}^{\text{H}_2\text{O}} \quad (80)$$

$$k_2^{\text{H}_2\text{O}} + k_2^{\text{i}} + K_a^{\text{T}}k_3^{\text{H}_2\text{O}}/a_{\text{H}^+} + K_a^{\text{T}}k_3^{\text{H}} \gg k_{-1}^{\text{H}}a_{\text{H}^+} \quad (81)$$

*Region III* (pH  $\sim 6$  to  $\sim 10$ ). In this pH range, equation (80) remains valid but equation (81) changes to equation (82) which means that the nucleophilic attack step is now a rapid

$$k_{-1}^H a_{H^+} \gg k_2^{H_2O} + k_2^i + K_a^T k_3^{H_2O} / a_{H^+} + K_a^T k_3^H \quad (82)$$

pre-equilibrium and hence  $k_{\text{obsd}}$  is given by equation (83), with  $K_1^{H_2O} = k_1^{H_2O} / k_{-1}^H$  being

$$k_{\text{obsd}} = \frac{k_1^{H_2O}}{a_{H^+}} (k_2^{H_2O} + k_2^i + K_a^T k_3) \quad (83)$$

the equilibrium constant for nucleophilic attack by water. The fact that the slope of the rate–pH profile is approximately unity indicates that neither the  $k_2^H a_{H^+}$  term nor the  $K_a^T k_3^{H_2O} / a_{H^+}$  term contribute significantly to  $k_{\text{obsd}}$  in this region and hence these two terms have been omitted from equations (82) and (83).

*Region IV* (pH  $\leq 6$ ). Below pH 6, the  $k_2^H a_{H^+}$  term finally becomes important; it now represents the dominant pathway for the rate-limiting collapse of  $T_{OH}^-$  (equation 84), equation (82) becomes equation (85), and equation (83) becomes equation (86).

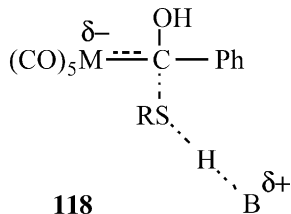
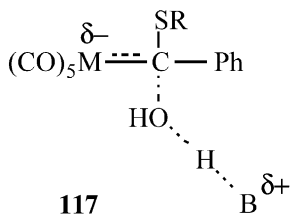
$$k_2^H a_{H^+} \gg k_2^{H_2O} + k_2^i + K_a^T k_3^H \quad (84)$$

$$k_{-1}^H a_{H^+} \gg k_2^H a_{H^+} \quad (85)$$

$$k_{\text{obsd}} = K_1^{H_2O} k_2^H \quad (86)$$

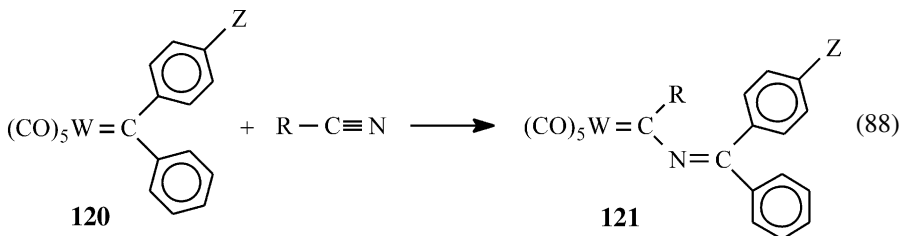
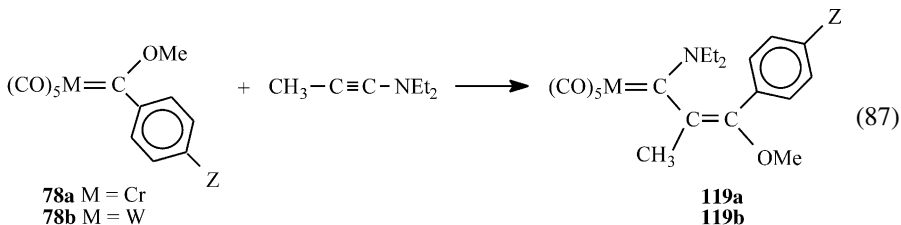
Why are the rate–pH profiles so different for complexes with thiomethyl compared to those with alkoxy leaving groups? For the hydrolysis of the alkoxy carbene complexes there are no changes from rate-limiting nucleophilic attack at high pH to rate-limiting collapse of  $T_{OH}^-$  at low pH, i.e., nucleophilic attack is rate limiting over the entire rate–pH profile. The key feature responsible for the difference between the two types of carbene complexes is that oxyanion ( $OH^-$  as well as  $RO^-$ ) departure from  $T_{OH}^-$  is very sensitive to  $H^+$  catalysis while for thiolate ion departure the sensitivity to  $H^+$  catalysis is much weaker. Hence, for the hydrolysis of the alkoxy carbene complexes,  $H^+$  catalysis of conversion of  $T_{OH}^-$  to products and of conversion back to reactants becomes important in similar pH ranges. This means that lowering the pH affects the rates of conversion of  $T_{OH}^-$  to reactants and products in a comparable way so that no change in rate-limiting steps occurs. In contrast, for the hydrolysis of thioalkyl carbene complexes,  $k_2^H$  is so small that at pH values where the  $k_{-1}^H a_{H^+}$  term starts to become important, the  $k_2^H a_{H^+}$  terms is still negligible. Hence in the pH range 6–10 where  $H^+$  catalysis of  $OH^-$  departure ( $k_{-1}^H a_{H^+}$ ) is already strong,  $H^+$  catalysis of  $RS^-$  departure ( $k_2^H a_{H^+}$ ) is insignificant which renders the ( $k_{-1}^H a_{H^+}$ ) process to be faster than the conversion of  $T_{OH}^-$  to products and leads to the observed change in rate-limiting step. As the pH is lowered further, the  $k_2^H a_{H^+}$  term eventually becomes significant but the  $k_{-1}^H a_{H^+}$  has also increased so that the collapse of  $T_{OH}^-$  to products remains rate limiting.

The lower sensitivity to  $H^+$  catalysis of thiolate compared to alkoxide ion departure has been observed in other reactions and is a general phenomenon; a detailed discussion has been presented in connection with the study of the acid-catalyzed breakdown of alkoxide and thiolate ion adducts of benzylidene Meldrum's acid type adducts.<sup>160</sup> The main reason for this reduced sensitivity appears to be the lower basicity of  $RS^-$  compared to  $RO^-$  or  $OH^-$  ions. However, the mechanism for  $H^+$  catalysis is probably the same for all leaving groups and most likely represents a concerted reaction with a transition state such as **117** or **118** ( $B = H_2O$ ).



#### INSERTION REACTIONS INITIATED BY NUCLEOPHILIC ATTACK

There are a number of reactions that involve insertion of an alkyne or nitrile between the metal and the carbene carbon that are initiated by a nucleophilic addition to the carbene carbon. Many of these reactions have been reviewed;<sup>1</sup> examples that have been subjected to kinetic investigations are shown in equations (87)<sup>161</sup> and (88).<sup>162-164</sup>



Rates of reaction (87) were measured for **78a** ( $Z = CF_3$  and H) and **78b** ( $Z = CF_3$ , Br, H, Me and MeO) at various temperatures in *n*-octane.<sup>161</sup> The reaction was found

**Table 22** Second-order rate constants and activation parameters for the reactions of  $(\text{CO})_5\text{Cr}=\text{C}(\text{OMe})\text{C}_6\text{H}_4\text{Z}$  (**78a**) and  $(\text{CO})_5\text{W}=\text{C}(\text{OMe})\text{C}_6\text{H}_4\text{Z}$  (**78b**) with  $\text{CH}_3\text{C}\equiv\text{CNEt}_2$  (equation 87) in *n*-octane at 20°C

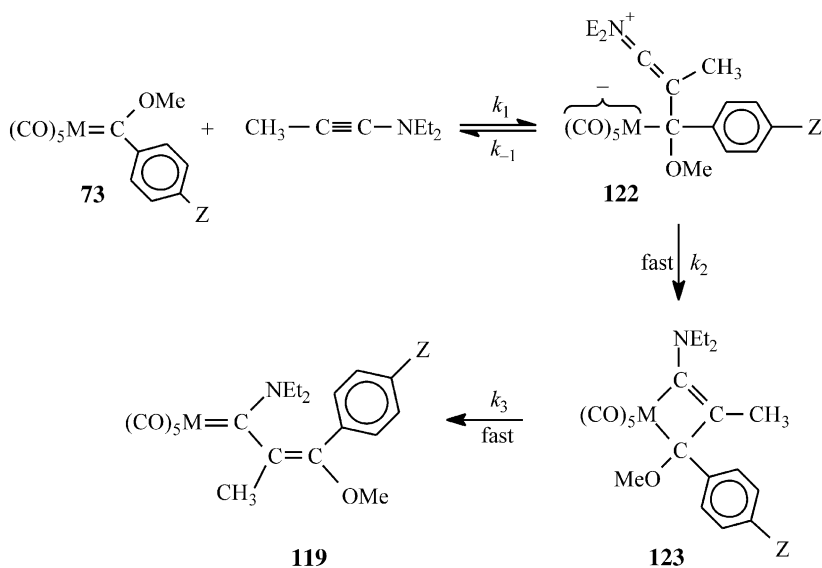
Carbene complex	$k = k_1^a$ ( $\text{M}^{-1} \text{s}^{-1}$ )	$\Delta H^\ddagger$ (kcal mol $^{-1}$ )	$\Delta S^\ddagger$ (cal mol $^{-1}$ deg $^{-1}$ )
<b>78a</b> Z = CF <sub>3</sub>	1.71	6.70	-34.7
<b>78a</b> Z = H	0.26	8.01	-34.0
<b>78b</b> Z = CF <sub>3</sub>	5.36	6.00	-34.7
<b>78b</b> Z = Br	1.76	7.56	-31.6
<b>78b</b> Z = H	0.873	7.82	-32.1
<b>78b</b> Z = Me	0.334	8.73	-31.1
<b>78b</b> Z = MeO	0.105	9.43	-30.9

Reference 161.

<sup>a</sup>See Scheme 13.

to be overall second order, i.e., first order in each of the reactants. Second-order rate constants at 20°C as well as  $\Delta H^\ddagger$  and  $\Delta S^\ddagger$  values are summarized in Table 22.

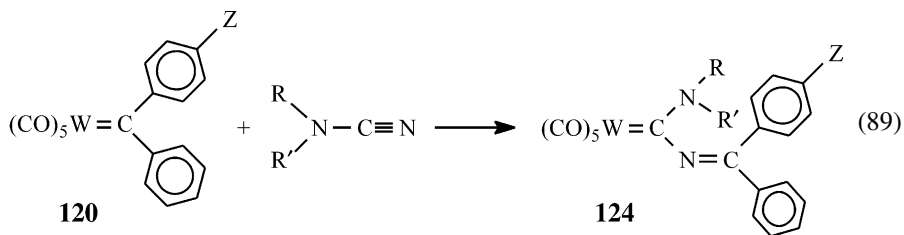
On the basis of these results the mechanism shown in Scheme 13 was proposed in which the  $k_1$  step is rate limiting. In support of rate-limiting nucleophilic attack, Fischer and Dötz<sup>161</sup> cite the fact that the second-order rate constants (Table 22) increase strongly as the Z substituent becomes more electron withdrawing (the reasons why electron withdrawing substituents enhance nucleophilic additions even with neutral nucleophiles have been discussed under “Phosphine and phosphite nucleophiles”), and that they correlate well with the equilibrium constants of (*n*-



Scheme 13

$\text{Bu}_3\text{P}$  addition to **63** (equation 52). The strongly negative  $\Delta S^\ddagger$  values are also consistent with a bimolecular reaction that leads to a zwitterionic intermediate such as **122**.

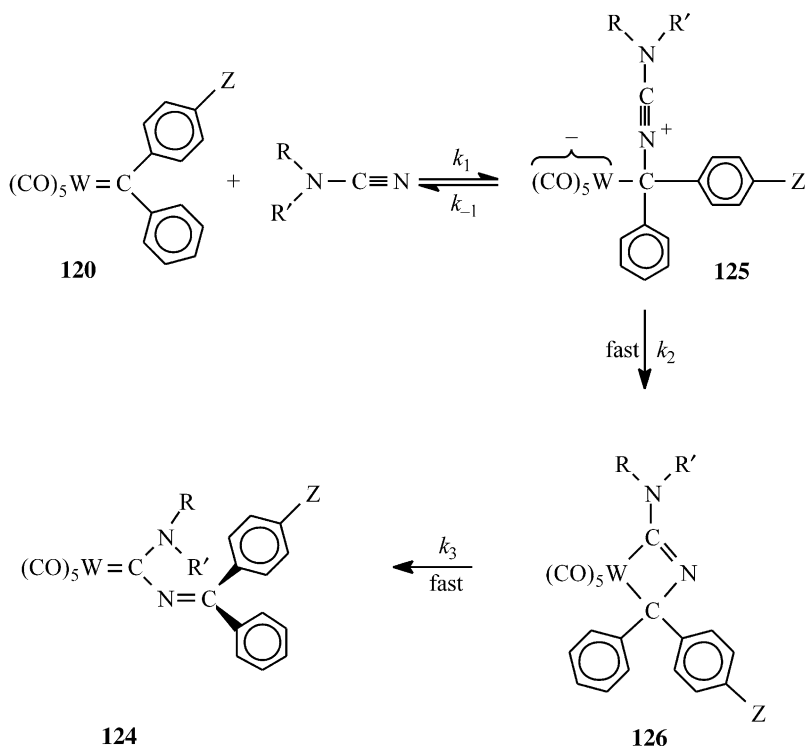
Three kinetic investigations have been reported on reactions of **120** with nitriles (equation 88). The first two involved dialkylcyanamides as the nitriles, equation (89), with  $\text{RR}' = \text{Me}_2, \text{MeEt}, (n\text{-Pr})_2$  and  $(i\text{-Pr})_2$ .<sup>162,163</sup> With  $\text{Me}_2\text{N}-\text{C}\equiv\text{N}$  rates were determined for five derivatives of **120** ( $\text{Z} = \text{CF}_3, \text{Br}, \text{H}, \text{Me}$  and  $\text{MeO}$ ) at different temperatures and also in a variety of solvents.



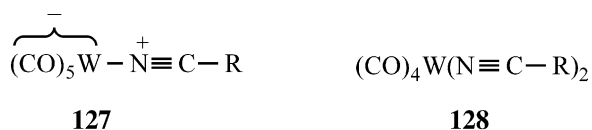
With the other nitriles the investigation was limited to **120** with  $\text{Z} = \text{H}$ . The reactions were again essentially second order, although in some cases a small first-order term was detected at high temperature. Using the same line of reasoning as for reaction (87) – strong acceleration by electron withdrawing substituents, large negative  $\Delta S^\ddagger$  values and correlation of  $k$  with the equilibrium constants of equation (52) – it was concluded that reaction (89) must involve a rate-limiting nucleophilic attack by the nitrile on the carbene carbon of **120** ( $k_1$ ) followed by rapid rearrangements as outlined in Scheme 14. The slight increase in the rate constants upon changing the methyl groups on the cyanamides to the more electron donating ethyl and propyl groups is also consistent with their mechanistic conclusion. As to the rearrangement of **125** into **124** via **126**, it is strongly analogous to that of **122** rearranging to **119** via **123** in Scheme 13.

In comparing the nucleophilic attack of  $\text{RR}'\text{N}-\text{C}\equiv\text{N}$  on **120** with that of  $\text{CH}_3\text{C}\equiv\text{N}(\text{Et})_2$  on **78b** one would expect the former reaction to be significantly faster because  $\text{RR}'\text{N}-\text{C}\equiv\text{N}$  should be a stronger nucleophile and **120** should be more reactive than **78b** since it lacks the strong  $\pi$ -donor stabilization by the methoxy group. However, comparison of the  $k$  values in Tables 22 and 23 reveals the opposite behavior. Even though Fischer<sup>162,163</sup> did not comment on this point, the most likely explanation of the observed reactivity patterns is that the two phenyl groups in **120** lead to strong steric crowding at the transition state of the  $k_1$  step. The importance of steric effects in reactions of carbene complexes with nucleophiles has been pointed out earlier (see the section on “Phosphine addition”).

The third kinetic study involved the reaction of **120** ( $\text{Z} = \text{H}$ ) with aryl nitriles and acetonitrile conducted in 1,1,2-trichloromethane at  $50.6^\circ\text{C}$ .<sup>164</sup> Even though **121** is the main product (equation 88), byproducts such as **127**, **128** and even traces of diphenylketene were detected.



Scheme 14



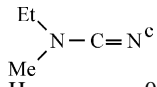
These byproducts are formed by a dissociative mechanism which is reflected in a rate law (equation 90) that includes a first-order term.

$$-\frac{d[\mathbf{120}]}{dt} = k_{\text{II}}[\mathbf{120}][\text{RCN}] + k_1[\mathbf{120}] \quad (90)$$

The following rate constants were obtained in 1,1,2-trichloroethane at 50.6°C:  $k_1 = 4.5 \times 10^{-4} \text{ s}^{-1}$ ;  $k_{\text{II}} = 0.6 \times 10^{-4} \text{ M}^{-1} \text{ s}^{-1}$  for MeCN,  $4.4 \times 10^{-4} \text{ M}^{-1} \text{ s}^{-1}$  for PhC≡N,  $7.9 \times 10^{-4} \text{ M}^{-1} \text{ s}^{-1}$  for *p*-MeOC<sub>6</sub>H<sub>4</sub>C≡N and  $1.97 \times 10^{-3} \text{ M}^{-1} \text{ s}^{-1}$  for *p*-Me<sub>2</sub>NC<sub>6</sub>H<sub>4</sub>C≡N. The trend in the  $k_{\text{II}}$  values for the aryl nitriles is consistent with increased nucleophilicity due to the electron donating substituents and with the increasing importance of the  $k_{\text{II}}$  pathway relative to the  $k_1$  pathway. The mechanism of the  $k_{\text{II}}$  pathway was assumed to be analogous to that in Scheme 14, again with nucleophilic attack being the rate-limiting step. The fact that  $k_{\text{II}}$  for the aryl nitriles is

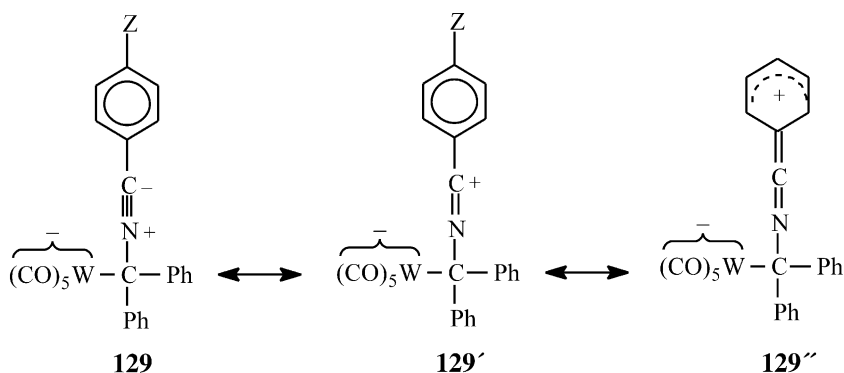


**Table 23** Second-order rate constants and activation parameters for the reactions of  $RR'N-C\equiv N$  with  $(CO)_5W=C(OMe)C_6H_4Z$  (**120**) in methylcyclohexane at 20°C

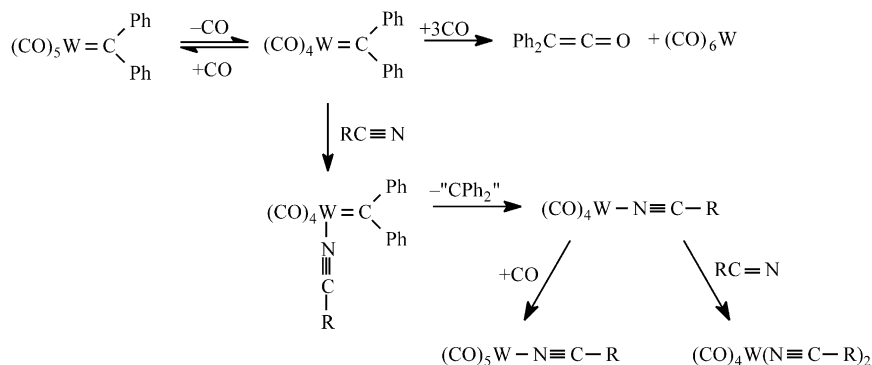
Z	$k = k_1^a$ ( $M^{-1} s^{-1}$ )	$\Delta H^\ddagger$ (kcal mol $^{-1}$ )	$\Delta S^\ddagger$ (cal mol $^{-1}$ deg $^{-1}$ )
$Me_2N-C\equiv N^b$			
MeO	0.0182	11.0	-28.9
Me	0.0459	10.6	-28.5
H	0.0836	9.3	-31.8
Br	0.130	9.1	-31.6
CF <sub>3</sub>	0.337	8.9	-30.4
			
H	0.120	9.7	-29.6
$(i-Pr)_2N-C\equiv N^c$			
H	0.192	9.5	-29.4
$(Pr)_2N-C\equiv N^c$			
H	0.214	9.0	-31.1

<sup>a</sup>See Scheme 14.<sup>b</sup>Reference 162.<sup>c</sup>Reference 163.

higher than for  $MeC\equiv N$ , despite their lower basicity, was attributed to the capability of the phenyl ring to delocalize the positive charge that forms on the nitrile fragment in the first intermediate ( $129 \leftrightarrow 129' \leftrightarrow 129''$ ).

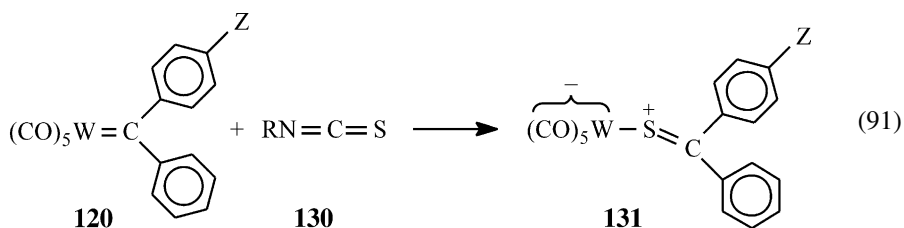


For the  $k_1$  pathway, dissociation of CO from the carbene complex was assumed to be rate limiting, in agreement with the fact that the measured  $k_1$  value is the same as the rate constant for thermolysis of **120** measured independently. The proposed mechanism for the dissociative pathway is shown in Scheme 15 (shown for  $Z = H$ ).



Scheme 15

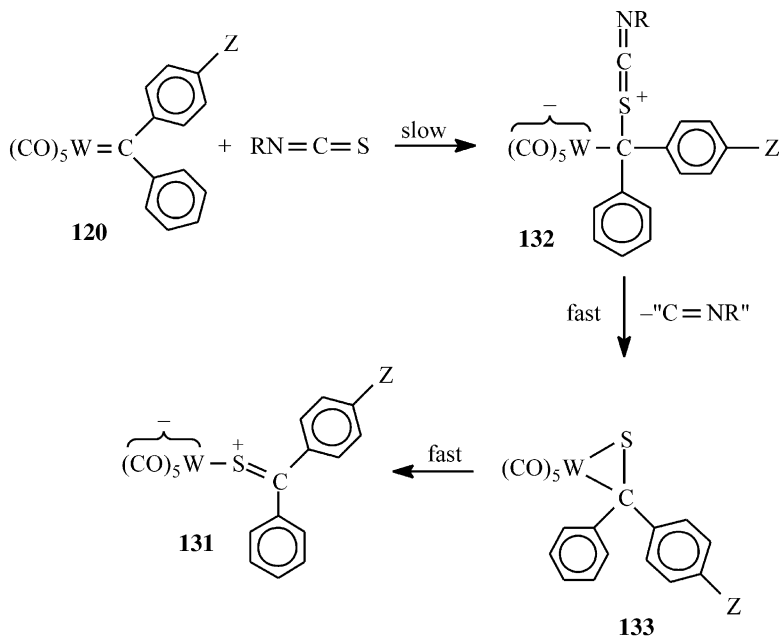
Another type of insertion reaction that is initiated by nucleophilic attack on the carbene carbon of **120** is shown in equation (91).



This reaction has been the subject of a kinetic study in dibutyl ether (R = Et with Z = MeO, Me, H, Br and CF<sub>3</sub>; R = Me with Z = H; R = Ph with Z = H) and *n*-octane (R = Et with Z = H).<sup>165</sup> In dibutyl ether the reaction is strictly second order, i.e., first order in **120** and first order in isothiocyanate, while in *n*-octane there is both a second- and a third-order term (equation 92).

$$-\frac{d[\mathbf{120}]}{dt} = k_{\text{II}}[\mathbf{120}][\mathbf{132}] + k_{\text{III}}[\mathbf{120}][\mathbf{130}]^2 \quad (92)$$

The dependence of  $k_{\text{II}}$  shows the same characteristics as for the nitrile insertions discussed above – acceleration by electron withdrawing Z substituents in the carbene complex, increased rates when the R group becomes more electron donating, correlation of  $k_{\text{II}}$  with the equilibrium constants of equation (52), and strongly negative  $\Delta S^\ddagger$  values – and suggests rate-limiting nucleophilic attack by the isothiocyanate on the carbene complexes. The proposed mechanism is shown in Scheme 16. Note that even though there is no direct evidence that the initial nucleophilic attack is through sulfur rather than nitrogen, the product strongly suggests that the former is the case.

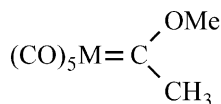


Scheme 16

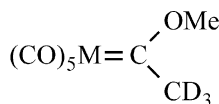
#### 4 Acid–base reactions at the $\alpha$ -carbon

##### GENERAL FEATURES AND METHODS

The first indication that Fischer carbene complexes of the type **40** or **68** have pronounced acidic properties was Kreiter's<sup>166</sup> observation of the rapid conversion of **68** to **134a** in dilute NaOMe/MeOD solutions. Casey and Anderson<sup>167</sup> subsequently showed that in THF the acidity of **68** is approximately the same as that of *p*-cyanophenol whose  $\text{p}K_{\text{a}}$  is about 8.<sup>168</sup> In quoting this work, a number of authors, as recently as in 2000,<sup>25</sup> have rather misleadingly referred to **68** as an acid with a  $\text{p}K_{\text{a}}$  of 8. This inference, of course, cannot be correct since *p*-cyanophenoxide ion and the conjugate base of **68** should respond differently to a solvent change from water to THF; indeed the  $\text{p}K_{\text{a}}^{\text{CH}}$  (the superscript CH will be used throughout this section to distinguish  $\text{p}K_{\text{a}}^{\text{CH}}$  from the  $\text{p}K_{\text{a}}$  of other acids) of **68** in water is 12.3,<sup>169</sup> not 8, and, in 50% MeCN–50% water (the standard solvent used for most  $\text{p}K_{\text{a}}^{\text{CH}}$  and proton transfer determinations of Fischer carbene complexes<sup>170</sup>), 12.5.<sup>171</sup> The problem in defining and determining  $\text{p}K_{\text{a}}^{\text{CH}}$  values in organic solvents such as THF will be taken up in more detail in a section titled “Thermodynamic acidities in organic solvents.”

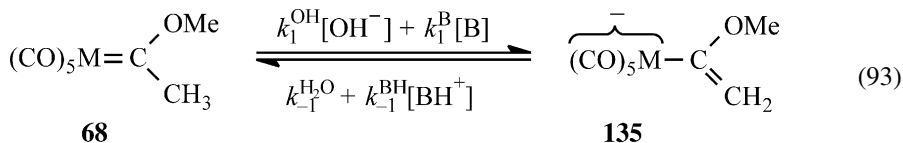


**68** M = Cr  
40 M = W



**134a** M = Cr  
**134b** M = W

It is perhaps surprising that no  $\text{p}K_{\text{a}}^{\text{CH}}$  measurements in water for even the most prototypical of all Fischer carbene complexes such as **68** had been reported before 1989.<sup>169</sup> The most likely explanation for this state of affairs is that in aqueous solution the conjugate anions of carbene complexes hydrolyze rapidly which precludes equilibrium determinations by classical photometric methods. In fact, most  $\text{p}K_{\text{a}}^{\text{CH}}$  values of Fischer complexes in aqueous solution were obtained by kinetic rather than equilibrium methods. For **68** the  $\text{p}K_{\text{a}}^{\text{CH}}$  was determined in KOH solution by applying the relationship  $K_{\text{a}}^{\text{CH}} = (k_1^{\text{OH}}/k_{-1}^{\text{H}_2\text{O}})K_{\text{w}}$  where  $k_1^{\text{OH}}$  is the rate constant for deprotonation of the carbene complex by  $\text{OH}^-$ ,  $k_{-1}^{\text{H}_2\text{O}}$  is the rate constant for protonation of the anion by water (equation 93) and  $K_{\text{w}}$  is the ionic product of the solvent;<sup>169,171</sup>  $k_1^{\text{OH}}$  and  $k_{-1}^{\text{H}_2\text{O}}$  were determined as the slope and intercept, respectively, of a plot of the observed pseudo-first-order rate constant for equilibrium approach versus  $[\text{OH}^-]$  (equation 94).



$$k_{\text{obsd}} = k_1^{\text{OH}}[\text{OH}^-] + k_{-1}^{\text{H}_2\text{O}} \quad (94)$$

This methodology was successfully applied to other carbene complexes with relatively high  $\text{p}K_{\text{a}}^{\text{CH}}$  values<sup>172-175</sup> but for the more acidic complexes it fails because  $k_{-1}^{\text{H}_2\text{O}}$  becomes very small relative to the  $k_1^{\text{OH}}[\text{OH}^-]$  term and hence cannot be evaluated accurately.<sup>171,176</sup> In these cases the  $\text{p}K_{\text{a}}^{\text{CH}}$  values were obtained by measuring proton transfer rates in buffer solutions ( $k_1^{\text{B}}[\text{B}]$  and  $k_{-1}^{\text{BH}}[\text{BH}]$  terms in equation 93) of buffers that have  $\text{p}K_{\text{a}}^{\text{BH}}$  values close to  $\text{p}K_{\text{a}}^{\text{CH}}$ . In such solutions  $k_{\text{obsd}}$  is given by equation (95) ( $K_{\text{a}}^{\text{BH}}$  is the acidity constant of BH) and the slope of a plot of  $k_{\text{obsd}}$  versus  $[\text{B}]$  is given by equation (95). From a plot of these slopes versus  $a_{\text{H}^+}$  according to equation (96) one then obtains  $k_1^{\text{B}}$  and  $k_{-1}^{\text{BH}}/K_{\text{a}}^{\text{BH}}$ :

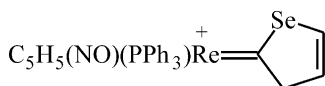
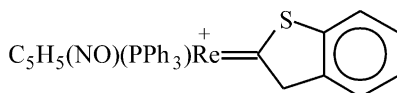
$$k_{\text{obsd}} = k_1^{\text{OH}}[\text{OH}^-] + k_{-1}^{\text{H}_2\text{O}} + \left( k_1^{\text{B}} + k_{-1}^{\text{BH}} \frac{a_{\text{H}^+}}{K_{\text{a}}^{\text{BH}}} \right) \quad (95)$$

$$\text{slope} = k_1^{\text{B}} + k_{-1}^{\text{BH}} \frac{a_{\text{H}^+}}{K_{\text{a}}^{\text{BH}}} \quad (96)$$

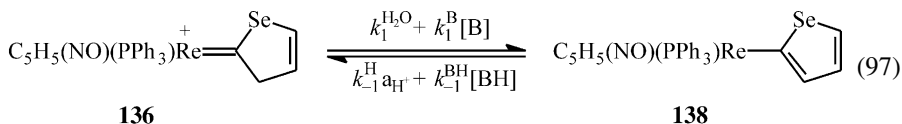
The kinetic experiments described above were typically extended to include numerous other buffers in order to provide the respective  $k_1^{\text{B}}$  and  $k_{-1}^{\text{BH}}$  values. For

buffers whose  $pK_a^{BH}$  values were significantly below the  $pK_a^{CH}$  of the carbene complex, the kinetic experiments had to be conducted in the direction  $\text{anion} + \text{BH} \rightarrow \text{carbene complex} + \text{B}$  in order to make the reaction thermodynamically favorable. This was achieved by generating the anion in a KOH solution prior to mixing it with the buffer. However, because of the very short lifetime of the anion which was typically a few seconds due to its rapid hydrolytic decomposition (more on this in the section on the hydrolysis of ionizable carbene complexes), these experiments had to be conducted in a double mixing stopped-flow apparatus. This apparatus allows mixing of the anion solution with the buffer solution within 20–30 ms after it has been generated in the presence of KOH, i.e., before significant decomposition can occur.

For the most acidic carbene complexes such as **136** ( $pK_a^{CH} = 4.18$ )<sup>177</sup> and **137** ( $pK_a^{CH} = -0.03$ ),<sup>177</sup> the proton transfer reactions were conducted in HCl and carboxylate buffer solutions.

**136****137**

In this case, the reaction pathways are the ones of equation (97)



with  $k_1^{\text{H}_2\text{O}}$  and  $k_{-1}^{\text{H}^+}$  referring to the deprotonation of the carbene complex by water and protonation of the anion by the hydronium ion, respectively, while  $k_1^{\text{B}}$  and  $k_{-1}^{\text{BH}}$  have the same meaning as in equation (93). For **137** the  $pK_a^{CH}$  was obtained in HCl solution where  $k_{\text{obsd}}$  is given by equation (98). Hence  $K_a^{CH} = k_1^{\text{H}_2\text{O}}/k_{-1}^{\text{H}^+}$  with  $k_1^{\text{H}_2\text{O}}$  and  $k_{-1}^{\text{H}^+}$  representing intercept and slope, respectively, of a plot of  $k_{\text{obsd}}$  versus  $a_{\text{H}^+}$ . For **136** the  $pK_a^{CH}$  was determined in chloroacetate buffers as described above for the amine buffers (equation 96).

$$k_{\text{obsd}} = k_1^{\text{H}_2\text{O}} + k_{-1}^{\text{H}^+} a_{\text{H}^+} \quad (98)$$

#### KINETIC AND THERMODYNAMIC ACIDITIES

As pointed out earlier, most data on  $pK_a^{CH}$  values and rate constants for proton transfer were obtained in 50% MeCN–50% water (v/v), a solvent that is essentially aqueous but which provides better solubility for some sparingly soluble Fischer carbene complexes. Some acidity measurements were reported in other solvents as

well, in particular in MeCN, THF, DMSO and acetone as will be elaborated upon in a later section.

Table 24 provides a summary of  $pK_a^{\text{CH}}$  values, the rate constants  $k_1^{\text{OH}}$  and  $k_{-1}^{\text{H}_2\text{O}}$  (e.g., equation 93), the rate constants  $k_1^{\text{H}_2\text{O}}$  and  $k_{-1}^{\text{H}}$  (e.g., equation 97), and the corresponding *intrinsic* rate constants  $k_0^{\text{OH}}$  (for the  $k_1^{\text{OH}}-k_{-1}^{\text{H}_2\text{O}}$  pathway) and  $k_0^{\text{H}_2\text{O}}$  (for the  $k_1^{\text{H}_2\text{O}}-k_{-1}^{\text{H}}$  pathway). These latter were estimated according to equations (99) and (100), respectively, where  $K_1^{\text{OH}}$  in equation (99) is defined as  $k_1^{\text{OH}}/k_{-1}^{\text{H}_2\text{O}} = K_a^{\text{CH}}/K_w$ .

$$\log k_0^{\text{OH}} = \log k_1^{\text{OH}} - 0.5 \log K_1^{\text{OH}} \quad (99)$$

$$\log k_0^{\text{H}_2\text{O}} = \log k_1^{\text{H}_2\text{O}} - 0.5 \log K_a^{\text{CH}} \quad (100)$$

It needs to be emphasized that the intrinsic rate constants obtained via equations (99) and (100) are subject to significant uncertainty, especially those for which  $\log K_1^{\text{OH}}$  or  $\log K_a^{\text{CH}}$  differ substantially from zero. This is because equations (99) and (100) are based on the simplest form of the Marcus<sup>119,120</sup> formalism (first two terms in equation 101) which may be a good approximation when  $\Delta G^\circ$  is close to zero but less so when  $|\Delta G^\circ|$  becomes large (third term in equation 101). The  $\log k_0$  values for these latter cases are identified by italics in the table.

$$\Delta G^\ddagger = \Delta G_0^\ddagger + 0.5\Delta G_0^\ddagger + \frac{(\Delta G^\circ)^2}{16\Delta G_0^\ddagger} \quad (101)$$

The kinetic data from the reactions conducted in buffers were also used to determine the corresponding intrinsic rate constants. They were calculated from statistically corrected Brønsted plots of  $\log(k_1^{\text{B}}/q)$  or  $\log(k_{-1}^{\text{BH}}/p)$  versus  $pK_a^{\text{BH}} - pK_a^{\text{CH}} + \log(p/q)$  where  $p$  is the number of equivalent protons on BH and  $q$  is the number of equivalent basic sites on B. Interpolation or extrapolation of such plots to  $pK_a^{\text{BH}} - pK_a^{\text{CH}} + \log(p/q) = 0$  yields  $\log k_0$ . Such  $\log k_0$  values for the reactions with primary aliphatic and secondary alicyclic amines as well as carboxylate ions are summarized in Table 25. In those cases where  $\log k_0$  could be obtained from interpolation or short extrapolations the  $\log k_0$  values can be assumed to be quite reliable but those obtained from long extrapolations are less accurate; the latter ones are again identified by italics.

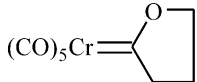
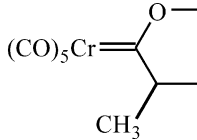
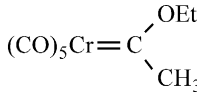
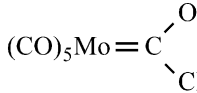
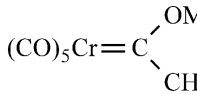
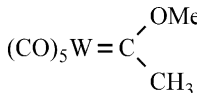
The significance of intrinsic rate constants in the context of our understanding chemical reactivity has already been discussed in a section titled “Alcohols and alkoxide ion nucleophiles” and will be further elaborated upon below.

#### EFFECT OF STRUCTURE ON $pK_a$ VALUES

##### *(CO)<sub>5</sub>M type complexes*

The  $pK_a^{\text{CH}}$  values of the neutral (CO)<sub>5</sub>M type complexes that are summarized in Table 24 and span a range 8.4–14.5; the two cationic rhenium carbene complexes which are substantially more acidic ( $pK_a^{\text{CH}} = 4.18$  and  $-0.03$ , respectively) will be dealt with below.

**Table 24** Summary of  $pK_a^{\text{CH}}$  values and rate constants for proton transfer from carbene complexes to  $\text{OH}^-$  in 50% MeCN–50% water (v/v) at 25°C

Entry		$pK_a^{\text{CH}}$	$k_1^{\text{OH}} (\text{M}^{-1} \text{s}^{-1})$	$k_{-1}^{\text{H}_2\text{O}} (\text{s}^{-1})$	$k_1^{\text{H}_2\text{O}} (\text{s}^{-1})$	$k_{-1}^{\text{H}} (\text{M}^{-1} \text{s}^{-1})$	$\log k_0^{\text{OH}}$	$\log k_0^{\text{H}_2\text{O}}$
1		(8) <sup>a</sup>	14.47	74.0	14.0		1.51	
2		(141) <sup>a</sup>	13.41	39.5	0.66		0.70	
3		(66) <sup>a</sup>	12.98	241	1.48		1.38	
4		(12) <sup>a</sup>	12.81	181	0.75		1.07	
5		(68) <sup>a</sup>	12.50	456	0.91		1.31	
6		(40) <sup>a</sup>	12.36	284	0.42		1.04	

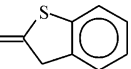
(continued on next page)

Table 24 (continued)

Entry		$pK_a^{CH}$	$k_1^{OH} (M^{-1} s^{-1})$	$k_{-1}^{H_2O} (s^{-1})$	$k_1^{H_2O} (s^{-1})$	$k_{-1}^H (M^{-1} s^{-1})$	$\log k_0^{OH}$	$\log k_0^{H_2O}$
7	$(CO)_5Cr=C \begin{matrix} \diagup OMe \\ \diagdown CH_2CH_3 \end{matrix}$	(145) <sup>a</sup>	12.32	46.8	$6.40 \times 10^{-2}$		-0.24	
8	$(CO)_5Cr=C \begin{matrix} \diagup OMe \\ \diagdown CH(CH_3)_2 \end{matrix}$	(146) <sup>a</sup>	12.27	2.97	$3.57 \times 10^{-3}$		-0.99	
9	$(CO)_5Cr=C \begin{matrix} \diagup OMe \\ \diagdown CH_2Ph \end{matrix}$	(144a) <sup>a</sup>	10.40	115	$1.90 \times 10^{-3}$	$4.10 \times 10^{-4}$ $1.02 \times 10^7$	-0.34	
10	$(CO)_5W=C \begin{matrix} \diagup OMe \\ \diagdown CH_2Ph \end{matrix}$	(144b) <sup>a</sup>	10.18	140	$1.35 \times 10^{-2}$		-0.35	$\approx 1.67$
11	$(CO)_5Cr=C \begin{matrix} \diagup SMe \\ \diagdown CH_3 \end{matrix}$	(139a) <sup>b</sup>	9.05	$1.20 \times 10^{-3}$	$8.30 \times 10^{-4}$	$1.61 \times 10^{-2}$ $1.73 \times 10^7$	0.01	$\approx 2.72$
12	$(CO)_5W=C \begin{matrix} \diagup SMe \\ \diagdown CH_3 \end{matrix}$	(139b) <sup>b</sup>	8.37	$8.37 \times 10^2$	$1.21 \times 10^{-4}$	$5.23 \times 10^{-2}$ $1.17 \times 10^7$	-0.49	$\approx 2.90$
13	$C_5H_5(NO)(PPh_3)Re^+ = C \begin{matrix} \diagup Se \\ \diagdown \text{cyclopentadienyl} \end{matrix}$	(136) <sup>c</sup>	4.18	$1.61 \times 10^4$	$3.07 \times 10^{-8}$	$1.85 \times 10^{-2}$ $2.80 \times 10^2$	$\approx -1.28$	0.36



Table 24 (continued)

Entry		$pK_a^{CH}$	$k_1^{OH} (M^{-1} s^{-1})$	$k_{-1}^{H_2O} (s^{-1})$	$k_1^{H_2O} (s^{-1})$	$k_{-1}^H (M^{-1} s^{-1})$	$\log k_0^{OH}$	$\log k_0^{H_2O}$
14	$C_5H_5(NO)(PPh_3)^+Re=$  <b>(137)<sup>c</sup></b>	-0.03	$\approx 10^5$	$\approx 6 \times 10^{-4}$	92.5	78.3	$\approx -2.61$	$\approx 1.95$

<sup>a</sup>Reference 170.<sup>b</sup>Reference 176.<sup>c</sup>Reference 177.

**Table 25** Summary of intrinsic rate constants and Brønsted  $\beta$  values for the proton transfer from carbene complexes to primary aliphatic amines ( $\text{RNH}_2$ ), secondary alicyclic amines ( $\text{R}_2\text{NH}$ ) and carboxylate ions in 50% MeCN–50% water (v/v) at 25°C

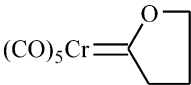
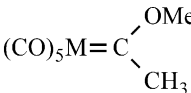
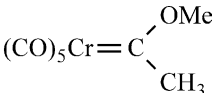
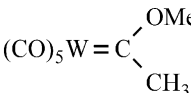
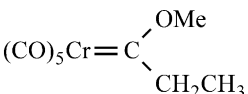
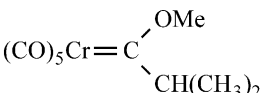
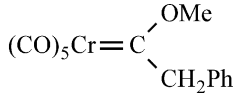
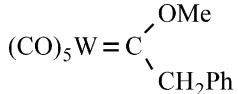
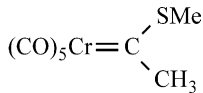
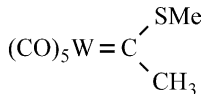
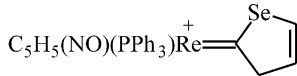
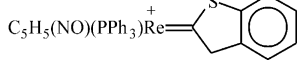
Entry	Carbene complex	$\text{p}K_{\text{a}}^{\text{CH}}$	$\log k_0^{\text{B}}(\beta)$		
			$\text{RNH}_2$	$\text{R}_2\text{NH}$	$\text{RCOO}^-$
1		(8) <sup>a</sup>	14.47		3.51 (0.62)
2		(12) <sup>a</sup>	12.81	2.95 (0.59)	3.73 (0.68)
3		(68a) <sup>a</sup>	12.50	3.04 (0.61)	3.70 (0.62)
4		(40) <sup>a</sup>	12.36	2.73 (0.64)	3.18 (0.49)
5		(145) <sup>a</sup>	12.32		2.34 (0.62)
6		(146) <sup>a</sup>	12.27		-0.11 (0.62)

Table 25 (continued)

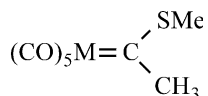
Entry	Carbene complex	$pK_a^{\text{CH}}$	$\log k_0^{\text{B}}(\beta)$			
			RNH <sub>2</sub>	R <sub>2</sub> NH	RCOO <sup>-</sup>	
7	 $(\text{CO})_5\text{Cr}=\text{C}\begin{matrix} \text{OMe} \\ \text{CH}_2\text{Ph} \end{matrix}$	(144a) <sup>a</sup>	10.40	1.51 (0.54)	1.86 (0.48)	0.79 (0.33)
8	 $(\text{CO})_5\text{W}=\text{C}\begin{matrix} \text{OMe} \\ \text{CH}_2\text{Ph} \end{matrix}$	(144b) <sup>a</sup>	10.18	1.55 (0.51)	1.93 (0.47)	
9	 $(\text{CO})_5\text{Cr}=\text{C}\begin{matrix} \text{SMe} \\ \text{CH}_3 \end{matrix}$	(139a) <sup>b</sup>	9.05	2.09 (0.48)	2.61 (0.45)	2.17 (0.44)
10	 $(\text{CO})_5\text{W}=\text{C}\begin{matrix} \text{SMe} \\ \text{CH}_3 \end{matrix}$	(139b) <sup>b</sup>	8.37	2.17 (0.47)	2.50 (0.49)	2.27 (0.43)
11	 $\text{C}_5\text{H}_5(\text{NO})(\text{PPh}_3)\text{Re}^+=\text{C}\begin{matrix} \text{Se} \\ \text{C}_4\text{H}_4 \end{matrix}$	(136) <sup>c</sup>	4.18	0.14 (0.53)	0.93 (0.49)	0.72 (0.28)
12	 $\text{C}_5\text{H}_5(\text{NO})(\text{PPh}_3)\text{Re}^+=\text{C}\begin{matrix} \text{S} \\ \text{C}_6\text{H}_4 \end{matrix}$	(137) <sup>c</sup>	-0.03	0.86 (0.33)		2.85 (0.12)

<sup>a</sup>Reference 170.<sup>b</sup>Reference 176.<sup>c</sup>Reference 177.

The powerful electron withdrawing effect of the  $(\text{CO})_5\text{M}$  moieties is best appreciated by comparing these  $\text{p}K_{\text{a}}^{\text{CH}}$  values with those of corresponding esters. For example,  $(\text{CO})_5\text{Cr}=\text{C}(\text{OEt})\text{CH}_3$  is 13.5  $\text{p}K_{\text{a}}$  units more acidic than  $\text{CH}_3\text{CO}_2\text{Et}$  ( $\text{p}K_{\text{a}}^{\text{CH}} = 26.5$ )<sup>178</sup> while  $(\text{CO})_5\text{Cr}=\text{C}(\text{SMe})\text{CH}_3$  is 12  $\text{p}K_{\text{a}}$  units more acidic than  $\text{CH}_3\text{COSEt}$  ( $\text{p}K_{\text{a}}^{\text{CH}} = 21.0$ );<sup>179</sup> the fact that the  $\text{p}K_{\text{a}}^{\text{CH}}$  values for the carbene complexes refer to 50% MeCN–50% water as the solvent is inconsequential since these  $\text{p}K_{\text{a}}^{\text{CH}}$  values are nearly the same as in water.<sup>171</sup>

The strong electron withdrawing effect of the  $(\text{CO})_5\text{M}$  groups is mainly the result of the stabilization of the conjugate anion by dispersion of the negative charge into the CO ligands, the same effect that enhances the equilibrium constants for nucleophilic addition to the carbene carbon discussed in this chapter. Regarding the variation of the  $\text{p}K_{\text{a}}^{\text{CH}}$  values with structure the following points are noteworthy.

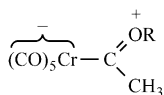
(1) The factor that affects the  $\text{p}K_{\text{a}}^{\text{CH}}$  values the most is the nature of the  $\pi$ -donor attached to the carbene carbon. For example, replacing the methoxy group in **68** or **40** with a thiomethyl group (**139**) (entry 5 versus 11 and 6 versus 12) lowers the  $\text{p}K_{\text{a}}^{\text{CH}}$  by 3.5–4.0 units.



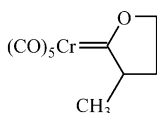
**139a** M = Cr

**139b** M = W

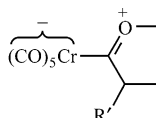
This increase in acidity is mainly the result of the weaker  $\pi$ -donor effect of the MeS ( $\sigma_{\text{R}} = -0.15$ )<sup>149</sup> compared to that of the MeO group ( $\sigma_{\text{R}} = -0.43$ )<sup>149</sup> which leads to a weaker stabilization of the neutral thia compared to the oxa carbene complexes. The higher  $\text{p}K_{\text{a}}^{\text{CH}}$  values of entries 1–3 compared to that of 5 can be attributed to  $\pi$ -donation by the respective oxygens in entries 1–3 that is stronger than in 5. In the case of entry 3, the ethyl group is a better stabilizer of the oxyanion resonance structure of the carbene complex (**140**). For the cyclic carbene complexes (entries 1 and 2), the  $\pi$ -donor effect is enhanced further because, by virtue of the cyclic structures of entries 1 and 2, the oxygen is locked into a position for better  $\pi$ -overlap with carbene carbon (**142**). <sup>53</sup>Cr NMR data are in agreement with this assessment.<sup>6</sup>



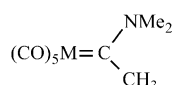
**140**



**141**



**142**



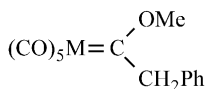
**143a** M = Cr

**143b** M = W

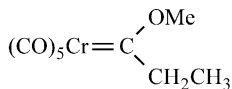
The notion that the  $\pi$ -donor effect is a dominant factor is also supported by the fact that **143a** and **143b** are not acidic enough to be deprotonated in 50% MeCN–

50% water although its acidity was determined in pure acetonitrile where its  $pK_a^{\text{CH}}$  is about 10 units higher than that of entry 5<sup>180</sup> (more on this under “Thermodynamic acidities in organic solvents”).

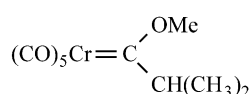
(2) Substituting one of the  $\alpha$  hydrogens by phenyl groups (**144**) increases the acidity by more than 2  $pK_a$ -units (entry 9 versus 5 and 10 versus 6). This acidifying effect is mainly the result of additional resonance stabilization of the anion provided by the phenyl group.



**144a** M = Cr  
**144b** M = W

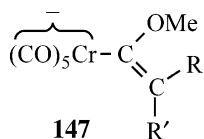


**145**



**146**

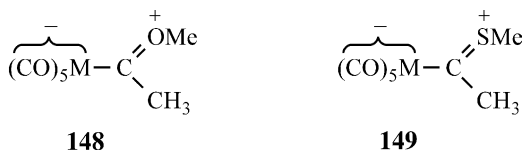
(3) Substituting one or two  $\alpha$  hydrogens by methyl groups (**145** or **146**) has an acidifying influence (entries 7 and 8 versus 5) that becomes more apparent when statistical corrections for the varying number of acidic protons are applied. These corrected  $pK_a^{\text{CH}}$  values are 12.98 for entry 5, 12.62 for 7 and 12.27 for 8. The acidity enhancement may be attributed to an increase in stability of the respective anions (entry 8 > entry 7 > entry 5) caused by the methyl groups. Assuming that the dominant resonance form of the anions has the negative charge mainly delocalized into the  $(\text{CO})_5\text{Cr}$  moiety (**147**) the increased anion stability in the order 8 > 7 > 5 simply reflects the well-known stabilization of alkenes by methyl groups.<sup>181,182</sup>



A similar situation exists when the  $pK_a^{\text{CH}}$  values of entry 1 (14.47) and entry 2 (13.41) are compared: here the acidifying effect of the methyl group is even more dramatic than in the comparison of entries 7 and 8 with 5, perhaps because  $\pi$  overlap in the anion is enhanced due to the cyclic nature of the carbene complex, which results in a more fully developed C=C double bond.

(4) The  $pK_a^{\text{CH}}$  values are not very sensitive to the metal. This is seen by a comparison of entries 4–6, of 9 with 10, and of 11 with 12. These results are reminiscent of the observations made in comparing equilibrium constants for the addition of nucleophiles to the carbene carbon (see, e.g., Tables 8, 9, 14, 17 and 19); they imply that the stabilization of the respective anions by the  $(\text{CO})_5\text{M}$  moiety depends little on the metal. The simplest explanation for this state of affairs is that it is mainly the CO ligands rather than the metal that are responsible for the stabilization of the anionic charge. It is also possible that we are dealing with a compensating effect between the influence of the metal on the stability of the anion

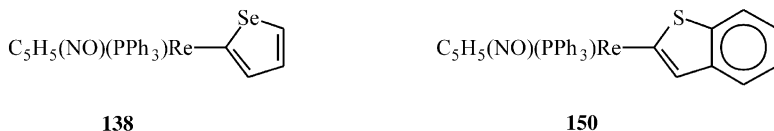
and that of the carbene complex. Thus, the  $(\text{CO})_5\text{W}$  moiety may be somewhat more effective in stabilizing negative charge of the anion than the  $(\text{CO})_5\text{Cr}$  moiety but there will also be greater stabilization of the negative charge on the resonance structure **148** ( $\text{M} = \text{W}$ ) of the carbene complex itself.



Because of this compensation effect the difference in the  $\text{p}K_{\text{a}}^{\text{CH}}$  values of entries 5 and 6 remains small. The fact that the  $\text{p}K_{\text{a}}^{\text{CH}}$  difference between entries 11 and 12 ( $\Delta\text{p}K_{\text{a}}^{\text{CH}} = 0.68$ ) is larger than that between entries 5 and 6 ( $\Delta\text{p}K_{\text{a}}^{\text{CH}} = 0.14$ ) supports this explanation: the resonance structure **149** of entries 11 and 12 is of lesser importance than **148** and hence there is less negative charge on the  $(\text{CO})_5\text{M}$  moieties of entries 11 and 12 than those of 5 and 6. As a result there is less compensation and less reduction in  $\Delta\text{p}K_{\text{a}}^{\text{CH}}$  between the chromium and tungsten carbene complex. The same type of compensating effects may be involved in explaining the small metal dependence of the equilibrium constants for nucleophilic addition to the carbene carbon (Tables 8, 9, 14, 17 and 19).

### Rhenium carbene complexes

The two rhenium carbene complexes are much more acidic than the  $(\text{CO})_5\text{M}$ -type carbene complexes. There are several reasons why they are so acidic. Probably the most important one is that they are cationic which makes the  $\text{C}_5\text{H}_5(\text{NO})(\text{PPh}_3)\text{Re}$  moiety a stronger  $\pi$ -acceptor than the  $(\text{CO})_5\text{M}$  moieties, despite the fact that in the latter there are five electron withdrawing CO ligands on the metal while there is only one electron withdrawing NO ligand in the rhenium complexes. Or, in other words, the dominant resonance structures of the conjugate bases of the rhenium complexes, **138** and **150**, respectively, are neutral molecules and hence more stable than the anionic conjugate bases of the  $(\text{CO})_5\text{M}$  type complexes.



An additional driving force for the deprotonation of the Re complexes is that their conjugate bases are aromatic, i.e., **138** is a selenophene, **150** a benzothiophene derivative. The fact that entry 14 ( $\text{p}K_{\text{a}}^{\text{CH}} = -0.3$ ) is substantially more acidic than entry 13 ( $\text{p}K_{\text{a}}^{\text{CH}} = 4.18$ ) is probably in large measure due to the stronger aromaticity of the benzothiophene moiety compared to the selenophene moiety.<sup>183</sup>

**Table 26** Intrinsic rate constants for the deprotonation of representative carbon acids in water at 25°C or 50% DMSO–50% water (v/v) at 20°C

Carbon acid	Solvent	$pK_a^{\text{CH}}$	$\log k_0^{\text{B}}$		
			RNH <sub>2</sub>	R <sub>2</sub> NH	RCOO <sup>-</sup>
HCN	H <sub>2</sub> O	9.0	~ 8.60		~ 9.1
CH <sub>2</sub> (CN) <sub>2</sub>	H <sub>2</sub> O	11.2		~ 7.0	
9-Cyanofluorene	50% DMSO	9.53	3.76	4.58	
Meldrum's acid	50% DMSO	4.70		3.90	
4-NO <sub>2</sub> C <sub>6</sub> H <sub>4</sub> CH <sub>2</sub> CN	50% DMSO	12.62		3.70	
1,3-Indandione	50% DMSO	6.35	2.44	3.13	3.18
CH <sub>2</sub> (COCH <sub>3</sub> ) <sub>2</sub>	50% DMSO	9.12	2.06	2.75	
2,4-(NO <sub>2</sub> ) <sub>2</sub> C <sub>6</sub> H <sub>3</sub> CH <sub>2</sub> CN	50% DMSO	8.06		2.75	
CH <sub>3</sub> NO <sub>2</sub>	50% DMSO	11.32		0.73	
PhCH <sub>2</sub> NO <sub>2</sub>	50% DMSO	7.93		-0.25	-0.59
CH <sub>3</sub> NO <sub>2</sub>	H <sub>2</sub> O	10.28		-0.59	
PhCH <sub>2</sub> NO <sub>2</sub>	H <sub>2</sub> O	6.88	-1.16	-0.86	

Taken from Ref. 122.

#### INTRINSIC RATE CONSTANTS FOR PROTON TRANSFER

##### *Comparisons with other carbon acids*

As discussed in the section “Alcohols and alkoxide ion nucleophiles,” the most useful measure of reactivity of a reaction system is its intrinsic barrier or intrinsic rate constant because, in comparing different systems, these quantities correct for potential differences in the thermodynamics of the reactions. A comparison of intrinsic rate constants for the deprotonation of Fischer carbene complexes by buffer bases with those for the deprotonation of other carbon acids is revealing. A representative list of such  $k_0^{\text{B}}$  values is given in Table 26. They show the well-known trend towards lower  $k_0^{\text{B}}$  values with increasing charge delocalization/resonance stabilization in the respective carbanions, a trend that results from the lag in the delocalization behind proton transfer at the transition state.

Most  $\log k_0^{\text{B}}$  values for the carbene complexes are between *ca.* 2.0 and 3.7 (Table 25) which places them into the midrange of the  $\log k_0^{\text{B}}$  values for the organic carbon acids listed in Table 26 but definitely above the intrinsic rate constants for the nitroalkanes. An interesting question is whether these findings allow the inference that the  $\pi$ -acceptor strength of the (CO)<sub>5</sub>M groups is comparable to that of 1,3-diones, 4-NO<sub>2</sub>C<sub>6</sub>H<sub>4</sub>CH<sub>2</sub>CN or 2,4-(NO<sub>2</sub>)<sub>2</sub>C<sub>6</sub>H<sub>3</sub>CH<sub>2</sub>CN but not quite at the level of nitro groups.

As already mentioned in the above referred sections, the  $k_0$ -reducing effect of resonance stabilization of the carbanion resulting from the deprotonation of organic carbon acids is the consequence of transition state imbalances. These imbalances manifest themselves in the Brønsted  $\alpha$  value being greater than the  $\beta$  value, with the

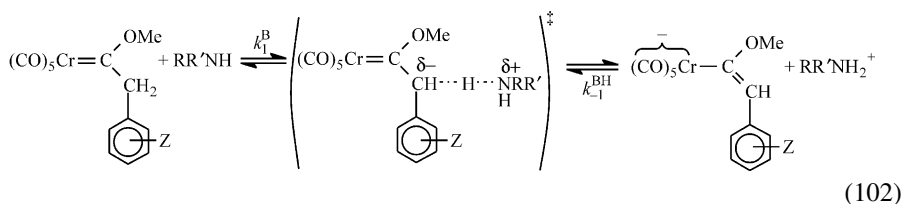
**Table 27** Brønsted  $\alpha$  and  $\beta$  values for the deprotonation of substituted benzyl carbene complexes (equation 102) in 50% MeCN–50% water at 25°C

Amine type	$\beta^a$	Amine	$\alpha^b$
RNH <sub>2</sub>	0.54 ± 0.04	<i>n</i> -BuNH <sub>2</sub>	0.56 ± 0.03
R <sub>2</sub> NH	0.48 ± 0.07	Piperidine	0.53 ± 0.03

Reference 184.

<sup>a</sup> $\beta = d \log k_1^B / d \log K_a^{BH}$  (Z = H).<sup>b</sup> $\alpha = d \log k_1^B / d \log K_a^{CH}$ .

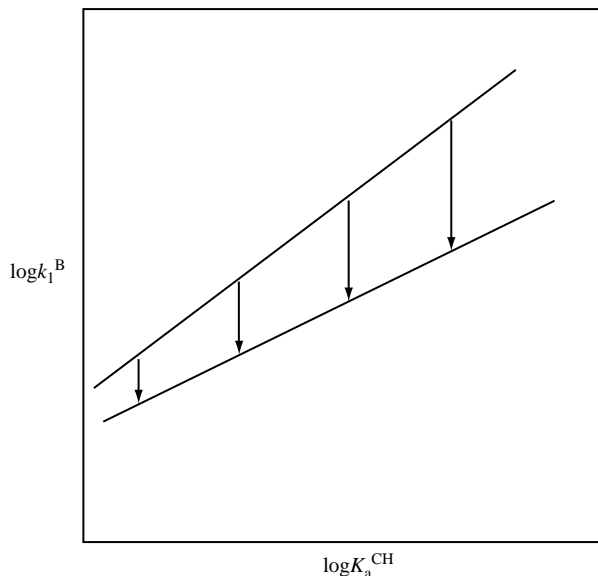
difference between  $\alpha$  and  $\beta$  correlating with the strength of the  $\pi$ -acceptor. Hence, if the same rules apply to Fischer carbene complexes, the transition state for their proton transfer reactions should also be imbalanced. However, a recent study of the reaction of substituted benzyl carbene complexes (equation 102) yielded  $\alpha$  and  $\beta$  values that, within their experimental uncertainty, are equal to each other (Table 27).<sup>184</sup>



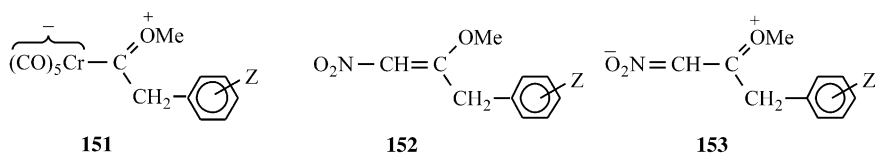
This result raised the question whether there is a fundamental difference between the (CO)<sub>5</sub>Cr moiety and purely organic  $\pi$ -acceptors in the way they affect intrinsic barriers, i.e., is it conceivable that the (CO)<sub>5</sub>Cr moiety would raise intrinsic barriers without a transition state imbalance? This seems unlikely.

A more reasonable hypothesis is that the transition state *is* imbalanced, as shown in equation (102), but that there is a structural feature characteristic of carbene complexes, absent from other carbon acids, that masks the imbalance by reducing  $\alpha$ . The most likely candidate is the  $\pi$ -donor effect of the methoxy group. Inasmuch as the contribution of **151** leads to resonance stabilization of the carbene complexes, this resonance is expected to add to the intrinsic barrier of proton transfer. This is because, as is true for resonance effects in general, its loss at the transition state should be ahead of the proton transfer.<sup>121–123</sup> As Z becomes more electron withdrawing, the greater electron deficiency of the carbene complex induces a stronger  $\pi$ -donor effect by the methoxy group. There are two consequences. One is that the increased contribution of the resonance structure **151** partially compensates for the destabilization of the electron deficient carbene carbon by the electron withdrawing inductive effect of Z. The second is that the increased resonance stabilization of the carbene complex increases the intrinsic barrier and hence the rate ( $k_1^B$ ) enhancement caused by the inductive effect of Z will be attenuated. This attenuation is proportional to the electron withdrawing strength of Z, as shown schematically in Fig. 8, and hence the slope of the Brønsted plot ( $\alpha_{\text{CH}}$ ) is reduced.





**Fig. 8** Schematic representation of how the Brønsted slope ( $\alpha_{\text{CH}}$ ) is lowered as a result of the  $\pi$ -donor effect of the MeO group. (Figure taken from Ref. 184, by permission from the American Chemical Society.)

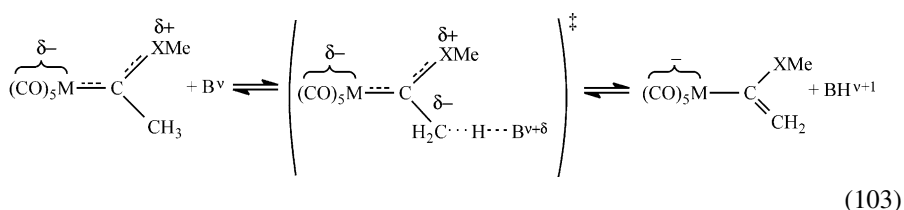


The notion that the  $\pi$ -donor effect of the methoxy group is responsible for the reduction in  $\alpha$  is supported by data on the deprotonation of **152** by amines which indicate a much smaller difference between  $\alpha$  and  $\beta$  than in the reaction of substituted phenylnitromethanes.<sup>185</sup> Again, the increased resonance stabilization by the  $\pi$ -donor effect of the MeO group (**153**) that results when Z is made more electron withdrawing is believed to be responsible for the reduced  $\alpha$  value.

#### *Dependence of $k_0$ on carbene complex structure*

For the  $(\text{CO})_5\text{M}$ -type carbene complexes, the intrinsic rate constants depend very little on the metal (Table 25, see entries 4–6), suggesting that the  $\pi$ -acceptor strength of the  $(\text{CO})_5\text{M}$  moiety is insensitive to the nature of the metal. This is true for the  $k_0^{\text{B}}$  (Table 25) as well as the  $k_0^{\text{OH}}$  values (Table 24); it is consistent with the fact that the  $\text{p}K_{\text{a}}^{\text{CH}}$  values also depend very little on M, as pointed out earlier.

The effect of changing the  $\pi$ -donor strength of alkoxy groups is also minimal, as is apparent by comparing entries 1, 3 and 5. On the other hand, the change from a MeO to a MeS group leads to a substantial lowering of  $k_0$  ( $\Delta\log k_0^{\text{OH}} = -1.30$ ,  $\Delta\log k_0^{\text{RNH}_2} = -0.95$  and  $\Delta\log k_0^{\text{R}_2\text{NH}} = -1.09$  for  $M = \text{Cr}$ ;  $\Delta\log k_0^{\text{OH}} = -1.53$ ,  $\Delta\log k_0^{\text{RNH}_2} = -0.56$  and  $\Delta\log k_0^{\text{R}_2\text{NH}} = -0.68$  for  $M = \text{W}$ ). There are probably several factors that contribute to the decrease in the  $k_0$  values. One such factor is the result of the imbalanced nature of the transition state which renders the intrinsic rate constants sensitive to the difference in the inductive/field effect of the MeO and MeS groups. These groups being closer to the negative charge at the transition state than in the anion (equation 103), their electron withdrawing effect should result in a transition state stabilization that is disproportionately strong relative to their stabilization of the anion. This will increase the intrinsic rate constant in both cases but more so for the MeO complex because of the stronger inductive effect of the MeO group compared to the MeS group.



A second factor is the larger size of the MeS group which probably reduces  $k_0$  for the MeS relative to the MeO complexes by a steric effect. As discussed in some detail elsewhere,<sup>176</sup> there is some independent evidence based on the relatively small differences between  $\log k_0^{\text{R}_2\text{NH}}$  and  $\log k_0^{\text{RNH}_2}$  for the reactions of entries 11 and 12 that steric effects indeed play a role in the reactions of these carbene complexes.

A third factor is electrostatic interaction between the base and the partial positive charge on the MeX group that arises from its  $\pi$ -donor effect. With amine bases ( $\nu = 0$ ) there is destabilization of the transition state by electrostatic repulsion. Since the  $\pi$ -donor effect of MeO is stronger than that of MeS and hence  $\delta^+$  on MeX is larger with  $X = \text{O}$  than  $X = \text{S}$ , the transition state destabilization will be greater for the MeO complexes. This will reduce  $|\Delta\log k_0^{\text{RNH}_2}|$  and  $|\Delta\log k_0^{\text{R}_2\text{NH}}|$ . With  $\text{OH}^-$  as the base ( $\nu = -1$ ) there is stabilization of the transition state that is more effective for the MeO complexes. This will enhance  $|\Delta\log k_0^{\text{OH}}|$ . The significantly more negative  $\Delta\log k_0^{\text{OH}}$  values compared to the  $\Delta\log k_0^{\text{RNH}_2}$  and  $\Delta\log k_0^{\text{R}_2\text{NH}}$  values are consistent with the above analysis. Interestingly, these electrostatic effects are strong enough to override the large steric effect expected for the amine reactions, especially those with the secondary amines, compared to that on the  $\text{OH}^-$  reactions.

Another factor that has a strong effect on the intrinsic rate constants is the substitution of a hydrogen on the  $\alpha$ -carbon by a phenyl or methyl group(s). The decrease in  $k_0$  that results from a phenyl group ( $\Delta\log k_0^{\text{OH}} = -1.65$ ,  $\Delta\log k_0^{\text{RNH}_2} = -1.53$ , and  $\Delta\log k_0^{\text{R}_2\text{NH}} = -1.84$  for  $M = \text{Cr}$ ;  $\Delta\log k_0^{\text{OH}} = -1.39$ ,  $\Delta\log k_0^{\text{RNH}_2} = -1.18$ , and  $\Delta\log k_0^{\text{R}_2\text{NH}} = -1.25$ ) can be mainly attributed to the



than entry 1 ( $pK_a^{\text{CH}} = 14.47$  in 50% MeCN–50% water). THF, a solvent commonly used in synthetic applications, allows ionization of even the least acidic carbene complexes but ion-pairing effects are so severe in this medium that quantitative measurements are strongly affected or distorted (more on this later). DMSO, a standard solvent for acidity determinations pioneered by Bordwell,<sup>187</sup> tends to oxidize Fischer carbene complexes quite rapidly.<sup>87,188</sup>

The most suitable solvent appears to be acetonitrile, which has also been used successfully for acidity measurements of hydrido transition metal complexes<sup>148,189</sup> and transition metal acyl compounds.<sup>190</sup> Fischer carbene complexes are quite stable in this solvent; its polarity is high enough that ion pairing is not a significant problem and  $pK_a$  values up to about 36 can be measured.<sup>191,192</sup>

### Acetonitrile

Table 28 summarizes  $pK_a^{\text{CH}}$  value determined in acetonitrile<sup>194</sup> along with  $pK_a^{\text{CH}}$  values in 50% MeCN–50% water for the complexes where these are available (values in parentheses). They were obtained spectrophotometrically from measurements of the equilibrium constants of the reaction of the carbene complex with strong amine bases such as TMG (1,1,2,2-tetramethylguanidine), DBU (1,8-diazabicyclo[5.4.0]undec-7-ene), BEMP (2-(*tert*-butylimino)-2-(diethylamino)-1,3-dimethylperhydro-1,3-diazaphosphine) and  $P_2\text{-Et}$  (1-*tert*-butyl-2,2,4,4,4-pentakis(dimethylamino)-2 $\lambda^5$ ,4 $\lambda^5$ -catenadi(phosphazene)).

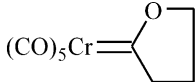
The  $pK_a^{\text{CH}}$  values in pure acetonitrile are, on average, 10.2 units higher than in 50% MeCN–50% water. This difference may be expressed by equation (104)

$$\begin{aligned} {}^{50}\Delta^A pK_a^{\text{CH}} &= pK_a^{\text{CH}}(\text{MeCN}) - pK_a(50\% \text{ MeCN} - 50\% \text{ water}) \\ &= \log {}^{50}\gamma_{\text{C}^-}^A + \log {}^{50}\gamma_{\text{H}^+}^A - \log {}^{50}\gamma_{\text{CH}}^A \end{aligned} \quad (104)$$

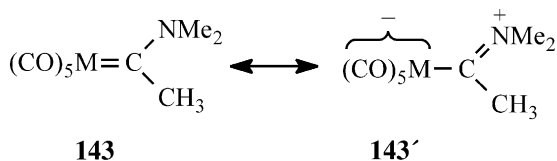
where  ${}^{50}\gamma_{\text{C}^-}^A$ ,  ${}^{50}\gamma_{\text{H}^+}^A$  and  ${}^{50}\gamma_{\text{CH}}^A$  are the solvent activity coefficients for the transfer of the anion  $\text{C}^-$ ,  $\text{H}^+$ , and the carbene complex (CH), respectively, from 50% MeCN–50% water (“50”) to pure MeCN (“A”).<sup>193</sup> The largest contributor to  ${}^{50}\Delta^A pK_a^{\text{CH}}$  must come from the  $\log {}^{50}\gamma_{\text{H}^+}^A$  term: for the transfer of  $\text{H}^+$  from pure water (“W”) to acetonitrile,  $\log {}^W\gamma_{\text{H}^+}^A = 8.1$ ,<sup>195,196</sup> reflecting the much weaker solvation of  $\text{H}^+$  in acetonitrile. The value of  $\log {}^{50}\gamma_{\text{H}^+}^A$  is not known but it is probably close to 8.1. This leaves a contribution of perhaps 2.5–3.0 log units of  ${}^{50}\Delta^A pK_a^{\text{CH}}$  to be accounted for by  $\log {}^{50}\gamma_{\text{C}^-}^A - \log {}^{50}\gamma_{\text{CH}}^A$  which must result from a combination of weaker solvation of  $\text{C}^-$  ( $\log {}^{50}\gamma_{\text{C}^-}^A > 0$ ) and a stronger solvation of CH ( $\log {}^{50}\gamma_{\text{CH}}^A < 0$ ) in pure acetonitrile.

The  $\text{Me}_2\text{N}$  derivatives (**143a** and **143b**) are seen to be the least acidic carbene complexes with  $pK_a^{\text{CH}}$  values (31.9 and 31.7, respectively) almost 10 units higher than for the methoxy analog **6** ( $pK_a^{\text{CH}} = 22.2$ ). The reduction in acidity reflects the strong  $\pi$ -donor effect at the  $\text{Me}_2\text{N}$  group, which stabilizes the carbene complex; the magnitude of the effect emphasizes the great importance of the resonance form **143'** in determining the electronic structure of Fischer carbene complexes.

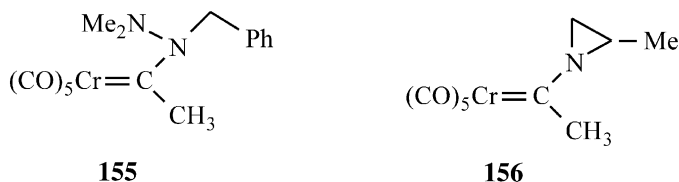
**Table 28** Summary of  $pK_a^{\text{CH}}$  values of Fischer carbene complexes in acetonitrile at 25°C

Carbene complex		$pK_a^{\text{CH}}$	Carbene complex		$pK_a^{\text{CH}}$
$(\text{CO})_5\text{Cr}=\text{C}(\text{NMe}_2)\text{CH}_3$	(143a)	31.9 <sup>a</sup>	$(\text{CO})_4\text{Cr}=\text{C}(\text{OMe})\text{CH}_3$   Ph <sub>3</sub> P	(158)	25.4 <sup>b</sup>
$(\text{CO})_5\text{W}=\text{C}(\text{NMe}_2)\text{CH}_3$	(143b)	31.7 <sup>a</sup>	$(\text{CO})_5\text{Cr}=\text{C}(\text{O})$ 	(8)	24.4 <sup>b</sup> (14.47) <sup>c</sup>
$(\text{CO})_5\text{Cr}=\text{C}(\text{N}(\text{Me}_2)\text{CH}_2\text{Ph})\text{CH}_3$	(155)	30.8	$(\text{CO})_5\text{Cr}=\text{C}(\text{OEt})\text{CH}_3$	(66)	25.2 <sup>b</sup> (12.98) <sup>c</sup>
$(\text{CO})_5\text{Cr}=\text{C}(\text{N}(\text{Me})\text{CH}_2\text{Me})\text{CH}_3$	(156)	27.6 <sup>b</sup>	$(\text{CO})_5\text{Cr}=\text{C}(\text{OMe})\text{CH}_2\text{CH}_3$	(145)	22.9 <sup>b</sup> (12.36) <sup>c</sup>
$(\text{CO})_4\text{Cr}=\text{C}(\text{OMe})\text{CH}_3$   (n-Bu) <sub>3</sub> P	(157)	26.5 <sup>b</sup>	$(\text{CO})_5\text{Cr}=\text{C}(\text{OMe})\text{CH}_3$	(68)	22.2 <sup>b</sup> (12.50) <sup>c</sup>

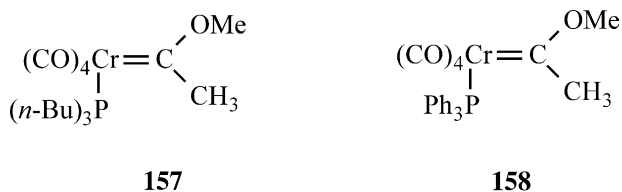
<sup>a</sup>Reference 180.<sup>b</sup>Reference 194.<sup>c</sup>In 50% MeCN–50% water (Table 24).



Replacing the methyl groups on the nitrogen by a  $\text{Me}_2\text{N}$  and a  $\text{PhCH}_2$  group increases the acidity only by about one  $\text{p}K_{\text{a}}$  unit (**155**), suggesting that the  $\pi$ -donor effect of the  $\text{N}(\text{Me}_2\text{N})\text{CH}_2\text{Ph}$  group is only slightly weaker than that of the  $\text{Me}_2\text{N}$  group. On the other hand, converting the  $\text{Me}_2\text{N}$  group into an aziridinyl group (**156**) leads to a 4.3 unit drop in  $\text{p}K_{\text{a}}^{\text{CH}}$  because the ring strain counteracts  $\text{sp}^2$  hybridization of the nitrogen and hence reduces its  $\pi$ -donor effect.



Substitution of one CO ligands by a phosphine (**157** and **158**) increases the  $\text{p}K_{\text{a}}^{\text{CH}}$  relative to that of  $(\text{CO})_5\text{Cr}=\text{C}(\text{OMe})\text{CH}_3$  (**68**), reflecting the reduced electron withdrawing effect of the  $(\text{CO})_4(\text{R}_3\text{P})\text{Cr}$  moiety relative to the  $(\text{CO})_5\text{Cr}$  moiety.



#### *Tetrahydrofuran and dimethyl sulfoxide*

Despite the drawbacks mentioned above, a small number of acidity measurements have been reported in THF<sup>167,197–199</sup> and in DMSO.<sup>29</sup> A major problem with THF is that there are no free ions in this solvent which makes it difficult to define a  $\text{p}K_{\text{a}}^{\text{CH}}$  that would be directly comparable to  $\text{p}K_{\text{a}}^{\text{CH}}$  values in polar solvents. Nevertheless, some of these acidity data have recently been summarized in terms of  $\text{p}K_{\text{a}}^{\text{CH}}$  values;<sup>29</sup> they are reported as “ $\text{p}K_{\text{a}}^{\text{CH}}$ ” in Table 29. The “ $\text{p}K_{\text{a}}^{\text{CH}}$ ” values for **68**, **8** and **141** in THF are based on equilibrium measurements of the reaction of the respective carbene complexes with the PPN (see footnote *b* in Table 29) salt of *p*-cyanophenoxide ion,<sup>167,197,198</sup> “ $\text{p}K_{\text{a}}^{\text{CH}}$ ” = 8 was deduced from the fact that the

**Table 29** Summary of  $pK_a^{\text{CH}}$  values of Fischer carbene complexes in THF and DMSO

Carbene complex		Solvent	Base	$pK_a^{\text{CH}}$
$(\text{CO})_5\text{Cr}=\text{C}(\text{OMe})(\text{CH}_3)$	(68)	THF	$\text{Li}^+\text{MeO}^-$	12 <sup>a</sup>
$(\text{CO})_5\text{Cr}=\text{C}(\text{O})\text{C}_2\text{H}_4$	(8)	THF	$\text{PPN}^{+b}4\text{-CNC}_6\text{H}_4\text{O}^-$ $\text{PPN}^{+b}4\text{-CNC}_6\text{H}_4\text{O}^-$	8 <sup>c</sup> 8 <sup>d</sup>
$(\text{CO})_5\text{Cr}=\text{C}(\text{O})\text{C}_2\text{H}_4\text{CH}_3$	(141)	THF	$\text{PPN}^{+b}4\text{-CNC}_6\text{H}_4\text{O}^-$	8 <sup>d</sup>
$(\text{CO})_4\text{Cr}=\text{C}(\text{OMe})(\text{CH}_3)(\text{n-Bu})_3\text{P}$	(157)	THF	$\text{Li}^+t\text{-BuO}^-$	18.8 <sup>e</sup>
$(\text{CO})_5\text{Cr}=\text{C}(\text{NMe}_2)(\text{CH}_3)$	(143a)	DMSO	$\text{K}^+2\text{-naphthylacetonitrile anion}$	20.4 <sup>f</sup>

<sup>a</sup>Reference 197.<sup>b</sup> $\text{PPN}^+$  = bis(triphenylphosphine)iminium ion.<sup>c</sup>Reference 167.<sup>d</sup>Reference 198.<sup>e</sup>Reference 199.<sup>f</sup>Reference 29.

equilibrium constants were about 1.0 for all three complexes while the aqueous  $pK_a$  of *p*-cyanophenol is 8.0. The “ $pK_a^{\text{CH}}$ ” value of 12 for **68**<sup>197</sup> was calculated on the basis of the equilibrium constant of the reaction of **68** with lithium methoxide and the  $pK_a$  of methanol. The “ $pK_a^{\text{CH}}$ ” value for **157** was derived from measurements with lithium *tert*-butoxide and the known  $pK_a$  of *tert*-butanol.<sup>199</sup>

The problem with the “ $pK_a^{\text{CH}}$ ” values in THF is that their absolute values have no well defined physical meaning. This is not only because of ion pairing effects but also because they are not based on  $pK_a$  values of the proton acceptors in THF but in solvents such as water or methanol. Even the *relative* “ $pK_a^{\text{CH}}$ ” values suffer from gross distortions which render their meaning questionable. For example, the “ $pK_a^{\text{CH}}$ ” value obtained for **68** strongly depends on the base system used for the deprotonation, i.e.,  $\text{PPN}^+/4\text{-CNC}_6\text{H}_4\text{O}^-$  versus  $\text{Li}^+/\text{MeO}^-$ . This must be the result of large differences in the tightness or stability of reactant and/or product ion pairs. Or, the “ $pK_a^{\text{CH}}$ ” values of **68**, **8** and **141** are all about the same in THF which

contrasts with the results in acetonitrile (Table 28) where the  $pK_a^{CH}$  of **8** is 2.2 units higher than that of **68** and the  $pK_a^{CH}$  of **141** is 1.5 units higher than that of **68**.

With respect to the “ $pK_a^{CH}$ ” of **143a** in DMSO (20.4), it is 11.5 units lower than in acetonitrile. This is a reasonable result. Carbon acids such as 4- $\text{NO}_2\text{C}_6\text{H}_4\text{CH}_2\text{NO}_2$  and 3,5- $(\text{NO}_2)_2\text{C}_6\text{H}_3\text{CH}_2\text{NO}_2$  have  ${}^D\Delta^A pK_a^{CH}$  values of 11.7, 12.0 and 11.2, respectively.<sup>200</sup> One may express  ${}^D\Delta^A pK_a^{CH}$  by equation (105) which is analogous to equation (104).

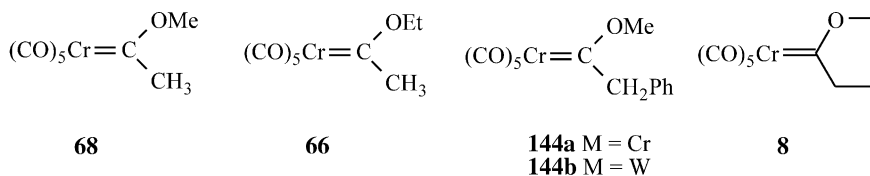
$$\begin{aligned} {}^D\Delta^A pK_a^{CH} &= pK_a^{CH}(\text{MeCN}) - pK_a^{CH}(\text{DMSO}) \\ &= \log {}^D\gamma_{\text{C}^-}^A + \log {}^D\gamma_{\text{H}^+}^A - \log {}^D\gamma_{\text{CH}}^A \end{aligned} \quad (105)$$

Again, as is the case for the comparison between pure acetonitrile and aqueous acetonitrile, the dominant contribution to the solvent effect on the  $pK_a^{CH}$  value comes from the much weaker solvation of the proton in acetonitrile, i.e.,  $\log {}^D\gamma_{\text{H}^+}^A = 11.4$ .<sup>195,196</sup>

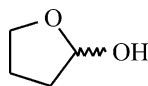
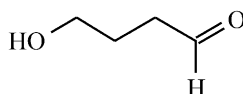
#### HYDROLYSIS OF IONIZABLE CARBENE COMPLEXES

##### *Thermal reactions*

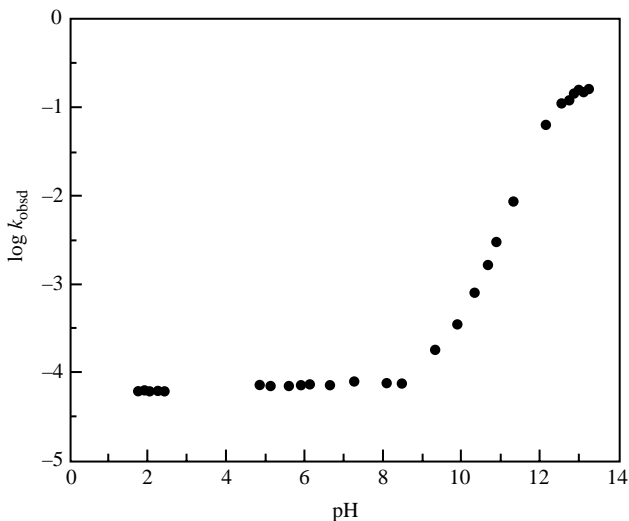
The hydrolysis of Fischer carbene complexes such as **11**, **13**, **42**, **87** and **112** has been discussed in the section “Hydroxide ion and water as nucleophiles” and proceeds by a standard nucleophilic addition–elimination mechanism (equation 74). On the other hand, carbene complexes with ionizable  $\alpha$ -carbons are hydrolyzed by a different mechanism which involves the deprotonated carbene complex as the key intermediate. This conclusion is based on a detailed kinetic investigation of the hydrolysis of **66**, **68**, **144** and **8** in 50% MeCN–50% water.<sup>201–204</sup>



The organic products of the hydrolysis reactions were: acetaldehyde and methanol for **68**,<sup>201</sup> acetaldehyde and ethanol for **66**,<sup>201</sup>  $\beta$ -methoxystyrene for **144**,<sup>202</sup> and 2-hydroxytetrahydrofuran (**159**) in equilibrium with small amounts of 4-hydroxybutanal (**160**) for **8**.<sup>203</sup>

**159****160**

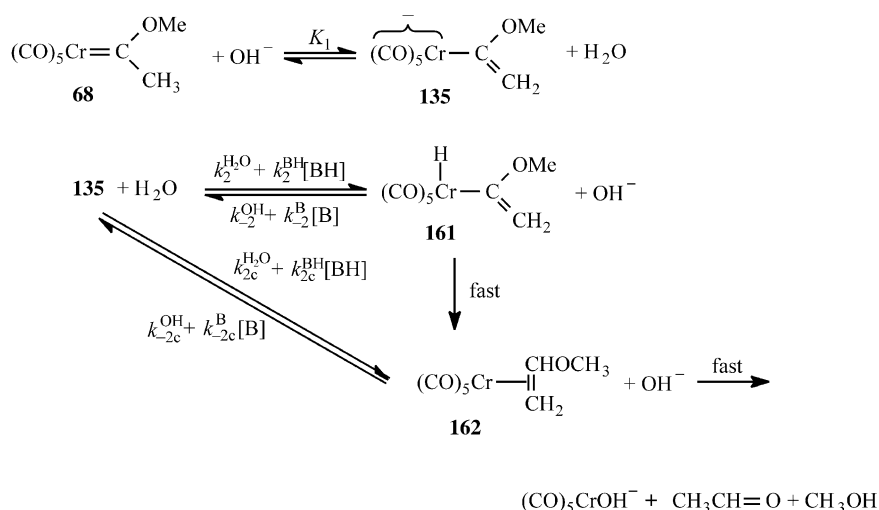




**Fig. 9** Rate–pH profile of the hydrolysis of  $(\text{CO})_5\text{M}=\text{C}(\text{OMe})\text{CH}_3$  (**68**) in 50% MeCN–50% water (v/v) at 25°C. (Figure taken from Ref. 201, by permission from the American Chemical Society.)

Figure 9 shows a typical rate–pH profile; the points below pH 8.5 represent a “water reaction,” those above 8.5 an  $\text{OH}^-$  catalyzed reaction while the leveling off at pH > 12 is due to the ionization of the carbene complex. The hydrolysis is subject to general base catalysis; the points on the pH–rate profile between pH 4.8 and 11.3 were obtained by extrapolation of buffer plots to zero buffer concentration.

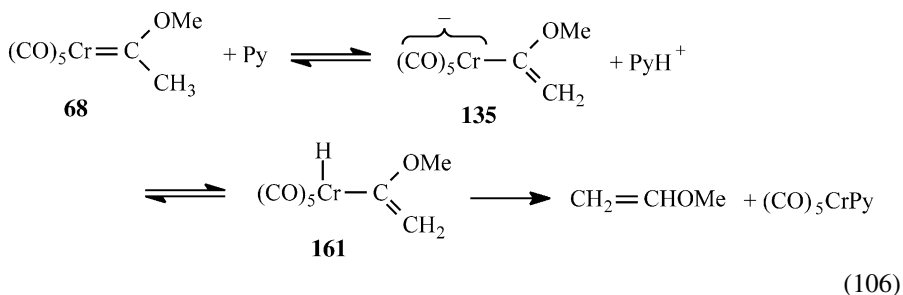
The pH dependence of the hydrolysis of all compounds studied is, in principle, consistent with the mechanism of Scheme 6 that applies to the alkoxyphenylcarbene complexes, and so are the products of the reactions of **68**, **66** and **8**. However, the products obtained in the hydrolysis of **144** and the fact that in basic solution the hydrolysis of all the compounds is subject to a substantial kinetic solvent isotope effect are inconsistent with Scheme 6, at least at pH > 8.5. The mechanism that accounts best for all experimental observations at pH > 8.5, including the isotope effect, is shown in Scheme 17 for the example of **68**. It involves rapid deprotonation of **68** followed either by slow protonation of **135** with water ( $k_2^{\text{H}_2\text{O}}$ ) or a buffer acid ( $k_2^{\text{BH}}[\text{BH}]$ ) and subsequent rapid conversion of **161** to **162**, or slow concerted water ( $k_{2c}$ ) or buffer acid catalyzed ( $k_{2c}^{\text{BH}}[\text{BH}]$ ) conversion of **135** to **162** (more on these two alternatives below). Complexation between  $(\text{CO})_5\text{Cr}$  and the enol ether activates the latter toward basic hydrolysis which rapidly leads to the vinyl alcohol and tautomerization to the aldehyde. Control experiments demonstrated that the kind of complexation indicated by **162** indeed promotes rapid hydrolysis of the enol ether.<sup>201</sup> In the reactions of **144** complexation of the enol ether ( $\beta$ -methoxystyrene) appears to be weak, presumably because of steric crowding, and hence the reaction



Scheme 17

essentially stops at the  $\beta$ -methoxystyrene stage although small amounts of  $\text{PhCH}_2\text{CH}=\text{O}$  could be detected with **144b**. Incidentally, in the absence of water, e.g., when **68** or **8** is reacted with pyridine or other tertiary amines, hydrolysis of **162** is not possible and the reaction always stops at the enol ether stage. This process has been exploited for the synthesis of complex enol ethers from alkoxy-carbene complexes.<sup>23</sup>

Regarding the conversion of **135** into **162**, there are two possible pathways, stepwise or concerted (Scheme 17). The stepwise pathway entails rate-limiting protonation on the metal followed by rapid reductive elimination while the concerted pathway involves protonation on the carbene carbon which is simultaneous with bond cleavage between the metal and the carbene carbon. For the reactions with tertiary amines, e.g., pyridine, in the absence of water, the stepwise analog of Scheme 17, i.e., equation (106), has been advocated<sup>23</sup> although no experimental evidence has been cited to exclude a concerted pathway.

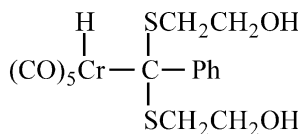


For the reactions in aqueous acetonitrile the concerted pathway is more plausible based on the following reasoning.

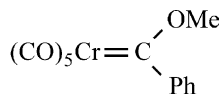
The rate constant for the conversion of **135** to **162** is  $0.16 \text{ s}^{-1}$ .<sup>201</sup> If the stepwise mechanism applies, this means  $k_2^{\text{H}_2\text{O}} = 0.16 \text{ s}^{-1}$ . If the concerted mechanism prevails, we have  $k_{2c}^{\text{H}_2\text{O}} = 0.16 \text{ s}^{-1}$ . If we assume that the  $\text{p}K_a^{\text{MH}}$  (metal proton) of **161** is comparable to that of **163**, i.e.,  $\text{p}K_a^{\text{MH}} \approx 0.7$ ,<sup>147</sup> one can estimate a  $k_{-2}^{\text{OH}}$  value based on equation (107)

$$k_{-2}^{\text{OH}} = k_2^{\text{H}_2\text{O}} \frac{K_a^{\text{MH}}}{K_w} \quad (107)$$

where  $K_w = 6.46 \times 10^{-16} \text{ M}^2$  is the ionic product of water in 50% MeCN–50% water.<sup>171</sup> One obtains  $k_{-2}^{\text{OH}} \approx 3.1 \times 10^{14} \text{ M}^{-1}$ , a nonsensical value that is about three orders of magnitude larger than the rate constant of a diffusion controlled proton transfer. Hence the step-wise mechanism must be discarded, at least in aqueous acetonitrile. The same conclusion is reached using similar arguments for the buffer catalyzed pathway.<sup>201</sup>

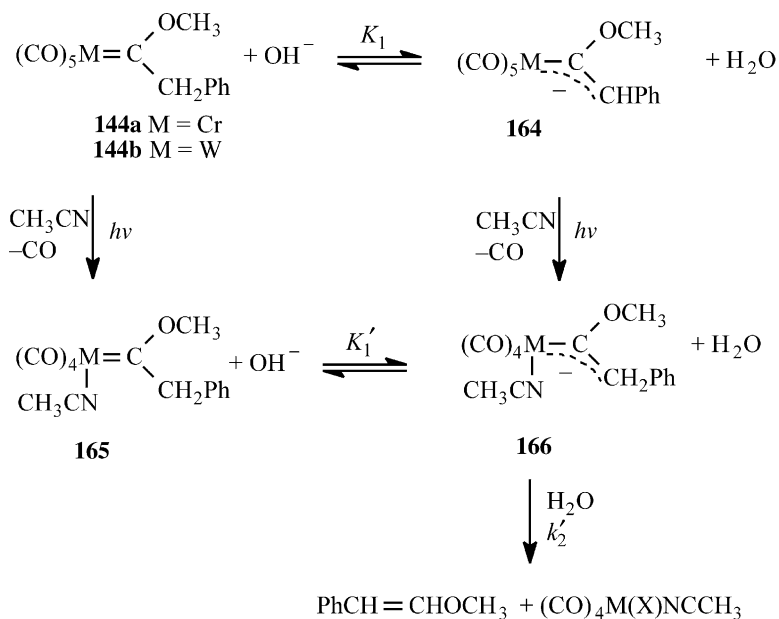
**163**

An interesting question is why the base catalyzed hydrolysis of ionizable carbene complexes proceeds by the mechanism of [Scheme 17](#) instead of that of [Scheme 11](#). Apparently [Scheme 17](#) is energetically more favorable than [Scheme 11](#). Detailed analysis indicates that for the nucleophilic mechanism to be competitive with [Scheme 17](#) in the case of **68**, the rate constant for  $\text{OH}^-$  attack on **68** would have to be at least 3-fold higher than for  $\text{OH}^-$  attack on the phenyl analog (**11**).<sup>157</sup> This contrasts with the expectation that it is **11** which should be the more reactive carbene complex, due to the electron withdrawing inductive effect of the phenyl group. The potential  $\pi$ -donor effect of the phenyl group which would counteract its inductive effect is negligible because this group was found to have an orthogonal orientation both in the solid state<sup>205</sup> and in solution.<sup>206</sup> The notion that the phenyl group in **11** is electron withdrawing relative to the methyl group in **68** is also supported by  $^{53}\text{Cr}$  NMR data.<sup>6</sup>

**11**

### Light-induced reactions

The hydrolysis of **144a** and **144b** is catalyzed by light.<sup>202</sup> Accelerations of the order of 5- to 6-fold in the presence of high light intensities have been observed. A



Scheme 18

possible mechanism for this photochemical process is shown in Scheme 18.<sup>202</sup> This mechanism is consistent with the fact that  $\text{PhCH}=\text{CHOCH}_3$  is the main organic product of the reaction, just as for the thermal reaction, and with a kinetic solvent isotope effect that is similar to that for the thermal process and suggests that reaction of **164** with water is rate limiting. The results did not, however, allow a distinction between the two pathways that lead to **166**. Note that the increased reactivity of **166** compared to **164** is consistent with a higher electron density induced by replacing one of the strongly electron withdrawing CO ligands by acetonitrile.

The hydrolysis of **146**<sup>207</sup> (isopropyl carbene) is also catalyzed by light although the effect is smaller than for **144a** or **144b** and the phenomenon was not studied in detail. On the other hand, no light-induced rate accelerations were observed for the hydrolysis of the cyclic carbene complexes **8**<sup>203</sup> and **141**,<sup>204</sup> or of the ethyl carbene complex **145**.<sup>174</sup> It is unclear at this point what structural factors power the photochemical reaction shown in Scheme 18.

## Acknowledgments

I gratefully acknowledge the tremendous contributions of all my co-workers whose names are cited in the references and who made it all possible. I also thank the National Science Foundation for its financial support (Grant CHE-0098553).

## References

1. Dötz, K.H., Fischer, H., Hofmann, P., Kreissl, F.R., Schubert, U. and Weiss, K. (1983). *Transition Metal Carbene Complexes*. Verlag Chemie, Weinheim
2. Taylor, T.E. and Hall, M.B. (1984). *J. Am. Chem. Soc.* **106**, 1576
3. Carter, E.A. and Goddard, W.A., III (1986). *J. Am. Chem. Soc.* **108**, 4746
4. Crabtree, R.H. (1988). *The Organometallic Chemistry of Transition Metals*, Chapter 11. Wiley, New York
5. Fischer, E.O. and Maasböl, A. (1967). *Chem. Ber.* **100**, 2445
6. Hafner, A., Hegedus, L.S., de Weck, G., Hawkins, B. and Dötz, K.H. (1988). *J. Am. Chem. Soc.* **110**, 8413
7. Marynick, D.S. and Kirkpatrick, C.M. (1985). *J. Am. Chem. Soc.* **107**, 1993
8. Dötz, K.H. (1984). *Angew. Chem. Int. Ed. Engl.* **13**, 587
9. Gallop, M.A. and Roper, W.R. (1986). *Adv. Organomet. Chem.* **25**, 121
10. Brookhart, M. and Studabaker, W.B. (1987). *Chem. Rev.* **87**, 411
11. Schubert, U. (ed.) (1988). *NATO ASI Series, Series C: Mathematical and Physical Sciences. Advances in Metal Carbene Chemistry*. **vol. 269**
12. Wulff, W.D. (1989). *Advances in Metal-Organic Chemistry*. Liebeskind, L.S. (ed.), **vol. 1**, p. 209–393. JAI, London
13. Dötz, K.H. (1990). *New J. Chem.* **14**, 433
14. Wulff, W.D. (1991). *Comprehensive Organic Synthesis*. Trost, R.H., Fleming, I. and Paquette, L.A. (eds), **vol. 5**, p. 1065–1113. Pergamon, Oxford
15. Reissig, H.-U. (1991). *Organic Synthesis Highlights*. Mulzer, J., Altenbach, H.-J., Braun, M., Krohn, K. and Reissig, H.-U. (eds), p. 168–191. VCH, Weinheim
16. Guerchais, V. (1994). *Bull. Soc. Chim. Fr.* **131**, 803
17. Hegedus, L.S. (1995). *Acc. Chem. Res.* **28**, 299
18. Wulff, W.D. (1995). *Comprehensive Organometallic Chemistry II*. Abel, E.W., Stone, F.G.A., Wilkinson, G. and Hegedus, L.S. (eds), **vol. 12**, p. 469–547. Pergamon, New York
19. Harvey, D.F. and Sigano, D.M. (1996). *Chem. Rev.* **96**, 271
20. de Meijere, A. (1996). *Pure Appl. Chem.* **68**, 61
21. Aumann, R. and Nienaber, H. (1997). *Adv. Organomet. Chem.* **41**, 163
22. Dörwald, F.Z. (1999). *Metal Carbenes in Organic Synthesis*. VCH, Weinheim
23. Hegedus, L.S. (1999). *Transition Metals in the Synthesis of Complex Organic Molecules* (2nd edn), Chapter 6. University Science Books, Sausalito, CA
24. Aumann, R. (2000). *Eur. J. Org. Chem.* 17
25. de Meijere, A., Schirmer, H. and Duetsch, M. (2000). *Angew. Chem. Int. Ed. Engl.* **39**, 3964
26. Casey, C.P. (1976). *Transition Metal Organometallics in Organic Synthesis*. Alper, H. (ed.), p. 190–223. Academic, New York
27. Lattuada, L., Licandro, E., Maiorana, S. and Papagni, A. (1991). *Organometallics* **10**, 807
28. Aumann, R. and Heinen, A. (1987). *Chem. Ber.* **120**, 537
29. Wulff, W.D., Anderson, B.A., Toole, A.J. and Xu, Y.-C. (1994). *Inorg. Chim. Acta* **220**, 215
30. Xu, Y.-C. and Wulff, W.D. (1987). *J. Org. Chem.* **52**, 3263
31. Fischer, E.O. and Massböl, A. (1968). *J. Organomet. Chem.* **12**, P15
32. Fischer, E.O. and Plabst, W. (1974). *Chem. Ber.* **107**, 3326
33. Casey, C.P. and Anderson, R.L. (1975). *J. Chem. Soc., Chem. Commun.* 895
34. Doyle, M.P. (1995). *Comprehensive Organometallic Chemistry II*. Abel, E.W., Stone, F.G.A. and Wilkinson, G. (eds), **vol. 12**, p. 387–395. Pergamon, Oxford
35. Dötz, K.H. and Fischer, E.O. (1972). *Chem. Ber.* **105**, 1356

36. Fischer, E.O. and Dötz, K.H. (1972). *Chem. Ber.* **105**, 3966
37. Casey, C.P. and Burkhardt, T.I. (1974). *J. Am. Chem. Soc.* **96**, 7808
38. Dötz, K.H. and Tomuschat, P. (1999). *Chem. Soc. Rev.* **28**, 187
39. Gut, H.-P., Welk, N., Link, U., Fischer, H. and Steiner, U.E. (2000). *Organometallics* **19**, 2354
40. Foley, H.C., Strubinger, L.M., Targos, T.S. and Geoffroy, G.L. (1983). *J. Am. Chem. Soc.* **105**, 3064
41. Collman, J.P., Hegedus, L.S., Norton, J.R. and Finke, R.G. (1987). *Principles and Applications of Organotransition Metal Chemistry*, Chapter 16. University Science Books, Mill Valley, CA
42. Schmidt, M.A., Miller, J.R. and Hegedus, L.S. (1991). *J. Organomet. Chem.* **413**, 143
43. Hegedus, L.S. (1997). *Tetrahedron* **53**, 4105
44. Casey, C.P. and Anderson, R.L. (1975). *J. Chem. Soc., Chem. Commun.* 895
45. Casey, C.P. and Cesa, M.C. (1982). *Organometallics* **1**, 87
46. Werner, H. and Rascher, H. (1968). *Helv. Chim. Acta* **51**, 1765
47. Fischer, H., Fischer, E.O., Kreiter, C.G. and Werner, H. (1974). *Chem. Ber.* **107**, 2459
48. Fischer, H. In Ref. **1**, p. 252
49. Fischer, H., Mühlemeier, J., Märkl, R. and Dötz, K.H. (1982). *Chem. Ber.* **115**, 1355
50. Torrent, M., Duran, M. and Solà, M. (1998). *Organometallics* **17**, 1492
51. Fischer, H. and Hofmann, P. (1999). *Organometallics* **18**, 2590
52. Fischer, H., Motsch, A. and Kleine, W. (1978). *Angew. Chem. Int. Ed. Engl.* **17**, 842
53. Fischer, H., Motsch, A., Märkl, R. and Ackermann, K. (1985). *Organometallics* **4**, 726
54. Fischer, H. and Motsch, A. (1981). *J. Organomet. Chem.* **220**, 301
55. Fischer, H., Fischer, E.O., Himmelreich, D., Cai, R., Schubert, U. and Ackermann, K. (1981). *Chem. Ber.* **114**, 3220
56. Fischer, H., Fischer, E.O., Cai, R. and Himmelreich, D. (1983). *Chem. Ber.* **116**, 1009
57. Fischer, H. (1980). *J. Organomet. Chem.* **195**, 55
58. Fischer, H., Fischer, E.O. and Cai, R. (1982). *Chem. Ber.* **115**, 2707
59. Fischer, E.O. and Fischer, H. (1974). *Chem. Ber.* **107**, 657
60. Casey, C.P. and Shusterman, A.J. (1970). *J. Mol. Catal.* **8**, 1
61. Casey, C.P., Scheck, D.M. and Shusterman, A.J. (1979). *Fundam. Res. Homogenous* **3**, 141
62. Casey, C.P., Shusterman, A.J., Vollendorf, N.W. and Haller, K.J. (1982). *J. Am. Chem. Soc.* **104**, 2417
63. Dahlgren, R.M. and Zink, J.I. (1977). *Inorg. Chem.* **16**, 3154
64. Edwards, B.H. and Rausch, M.D. (1981). *J. Organomet. Chem.* **210**, 91
65. Foley, H.C., Strubinger, L.M., Targos, T.S. and Geoffroy, G.L. (1983). *J. Am. Chem. Soc.* **105**, 3064
66. Bechara, J.N., Bell, S.E.J., McGarvey, J.J. and Rooney, J.J. (1986). *J. Chem. Soc., Chem. Commun.* 1785
67. Bell, S.E.J., Gordon, K.C. and McGarvey, J.J. (1988). *J. Am. Chem. Soc.* **110**, 3107
68. Servaas, P.C., Stufkens, D.J. and Oskam, A. (1990). *J. Organomet. Chem.* **390**, 61
69. Rooney, A.D., McGarvey, J.J. and Gordon, K.C. (1995). *Organometallics* **14**, 107
70. Rooney, A.D., McGarvey, J.J., Gordon, K.C., McNicholl, R.-A., Schubert, U. and Hepp, W. (1993). *Organometallics* **12**, 1277
71. Gut, H.-P., Welte, N., Link, U., Fischer, H. and Steiner, U.E. (2000). *Organometallics* **19**, 2354
72. Klabunde, U. and Fischer, E.O. (1967). *J. Am. Chem. Soc.* **89**, 7141
73. Connor, J.A. and Fischer, E.O. (1969). *J. Chem. Soc. A* 578
74. Fischer, E.O. and Kollmeier, H.-J. (1971). *Chem. Ber.* **104**, 1339
75. Fischer, E.O. and Leupold, M. (1972). *Chem. Ber.* **105**, 599
76. Fischer, E.O., Heckl, B. and Werner, H. (1971). *J. Organomet. Chem.* **28**, 359

77. Fischer, E.O. and Aumann, R. (1968). *Chem. Ber.* **101**, 963
78. Fischer, E.O. and Knauss, L. (1970). *Chem. Ber.* **103**, 1262
79. Kreiter, C.G. (1968). *Angew. Chem. Int. Ed. Engl.* **7**, 390
80. Fischer, E.O., Leupold, M., Kreiter, C.G. and Müller, J. (1972). *Chem. Ber.* **105**, 150
81. Lam, C.T., Senoff, C.V. and Ward, J.E.H. (1974). *J. Organomet. Chem.* **70**, 273
82. Aumann, R. and Schröder, J. (1990). *Chem. Ber.* **123**, 2053
83. Burkhardt, T.J. and Casey, C.P. (1973). *J. Am. Chem. Soc.* **95**, 5833
84. Fischer, E.O. and Riedmuller, S. (1976). *Chem. Ber.* **109**, 3358
85. Fischer, E.O., Held, W. and Kreissl, F.R. (1977). *Chem. Ber.* **110**, 3842
86. Fischer, E.O., Held, W., Kreissl, F.R., Frank, A. and Haltner, G. (1977). *Chem. Ber.* **110**, 656
87. Casey, C.P., Burkhardt, T.J., Bunnell, C.A. and Calabrese, J.C. (1977). *J. Am. Chem. Soc.* **99**, 2127
88. Fischer, E.O., Kreis, G., Kreissl, F.R., Kreiter, C.G. and Müller, J. (1973). *Chem. Ber.* **106**, 3910
89. Casey, C.P. and Brunsvold, W.P. (1977). *Inorg. Chem.* **16**, 391
90. Bell, R.A., Chisholm, M.H., Couch, D.A. and Rankel, L.A. (1977). *Inorg. Chem.* **16**, 677
91. Heckl, B., Werner, H. and Fischer, E.O. (1968). *Angew. Chem. Int. Ed. Engl.* **7**, 817
92. Werner, H., Fischer, E.O., Heckl, B. and Kreiter, C.G. (1971). *J. Organomet. Chem.* **28**, 367
93. Steinmetz, A.L., Hershberger, S.A. and Angelici, R.J. (1984). *Organometallics* **3**, 461
94. Pickering, R.A. and Angelici, R.J. (1981). *Inorg. Chem.* **20**, 2977
95. Kreissl, F.R., Fischer, E.O., Kreiter, C.G. and Weiss, K. (1973). *Angew. Chem. Int. Ed. Engl.* **12**, 563
96. Kreissl, F.R. and Fischer, E.O. (1974). *Chem. Ber.* **107**, 103
97. Bernasconi, C.F. and Stronach, M.W. (1993). *J. Am. Chem. Soc.* **115**, 1341
98. Bernasconi, C.F., Whitesell, C. and Johnson, R.A. (2000). *Tetrahedron* **56**, 4917
99. Satterthwait, A.C. and Jencks, W.P. (1974). *J. Am. Chem. Soc.* **96**, 7018
100. Gresser, M.J. and Jencks, W.P. (1977). *J. Am. Chem. Soc.* **99**, 6963
101. Yang, C.C. and Jencks, W.P. (1988). *J. Am. Chem. Soc.* **110**, 2972
102. Bernasconi, C.F., Rossi, R.H. and Schmid, P. (1977). *J. Am. Chem. Soc.* **99**, 4090
103. Bernasconi, C.F. (1978). *Acc. Chem. Res.* **11**, 147
104. Terrier, F. (1991). *Nucleophilic Aromatic Displacement*, p. 55. VCH, New York
105. Bernasconi, C.F., Fassberg, J., Killion, R.B. and Rappoport, Z. (1990). *J. Org. Chem.* **55**, 4568
106. Bernasconi, C.F., Leyes, A.E., Evantova, I. and Rappoport, Z. (1995). *J. Am. Chem. Soc.* **117**, 1703
107. Eigen, M. (1964). *Angew. Chem. Int. Ed. Engl.* **3**, 1
108. Ahrens, M.-L. and Maass, G. (1968). *Angew. Chem. Int. Ed. Engl.* **7**, 818
109. Kreissl, F.R., Kreiter, C.G. and Fischer, E.O. (1972). *Angew. Chem. Int. Ed. Engl.* **11**, 643
110. Kreissl, F.R. and Held, W. (1975). *J. Organomet. Chem.* **86**, C10
111. Kreissl, F.R., Fischer, E.O., Kreiter, C.G. and Fischer, H. (1973). *Chem. Ber.* **106**, 1262
112. Fischer, H. (1979). *J. Organomet. Chem.* **170**, 309
113. Choi, H.S. and Sweigart, D.A. (1982). *J. Organomet. Chem.* **228**, 249
114. Pickering, R.A. and Angelici, R.J. (1982). *J. Organomet. Chem.* **225**, 253
115. Kreiter, C.G. (1968). *Angew. Chem. Int. Ed. Engl.* **7**, 390
116. Schubert, U. and Fischer, E.O. (1975). *Justus Liebig's Ann. Chem.* 393
117. Fischer, E.O., Schubert, U., Kalbfus, W. and Kreiter, C.G. (1975). *Z. Anorg. Allg. Chem.* **416**, 135
118. Bernasconi, C.F., Flores, F.X., Gandler, J.R. and Leyes, A.E. (1994). *Organometallics* **13**, 2186

119. Marcus, R.A. (1965). *J. Chem. Phys.* **43**, 679
120. Marcus, R.A. (1968). *J. Phys. Chem.* **72**, 891
121. Bernasconi, C.F. (1987). *Acc. Chem. Res.* **20**, 301
122. Bernasconi, C.F. (1992). *Adv. Phys. Org. Chem.* **27**, 119
123. Bernasconi, C.F. (1992). *Acc. Chem. Res.* **25**, 9
124. Bordwell, F.G. and Boyle, W.J., Jr. (1972). *J. Am. Chem. Soc.* **94**, 3907
125. Leffler, J.E. and Grunwald, E. (1963). *Rates and Equilibria of Organic Reactions*, p. 156. Wiley, New York
126. Kresge, A.J. (1975). *Acc. Chem. Res.* **8**, 354
127. Jencks, W.P. (1985). *Chem. Rev.* **85**, 511
128. Bernasconi, C.F. (1989). *Tetrahedron* **45**, 4017
129. Bernasconi, C.F. and Renfrow, R.A. (1987). *J. Org. Chem.* **52**, 3035
130. Terrier, F., Millot, F. and Morel, G. (1976). *J. Org. Chem.* **41**, 3892
131. Bernasconi, C.F., Fassberg, J., Killion, R.B., Schuck, D.F. and Rappoport, Z. (1991). *J. Am. Chem. Soc.* **113**, 4937
132. Bernasconi, C.F. and García-Río, L. (2000). *J. Am. Chem. Soc.* **122**, 3821
133. Bernasconi, C.F., Flores, F.X. and Kittredge, K.W. (1998). *J. Am. Chem. Soc.* **120**, 7983
134. Bernasconi, C.F., Kittredge, K.W. and Flores, F.X. (1999). *J. Am. Chem. Soc.* **121**, 6630
135. Guthrie, J.P. (1978). *J. Am. Chem. Soc.* **100**, 5892
136. Pearson, R.G. and Songstad, J. (1967). *J. Am. Chem. Soc.* **89**, 1827
137. Pearson, R.G. (1969). *Surv. Prog. Chem.* **5**, 1
138. Sander, E.G. and Jencks, W.P. (1968). *J. Am. Chem. Soc.* **90**, 6154
139. Hine, J. (1975). *Structural Effects on Equilibria in Organic Chemistry*, p. 225. Wiley, New York
140. Hupe, D.J. and Jencks, W.P. (1977). *J. Am. Chem. Soc.* **99**, 451
141. Jencks, W.P., Brant, S.R., Gandler, J.R., Fendrich, G. and Nakamura, C. (1982). *J. Am. Chem. Soc.* **104**, 7054
142. Bernasconi, C.F. and Killion, R.B. (1988). *J. Am. Chem. Soc.* **110**, 7506
143. Jencks, W.P., Haber, M.T., Herchlag, D. and Nazaretian, K.L. (1986). *J. Am. Chem. Soc.* **108**, 479
144. Richard, J.P. (1987). *J. Chem. Soc., Chem. Commun.* 1768
145. McClelland, R.A., Kanagasabapathy, V.M., Banait, N.S. and Steenken, S. (1992). *J. Am. Chem. Soc.* **114**, 1816
146. Andraos, J. and Kresge, A.J. (1992). *J. Am. Chem. Soc.* **114**, 5643
147. Bernasconi, C.F. and Ali, M. (1999). *J. Am. Chem. Soc.* **121**, 11384
148. Kristjánsdóttir, S.S. and Norton, J.P. (1992). *Transition Metal Hydrides*. Dedieu, A. (ed.), p. 309. Verlag Chemie, New York
149. Hansch, C., Leo, A. and Taft, R.W. (1991). *Chem. Rev.* **91**, 165
150. Unger, S.H. and Hansch, S.C. (1976). *Prog. Phys. Org. Chem.* **12**, 9
151. Bernasconi, C.F. and Ali, M. (2001). *Organometallics* **20**, 3383
152. Bernasconi, C.F., Ali, M. and Lu, F. (2000). *J. Am. Chem. Soc.* **122**, 1352
153. Kirby, A.J. (1980). *Adv. Phys. Org. Chem.* **17**, 183
154. Mandolini, L. (1986). *Adv. Phys. Org. Chem.* **22**, 1
155. Aumann, R., Hinterding, P., Krüger, C. and Goddard, R. (1993). *J. Organomet. Chem.* **459**, 145
156. Fischer, E.O., Kreiss, G. and Kreissl, F.R. (1973). *J. Organomet. Chem.* **56**, C37
157. Bernasconi, C.F., Flores, F.X. and Kittredge, K.W. (1997). *J. Am. Chem. Soc.* **119**, 2103
158. Jencks, W.P. (1972). *J. Am. Chem. Soc.* **94**, 4731
159. Bernasconi, C.F. and Perez, G.S. (2000). *J. Am. Chem. Soc.* **122**, 12441
160. Bernasconi, C.F., Ketner, R.J., Brown, S.D., Chen, X. and Rappoport, Z. (1999). *J. Org. Chem.* **64**, 8829
161. Fischer, H. and Dötz, K.H. (1980). *Chem. Ber.* **113**, 193



162. Fischer, H. (1980). *J. Organomet. Chem.* **197**, 303
163. Fischer, H. and Märkl, R. (1985). *Chem. Ber.* **118**, 3683
164. Fischer, H. and Zeuner, S. (1987). *J. Organomet. Chem.* **327**, 63
165. Fischer, H. (1981). *J. Organomet. Chem.* **222**, 241
166. Kreiter, C.G. (1968). *Angew. Chem. Int. Ed. Engl.* **7**, 390
167. Casey, C.P. and Anderson, R.L. (1974). *J. Am. Chem. Soc.* **96**, 1230
168. Fickling, M.M., Fischer, A., Mann, B.R., Packer, J. and Vaughan, J. (1959). *J. Am. Chem. Soc.* **81**, 4226
169. Gandler, J.R. and Bernasconi, C.F. (1989). *Organometallics* **8**, 2282
170. Bernasconi, C.F. (1997). *Chem. Soc. Rev.* **26**, 299
171. Bernasconi, C.F. and Sun, W. (1993). *J. Am. Chem. Soc.* **115**, 12526
172. Bernasconi, C.F. and Sun, W. (1997). *Organometallics* **16**, 1926
173. Bernasconi, C.F. and Leyes, A.E. (1997). *J. Am. Chem. Soc.* **119**, 5169
174. Bernasconi, C.F., Sun, W., García-Río, L., Kin-Yan, and Kittredge, K. (1997). *J. Am. Chem. Soc.* **119**, 5583
175. Bernasconi, C.F., Leyes, A.E. and García-Río, L. (1998). *Organometallics* **17**, 4940
176. Bernasconi, C.F. and Ali, M. (1999). *J. Am. Chem. Soc.* **121**, 3039
177. Bernasconi, C.F. and Ragains, M.L. (2001). *J. Am. Chem. Soc.* **123**, 11890
178. Amyes, T.L. and Richard, J.P. (1996). *J. Am. Chem. Soc.* **118**, 3129
179. Amyes, T.L. and Richard, J.P. (1992). *J. Am. Chem. Soc.* **114**, 10257
180. Bernasconi, C. F.; Ragains, M. L. Unpublished results
181. Bruice, P.Y. (2001). *Organic Chemistry* (3rd edn), p. 169. Prentice-Hall, Upper Saddle River, NJ
182. Jones, M., Jr. (2000). *Organic Chemistry* (2nd edn), p. 111. W.W. Norton, New York
183. Chesnut, D.B. and Bartolotti, L.J. (2000). *Chem. Phys.* **253**, 1
184. Bernasconi, C.F. and Sun, W. (2002). *J. Am. Chem. Soc.* **124**, 2299
185. Bernasconi, C. F.; Ali, M. Unpublished observations
186. Kresge, A.J. (1974). *Can. J. Chem.* **52**, 1897
187. Bordwell, F.G. (1988). *Acc. Chem. Res.* **21**, 456
188. Wulff, W.D. and Yang, D.C. (1983). *J. Am. Chem. Soc.* **105**, 6726
189. Moore, E.J., Sullivan, J.M. and Norton, J.R. (1986). *J. Am. Chem. Soc.* **108**, 2257
190. Fermin, M.C., Thiyagarajan, B. and Bruno, J.W. (1993). *J. Am. Chem. Soc.* **115**, 974
191. Schwesinger, R. (1985). *Chimia* **39**, 269
192. Schwesinger, R. and Schlemper, H. (1987). *Angew. Chem. Int. Ed. Engl.* **26**, 1167
193. Parker, A.J. (1969). *Chem. Rev.* **69**, 1
194. Bernasconi, C.F., Leyes, A.E., Ragains, M.L., Shi, Y., Wang, H. and Wulff, W.D. (1998). *J. Am. Chem. Soc.* **120**, 8632
195. Koltthoff, I.M. and Chantooni, M.K. (1972). *Anal. Chem.* **44**, 194
196. Koltthoff, I.M. and Chantooni, M.K. (1972). *J. Phys. Chem.* **76**, 2026
197. Anderson, R. L. Ph.D. Thesis, University of Wisconsin, Madison, WI, 1974
198. Casey, C.P. and Brunsvold, W.R. (1976). *J. Organomet. Chem.* **118**, 309
199. Xu, Y.-C. and Wulff, W.D. (1987). *J. Org. Chem.* **52**, 3263
200. Gandler, J.R. and Bernasconi, C.F. (1992). *J. Am. Chem. Soc.* **114**, 631
201. Bernasconi, C.F., Flores, F.X. and Sun, W. (1995). *J. Am. Chem. Soc.* **117**, 4875
202. Bernasconi, C.F. and Sun, W. (1995). *Organometallics* **14**, 5615
203. Bernasconi, C.F. and Leyes, A.E. (1997). *J. Chem. Soc., Perkin Trans. 2* 1641
204. Bernasconi, C.F., Leyes, A.E. and García-Río, L. (1998). *Organometallics* **17**, 4940
205. Mills, O.S. and Redhouse, A.D. (1968). *J. Chem. Soc. A* 642
206. Amin, S.R., Jayaprakash, K.N., Nandi, M., Sathe, K.M. and Sarkar, A. (1996). *Organometallics* **15**, 3528
207. Bernasconi, C.F., García-Río, L., Sun, W., Yan, K. and Kittredge, K.W. (1997). *J. Am. Chem. Soc.* **119**, 5583

# Thermodynamic Stabilities of Carbocations

JOSÉ-LUIS M. ABBOUD,<sup>†</sup> IBON ALKORTA,<sup>‡</sup> JUAN Z. DÁVALOS,<sup>†</sup> PAUL MÜLLER<sup>§</sup> and ESTHER QUINTANILLA<sup>†</sup>

<sup>†</sup>*Instituto de Química Física “Rocasolano”, CSIC, Madrid, Spain*

<sup>‡</sup>*Instituto de Química Médica, CSIC, Madrid, Spain*

<sup>§</sup>*Department of Organic Chemistry, University of Geneva, Geneva, Switzerland*

*Dedicated to Professor Edward M. Arnett*

- 1 Introduction 57
- 2 Quantitative thermodynamic criteria of stability in the gas phase 58
  - Definitions and experimental techniques 58
  - The specific case of carbocations 61
- 3 Theoretical calculations 64
- 4 Uncertainties 65
- 5 Thermodynamics and structure of selected species 67
  - Carbocations C1–C4 67
    - Aliphatic carbocations with more than four carbon atoms 75
    - Cyclic species without formal  $\pi$  systems 79
    - Cyclopropyl-substituted carbocations 83
    - Secondary and tertiary carbocations derived from cage hydrocarbons 89
    - Carbenium ions with formal  $\pi$  systems 98
    - Two-electron aromatic and homoaromatic ions 101
    - Six-electron aromatic ions 108
    - Phenyl-substituted carbocations 110
- 6 Solution reactivity 116
  - Thermodynamic properties 118
  - Reaction kinetics 122
- 7 Conclusion 126
  - Acknowledgments 127
  - References 127

## 1 Introduction

Small ions such as methylium ( $\text{CH}_3^+$ ), methanium ( $\text{CH}_5^+$ ) and ethylium ( $\text{C}_2\text{H}_5^+$ )<sup>1,2</sup> are long-time favorites of experimental chemical physicists and theoretical chemists. Some of their work is reflected in this chapter. Furthermore, these and/or other cognate species such as vinylum ( $\text{C}_2\text{H}_3^+$ ) and cyclopropenylium ( $c\text{-C}_3\text{H}_3^+$ ) ions have been either detected or postulated to be significant constituents of the interstellar space<sup>3</sup> and the stratospheres of the outer planets and some of their satellites<sup>4,5</sup> as a result of the ionization of hydrocarbons.<sup>6</sup> Even larger species have recently been considered.<sup>7</sup> So, a great deal of experimental and computational information on their

structure, molecular spectra and energetics is available and part of it is summarized here. On the other hand, many of these species are far too reactive to be experimentally observed in solution, let alone the solid state. At the other end of the “stability spectrum” we have species such as substituted triarylmethylium, cyclopropenylium and tropylium ions, which form authentic hydrocarbon salts. A series of these and other remarkable carbocations has recently been reviewed.<sup>8</sup> The cyclopropenylium and tropylium ions are aromatic species with highly delocalized  $\pi$ -electron systems.<sup>9</sup>

A number of carbenium ions lies between these two extremes, including secondary and tertiary alkyl carbocations as well as protonated aromatic hydrocarbons, many of them identified in solution, and more recently, as relatively stable solid salts (some representative examples are examined here). The study of all these species has long been a very important part of physical organic chemistry. Their industrial importance has promoted a great deal of research, both experimental<sup>10–15</sup> and theoretical.<sup>16–20</sup>

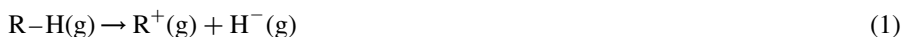
This chapter essentially addresses the following topics:

- (1) The quantification of the concept of “stability”. More precisely, thermodynamic criteria are applied in order to rank carbenium ions on the basis of their intrinsic stabilities, that is, stabilities in the absence of solvent. Both experimental and computational data are used.
- (2) The relationship between the intrinsic thermodynamic stability of these species and their reactivity in solution, from both the thermodynamic and the kinetic points of view.
- (3) Relevant structural features of these species, as revealed by experimental or computational methods data, are reviewed. Furthermore, quantum mechanical calculations at the highest possible levels (within our computational capabilities) were performed on most of these species. The scope of this chapter is limited to a relatively small number of ions that illustrate some representative examples of structural effects.

## 2 Quantitative thermodynamic criteria of stability in the gas phase

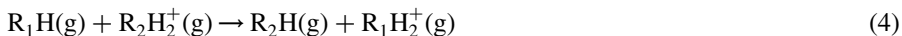
### DEFINITIONS AND EXPERIMENTAL TECHNIQUES

We are concerned here with the thermodynamic stability of carbocations. For the sake of generality, we formally consider that they derive from a neutral molecule R–H, which can either lose a hydride or be protonated in the gas phase, reactions (1) and (2):



A quantitative ranking of stabilities for any two of these species (e.g.,  $\text{R}_1^+$  and  $\text{R}_2^+$ ) can be defined through the thermodynamic state functions for the hydride- or proton-

exchange processes (3a) and (4):<sup>21,22</sup>



The standard enthalpies and Gibbs energy changes for these reactions at some temperature  $T$ , respectively,  $\Delta_r H^\circ_T$  and  $\Delta_r G^\circ_T$ , involve the corresponding standard magnitudes for the various reactants and products.

For example, the standard enthalpy change for reaction (3a) at 298.15 K is given by equation (3b):

$$\begin{aligned} \Delta_r H^\circ(3a) = & \Delta_f H^\circ_m[R_2H(g)] + \Delta_f H^\circ_m[R_1^+(g)] - \Delta_f H^\circ_m[R_1H(g)] \\ & - \Delta_f H^\circ_m[R_2^+(g)] \end{aligned} \quad (3b)$$

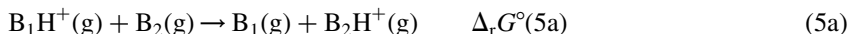
wherein the various  $\Delta_f H^\circ_m$  terms are the standard enthalpies of formation of the various species involved in the reaction.

Experimental values of the standard enthalpies of formation of the neutral species, generally obtained by thermochemical or kinetic techniques,<sup>23–25</sup> are frequently available and there are some excellent critical compilations of these data<sup>26–31</sup> that can be eventually estimated empirically<sup>32–35</sup> or computationally (see later).

Several methods exist that allow the determination of the standard enthalpies of formation of the ionic species. The reader is referred to two recent rigorous and detailed chapters by Lias and Bartmess<sup>36</sup> and Ervin.<sup>37</sup> The vast majority of the experimental data reported here are obtained by means of Fourier transform ion cyclotron resonance spectroscopy (FT ICR), high-pressure mass spectrometry (HPMS), selected ion flow tube (SIFT), and pulsed-field ionization (PFI) techniques, particularly pulsed-field ionization photoelectron photoion coincidence (PFI-PEPICO). All these experimental techniques have been examined quite recently, respectively, by Marshall,<sup>38</sup> Kebarle,<sup>39</sup> Böhme,<sup>40</sup> Ng<sup>41</sup> and Baer.<sup>42</sup> These chapters appear in a single (remarkable) issue of the *International Journal of Mass Spectrometry*. An excellent independent discussion of the thermochemical data of ions, with a careful survey of these and other experimental methods, is given in Ref. 37.

From these techniques the following raw experimental data are obtained:

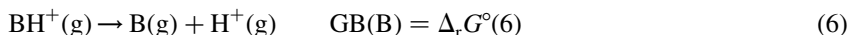
- (1) FT ICR, HPMS and SIFT yield the standard Gibbs energy change,  $\Delta_r G^\circ(5a)$  for reaction (5a), the proton exchange between two bases,  $B_1$  and  $B_2$ ,



$\Delta_r G^\circ(5a)$  is given by the difference between  $\Delta_r G^\circ(5b)$  and  $\Delta_r G^\circ(5c)$  pertaining, respectively, to reactions (5b) and (5c):



The standard Gibbs energy change for reaction (6) is known as the gas-phase basicity of base B, GB(B):



From this it follows that the unknown GB of a base, say B<sub>1</sub>, can be obtained from the experimental values of  $\Delta_r G^\circ(5a)$  and GB(B<sub>2</sub>), B<sub>2</sub> being an appropriate reference base.<sup>43,44</sup>

- (2) SIFT and HPMS experiments performed at different temperatures provide the standard enthalpy change for reaction (5a),  $\Delta_r H^\circ(5a)$ . As before, combination of this datum with  $\Delta_r H^\circ(5b)$  leads to  $\Delta_r H^\circ(5c)$ , also known as the proton affinity of B<sub>1</sub>, PA(B<sub>1</sub>).<sup>43,44</sup>
- (3) Ionization techniques are extremely important sources of thermochemical data for ions. Excellent chapters are given in Refs. 37, 41 and 42.

Here, we simply consider that they yield (*inter alia*) the adiabatic ionization energies (IE) and appearance energies (AE) defined as the standard energy changes at 0 K for reactions (7) and (8) (assuming for the latter that there is no potential barrier in the reaction coordinate and little or no kinetic shift):



Extracting  $\Delta_f H^\circ_m(\text{R}^+)$  or  $\Delta_f H^\circ_m(\text{A}^+)$  at finite temperatures from IE or AE, respectively, requires the corresponding  $\Delta_f H^\circ_m$  values for the appropriate neutral species as well as their corresponding integrated heat capacities. The latter can be obtained from compilations (see above) or else computed by quantum chemical methods. Several conventions, clearly presented and compared in Refs. 36 and 37, exist for the determination of  $\Delta_f H^\circ_m(\text{e}^-)$ . Here, we follow the so-called “ion convention” because it is used in a number of important sources of thermochemical data for ions. In this convention, the enthalpy of formation of the electron is defined as equal to its integrated heat capacity at all temperatures. Note that as indicated by Bartmess,<sup>45,46</sup> the most rigorous approach is to treat the electron as a fermion and to apply Fermi–Dirac statistics to compute its integrated heat capacity and entropy. We suggest that institutions such as IUPAC ought to officially recommend this treatment.

Directly determined experimental standard entropies for carbenium ions in the gas phase,  $S^\circ_m$ , are seldom available. Those we present here are derived generally from the combination of experimental gas phase  $\Delta_r G^\circ_m$  and  $\Delta_r H^\circ_m$  values. We also report the data obtained by quantum mechanical methods. A careful discussion of these data is given in Ref. 47. When needed,  $S^\circ_m$  values for neutral species were taken from compilations<sup>29,30,48</sup> or computed.

## THE SPECIFIC CASE OF CARBOCATIONS

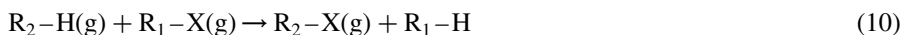
*Hydride, halide and proton exchanges*

The quantitative ranking of stabilities can sometimes be obtained directly by HPMS or FT ICR. In both these cases the main condition is the absence of isomerization or other extraneous processes.

Carbocations can exchange hydride, as in reaction (3a),<sup>49</sup> or halide anions (mostly chlorides and bromides),<sup>50</sup> as in reaction (9):

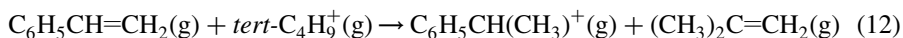
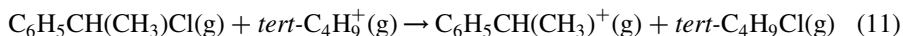


As we show below, exchanges of other species can be studied, at least formally. In all cases, the rankings defined through equations (3a) and (9) are linked through equation (10):



This is an isodesmic process involving the neutral species only. In principle,  $\Delta_r G^\circ(10)$  and  $\Delta_r H^\circ(10)$  can be obtained experimentally. Otherwise, this “leaving group correction” can be obtained by quantum chemical calculations. Here, we use both methods.

Equilibrium proton exchange between ethylenic compounds is ideally suited whenever isomerization and/or other processes cannot compete with proton exchange. If contributions from the neutral species are very small, rankings obtained by this method and by chloride exchange are essentially identical. For example, the standard Gibbs energy changes for reactions (11) and (12) are, respectively,<sup>51</sup>  $-7.7$  and  $-7.5$  kcal mol<sup>-1</sup>:



Other important examples are also known.<sup>52</sup>

*The dissociative proton attachment method*

The construction of a quantitative scale of carbocation stabilities based on hydride or halide exchanges would require the systematic overlapping equilibration<sup>44</sup> of a large number of species (as in reactions (11) and (12)). This was the time-honored procedure for the construction of the gas-phase proton basicity scale.<sup>43</sup> In the present case, this is difficult to achieve because of the widely different stabilities involved and because of the possibility of rearrangement of the ions.

It has long been known that in the gas phase, R-X compounds (X = OH, halogen, SH, etc.) can react with protonated bases, BH<sup>+</sup>, to undergo a “dissociative proton

attachment process" (DPA), as shown in reaction (13):



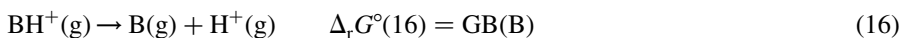
Lias and Ausloos<sup>53</sup> have summarized earlier literature on these processes.

We have recently shown that by varying the strength of the bases (B), it is possible to determine the onset for reaction (13) fairly accurately.<sup>54</sup> This is conveniently done by means of FT ICR. Full experimental details are given in Refs. 54 and 55. Briefly stated,  $\text{BH}^+(\text{g})$  is formed by chemical ionization following the electron ionization of a mixture of  $\text{B}(\text{g})$  and  $\text{R-X}(\text{g})$  (in general, fragment ions from B and/or  $\text{R-X}$  act as proton sources) and then isolated by ion ejection techniques and allowed to react. The formation/absence of  $\text{R}^+(\text{g})$  is monitored for periods ranging from 1 to (sometimes) 60 s.

The dissociative proton transfer from  $\text{BH}^+(\text{g})$  to  $\text{R-X}$  under a pressure  $P$ , reaction (13), will take place spontaneously (assuming a negligible dissociation barrier) when  $\Delta_r G^P(13) < 0$ . It can be easily shown that  $\Delta_r G^P(13)$  is given by equation (14):

$$\Delta_r G^P(13) = \Delta_r G^P(15) + \Delta_r G^P(16) \quad (14)$$

wherein  $\Delta_r G^P(15)$  and  $\Delta_r G^P(16)$  pertain, respectively, to reactions (15) and (16):



The experimentally determined onset for reaction (13) satisfies the condition  $\Delta_r G^P(13) \approx 0$ . It then follows that  $\Delta_r G^P(15) \approx -\Delta_r G^P(16)$ .

Let  $\text{R}_1\text{-X}$  and  $\text{R}_2\text{-X}$ , respectively, stand for two halides (or alcohols or other derivatives) and  $\text{B}_1$  and  $\text{B}_2$  two reference bases defining their respective DPA onsets. The position of equilibrium (17) as determined by  $\Delta_r G^\circ(17)$  is a quantitative measure of the relative stabilities of  $\text{R}_1^+(\text{g})$  and  $\text{R}_2^+(\text{g})$ :



It can be readily shown that  $\Delta_r G^\circ(17) = \Delta_r G^P(17)$ . Then, and from the discussion given above, equation (18) follows:

$$\Delta_r G^\circ(17) \approx \text{GB}(\text{B}_2) - \text{GB}(\text{B}_1) \quad (18)$$

This expression reduces the determination of the relative stabilities of  $\text{R}_1^+(\text{g})$  and  $\text{R}_2^+(\text{g})$  through the formal exchange of the halide, hydroxide or other anions, reaction (17), to the actual determination of the DPA onsets for the corresponding neutral precursors, reaction (13).

These are bracketing experiments and their precision (estimated at *ca.* 2 kcal mol<sup>-1</sup>) is lower than that achieved under "true" equilibrium conditions. They have, however, the following advantages: (1) ions are formed under extremely mild conditions (see later); (2) the acidity of the protonating species  $\text{BH}^+(\text{g})$  can be varied within very wide limits by an appropriate choice of  $\text{B}(\text{g})$ ; (3) gas-phase basicities are available for hundreds of compounds.

Over the last several years, the DPA method has been applied to a number of systems. The following illustrates its scope and the reliability of the data derived therefrom.

- (1) We have applied DPA to *tert*-butyl and *sec*-butyl chlorides.<sup>55,56</sup> As discussed in other sections, the difference in stabilities we obtained was in excellent agreement with that provided by other methods. The most important point, however, is that the DPA onset for *sec*-BuCl could be clearly determined, in spite of the fact that *sec*-Bu<sup>+</sup> readily rearranges to *tert*-Bu<sup>+</sup>. This is explained by the fact that the DPA are *entropy-driven, endoergic reactions*. This makes DPA extremely valuable for the study of relatively unstable species.<sup>55,57,58</sup> Examples of such processes are known.<sup>59–61</sup> They are currently under study in our laboratories.
- (2) We have applied DPA to a set of halomethanes.<sup>62</sup> A value of  $201.9 \pm 2.0$  kcal mol<sup>-1</sup> for  $\Delta_f H_m^\circ(\text{CCl}_3^+)$  was obtained from that study.<sup>63,64</sup> From the most recent  $\Delta_f H_m^\circ$  and adiabatic ionization energy for the trichloromethyl radical, respectively,  $17.0 \pm 0.6$  kcal mol<sup>-1</sup><sup>65</sup> and  $8.06 \pm 0.02$  eV,<sup>66</sup> one gets  $\Delta_f H_m^\circ(\text{CCl}_3^+) = 202.7 \pm 0.8$  kcal mol<sup>-1</sup>. Using instead the computed ionization energy (CEPA-1 level with triple- $\zeta$  equivalent basis set) of 7.990 eV,<sup>67</sup>  $\Delta_f H_m^\circ(\text{CCl}_3^+)$  becomes  $201.0 \pm 2.0$  kcal mol<sup>-1</sup>. Other examples exist showing that the accuracy of the thermodynamic data obtained by DPA is sufficient for the purposes of this study.
- (3) Consider reaction (17). For DPA results to be acceptable, one has to ensure that rankings of carbocation stabilities obtained by using different precursor species (i.e., different X) are self-consistent. For example, let us suppose we compare the stabilities of R<sub>1</sub><sup>+</sup>(g) and R<sub>2</sub><sup>+</sup>(g) through DPA studies of the respective chlorides and alcohols (X = Cl and X = OH). The corresponding experimental  $\Delta_r G^\circ(17)$  values are noted,  $\Delta_r G^\circ(17, X = \text{Cl})$  and  $\Delta_r G^\circ(17, X = \text{OH})$ . They must satisfy equation (19):

$$\Delta_r G^\circ(17, X = \text{OH}) = \Delta_r G^\circ(17, X = \text{Cl}) + \Delta_r G^\circ(20) \quad (19)$$

wherein  $\Delta_r G^\circ(20)$  pertains to reaction (20), an isodesmic process involving the neutral precursors and having the meaning of a leaving group correction:

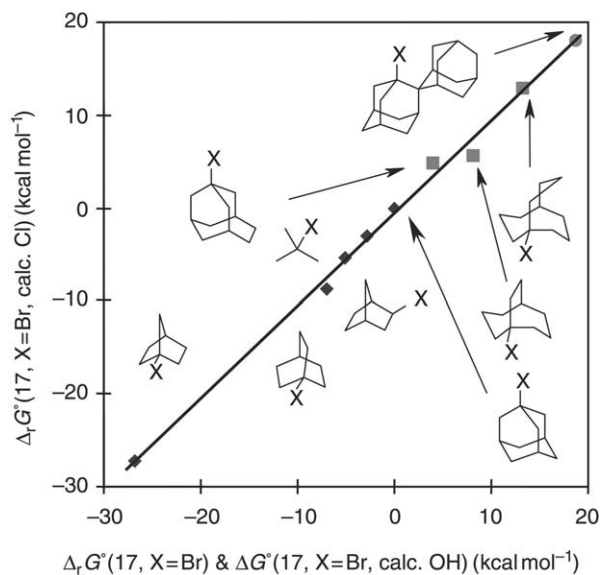


We have recently reported results of a systematic DPA study of bridgehead carbocations using as precursors alcohols, chlorides and bromides.<sup>58</sup> Figure 1 is a plot of  $\Delta_r G^\circ(17, X = \text{Br, calc. Cl})$ , i.e., values of  $\Delta_r G^\circ(17, X = \text{Br})$  obtained from experimental  $\Delta_r G^\circ(17, X = \text{Cl})$  and corrected as indicated above, versus the experimental  $\Delta_r G^\circ(17, X = \text{Br})$  and  $\Delta_r G^\circ(17, X = \text{Br, calc. OH})$ . It shows that the self-consistency is excellent.

The same was found to hold with a series of tertiary alkyl cations obtained from their chlorides and alcohols.<sup>68</sup>

- (4) Reaction (3a) is one of the key reference processes used here.  $\Delta_r G^\circ(3a)$  can also be obtained computationally. In keeping with previous studies,  $\Delta_r G^\circ(3a)$  is





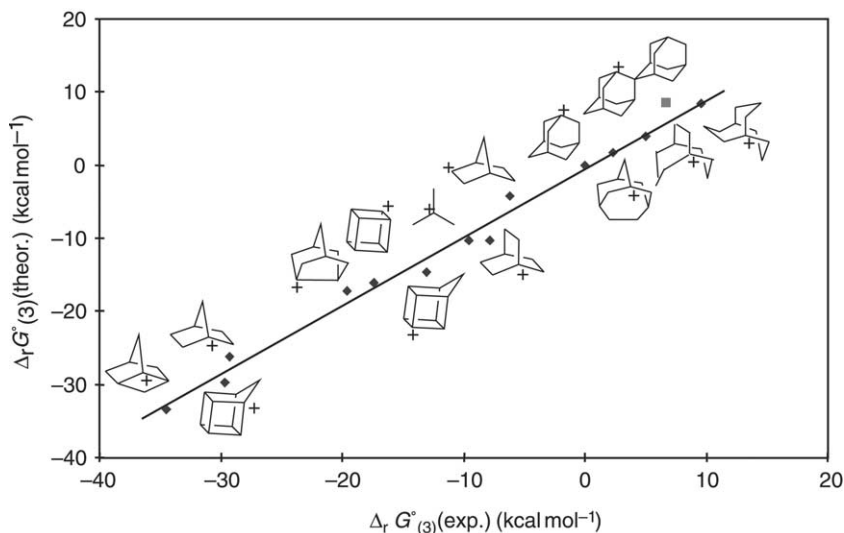
**Fig. 1** Self-consistency of DPA results. Correction of leaving group effects.

referred to 1-adamantyl cation ( $R_2^+$ ). A most stringent test of the self-consistency of the DPA method is the comparison of the  $\Delta_r G^\circ(3a)$  values derived from experiment (upon the appropriate leaving group correction) with those obtained by purely computational methods (ranging from MP2(full)/6-31G(d) to G2(MP2) levels). [Figure 2](#) is an example of the quality of the agreement.

### 3 Theoretical calculations

Enthalpies and Gibbs free energies for the experimental processes of the systems involved were evaluated using high-level *ab initio* calculations. The results reported herein are based on G2<sup>69</sup> calculations for the smallest systems (up to five heavy atoms) and G2(MP2)<sup>70</sup> for the intermediate ones (between six and eight heavy atoms). Larger systems were optimized at the MP2(full)/6-31G(d) level. Thermodynamic corrections were generally calculated at the RHF/6-31G(d) level, with the scaling used in the G-n family of calculations. Thus, the results obtained for all the molecules can be compared at the same level, if necessary, since the calculations at the lowest levels are embedded in the G2 and G2(MP2) methodologies. In the same way, calculations at lower levels can be upgraded easily when the necessary computational resources become available.

The G2 and G2(MP2) computational methods used here provide molecular energies with deviations from the experimental data similar, in many cases, to the



**Fig. 2** Computed Gibbs energy changes for reaction (3a) versus DPA-based results.

accuracy of the latter. The reported average deviations are 1.21 and 1.52 kcal mol<sup>-1</sup> for the G2 and G2(MP2) calculations, respectively.<sup>69,70</sup>

## 4 Uncertainties

From the inspection of reactions (3a), (4), (7) and (8), it follows immediately that the uncertainties on the standard enthalpies of formation of gaseous ions are determined by those affecting the thermochemical data for the relevant neutral species (molecules or free radicals) and the specific method used for ion generation. The uncertainty assigned to the standard enthalpy of formation of a gaseous ion is the root-sum-of-squares combination of the individual uncertainties of the various contributions.<sup>43</sup>

Perusal of the data presented in the following sections would show that extremely accurate (better than 0.01 kcal mol<sup>-1</sup>) ionization energies can be obtained with state-of-the-art optical spectroscopy and photoionization and electron ionization techniques.

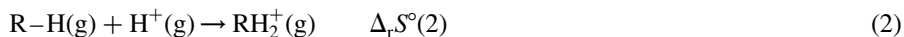
The uncertainties affecting experimental *differences* in GB values as determined by equilibrium methods are frequently in the range 0.1–0.3 kcal mol<sup>-1</sup>. Individual differences in PA values obtained by van't Hoff plots of equilibrium constants for processes such as proton or halide exchange reactions are accurate to within a 1–2 kcal mol<sup>-1</sup> range as indicated by Kebarle and co-workers.<sup>71</sup> The usual multiple-overlap technique likely halves these uncertainties in the case of data originating in the same laboratory. As indicated in the discussion of reactions (5a) and (6),

“absolute” GB and PA values must be anchored to some specific reference values. Overall, and unless warranted by other evidence, we take the accuracy of “absolute” GB and PA values as *ca.* 2 kcal mol<sup>-1</sup>.<sup>43</sup> In many cases this is practically the main contributor to the uncertainty on  $\Delta_f H_m^\circ$  values for ions. Note, however, that in some cases this is perhaps too conservative an estimate, in view of the excellent level of agreement that often exists between independent  $\Delta_f H_m^\circ$  values obtained from ionization and equilibrium techniques.

DPA onsets are estimated to be known within 2 kcal mol<sup>-1</sup>. These values must also be anchored to some reference. This leads to an estimated uncertainty of *ca.* 2.8 kcal mol<sup>-1</sup> on the formal  $\Delta_f G_m^\circ(17)$  values. Furthermore, in order to extract  $\Delta_f H_m^\circ$  values for ions, leaving group and entropy corrections are needed. With few exceptions, and because of the scarcity of experimental data, these corrections are determined computationally by means of isodesmic reactions.<sup>57,58,68</sup> We estimate that the leaving group correction introduces an extra 1 kcal mol<sup>-1</sup> uncertainty. Unless otherwise stated, we anchor DPA onsets obtained from chlorides and alcohols to the onsets for the corresponding 1-adamantyl derivatives. We have recently introduced the DPA of methyl ethers as an appropriate tool for the study of very stable species (see later); their corresponding onsets are anchored to that for the methyl ether of tricyclopropyl carbinol.

Uncertainties on the experimental standard enthalpies of formation of neutral species vary widely. For most hydrocarbons and radicals they are in the 0.1–1.0 and 0.5–2.0 kcal mol<sup>-1</sup> ranges, respectively.

Very few standard entropies for ions relevant to this study are available that derive from purely experimental data. These data can be obtained, at least formally, from the combination of PA and GB values for processes such as reaction (2):



The accuracy of  $\Delta_r S^\circ(2)$  is estimated at 1–2.5 cal mol<sup>-1</sup> K<sup>-1</sup>.  $S^\circ[\text{RH}_2^+(\text{g})]$  is even less accurate, because of the contribution from the uncertainty on  $S^\circ[\text{RH(g)}]$ .

A recent study<sup>47</sup> indicates that quantum mechanical calculations of moderate to high level are able to provide values of  $\Delta_r S^\circ(2)$  accurate to within 0.3–0.6 cal mol<sup>-1</sup> K<sup>-1</sup>. As regards the standard entropies for individual ions, we estimate that the accuracy of the scaled HF/6-31G(d) values used in the G-n family calculations<sup>69,70</sup> (see above) is about 2 cal mol<sup>-1</sup> K<sup>-1</sup>, based on the differences between values computed at this level and experimental or high-level computational data.

The accuracy of the data we present is not homogeneous and it is rather low in some cases, largely because of the unavailability of thermodynamic state functions for neutral species. Obviously, the spirit of this work is quite different from that of the excellent databases from NIST. Thus, while we have striven to provide the “best” possible thermodynamic values, we have also considered that even a “low-resolution” study of the relationships between structure, intrinsic (gas phase) stability and solution reactivity of carbocations is bound to provide useful results.

## 5 Thermodynamics and structure of selected species

### CARBOCATIONS C1–C4

#### Methylium ion ( $\text{CH}_3^+$ ) (**1**)

Spectroscopic studies in the gas phase<sup>72–76</sup> and very high level *ab initio* calculations<sup>77</sup> indicate that this species is an oblate symmetric top belonging to the  $D_{3h}$  molecular point group (Fig. 3). The experimentally estimated C–H distance is 1.087 Å, the computed value (1.089 Å) being in excellent agreement.

The standard enthalpy of formation given in Table 1 is based on the experimental value of the adiabatic ionization potential of the methyl radical<sup>78</sup> and has been adjusted<sup>79</sup> to a series of fundamental enthalpies of formation. Very recently,<sup>80</sup> the onset of the formation of  $\text{CH}_3^+$  from methane was determined quite accurately by means of the PFI-PEPICO technique. This datum, combined with other experimental results, yields the accurate 0 K dissociation energies ( $D_0$ ) for  $\text{CH}_4$  and  $\text{CH}_4^+$ ,  $D_0(\text{H}-\text{CH}_3) = 103.479 \pm 0.023$  and  $D_0(\text{H}-\text{CH}_3^+) = 39.321 \pm 0.092$  kcal mol<sup>-1</sup>.

#### Methanium ion ( $\text{CH}_5^+$ ) (**2**)

Reliable experimental values for  $\text{PA}(\text{CH}_4)$  and  $\text{GB}(\text{CH}_4)$  are available, particularly from HPMS and flowing afterglow studies.<sup>81,82</sup> When combined with the (rather accurate) data for the neutral species, they provide the thermodynamic data given in Table 1. The results of G2 *ab initio* calculations (Ref. 83 and this study) are also reported.

Within the Born–Oppenheimer approximation, computational studies at extremely high levels<sup>84,85</sup> show that the global minimum, **2a**( $C_s$ ), has a  $C_s$  symmetry and that it can be viewed as an  $\text{H}_2$  molecule tightly bound to a methyl cation (three-center two-electron bonds). Two other structures, **2b**( $C_s$ ) and **2c**( $C_v$ ), respectively, of symmetries  $C_s$  and  $C_{2v}$ , are transition states. **2b**( $C_s$ ) involves the rotation of the  $\text{H}_2$  moiety and allows the exchange of the two hydrogen atoms.

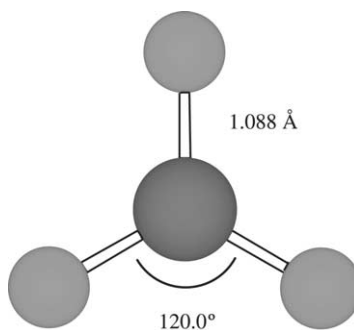


Fig. 3 Structure of methylium ion, **1**, optimized at the MP2(full)/6-31G(d) level.

**Table 1** Thermodynamic data for selected carbocations, C1–C4

Cations	$\Delta_f H_m^\circ(\text{g})^a$	$S_m^\circ(\text{g})^b$
Methylium, $\text{CH}_3^+$ (1)	$261.83 \pm 0.06^c$	$44.59 \pm 0.06^d$
Methanium, $\text{CH}_5^+$ (2)	$218.0 \pm 2.0^e$ $220.3 \pm 2.0^g$	$54.2 \pm 1.2^f$ $53.8 \pm 2.0^h$
Ethylum, $\text{C}_2\text{H}_5^+$ (3)	$215.6 \pm 2.0^i$ $215.17 \pm 0.50^k$ $215.25 \pm 0.50^m$ $215.2 \pm 2.0^n$	$55.2 \pm 2.0^j$ $55.3 \pm 2.0^l$
Propan-2-ylum, <i>iso</i> - $\text{C}_3\text{H}_7^+$ (4)	$193.04 \pm 0.36^o$ $192.2 \pm 2.0^q$ $192.7 \pm 2.0^s$ $194.4 \pm 2.0^t$	$68.0 \pm 2.0^p$ $66.23 \pm 0.24^r$
Butan-2-ylum ( <i>sec</i> -butyl), <i>sec</i> - $\text{C}_4\text{H}_9^+$ (5)	$184.5 \pm 1.3^u$ $182.4 \pm 2.0^v$ $183.0 \pm 2.0^y$ $183.4 \pm 2.0^z$	$69.8 \pm 2.0^v$ $71.2 \pm 2.0^x$
2-Methylpropan-2-ylum ( <i>tert</i> -butyl), <i>tert</i> - $\text{C}_4\text{H}_9^+$ (6)	$169.9 \pm 0.9^{aa}$ $170.03 \pm 0.26^{ac}$ $169.7 \pm 0.6^{ae}$ $169.2 \pm 1.7^{af}$	$73.4 \pm 2.0^{ab}$ $74.04 \pm 0.26^{ad}$

<sup>a</sup>In kcal mol<sup>-1</sup>.<sup>b</sup>In cal mol<sup>-1</sup> K<sup>-1</sup>.<sup>c</sup> $\Delta_f H_m^\circ(\text{g})$  from Ref. 79, based on the experimentally resolved threshold PE spectrum of  $\text{CH}_3$  (Ref. 78) and vibrational data summarized in Chase, M. W., Jr. NIST-JANAF Thermochemical Tables, 4th edn (1998). J. Phys. Chem. Ref. Data, Monograph No. 9. The very high level calculation of the ionization energy of  $\text{CH}_3$  (Ref. 77) agrees with experiment within 0.02 kcal mol<sup>-1</sup>.<sup>d</sup>Obtained in this work using the smoothed experimental vibrational frequencies and C–H bond length given in Ref. 77.<sup>e</sup>From the averaged experimental PA( $\text{CH}_4$ ) taken from Ref. 43 and  $\Delta_f H_m^\circ(\text{CH}_4) = -17.80 \pm 0.10$  kcal mol<sup>-1</sup>.<sup>26</sup><sup>f</sup>From the experimental  $S_m^\circ(\text{g})$  value for  $\text{CH}_4$ ,  $45.09 \pm 0.10$  cal mol<sup>-1</sup> K<sup>-1</sup> (Ref. 26) and the recommended experimental values<sup>43</sup> for PA and GB( $\text{CH}_4$ ). Uncertainties are estimated from the differences between the experimental values determined.<sup>81</sup><sup>g</sup>From  $\Delta_f H_m^\circ(\text{CH}_4)$  and the computed (G2) PA( $\text{CH}_4$ ), 127.6 kcal mol<sup>-1</sup> (this work).<sup>h</sup>Scaled, symmetry-corrected value from this work [HF/6-31G(d)].<sup>i</sup>From the experimental PA( $\text{C}_2\text{H}_4$ ) = 162.6 kcal mol<sup>-1</sup> (Ref. 81) and  $\Delta_f H_m^\circ(\text{C}_2\text{H}_4) = 12.54 \pm 0.25$  kcal mol<sup>-1</sup>.<sup>26</sup><sup>j</sup>From the experimental GB( $\text{C}_2\text{H}_4$ ) and PA( $\text{C}_2\text{H}_4$ ) from Refs. 43 and 81.<sup>k</sup>From the adiabatic ionization potential of ethyl radical,  $8.117 \pm 0.008$  eV determined by photoionization mass spectrometry<sup>95</sup> and  $\Delta_f H_m^\circ(\text{C}_2\text{H}_5) = 28.35 \pm 0.41$  kcal mol<sup>-1</sup> from Ref. 96. Thermal corrections as in Ref. 95.<sup>l</sup>From the *ab initio* scheme by Radom and co-workers.<sup>47</sup><sup>m</sup>From PFI-PE spectroscopy and ion coincidence detection using multi-bunch synchrotron radiation.<sup>97</sup><sup>n</sup>From the experimental  $\Delta_f H_m^\circ(\text{C}_2\text{H}_4)$  and PA( $\text{C}_2\text{H}_4$ ) = 162.98 kcal mol<sup>-1</sup> computed at the G2 level.<sup>47</sup><sup>o</sup>PFI-PEPICO TOF experiments and experimental  $\Delta_f H_m^\circ(\text{g})$  for the various precursor species.<sup>102</sup><sup>p</sup>From the experimental  $S_m^\circ$ , (Ref. 26) PA and GB for  $\text{C}_3\text{H}_6$ .

<sup>g</sup>From the experimental PA of propene ( $178.4 \text{ kcal mol}^{-1}$ )<sup>81</sup> and its  $\Delta_f H_m^\circ(\text{g})$  value,  $4.879 \text{ kcal mol}^{-1}$ .<sup>26</sup>

<sup>h</sup>*Ab initio* computed value, from Ref. 47.

<sup>i</sup>From the experimental  $\Delta_f H_m^\circ(\text{g})$  of  $\text{C}_3\text{H}_6$  and its G2-computed PA.<sup>47,83</sup>

<sup>j</sup>Computed (CBSQ, atomization).<sup>99</sup>

<sup>k</sup>From  $\Delta_f H_m^\circ(\text{tert-C}_4\text{H}_9^+) = 169.9 \pm 0.9 \text{ kcal mol}^{-1}$  (see later) and the experimental enthalpy of isomerization  $\text{sec-C}_4\text{H}_9^+ \rightarrow \text{tert-C}_4\text{H}_9^+$ ,  $-14.55 \pm 0.50 \text{ kcal mol}^{-1}$ .<sup>108,109</sup> This value pertains to the formation of an equilibrating mixture of isomers **I** and **II** in solution.

<sup>l</sup>Scaled, symmetry-corrected value for structure **I**, computed at the MP2(full)/6-31G(d) level (this work).

<sup>m</sup>From the experimental  $\Delta_f H_m^\circ$  (Ref. 26) and  $S_m^\circ(E\text{-C}_4\text{H}_8)$ <sup>29</sup> and  $\text{GB}(E\text{-C}_4\text{H}_8) = -172.5 \pm 1.1 \text{ kcal mol}^{-1}$  (Ref. 107) corrected with the computed  $S_m^\circ$  values for structures **I** and **II**. This value pertains to the formation of an equilibrating mixture of isomers **I** and **II** in the gas phase.

<sup>n</sup>Scaled value for structure **II**, computed at the MP2(full)/6-31G(d) level (this work).

<sup>o</sup>From the experimental  $\Delta_f H_m^\circ(E\text{-C}_4\text{H}_8) = -2.58 \text{ kcal mol}^{-1}$  (Ref. 26) and the G2-computed PA( $E\text{-C}_4\text{H}_8$ ) to yield structure **I** (this work).

<sup>p</sup>From the experimental  $\Delta_f H_m^\circ(E\text{-C}_4\text{H}_8)$  and the G2-computed PA( $E\text{-C}_4\text{H}_8$ ) to yield structure **II** (this work).

<sup>aa</sup>From PEPICO studies.<sup>113</sup>

<sup>ab</sup>From the experimental  $\text{GB}(iso\text{-C}_4\text{H}_8) = 185.4 \text{ kcal mol}^{-1}$  (Ref. 115) and  $\text{PA}(iso\text{-C}_4\text{H}_8)$ .<sup>81</sup>

<sup>ac</sup>From photoionization mass spectrometry.<sup>114</sup>

<sup>ad</sup>Computed value.<sup>47</sup>

<sup>ae</sup>From  $\Delta_f H_m^\circ(iso\text{-C}_4\text{H}_8) = -4.29 \pm 0.26 \text{ kcal mol}^{-1}$ , (Ref. 26) and  $\text{PA}(iso\text{-C}_4\text{H}_8) = 191.7 \pm 0.5 \text{ kcal mol}^{-1}$ .<sup>81</sup>

<sup>af</sup>From the experimental  $\Delta_f H_m^\circ$  and  $S_m^\circ$  for  $iso\text{-C}_4\text{H}_8$ , from Ref. 26 and the calculated (G2) values for the PA and GB of  $iso\text{-C}_4\text{H}_8$ , respectively,  $192.2$  and  $185.6 \text{ kcal mol}^{-1}$ .<sup>47,83</sup>

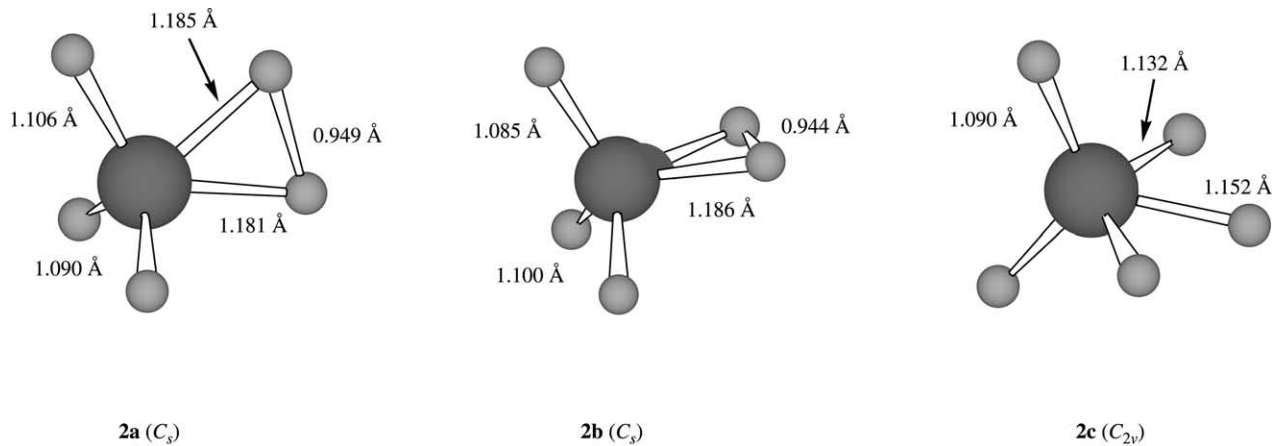
**2c**( $C_v$ ) allows the exchange between these hydrogens and those of the methyl tripod (Fig. 4).

These calculations also show that, in terms of electronic energies, structures **2b**( $C_s$ ) and **2c**( $C_v$ ) are some  $0.1$  and  $0.8 \text{ kcal mol}^{-1}$  above structure **2a**( $C_s$ ). Inclusion of the vibrational contributions makes the barrier heights vanishingly small and raises some intriguing questions. In any case, these results suggest an extremely floppy structure and the possibility of easy scrambling of the hydrogen atoms.

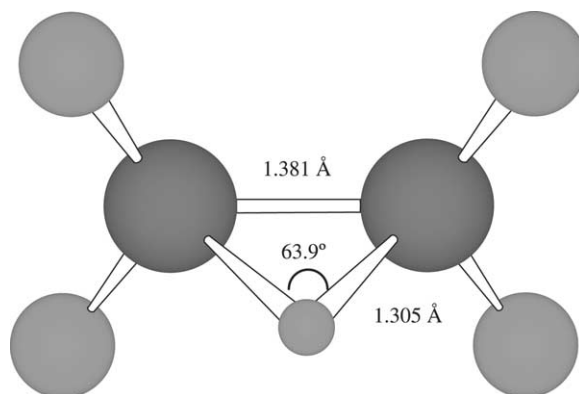
Recently,<sup>86,87</sup>  $\text{CH}_5^+$  has been the subject of *ab initio* integral path calculations, which include nuclear quantum effects such as zero-point motion and tunneling in full dimensionality and go beyond the harmonic approximation. These studies confirm the above results, in that while protons undergo large-amplitude pseudorotational motion and become scrambled and statistically equivalent, this motion is concerted and the situations in which the vibrating nuclear skeleton having an  $\text{H}_2$  moiety attached to a  $\text{CH}_3$  tripod are the most important contributors to the overall appearance of the cation.

At this point, however, the situation is far from being entirely clear, because of the following facts:

- (1) The experimental (gas phase) IR spectrum of the C–H stretching region of  $\text{CH}_5^+$  has been obtained.<sup>88</sup> It portrays some 900 lines and has not yet been interpreted.
- (2) Mass spectrometric studies<sup>89</sup> seem to indicate that, in the absence of intermolecular collisions,  $\text{CH}_4\text{D}^+$  and  $\text{CD}_4\text{H}^+$  do not show any rearrangement.



**Fig. 4** Possible structures (Born–Oppenheimer approximation), for methanium ion, **2**, optimized at the MP2(full)/6-31G(d) level. **2a** is the absolute minimum; **2b** and **2c** are transition states.



**Fig. 5** Structure of ethylium ion, **3**, optimized at the MP2(full)/6-31G(d) level.

This situation has prompted a lively debate<sup>90</sup> but still remains a “tough test for experiment and theory”.<sup>91</sup>

#### *Ethylium ion, ethyl cation* ( $C_2H_5^+$ ) (**3**)

It has long been known<sup>92,93</sup> that this ion has a non-classical, bridged  $C_{2v}$  structure and that the classical  $C_s$  form is a saddle point on the potential energy surface of the  $C_2H_5^+$  manifold<sup>94</sup> (Fig. 5).

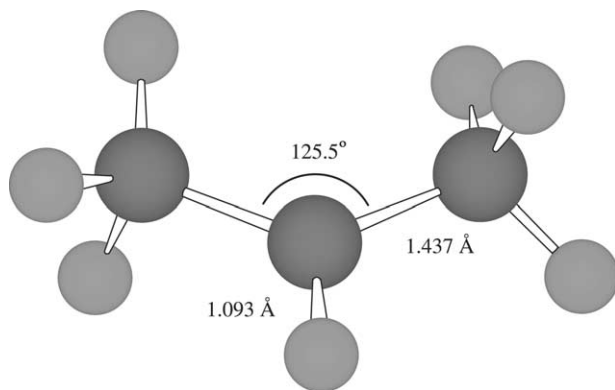
The rewardingly coincident  $\Delta_f H_m^\circ(g)$  values for this ion, reported in Table 1, were obtained from three experimental sources: (1) the proton affinity of ethylene;<sup>43, 81</sup> (2) the ionization energy of the ethyl radical;<sup>95</sup> (3) the PFI-PE spectrum of  $C_2H_5Br$ ,<sup>96</sup> combined with the  $\Delta_f H_m^\circ(g)$  of the appropriate neutral<sup>26,97</sup> species.  $S_m^\circ(g)$ , as obtained from the experimental PA and GB values for  $C_2H_4$  together with the experimental  $S_m^\circ(C_2H_4)$ , is presented in Table 1 together with the computational value.

#### *Propan-2-ylum ion, iso-propyl cation* (*iso*- $C_3H_7^+$ ) (**4**)

According to theoretical calculations and experimental evidence in solution,<sup>22,98,99</sup> this species has a *chiral* structure with  $C_2$  symmetry but very low methyl rotation barriers (Fig. 6). Cation **4** has been studied in solution by NMR<sup>100,101</sup> but no data seem to be available for this ion in the solid state.

$\Delta_f H_m^\circ(\mathbf{4})$  has been obtained experimentally from the dissociative ionization onset for the 2-propyl chloride, bromide and iodide PFI-PEPICO TOF.<sup>102</sup> The experimental value of the PA of propene<sup>81</sup> leads to a very close result. These data are summarized in Table 1. The reader is referred to Ref. 102 for an extremely careful discussion on the experimental and calculated values of  $\Delta_f H_m^\circ(\mathbf{4})$ . High-level theoretical calculations using various methods,<sup>47,83,98,99</sup> are also in good





**Fig. 6** Structure of propan-2-ylum ion, **4**, optimized at the MP2(full)/6-31G(d) level.

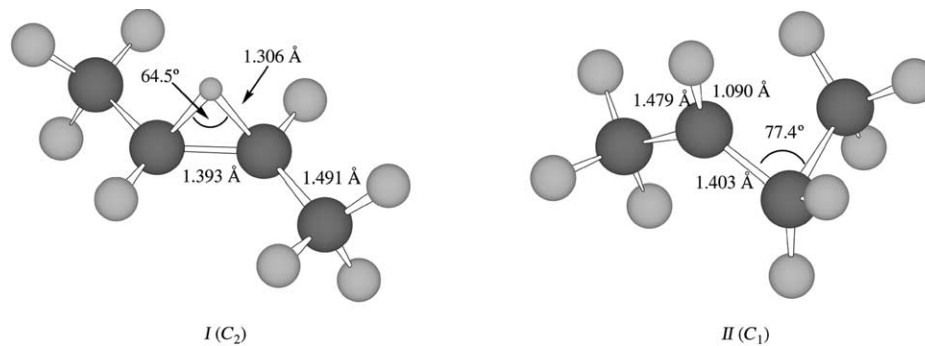
agreement with these results. They are presented in Table 1.  $S_m^\circ(\mathbf{4})$  given in Table 1 is computed at the E3 level.<sup>47</sup>

The classical structures of propan-1-ylum ion (1-propyl cation) are not minima on the potential energy surface of the  $C_3H_7^+$  manifold.<sup>22,98</sup> They are some 20 kcal mol<sup>-1</sup> above **4**, as determined computationally.<sup>98</sup> This result is in fair agreement with gas-phase photoionization experiments on the *n*-propyl radical by Schultz,<sup>103</sup> and Dyke and co-workers.<sup>104</sup> These structures are transition states involved in the hydrogen scrambling of **4** in superacidic media.<sup>22,105</sup>

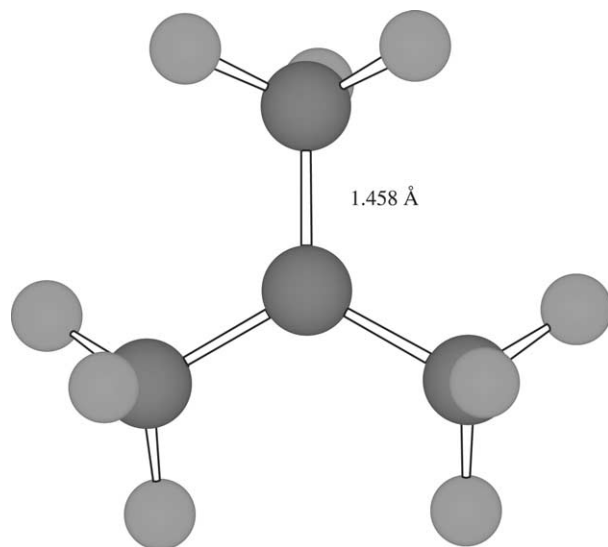
#### *Butan-2-ylum ion, sec-butyl cation (sec-C<sub>4</sub>H<sub>9</sub><sup>+</sup>) (5)*

Experimental evidence (essentially IR and NMR data) in solution at low temperatures, summarized in Ref. 106, as well as high-level *ab initio* calculations<sup>106</sup> indicate that this ion exists as a mixture of structures **I** and **II**, of, respectively,  $C_2$  and  $C_1$  point group symmetries (Fig. 7).

The GB of *E*-C<sub>4</sub>H<sub>8</sub> has been determined experimentally by ICR, using bracketing techniques.<sup>107</sup> We have carried out G2 calculations providing computed GB values for *E*-C<sub>4</sub>H<sub>8</sub> and leading to structures **I** and **II**. These calculations show: (1) that the thermodynamic stabilities of *both* structures are extremely close and, more precisely, that a gaseous sample of *sec*-C<sub>4</sub>H<sub>9</sub><sup>+</sup> in thermal equilibrium at 298.15 K is very nearly a 1:1 mixture of isomers **I** and **II**; (2) that these computed GB values are in extremely good agreement with experiment. We have combined the experimental GB,  $\Delta_f H_m^\circ$  and  $S_m^\circ$  for *E*-C<sub>4</sub>H<sub>8</sub> and the computed  $S_m^\circ$  values for structures **I** and **II** to derive the corresponding values for  $\Delta_f H_m^\circ(\mathbf{5})$  (Table 1). Arnett and co-workers<sup>108,109</sup> used low-temperature calorimetry in superacids to determine the standard enthalpy change for the isomerization *sec*-C<sub>4</sub>H<sub>9</sub><sup>+</sup>  $\rightarrow$  *tert*-C<sub>4</sub>H<sub>9</sub><sup>+</sup>. This datum, combined with  $\Delta_f H_m^\circ(\textit{tert}\text{-C}_4\text{H}_9^+)$ , provides an “apparent” value (assuming negligible differential solvation effects) of  $\Delta_f H_m^\circ(\mathbf{5})$  quite consistent with the independent results reported above for the gas phase.



**Fig. 7** Isomeric structures **I** and **II** of butan-2-ylum ion, **5**, optimized at the MP2(full)/6-31G(d) level.



**Fig. 8** Structure of 2-methylpropan-2-ylum ion, **6**, optimized at the MP2(full)/6-31G(d) level.

The primary cations  $n\text{-C}_4\text{H}_9^+$  and  $iso\text{-C}_4\text{H}_9^+$  are not on the minima on the PES of the  $\text{C}_4\text{H}_9^+$  manifold.<sup>106</sup> The stability of these species can be estimated from vertical ionization potentials of appropriate substrates.<sup>110</sup> The corresponding  $\Delta_f H_m^\circ$  values are some  $30 \text{ kcal mol}^{-1}$  more positive than  $\Delta_f H_m^\circ(\text{tert-C}_4\text{H}_9^+)$ .

### 2-Methylpropan-2-ylum ion, *tert*-butyl cation ( $\text{tert-C}_4\text{H}_9^+$ ) (**6**)

Solid state nutation NMR spectroscopy<sup>111</sup> and X-ray diffraction,<sup>112</sup> show that this ion has a trigonal structure with 1.46 and 2.51 Å for central-methyl and C–C methyl–methyl distances (Fig. 8).

Remarkably coincident experimental values for  $\Delta_f H_m^\circ(\mathbf{6})$  can be obtained from: (1) PEPICO studies on *tert*-butyl iodide;<sup>113</sup> (2) appearance energies for the formation of **6** from isobutane, neopentane and *tert*-butyl iodide (threshold photoionization mass spectrometry);<sup>114</sup> (3) the PA of *iso*-butene.<sup>81</sup> They are presented in Table 1, together with  $S_m^\circ(\mathbf{6})$  determined from the experimental values of PA and GB(*iso*- $\text{C}_4\text{H}_8$ ),<sup>115</sup> together with  $\Delta_f H_m^\circ(\text{iso-C}_4\text{H}_8)$  and  $S_m^\circ(\text{iso-C}_4\text{H}_8)$ .

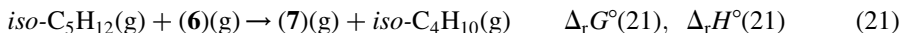
G2 values for the PA and GB of *iso*- $\text{C}_4\text{H}_8$ , particularly with entropies treated according to Ref. 47, lead to thermodynamic data in excellent agreement with experiment. Recent very high-level calculations<sup>116</sup> on the *tert*-butyl radical also provide extremely consistent results. Our *ab initio* [MP2(full)/6-31G(d)] geometries are in excellent agreement with experimental data.

## ALIPHATIC CARBOCATIONS WITH MORE THAN FOUR CARBON ATOMS

*2-Methylbutan-2-ylum ion (tert-C<sub>5</sub>H<sub>11</sub><sup>+</sup>) (7)*

To our knowledge, there are no X-ray data on the structure of this ion. Its <sup>13</sup>C NMR spectrum in solution has long been known.<sup>117</sup>

The experimental  $\Delta_f H_m^\circ(7)$  and  $S_m^\circ(7)$  values reported in Table 2 were obtained from the experimental standard enthalpy and Gibbs energy changes for the hydride exchange between ions **6** and **7** (reaction (21)) as determined by pulsed HPMS:<sup>118,119</sup>



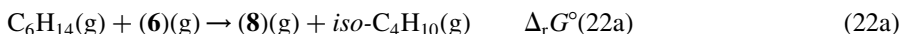
The structure of this ion, shown in Fig. 9, was fully optimized at the MP2(full)/6-31G(d) level (this work) and belongs to the C<sub>s</sub> symmetry point group. Schleyer and co-workers<sup>120</sup> pointed out two important properties of this structure: (1) the lengthening of the C3–C4 bond to *ca.* 1.58 Å, indicative of hyperconjugation; (2) the reduction of the C4–C3–C2<sup>+</sup> angle to 101.5°, showing distortion of the C–C hyperconjugating form toward bridging. This implies some “non-classical” character for **7**.

The computed <sup>13</sup>C NMR shifts for this structure are in excellent agreement with experiment. This is not the case for other conformations, close in energy but not displaying this incipient bridging.<sup>120</sup>

We have computed  $\Delta_r G^\circ(21)$  and  $\Delta_r H^\circ(21)$  at the G2(MP2) level. They are in excellent agreement with experiment and lead to  $\Delta_f H_m^\circ(7)$  and  $S_m^\circ(7)$  values, also given in Table 2.

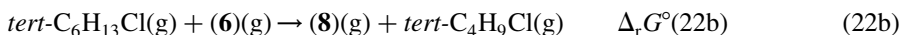
*2-Methylpentan-2-ylum ion (tert-C<sub>6</sub>H<sub>13</sub><sup>+</sup>) (8)*

To our knowledge, no experimental structural data are available for this species. The experimental  $\Delta_f H_m^\circ(8)$  and  $S_m^\circ(8)$  were obtained from the experimental standard enthalpy and Gibbs energy changes for the hydride exchange between ions **6** and **8**, reaction (22a), as determined by pulsed HPMS:<sup>119,121</sup>



Fully independent values of  $\Delta_f H_m^\circ(8)$  and  $S_m^\circ(8)$ , also reported in Table 2, were obtained as follows:

(1) We applied the DPA technique to 2-chloro-2-methylpentane and to other tertiary alkyl chlorides.<sup>68</sup> These data lead to  $\Delta_r G^\circ(22b)$ :



Upon the appropriate leaving group corrections, this immediately provides  $\Delta_r G^\circ(22a)$ . This datum, corrected for the entropy terms, yields  $\Delta_r H^\circ(22a)$ , which in turn, upon combination with the experimental  $\Delta_f H_m^\circ$  for 2-methylpentane, **6** and *iso*-C<sub>4</sub>H<sub>10</sub>(g) leads to a value of  $\Delta_f H_m^\circ(8)$  in very good agreement with the results presented above.

(2) All the species involved in reaction (22a) were studied at the MP2/6-311G(d,p) level in Ref. 68;  $\Delta_r H^\circ(22a)$  obtained from these calculations provides a value of  $\Delta_f H_m^\circ(8)$  in satisfactory agreement with experiment.

**Table 2** Thermodynamic data for selected aliphatic carbocations with five and more carbon atoms

Cations	$\Delta_f H_m^\circ(\text{g})^a$	$S_m^\circ(\text{g})^b$
2-Methylbutan-2-ylum ( <i>tert</i> -C <sub>5</sub> H <sub>11</sub> <sup>+</sup> ) ( <b>7</b> )	162.4 ± 2.0 <sup>c</sup>	83.3 ± 2.0 <sup>c</sup>
	164.1 ± 2.0 <sup>d</sup>	85.2 ± 2.0 <sup>e</sup>
2-Methylpentan-2-ylum ( <i>tert</i> -C <sub>6</sub> H <sub>13</sub> <sup>+</sup> ) ( <b>8</b> )	156.2 ± 2.0 <sup>f</sup>	92.2 ± 2.0 <sup>g</sup>
	155.0 ± 3.0 <sup>h</sup>	91.1 ± 2.0 <sup>i</sup>
	154.3 ± 2.0 <sup>j</sup>	
2,4-Dimethylpentan-2-ylum (C <sub>7</sub> H <sub>15</sub> <sup>+</sup> ) ( <b>9</b> )	147.4 ± 2.1 <sup>k</sup>	96.1 ± 2.0 <sup>l</sup>
	146.7 ± 2.0 <sup>m</sup>	
2,4,4-Trimethylpentan-2-ylum (C <sub>8</sub> H <sub>17</sub> <sup>+</sup> ) ( <b>10</b> )	139.8 ± 2.1 <sup>n</sup>	101.0 ± 2.0 <sup>o</sup>
	140.5 ± 2.1 <sup>p</sup>	
	139.2 ± 2.1 <sup>q</sup>	
3-Ethyl-5,5-dimethylhexan-3-ylum (C <sub>10</sub> H <sub>21</sub> <sup>+</sup> ) ( <b>11</b> )	128.3 ± 2.1 <sup>r</sup>	113.2 ± 2.0 <sup>s</sup>
	129.0 ± 2.1 <sup>t</sup>	
	126.8 ± 2.0 <sup>u</sup>	
2,2,4,6,6-Pentamethylheptan-4-ylum (C <sub>12</sub> H <sub>25</sub> <sup>+</sup> ) ( <b>12</b> )	112.0 ± 2.1 <sup>v</sup>	125.1 ± 2.0 <sup>w</sup>
	113.3 ± 2.1 <sup>x</sup>	
	110.8 ± 2.0 <sup>y</sup>	

<sup>a</sup>In kcal mol<sup>-1</sup>.<sup>b</sup>In cal mol<sup>-1</sup> K<sup>-1</sup>.<sup>c</sup>From  $\Delta_f H^\circ(21) = -2.6 \pm 1.0$  and  $\Delta_f G^\circ(21) = -1.9 \pm 0.5$  kcal mol<sup>-1</sup>, respectively; averages of data from Refs. 118 and 119.  $\Delta_f H_m^\circ(\text{C}_5\text{H}_{12}) = -36.73 \pm 0.14$  kcal mol<sup>-1</sup> (Ref. 43) and  $S^\circ(\text{C}_5\text{H}_{12}) = 82.2$  cal mol<sup>-1</sup> K<sup>-1</sup>.<sup>29</sup><sup>d</sup>From  $\Delta_f H^\circ(21) = -0.93 \pm 1.0$  kcal mol<sup>-1</sup> at the G2(MP2) level (this work).<sup>e</sup>Scaled HF/6-31G(d) value from the calculations in (d).<sup>f</sup>From  $\Delta_f H^\circ(22a) = -4.2 \pm 1.0$  and  $\Delta_f G^\circ(22a) = -4.1 \pm 0.5$  kcal mol<sup>-1</sup>, respectively; averages of data from Refs. 119 and 121.  $\Delta_f H_m^\circ(\text{C}_6\text{H}_{14}) = -41.66 \pm 0.25$  kcal mol<sup>-1</sup> (Ref. 43) and  $S^\circ(\text{C}_6\text{H}_{14}) = 91.1$  cal mol<sup>-1</sup> K<sup>-1</sup>.<sup>29</sup><sup>g</sup>From the data in (f).<sup>h</sup>Based on  $\Delta_f H^\circ(22a) = -5.4 \pm 2.8$  kcal mol<sup>-1</sup> from DPA experiments<sup>68</sup> treated as indicated in the text.<sup>i</sup>Scaled HF/6-31G(d) value from the calculations in Ref. 68.<sup>j</sup>From the MP2/6-311G(d,p) value of  $\Delta_f H^\circ(22a)$ .<sup>68</sup><sup>k</sup>Determined from the DPA results for chlorides<sup>68</sup> with the appropriate leaving group and entropy corrections indicated in the text.<sup>l</sup>Scaled, computed HF/6-31G(d) value from data in Ref. 68.<sup>m</sup>Based on the MP2/6-311G(d,p) data anchored, to the experimental  $\Delta_f H_m^\circ[\text{C}_7\text{H}_{16}(\text{g})]$ ,  $-48.30 \pm 0.23$  kcal mol<sup>-1</sup>.<sup>26</sup><sup>n</sup>Determined from the DPA results for chlorides<sup>68</sup> with the appropriate leaving group and entropy corrections indicated in the text.<sup>o</sup>Scaled, computed HF/6-31G(d) value from data in Ref. 68.<sup>p</sup>As in (n) but based on the DPA of the corresponding alcohol.<sup>q</sup>Based on the MP2/6-311G(d,p) data anchored to the experimental  $\Delta_f H_m^\circ[\text{C}_8\text{H}_{18}(\text{g})]$ ,  $-53.57 \pm 0.32$  kcal mol<sup>-1</sup>.<sup>26</sup><sup>r</sup>Determined from the DPA results for chlorides<sup>68</sup> with the appropriate leaving group and entropy corrections indicated in the text.<sup>s</sup>Scaled, computed HF/6-31G(d) value from data in Ref. 68.

<sup>f</sup>As in (a) but based on the DPA of the corresponding alcohol.

<sup>g</sup>Based on the MP2/6-311G(d,p) data anchored to the experimental  $\Delta_f H_m^\circ[\text{C}_{10}\text{H}_{22}(\text{g})]$ ,  $-62.72 \pm 0.50 \text{ kcal mol}^{-1}$ .<sup>28</sup>

<sup>h</sup>Determined from the DPA results for chlorides<sup>68</sup> with the appropriate leaving group and entropy corrections indicated in the text.

<sup>i</sup>Scaled, computed HF/6-31G(d) value from data in Ref. 68.

<sup>x</sup>As in (v) but based on the DPA of the corresponding alcohol.

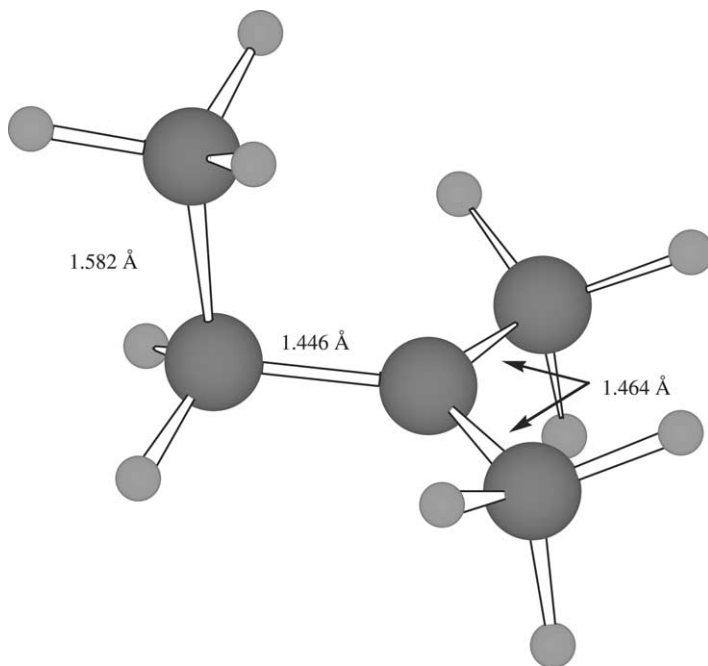
<sup>y</sup>Based on the MP2/6-311G(d,p)//MP2/6-31G(d) data anchored to the experimental  $\Delta_f H_m^\circ[\text{C}_{12}\text{H}_{26}(\text{g})]$ ,  $-75.43 \pm 0.50 \text{ kcal mol}^{-1}$ .<sup>28</sup>

Notice in Fig. 10 that the C3–C4 bond is elongated as in the case of 7. This can also be taken as implying some contribution from hyperconjugation.<sup>120</sup>

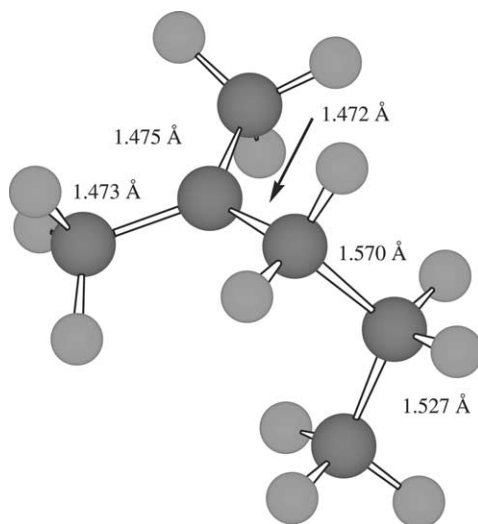
*2,4-Dimethylpentan-2-ylum* ( $\text{C}_7\text{H}_{15}^+$ ) (**9**), *2,4,4-trimethylpentan-2-ylum* ( $\text{C}_8\text{H}_{17}^+$ ) (**10**), *3-ethyl-5,5-dimethylhexan-3-ylum* ( $\text{C}_{10}\text{H}_{21}^+$ ) (**11**) and *2,2,4,6,6-pentamethylheptan-4-ylum* ( $\text{C}_{12}\text{H}_{25}^+$ ) (**12**) ions

To our knowledge, no experimental structural information is available for these species (Chart 1).

Experimental thermodynamic information on these ions was obtained by DPA using chlorides and alcohols as substrates.<sup>68</sup> Treatment of the experimental data by

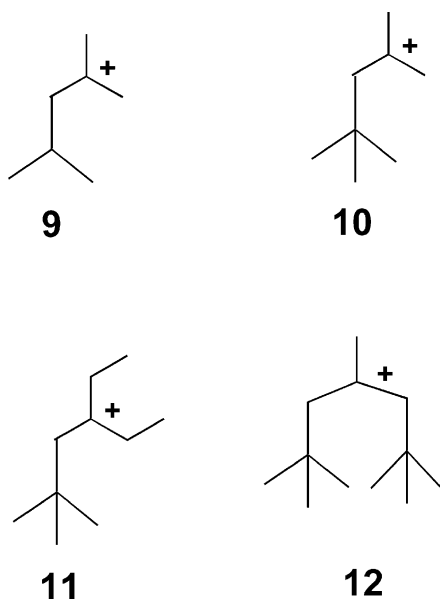


**Fig. 9** Structure of 2-methylbutan-2-ylum ion, 7, optimized at the MP2(full)/6-31G(d) level.



**Fig. 10** Structure of 2-methylpentan-2-ylum ion, **8**, optimized at the MP2(full)/6-31G(d) level.

the methods indicated above led to the  $\Delta_f H_m^\circ$  values summarized in [Table 2](#). Relevant structural features of these ions, as determined by *ab initio* methods shall be reported in due course. Here, we notice that the experimental  $\Delta_f H_m^\circ$  values are in good agreement with the MP2/6-311G(d,p) data, as shown in [Table 2](#).



**Chart 1**

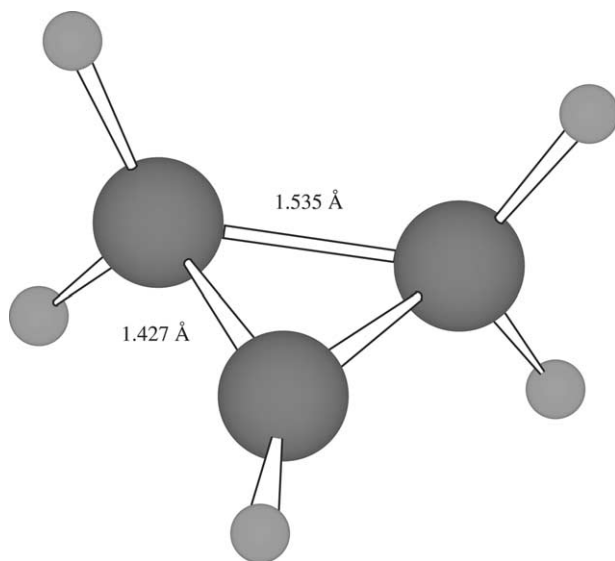
CYCLIC SPECIES WITHOUT FORMAL  $\pi$  SYSTEMS*Cyclopropylium ion* ( $c\text{-C}_3\text{H}_5^+$ ) (**13**)

In principle, the species of  $C_{2v}$  symmetry,<sup>99,122</sup> Fig. 11, can be formed in the gas phase by protonation of cyclopropene<sup>21</sup> and by photoionization of the cyclopropyl radical.<sup>104</sup>

These methods lead to rather different values of  $\Delta_f H_m^\circ(\mathbf{13})$ . Thus, using  $\Delta_f H_m^\circ(c\text{-C}_3\text{H}_4) = 66.22 \pm 0.60 \text{ kcal mol}^{-1}$  (Ref. 27) and  $\text{PA}(c\text{-C}_3\text{H}_4) = -195.6 \text{ kcal mol}^{-1}$ , (Ref. 43) we get  $\Delta_f H_m^\circ(\mathbf{13}) \approx 236.3 \text{ kcal mol}^{-1}$ . Combining the ionization energy of the cyclopropyl radical,  $8.18 \pm 0.03 \text{ eV}$ ,<sup>104</sup> with  $\Delta_f H_m^\circ(c\text{-C}_3\text{H}_5) = 63.7 \pm 2.7 \text{ kcal mol}^{-1}$  based on the experimental ICR data from Ref. 123, we obtain  $\Delta_f H_m^\circ(\mathbf{13}) \approx 252.7 \text{ kcal mol}^{-1}$ .

High-level *ab initio* calculations fully rationalize these discrepancies. Thus, it has been shown that the cyclic  $C_{2v}$  structure is not a minimum on the potential energy surface of the  $c\text{-C}_3\text{H}_5^+$  manifold.<sup>124,125</sup> We have confirmed at the MP2(full)/6-311 + G(d,p) level that this is indeed the case. As indicated by Glukhovtsev *et al.*<sup>122</sup> the cyclic  $C_{2v}$  structure appears as a shallow minimum at the HF/6-31G(d) level. We took advantage of this to estimate the PA of  $c\text{-C}_3\text{H}_4$  at the standard G2 level. The value we obtain,  $171.3 \text{ kcal mol}^{-1}$ , puts  $\Delta_f H_m^\circ(\mathbf{13})$  at about  $260.6 \text{ kcal mol}^{-1}$ . Notice that the meaning of the apparent  $\text{PA}(c\text{-C}_3\text{H}_4)$  has been recently re-interpreted.<sup>126</sup>

All these facts are perfectly consistent with solution chemistry results showing the essentially barrierless electrocyclic disrotatory ring opening of cyclopropyl cations



**Fig. 11** Structure of cyclopropylium ion, **13**, optimized at the HF/6-31G(d) level. This structure is not a minimum at correlated levels.



to yield allylic cations in solvolytic processes,<sup>127</sup> this being a classical example of a pericyclic reaction.<sup>128</sup> To our knowledge, only a single-substituted cyclopropylium ion has been observed by NMR (in  $\text{SbF}_5\text{-SO}_2\text{ClF}$  solution between  $-120$  and  $-60^\circ\text{C}$ ), the 11-methyl-tricyclo[4.4.1.0<sup>1,6</sup>]undec-11-yl cation.<sup>129</sup>

#### Cyclobutylium ( $c\text{-C}_4\text{H}_7^+$ ) (**14**) and cyclopropylmethylium ( $c\text{-C}_3\text{H}_5\text{CH}_2^+$ ) (**15**) ions

Because of their relevance in physical organic chemistry a great deal of experimental information is available on these species, an excellent summary being given in Ref. 131. According to high-level calculations,<sup>130,131</sup> **14** has a puckered structure (symmetrical, non-classical bicyclobutonium,  $C_s$  point group), as shown in Fig. 12.

It is known experimentally<sup>130</sup> that in solution at low temperature, **14** is in equilibrium with the bisected ( $C_s$  symmetry point group) **15**, (Fig. 13), and that the interconversion barrier is small (*ca.* 2 kcal mol<sup>-1</sup>).

Notice that the bisected structure of **15** is taken to reflect the stabilizing interaction<sup>132-134</sup> between the empty p orbital of the  $\text{CH}_2^+$  moiety and the Walsh orbital<sup>135-139</sup> of the cyclopropyl ring.

As regards the thermodynamic state functions for the equilibrating mixture of these two ions in the gas phase, we believe that the only piece of information available so far is the GB of cyclobutene.<sup>26</sup> This datum, combined with the experimental  $S_m^\circ(c\text{-C}_4\text{H}_6)$  and the computed  $S_m^\circ(\mathbf{14})$  (this work) leads to  $\Delta_f H_m^\circ(\mathbf{14})$  (Table 3).

Our G2 calculations provide PA and GB values for  $c\text{-C}_4\text{H}_6$  to yield **14** which, once combined with the experimental thermodynamic data for  $c\text{-C}_4\text{H}_6$ , lead to the

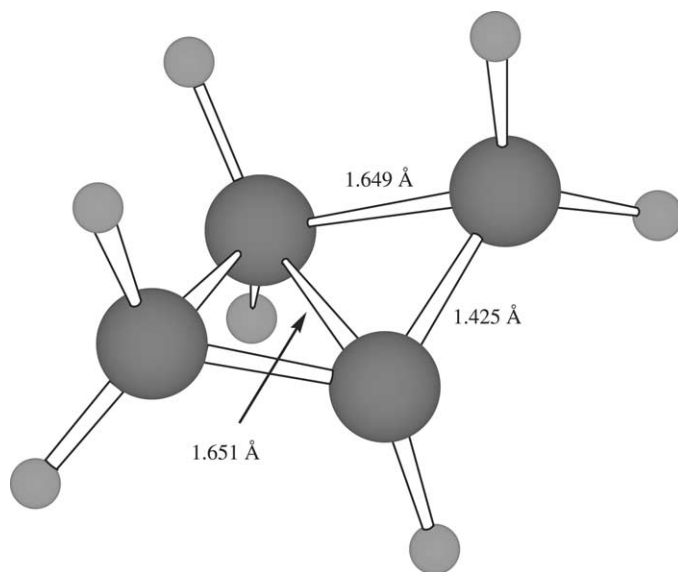
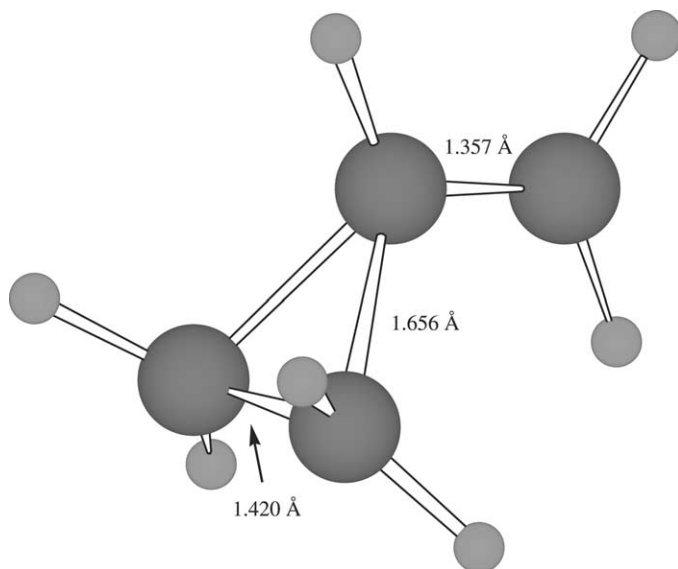


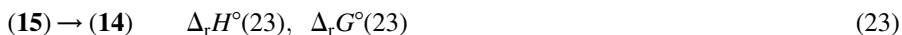
Fig. 12 Structure of cyclobutylium ion, **14**, optimized at the MP2(full)/6-31G(d) level.



**Fig. 13** Structure of cyclopropylmethyl cation, **15**, optimized at the MP2(full)/6-31G(d) level.

value of  $\Delta_f H_m^\circ(\mathbf{14})$  reported in Table 3. As can be seen, the agreement with experiment is only moderately good.

High-level *ab initio* calculations<sup>130,131</sup> have already indicated that species **14** and **15** have very close thermodynamic stabilities. Our own investigations show that, at the G2 level,  $\Delta_f H^\circ(23)$  and  $\Delta_f G^\circ(23)$  are, respectively, equal to  $-0.5$  and  $0.0$  kcal mol<sup>-1</sup>:



That  $\Delta_f G_m^\circ(23) \approx 0$  kcal mol<sup>-1</sup> is in remarkably good agreement with the results of solvolytic studies.<sup>130,140</sup> This and  $\Delta_f H_m^\circ(23) = -0.5$  kcal mol<sup>-1</sup> imply that in solution at  $-132^\circ\text{C}$ , an equilibrating mixture of these cations contains about 72 and 28%, respectively, of isomers **14** and **15**, in very fair agreement with experiment.<sup>130</sup>

It has just been reported<sup>141</sup> that two different  $\text{C}_4\text{H}_7^+$  ions can be generated in the gas phase from cyclobutyl and cyclopropylcarbinyl chlorides. When sampled shortly (*ca.*  $10^{-6}$  s) after their formation and in the absence of excitation, they display different patterns of reactivity, quite consistent with the structures given above for **14** and **15**.

### Cyclopentylum ion (*c*- $\text{C}_5\text{H}_9^+$ ) (**16**)

This ion is known in solution at low temperature and has been studied in superacid media<sup>142</sup> and even at 70 K in the solid state.<sup>143</sup>

**Table 3** Thermodynamic data for cyclic carbocations C4 and C5

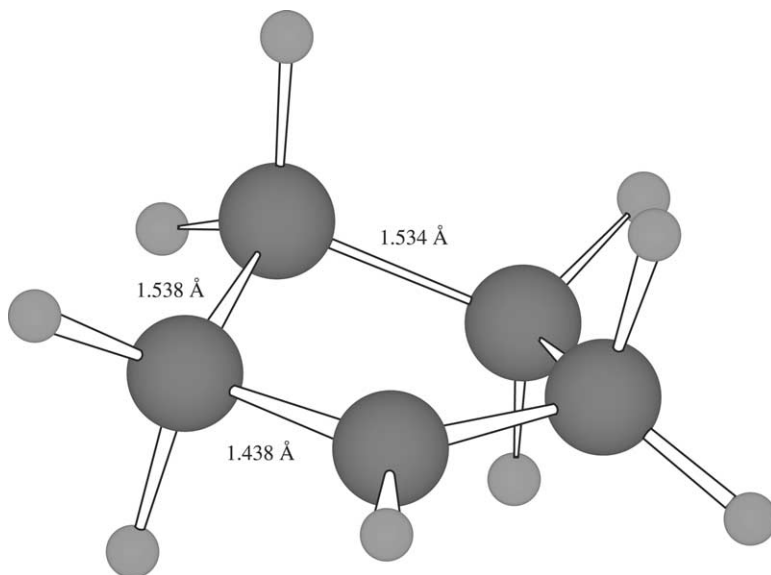
Cations	$\Delta_f H_m^\circ(\text{g})^a$	$S_m^\circ(\text{g})^b$
Cyclobutylum, $c\text{-C}_4\text{H}_7^+$ ( <b>14</b> )	$216.3 \pm 2.2^c$	$67.6 \pm 2.0^d$
	$212.2 \pm 2.2^{e,f}$	
	$212.0 \pm 2.3^{f,g}$	
Cyclopropylmethylum, $c\text{-C}_3\text{H}_5\text{CH}_2^+$ ( <b>15</b> )	$218.4 \pm 2.2^h$	$69.5 \pm 2.0^j$
	$214.4 \pm 2.2^{f,i}$	
	$213.0 \pm 2.3^{f,k}$	
Cyclopentylum, $c\text{-C}_5\text{H}_9^+$ ( <b>16</b> )	$193.1 \pm 2.0^l$	$69.7 \pm 2.0^n$
	$193.7 \pm 2.0^m$	
	$191.9 \pm 2.0^o$	

<sup>a</sup>In kcal mol<sup>-1</sup>.<sup>b</sup>In cal mol<sup>-1</sup> K<sup>-1</sup>.<sup>c</sup>From the experimental GB( $c\text{-C}_4\text{H}_6$ ), 180.1 kcal mol<sup>-1</sup> (Ref. 21),  $\Delta_f H_m^\circ(c\text{-C}_4\text{H}_6) = 37.5 \pm 0.4$  kcal mol<sup>-1</sup> (Ref. 26) and  $S_m^\circ(c\text{-C}_4\text{H}_6) = 62.6 \pm 2.0$  cal mol<sup>-1</sup> K<sup>-1</sup> (Ref. 30) and the computed [MP2(FC)/6-311G(d,p)], scaled  $S_m^\circ(\mathbf{14})$ ,  $67.6 \pm 2.0$  cal mol<sup>-1</sup> K<sup>-1</sup>.<sup>d</sup>Computed, scaled MP2(FC)/6-311G(d,p) value.<sup>e</sup>From the computed PA( $c\text{-C}_4\text{H}_6$ ) to yield **14**, 190.8 kcal mol<sup>-1</sup> and the experimental  $\Delta_f H_m^\circ(c\text{-C}_4\text{H}_6)$ .<sup>f</sup>These values seem more reliable than those based on the experimental GB( $c\text{-C}_4\text{H}_6$ ).<sup>g</sup>G2-computed value.<sup>h</sup>From the experimental GB( $c\text{-C}_4\text{H}_6$ ),  $\Delta_f H_m^\circ(c\text{-C}_4\text{H}_6)$  and  $S_m^\circ(c\text{-C}_4\text{H}_6)$ , and the computed [MP2(FC)/6-311G(d,p)], scaled  $S_m^\circ(\mathbf{15})$ ,  $69.5 \pm 2.0$  cal mol<sup>-1</sup> K<sup>-1</sup> and assuming  $\Delta_f G_m^\circ(\mathbf{14}) = \Delta_f G_m^\circ(\mathbf{15})$ , on the basis of G2 calculations.<sup>i</sup>From the G2-computed PA( $c\text{-C}_4\text{H}_6$ ) to yield **15**, 190.3 kcal mol<sup>-1</sup> and the experimental  $\Delta_f H_m^\circ(c\text{-C}_4\text{H}_6)$ .<sup>j</sup>Computed, scaled MP2(FC)/6-311G(d,p) value.<sup>k</sup>G2-computed value.<sup>l</sup>From the experimental  $\Delta_f H_m^\circ(c\text{-C}_5\text{H}_8) = -18.36 \pm 0.36$  kcal mol<sup>-1</sup> (Ref. 26),  $S_m^\circ(c\text{-C}_5\text{H}_8) = 69.2$  cal mol<sup>-1</sup> K<sup>-1</sup> (Ref. 30),  $\Delta_f H_m^\circ(\mathbf{24})$  and  $\Delta_f G_m^\circ(\mathbf{24})$  from Ref. 149 and the appropriate data for  $iso\text{-C}_3\text{H}_7^+(\text{g})$  (Table 1).<sup>m</sup>As above, but using data from Refs. 117, 147 and 148.<sup>n</sup>Scaled, symmetry-corrected value from the calculations in (o).<sup>o</sup>As above, using our computed G2(MP2) values of  $\Delta_f H_m^\circ(\mathbf{24})$  and  $\Delta_f G_m^\circ(\mathbf{24})$ .

<sup>1</sup>H and <sup>13</sup>C NMR spectra show **16** to have a highly fluxional structure, this being a consequence of very rapid 1,2-hydride shifts.<sup>144,145</sup>

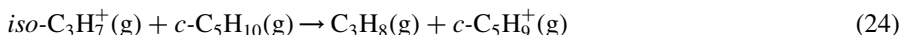
Its structure in the gas phase, as obtained at various correlated *ab initio* levels<sup>146</sup> is twisted ( $C_2$  symmetry), as shown in Fig. 14. This is important because: (1) It shows, as shown in Fig. 14, that the C(1)–C(2)–H<sub>a</sub> and C(1)–C(2)–H<sub>c</sub> angles are quite different and the C–H<sub>a</sub> bond lengths are relatively large, as they fit to partial hydrogen bonding and to a hyperconjugative effect. The same holds for the hydrogens bound to C(5); (2) this structure is able to account for the experimental <sup>13</sup>C NMR spectra of **16** in solution and in the solid state.

Experimental standard thermodynamic state functions for this ion in the gas phase can be obtained from the following sources: the GB of cyclopentene, an ICR



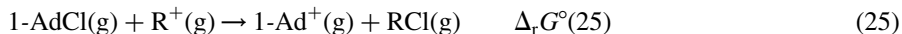
**Fig. 14** Structure of cyclopentylum ion, **16**, optimized at the MP2(full)/6-31G(d) level.

bracketing value from Ref. 107 and the standard Gibbs energy change and enthalpy for reaction (24)<sup>121,148,149</sup> as determined by HPMS:



These thermodynamic data are collected in Table 3, together with the results of our G2(MP2) calculations. The agreement is reasonable.

For the purposes of linking the present results to those obtained by the DPA technique, the standard Gibbs energy change for reaction (25), a chloride ion exchange between a carbocation ( $R^+$ ) (**16** in this case) and 1-adamantyl cation (1-Ad<sup>+</sup>), is necessary. We obtained this datum by combining the experimental  $\Delta_r G^\circ(24)$  with the computed value of the standard Gibbs energy change for the chlorine exchange between 1-adamantyl chloride and cyclopentane, no experimental data being available for cyclopentyl chloride. The result is reported in Table 4:



Notice that in some cases, *tert*-C<sub>4</sub>H<sub>9</sub>Cl has been used instead of 1-AdCl as a reference.

#### CYCLOPROPYL-SUBSTITUTED CARBOCATIONS

The stabilizing interactions between the empty p orbital in the methyl cation and the Walsh orbital of cyclopropane reported in the case of **15** are also present in other cognate ions. Some examples are as follows.

**Table 4** Standard Gibbs energy changes for reaction (25),  $\Delta_r G_m^\circ(25)$ 

Cation	$\Delta_r G_m^\circ(25)$
Methylium ( $\text{CH}_3^+$ ) (1)	$-77.4 \pm 2.8^a$
Propan-2-ylum ( <i>iso</i> - $\text{C}_3\text{H}_7^+$ ) (4)	$-22.7 \pm 3.0^a$
Butan-2-ylum ( <i>sec</i> - $\text{C}_4\text{H}_9^+$ ) (5)	$-18.9 \pm 3.0^a$
2-Methylpropan-2-ylum ( <i>tert</i> - $\text{C}_4\text{H}_9^+$ ) (6)	$-6.0 \pm 1.0^b$
2-Methylpentan-2-ylum ( <i>tert</i> - $\text{C}_6\text{H}_{13}^+$ ) (8)	$-1.1 \pm 2.8^c$
2,4-Dimethylpentan-2-ylum ( $\text{C}_7\text{H}_{15}^+$ ) (9)	$1.9 \pm 2.8^c$
2,4,4-Trimethylpentan-2-ylum ( $\text{C}_8\text{H}_{17}^+$ ) (10)	$4.9 \pm 2.8^c$
3-Ethyl-5,5-dimethylhexan-3-ylum ( $\text{C}_{10}\text{H}_{21}^+$ ) (11)	$7.6 \pm 2.8^c$
2,2,4,6,6-Pentamethylheptan-4-ylum ( $\text{C}_{12}\text{H}_{25}^+$ ) (12)	$13.3 \pm 2.8^c$
Cyclopropylmethylium ( <i>c</i> - $\text{C}_3\text{H}_5\text{-CH}_2^+$ ) (15)	$-7.1 \pm 2.0^d$
Cyclopentylum ( <i>c</i> - $\text{C}_5\text{H}_9^+$ ) (16)	$-13.6 \pm 2.5^a$
1-Cyclopropylethan-1-ylum ( <i>c</i> - $\text{C}_3\text{H}_5\text{-CHCH}_3^+$ ) (17)	$2.0 \pm 2.0^d$
2-Cyclopropylpropan-2-ylum ( <i>c</i> - $\text{C}_3\text{H}_5\text{-C}(\text{CH}_3)_2^+$ ) (18)	$14.2 \pm 2.0^d$
Dicyclopropylmethylium [ <i>(c</i> - $\text{C}_3\text{H}_5)_2\text{-CH}^+$ ] (19)	$12.0 \pm 2.0^d$
1,1-Dicyclopropylethan-1-ylum [ <i>(c</i> - $\text{C}_3\text{H}_5)_2\text{CCH}_3^+$ ] (20)	$22.1 \pm 2.0^d$
Tricyclopropylmethylium [ <i>(c</i> - $\text{C}_3\text{H}_5)_3\text{C}^+$ ] (21)	$29.0 \pm 3.0^c$
Norbornan-1-ylum (1-Nb <sup>+</sup> ) ( $\text{C}_7\text{H}_{11}^+$ ) (22)	$-27.3 \pm 2.8^c$
Norbornan-2-ylum (2-Nb <sup>+</sup> ) ( $\text{C}_7\text{H}_{11}^+$ ) (23)	$-3.0 \pm 1.0^b$
Norbornan-7-ylum (7-Nb <sup>+</sup> ) ( $\text{C}_7\text{H}_{11}^+$ ) (24)	$-22.2 \pm 2.8^c$
Bicyclo[2.2.2]octan-1-ylum ( $\text{C}_8\text{H}_{13}^+$ ) (26)	$-7.4 \pm 2.8^c$
Noradamantan-3-ylum ( $\text{C}_{10}\text{H}_{15}^+$ ) (27)	$-17.4 \pm 2.8^c$
Adamantan-1-ylum ( $\text{C}_{10}\text{H}_{15}^+$ ) (28)	0.00 (by definition)
Adamantan-2-ylum ( $\text{C}_{10}\text{H}_{15}^+$ ) (29)	$-7.6 \pm 2.8^c$ ( $-11.3 \pm 3.0$ ) <sup>e</sup>
Bicyclo[3.3.2]decan-1-ylum ( $\text{C}_{10}\text{H}_{17}^+$ ) (30)	$10.4 \pm 3.3^c$
Homoadamantan-3-ylum ( $\text{C}_{11}\text{H}_{17}^+$ ) (31)	$4.7 \pm 2.8^c$
Homoadamantan-4-ylum ( $\text{C}_{11}\text{H}_{17}^+$ ) (32)	$-0.9 \pm 3.0^c$
Bicyclo[3.3.3]undecan-1-ylum ( $\text{C}_{11}\text{H}_{17}^+$ ) (33)	$13.2 \pm 2.8^c$
[1]Diadamantan-1-ylum ( $\text{C}_{19}\text{H}_{27}^+$ ) (34)	$16.7 \pm 2.8^c$
Cyclopropenylium ( $\text{C}_3\text{H}_3^+$ ) (38)	$5.2 \pm 2.0^c$
1,2-Dipropylcyclopropenylium [ <i>c</i> - $\text{C}_3\text{H}(\text{C}_3\text{H}_7)_2^+$ ] (40)	$32.3 \pm 3.4^c$
Tripropylcyclopropenylium [ <i>c</i> - $\text{C}_3(\text{C}_3\text{H}_7)_3^+$ ] (41)	$41.5 \pm 3.4^c$
Norbornen-7-ylum ( $\text{C}_7\text{H}_9^+$ ) (43)	$1.3 \pm 2.8^c$
Norbornadien-7-ylum ( $\text{C}_7\text{H}_7^+$ ) (44)	$6.9 \pm 2.8^c$
Cycloheptatrienylium (Tropylium) ( $\text{C}_7\text{H}_7^+$ ) (45)	$29.8 \pm 2.0^d$ ( $32.3 \pm 3.4$ ) <sup>c</sup>
Benzylum ( $\text{C}_7\text{H}_7^+$ ) (46)	$-5.8 \pm 2.0^b$
4-Nitrobenzylum (4- $\text{NO}_2\text{-C}_6\text{H}_4\text{-CH}_2^+$ )	$-17.2 \pm 2.0^b$
4-Methoxybenzylum (4- $\text{MeO-C}_6\text{H}_4\text{-CH}_2^+$ )	$7.7 \pm 2.0^b$
1-Phenylethan-1-ylum ( $\text{C}_8\text{H}_9^+$ ) (47)	$1.7 \pm 2.0^b$
2-[4-Methoxyphenyl]propan-2-ylum [4- $\text{MeO-C}_6\text{H}_5\text{C}(\text{CH}_3)_2^+$ ]	$16.7 \pm 2.0^b$
2-[3-Nitrophenyl]propan-2-ylum [3- $\text{NO}_2\text{-C}_6\text{H}_5\text{C}(\text{CH}_3)_2^+$ ]	$-3.2 \pm 2.0^b$
2-Phenylpropan-2-ylum ( $\text{C}_9\text{H}_{11}^+$ ) (48)	$6.4 \pm 1.0^b$
Diphenylmethanylium ( $\text{C}_{13}\text{H}_{11}^+$ ) (49)	$13.4 \pm 3.0^f$
1,1-Diphenylethan-1-ylum ( $\text{C}_{14}\text{H}_{13}^+$ ) (50)	$23.5 \pm 3.0^f$
Triphenylmethanylium ( $\text{C}_{19}\text{H}_{15}^+$ ) (51)	$28.4 \pm 3.0^f$

All values in  $\text{kcal mol}^{-1}$ . Specific details for each ion are given in the text.

<sup>a</sup>From the  $\Delta_f H_m^\circ(\text{g})$  and  $S_m^\circ(\text{g})$  values for ions, as reported in the various tables. Whenever a choice was possible, the most accurate value was used. Data for 1-AdCl and **28** are from Ref. 64. Data for other neutral species are either experimental or computed as indicated in the text.

<sup>b</sup>Direct experimental value (equilibrium techniques).

<sup>c</sup>From DPA experiments and, when necessary, the appropriate leaving group correction for chloride, (see text).

<sup>d</sup>Calculated at the G2(MP2) level.

<sup>e</sup>With leaving group correction for OTs.

<sup>f</sup>From the computed  $\Delta_f H_m^\circ(g)$ <sup>155</sup> and the leaving group correction for chloride.

### 1-Cyclopropylethan-1-ylum ion (*c*-C<sub>3</sub>H<sub>5</sub>CHCH<sub>3</sub><sup>+</sup>) (**17**)

Compound **17** has been obtained at low temperature in superacid media.<sup>150</sup> Both its <sup>1</sup>H and <sup>13</sup>C NMR spectra are known.<sup>151</sup>

NMR evidence indicates that it has a bisected structure (*C<sub>s</sub>* symmetry), the most stable isomer having the methyl group in position *trans* relative to the ring (see Fig. 15).

$\Delta_f H_m^\circ(\mathbf{17})$  as reported in Table 5 was obtained from the experimental standard enthalpy of formation<sup>31</sup> and the PA of vinylcyclopropane as given in Ref. 43, based on (ICR) GB data from Taft's group.

G2(MP2) calculations (this work) provide thermodynamic data also reported there. Interestingly, the computed  $\Delta_f H_m^\circ$  value for gaseous vinylcyclopropane is in excellent agreement with the literature data.<sup>31,35</sup> The structure for the *trans* form of the ion at the MP2(full)/6-31G(d) level is portrayed in Fig. 15.  $\Delta_r G_m^\circ(\mathbf{25})$  is given in Table 4.

### 2-Cyclopropylpropan-2-ylum ion (*c*-C<sub>3</sub>H<sub>5</sub>C(CH<sub>3</sub>)<sub>2</sub><sup>+</sup>) (**18**)

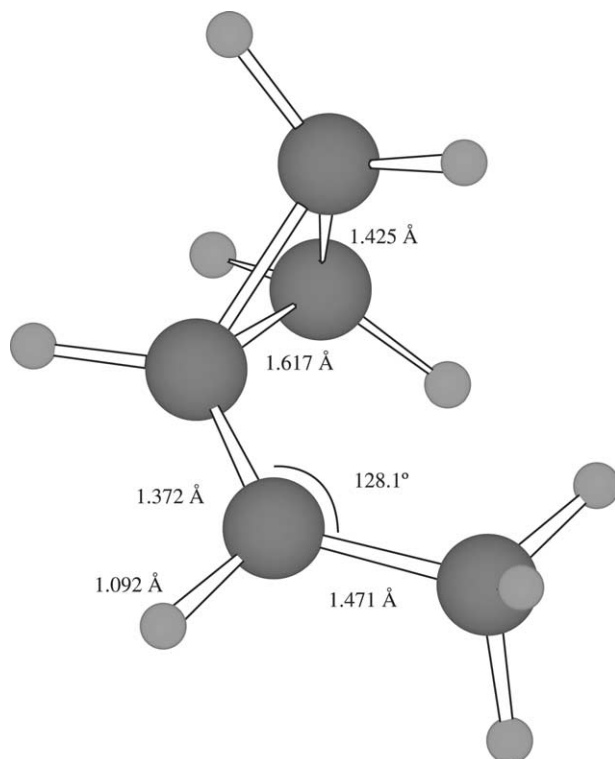
This ion has been generated in solution at low temperature in superacid medium.<sup>150</sup> The <sup>1</sup>H and <sup>13</sup>C NMR spectra of this and cognate ions are reported and discussed in Refs. 151 and 152.

Theoretical calculations, such as those performed in this work, lead to the structure presented in Fig. 16, in which the plane defined by the carbons of the 2-propyl moiety is a perpendicular bisector of the cyclopropyl ring, as in the case of the 1-cyclopropylethyl cation. This is an important result, in full agreement with the NMR spectrum of the ion. Furthermore, rotation around the C(1)–C( $\alpha$ ) bond involves a barrier of *ca.* 13.7 kcal mol<sup>-1</sup>.<sup>153</sup> These structural features, as well as those presented by **15** and **17**, are consequences of the stabilizing interaction between the strained C–C bonds of the cyclopropane moiety and the formally empty *p* orbital of the alkyl moiety.<sup>135–140</sup>

The value of  $\Delta_f H_m^\circ(\mathbf{18})$  given in Table 5 was obtained from the experimental PA of 2-propenylcyclopropane. This value is that recommended in Ref. 43, based on scaled data from Taft's group and Ref. 21. We also report  $\Delta_f H_m^\circ[c\text{-C}_3\text{H}_5\text{C}(\text{CH}_3)_2]^+$  from our G2(MP2) calculations.  $\Delta_r G_m^\circ(\mathbf{25})$  is given in Table 4.

### Dicyclopopylmethylum ion [(*c*-C<sub>3</sub>H<sub>5</sub>)<sub>2</sub>CH<sup>+</sup>] (**19**)

The <sup>1</sup>H NMR spectrum of **19** in solution in superacid media was reported in 1970.<sup>153</sup> As far as we know, its structure in the solid state is not yet available. The X-ray



**Fig. 15** Structure of 1-cyclopropylethan-1-ylum ion, **17**, optimized at the MP2(full)/6-31G(d) level.

structure of the hexafluoroantimonate of hydroxycyclopropylmethylum is known, however,<sup>154</sup> and shows that both rings adopt an essentially “bisected” structure. The structure of **19**, optimized at the MP2(full)/6-31G(d) level, has  $C_2$  symmetry (Fig. 17) and also shows this feature.

No thermodynamic data seem to be available for this species in the gas phase. The data reported in Table 5 were obtained computationally at the MP4(SDQ)/6-31G(d)//MP2(full)/6-31G(d) level.<sup>155</sup> The computed  $\Delta_f G^\circ(25)$  is given in Table 4.

#### *1,1-Dicyclopropylethan-1-ylum ion* [(*c*-C<sub>3</sub>H<sub>5</sub>)<sub>2</sub>CCH<sub>3</sub><sup>+</sup>] (**20**)

We are not aware of experimental structural data on this species. The structure we present here (Fig. 18) is that optimized at the MP2(full)/6-31G(d) level and has a  $C_s$  symmetry clearly showing the bisected positions of the cyclopropyl rings.

The value of  $\Delta_f H_m^\circ[(c-C_3H_5)_2CCH_3^+]$  given in Table 5 was obtained from the experimental PA of [(*c*-C<sub>3</sub>H<sub>5</sub>)<sub>2</sub>C=CH<sub>2</sub>] and the computed (this work)  $\Delta_f H_m^\circ(g)$  for

**Table 5** Thermodynamic data for selected cyclopropyl-containing carbocations

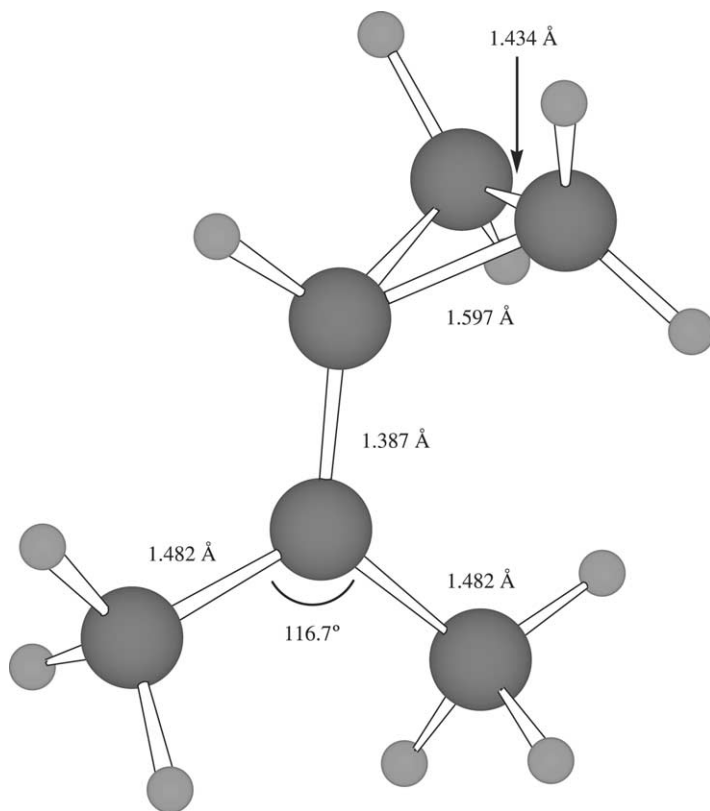
Cations	$\Delta_f H_m^\circ(\text{g})^a$	$S_m^\circ(\text{g})^b$
1-Cyclopropylethan-1-ylum ( $c\text{-C}_3\text{H}_5\text{CHCH}_3^+$ ) ( <b>17</b> )	201.1 $\pm$ 2.1 <sup>c</sup> 197.6 $\pm$ 2.1 <sup>e,f</sup> 194.5 $\pm$ 2.1 <sup>f,g</sup>	77.6 $\pm$ 2.0 <sup>d</sup>
2-Cyclopropylpropan-2-ylum ( $c\text{-C}_3\text{H}_5\text{C}(\text{CH}_3)_2^+$ ) ( <b>18</b> )	178.8 $\pm$ 2.1 <sup>h</sup> 180.0 $\pm$ 2.1 <sup>i</sup> 181.2 $\pm$ 2.1 <sup>k</sup>	84.6 $\pm$ 2.0 <sup>j</sup>
Dicyclopropylmethylium ( $(c\text{-C}_3\text{H}_5)_2\text{CH}^+$ ) ( <b>19</b> )	217.5 $\pm$ 2.0 <sup>l</sup>	82.0 $\pm$ 2.0 <sup>m</sup>
1,1-Dicyclopropylethan-1-ylum ( $(c\text{-C}_3\text{H}_5)_2\text{CCH}_3^+$ ) ( <b>20</b> )	199.3 $\pm$ 4.0 <sup>n</sup>	92.9 $\pm$ 2.0 <sup>o</sup>
Tricyclopropylmethylium ( $(c\text{-C}_3\text{H}_5)_3\text{C}^+$ ) ( <b>21</b> )	232.0 $\pm$ 4.0 <sup>p</sup>	97.8 $\pm$ 2.0 <sup>q</sup>

<sup>a</sup>In kcal mol<sup>-1</sup>.<sup>b</sup>In cal mol<sup>-1</sup> K<sup>-1</sup>.<sup>c</sup>From the experimental PA of vinylcyclopropane,<sup>43</sup> 195.1  $\pm$  2.0 kcal mol<sup>-1</sup> and  $\Delta_f H_m^\circ(c\text{-C}_3\text{H}_5\text{CHCH}_2) = 30.40 \pm 0.30$  kcal mol<sup>-1</sup>.<sup>35</sup><sup>d</sup>Scaled HF/6-31G(d) value from this work.<sup>e</sup>From the computed (G2MP2) PA of  $c\text{-C}_3\text{H}_5\text{CHCH}_2$ , 199.0 kcal mol<sup>-1</sup> and the experimental  $\Delta_f H_m^\circ(c\text{-C}_3\text{H}_5\text{CHCH}_2)$ .<sup>f</sup>Values more reliable than those based on the experimental PA of vinylcyclopropane. See Ref. 126.<sup>g</sup>From the computed  $\Delta_f H_m^\circ$  for the hydride exchange between **17** and **4** together with the experimental value of  $\Delta_f H_m^\circ(c\text{-C}_3\text{H}_5\text{CH}_2\text{CH}_3)$ .<sup>h</sup>From the experimental PA of 2-propenylcyclopropane,<sup>43</sup> 208.3  $\pm$  2.0 kcal mol<sup>-1</sup> and  $\Delta_f H_m^\circ(c\text{-C}_3\text{H}_5\text{CCH}_2\text{CH}_3) = 21.4 \pm 0.5$  kcal mol<sup>-1</sup> from Refs. 31 and 35.<sup>i</sup>From the computed (G2MP2) PA of  $c\text{-C}_3\text{H}_5\text{CCH}_2\text{CH}_3$ , 207.0 kcal mol<sup>-1</sup> and the experimental and  $\Delta_f H_m^\circ(c\text{-C}_3\text{H}_5\text{CCH}_2\text{CH}_3)$ .<sup>j</sup>Scaled HF/6-31G(d) value extracted from the G2(MP2) calculation.<sup>k</sup>From the computed [G2(MP2)]  $\Delta_f H_m^\circ$  for the hydride exchange between 2-cyclopropyl-2-propyl cation and *tert*-butyl cation and the experimental  $\Delta_f H_m^\circ$  values for all the other species.<sup>l</sup>Computed at the G2(MP2) level (this work).<sup>m</sup>Scaled HF/6-31G(d) value from this work.<sup>n</sup>From the experimental PA[( $c\text{-C}_3\text{H}_5$ )<sub>2</sub>C=CH<sub>2</sub>], 216.2 kcal mol<sup>-1</sup><sup>43</sup> and the computed  $\Delta_f H_m^\circ[(c\text{-C}_3\text{H}_5)_2\text{C}=\text{CH}_2]$  (see text).<sup>o</sup>Scaled, symmetry-corrected HF/6-31G(d) value from this work.<sup>p</sup>From the DPA onset of tricyclopropylcarbinol and the computed  $\Delta_f H_m^\circ[(c\text{-C}_3\text{H}_5)_3\text{CH}]$  (this work).<sup>q</sup>Scaled, symmetry-corrected HF/6-31G(d) value from this work.

this species. The former is taken from Ref. 43 and is based on experimental ICR data from Taft's group and Ref. 21.  $\Delta_f H_m^\circ[(c\text{-C}_3\text{H}_5)_2\text{C}=\text{CH}_2]$  was estimated through the combination of experimental  $\Delta_f H_m^\circ$ (vinylcyclopropane, g) and the enthalpy of the isodesmic reaction (26) computed at the MP4(SDQ)/6-31G(d)//MP2(full)/6-31G(d) level.<sup>156</sup> It is difficult to assess the uncertainty of this value, but it might reach some 2–3 kcal mol<sup>-1</sup>. The computed  $\Delta_f G_m^\circ(25)$  is given in Table 4:







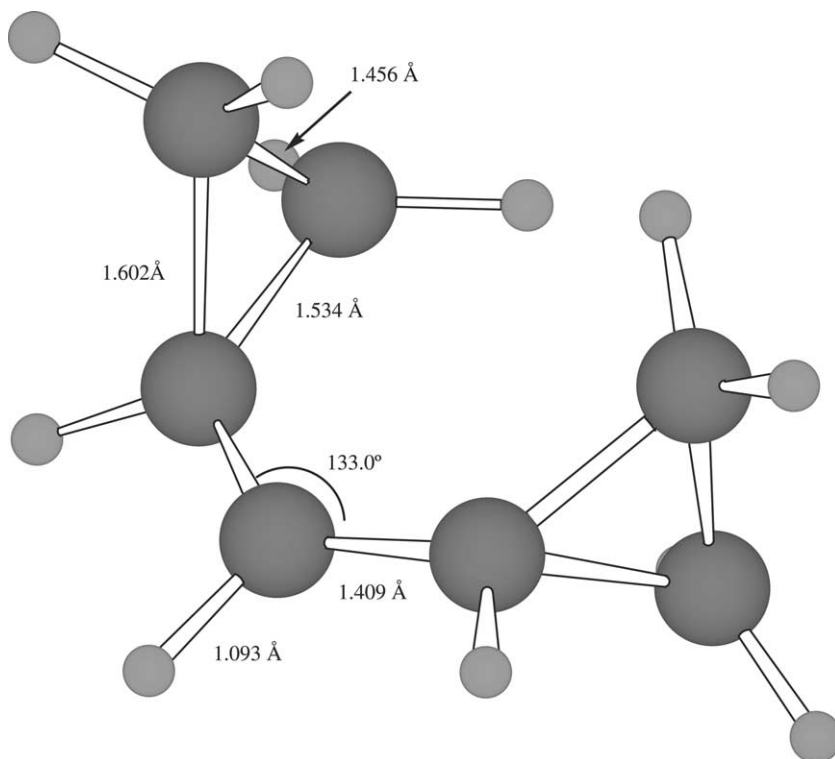
**Fig. 16** Structure of 2-cyclopropylpropan-2-ylum ion, **18**, optimized at the MP2(full)/6-31G(d) level.

### *Tricyclopropylmethylium ion* [(*c*-C<sub>3</sub>H<sub>5</sub>)<sub>3</sub>C<sup>+</sup>] (**21**)

This is a remarkably stable ion, already observed in 1955.<sup>157</sup> Its first <sup>1</sup>H NMR spectrum (in H<sub>2</sub>SO<sub>4</sub> at room temperature!) was reported in 1962<sup>158</sup> and so were a little later, the spectra of a variety of cyclopropyl carbocations in superacid media.<sup>159</sup> Its <sup>13</sup>C spectrum has been carefully analyzed.<sup>160,161</sup>

The structure computed at the MP2(full)/6-31G(d) level (this work) and portrayed in Fig. 19 is propeller-shaped and has *C*<sub>3*h*</sub> symmetry. It obviously minimizes internal repulsions between the rings while allowing for maximal simultaneous overlap between the empty p orbital of the central carbon and the Walsh orbitals of the rings. This situation is to be compared to that prevailing in the trityl cation, which is much less favorable.

No thermodynamic data for this ion in the gas phase seem to be available so far. We have carried out DPA studies of tricyclopropyl carbinol and its methyl ether. This provides  $\Delta_f H_m^\circ(\mathbf{21})$ . Unfortunately, the associated uncertainty is somewhat



**Fig. 17** Structure of dicyclopropylmethyl cation, **19**, optimized at the MP2(full)/6-31G(d) level.

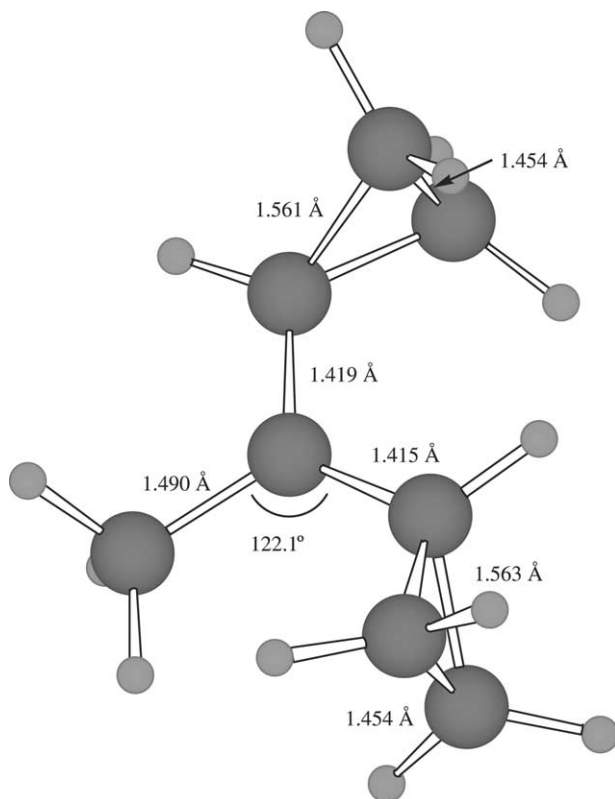
large because of the unavailability of experimental enthalpies of formation for tricyclopropylmethane and other relevant species. As in the previous case, no G2-type calculations could be performed on these species because of their size. Instead, the enthalpy of the isodesmic reaction (27) was computed at the MP4(SDQ)/6-31G(d)/MP2(full)/6-31G(d) level<sup>156</sup> and combined with the experimental value of  $\Delta_f H_m^\circ(c\text{-C}_3\text{H}_5\text{CH}_3)$  to obtain  $\Delta_f H_m^\circ[(c\text{-C}_3\text{H}_5)_3\text{CH}]$ . The computed  $\Delta_f G_m^\circ(25)$  is given in Table 4:



#### SECONDARY AND TERTIARY CARBOCATIONS DERIVED FROM CAGE HYDROCARBONS

##### *Norboman-1-ylum ion* (1-Nb<sup>+</sup>) (C<sub>7</sub>H<sub>11</sub><sup>+</sup>) (**22**)

To our knowledge, this highly strained ion<sup>57,58,162,163</sup> has not been observed in solution or in the solid state. It is known that in solution under stable ion



**Fig. 18** Structure of 1,1-dicyclopropylethan-1-ylum ion, **20**, optimized at the MP2(full)/6-31G(d) level.

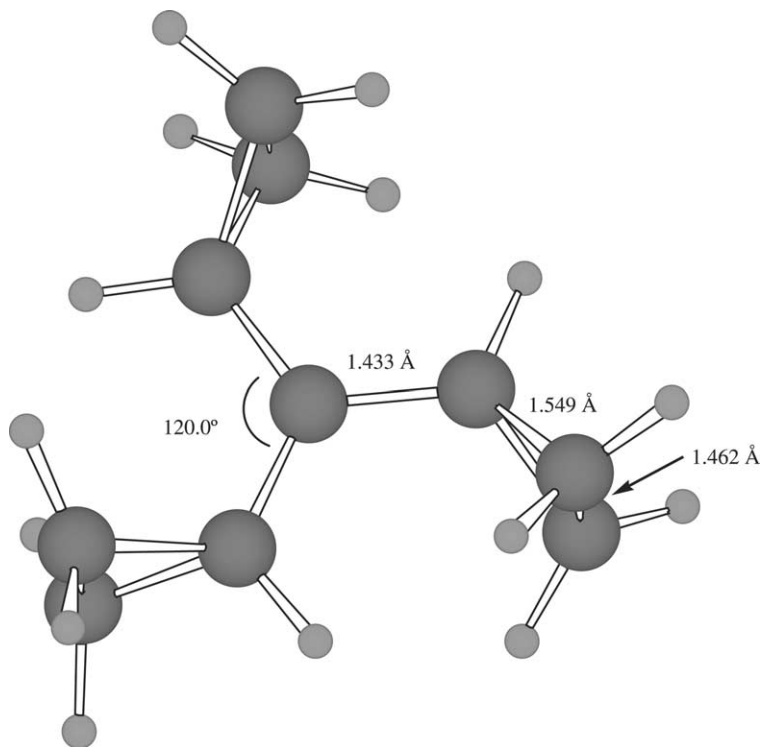
conditions, it is not observed and it rearranges to yield a 2-norbornyl cation.<sup>164</sup> No high-level *ab initio* studies seem to have been published by other workers on this species. Figure 20 portrays its optimized structure at the MP2(full)/6-31G(d) level.

The stability of this ion was experimentally estimated by DPA<sup>57,58</sup> using as substrates the corresponding chloride and bromide. The experimental  $\Delta_r G^\circ(25)$ , is reported in Table 4.

The DPA onset for 1-NbCl, subject to leaving group and entropy corrections similar to those used for **6**, led to the value of  $\Delta_r H^\circ(22)$  reported in Table 6. This table also presents  $\Delta_r H^\circ(22)$  obtained at the G2(MP2) level.

#### Norbornan-2-ylum ion (2-Nb<sup>+</sup>) (C<sub>7</sub>H<sub>11</sub><sup>+</sup>) (**23**)

Few species have raised so much interest and for such a long period of time as **23**.<sup>165–170</sup>



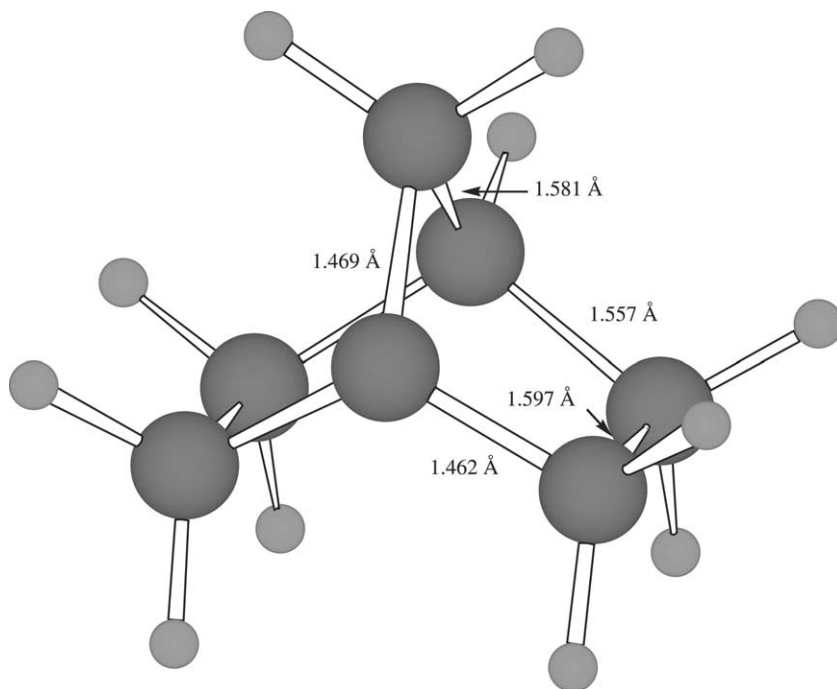
**Fig. 19** Structure of tricyclopropylmethyl cation, **21**, optimized at the MP2(full)/6-31G(d) level.

$^{13}\text{C}$  and  $^1\text{H}$  NMR spectra of this ion in superacid media at low temperatures,<sup>171,172</sup> as well as in the solid state at 5 K,<sup>173</sup> strongly indicate that this ion has the “non-classical” structure depicted in Fig. 21.

The IR<sup>174</sup> and ESCA<sup>175</sup> spectra of this ion at low temperature also support this contention.

High-level *ab initio* calculations in Ref. 176 and references therein agree with these results. Our own G2(MP2) data, based on this non-classical structure, lead to energetic values in excellent agreement with experiment (see Table 6). It is interesting that these concepts have been challenged very recently.<sup>177</sup>

The experimental thermodynamic state functions presented in Table 6 have been obtained from the following sources: (1) the averaged, selected experimental values of PA and GB for norbornene;<sup>43</sup> (2) the experimental HPMS standard Gibbs energy change for the hydride exchange between *tert*-butyl and 2-norbornyl cations;<sup>149</sup> (3) the standard Gibbs energy change for the chloride exchange between *tert*-butyl and 2-norbornyl cations as determined from DPA results<sup>57,58</sup> (see Table 4) and the appropriate leaving group and entropy corrections. All these results are extremely self-consistent.



**Fig. 20** Structure of norbornan-1-ylum ion, **22**, optimized at the MP2(full)/6-31G(d) level.

#### *Norbornan-7-ylum ion* (7-Nb<sup>+</sup>) (C<sub>7</sub>H<sub>11</sub><sup>+</sup>) (**24**)

To our knowledge, this ion has not been observed in solution in superacid media although its IR spectrum, using the SbF<sub>5</sub> matrix technique at very low temperatures, has been obtained from various precursors, including 7-norbornyl chloride.<sup>178,179</sup> These experiments, together with high-level *ab initio* calculations,<sup>179,180</sup> indicate that **24** has the non-classical (C<sub>1</sub> symmetry) structure portrayed in Fig. 22.

7-Norbornyl chloride was subject to DPA treatment in the gas phase.<sup>181</sup> As in the cases discussed above, its reaction onset was used to estimate  $\Delta_r G^\circ(25)$  (Table 4). Also, applying the same kind of leaving group and entropy corrections, the value of  $\Delta_f H_m^\circ(24)$  reported in Table 6 was obtained.  $\Delta_f H_m^\circ(24)$  computed at the G2(MP2) level is also given in Table 6.

#### *Cubylum ion* (C<sub>8</sub>H<sub>7</sub><sup>+</sup>) (**25**)

The stability of this ion (Chart 2) was obtained by direct bromide exchange with 3-noradamantyl cation, prepared in turn by DPA of the 3-bromonoradamantane.<sup>57,58</sup> For the sake of consistency with the treatment in Refs. 57 and 58,  $\Delta_f H_m^\circ(25)$  reported in Table 6 was anchored to that for the 1-adamantyl cation, using for the

**Table 6** Thermodynamic data for secondary and tertiary carbocations derived from cage hydrocarbons

Cations	$\Delta_f H_m^\circ(\text{g})^a$	$S_m^\circ(\text{g})^b$
Norbornan-1-ylum ( $\text{C}_7\text{H}_{11}^+$ ) ( <b>22</b> )	$208.7 \pm 3.1^c$ $204.8 \pm 2.0^e$	$77.0 \pm 2.0^d$
Norbornan-2-ylum ( $\text{C}_7\text{H}_{11}^+$ ) ( <b>23</b> )	$186.1 \pm 2.1^f$ $185.8 \pm 2.1^g$ $186.3 \pm 3.0^i$ $187.1 \pm 2.0^j$	$78.8 \pm 2.0^h$
Norbornan-7-ylum ( $\text{C}_7\text{H}_{11}^+$ ) ( <b>24</b> )	$205.6 \pm 3.0^k$ $203.2 \pm 2.0^l$	$76.4 \pm 2.0^m$
Cubylum ( $\text{C}_8\text{H}_7^+$ ) ( <b>25</b> )	$360.2 \pm 3.8^n$ $358.9 \pm 3.2^o$	$85.6 \pm 2.0^p$
Bicyclo[2.2.2]octan-1-ylum ( $\text{C}_8\text{H}_{13}^+$ ) ( <b>26</b> )	$174.2 \pm 3.0^q$ $176.1 \pm 3.0^r$	$78.7 \pm 2.0^s$
Adamantan-1-ylum ( $\text{C}_{10}\text{H}_{15}^+$ ) ( <b>28</b> )	$162.6 \pm 3.0^t$ $164.1 \pm 3.2^u$ $162.9 \pm 3.2^v$ $160.7 \pm 3.7^x$	$81.07 \pm 2.0^w$
Adamantan-2-ylum ( $\text{C}_{10}\text{H}_{15}^+$ ) ( <b>29</b> )	$171 \pm 3^y$ $171.9 \pm 1.1^z$ $172.1 \pm 1.1^{ab}$	$84.45 \pm 2.0^{aa}$
Bicyclo[3.3.2]decan-1-ylum ( $\text{C}_{10}\text{H}_{17}^+$ ) ( <b>30</b> )	$160.5 \pm 3.5^{ac}$ $161.6 \pm 3.0^{ad}$	$85.3 \pm 2.0^{ae}$
Bicyclo[3.3.3]undecan-1-ylum ( $\text{C}_{11}\text{H}_{19}^+$ ) ( <b>33</b> )	$161.7 \pm 3.0^{af}$ $160.2 \pm 3.0^{ag}$	$86.6 \pm 2.0^{ah}$

<sup>a</sup>In kcal mol<sup>-1</sup>.<sup>b</sup>In cal mol<sup>-1</sup> K<sup>-1</sup>.<sup>c</sup>From the DPA results on 1-NbCl and *tert*-BuCl with the computed leaving group and entropy corrections<sup>57,58</sup> and the  $\Delta_f H_m^\circ$  values for *tert*-C<sub>4</sub>H<sub>9</sub>Cl and *iso*-C<sub>4</sub>H<sub>10</sub>, respectively,  $-42.99 \pm 0.50$  and  $-32.25$  kcal mol<sup>-1</sup>.<sup>26</sup>  $\Delta_f H_m^\circ(\mathbf{6})$  is from Table 1.<sup>d</sup>Scaled value at the HF/6-31G\* level.<sup>e</sup>G2(MP2) computed value (this work).<sup>f</sup>From the averaged, selected experimental values of PA and GB for norbornene<sup>43</sup> and the experimental  $\Delta_f H_m^\circ(\text{C}_7\text{H}_{10})$ ,  $19.7 \pm 0.50$  kcal mol<sup>-1</sup> (Ref. 26) and  $S^\circ(\text{C}_7\text{H}_{10}) = 74.3 \pm 2.0$  cal mol<sup>-1</sup> K<sup>-1</sup> (Walsh, R. and Wells, J. M. (1976) *J. Chem. Thermodyn.* 8, 55).<sup>g</sup>From the experimental HPMS<sup>149</sup> standard Gibbs energy change for the hydride exchange between *tert*-butyl and 2-norbornyl cations with scaled entropy corrections for all species from our G2(MP2) calculations.<sup>h</sup>Scaled value at the HF/6-31G\* level.<sup>i</sup>From the standard Gibbs energy change for the chloride exchange between *tert*-butyl and 2-norbornyl cations as determined from DPA results<sup>57,58</sup> and the appropriate leaving group and entropy corrections, the latter as in (g).<sup>j</sup>As in (f) but using the computed [G2(MP2)] PA and GB of norbornene.

<sup>k</sup>From the standard Gibbs energy change for the chloride exchange between *tert*-butyl and 7-norbornyl cations as determined from DPA results<sup>181</sup> with the appropriate leaving group corrections (at the MP2(full)/6-31G(d) level). Entropy corrections are scaled, values at the HF/6-31G(d) level. Ancillary experimental data for the other species are from Tables 1 and 3.  $\Delta_f H_m^\circ(\text{norbornane}) = 13.30 \pm 0.50$  kcal mol<sup>-1</sup>.<sup>26</sup>

<sup>l</sup>G2(MP2) value.

<sup>m</sup>The value of  $S^\circ(\mathbf{24})$  is a scaled MP2(FU)/6-31G(d) value from this work.

<sup>n</sup>Experimental value obtained as indicated in the text. Leaving group correction at the HF/6-31G(d) level.  $\Delta_f H_m^\circ(\text{adamantane}) = -32.0 \pm 0.50$  kcal mol<sup>-1</sup>,<sup>26</sup>  $\Delta_f H_m^\circ(\text{cubane}) = 148.7 \pm 1.0$  kcal mol<sup>-1</sup>,<sup>26</sup>  $\Delta_f H_m^\circ(\text{1-adamantyl}) = -162.0 \pm 2.0$  kcal mol<sup>-1</sup>.<sup>64</sup>

<sup>o</sup>Computed at the MP2/6-311G(d,p) level. Anchored to experimental data as indicated in the text.

<sup>p</sup>Symmetry-corrected HF/6-31G(d) value.<sup>57</sup>

<sup>q</sup>From the standard Gibbs energy change for the chloride exchange between *tert*-butyl and bicyclo[2.2.2]octyl cations as determined from DPA results<sup>57</sup> and the appropriate leaving group corrections (at the HF/6-31G(d) level). Entropy corrections at the HF/6-31G(d) level. Ancillary experimental data for the other species are from Tables 1 and 3.

<sup>r</sup>Computed values at the MP2/6-311G(d,p) level for the hydride exchange between *tert*-butyl and bicyclo[2.2.2]octyl cations and anchored to the experimental data for *tert*-butyl cation and *iso*-butane. Entropy corrections at the HF/6-31G(d) level.

<sup>s</sup>Symmetry-corrected HF/6-31G(d) value.<sup>57</sup>

<sup>t</sup>From HPMS data<sup>186</sup> for hydride exchange between *tert*-Bu<sup>+</sup> and 1-Ad<sup>+</sup> together with data from Ref. 26 for the neutral species.

<sup>u</sup>From the same source, for the homologous chloride anion exchange, together with  $\Delta_f H_m^\circ(\text{tert-C}_4\text{H}_9\text{Cl}) = 42.99 \pm 0.50$  kcal mol<sup>-1</sup> (Ref. 26) and  $\Delta_f H_m^\circ(\text{1-AdCl}) = -42.45 \pm 0.60$  kcal mol<sup>-1</sup>.<sup>64</sup>

<sup>v</sup>From the DPA and FT ICR equilibrium study of the same process with the entropy corrections (scaled, symmetry-corrected HF/6-31G(d) values) from Ref. 64.

<sup>w</sup>Scaled, symmetry-corrected HF/6-31G(d) value from Ref. 64.

<sup>x</sup>Average of the G2(MP2) calculations for hydride and chloride exchanges, anchored to the experimental  $\Delta_f H_m^\circ(\text{g})$  values for the neutral species.

<sup>y</sup>From Ref. 189.

<sup>z</sup>From Ref. 190 and ancillary data from Ref. 192.

<sup>aa</sup>Computed [HF/6-31G(d)], scaled value.

<sup>ab</sup>G2(MP2) value anchored to experimental data for *iso*-C<sub>3</sub>H<sub>7</sub><sup>+</sup> (Table 1) and *iso*-C<sub>3</sub>H<sub>7</sub> (Ref. 26), see Ref. 192.

<sup>ac</sup>From the standard Gibbs energy change for the chloride or hydroxyl exchanges between *tert*-butyl and bicyclo[3.3.2]decyl cations as determined from DPA results<sup>57</sup> and the appropriate leaving group corrections [at the HF/6-31G(d) level]. Entropy corrections are symmetry-corrected values at the HF/6-31G(d) level. Ancillary experimental data for the other species are from Tables 1 and 3.  $\Delta_f H_m^\circ(\text{g})$  for bicyclo[3.3.2]decane is  $-25.3 \pm 0.50$  kcal mol<sup>-1</sup>.<sup>26</sup>

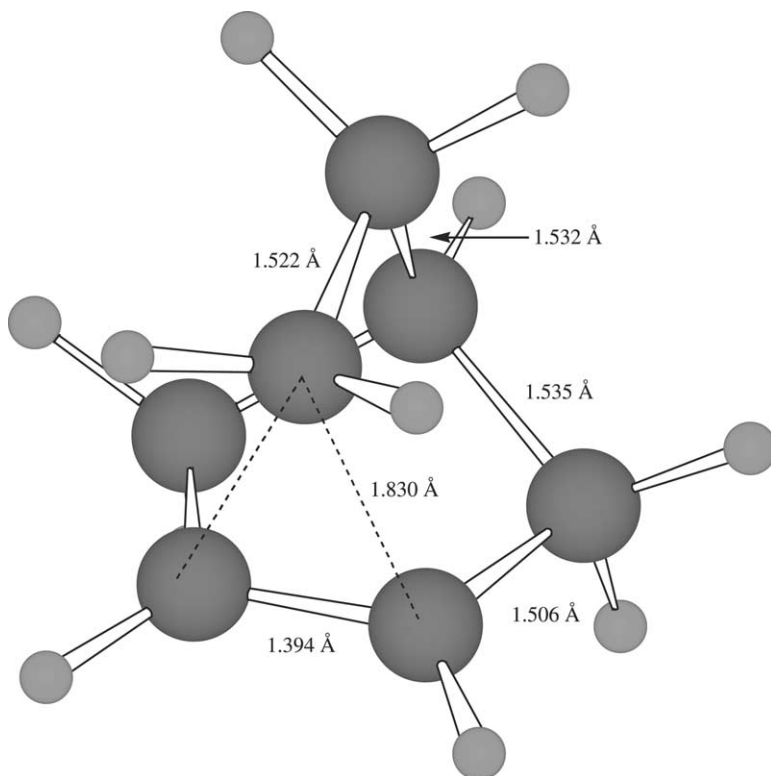
<sup>ad</sup>Computed values at the MP2/6-311G(d,p) level for the hydride exchange between *tert*-butyl and bicyclo[3.3.2]decyl cations and anchored to the experimental data for *tert*-butyl cation and *iso*-butane. Entropy values are symmetry-corrected at the HF/6-31G(d) level.

<sup>ae</sup>Computed [HF/6-31G(d)] value.

<sup>af</sup>From the averaged standard Gibbs energy changes for the chloride or hydroxyl exchanges between *tert*-butyl and bicyclo[3.3.3]undecyl cations as determined from DPA results<sup>57</sup> and the appropriate leaving group corrections [at the HF/6-31G(d) level].<sup>57</sup> Entropy corrections are symmetry-corrected values at the HF/6-31G(d) level. Ancillary experimental data for the other species are from Tables 1 and 3.  $\Delta_f H_m^\circ(\text{g})$  for bicyclo[3.3.3]undecane is  $-21.2 \pm 0.50$  kcal mol<sup>-1</sup>.<sup>26</sup>

<sup>ag</sup>Computed values at the MP2/6-311G(d,p) level for the hydride exchange between *tert*-butyl and bicyclo[3.3.3]undecyl cations and anchored to the experimental data for *tert*-butyl cation and *iso*-butane. Entropy values are symmetry-corrected at the HF/6-31G(d) level.

<sup>ah</sup>Computed [HF/6-31G(d)] value.



**Fig. 21** Structure of norbornan-2-ylum ion, **23**, optimized at the MP2(full)/6-31G(d) level.

latter  $\Delta_f H_m^\circ = 162.0 \pm 2.0 \text{ kcal mol}^{-1}$ .<sup>64</sup> We also report the results computed at the MP2/6-311G(d,p) level.<sup>57,58</sup>

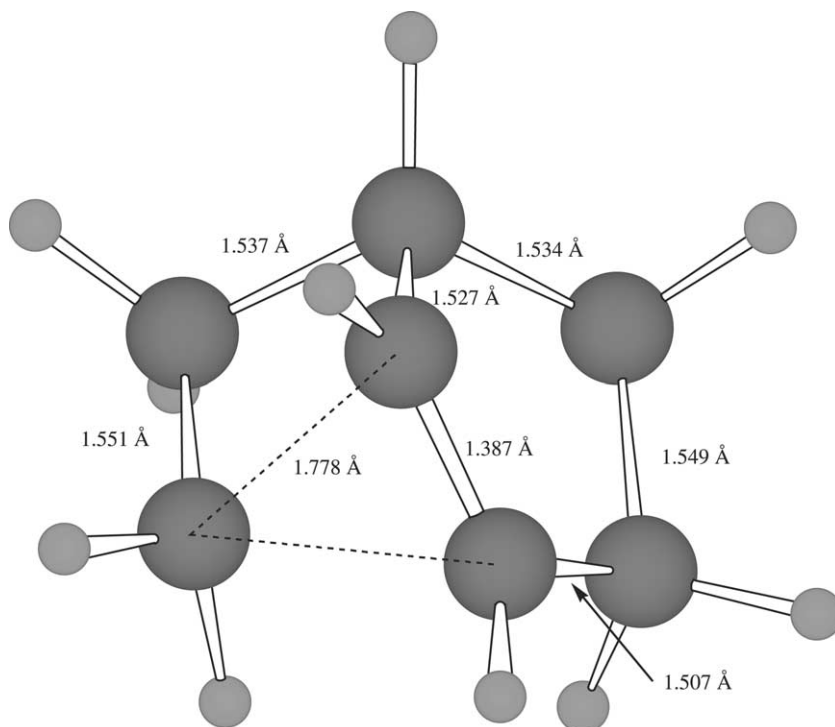
*Bicyclo[2.2.2]octan-1-ylum ion (C<sub>8</sub>H<sub>7</sub><sup>+</sup>) (26)*

$\Delta_f H_m^\circ$ (**26**) (see [Chart 2](#)) presented in [Table 6](#) is based on the DPA study of the 1-chlorobicyclo[2.2.2]octane<sup>57</sup> (see also [Table 4](#)). These results were shown to be in excellent agreement with those obtained from the corresponding bromide.<sup>58</sup> Experimental data were treated exactly as in the case of **25**. Computational results at the MP2/6-311G(d,p) level are also given in [Table 6](#).

*Noradamantan-3-ylum ion (C<sub>10</sub>H<sub>13</sub><sup>+</sup>) (27)*

The  $\Delta_f G^\circ$ (**25**) value given in [Table 4](#) was obtained from the DPA study of 3-noradamantyl bromide with the appropriate leaving group corrections<sup>57,58</sup> (see [Chart 2](#)).





**Fig. 22** Structure of norbornan-7-ylum ion, **24**, optimized at the MP2(full)/6-31G(d) level.

#### *Adamantan-1-ylum ion* ( $C_{10}H_{15}^+$ ) (**28**)

This ion (see [Chart 2](#)) is of both historical and chemical importance. It was one of the first tertiary carbocations to be identified in solution in superacid media,<sup>182</sup> studied by  $^1\text{H}$  and  $^{13}\text{C}$  NMR in solution,<sup>183</sup> prepared as a stable solid salt,<sup>184</sup> and characterized by its IR spectrum in cryogenic  $\text{SbF}_5$  matrices.<sup>185</sup> It was amongst the first ions to be studied by ICR through halide exchange reactions<sup>50,186</sup> and also the first tertiary carbocation to undergo a systematic treatment by means of DPA.<sup>54</sup>

$\Delta_f H_m^\circ(\mathbf{28})$ , presented in [Table 6](#), is based on the most recent HPMS and FT ICR studies by hydride and halide exchanges<sup>58,60,187</sup> (see [Table 4](#)). These results have been shown to be quite consistent with the G2(MP2) studies of both kinds of processes.<sup>64</sup> The value of  $\Delta_f H_m^\circ(\mathbf{28})$  used here is  $162.0 \pm 2.0 \text{ kcal mol}^{-1}$ , simultaneously consistent with these experimental and computational data.

#### *Adamantan-2-ylum ion* ( $C_{10}H_{15}^+$ ) (**29**)

As far as we know, this ion ([Chart 2](#)) has not been observed in solution or in the solid state. It has, however, been studied in the gas phase<sup>186</sup> and computationally at the MP2/6-31G(d)//6-31G(d) + ZPVE6-31G(d) level.<sup>188</sup>

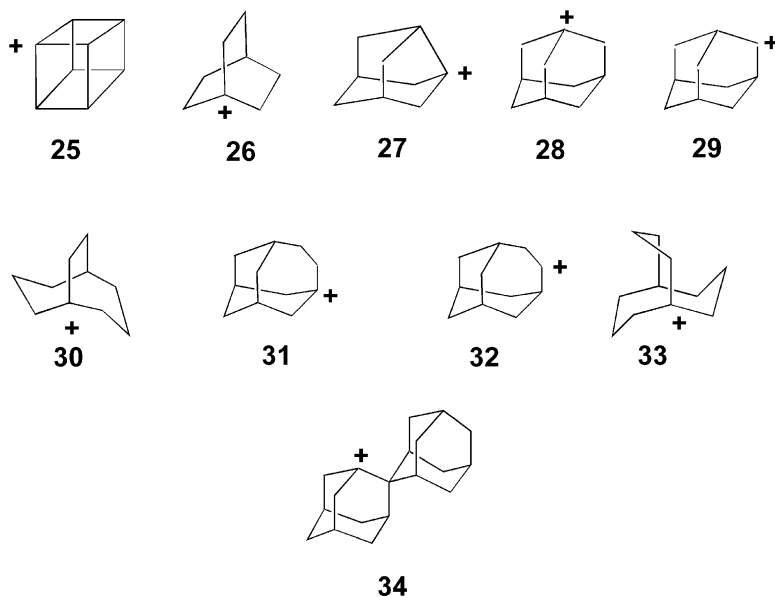


Chart 2

Thermodynamic experimental data for this ion comes from three sources: (1) its appearance energy from a variety of precursors;<sup>189</sup> (2) the adiabatic ionization energy of the 2-adamantyl radical;<sup>190</sup> (3) the DPA study of 2-adamantyl chloride and 2-adamantyl alcohol.<sup>191</sup>

On the basis of a G2(MP2) study of 1- and 2-adamantyl radicals and cations,<sup>192</sup> the results by Aubry *et al.*<sup>189</sup> and Kruppa and Beauchamp<sup>190</sup> seem quite consistent,<sup>191</sup> they are also in very good agreement with DPA studies of 2-adamantanol and 2-adamantyl chloride. The results are summarized in Table 6 (see also Table 4).

A value for  $\Delta_f H_m^\circ(\mathbf{29})$  of  $171.9 \pm 2.0$  kcal mol<sup>-1</sup> is simultaneously consistent with these experimental and computational data.

#### *Bicyclo[3.3.2]decan-1-ylum ion* (C<sub>11</sub>H<sub>17</sub><sup>+</sup>) (**30**)

The thermodynamic data for this ion presented in Table 6 were obtained from the DPA study of the corresponding alcohol and chloride.<sup>57,58</sup> The average  $\Delta_f G^\circ(25)$  is given in Table 4. Leaving group and entropy corrections were applied as in previous cases. Values obtained at the MP2/6-311G(d,p) level are reported in Table 4.

#### *Homoadamantan-3-ylum ion* (C<sub>11</sub>H<sub>17</sub><sup>+</sup>) (**31**)

This ion (see Chart 2) was obtained from the DPA of the corresponding chloride and alcohol.<sup>57,58</sup> The value of  $\Delta_f G^\circ(25)$  given in Table 4 is the average of both results (with the appropriate leaving group correction).

*Homoadamantan-4-ylum ion* ( $C_{11}H_{17}^+$ ) (**32**)

This ion ([Chart 2](#)) was obtained from the DPA of the corresponding chloride.<sup>193</sup> The experimental  $\Delta_f G^\circ(25)$  value is given in [Table 4](#).

*Bicyclo[3.3.3]undecan-1-ylum ion* ( $C_{10}H_{17}^+$ ) (**33**)

This ion was obtained from the DPA of the corresponding chloride and alcohol.<sup>57,58</sup> The value of  $\Delta_f G^\circ(25)$  given in [Table 4](#) is the average of both highly consistent results (with the appropriate leaving group correction).  $\Delta_f H_m^\circ(\mathbf{33})$  derived therefrom is given in [Table 6](#) together with the results obtained at the MP2/6-311G(d,p) level.

*Diadamantan-1-ylum ion* ( $C_{19}H_{27}^+$ ) (**34**)

This ion was obtained from the DPA of the corresponding chloride and alcohol.<sup>58</sup> The value of  $\Delta_f G^\circ(25)$  given in [Table 4](#) is the average of both highly consistent results. Because of the size of the system, leaving group corrections were computed at the AM1 level.

CARBENIUM IONS WITH FORMAL  $\pi$  SYSTEMS*Vinylium ion* ( $C_2H_3^+$ ) (**35**)

Experimental values for the standard enthalpy of formation of this ion, as reported in [Table 7](#), are in fair agreement. They originate in: (1) the proton affinity of acetylene<sup>194</sup> obtained in SIFT experiments; and (2) the adiabatic ionization energy of the vinyl radical<sup>195</sup> combined with its standard enthalpy of formation.<sup>25</sup>

We have obtained  $\Delta_f H_m^\circ(g)$  values for  $C_2H_3^+$  by combining the standard enthalpy of protonation of acetylene as computed at the G2 level (this work) with the experimental  $\Delta_f H_m^\circ(C_2H_2)$ . Also used was the computed (G2) ionization energy of vinyl radical together with the experimental value of  $\Delta_f H_m^\circ(C_2H_3)$  to obtain  $\Delta_f H_m^\circ(C_2H_3^+)$ . These values are presented in [Table 7](#). (see also Ref. 196).

Experimental spectroscopic studies in the millimeter wavelength region<sup>3,197,198</sup> provided rotational constants and the inertial defect for this ion. These data show that the ground state of this species is planar and has a non-classical  $C_{2v}$  structure (**1**, [Fig. 23](#)). Near-IR studies of  $C_2H_3^+$  led to results<sup>199,200</sup> also in agreement with this non-classical structure. Furthermore, the splitting of the spectral lines was interpreted in terms of the tunneling of protons between the nonequivalent axial and apical positions. This tunneling takes place through the classical structure **2** ([Fig. 23](#)). From the most recent work,<sup>198</sup> the difference in stability between these structures has been estimated at 4.7 kcal mol<sup>-1</sup>.

The computed difference in standard enthalpies of formation between structures **1** and **2** amounts to 4.3 kcal mol<sup>-1</sup>. High-level structural studies<sup>201</sup> reveal a small upward tilting (0.3°) of the axial hydrogens with respect to the internuclear C–C

**Table 7** Thermodynamic data for non-aromatic carbocations with formal  $\pi$  bonds

Cations	$\Delta_f H_m^\circ(\text{g})^a$	$S_m^\circ(\text{g})^b$
Vinylum ( $\text{C}_2\text{H}_3^+$ ) (35)	$266.6 \pm 3.2^c$	$52.4 \pm 2.0^e$
	$269.9 \pm 1.9^d$	
	$265.7 \pm 2.5^f$	
	$266.8 \pm 2.0^g$	
2-Propargylium ( $\text{C}_3\text{H}_3^+$ ) (36)	$280.8 \pm 1.1^h$	$59.3 \pm 2.0^i$
	$279.6 \pm 2.0^j$	
2-Propenylium, allyl ( $\text{C}_3\text{H}_5^+$ ) (37)	$228.9 \pm 0.6^k$	$60.4 \pm 2.0^m$
	$226.0 \pm 2.0^l$	
	$228.7 \pm 2.0^n$	

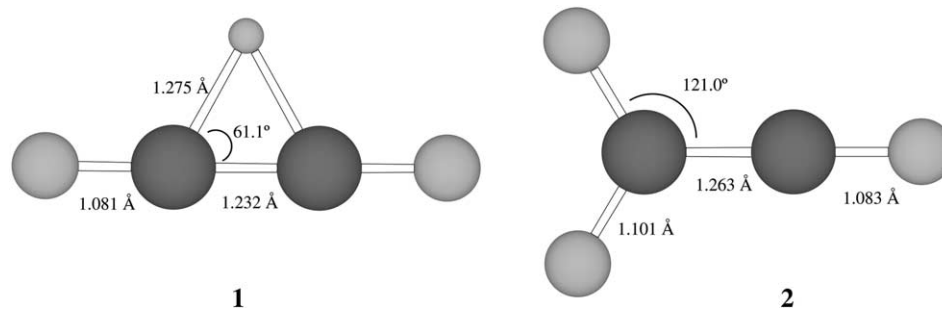
<sup>a</sup>In kcal mol<sup>-1</sup>.<sup>b</sup>In cal mol<sup>-1</sup> K<sup>-1</sup>.<sup>c</sup>From the experimental PA( $\text{C}_2\text{H}_2$ ),  $153.3 \pm 3.2$  kcal mol<sup>-1</sup> (Ref. 194) and  $\Delta_f H_m^\circ(\text{C}_2\text{H}_2)$ ,  $54.190$  kcal mol<sup>-1</sup>.<sup>26</sup><sup>d</sup>From the adiabatic ionization energy of vinyl radical,  $8.59 \pm 0.03$  eV (Ref. 195) and  $\Delta_f H_m^\circ(\text{C}_2\text{H}_3) = 71.5 \pm 1.5$  kcal mol<sup>-1</sup>.<sup>25</sup> See also Berkowitz, J., Ellison, G. B. and Gutman, D. (1994) *J. Phys. Chem.* 98, 2744 for a detailed discussion of the matter.<sup>e</sup>Symmetry-corrected, scaled value at the HF/6-31G(d) level (this work).<sup>f</sup>From the G2-computed ionization energy of vinyl radical ( $194.1$  kcal mol<sup>-1</sup> at 0 K) and the experimental  $\Delta_f H_m^\circ(\text{C}_2\text{H}_3)$  (this work).<sup>g</sup>From the G2-computed PA( $\text{C}_2\text{H}_2$ ) (this work) ( $153.1$  kcal mol<sup>-1</sup>) and the experimental  $\Delta_f H_m^\circ(\text{C}_2\text{H}_2)$ .<sup>h</sup>From the ionization energy of the propargyl radical<sup>207</sup> and  $\Delta_f H_m^\circ(\text{C}_3\text{H}_3) = 81.0 \pm 1.0$  kcal mol<sup>-1</sup> from Ref. 25. Thermal corrections from this work.<sup>i</sup>Scaled, corrected HF/6-31G(d) value from this work.<sup>j</sup>This work, using the computed (G2) ionization energy of  $\text{C}_3\text{H}_3$  ( $8.673$  eV)<sup>207</sup> and  $\Delta_f H_m^\circ(\text{C}_3\text{H}_3) = 81.0 \pm 1.0$  kcal mol<sup>-1</sup>.<sup>25</sup> Thermal corrections from this work.<sup>k</sup>From Ref. 212.<sup>l</sup>From the experimental  $\Delta_f H_m^\circ(\text{g})$  of allene,  $45.6 \pm 0.2$  kcal mol<sup>-1</sup> (Ref. 27) and its experimental PA,  $185.3$  kcal mol<sup>-1</sup>.<sup>191</sup><sup>m</sup>HF/6-31G(d) value from this work, scaled and symmetry corrected.<sup>n</sup>This work, using the experimental  $\Delta_f H_m^\circ(\text{g})$  for allene and its G2-calculated PA ( $184.0$  kcal mol<sup>-1</sup>).

axis. Theory and computation on vinyl cations have been reviewed.<sup>202</sup> Studies on medium effects on acetylene and vinyl cation have been reported recently.<sup>203</sup>

*Ab initio* molecular dynamics<sup>204,205</sup> calculations performed on vinyl cation confirm that the ground-state structure of  $\text{C}_2\text{H}_3^+$  is best described as a quasi-planar bridged structure broadened significantly by anisotropic delocalization of the protons due to zero point motion.

### 2-Propargylium ion ( $\text{C}_3\text{H}_3^+$ ) (36)

To our knowledge, no direct experimental spectroscopic data are available for the propargyl cation. Very large scale *ab initio* calculations have been carried out on both this ion and on the propargyl radical.<sup>206</sup> They lead to vibrational frequencies for the latter in excellent agreement with experiment and to an adiabatic ionization



**Fig. 23** Structure of vinylium ion, **35**, optimized at the MP2(full)/6-31G(d) level. Structure **1** is the absolute minimum. Structure **2** is a transition state.

potential for this radical (8.650 eV) pleasantly close to the experimental value (8.673 eV).<sup>207,208</sup>  $\Delta_f H_m^\circ(\mathbf{36})$  (Table 7) can be obtained experimentally from the standard enthalpy of formation of the propargyl radical<sup>25</sup> and the zero kinetic energy photoelectron spectrum (ZEKE) of this species.<sup>207</sup>

Recent calculations at the CBS-Q level<sup>99</sup> as well as our present G2 computations lead to values of  $\Delta_f H_m^\circ(\mathbf{36})$  in excellent agreement with experiment (Table 7). They all confirm the  $C_{2v}$  symmetry of **36** (Fig. 24).

### 2-Propenylium ion, allyl cation ( $C_3H_5^+$ ) (**37**)

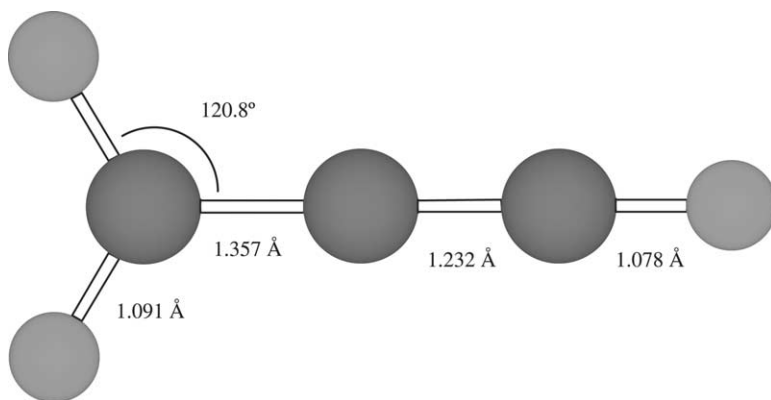
According to careful *ab initio* calculations, this species is planar and has a  $C_{2v}$  symmetry (Fig. 25).<sup>209,210</sup> According to Ref. 210, this planarity seems to be enforced by the  $\sigma$  framework although the contribution from the  $\pi$  conjugation is also relevant.

Based on the adiabatic ionization energy of the allyl radical as determined by Houle and Beauchamp<sup>211</sup> and on its own work, the Boulder group<sup>212</sup> determined a value of  $\Delta_f H_m^\circ(\mathbf{37})$  in remarkable agreement with that obtained much earlier by Lossing<sup>213</sup> by means of appearance energies.  $\Delta_f H_m^\circ(\mathbf{37})$  can also be derived from the experimental GB of allene (upon appropriate correction of entropy effects; see Table 7) obtained by ICR, using a bracketing technique.<sup>214</sup>  $\Delta_f H_m^\circ(\mathbf{37})$  computed at the CBS-Q level<sup>99</sup> is in very nice agreement with the datum from Ref. 212. So is our own G2 result (see Table 7).

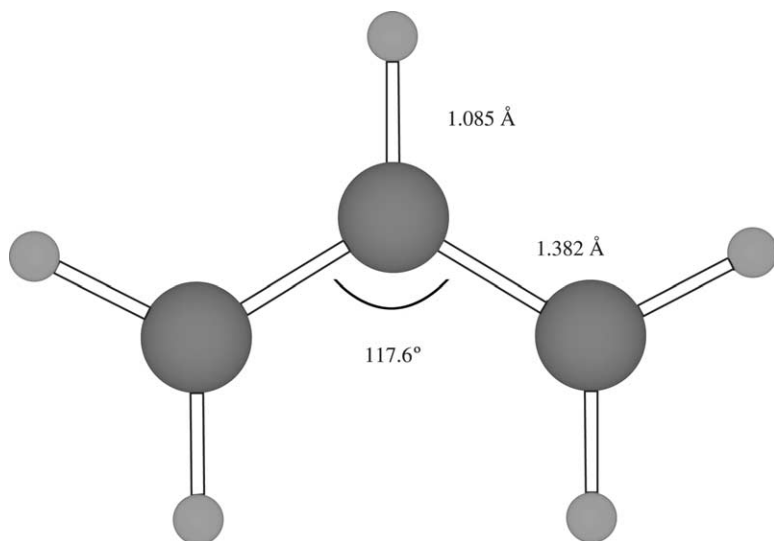
### TWO-ELECTRON AROMATIC AND HOMOAROMATIC IONS

#### Cyclopropenylium ion ( $C_3H_3^+$ ) (**38**)

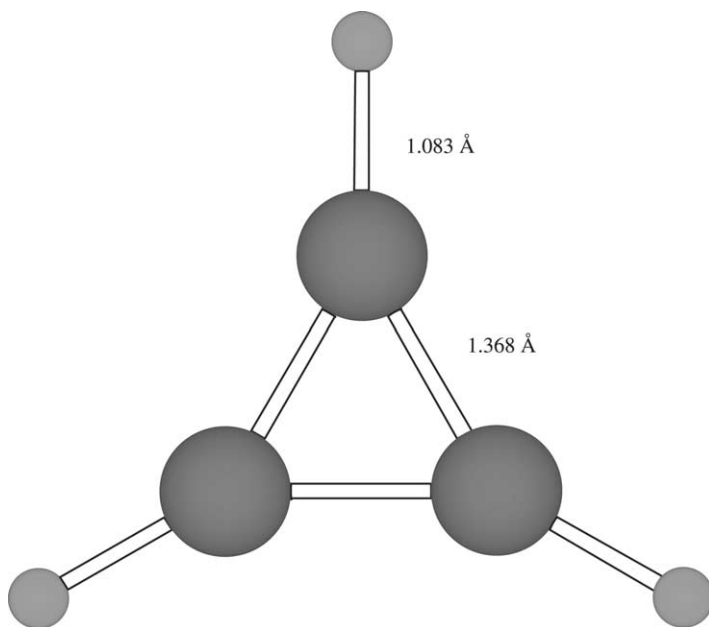
This species, an “archetypal aromatic cation”<sup>122</sup> has a planar, fully symmetrical structure ( $D_{3h}$  symmetry point group) (Fig. 26) as confirmed by the systematic



**Fig. 24** Structure of 2-propenylium ion, **36**, optimized at the MP2(full)/6-31G(d) level.



**Fig. 25** Structure of 2-propenylium ion, **37**, optimized at the MP2(full)/6-31G(d) level.



**Fig. 26** Structure of cyclopropenylium ion, **38**, optimized at the MP2(full)/6-31G(d) level.

experimental study of the IR and Raman spectra of some of its salts (in liquid sulfur dioxide solution and in polycrystalline state).<sup>215</sup>

$\Delta_f H_m^\circ(\mathbf{38})$  has been obtained experimentally through the determination of the appearance potential of this ion from a variety of neutral precursors including several molecules.<sup>213</sup> These studies lead to the values reported in Table 8.

No experimental value of  $S_m^\circ(\mathbf{38})$  seems to be presently available. That given in Table 8 was calculated in this work.

Compound **38** has been the subject of a large number of theoretical studies, the most recent ones being listed in Refs. 216–218. The relevant C–C and C–H distances, as obtained at the MP4/6-311G 4\* + level,<sup>216</sup> are, respectively,

**Table 8** Thermodynamic data for aromatic and homoaromatic two- and six- $\pi$ -electron carbenium ions

Cations	$\Delta_f H_m^\circ(\text{g})^a$	$S_m^\circ(\text{g})^b$
Cyclopropenylium ( $\text{C}_3\text{H}_3^+$ ) ( <b>38</b> )	257.0 $\pm$ 2.0 <sup>c</sup> 256.7 $\pm$ 2.0 <sup>e</sup> 257.2 $\pm$ 2.0 <sup>f</sup>	54.8 $\pm$ 2.0 <sup>d</sup>
Propylcyclopropenylium ( <i>c</i> - $\text{C}_3\text{H}_2$ - $\text{C}_3\text{H}_7^+$ ) ( <b>39</b> )	222.5 $\pm$ 2.9 <sup>g</sup>	85.43 $\pm$ 2.0 <sup>h</sup>
Cyclobutenylium ( $\text{C}_4\text{H}_5^+$ ) ( <i>c</i> - $\text{C}_4\text{H}_5^+$ ) ( <b>42</b> )	210.1 $\pm$ 2.9 <sup>i</sup>	59.6 $\pm$ 2.0 <sup>j</sup>
Norbornen-7-ylum ( $\text{C}_7\text{H}_9^+$ ) ( <b>43</b> )	215.7 $\pm$ 3.3 <sup>k</sup> 215.2 $\pm$ 2.6 <sup>m</sup>	74.2 $\pm$ 2.0 <sup>l</sup>
Norbornadien-7-ylum ( $\text{C}_7\text{H}_7^+$ ) ( <b>44</b> )	247.9 $\pm$ 3.8 <sup>n</sup> 249.9 $\pm$ 2.0 <sup>p</sup>	71.4 $\pm$ 2.0 <sup>o</sup>
Cycloheptatrienylium, tropylium ( $\text{C}_7\text{H}_7^+$ ) ( <b>45</b> )	211.4 $\pm$ 3.8 <sup>q</sup> 209.8 $\pm$ 2.0 <sup>s</sup>	69.8 $\pm$ 2.0 <sup>r</sup>

<sup>a</sup>In kcal mol<sup>-1</sup>.

<sup>b</sup>In cal mol<sup>-1</sup> K<sup>-1</sup>.

<sup>c</sup>From appearance energies.<sup>213</sup>

<sup>d</sup>From the scaled, symmetry-corrected HF/6-31G\* value taken from the G2 calculation (this work).

<sup>e</sup>From G2 computations.<sup>99</sup>

<sup>f</sup>From CBS-Q calculations.<sup>99</sup>

<sup>g</sup>Computed at the G2(MP2) level (this work); see text.

<sup>h</sup>Symmetry-corrected HF/6-31G(d) value taken from the G2(MP2) calculation (this work).

<sup>i</sup>Computed at the G2 level (this work); see text.

<sup>j</sup>Symmetry-corrected HF/6-31G(d) value taken from the G2(MP2) calculation (this work).

<sup>k</sup>Obtained from the DPA study of the corresponding alcohol and chloride.<sup>182</sup>

<sup>l</sup>Scaled HF/6-31G(d) value taken from the G2(MP2) calculation (this work).

<sup>m</sup>Computed at the G2(MP2) level (this work).

<sup>n</sup>Obtained from the DPA study of the corresponding alcohol.<sup>182</sup>

<sup>o</sup>Scaled HF/6-31G(d) value taken from the G2(MP2) calculation (this work).

<sup>p</sup>Computed at the G2(MP2) level (this work).

<sup>q</sup>From DPA studies.<sup>156</sup>

<sup>r</sup>Scaled, symmetry-corrected HF/6-31G(d) value (this work).

<sup>s</sup>Computational value from Ref. 242.



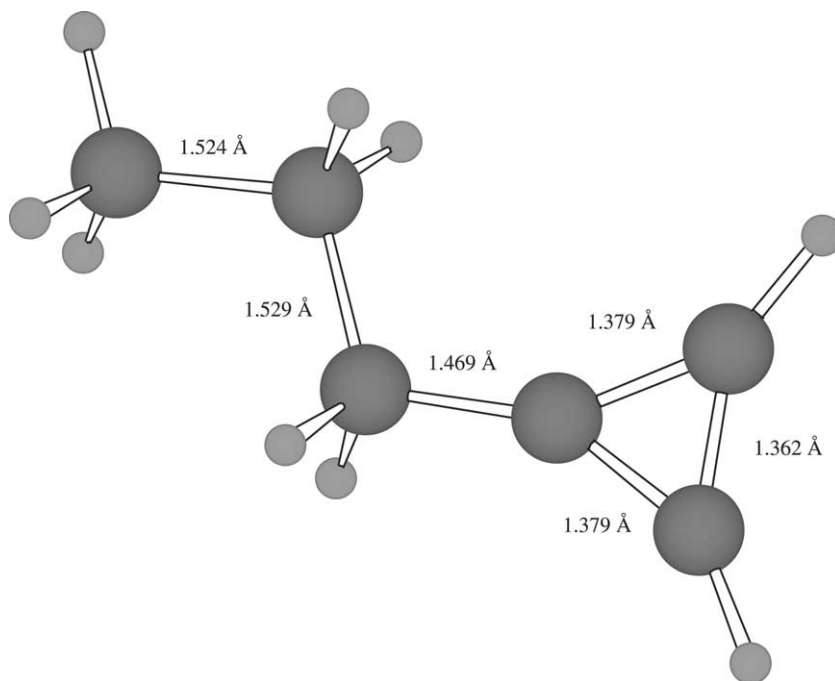
1.363<sub>2</sub> and 1.079<sub>5</sub> Å. While the latter is close to that in benzene, the former is significantly shorter (C–C bond length of 1.397 Å for benzene). The various vibrational frequencies, including anharmonicity effects and Fermi resonance pairs for this ion and all its deuterated isotopomers, have been computed at extremely high levels and are in excellent agreement with experiment whenever a comparison has been possible.<sup>216,217</sup>

The fact that the C–C bond lengths are shorter and the C–C stretching frequencies and the delocalization energies per  $\pi$  electron are higher for cyclopropenium than for benzene, is taken as an indication of “superaromaticity”.<sup>122,215</sup>

The  $\Delta_f H_m^\circ(\mathbf{38})$  values computed using G2 methodology<sup>122</sup> and Petersson’s complete basis technique (CBS-Q)<sup>99</sup> are nicely consistent and in excellent agreement with experiment (see Table 8).

### *1-Propylcyclopropen-2-ylum ion (c-C<sub>3</sub>H<sub>2</sub>C<sub>3</sub>H<sub>7</sub><sup>+</sup>) (39)*

To our knowledge, no experimental structural data seem to be available for this ion. The value of  $\Delta_f H_m^\circ(\mathbf{39})$  reported in Table 8 was obtained computationally at the G2(MP2) level. The fully optimized structure (of  $C_s$  symmetry) portrayed in Fig. 27 derives from these calculations.



**Fig. 27** Structure of 1-propylcyclopropenyl cation, **39**, optimized at the MP2(full)/6-31G(d) level.

*1,2-Dipropylcyclopropen-3-ylum* [ $c\text{-C}_3\text{H}(\text{C}_3\text{H}_7)_2^+$ ] (**40**) and *tripropylcyclopropenylum* [ $c\text{-C}_3(\text{C}_3\text{H}_7)_3^+$ ] (**41**) ions

Again, no structural data seem to be available for these species. Their optimized structures [MP2(full)/6-31G(d) level; this work], of  $C_s$  symmetry, are given in Figs. 28 and 29.

Compounds **40** and **41** were generated by DPA of the corresponding precursors,<sup>156</sup> namely the methyl ethers of 1,2-dipropylcyclopropen-3-ol and tripropylcyclopropen-1-ol. These onsets were anchored to that of the methyl ether of 1,1,1-tricyclopropylcarbinol. An independent onset for 1,1,1-tricyclopropylcarbinol is available so that the onsets of **40** and **41** can be ultimately referred to that of the 1-adamantyl cation. These results, upon the appropriate leaving group correction, provide the values of  $\Delta_r G^\circ(25)$  given in Table 4.

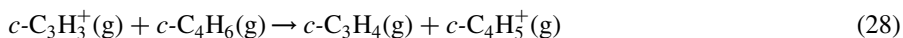
*Cyclobutenylum ion* ( $c\text{-C}_4\text{H}_5^+$ ) (**42**)

In classical studies, Olah and co-workers<sup>219</sup> obtained this cation in solution and were able to show that at  $-110^\circ\text{C}$  it has a puckered structure (Fig. 30) displaying true aromatic delocalization. Compound **42** is thus the simplest homoaromatic system.<sup>220–222</sup>

This aromatic character was confirmed by an extensive series of high-level quantum mechanical studies (structure, energetics and NMR chemical shifts) by Schleyer and co-workers.<sup>223</sup>

G2 studies have been recently performed on **42** and cyclobutadiene.<sup>224</sup>

To our knowledge, there is no experimental information on the thermodynamics of this ion. The results we present in Table 8 are based on our own G2 calculations for reaction (28), the hydride exchange between cyclopropenylum and cyclobutenylum ions:



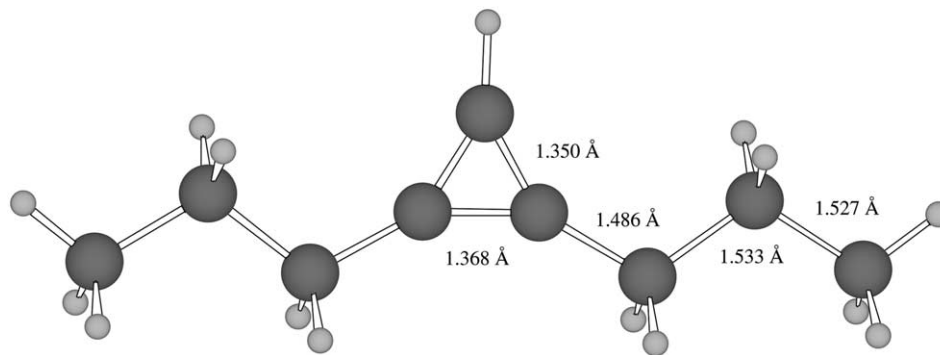
*Norbornen-7-ylum ion* ( $\text{C}_7\text{H}_9^+$ ) (**43**)

The discovery by Winstein, Woodward, and coworkers of a  $10^{11}$  rate enhancement in the solvolysis of *anti*-7-norbornenyl tosylate relative to that of 7-norbornyl tosylate<sup>225</sup> led to extensive investigations of this ion.

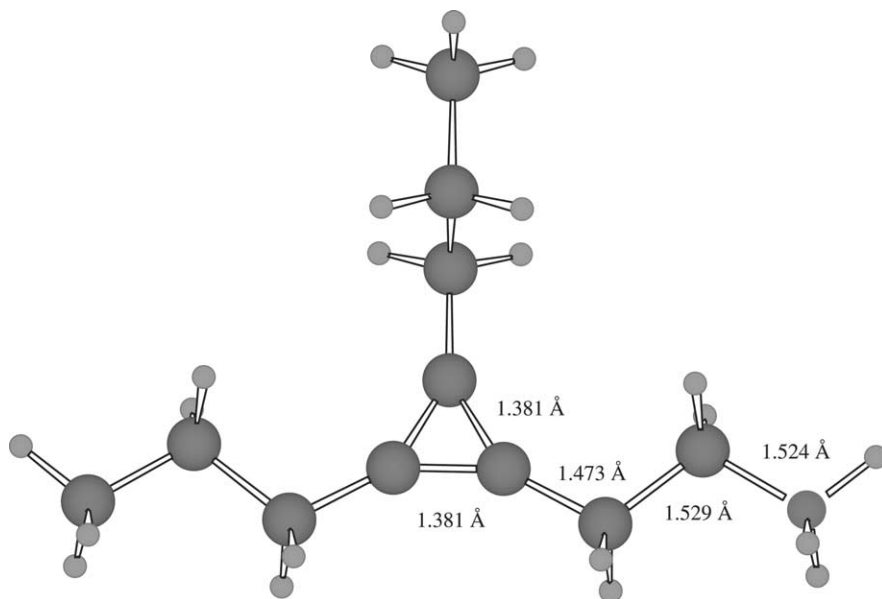
The  $^1\text{H}$ <sup>226,227</sup> and  $^{13}\text{C}$  NMR spectra of **43**<sup>228</sup> and some of its derivatives<sup>229</sup> in solution at low temperature are known. These spectra as well as the X-ray structure of 7-phenyl-2,3-dimethyl-7-norbornenyl cation<sup>230</sup> indicate that C(7) in **43** is “canted” towards the formal double bond, implying a significant degree of homoconjugation (Fig. 31).

*Ab initio* studies<sup>231,232</sup> fully agree with these contentions and further, through computation of the  $^{13}\text{C}$  NMR shifts, lead to an entirely consistent image of this ion as a species of  $C_s$  symmetry.

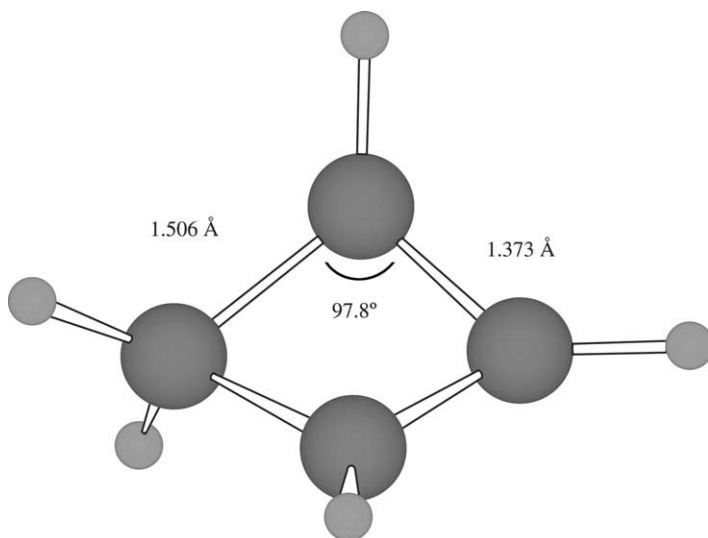
Thermodynamic data for this species (see Table 8) were obtained from the DPA study of *anti*-7-norbornenyl chloride and *anti*-7-norbornenol<sup>182</sup> with the appropriate



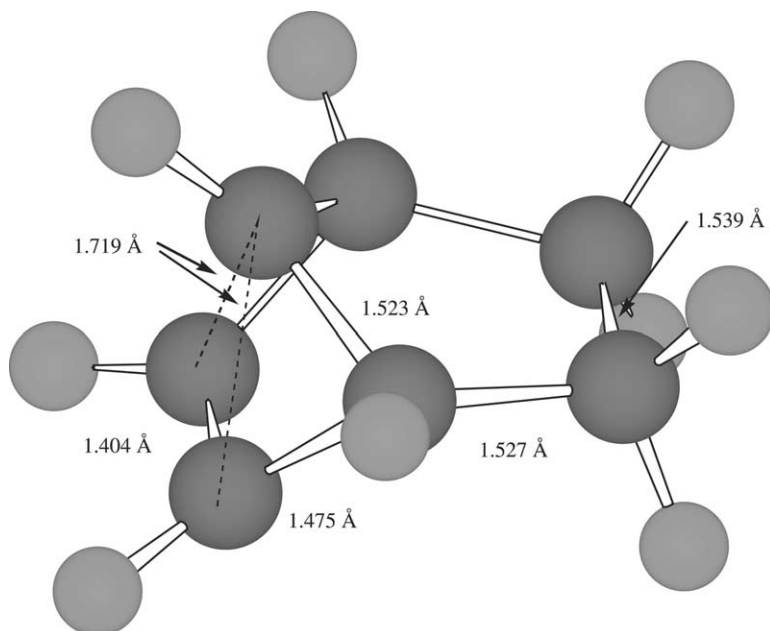
**Fig. 28** Structure of 1,2-Dipropylcyclopropen-3-ylum ion, **40**, optimized at the MP2(full)/6-31G(d) level.



**Fig. 29** Structure of tripropylcyclopropenyl, **41**, optimized at the MP2(full)/6-31G(d) level.



**Fig. 30** Structure of cyclobutenyl cation, **42**, optimized at the MP2(full)/6-31G(d) level.



**Fig. 31** Structure of norbornen-7-ylum ion, **43**, optimized at the MP2(full)/6-31G(d) level.

corrections. We present in [Table 8](#) thermodynamic data for **43** obtained at the G2(MP2) level in this work. The results are extremely consistent.  $\Delta_r G_m^\circ(25)$  is given in [Table 4](#).

#### Norbornadien-7-ylum ion ( $C_7H_7^+$ ) (**44**)

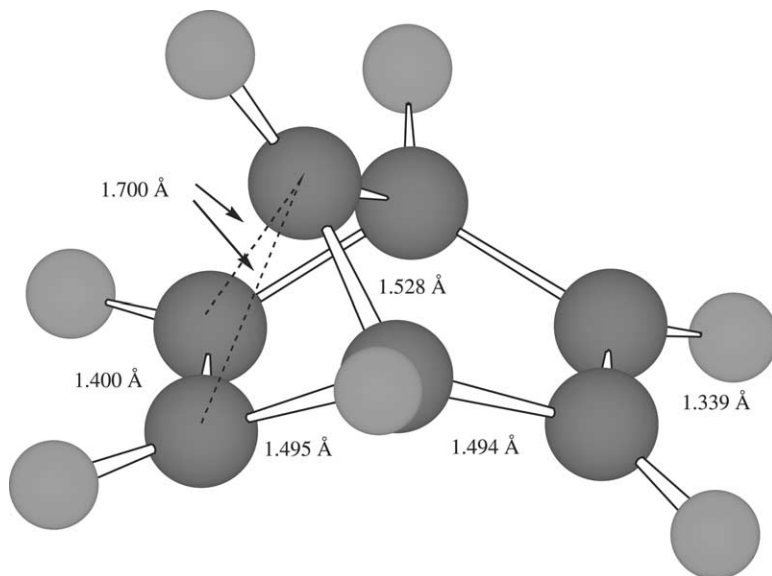
7-Norbornadienyl chloride solvolyzes some  $10^3$  times faster than *anti*-7-norbornenyl chloride.<sup>233</sup> This enormous neighboring group participation is associated with the intrinsic stability of **44**. This ion has also been studied by NMR in solution at low temperature.<sup>226,227</sup> These experiments as well as *ab initio* studies<sup>231,232</sup> indicate that the most stable structure of **44** corresponds to that presented in [Fig. 32](#). This is a structure of  $C_s$  symmetry, the more symmetrical  $C_{2v}$  structure being the transition state between the two  $C_s$  mirror images.<sup>234</sup>

Experimental thermodynamic data for **44** (see [Table 8](#)) were obtained from the DPA study of 7-norbornadienol.<sup>182</sup>  $\Delta_r G_m^\circ(25)$  is given in [Table 4](#). Thermodynamic data for **44** obtained at the G2(MP2) level in this work are given in [Table 8](#).

#### SIX-ELECTRON AROMATIC IONS

#### Cycloheptatrienylium ion (tropylium) ( $C_7H_7^+$ ) (**45**)

The synthesis and description of some important properties (including its very simple IR spectrum, a consequence of the  $D_{7h}$  symmetry) of this ion were carried out



**Fig. 32** Structure of norbornadien-7-ylum ion, **44**, optimized at the MP2(full)/6-31G(d) level.

in 1954 by Doering and Knox<sup>235</sup> even though it was actually prepared unintentionally, but not identified, in 1881.<sup>236</sup> Interest in this and other species originates in Hückel's classical studies<sup>237</sup> ( $4n + 2\pi$ -electron rule).

The remarkably simple  $^1\text{H}$  and  $^{13}\text{C}$  NMR spectra of **45** in solution are known<sup>238, 239</sup> as is its X-ray structure (in salts).<sup>240,241</sup>

The thermodynamic data for this ion as reported in Table 8 were obtained from the following sources:

- (1) The DPA study of tropylium methyl ether,  $\text{C}_7\text{H}_7\text{OCH}_3$ , with the appropriate leaving group corrections.<sup>156</sup>
- (2) The G2(MP2) results from Nicolaides and Radom.<sup>242</sup>

The experimental determination of  $\Delta_f H_m^\circ(\mathbf{45})$  has long been marred, *inter alia*, by the interconversion of the molecular ions of toluene and cycloheptatriene prior to dissociation.<sup>243,244</sup> The experimental adiabatic ionization energy of the tropylium radical,<sup>245,246</sup> has been found to be in excellent agreement with the result of high-level *ab initio* calculations,<sup>247,248</sup> but the computed standard enthalpy of formation of the radical seems significantly different from the reported experimental value.<sup>247,248</sup> It is thus rewarding to find that both DPA and computed values are in excellent agreement. The structure portrayed in Fig. 33 was optimized at the MP2(full)/6-31G(d) level in this work. The value of  $\Delta_r G^\circ(25)$  reported in Table 4 is from our DPA studies corrected with the corresponding leaving group corrections.

## PHENYL-SUBSTITUTED CARBOCATIONS

*Benzylum ion* ( $C_7H_7^+$ ) (**46**)

To our knowledge, **46** has never been observed in solution under stable conditions, even at low temperature. Pulse radiolysis<sup>249</sup> of benzyl chloride as well as flash photolysis<sup>250</sup> of several derivatives in HFIP have allowed the observation of the electronic absorption spectra of benzyl and its 4-methyl and 4-methoxy derivatives. The  $^1H$  and  $^{13}C$  NMR spectra of the 2,4,6-trimethylbenzyl cation and other more heavily substituted benzyl cations, however, have been studied at low temperature in superacid media.<sup>251</sup> In the gas phase, cold benzyl radical has been probed by two-color, resonant two-photon ionization techniques, thus providing very accurate vibrational frequencies below  $650\text{ cm}^{-1}$  for the benzyl cation.<sup>252</sup> Furthermore, the adiabatic ionization energy of benzyl radical and several isotopomers in the ground state were determined from their threshold photoionization spectra using resonant two-photon excitation and detection of electrons by pulsed field ionization.<sup>253</sup> This information, combined with  $\Delta_f H_m^\circ(C_6H_5CH_2)$  from Ref. 212 leads to the value of  $\Delta_f H_m^\circ(\mathbf{46})$  reported in Table 9.

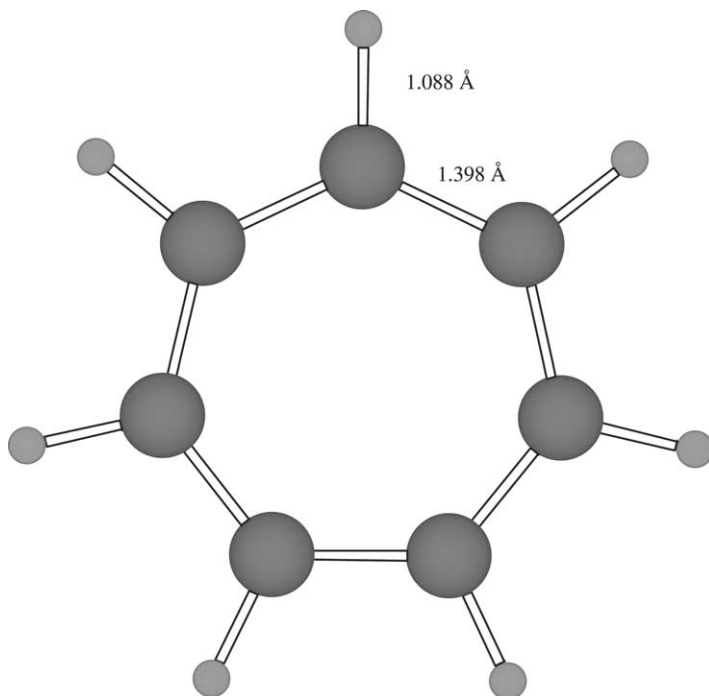
Data for this ion were also obtained through the study of hydride and chloride exchange with ions of known stability using both HPMS<sup>254</sup> and FT ICR.<sup>51,52</sup> These results, also reported in Tables 9 and 4, respectively, are rewardingly coincident. This is particularly important because it tends to indicate that the well-known benzyl/tropylium isomerization problem<sup>244</sup> does not seem to affect significantly these results

The study of substituent effects on the stability of substituted benzyl cations<sup>51,52,149</sup> is important as a source of thermodynamic information as well as a means to provide a conceptual link between the stabilities of a number of important carbocations. Mishima's study,<sup>51</sup> in particular, shows that the stabilities in terms of standard Gibbs energy for 4-methoxy- and 4-nitro-substituted benzyl cations differ by some  $24.9\text{ kcal mol}^{-1}$ . The former has a stability comparable to that of bicyclo[3.3.3]undecyl (manxyl) cation, while the latter is comparable to the *c*-pentyl cation. We present these two extreme cases in Table 4. The relative stabilities of other substituted benzyl cations are given in Refs. 50 and 51.

The results of high-level *ab initio* calculations on this  $C_{2v}$  ion (Fig. 34) are also summarized in Table 9. G2-level computations lead to  $\Delta_f H_m^\circ(g)$  values in excellent agreement with experiment.<sup>242</sup> Equally satisfactory are the results obtained at the G2(MP2,SVP) level for the ionization potential of benzyl radical.<sup>248</sup>

*1-Phenylethan-1-ylum ion,  $\alpha$ -phenethyl cation* ( $C_8H_9^+$ ) (**47**)

As far as we are aware, **47** has not been observed as a stable species in solution, although flash photolysis<sup>250</sup> of ethylbenzene and several of its derivatives in HFIP has allowed the detection of their electronic absorption spectra in the near-UV-visible region.



**Fig. 33** Structure of cycloheptatrienylium (tropylium) ion, **45**, optimized at the MP2(full)/6-31G(d) level.

$\Delta_f H_m^\circ(\mathbf{47})$  can be obtained from the experimental PA and GB of styrene. Over the years, a number of values has been obtained, essentially by HMPS and ICR. Here, we use the average value recommended in Ref. 43. Values are also available from the FT ICR study<sup>51</sup> of chloride exchange between this ion and the *tert*-butyl cation (through the appropriate ladder of experimental values). As shown in Table 9, the results are extremely self-consistent.

We present in Fig. 35 the structure ( $C_s$  symmetry) optimized at the MP2(full)/6-31G(d) level (this work). Recently, a large computational study has been published on benzyl and larger carbocations.<sup>155</sup> It uses both the optimized force field MMP2 extended to carbocations and MP4sdq/6-31G(d)//MP2(full)/6-31G(d) calculations. It provides, *inter alia*, valuable estimates of standard heats of formation. In this case, the difference in stability between phenethyl and 4-methylbenzyl cations (1.7 by *ab initio* computations and 2.9 kcal mol<sup>-1</sup> by MMP2) is in good agreement with the experimental results in Ref. 51. Our own G2(MP2) results are presented in Table 9.

The experimental  $\Delta_f G^\circ(25)$  for this ion is given in Table 4.



**Table 9** Thermodynamic data for phenyl-substituted carbocations

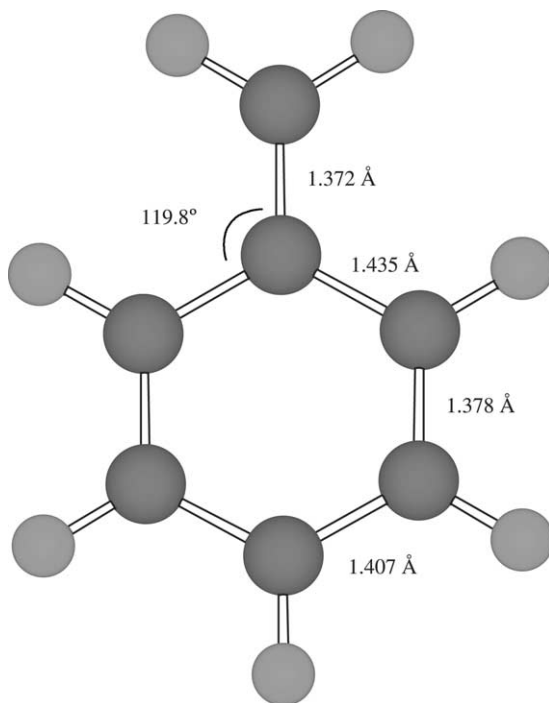
Cations	$\Delta_f H_m^\circ(\text{g})^a$	$S_m^\circ(\text{g})^b$
Benzylum ( $\text{C}_7\text{H}_7^+$ ) ( <b>46</b> )	$216.8 \pm 0.6^c$ $216.8 \pm 2.0^e$	$74.6 \pm 2.0^d$
1-Phenylethan-1-ylum ( $\text{C}_8\text{H}_9^+$ ) ( <b>47</b> )	$200.2 \pm 2.0^f$ $200.6 \pm 2.0^g$ $198.7 \pm 2.0^i$	$84.7 \pm 2.0^h$
2-Phenylpropan-2-ylum ( $\text{C}_9\text{H}_{11}^+$ ) ( <b>48</b> )	$187.4 \pm 2.0^j$ $187.2 \pm 2.0^k$	$93.1 \pm 2.0^l$
Diphenylmethanylium ( $\text{C}_{13}\text{H}_{11}^+$ ) ( <b>49</b> )	$225.7 \pm 2.0^m$	$99.7 \pm 2.0^n$
1,1-Diphenylethan-1-ylum ( $\text{C}_{14}\text{H}_{13}^+$ ) ( <b>50</b> )	$212.7 \pm 2.3^o$ $214.1 \pm 2.0^q$	$107.9 \pm 2.0^p$
Triphenylmethanylium ( $\text{C}_{19}\text{H}_{15}^+$ ) ( <b>51</b> )	$243.7 \pm 2.0^r$	$123.8 \pm 2.0^s$

<sup>a</sup>In kcal mol<sup>-1</sup>.<sup>b</sup>In cal mol<sup>-1</sup> K<sup>-1</sup>.<sup>c</sup>From Ref. 212. See text.<sup>d</sup>Scaled, symmetry-corrected HF/6-31G(d) value (this work).<sup>e</sup>Computed (G2) value from Ref. 242.<sup>f</sup>From the averaged experimental GB(styrene), 193.4 kcal mol<sup>-1</sup> (Ref. 43), and the entropy correction from the same reference.<sup>g</sup>From the standard Gibbs energy change for the formal hydride exchange between  $\alpha$ -phenethyl and *tert*-butyl cations as determined by FT ICR in Ref. 51. Entropies corrected using the experimental values for *iso*-butene<sup>26</sup> and styrene<sup>26</sup> (82.48 cal mol<sup>-1</sup> K<sup>-1</sup>) and our computed value for the phenethyl cation.<sup>h</sup>Scaled HF/6-31G(d) value from this work.<sup>i</sup>Combining experimental values for  $\Delta_f H_m^\circ$ , C<sub>6</sub>H<sub>5</sub>-CH<sub>2</sub>CH<sub>3</sub>, *iso*-butane and **6** with the standard enthalpy for the hydride exchange between **6** and **47**.<sup>j</sup>From the averaged experimental PA( $\alpha$ -methyl styrene), 206.6 kcal mol<sup>-1</sup> (Ref. 43) and  $\Delta_f H_m^\circ$  (C<sub>9</sub>H<sub>10</sub>) = 28.27  $\pm$  0.34 kcal mol<sup>-1</sup>.<sup>26</sup><sup>k</sup>Computed (MMP2) value from Ref. 155.<sup>l</sup>Scaled, symmetry-corrected value at the HF/6-31G(d) level (this work).<sup>m</sup>MMP2 value from Ref. 155.<sup>n</sup>Scaled, symmetry-corrected value at the HF/6-31G(d) level (this work).<sup>o</sup>From the averaged experimental PA (1,1-diphenylethylene), 211.7 kcal mol<sup>-1</sup> (Ref. 43) and  $\Delta_f H_m^\circ$  (C<sub>14</sub>H<sub>12</sub>) = 58.7  $\pm$  1.1 kcal mol<sup>-1</sup>.<sup>26</sup><sup>p</sup>Scaled, symmetry-corrected value at the HF/6-31G(d) level (this work).<sup>q</sup>MMP2 value from Ref. 155.<sup>r</sup>MMP2 value from Ref. 155.<sup>s</sup>Scaled, symmetry-corrected value at the HF/6-31G(d) level (this work).

### 2-Phenylpropan-2-ylum ion, cumyl cation (C<sub>9</sub>H<sub>11</sub><sup>+</sup>) (**48**)

This ion as well as its derivatives have played a key role in the development of current concepts and quantitative treatment of substituent effects on organic reactivity.<sup>256,257</sup>

The UV-visible absorption spectra of **48** and some 4-substituted derivatives have been obtained in HFIP solution using laser flash photolysis techniques.<sup>258</sup> The <sup>1</sup>H



**Fig. 34** Structure of benzylum ion, **46**, optimized at the MP2(full)/6-31G(d) level.

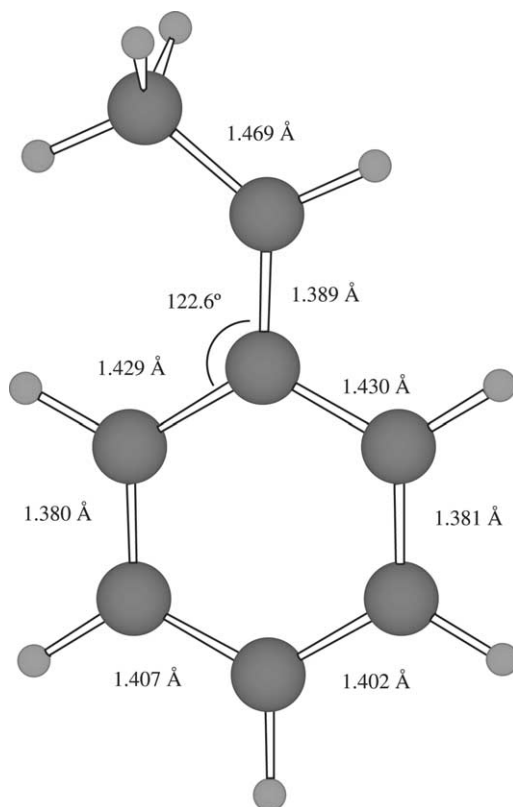
NMR spectrum of this ion at low temperature and in superacid media was obtained in 1964<sup>259,260</sup> and carefully analyzed in 1966.<sup>261</sup> The X-ray structure of its hexafluoroantimonate(V) salt was obtained much more recently<sup>262</sup> and it reveals significant benzylic delocalization.

The  $\Delta_f H_m^\circ(\text{g})$  value reported in Table 9 was obtained from the PA recommended in Ref. 43, based on ICR data from Taft's and Marshall's groups.

We present in Fig. 36 the  $C_{2v}$  structure of **48**, obtained at the MP2(full)/6-31G(d) level (this work).

The experimental  $\Delta_f H_m^\circ(\mathbf{48})$  is in quite good agreement with the computed MMP2 and MP4sdq/6-31G(d)//MP2(full)/6-31G\* results from Ref. 155 (see Table 9).

We report in Table 4 the experimental  $\Delta_f G^\circ(25)$  for this ion as given in Refs. 51 and 52. Also reported are values for 4-methoxy and 3-nitro cumyl cations, taken from the same references. These are extreme cases of substituent effects in these systems and span a range of stabilities somewhat smaller than that of the homologous benzyl derivatives (19.9 versus 24.3 kcal mol<sup>-1</sup>). Still, this yields a stability for the 4-methoxy derivative quite close to that of trityl cation.



**Fig. 35** Structure of 1-phenylethan-1-ylum ion, **47**, optimized at the MP2(full)/6-31G(d) level.

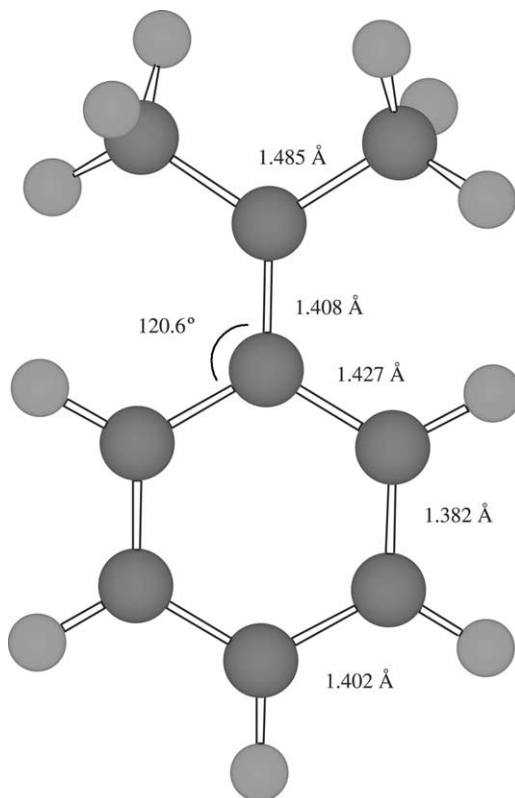
### *Diphenylmethanylium ion, benzhydryl cation* ( $C_{13}H_{11}^+$ ) (**49**)

The  $^1H$  NMR spectrum of this ion was reported in the early 1960s<sup>259,260</sup> and analyzed a little later.<sup>261</sup>

This ion and several ring-substituted derivatives have been generated by nanosecond laser flash photolysis in solution.<sup>263</sup>

As far as we know, **49** has not yet been studied in the solid state.

Direct experimental determinations of its thermodynamic state functions are still missing. Fortunately, a fairly reliable value for  $\Delta_f H_m^\circ(\mathbf{49})$  is available thanks to the MMP2 and MP4sdq/6-31G(d)//Mp2(full)/6-31G(d) calculations in Ref. 155. This value is presented in Table 9. The value of  $\Delta_r G^\circ(25)$  given in Table 4 as well as the structure in Fig. 37 were obtained in this study.



**Fig. 36** Structure of 2-phenylpropan-2-ylum ion, **48**, optimized at the MP2(full)/6-31G(d) level.

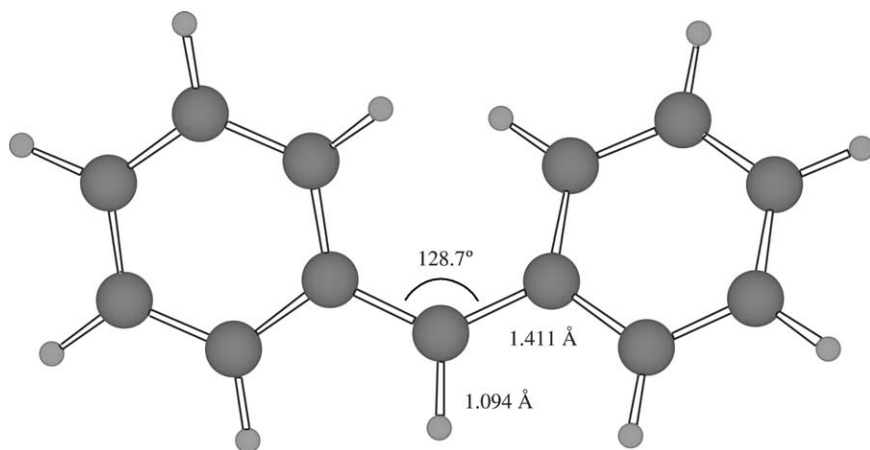
### *1,1-Diphenylethan-1-ylum ion* ( $C_{14}H_{13}^+$ ) (**50**)

This ion is known in solution at low temperature in strongly acidic media and was generally studied together with benzhydryl cation.<sup>259–261</sup>

Its UV–visible spectrum has been obtained by laser flash photolysis techniques.<sup>258</sup> Interestingly, it has recently been generated and studied encapsulated in zeolites<sup>264</sup> and at ambient temperature in superacid molten salts.<sup>265</sup>

The experimental  $\Delta_f H_m^\circ(\mathbf{50})$  given in Table 9 was obtained from the GB of 1,1-diphenylethane as determined by Taft's group and reported in Ref. 43. This value is in agreement with the computational result from Ref. 155.

We present in Table 4 the  $\Delta_r G^\circ(25)$  obtained in this study and based on the experimental data indicated above. The structure optimized at the MP2(full)/6-31G(d) level portrayed in Fig. 38 was also obtained in this work.



**Fig. 37** Structure of diphenylmethanylium ion, **49**, optimized at the MP2(full)/6-31G(d) level.

### *Triphenylmethanylium ion, triphenyl methyl cation* ( $C_{19}H_{15}^+$ ) (**51**)

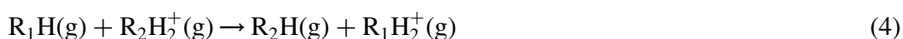
This species<sup>266–268</sup> as well as the salt character of some of its derivatives have long been known.<sup>269,270</sup> Structure **51** has been studied by UV–visible<sup>271</sup> and IR<sup>272</sup> spectroscopies. Its  $^1H$  NMR spectrum in solution was reported in 1959<sup>273</sup> and its features carefully discussed in 1966.<sup>261</sup> The  $^{13}C$  NMR spectrum in superacid solution was also reported in 1964.<sup>274</sup> It has also been obtained in the solid state, trapped in a zeolite.<sup>275</sup> The  $^{13}C$  NMR spectra of a number of other triaryl and heteroaryl ions have also been reported.<sup>276</sup>

All these techniques as well as the X-ray spectra of its salts<sup>277</sup> agree on the twisting of the phenyl rings out of the central carbon plane by *ca.* 33°. Figure 39 presents the structure of this ion (symmetry group  $D_3$ ) obtained at the MP2(full)/6-31G(d) level in this work. Our calculated structure agrees nicely with this result and with the MMP2 structure.<sup>155</sup>

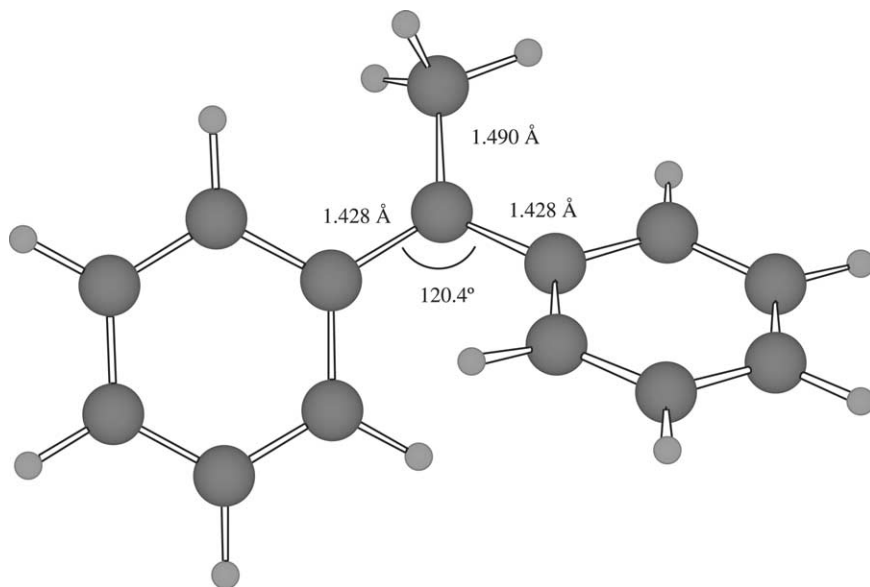
The  $\Delta_f H_m^\circ(\mathbf{51})$  given in Table 9 was obtained computationally at the MMP2 level<sup>155</sup> and was used to estimate the value of  $\Delta_r G^\circ(25)$  given in Table 4.

## 6 Solution reactivity

Consider reactions (3a) and (4):

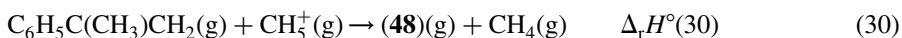
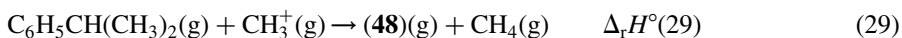


For comparison purposes it seems useful to take the cumyl cation **48** as a reference ion, on account of the fact that it can be obtained through reactions (29) and (30) and



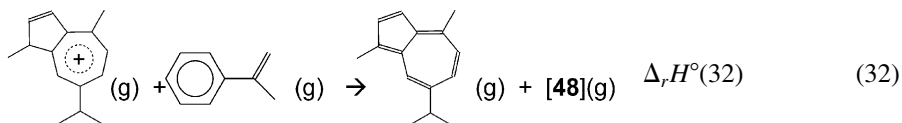
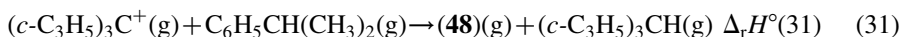
**Fig. 38** Structure of 1,1-diphenylethan-1-ylum ion, **50**, optimized at the MP2(full)/6-31G(d) level.

that in both cases, fairly reliable thermodynamic data are available for reactants and products:



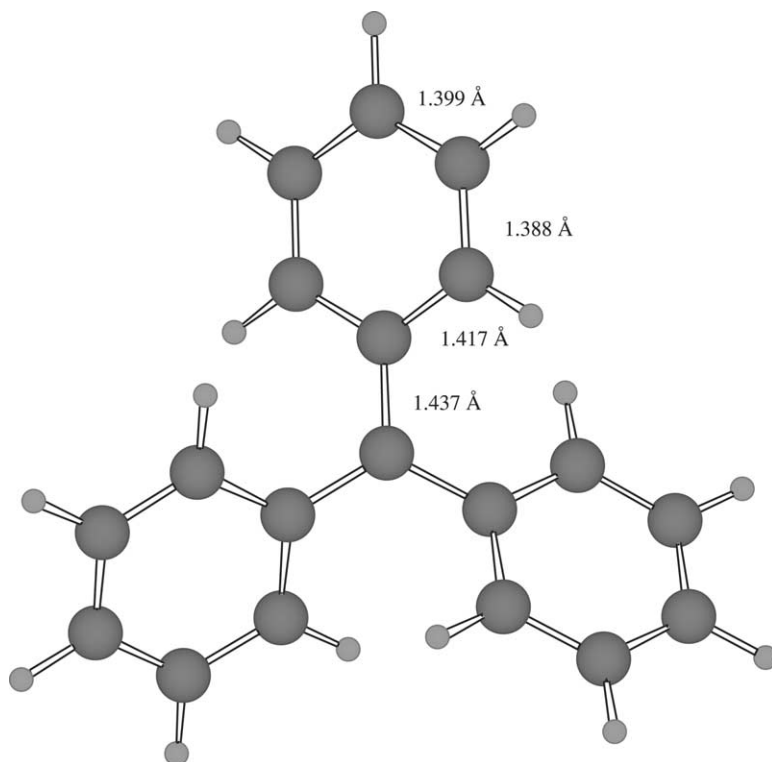
Using data given in the previous sections, we get  $\Delta_r H^\circ(29) = -93.3 \pm 2.1$  and  $\Delta_r H^\circ(30) = -76.8 \pm 2.2 \text{ kcal mol}^{-1}$ .

Let us now examine two rather extreme cases: the hydride exchange between tricyclopropylmethyl and cumyl cations and the proton exchange between guaiazulene<sup>278</sup> and  $\alpha$ -methylstyrene, respectively (reactions 31 and 32):



The corresponding  $\Delta_r H^\circ(31)$  and  $\Delta_r H^\circ(32)$  are, respectively,  $-11.0 \pm 4.1$  and  $28.4 \pm 2.8 \text{ kcal mol}^{-1}$ .<sup>279</sup>

These results show that the range of structural effects on the intrinsic (gas phase) stability of carbenium ions amounts to at least  $110 \text{ kcal mol}^{-1}$ . Let us see now how



**Fig. 39** Structure of triphenylmethylium ion, **51**, optimized at the MP2(full)/6-31G(d) level.

the differences in intrinsic stability affect solution (“real world”?) reactivity. As in the previous section, thermodynamic criteria seem well suited for this purpose and so are kinetic data, through formally straightforward extra thermodynamic relationships.

#### THERMODYNAMIC PROPERTIES

##### *The $pK_{R^+}$ and $pK_a$ scales*

The use of reaction (33) in solution as a quantitative tool for the ranking of carbocation stability is at least half-a-century old:<sup>280</sup>



The concept is extremely simple, as it takes as its starting point the equilibrium constant for this reaction,  $K_{R^+}$ <sup>157,281,282</sup>

$$K_{R^+} = a_{R^+}a_{H_2O}/a_{ROH}a_{H^+} \quad (34)$$

Given two alcohols, respectively,  $R_1OH$  and  $R_2OH$ , the position of equilibrium (35)



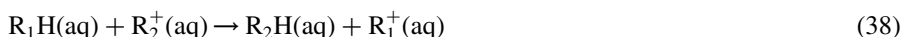
is simply given by  $K_{35}$ , equation (36):

$$K_{35} = K_{R(1)^+} / K_{R(2)^+} \quad (36)$$

or

$$\log K_{35} = pK_{R(1)^+} - pK_{R(2)^+} \quad (37)$$

Reaction (38) is also suitable for comparison purposes. Following the same procedure as above,  $\log K_{38}$  is given by equation (39):



$$\log K_{38} = pK_a(R_1) - pK_a(R_2) \quad (39)$$

From an operational point of view, difficulties might arise from the fact that rather high acid concentrations and/or aqueous-organic solvents are often used in these studies, the reference state being the pure water solution. These shortcomings can be averted by the use of appropriate methods, recently reviewed by Cox in this series.<sup>283</sup>

In what follows we shall use both the  $pK_{R^+}$  and  $pK_a$  scales for the quantitative comparison of carbenium ions, without attempting any correction for aqueous-organic medium effects. All data are anchored to **48**. Taft and co-workers already compared gas phase and solution basicities of ethylenic and aromatic hydrocarbons.<sup>278,284</sup> Now the  $pK_{R^+}$  scale has been widely extended<sup>285,286</sup> through the determination of  $K_{R^+}$  from the reaction rate constants for the forward and reverse processes in reaction (33). This is a very important breakthrough. Also, a number of new data for other species in the gas phase has become available.

We can now carry out a comparison of solution and gas-phase rankings of stabilities, respectively, using  $\Delta pK_{R^+}$  and  $\Delta pK_a$  values; i.e., referred to processes leading to **48**. The reference processes in the gas phase are the chloride exchange between **48** and the relevant ion, i.e. reaction (40), and the proton exchange between  $\alpha$ -methylstyrene and the relevant base, i.e. reaction (41).  $\Delta_r G^\circ$  values for both reactions are given, respectively, by the differences in  $\Delta_r G^\circ(25)$  for the corresponding chloride and cumyl chloride (data from Table 4) and the difference in GB values between the relevant base and  $\alpha$ -methylstyrene. Formally, very similar processes are compared as they only differ in the leaving group:

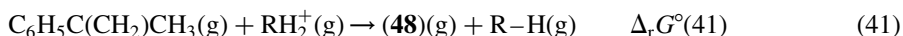
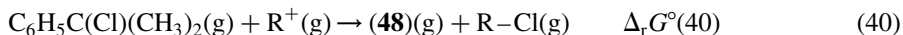


Figure 40 is a joint plot of  $\Delta pK_{R^+}$  and  $\Delta pK_a$  (using data from Refs. 278, 284–287) against  $\Delta_r G^\circ(40)$  and  $\Delta_r G^\circ(41)$ . Squares denote  $\Delta pK_a / \Delta_r G^\circ(41)$  and open circles denote  $\Delta pK_{R^+} / \Delta_r G^\circ(40)$ . They define a straight line of very good statistical quality involving ranges of some 45 kcal mol<sup>-1</sup> and 27 log units, respectively. The level of



self-consistency of these results is both rewarding and surprising, on account of the variety of experimental methods involved. Conversion of log units to Gibbs energies leads to a slope of 0.77.

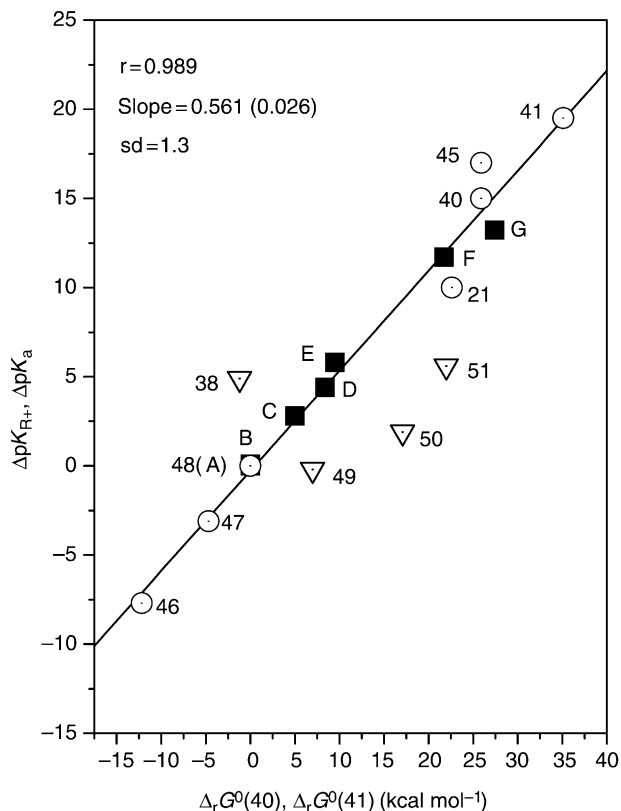
We take this result as implying that: (1) the ranking of intrinsic stabilities of these ions is faithfully reproduced in solution with a moderate attenuation (*ca.* 24%); (2) the ionic systems described by this line follow a constant pattern of solvation which we call “general” for the sake of simplicity. This does not mean that these effects are small in absolute value but rather, that *differential* solvation effects are likely to be small; and (3) the fact that the slope is smaller than unity suggests that solvation energetics are not exactly constant and that the less stable ions interact more strongly with the solvent. The correlation spans a range of stabilities going all the way from benzylium to tripropylcyclopropenylium ion. Table 4 shows that this range includes most tertiary alkyl cations, several stabilized secondary ones, a number of bridgehead carbocations and phenyl- and cyclopropyl-stabilized methyl cations. This correlation appears, therefore, as a very powerful and simple unifying factor.

Ions **38**, **49**–**51** do not seem to follow the “general” pattern and were not included in the correlation. Interestingly, at least the gas-phase data for **38**, the cyclopropenylium ion, seem quite reliable. This ion, however, is small and readily accessible to solvent molecules. Furthermore, *ab initio* calculations indicate that **38** is a strong hydrogen bond donor to water. It seems reasonable to attribute at least part of this enhanced stability in solution to hydrogen bonding to the solvent. A plot similar to Fig. 40 but involving standard Gibbs energy changes for hydroxide instead of chloride exchange is also nicely linear and, once again, **38** is deviant but **49**–**51** are now “well behaved”. This is important, inasmuch as the  $pK_{R^+}$  is based on the protonation of alcohols and strongly suggests that these ions do not display any abnormal behavior in solution. It follows that the departures shown in Fig. 40 originate in the leaving group correction for the corresponding chlorides. At this point, unfortunately, the possibility for these corrections being affected by computational artifacts cannot be ruled out.

Ions with  $pK_{R^+}$  values of about 14 have recently been synthesized.<sup>288</sup> Assuming that the linearity extends up to these ions, this would bring the range of structural effects on stabilities of carbenium ions to at least 120 kcal mol<sup>-1</sup>.

### *Solution thermochemistry*

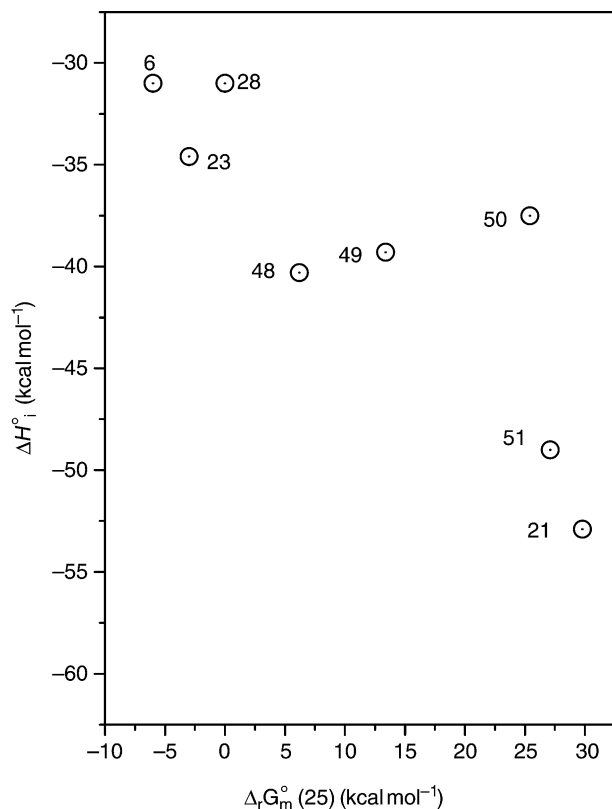
The quantitative thermodynamic study of the ionization of appropriate precursors R–X (X = OH, halogen) by superacidic species (FSO<sub>3</sub>H, SbF<sub>5</sub>, FSO<sub>3</sub>H–SbF<sub>5</sub> mixtures) in low nucleophilicity solvents [SO<sub>2</sub>(l), SO<sub>2</sub>ClF, CH<sub>2</sub>Cl<sub>2</sub>] at low temperatures was carried out during the 1970s and early 1980s by Arnett and co-workers.<sup>289</sup> The basic concept behind this effort was “to provide the basis for a single stability scale in solution ranging from the relatively unstable secondary ions (e.g., isopropyl or cyclopentyl) to the more familiar triarylmethylcarbenium ions. If this were accomplished, future workers could use a scale to interpolate and include



**Fig. 40** Plot of  $\Delta pK_{R^+}$  and  $\Delta pK_a$  (i.e., values relative to **48** and  $\alpha$ -methylstyrene) versus  $\Delta_r G^\circ(40)$  and  $\Delta_r G^\circ(41)$ . Open circles denote  $\Delta pK_{R^+}/\Delta_r G^\circ(40)$  and full squares denote  $\Delta pK_a/\Delta_r G^\circ(41)$ . A =  $\alpha$ -methylstyrene; B = hexamethylbenzene; C = 1,1-diphenylethylene; D = 1,1'-ethenyldienebis-[4-methyl-benzene]; E = 1,1-dicyclopropylethylene; F = azulene; G = guaiazulene.

almost any ion whose ionization energy can be related directly or indirectly to the gas phase scale, the  $pK_R$  scale, thermochemical scales or solvolysis rates".<sup>290</sup>

We present in Fig. 41 a plot of the ionization enthalpies of alcohols in a 1:1 mixture of  $SbF_5$  and  $FSO_3H$  in  $SO_2ClF$  solution,<sup>290</sup>  $\Delta H_i^\circ$ , against  $\Delta_r G^\circ(25)$ . The proportionality is very clear but the scatter is significant. More limited groups of ions yield better correlations, particularly in the case of the ionization of chlorides by  $SbF_5$ .<sup>291</sup> Entropic factors might play a role, as well as, in some cases, ion-pairing. Differential solvation effects in these systems are well known. Thus, adamantyl appears as less stable than the *tert*-butyl cation while the opposite occurs in the gas phase. We have recently shown computationally that at least part of this reversal can be largely attributed to solvation effects.<sup>68</sup> It was shown, much earlier, that the



**Fig. 41** Enthalpies of ionization,  $\Delta H_i^\circ$  for alcohols with 1:1 mixtures of  $\text{SbF}_5$  and  $\text{FSO}_3\text{H}$  in  $\text{SO}_2\text{ClF}$  solution versus  $\Delta_r G^\circ(25)$ .

ranking of basicities of alkylbenzenes was reversed on going from the gas phase to superacid solutions,<sup>292</sup> a fact also consistent with solvation effects.

As things stand now, a more complete understanding of the situation still requires considerable work.

#### REACTION KINETICS

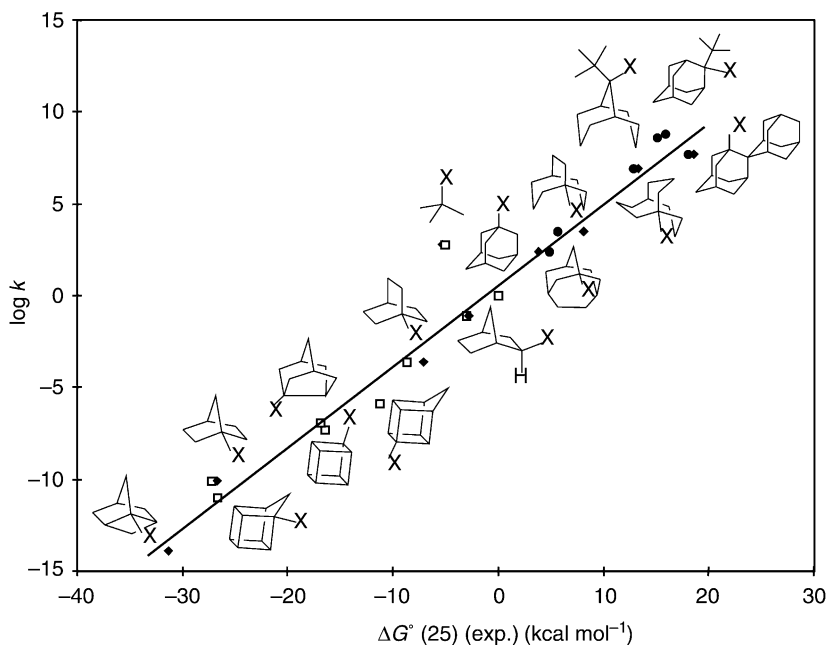
It is generally accepted that  $\text{S}_{\text{N}}1$  solvolysis rates for a series of similar compounds under similar conditions reflect directly the stability of their carbocationoid intermediates.<sup>166,293</sup> However, the lack of reliable experimental data for stabilities of carbenium ions prevented verification of this hypothesis for a long time. Several approaches at various levels of sophistication were advanced to estimate these ion stabilities: their strain was estimated via empirical correlations with IR-stretching frequencies of the respective carbonyl groups, and non-bonded interactions from molecular models or, subsequently, by empirical force-field calculations.<sup>294–302</sup>

However, owing to the empirical nature of these methods, the significance of the results could not be truly assessed. More recently, Arnett *et al.*<sup>109,290</sup> reported heats of ionization ( $\Delta H_i$ ) of alkyl chlorides to stable carbocations in  $\text{SbF}_5$ -solvent mixtures. Correlation of the heats of ionization with the respective free energies of activation for ethanolysis afforded a straight line over a range of  $22 \text{ kcal mol}^{-1}$  for  $\Delta H_i$ .

Initial attempts to establish an analogous correlation between solvolytic reactivity for a limited series of bridgehead halides and stability of the respective carbenium ions in the gas phase by ion cyclotron resonance (ICR) were met by only limited success owing to apparent rearrangement of some of the ions under the conditions of the ICR experiments.<sup>303</sup> Although highly strained ions such as 1-norbornyl were particularly prone to undergo such rearrangements, the ICR measurements alone did not allow a distinction between unrearranged and rearranged ions. However, when ions were generated by DPA rather than on electron impact, they are not significantly vibrationally excited and, hence, are less prone to undergo rearrangement. As shown above for bridgehead derivatives, the experimental ion stabilities as determined by DPA and adjusted with the appropriate leaving group correction correlate well with the stabilities calculated by *ab initio* methods (MP2/6-311G\*\*).<sup>57,58</sup> Figure 42 shows the correlation between the rate constants for solvolysis of a series of representative bridgehead bromides under standard conditions ( $\log k$  for tosylate solvolysis relative to 1-adamantyl in 80% ethanol at  $70^\circ\text{C}$ )<sup>304</sup> versus ion stabilities [ $\Delta_r G^\circ(25)$ ].<sup>55</sup>

The correlation in Fig. 42 is given by  $\log k = 0.427\Delta_r G^\circ(25) + 0.41$  ( $r^2 = 0.986$ ,  $\sigma = 0.75$ , non-bridgehead ions excluded from the correlation). It spans *ca.*  $50 \text{ kcal mol}^{-1}$  in  $\Delta_r G^\circ(25)$ . Conversion of  $\log k$  in units of free energies of activation results in a slope of 0.67, in reasonable agreement with the slopes reported by Arnett ( $-0.89$  in  $\text{SO}_2\text{ClF}$ ,  $-1.02$  in  $\text{CH}_2\text{Cl}_2$  and  $-0.95$  in  $\text{SO}_2$ ). The lower value of the slope in the gas phase may be attributed to the absence of stabilization by solvent.

The bridgehead derivatives represent a mechanistically homogenous series of model compounds. Nucleophilic solvent participation (NSP) and E1-pathways upon solvolysis are excluded for skeletal reasons, and relative rate constants are independent of leaving group and solvent. This is not necessarily so in the general case of solvolysis. DPA has now been applied to halides and alcohols leading to carbenium ions representative of various classes, such as secondary aliphatic, strained bicyclic, homoaromatic, benzyl- and cyclopropyl-stabilized ions. The relative ion stabilities are reported in Table 4. The rate constants for solvolysis of the respective halides, *p*-toluenesulfonates or *p*-nitrobenzoates are available in the literature. For reasons of consistency with the plot shown in Fig. 42, they are extrapolated to  $70^\circ\text{C}$  and expressed relative to 1-adamantyl solvolysis under the same conditions, assuming relative rates to be independent of leaving groups and solvent, as in the bridgehead series. These assumptions are not always justified, however. For example, significant variations in the relative rates in different solvents occur in the case of benzylic derivatives, but no systematic study was undertaken in

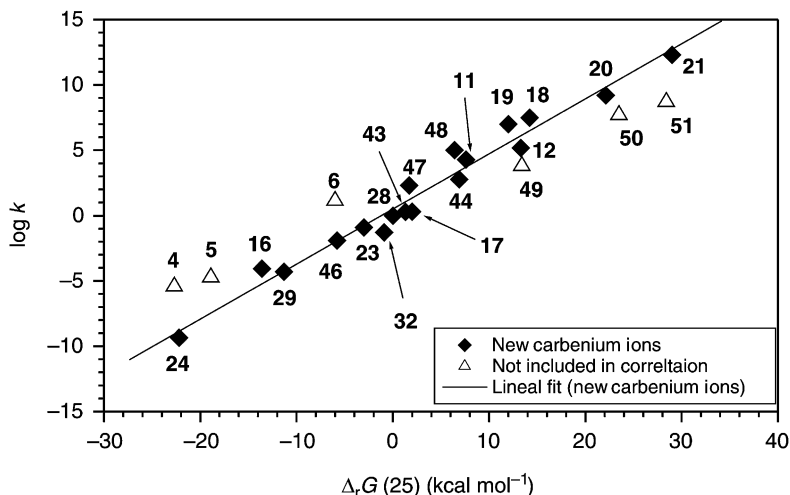


**Fig. 42** Plot of  $\log k$  for bridgehead derivatives versus  $\Delta_r G^\circ(25)$  ( $X = \text{Br}$ ), open squares,  $\Delta_r G^\circ(29)$  ( $X = \text{Br}$ , calculated Cl), diamonds, and  $\Delta_r G^\circ(25)$  ( $X = \text{Br}$ , calculated OH), filled circles.

order to determine which data are most representative. In order to minimize complications owing to NSP, rate constants for acetolysis were used in preference to data from other solvent systems. Details will be reported in a forthcoming publication.<sup>305</sup>

As indicated earlier, the experimental or computed gas-phase data were subject whenever necessary to the appropriate leaving correction in order to generate a homogeneous set of Gibbs energy changes based on chloride exchange,  $\Delta_r G^\circ(25)$  (summarized in Table 4). For some non-bridgehead derivatives, specific leaving group corrections for *p*-toluenesulfonates were applied in order to compare exactly the same systems in the gas phase and in solution.<sup>191</sup>

In Fig. 43,  $\log k$  for 24 substrates versus the appropriate  $\Delta_r G^\circ(25)$  values are represented. A subset of 18 substrates follow the correlation equation  $\log k = 0.422\Delta_r G^\circ(25) + 0.50$  ( $r^2 = 0.9686$ ,  $\sigma = 0.97$ ). This correlation spans over 50 kcal mol<sup>-1</sup> in  $\Delta_r G^\circ(25)$ . Most important is the fact that the slope is practically identical to that found for bridgehead derivatives (Fig. 42), while the quality of the fit is also excellent. While consistent behavior of bridgehead and bicyclic secondary derivatives such as 7-norbornyl (**24**), 2-adamantyl (**29**), or 4-homoadamantyl (**32**) upon solvolysis might be expected on the grounds of structural similarities and the absence of NSP, that of the other compounds of this series is surprising. The stability



**Fig. 43**  $\log k$  for 24 substrates relative to 1-adamantyl chloride (computed as tosylates in 80% ethanol at 70°C), versus  $\Delta_r G^\circ(25)$ .

of the bicyclic secondary ions is mainly determined by strain effects. The 2-norbornyl cation (**23**) is stabilized by  $\sigma$ -participation, and the 7-norbornenyl (**43**) and 7-norbornadienyl (**44**) cations are homoaromatic and bishomoaromatic, respectively. In the cyclopropylcarbiny cations **17–21** stabilization occurs through the Walsh orbitals of the cyclopropane rings, while the phenyl-substituted cations **46–51** profit from resonance stabilization. Despite these different causes for ion stability, the correlation suggests ion stability as by far the predominant factor determining solvolytic reactivity of secondary and tertiary derivatives. At the same time, the correlation confirms the qualitative concepts of strain and anchimeric participation, which have been developed over the years in the context of solvolysis.

Out of the 24 compounds represented in Fig. 43, there are six which fall outside the correlation. The low rate of triphenylmethyl chloride (**51**) in comparison to that of diphenylmethyl (**49**) or 1,1-diphenylethyl chloride (**50**) has been known for more than 35 years<sup>306</sup> but, to our knowledge, has not been rationalized. However, if  $\log k$  is correlated with the  $pK_{R^+}$  values of the corresponding alcohols in condensed phase, the corresponding cations, **49–51**, are well behaved (exactly as discussed in the previous section), so that their deviations in Fig. 43 must be attributed to a solvation effect. The deviations observed with the 2-propyl (**4**), 2-butyl (**5**), and *tert*-butyl (**6**) derivatives are more significant. The rate constants for these compounds, and also that of cyclopentyl (**16**) refer to tosylate acetolysis and are corrected for NSP.<sup>303</sup> This NSP correction brings **16** on to the correlation line, but the other compounds react still significantly faster than predicted on the grounds of the stability of the respective carbenium ions. According to the definition used here,<sup>303</sup> NSP is defined as the rate enhancement experienced by a substrate, relative to 1-adamantyl, upon

solvent change from trifluoroacetic acid to the solvent of interest. Solvents other than trifluoroacetic acid may be used as reference, but this does not fundamentally change the problem. NSP occurs in solvolysis reactions that lead to small, undelocalized carbenium ions. As shown by Takeuchi and colleagues<sup>68</sup> for tertiary solvolysis, NSP vanishes upon an increase of steric crowding around the reaction center, and upon increased stabilization of the positive charge by alkyl substitution. Even in the most limiting solvent HFIP, *tert*-butyl derivatives react still significantly faster than predicted on the grounds of the stability of the *tert*-butyl cation. In other words, NSP alone does not account for the total of the rate enhancement of *tert*-butyl derivatives, and the same phenomenon occurs with 2-propyl and 2-butyl. Although the transition state for solvolysis is close to the carbenium ion with respect to structure and energy, less charge is developed owing to the proximity of the leaving group and also to solvation. Apparently, these stabilizing effects are more important in the case of reactions leading to small ions such as 2-propyl or *tert*-butyl where charge is strongly localized, than to larger ions, where charge may be dispersed over a large number of atoms. For this reason, Arnett's heats of ionization of halides in the condensed phase are a more realistic model for the solvolysis reaction than is ion stability in the gas phase because they contain contributions for solvation and, although to some unknown degree, stabilization by the counter-ion.<sup>290</sup> However, as Figs. 42 and 43 show, for ions having a sufficiently large number of atoms, the gas-phase stability of the carbenium ions is reflected to the same degree in the transition state for solvolysis over a very large range of reactivities, and the discrepancies between ion stabilities as determined in solution and in the gas phase are of minor significance considering the overall consistency of the data over the large range of ion stabilities.

## 7 Conclusion

This "low resolution" overview of the gas-phase stabilities of a variety of carbenium ions shows that they are by no means exotic data unrelated to solution reactivity. Quite on the contrary, they are the fundamental factor determining the relative stabilities of the same species in solution (as determined by the  $pK_R$  and  $pK_a$  scales, for example). Furthermore, the ranking of solvolysis rates of compounds  $R-X$  is largely dependent on the intrinsic stability of  $R^+$ . While this was already known in the case of bridgehead carbocations, we see now that this applies also to non-bridgehead tertiary cations as well as to a variety of secondary cations, even sometimes in cases wherein the access of solvent to the reaction center is not hindered. Intrinsic stability of carbocations thus appears as a very powerful unifying factor.

A number of significant problems obviously remains to be solved:

- (1) It seems highly desirable to extend both the accuracy and the size of the data base. This implies the need for more and more accurate *experimental* data.

- (2) The very existence of a remarkably simple and extensive relationship between thermodynamic and kinetic reactivity in solution and intrinsic stability is intriguing, on account of the variety of stabilities, structures and exposures to solvent involved. This raises important questions about, *inter alia*, the role of C–H...solvent hydrogen bonding interactions of carbocations in solution as well as charge delocalization effects within hydrocarbon frameworks of the carbocations.
- (3) The recent development of important quantitative empirical treatments of electrophilicity–nucleophilicity in solution<sup>307,308</sup> calls for an investigation of the relationship between intrinsic stability and solution electrophilicity.

## Acknowledgments

This work was supported by grants PB96-0927-C02-01 and BQU2000-1497 of the Spanish DGES, 20-52581.97 and 2000-058801.99 of the Swiss National Science Foundation. Valuable assistance from M. Jean-Claude Rossier is greatly appreciated. Interesting discussions with Profs J. F. Liebman and H. Mayr are acknowledged.

## References

1. Regarding the IUPAC nomenclature for these species, see Powell, W.H. (1993). *Pure Appl. Chem.* **65**, 1357
2. Regarding the IUPAC nomenclature for general physical organic chemistry, see Müller, P. (1994). *Pure Appl. Chem.* **66**, 1077
3. Glassgold, A.E., Omont, A. and Guelin, M. (1992). *Astrophys. J.* **396**, 115
4. Banaszekiewicz, M., Lara, L.M., Rodrigo, R., López-Moreno, J. and Molina-Cuberos, G.J. (2000). *Icarus* **147**, 386
5. Anicich, V.G., Milligan, D.B., Fairley, D.A. and McEwan, M.J. (2000). *Icarus* **146**, 118
6. Encrenaz, T.H., Drossart, P., Feuchtgruber, H., Lellouch, E., Bezaud, B., Fouchet, T. and Atreya, S.K. (1999). *Planet. Space Sci.* **47**, 1225
7. Thaddeus, P., McCarthy, M.C., Travers, M.J., Gottlieb, C.A. and Chen, W. (1998). *Faraday Discuss.* **109**, 121
8. Okamoto, K., Takeuchi, K. and Kitagawa, T. (1995). *Adv. Phys. Org. Chem.* **30**, 173
9. Tanaka, T., Kitagawa, T., Komatsu, K. and Takeuchi, K. (1997). *J. Am. Chem. Soc.* **119**, 9313
10. Asensi, M.A., Corma, A., Martínez, A. and Martínez, C. (1996). *Prepr. Am. Chem. Soc. Div. Pet. Chem.* **41**, 692
11. Corma, A., Martínez, A. and Martínez, C. (1996). *J. Catal.* **164**, 422
12. Corma, A. and García, H. (1997). *Catal. Today* **38**, 257
13. Corma, A. and García, H. (1998). *Top. Catal.* **6**, 127
14. Corma, A. and Martínez, A. (1998). *NATO ASI Series 3.* **44**. Kluwer Academic Publishers, Dordrecht, Holland
15. Corma, A. and García, H. (2000). *Dalton* 1381
16. Farcasiu, D. and Lukinskas, P. (1998). *J. Phys. Chem. A* **102**, 10436
17. Farcasiu, D. and Hancu, D. (1999). *J. Am. Chem. Soc.* **121**, 7173
18. Farcasiu, D. and Lukinskas, P. (2000). *J. Phys. Chem. A* **104**, 1944



19. Farcasiu, D., Norton, S.H. and Hancu, D. (2000). *J. Am. Chem. Soc.* **122**, 668
20. Boronat, M., Viruela, P. and Corma, A. (2000). *Phys. Chem. Chem. Phys.* **2**, 3327
21. Aue, D.H. and Bowers, M.T. (1979). *Gas Phase Ion Chemistry*. Bowers, M.T. (ed.), **vol. 2**, Chapter 1. Academic Press, New York
22. Raghavachari, K., Whiteside, R.A., Pople, J.A. and Schleyer, P.v.R. (1981). *J. Am. Chem. Soc.* **103**, 5649
23. Pilhaja, K. (1987). Thermochemical Methods in the Structural Analysis of Organic Compounds. *Molecular Structure and Energetics. Physical Measurements*. Liebman, J.F. and Greenberg, A. (eds), **2**, Chapter 5. VCH Publishers, New York
24. Chickos, J.S. (1987). Heats of Sublimation. *Molecular Structure and Energetics. Physical Measurements*. Liebman, J.L. and Greenberg, A. (eds), **2**, Chapter 3. VCH Publishers, New York
25. Tsang, W. (1996). *Heats of Formation of Organic Free Radicals by Kinetic Methods in Energetics of Organic Free Radicals*. Martinho Simões, J.A., Greenberg, A. and Liebman, J.F. (eds), . Blackie Academic and Professional, London
26. Afeefy, H.Y., Liebman, J.F. and Stein, S.E. (2000). Neutral Thermochemical Data in NIST Chemistry WebBook. *NIST Standard Reference Database Number 69*. Mallard, W.G. and Linstrom, P.J. (eds), (<http://webbook.nist.gov>). National Institute of Standards and Technology, Gaithersburg, MD
27. Pedley, J.B., Naylor, R.D. and Kirby, S.P. (eds) (1986). *Thermochemical Data of Organic Compounds* (2nd ed). Chapman & Hall, New York
28. Pedley, J.B. (ed.), (1994). *Thermochemical Data and Structures of Organic Compounds. vol. 1*. Thermodynamics Research Center, College Station, TX, USA
29. *TRC Thermodynamic Tables*. Thermodynamic Research Center, The Texas A&M University System, USA. These tables are being updated continuously
30. Dorofeeva, O.V., Gurvich, L.V. and Jorish, S.V. (1986). *J. Phys. Chem. Ref. Data* **15**, 438
31. Liebman, J.F. and Greenberg, A. (1989). *Chem. Rev.* **89**, 1225
32. Domalski, E.S. and Hearing, E.D. (1990). *J. Phys. Chem. Ref. Data* **19**, 881
33. Domalski, E.S. and Hearing, E.D. (1996). *J. Phys. Chem. Ref. Data* **25**, 1
34. Domalski, E.S. (ed.), (1993). NIST Estimation of the Thermodynamic Properties for Organic Compounds at 298.15 K—Compounds Containing the Elements C,H,N,O,S, and Halogens. National Institute of Standards and Technology, Washington, DC
35. Roth, W.R., Adamczak, O., Breuckmann, R., Lennartz, H.-W. and Boese, R. (1991). *Chem. Ber.* **124**, 2499
36. Lias, S.G. and Bartmess, J.E. (2000). NIST Chemistry WebBook. *NIST Standard Reference Database Number 69*. Mallard, W.G. and Linstrom, P.J. (eds), (<http://webbook.nist.gov>). National Institute of Standards and Technology, Gaithersburg, MD, USA
37. Ervin, K.M. (2001). *Chem. Rev.* **101**, 391
38. Marshall, A.G. (2000). *Int. J. Mass Spectrom.* **200**, 331
39. Kebarle, P. (2000). *Int. J. Mass Spectrom.* **200**, 313
40. Böhme, D.K. (2000). *Int. J. Mass Spectrom.* **200**, 97
41. Ng, C.Y. (2000). *Int. J. Mass Spectrom.* **200**, 357
42. Baer, T. (2000). *Int. J. Mass Spectrom.* **200**, 443
43. Hunter, E.P.L. and Lias, S.G. (1998). *J. Phys. Chem. Ref. Data* **27**, 413
44. Abboud, J.-L.M. and Notario, R. (1999). Energetics of Stable Molecules and Reactive Intermediates. *NATO Science Series*. Minas da Piedade, M.E. (ed.), **535**. Kluwer Academic Publishers, Dordrecht
45. Bartmess, J.E. (1994). *J. Phys. Chem.* **98**, 6420
46. Bartmess, J.E. (1995). *J. Phys. Chem.* **99**, 6755
47. East, A.L.L., Smith, B.J. and Radom, L. (1997). *J. Am. Chem. Soc.* **119**, 9014

48. Yungman, V.S. (2000). Entropy and Heat Capacity of Organic Compounds in NIST Chemistry WebBook. *NIST Standard Reference Database Number 69*. Mallard, W.G. and Linstrom, P.J. (eds), (<http://webbook.nist.gov>). National Institute of Standards and Technology, Gaithersburg, MD
49. Solomon, J.J. and Field, F.H. (1973). *J. Am. Chem. Soc.* **95**, 4483
50. Staley, R.H., Wieting, R.D. and Beauchamp, J.L. (1977). *J. Am. Chem. Soc.* **99**, 5964
51. Mishima, M., Arima, K., Inoue, H., Usui, S., Fujio, M. and Tsuno, Y. (1995). *Bull. Chem. Soc. Jpn* **68**, 3199
52. Chuchani, G., Mishima, M., Notario, R. and Abboud, J.-L.M. (1999). *Advances in Quantitative Structure–Property Relationships*. Charton, M. and Charton, B.I. (eds), **2**. JAI Press, Standford, Conn
53. Lias, S.G. and Ausloos, P. (1977). *Int. J. Mass Spectrom. Ion Phys.* **23**, 273
54. Abboud, J.-L.M., Notario, R., Ballesteros, E., Herreros, M., M6, O., Yáñez, M., Elguero, J., Boyer, G. and Claramunt, R. (1994). *J. Am. Chem. Soc.* **116**, 2486
55. Abboud, J.-L.M., Castaño, O., Herreros, M., Leito, I., Notario, R. and Sak, K. (1998). *J. Org. Chem.* **63**, 8995
56. Abboud, J. -L. M.; Leito, I.; Kaljurand, I.; Notario, R. Unpublished results
57. Abboud, J.-L.M., Castaño, O., Della, E.W., Herreros, M., Müller, P., Notario, R. and Rossier, J.C. (1997). *J. Am. Chem. Soc.* **119**, 2262
58. Abboud, J.-L.M., Herreros, M., Notario, R., Lomas, J.S., Mareda, J., Müller, P., Notario, R. and Rossier, J.C. (1999). *J. Org. Chem.* **64**, 6401
59. Meot-Ner, M. (1987). *NATO ASI Series C* **193**, 383
60. Meot-Ner, M. (1991). *J. Phys. Chem.* **95**, 6580
61. Irikura, K.K. (1999). *J. Am. Chem. Soc.* **121**, 7689
62. Abboud, J.-L.M., Castaño, O., Elguero, J., Herreros, M., Jagerovic, N., Notario, R. and Sak, K. (1998). *Int. J. Mass Spectrom. Ion Proc.* **175**, 35
63. Using the updated GB values from Ref. 43 and  $\Delta_f H_m^\circ$  for 1-adamantyl cation from Ref. 64.
64. Flores, H., Dávalos, J.Z., Abboud, J.-L.M., Castaño, O., Gomperts, R., Jiménez, P., Notario, R. and Roux, M.V. (1999). *J. Phys. Chem. A* **103**, 7555
65. Hudgens, J.W., Johnson, R.D., Tsai, B.P. and Kafafi, S.A. (1990). *J. Am. Chem. Soc.* **112**, 5763
66. Robles, E.S.J. and Chen, P. (1994). *J. Phys. Chem.* **98**, 6919
67. Horn, M. and Botschwina, P. (1994). *Chem. Phys. Lett.* **228**, 259
68. Takeuchi, K., Takasuka, M., Shiba, E., Kinoshita, T., Okazaki, T., Abboud, J.-L.M., Notario, R. and Castaño, O. (2000). *J. Am. Chem. Soc.* **122**, 7351
69. Curtiss, L.A. and Pople, J.A. (1991). *J. Chem. Phys.* **94**, 7221
70. Curtiss, L.A., Raghavachari, K. and Pople, J.A. (1993). *J. Chem. Phys.* **98**, 1293
71. Sharma, R.B., Sen Sharma, D.K., Hiraoka, K. and Kebarle, P. (1985). *J. Am. Chem. Soc.* **107**, 3747
72. Jacox, M.E. (1994). *J. Phys. Chem. Ref. Data, Monograph No. 3* 124
73. Koenig, T., Balle, T. and Snell, W. (1975). *J. Am. Chem. Soc.* **97**, 662
74. Dyke, J., Jonathan, N., Lee, E. and Morris, A. (1976). *J. Chem. Soc. Faraday Trans. 2* **72**, 1385
75. Crofton, M.W., Kreiner, W.A., Jagod, J.F., Rehfuss, G.D. and Oka, T. (1985). *J. Chem. Phys.* **83**, 3702
76. Crofton, M.W., Jagod, J.F., Rehfuss, G.D., Kreiner, W.A. and Oka, T. (1988). *J. Chem. Phys.* **88**, 666
77. Dixon, D.A., Feller, D. and Peterson, K.A. (1997). *J. Phys. Chem. A* **101**, 9405
78. Blush, J.A., Chen, P., Wiedmann, R.T. and White, M.G. (1993). *J. Chem. Phys.* **98**, 3557
79. Ruscic, B., Litorja, M. and Asher, R.L. (1999). *J. Phys. Chem. A* **103**, 8625

80. Weitzel, K.-M., Malow, M., Jarvis, G.K., Baer, T., Song, Y. and Ng, C.Y. (1999). *J. Chem. Phys.* **111**, 8267
81. Szulejko, J.E. and McMahon, T.B. (1993). *J. Am. Chem. Soc.* **115**, 7839
82. Hemsworth, R.S., Rundle, H.W., Böhme, D.K., Schiff, H.I., Dunkin, D.B. and Fehsenfeld, F.C. (1973). *J. Chem. Phys.* **59**, 61
83. Smith, B.J. and Radom, L. (1993). *J. Am. Chem. Soc.* **115**, 4885
84. Schreiner, P.R., Kim, S.-J., Schaefer, H.F., III and Schleyer, P.v.R. (1993). *J. Chem. Phys.* **99**, 3716
85. Müller, H., Kutzelnigg, W. and Klopper, W. (1997). *J. Chem. Phys.* **106**, 1863
86. Marx, D. and Parrinello, M. (1995). *Nature* **375**, 216
87. Marx, D. and Parrinello, M. (1999). *Science* **284**, 59
88. White, E.T., Tang, J. and Oka, T. (1999). *Science* **284**, 135
89. Heck, A.J.R., de Konig, L.J. and Nibbering, N.M.M. (1991). *J. Am. Soc. Mass Spectrom.* **2**, 453
90. Kramer, G.M., Oka, T., White, E.T., Marx, D. and Parrinello, M. (1999). *Science* **286**, 1051a
91. Schreiner, P.R. (2000). *Angew. Chem. Int. Ed.* **39**, 3239
92. Hariharan, P.C., Lathan, W.A. and Pople, J.A. (1972). *Chem. Phys. Lett.* **4**, 385
93. Zurawski, B., Ahlrichs, R. and Kutzelnigg, W. (1973). *Chem. Phys. Lett.* **21**, 309
94. Perera, S.A., Bartlett, R.J. and Schleyer, P.v.R. (1995). *J. Am. Chem. Soc.* **117**, 8476 and references therein
95. Ruscic, B., Berkowitz, J., Curtiss, L.A. and Pople, J.A. (1989). *J. Chem. Phys.* **91**, 114
96. Baer, T., Song, Y., Liu, J., Chen, W. and Ng, Y. (2000). *Faraday Discuss.* **115**, 137
97. Brouard, M., Lightfoot, P.D. and Pilling, M.J. (1986). *J. Phys. Chem.* **90**, 445
98. Koch, W., Liu, B. and Schleyer, P.v.R. (1989). *J. Am. Chem. Soc.* **111**, 3479
99. Jursic, B.S. (1999). *J. Mol. Struct. (Theochem)* **491**, 193
100. Saunders, M., Hagen, E.L. and Rosenfeld, J. (1968). *J. Am. Chem. Soc.* **90**, 6881
101. Saunders, M., Vogel, P., Hagen, E.L. and Rosenfeld, J. (1973). *Acc. Chem. Res.* **6**, 53
102. Baer, T., Song, Y., Ng, C.Y., Liu, J. and Chen, W. (2000). *J. Phys. Chem. A* **104**, 1959
103. Schultz, J.C., Houle, F.A. and Beauchamp, J.L. (1984). *J. Am. Chem. Soc.* **106**, 3917
104. Dyke, J., Ellis, A., Jonathan, N. and Morris, A. (1985). *J. Chem. Soc. Faraday Trans. 2* **81**, 1573
105. Saunders, M., Vogel, P., Hagen, L. and Rosenfeld, J. (1973). *Acc. Chem. Res.* **6**, 53
106. Sieber, S., Buzek, P., Schleyer, P.v.R., Koch, W. and de M. Carneiro, J.W. (1993). *J. Am. Chem. Soc.* **115**, 259
107. Lias, S.G., Shold, D.M. and Ausloos, P. (1980). *J. Am. Chem. Soc.* **102**, 2540
108. Bittner, E.W., Arnett, E.M. and Saunders, M. (1976). *J. Am. Chem. Soc.* **98**, 3734
109. Arnett, E.M. and Petro, C. (1978). *J. Am. Chem. Soc.* **100**, 5408
110. Lossing, F.P. and Semeluk, G.P. (1970). *Can. J. Chem.* **48**, 955
111. Yannoni, C.S., Kendrick, R.D., Myhre, P.C., Bébout, D.C. and Peterson, B.L. (1989). *J. Am. Chem. Soc.* **111**, 6440
112. Hollenstein, S. and Laube, T. (1993). *J. Am. Chem. Soc.* **115**, 7240
113. Keister, J.W., Riley, J.S. and Baer, T. (1993). *J. Am. Chem. Soc.* **115**, 12613
114. Traeger, J.C. (1996). *Rapid Commun. Mass Spectrom.* **10**, 119
115. Value from Prof. Taft's group as anchored to other data in Ref. 43.
116. Smith, B.J. and Radom, L. (1998). *J. Phys. Chem. A* **102**, 10787
117. Olah, G.A. and Donovan, D.J. (1978). *J. Am. Chem. Soc.* **100**, 5163
118. Solomon, J.J., Meot-Ner, M. and Field, F.H. (1974). *J. Am. Chem. Soc.* **96**, 3727
119. Goren, A. and Munson, B. (1976). *J. Phys. Chem.* **80**, 2848
120. Schleyer, P.v.R., de M. Carneiro, J.W., Koch, W. and Forsyth, D.A. (1991). *J. Am. Chem. Soc.* **113**, 3990
121. Solomon, J.J. and Field, F.H. (1975). *J. Am. Chem. Soc.* **97**, 2625

122. Glukhovtsev, M.N., Laiter, S. and Pross, A. (1996). *J. Phys. Chem.* **100**, 17801
123. DeFrees, D.J., McIver, R.T., Jr. and Hehre, W.J. (1980). *J. Am. Chem. Soc.* **102**, 3334
124. Taylor, C.A., Zerner, M.C. and Ramsey, B. (1986). *J. Organomet. Chem.* **317**
125. Schleyer, P.v.R. and Berner, M. (1988). *J. Org. Chem.* **53**, 2362
126. Aue, D.H. (1997). In *Dicoordinated Carbocations and Related Species*. Rappoport, Z. and Stang, P.J. (eds), Wiley, New York
127. Carey, F.A. and Sundberg, R.J. (2000). *Advanced Organic Chemistry, Part A* (4th ed), p. 617. Plenum Press, New York
128. Woodward, R.B. and Hoffmann, R. (1970). *The Conservation of Orbital Symmetry*. Academic Press, New York
129. Olah, G.A., Liang, G., Ledlie, D.B. and Costopoulos, M.G. (1977). *J. Am. Chem. Soc.* **99**, 4196
130. Saunders, M., Laidig, K.E., Wiberg, K.B. and Schleyer, P.v.R. (1988). *J. Am. Chem. Soc.* **110**, 7652
131. Koch, W., Liu, B. and DeFrees, D.J. (1988). *J. Am. Chem. Soc.* **110**, 7325
132. Hoffmann, R. (1964). *J. Chem. Phys.* **40**, 2480
133. Hehre, W.J., Radom, L., Schleyer, P.v.R. and Pople, J.A. (1986). *Ab Initio Molecular Orbital Theory*, p. 390. Wiley, New York
134. Jorgensen, W.L. and Salem, L. (1973). *The Organic Chemist's Book of Orbitals*, p. 35. Academic Press, New York
135. Walsh, A.D. (1947). *Nature* **159**, 712
136. Walsh, A.D. (1949). *Trans. Faraday Soc.* **45**, 179
137. de Meijere, A. (1979). *Angew. Chem. Int. Ed. Engl.* **18**, 809
138. Sugden, T.M. (1947). *Nature (London)* **160**, 367
139. Honegger, M., Heilbronner, E. and Schwenger, A. (1982). *Nouv. J. Chim.* **6**, 519
140. Saunders, M. and Siehl, H.U. (1980). *J. Am. Chem. Soc.* **102**, 6868
141. Holman, R.W., Plocica, J., Blair, L., Giblin, D. and Gross, M.L. (2001). *J. Phys. Org. Chem.* **14**, 17
142. Olah, G.A. and White, A.M. (1969). *J. Am. Chem. Soc.* **91**, 3954
143. Myrhe, P.C., Kruger, J.D., Hammond, B.L., Lok, S.M., Yannoni, C.S., Macho, V., Limbach, H.H. and Vieth, H.M. (1984). *J. Am. Chem. Soc.* **106**, 6079
144. Saunders, M. and Vogel, P. (1971). *J. Am. Chem. Soc.* **93**, 2559
145. Saunders, M. and Kates, M.R. (1978). *J. Am. Chem. Soc.* **100**, 7082
146. Schleyer, P.v.R., de M. Carneiro, J.W., Koch, W. and Raghavachari, K. (1989). *J. Am. Chem. Soc.* **111**, 5475
147. Solomon, J.J. and Field, F.H. (1976). *J. Am. Chem. Soc.* **98**, 1567
148. Meot-Ner, M., Solomon, J.J. and Field, F.H. (1976). *J. Am. Chem. Soc.* **98**, 1025
149. Sharma, R.B., Sen Sharma, D.K., Hiraoka, K. and Kebarle, P. (1985). *J. Am. Chem. Soc.* **107**, 3747
150. Olah, G.A., Kelly, D.P., Jeuell, G.L. and Porter, R.D. (1970). *J. Am. Chem. Soc.* **92**, 2544
151. Falkenberg-Andersen, C., Ranganayakulu, K., Schmitz, L.R. and Sorensen, T.S. (1984). *J. Am. Chem. Soc.* **106**, 178
152. Olah, G.A. and Liang, G. (1973). *J. Am. Chem. Soc.* **95**, 3792
153. Kabakoff, D.S. and Namanworth, E.J. (1970). *J. Am. Chem. Soc.* **92**, 3234
154. Childs, R.F., Faggiani, R., Lock, C.J.L., Mahendran, M. and Zweep, S.D. (1986). *J. Am. Chem. Soc.* **108**, 1962
155. Reindl, B., Clark, T. and Schleyer, P.v.R. (1998). *J. Phys. Chem. A* **102**, 8953
156. Abboud, J. -L. M.; Alkorta, I.; Dávalos, J.; Müller, P.; Quintanilla, E.; Rossier, J.-C.; Submitted for publication
157. Deno, N.C., Jaruzelski, J.J. and Schriesheim, A. (1955). *J. Am. Chem. Soc.* **77**, 3044
158. Deno, N.C., Richey, H.G., Jr., Liu, J.D., Hodge, J.D., Houser, J.J. and Wisotsky, M.J. (1962). *J. Am. Chem. Soc.* **84**, 1962

159. Pittman, C.U., Jr. and Olah, G.A. (1965). *J. Am. Chem. Soc.* **87**, 5123
160. Olah, G.A., Prakash, R.V., Rasul, G. and Prakash, G.K.S. (1999). *J. Am. Chem. Soc.* **121**, 9994
161. Schindler, M. (1987). *J. Am. Chem. Soc.* **109**, 1020
162. Müller, P. and Mareda, J. (1995). *J. Phys. Org. Chem.* **8**, 507
163. Müller, P. and Mareda, J. (1990). *Cage Hydrocarbons*. Olah, G.A. (ed.), Chapter 6. Wiley, New York
164. Schleyer, P.v.R., Fort, R.C., Watts, W.E., Comisarow, M.B. and Olah, G.A. (1964). *J. Am. Chem. Soc.* **86**, 5679
165. Winstein, S. and Trifan, D.S. (1949). *J. Am. Chem. Soc.* **71**, 2953
166. Schleyer, P.v.R. (1964). *J. Am. Chem. Soc.* **86**, 1856
167. Brown, H.C. (1977). *The Nonclassical Ion Problem*. Plenum Press, New York
168. Grob, C.A. (1983). *Acc. Chem. Res.* **16**, 426
169. Olah, G.A., Surya Prakash, G.K. and Saunders, M. (1983). *Acc. Chem. Res.* **16**, 440
170. Brown, H.C. (1983). *Acc. Chem. Res.* **16**, 432
171. Olah, G.A., Prakash, G.K.S., Arvaggi, M. and Anet, F.A. (1985). *J. Am. Chem. Soc.* **107**, 3747
172. Jarret, R.M. and Saunders, M. (1987). *J. Am. Chem. Soc.* **109**, 3365
173. Yannoni, C.S., Macho, V. and Myhre, P.C. (1982). *J. Am. Chem. Soc.* **104**, 7380
174. Koch, W., Liu, B., DeFrees, D.J., Sunko, D.E. and Vancik, H. (1990). *Angew. Chem. Int. Ed. Engl.* **29**, 183
175. Johnson, S.A. and Clark, D.T. (1988). *J. Am. Chem. Soc.* **110**, 4112
176. Perera, S.A. and Bartlett, R.J. (1996). *J. Am. Chem. Soc.* **118**, 7849
177. Werstiuk, N.H. and Muchall, H.M. (2000). *J. Phys. Chem. A* **104**, 2054
178. Mesić, M., Sunko, D.E. and Vančik, H. (1994). *J. Chem. Soc. Perkin Trans.* **2**, 1135
179. Sieber, S., Schleyer, P.v.R., Vančik, H., Mesić, M. and Sunko, D.E. (1993). *Angew. Chem. Int. Ed. Engl.* **32**, 1604
180. Schleyer, P.v.R. and Sieber, S. (1993). *Angew. Chem. Int. Ed. Engl.* **32**, 1606
181. Abboud, J.-L. M.; Alkorta, I.; Dávalos, J.; Müller, P.; Rossier, J.-C. Submitted for publication
182. Schleyer, P.v.R., Fort, R.C., Jr., Watts, W.E., Comisarow, M.B. and Olah, G.A. (1964). *J. Am. Chem. Soc.* **86**, 4195
183. Olah, G.A., Prakash, G.K.S., Shih, J.G., Krishnamurty, V.V., Mateescu, G.D., Liang, G., Sipos, G., Buss, V., Gund, T.M. and Schleyer, P.v.R. (1985). *J. Am. Chem. Soc.* **107**, 2764
184. Olah, G.A., Svoboda, J.J. and Ku, A.T. (1973). *Synthesis* 492
185. Vančik, H., Percac, K. and Sunko, D.E. (1990). *J. Am. Chem. Soc.* **112**, 7418
186. Houriet, R. and Schwarz, H. (1979). *Angew. Chem. Int. Ed. Engl.* **91**, 1018
187. Sharma, R.B., Sen Sharma, D.K., Hiraoka, K. and Kebarle, P. (1982). *J. Am. Chem. Soc.* **104**, 7105
188. Dutler, R., Rauk, A., Sorensen, T.S. and Whitworth, S.M. (1989). *J. Am. Chem. Soc.* **111**, 9024
189. Aubry, C., Holmes, J.L. and Walton, C.W. (1998). *J. Phys. Chem. A* **102**, 1389
190. Kruppa, G.H. and Beauchamp, J.L. (1986). *J. Am. Chem. Soc.* **108**, 2162
191. Abboud, J.-L.M., Castaño, O., Dávalos, J.Z., Jiménez, P., Gomperts, R. and Roux, M.V. (2002). *J. Org. Chem.* **67**, 1057
192. Abboud, J.-L.M., Castaño, O., Dávalos, J.Z. and Gomperts, R. (2001). *Chem. Phys. Lett.* **337**, 327
193. Abboud, J.-L. M.; Alkorta, I.; Dávalos, J.; Müller, P.; Rossier, J. C. Submitted for publication
194. Smith, D., Adams, N.G. and Ferguson, E.E. (1984). *Int. J. Mass Spectrom. Ion Proc.* **61**, 15

195. Berkowitz, J., Mayhew, C.A. and Rušćic, B. (1988). *J. Chem. Phys.* **88**, 7396
196. Glukhovtsev, M.N. and Bach, R.D. (1998). *Chem. Phys. Lett.* **286**, 51
197. Bogey, M., Cordonnier, M., Demuynck, C. and Destombes, J.L. (1992). *Astrophys. J.* **399**, L103
198. Bogey, M., Bolvin, H., Cordonnier, M., Demuynck, C., Destombes, J.L., Escribano, R. and Gómez, P.C. (1994). *Can. J. Phys.* **72**, 967
199. Crofton, M.W., Jagod, M.-F., Rehfuss, B.D. and Oka, T. (1989). *J. Chem. Phys.* **91**, 5139
200. Gabrys, C.M., Uy, D., Jagod, M.-F. and Oka, T. (1995). *J. Phys. Chem.* **99**, 15611
201. Lammerstma, K. and Ohwada, T. (1996). *J. Am. Chem. Soc.* **118**, 7247
202. Apeloig, Y. and Muller, T. (1997). In *Dicoordinated Carbocations and Related Species*. Rappoport, Z. and Stang, P.J. (eds), Wiley, New York
203. Bagno, A. and Modena, G. (1999). *Eur. J. Org. Chem.* 2893
204. Tse, J.S., Klug, D.D. and Laasonen, K. (1995). *Phys. Rev. Lett.* **74**, 876
205. Marx, D. and Parrinello, M. (1996). *Science* **271**, 179
206. Botschwina, P., Oswald, R., Flügge, J. and Horn, M. (1995). *Z. Phys. Chem.* **188**, 29
207. Gilbert, T., Pfab, R., Fischer, I. and Chen, P. (2000). *J. Chem. Phys.* **112**, 2575
208. Harkless, J.A.W. and Lester, A.W., Jr. (2000). *J. Chem. Phys.* **113**, 2680
209. Gobbi, A. and Frenking, G. (1994). *J. Am. Chem. Soc.* **110**, 9275
210. Mo, Y., Lin, Z., Wu, W. and Zhang, Q. (1996). *J. Phys. Chem.* **100**, 6469
211. Houle, F.A. and Beauchamp, J.L. (1978). *J. Am. Chem. Soc.* **100**, 3290
212. Ellison, G.B., Davico, G.E., Bierbaum, V.M. and DePuy, C.H. (1996). *Int. J. Mass. Spectrom. Ion Proc.* **156**, 109
213. Lossing, F.P. (1972). *Can. J. Chem.* **50**, 3973
214. Value reported in Ref. 43 as "Unpublished results by Ausloos, P., and Lias, S. G."
215. Craig, N.C., Pranata, J., Reinganum, S.J., Sprague, J.R. and Stevens, P.S. (1986). *J. Am. Chem. Soc.* **108**, 4378. This study includes all the possible deuterated isotopomers.
216. Xie, Y. and Boggs, J.E. (1989). *J. Chem. Phys.* **90**, 4320
217. Lee, T.J., Willetts, A., Gaw, J.F. and Handy, N.C. (1989). *J. Chem. Phys.* **90**, 4330
218. Salcedo, R. and Olvera, C. (1999). *J. Mol. Struct (Theochem)* **460**, 221
219. Olah, G.A., Staral, J.S., Spear, R.J. and Liang, G. (1975). *J. Am. Chem. Soc.* **97**, 5489
220. Haddon, R.C. (1975). *J. Am. Chem. Soc.* **97**, 3608 and references therein
221. Krygowski, T.M., Cyrański, M.K., Czarnocki, Z., Häfelfinger, G. and Katritzky, A.R. (2000). *Tetrahedron* **56**, 1783. This important report contains a wealth of references to previous studies on aromaticity and cognate subjects
222. Minkin, V.I., Glukhovtsev, M.N. and Simkin, B.Ya. (1994). *Aromaticity, and Antiaromaticity. Electronic and Structural Effects*, Chapter 6. Wiley, New York
223. Sieber, S., Schleyer, P.v.R., Otto, A.H., Gauss, J., Reichel, F. and Cremer, D. (1993). *J. Phys. Org. Chem.* **6**, 445
224. Maksic, Z.B., Kovacevic, B. and Lesar, A. (2000). *Chem. Phys.* **253**, 59
225. Winstein, S., Shatavsky, M., Norton, C. and Woodward, R.B. (1955). *J. Am. Chem. Soc.* **77**, 4183
226. Richey, H.G., Jr. and Lustgarten, R.K. (1966). *J. Am. Chem. Soc.* **88**, 3136
227. Brookhart, M., Diaz, A. and Winstein, S. (1966). *J. Am. Chem. Soc.* **88**, 3135
228. Olah, G.A., Liang, G., Mateescu, G.D. and Riemenschneider, J.L. (1973). *J. Am. Chem. Soc.* **95**, 8698
229. Olah, G.A. and Liang, G. (1975). *J. Am. Chem. Soc.* **97**, 6803
230. Laube, T. (1989). *J. Am. Chem. Soc.* **111**, 9224
231. Bremer, M., Schötz, K., Schleyer, P.v.R., Fleischer, U., Schindler, M., Kutzelnigg, W., Koch, W. and Pulay, P. (1989). *Angew. Chem. Int. Ed. Engl.* **28**, 1042
232. Schulman, J.M., Disch, R.L., Schleyer, P.v.R., Bühl, M., Bremer, M. and Koch, W. (1992). *J. Am. Chem. Soc.* **114**, 7897
233. Winstein, S. and Ordonneau, C. (1960). *J. Am. Chem. Soc.* **82**, 2084

234. Vogel, P. (1985). *Carbocation Chemistry*, p. 256. Elsevier, Amsterdam
235. Doering, W.v.E. and Knox, L.H. (1954). *J. Am. Chem. Soc.* **76**, 3203
236. Merling, G. (1881). *Chem. Ber.* **24**, 3108
237. Hückel, E.Z. (1931). *Z. Phys.* **70**, 204
238. Spiessacke, H. and Schneider, W.G. (1961). *Tetrahedron Lett.* 468
239. Garratt, P.J. (1986). *Aromaticity*. Wiley, New York
240. Engel, P., Keller, U.M., Bigler, P. and Neunschwander, M. (1976). *Helv. Chim. Acta* **59**, 2344
241. Takahashi, Y., Sankararaman, S. and Kochi, J.K. (1989). *J. Am. Chem. Soc.* **111**, 2954
242. Nicolaides, A. and Radom, L. (1996). *J. Am. Chem. Soc.* **118**, 10561
243. Moon, J.H., Choe, J.C. and Kim, M.S. (2000). *J. Phys. Chem. A* **104**, 458
244. Lifshitz, C. (1994). *Acc. Chem. Res.* **27**, 138
245. Elder, F.A. and Parr, A.C. (1969). *J. Chem Phys.* **50**, 1027
246. Thrush, B.A. and Zwonienik, J.J. (1963). *Discuss. Faraday Soc.* **35**, 196
247. Lee, E.P.F. and Wright, T.G. (1998). *J. Phys.Chem. A* **102**, 4007
248. Smith, B.J. and Hall, N.E. (1997). *Chem. Phys. Lett.* **279**, 165
249. Fujisaki, N., Comte, P. and Gäuman, T. (1993). *J. Chem. Soc. Chem. Commun.* 848
250. McClelland, R.A., Chan, C., Cozens, F., Modro, A. and Steenken, S. (1991). *Angew. Chem. Int. Ed. Engl.* **30**, 1337
251. Olah, G.A., Shamma, T., Burrichter, A., Rasul, G. and Surya Prakash, G.K. (1997). *J. Am. Chem. Soc.* **119**, 12923
252. Eiden, G.C., Weinhold, F. and Weisshaar, J.C. (1991). *J. Chem. Phys.* **95**, 8665
253. Eiden, G.C., Lu, K.-T., Badenhoop, J., Weinhold, F. and Weisshaar, J.C. (1996). *J. Chem. Phys.* **104**, 8886
254. Sen Sharma, D.K. and Kebarle, P. (1981). *Can. J. Chem.* **59**, 159
255. Smith, B.J. and Hall, N.E. (1997). *Chem. Phys. Lett.* **279**, 165
256. Brown, H.C. and Okamoto, Y. (1958). *J. Am. Chem. Soc.* **80**, 4979
257. Takeuchi, K., Takasuka, M., Ohga, Y. and Okazaki, T. (1999). *J. Org. Chem.* **64**, 2375
258. Cozens, F.L., Kanagasabapathy, V.M., McClelland, R.A. and Steenken, S. (1999). *Can. J. Chem.* **77**, 2069
259. Olah, G.A. (1964). *J. Am. Chem. Soc.* **86**, 932
260. Farnum, D.G. (1964). *J. Am. Chem. Soc.* **86**, 934
261. Farnum, D.G. (1966). *J. Am. Chem. Soc.* **88**, 2970
262. Laube, T., Olah, G.A. and Bau, R. (1997). *J. Am. Chem. Soc.* **119**, 3087
263. McClelland, R.A., Kanagasabapathy, V.M., Banait, N.S. and Steenken, S. (1989). *J. Am. Chem. Soc.* **111**, 3966
264. Ma, M. and Johnson, K.E. (1995). *J. Am. Chem. Soc.* **117**, 1508
265. Pitchumani, K., Lakshminarasimhan, P.H., Prevost, N., Corbin, D.R. and Ramamurthy, V. (1997). *Chem. Commun.* 181
266. Norris, F.F. and Sanders, W.W. (1901). *J. Am. Chem. Soc.* **25**, 54
267. Kehrmann, F. and Wentzel, F. (1901). *Ber. Dtsch. Chem. Ges.* **34**, 3815
268. Gomberg, M. (1901). *J. Am. Chem. Soc.* **25**, 328
269. v. Baeyer, A. (1905). *Ber. Dtsch. Chem. Ges.* **38**, 569
270. This was confirmed by cryoscopy:Hantzsch, A. (1907). *Z. Phys. Chem.* **61**, 257
271. Ferguson, L.N. (1948). *Chem. Rev.* **43**, 385
272. Sharp, D.W.A. and Sheppard, N. (1957). *J. Chem. Soc.* 674
273. Moodie, R.B., Connor, T.M. and Stewart, R. (1959). *Can. J. Chem.* **37**, 1402
274. Olah, G.A., Baker, E.B. and Comisarow, M.B. (1964). *J. Am. Chem. Soc.* **86**, 1265
275. Tao, T. and Maciel, G.E. (1995). *J. Am. Chem. Soc.* **117**, 12889
276. Avendaño, C., de Diego, C. and Elguero, J. (1990). *Magn. Reson. Chem.* **28**, 1011
277. Gomes da Mesquita, A.H., MacGillvary, C.H. and Eriks, H. (1965). *Acta Crystallogr.* **18**, 437

278. Wolf, J.F., Abboud, J.-L.M. and Taft, R.W. (1977). *J. Org. Chem.* **42**, 3316
279. Using scaled data from Ref. 43 and data for neutrals from Ref. 26
280. Gold, V. and Hawes, B.W.V. (1951). *J. Chem. Soc.* 2102
281. Deno, N.C. and Schriesheim, A. (1954). *J. Am. Chem. Soc.* **77**, 3051
282. Arnett, E.M. and Bushick, R.D. (1964). *J. Am. Chem. Soc.* **86**, 1564
283. Cox, R.A. (2000). *Adv. Phys. Org. Chem.* **35**, 1
284. Wolf, J.F., Harch, P. and Taft, R.W. (1975). *J. Am. Chem. Soc.* **97**, 2904
285. Amyes, T.L., Richard, J.P. and Novak, M. (1992). *J. Am. Chem. Soc.* **114**, 8032
286. Richard, J.P., Amyes, T.L., Lin, S.-S., O'Donoghue, A., Toteva, M.M., Tsuji, Y. and Williams, K.B. (2000). *Adv. Phys. Org. Chem.* **35**, 67
287. Hine, J. (1975). *Structural Effects on Equilibria in Organic Chemistry*, Chapter 7. Wiley, New York
288. Ito, S., Morita, N. and Asao, T. (1994). *Tetrahedron Lett.* **35**, 751
289. Arnett, E.M. (1999). *J. Chem. Thermodyn.* **31**, 711. This recent paper contains a number of references to the vast and fundamental work of this author in the field of solution thermochemistry of carbenium ions
290. Arnett, E.M. and Hofelich, T.C. (1983). *J. Am. Chem. Soc.* **105**, 2889
291. Arnett, E.M. and Pienta, N.J. (1980). *J. Am. Chem. Soc.* **102**, 3328
292. Arnett, E.M. and Abboud, J.-L.M. (1975). *J. Am. Chem. Soc.* **97**, 3865
293. Foote, C.S. (1964). *J. Am. Chem. Soc.* **86**, 1853
294. Bingham, C.R. and Schleyer, P.v.R. (1971). *J. Am. Chem. Soc.* **93**, 3189
295. Parker, W., Trauter, R.L., Watt, C.I.F., Chang, L.W.K. and Schleyer, P.v.R. (1974). *J. Am. Chem. Soc.* **96**, 7121
296. Schneider, H.J. and Thomas, F. (1980). *J. Am. Chem. Soc.* **102**, 1424
297. Schneider, H.J., Schmidt, G. and Thomas, F. (1983). *J. Am. Chem. Soc.* **105**, 3356
298. Müller, P., Blanc, J. and Perlberger, J.C. (1982). *Helv. Chim. Acta* **65**, 1418
299. Müller, P., Mareda, J. and Milin, D. (1995). *J. Phys. Org. Chem.* **8**, 507
300. Smith, M.R. and Harris, J.M. (1978). *J. Org. Chem.* **43**, 3588
301. Farcasiu, D. (1978). *J. Org. Chem.* **43**, 3878
302. Lenoir, D. and Frank, R.M. (1981). *Chem. Ber.* **114**, 3336
303. Müller, P., Milin, D., Feng, W.Q., Houriet, R. and Della, E.W. (1992). *J. Am. Chem. Soc.* **114**, 6169
304. Bentley, T.W. and Roberts, K. (1985). *J. Org. Chem.* **50**, 5852
305. Müller, P.; Abboud, J.-L. M.; Rossier, J.-C. Unpublished
306. Brown, H.C. and Rei, M.-H. (1964). *J. Am. Chem. Soc.* **86**, 5008
307. Mayr, H., Bug, T., Gotta, M.F., Hering, N., Irrgang, B., Janker, B., Kempf, B., Loos, R., Offial, A.R., Remennikov, G. and Schimmel, H. (2001). *J. Am. Chem. Soc.* **123**, 9500
308. Mayr, H. and Patz, M. (1994). *Angew. Chem. Int. Ed. Engl.* **33**, 938



# Transition State Analysis Using Multiple Kinetic Isotope Effects: Mechanisms of Enzymatic and Non-enzymatic Glycoside Hydrolysis and Transfer

PAUL J. BERTI<sup>†</sup> and KELLY S.E. TANAKA<sup>‡</sup>

<sup>†</sup>*Departments of Chemistry and Biochemistry and the Antimicrobial Research Centre, McMaster University, 1280 Main Street W., Hamilton, Ontario, Canada*

<sup>‡</sup>*Department of Biochemistry, Albert Einstein College of Medicine, 1300 Morris Park Avenue, Bronx, New York, USA*

- 1 Introduction 240
  - Glycoside chemistry 240
  - Enzymatic versus non-enzymatic transition states 241
  - The practice of TS analysis 242
  - TS analysis and inhibitor design 244
  - Mechanism nomenclature 244
  - Kinetically significant steps: irreversible steps and rate-limiting steps 245
- 2 TS analysis: principles and procedures 247
  - The meaning of KIEs in enzymatic reactions 247
  - The reaction coordinate and the structure of the transition state 249
  - Very low bond orders 250
  - Observable KIEs for stepwise reactions 250
  - From experimental KIEs to transition states 251
- 3 TS analysis: results and recent developments 255
  - The nature of the oxocarbenium ion 255
  - Non-chemical steps 259
  - Transition state imbalance 261
  - Secondary KIEs 266
  - Catalytic strategies 273
- 4 Specific reactions 283
  - Glucoside and xyloside hydrolysis and glucosidases 283
  - Sialidases and sialyltransferases 288
  - Bacterial ADP-ribosylating toxins and non-enzymatic NAD<sup>+</sup> hydrolysis 291
  - Nucleoside and AMP hydrolases 294
  - Phosphorylase and pyrophosphorylase reactions 297
  - DNA and RNA 301
- 5 Conclusions and future directions 306
  - The immediate future 306
  - Crucial questions 307
  - Acknowledgments 308
  - References 308

## 1 Introduction

This chapter addresses both the principles and practice of transition state (TS<sup>#1</sup>) analysis and recent advances in our understanding of hydrolysis and glycosyl transfer reactions of *N*- and *O*-glycosides. By transition state analysis, we mean specifically the use of multiple (or families of) kinetic isotope effects (KIEs) to define transition states in atomic detail. In the best cases, it has been possible to determine the structure of the transition state, a species that exists for less than a single bond vibration (*ca.*  $10^{-13}$  s), with accuracy that rivals that of X-ray crystallography of stable molecules. These studies have elucidated both the chemistry of these reactions and the strategies used by enzymes to promote catalysis. The use of TS analysis to build quantitative, atomic resolution transition state models is still a relatively new technique. In this chapter, we describe the techniques of TS analysis as applied to glycoside chemistry and recent results that have emerged from these studies.

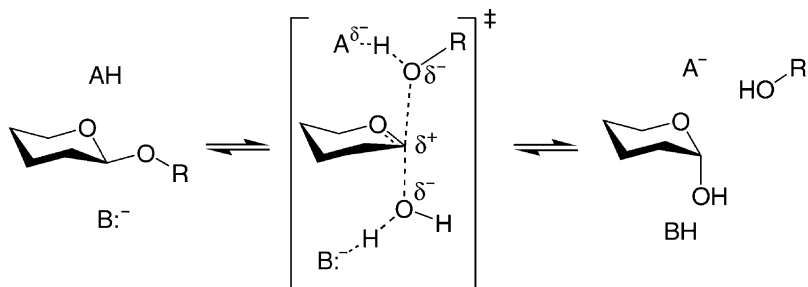
### GLYCOSIDE CHEMISTRY

There is a long history of exploration of *O*- and *N*-glycoside chemistry by physical organic chemists.<sup>1–5</sup> Biologists have long been interested in systems involving glycoside chemistry, such as cell–cell contacts and signaling; nucleic acid synthesis, repair and recycling; glycoprotein maturation, folding, and degradation; intracellular signaling; microbial (viral, bacterial and fungal) pathogenicity; apoptosis; cancer; lysosomal storage diseases; and even wood degradation.<sup>6–8</sup> Recent advances in chemical and enzymatic synthesis and characterization (e.g., see Ref. 9) have made complex oligosaccharides experimentally accessible. The division of glycoside chemistry into pyranosides and furanosides coincides well with the division between *O*-glycosides (pyranosides), and *N*-glycosides (furanosides). The notable exception is the study of cationic *N*-glucosides by Bennet and coworkers, which have shed light on both classes of sugars.

We discuss in this chapter how TS analysis allows chemists to ask sophisticated and subtle questions of enzymatic and non-enzymatic glycoside hydrolysis and transfer reactions. It is now becoming possible to measure routinely (if perhaps not

---

<sup>#1</sup>  $\alpha_n$ , the intrinsic KIE on rate constant  $k_n$ ;  $\psi$ U, pseudouridine; ADP, adenosine 5'-diphosphate; AMP, adenosine 5'-monophosphate; ATP, adenosine 5'-triphosphate; BOVA, bond order vibrational analysis; CMP-NeuAc, cytidine monophosphate glycoside of *N*-acetylneuraminic acid; DFT, density functional theory, DTA, diphtheria toxin A-chain; EIE, equilibrium isotope effect; IE, isotope effect; immucillin H, (1S)-1-(9-deazahypoxanthin-9-yl)-1,4-dideoxy-1,4-imino-D-ribitol; IU-NH, inosine–uridine-specific nucleoside hydrolase; KIE, kinetic isotope effect; MP2, second order Moller–Plesset perturbation theory; NAD<sup>+</sup>, oxidized nicotinamide adenine dinucleotide;  $n_{LG}$ ,  $n_{Nu}$ , Pauling bond order to the leaving group or nucleophile; OPRTase, orotate phosphoribosyltransferase; pAPIR, *p*-aminophenyl iminoribitol; PNP, purine nucleoside phosphorylase; RTA, ricin toxin A-chain; SDKIE, solvent deuterium KIE; TS, transition state; UDG, uracil DNA glycosylase; UMP, uridine 5'-monophosphate.



**Fig. 1** Simultaneous general acid and general base catalysis of glycoside hydrolysis.

yet easily) experimental KIEs and from them deduce in detail the structure and other essential features of the transition state.

#### ENZYMATIC VERSUS NON-ENZYMATIC TRANSITION STATES

Enzymes catalyze reactions by binding to transition states, lowering their energy. However, the transition state to which the enzyme binds is not necessarily the same as for the non-enzymatic reaction. TS analysis has shown that various enzymes can give different TS structures for the same reaction, which are in turn different from their non-enzymatic counterparts. Enzymes often do not merely stabilize the transition state; they change it. This is a reflection of the fact that the environment of an enzyme active site is different from aqueous solution. One crucial difference between an enzyme active site and aqueous solution is that the former can be viewed as a pre-organized “supersolvent”.<sup>10</sup> Using the example of *O*-glycoside hydrolysis, there would be catalytic advantage to protonating the alkoxide leaving group and deprotonating the water nucleophile simultaneously (Fig. 1), but such a transition state is highly unlikely in solution. The probability of these events happening simultaneously is vanishingly small because of the high entropic cost of forming a tetramolecular transition state (glycoside, nucleophile, general acid, general base), and the unlikelihood of having solvent molecules acting as both a general acid and a general base in a single solution. In an enzyme, however, suitably positioned functionalities in the active site can act as general acids and bases simultaneously. The entropic cost of transition state formation is mitigated by: (1) the need to form only a termolecular transition state (glycoside, nucleophile, enzyme); (2) the use of binding energy with the substrates to compensate for the entropic cost.

Retaining and inverting *O*-glycosidases make use of a general acid/general base pair comprised of a carboxylic acid and carboxylate of aspartic acid or glutamic acid side chains (see also Fig. 21). These side chains have similar  $pK_a$  values in solution; but the micro-environments of enzyme active sites allow each  $pK_a$  to be tuned so that each side chain is in the correct protonation state. This makes it possible for a carboxylate and a carboxylic acid to exist in the active site simultaneously.

Enzymes do not merely stabilize transition states, but can alter their structures, even whole reaction pathways to achieve catalysis. We can probe the potential energy surface of a reaction directly through computations or indirectly through experimental studies, but TS analysis can show how the potential energy surface itself is modified to promote catalysis.

#### THE PRACTICE OF TS ANALYSIS

##### *Overview of TS analysis*

TS analysis involves a number of steps. It is necessary that the kinetic mechanism of the reaction be thoroughly characterized. Conditions must be found where the experimental KIEs reflect the chemical steps of the reaction rather than binding events or conformational changes. Isotopically labeled substrates are then synthesized and KIEs measured.

*Advances in measurement.* Recent emphasis on biologically relevant systems has created special challenges and unique solutions to the challenges of KIE measurement. Synthesis of complex molecules labeled at a variety of positions has been made possible by the routine availability of recombinant enzymes to build up complex biosynthetic pathways in a test tube. The “traditional” techniques of measuring KIEs by isotope ratio mass spectrometry<sup>11</sup> or scintillation counting of radiolabeled compounds,<sup>12</sup> are now being complemented by methods such as whole-molecule mass spectrometry,<sup>13–17</sup> short-lived isotopes<sup>18</sup> and novel spectrophotometric techniques.<sup>19–21</sup> These new methods hold the promise of greater versatility than isotope ratio mass spectrometry and both easier synthesis and faster measurements than radiolabeling techniques. One approach that holds great promise is the determination of KIEs on natural abundance isotopes (i.e. unlabeled compounds) using NMR to measure relative isotopic abundances in residual substrate after the reaction has been run to 90–99% completion.<sup>22,23</sup> By eliminating the need to synthesize labeled compounds and offering the promise of measuring KIEs on every non-exchangeable nucleus in a single reaction, the technique of Singleton and coworkers holds great promise.

*Advances in interpretation.* Experimental KIEs are interpreted using quantum mechanical and/or bond order vibrational analysis (BOVA) approaches to yield the experimental transition state. In systems that are well understood, the accuracy of experimental TS structures derived using a BOVA “unified model” rivals X-ray crystallography of stable molecules. The largest advance in KIE interpretation since the description of BOVA by Sims and Lewis<sup>24,25</sup> has been the increase in computational power available to the average chemist. Previously, vibrational models were reduced to a minimal number of atoms to make them computationally tractable. Today, a desktop computer can perform BOVA calculations with hundreds of atoms. The accessibility of post-Hartree–Fock calculations to the average chemist has made *ab initio* calculations a routine part of TS analysis, and made possible the structure interpolation approach to BOVA.

If possible, one of the transition states solved should be the non-enzymatic analogue of the enzymatic reaction. The non-enzymatic reaction acts as a reference for which there is frequently a variety of other experimental evidence to guide KIE interpretation and help validate the experimental transition state. In addition, the difference between the transition state for the enzymatic and non-enzymatic reactions reflects the interaction between the substrate's intrinsic reaction pathway<sup>#2</sup> and the enzyme's use of binding energy to lower the energetic barrier to the transition state.

The theoretical and practical challenges of TS analysis remain formidable, but the increase in our understanding of chemical systems from each experimental transition state, and the impossibility of achieving these results by any other technique, fully justify the effort.

### *TS analysis as part of a research program*

As powerful as TS analysis is, no single experimental technique can provide all the information required to understand an enzymatic system in detail. TS analysis is part of a suite of techniques that are necessary to characterize the structure and catalytic activity of enzymes.

A recent publication on purine nucleoside phosphorylase (PNP)<sup>26</sup> represents the end result of a systematic program of TS analysis<sup>27,28</sup> combined with protein dynamic,<sup>29</sup> structural<sup>30</sup> and functional analyses<sup>31,32</sup> that have yielded profound insights into the catalytic mechanisms of this enzyme, as well as powerful inhibitors with therapeutic potential.<sup>32,33</sup> TS analysis demonstrated that the reaction proceeded with a highly dissociative<sup>#3</sup>  $A_ND_N$  mechanism, passing through an oxocarbenium ion-like (but still bimolecular) transition state. Cycles of inhibitor design and testing, as well as theoretical prediction of inhibition constants, resulted in a PNP inhibitor, immucillin H, with a dissociation constant of 23 pM. This inhibitor showed third-of-sites reactivity, consistent with being a good TS mimic, and was shown through solvent-exchange experiments to decrease protein dynamics. TS analysis, combined with the crystal structures of PNP-immucillin H cocrystals, as well as cocrystals of a Michaelis complex analogue (substituting sulfate for phosphate) and the reaction products, along with docking of the experimental TS structure, resulted in convincing evidence for an "electrophile migration" mechanism. This is distinct from a more conventional view of nucleophilic substitutions proceeding through nucleophile approach to the electrophilic center concerted with leaving group departure. It is hard to imagine how these results could have been achieved without the use of TS analysis.

<sup>#2</sup> This is not to say that the non-enzymatic transition state is the "intrinsic" transition state. It will reflect interactions of the molecule with solvent water, salts and other solutes. The intrinsic reaction *in vacuo* is generally not experimentally accessible for biologically relevant molecules.

<sup>#3</sup> Several meanings of the word "dissociative" have been used. We use it to mean that the sum of nucleophile and leaving group bond orders at an  $A_ND_N$  transition state are less than the corresponding bond orders in the reactants or products.

## TS ANALYSIS AND INHIBITOR DESIGN

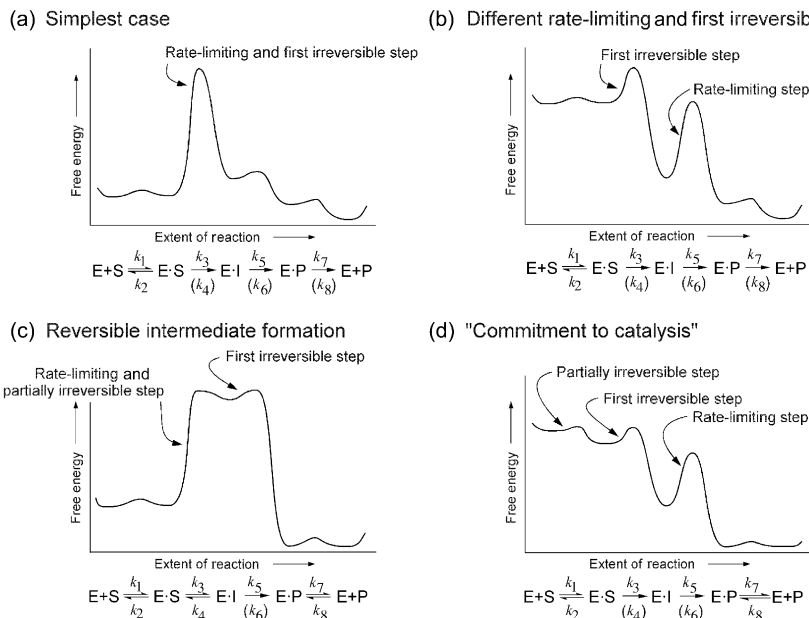
From a biological perspective, one of the primary motivations for studying enzymatic mechanisms is inhibitor design. The relevance of the transition state to inhibitor design stems from the application of TS theory to catalysis, which states that enzymes catalyze reactions by binding tightly to the transition state in preference to any other species, thereby stabilizing it.<sup>34,35</sup> Enzymes typically bind reactants and products with equilibrium dissociation constants in the  $10^{-3}$ – $10^{-6}$  M range. Tighter binding would interfere with product release at the end of the catalytic cycle. In contrast, the inferred equilibrium dissociation constant of the enzyme·TS complex for the reaction catalyzed by orotidine-5'-phosphate decarboxylase is  $10^{-24}$  M.<sup>36</sup> Exploiting the enzyme's affinity for the transition state by synthesizing TS analogues as inhibitors, or in other ways designing mechanism-based inhibitors that rely on the catalytic powers of the enzyme to effect inhibition ( $\beta$ -lactam antibiotics being the classic example) is an effective means to inhibit enzymes.

Resistance is an additional consideration in the design of inhibitors as antimicrobial compounds. With the advent of vancomycin resistance, once thought to be the single antibiotic against which resistance would never arise,<sup>37</sup> it is now clear that resistance will eventually arise to every antibiotic. However, it is possible to consider designing TS analogues that are "resistance resistant antibiotics". An enzyme cannot lose affinity for its cognate transition state without also losing its catalytic ability. Thus, resistance to TS analogues must arise through specificity against remote parts of the inhibitor molecule. As long as the target enzyme has catalytic activity, it should be possible in principle to modify the TS analogue to counter changes in the enzyme's specificity.

## MECHANISM NOMENCLATURE

According to IUPAC nomenclature,<sup>38–40</sup> a reaction mechanism is divided into elementary steps, with  $A_N$  representing a nucleophilic addition and  $D_N$  representing a nucleophilic dissociation. A bimolecular ( $S_N2$ ) reaction is represented as  $A_N D_N$ .  $D_N + A_N$  and  $D_N * A_N$  mechanisms are stepwise ( $S_N1$ ), with a discrete intermediate formed between leaving group departure and nucleophile approach. A  $D_N + A_N$  reaction has a cationic intermediate that is sufficiently long-lived for the leaving group to diffuse away into solution. A  $D_N * A_N$  mechanism involves an intermediate that is too short-lived to separate diffusively from the leaving group. In an enzyme-catalyzed reaction, the lifetime *per se* of the intermediate may not be relevant if the leaving group is bound to the enzyme and cannot diffuse away.

Oxocarbenium ions do not generally have a long enough lifetime in solution for diffusive separation of the leaving group. Thus, in the case of enzymatic reactions where an oxocarbenium ion intermediate is formed, it will not be possible for it to diffusively separate from the enzyme and leaving group, so the mechanistic description  $D_N * A_N$  will be used by default for stepwise enzymatic reactions. From the point of view of KIEs,  $D_N + A_N$  and  $D_N * A_N$  mechanisms are indistinguishable.



**Fig. 2** Free energy profiles for enzyme-catalyzed reactions. The rate-limiting, partially irreversible and first irreversible steps are labeled for each reaction profile: (a) the simplest case where the rate-limiting and first irreversible steps are the same; (b) the first irreversible step occurring before the rate-limiting step; (c) a high-energy intermediate where its formation is rate-limiting and partially irreversible, while its breakdown is the first (fully) irreversible step; (d) external commitment to catalysis, where formation of the non-covalent Michaelis complex is partially irreversible, and  $k_3$  is the first irreversible step. Each reaction involves association of free enzyme and a single substrate ( $E + S$ ) to form a non-covalent Michaelis complex ( $E \cdot S$ ), which then undergoes two chemical steps to first form an intermediate complex ( $E \cdot I$ ), then the enzyme-product complex ( $E \cdot P$ ) before dissociation to give free enzyme and product ( $E + P$ ). In the kinetic mechanisms, irreversible steps are indicated by a single headed arrow, and the reverse rate constants in parentheses.

In stepwise reactions, the double dagger symbol, ‡, is used to indicate the rate-limiting step when it is known.

Some authors have referred to highly dissociative  $A_N D_N$  reactions as being “ $S_N1$ -like”. If the transition state is bimolecular, with both the nucleophile and the leaving group in the reaction coordinate, then the reaction has an  $A_N D_N$  mechanism, regardless of the extents of bond loss or formation at the transition state. In this chapter, we will refer to highly dissociative  $A_N D_N$  transition states as being “oxocarbenium ion-like” rather than “ $S_N1$ -like”.

#### KINETICALLY SIGNIFICANT STEPS: IRREVERSIBLE STEPS AND RATE-LIMITING STEPS

When performing TS analysis, it is crucially important to know which step(s) of the reaction are being probed by the experimental KIEs. The meaning of KIEs is

different depending on whether they are measured by the competitive or non-competitive (direct) methods (see below).

Competitive KIEs reflect steps up to and including the first irreversible step of the reaction. In contrast, non-competitive KIEs reflect the rate-limiting step(s). In the simplest case, one step in the kinetic mechanism is both the rate-limiting and the first irreversible step (Fig. 2a). In enzymatic reactions, however, it is common for different steps in the kinetic mechanism to correspond to the rate-limiting step and the first irreversible step (e.g., Fig. 2b). A classic example is the hydrolysis of *p*-nitrophenyl acetate by chymotrypsin.<sup>41</sup> In this reaction, the acylation step ( $k_3$ ) to form the covalent acetyl-chymotrypsin intermediate is much faster than deacylation ( $k_5$ ), but is effectively irreversible because the other product, *p*-nitrophenol, can diffuse away into solution. Under these conditions, the first irreversible step is different from the rate-limiting step. This type of situation is relatively common, and is observed, e.g., in enzymes where product release is the rate-limiting step, but the chemical step is effectively irreversible. Competitive KIEs measured on this reaction would include no contribution from the rate-limiting step and would reflect the reaction only up to the transition state of the first irreversible step. In contrast, non-competitive KIEs would reflect only the rate-limiting step and would include no contribution from the acylation step.

Just as reactions may have more than one partially rate-limiting step, similarly, they may have more than one partially irreversible step.<sup>#4</sup> One common example in both enzymatic and non-enzymatic reactions is where a high-energy intermediate is formed that can then partition in both the forward ( $k_5$ ) and reverse ( $k_4$ ) directions (Fig. 2c). In this example, intermediate formation ( $k_3$ ) is rate-limiting and partially irreversible, while its breakdown ( $k_5$ ) is the first (fully) irreversible step. The degree of irreversibility of a given step is determined by the partitioning of the subsequent species forward or backward. In the previous examples (Fig. 2a and b), the energetic barriers after the E·I intermediate ensure it partitions overwhelmingly in the forward direction. In Fig. 2c, steps  $k_3$  and  $k_5$  are both partially irreversible, and competitive KIEs for this reaction would include contributions from both steps. With two different steps contributing to the experimental KIEs, it is likely that they would be uninterpretable for transition state analysis (but see the ricin-catalyzed reactions in Section 4). In contrast, non-competitive KIEs on this reaction would reflect only  $k_3$ , the rate-limiting step.

We use the expression “kinetically significant step” throughout this chapter. Its meaning is context dependent. When the rate-limiting step is under consideration, then if one step is much slower than all others, it is the only kinetically significant step ( $k_3$  in Fig. 2a). If the rates of two steps are similar to each other and much slower than all others, then both are partially rate-limiting and both are kinetically significant. In another context “kinetically significant” will refer to the irreversibility of steps. If every step before the first irreversible step is freely reversible and

<sup>#4</sup> The expression “partially irreversible” is grammatically suspect, but the alternatives sacrifice clarity for correctness.



therefore at equilibrium (Fig. 2a and b), then it is the only kinetically significant step. If, however, an intermediate is formed that partitions significantly in both directions, then there are two partially irreversible steps ( $k_3$  and  $k_5$  in Fig. 2c), and both steps are kinetically significant. The partitioning ratio (i.e.  $k_5$  versus  $k_4$ ) determines the degree of irreversibility of formation of an intermediate.

The term “commitment to catalysis”<sup>42</sup> is unique to KIE studies on enzymes and not widely used in the chemical literature. “External commitment to catalysis” refers to the partitioning of the first intermediate of the reaction, the non-covalent enzyme-substrate (E·S) intermediate. Some enzymes are such efficient catalysts that nearly every molecule of substrate that binds proceeds forward to products (i.e.  $k_3 \gg k_2$ ). Under these conditions, the first irreversible step of the reaction is substrate binding. If competitive isotope effects are measured, they will only reflect binding isotope effects, and have no contribution from the chemical steps of the reaction. In less extreme cases (Fig. 2d), both substrate binding ( $k_1$ ) and the chemical step ( $k_3$ ) are partially irreversible. “Internal commitment to catalysis” simply refers to the partitioning of any intermediate enzyme-bound species.

## 2 TS analysis: principles and procedures

### THE MEANING OF KIEs IN ENZYMATIC REACTIONS

*Competitive versus non-competitive KIEs.* KIE measurements can be made in a competitive or non-competitive manner.<sup>12</sup> In the non-competitive (or direct) methodology, kinetic constants are determined with the labeled and unlabeled compound in separate experiments, and the ratios of rate constants are compared to give the experimental KIEs. Non-competitive KIEs are generally not sufficiently accurate for transition state analysis, although recently the groups of Huskey and Toney have described methods for accurate measurement of non-competitive KIEs.<sup>19,20</sup> The advantage of non-competitive KIEs is that it is possible in principle to measure isotope effects on every kinetic parameter (e.g.,  $k_{\text{cat}}/K_M$ ,  $k_{\text{cat}}$ , and  $K_M$ ) individually.

It is generally necessary to measure competitive KIEs to achieve the confidence intervals of  $\pm 0.002$  to  $\pm 0.005$  needed to accurately describe a transition state. In competitive measurements, labeled and unlabeled reactants are combined in a single reaction mixture and allowed to react as competitive substrates in the enzymatic reactions (or as competitive reactants in non-enzymatic reactions). If there is an isotope effect at the labeled position, the faster reacting isotope will become depleted in the reactant and enriched in the product and the isotope ratio (unlabeled:labeled) will change. It is this change in isotopic composition that is measured to determine KIEs.

Competitive KIEs in enzymatic reactions are isotope effects on the second-order rate constant  $k_{\text{cat}}/K_M$ , also called the “specificity constant”.<sup>35</sup> The value of  $k_{\text{cat}}/K_M$  reflects, in the simplest case, the difference between the energy of the free substrate

in solution and the transition state of the *first irreversible step* of the reaction (e.g., Fig. 2a and b).<sup>43</sup> After the first irreversible step, the reaction is committed to continuing forward and no further isotopic discrimination can occur. This assumes that all steps before the irreversible step are freely reversible and therefore at equilibrium. If this is not true and there are several partially irreversible steps, each one will contribute to the observed KIE (Fig. 2c and d).

*Multiple kinetically significant steps.* If a reaction has several steps that are kinetically significant (partially rate-limiting or partially irreversible), then an incremental change in any one of those steps will not be fully reflected in the macroscopic rate constant for the reaction. The practical upshot is that an isotope effect on one microscopic rate constant,  $k_n$ , will be reflected in the macroscopic rate constant *only* if  $k_n$  is the only kinetically significant step. If there is more than one kinetically significant step, the observed KIE will be less than the KIE on  $k_n$ . In the jargon of the field, the KIE on  $k_n$  would be “suppressed by kinetic complexity”.

*Intrinsic KIEs.* The phrase “intrinsic KIEs” is often used. This refers to the situation where only chemical steps are kinetically significant, i.e. irreversible or rate-limiting, depending on the context. As the goal of TS analysis is to understand the chemical mechanisms of catalysis, the goal is always to measure intrinsic KIEs that do not contain contributions from non-chemical, isotopically insensitive steps.

*Commitment to catalysis.* “External commitment to catalysis”, or often just “commitment to catalysis” occurs when an enzyme is so efficient that most of the Michaelis complex (E·S) partitions forward to undergo catalysis. When this occurs, substrate association is the first irreversible step, or partially irreversible step. The classic example of this is catalase, where the reaction is close to diffusion rate-limited, and  $k_{\text{cat}}/K_M = 4 \times 10^7 \text{ s}^{-1}$ .<sup>35</sup> It is possible to test for commitment to catalysis using the isotope-trapping methodology of Rose.<sup>44</sup> If it is not close to zero, conditions may be modified to achieve this, such as using alternate substrates, adjusting reaction conditions, or using mutant enzymes. When commitment to catalysis is close to zero, this implies that substrate association is fully reversible and at equilibrium. The observable KIEs are those of the chemical step(s). If conditions are found where commitment to catalysis is moderate, it can be quantitated and the experimental KIEs corrected numerically,<sup>44,45</sup> although this correction is only approximate as it does not take into account binding isotope effects (IEs) on association.

*Conformational change.* Another situation where a non-chemical step can contribute to the experimental KIEs is if a conformational change, such as a loop movement in the protein, is kinetically significant. Kinetically significant conformational changes are not rare in enzymology in general, and have (apparently) been observed in at least four TS analysis studies.<sup>46–49</sup> Again, if possible, conditions are found where the conformational change is no longer kinetically significant.

*Intermediates.* Another complication is when an intermediate is formed that partitions to a significant extent both forward and backward. The observable KIEs will be a function of the intermediate partitioning.<sup>43</sup> Again, it may be possible to

adjust reaction conditions such that the intermediate partitions predominantly in one direction.

For non-enzymatic reactions, some of the same concerns apply. Kinetically significant substrate binding is not a concern, and conformational change is much less likely to be kinetically significant, however, partitioning of intermediates may have to be considered. In particular, glucopyranosides<sup>50–53</sup> and sialylpyranosides<sup>54,55</sup> have been shown to proceed through several simultaneous pathways, including direct nucleophilic displacement, formation of intimate ion pairs (or ion-neutral complexes) and solvent-separated ion pairs.

In spite of all these potential complications, it has proven possible in the majority of cases examined to generate experimental KIEs that reflect the chemical steps of the enzymatic reaction. Thus, one may embark on a TS analysis study with a good expectation of obtaining an experimental transition state.

#### THE REACTION COORDINATE AND THE STRUCTURE OF THE TRANSITION STATE

*KIEs on the reaction coordinate.* All the experimental and theoretical evidence gathered to date has supported the view that nucleophilic substitutions on glycosides proceed through transition states on the border between  $A_N D_N$  and  $D_N * A_N$ . In conventional physical organic experiments, it is often difficult to distinguish between mechanisms for reactions that are very close to the borderline. In isotope effect studies, however, it is possible to unambiguously make this distinction. In some highly dissociative  $A_N D_N$  transition states, the residual bond order<sup>#5</sup> to the leaving group and the incipient bond order to the incoming nucleophile are so low ( $< 0.05$ ) that it seems they should have little or no observable effect on the KIEs. The question then arises whether these groups are present in the transition state at all. The reaction coordinate<sup>#6</sup> motion makes a contribution to the primary carbon KIE of  $\geq 1.01$  in addition to the zero point energy and excited state contributions of other vibrational modes. As such, there is a significant difference in calculated isotope effects for the same structure if either the nucleophile or leaving group is left out of the reaction coordinate.  $A_N D_N$  reactions are traditionally expected to give primary carbon KIEs in the range of  $^{13}\text{C}$  KIE = 1.03–1.08 or  $^{14}\text{C}$  KIE = 1.06–1.16, while  $D_N * A_N$  mechanisms would give  $^{13}\text{C}$  KIE = 1.00–1.01 or  $^{14}\text{C}$  KIE = 1.00–1.02.<sup>57</sup> More recent calculations on *N*-(deoxy-)ribofuranosides have indicated approximate limits of  $^{13}\text{C}$  KIE = 1.013–1.04 or  $^{14}\text{C}$  KIE = 1.025–1.075 for  $A_N D_N$  mechanisms, and  $^{13}\text{C}$  KIE = 1.008–1.010 or  $^{14}\text{C}$  KIE = 1.015–1.018 for  $D_N * A_N$  mechanisms.<sup>58</sup> As discussed in Section 4, examples have been found of both highly

<sup>#5</sup> The Pauling bond order between atoms  $i$  and  $j$ ,  $n_{ij}$ , is  $n_{ij} = e^{(r_1 - r_{ij})/0.3}$ , where  $r_{ij}$  is the bond length between atoms  $i$  and  $j$  and  $r_1$  is the bond length for a single bond between atoms  $i$  and  $j$ .<sup>24,56</sup>

<sup>#6</sup> In this chapter, “reaction coordinate” refers specifically to the vibrational normal mode at the transition state that has an imaginary frequency. Displacement of atoms along this normal mode in either direction results in a decrease in energy and movement of the molecule either forward toward products, or back towards reactants. In an  $A_N D_N$  mechanism, the reaction coordinate involves coordinated departure of the leaving group and approach of the nucleophile.

dissociative  $A_N D_N$  and true stepwise  $D_N * A_N$  reactions for both enzymatic and non-enzymatic reactions.

*The structure of the transition state.* TS analysis tends to emphasize enzyme–substrate contacts that promote catalysis, and on exploiting these interactions in designing inhibitors. The focus therefore tends to be on the structure of the transition state. However, an experimental transition state necessarily includes information on the reaction coordinate. Even though the focus of TS analyses tends to be on structure, there is more information about catalysis inherently available from the TS determination process.

#### VERY LOW BOND ORDERS

Glycoside hydrolysis and transfer reactions with  $A_N D_N$  mechanisms are highly dissociative, with leaving group and nucleophile bond orders often in the range of 0.005–0.05. Because KIEs are a roughly logarithmic function of bond order,<sup>#7</sup> a bond order of 0.005 is different than 0.01 from a vibrational point of view, even though it may not be clear what this means structurally. The concept of Pauling bond order arises from empirical observations of molecular structure (e.g., see Ref. 56), which necessarily involved studying bonds in stable molecules. The validity of the concept of bond order for very weak bonds has not been verified experimentally. Some workers have suggested that the usual factor of  $c = 0.3$  used in calculating the Pauling bond order ( $n_{ij} = e^{(r_1 - r_{ij})/c}$ ) should be replaced by  $c \geq 0.6$  for bond orders less than 1.<sup>59,60</sup> The inclusion of leaving groups and nucleophiles with very low bond orders in the TS structure is necessary because of their contribution to the  $A_N D_N$  reaction coordinate KIE; however, the structural interpretation of such low bond orders should be approached with caution.

#### OBSERVABLE KIEs FOR STEPWISE REACTIONS

In an  $A_N D_N$  mechanism only one chemical step is kinetically significant, the concerted approach of the nucleophile and departure of the leaving group. In stepwise mechanisms, either step, or both, may be kinetically significant and contribute to the observable KIEs. In a  $D_N * A_N$  mechanism, the irreversible step can be either leaving group dissociation ( $D_N^\ddagger * A_N$ ) or nucleophilic attack ( $D_N * A_N^\ddagger$ ); or, if the oxocarbenium ion intermediate partitions in both directions, both steps will be partially irreversible and contribute to the observable KIEs. As competitive KIEs always reflect  $k_{cat}/K_M$ , the observable KIEs for a  $D_N * A_N$  kinetic mechanism (equation 1) will reflect changes in this kinetic parameter (equation 2), and are given by equation (3), assuming that  $k_2 \gg k_3$ <sup>58</sup>



<sup>#7</sup> Unpublished data.

$$\frac{k_{\text{cat}}}{K_{\text{M}}} = \frac{k_1 k_3 k_5}{k_2 k_4 \left( 1 + \frac{k_5}{k_4} \left( 1 + \frac{k_3}{k_2} \right) \right)} \quad (2)$$

$$\text{KIE} = \frac{\frac{\alpha_1 \alpha_3}{\alpha_2} \left( \frac{\alpha_5}{\alpha_4} + \frac{k_5}{k_4} \right)}{1 + \frac{k_5}{k_4}} \quad (3)$$

where  $\alpha_n$  is the intrinsic KIE on step  $n$ .

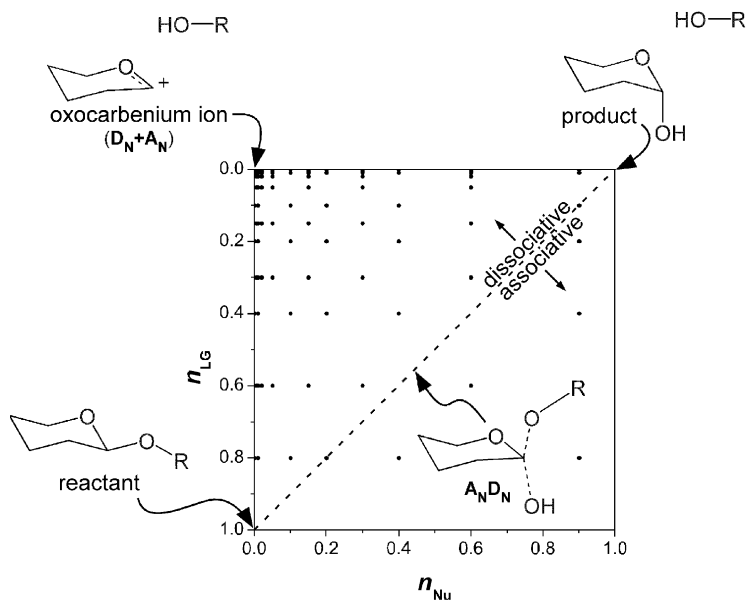
The observable KIEs depend on the partitioning of the oxocarbenium ion intermediate, i.e.  $k_5/k_4$  (equation 3). If the intermediate partitions completely forward to products, then  $k_3$  is the first irreversible step,  $k_5 \gg k_4$ , and  $\text{KIE} = \alpha_1 \alpha_3 / \alpha_2$ . If it is in equilibrium with the reactant, then  $k_5$  is the first irreversible step,  $k_4 \gg k_5$ , and  $\text{KIE} = (\alpha_1 \alpha_3 \alpha_5) / (\alpha_2 \alpha_4)$ .

#### FROM EXPERIMENTAL KIEs TO TRANSITION STATES

The physical basis of IEs has been described in several excellent reviews.<sup>57,61,62</sup> IEs are vibrational phenomena. They reflect the change in vibrational environment of an atom between the initial and final state (reactant and transition state for KIEs, reactant and product for equilibrium isotope effects (EIEs)). If there is a change in the structure of the molecule between the initial and final states, there will be a corresponding change in force constants ( $\approx$  bond strengths) in the bonds making up the molecule. These cause changes in the vibrational normal modes of the molecule, which in turn result in IEs. In deducing a transition state from experimental KIEs, one is, in essence, deducing the (experimentally inaccessible) vibrational spectrum of the transition state.

#### *Electronic structure methods*

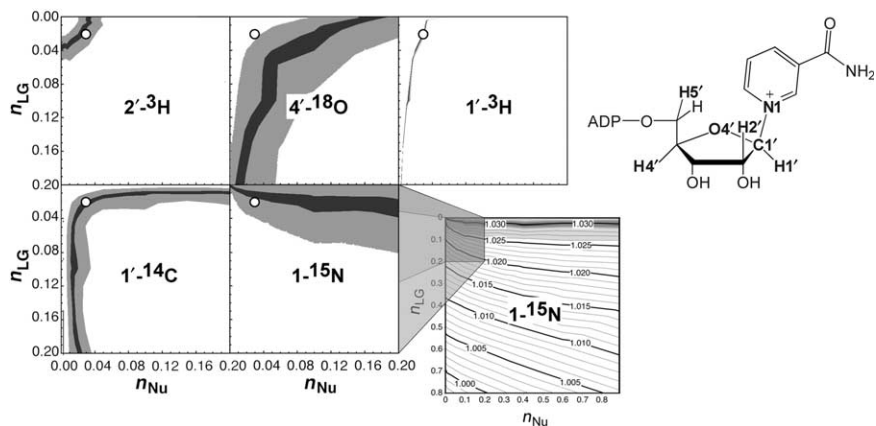
Using electronic structure calculations, it is possible to calculate the structures and vibrational frequencies of reactant and TS molecules. From these, one may calculate IEs. Some authors have suggested it is necessary to use *ab initio* methods at the post-Hartree–Fock level to obtain vibrational frequencies accurate enough for IE calculations.<sup>63,64</sup> Calculations at these levels are computationally expensive, so the “cheapest” available methods are generally used, namely MP2 or density functional theory (DFT) methods. At this level of theory, vibrational frequency calculations can be quite accurate, with overall root mean square errors as low as  $34 \text{ cm}^{-1}$ .<sup>65</sup> Because the frequencies calculated by quantum mechanical methods for a given structure are generally quite accurate, the factor limiting the accuracy of computed IEs is the accuracy of the structure. Thus, one may presume that if calculated and experimental KIEs agree well, then the calculated TS structure is accurate. However, calculated TS structures of reactions in the condensed phase are often not



**Fig. 3** Reaction space for hydrolysis of a glycoside. In this More O'Ferrall–Jencks diagram, the axes are leaving group ( $n_{LG}$ ) and nucleophile ( $n_{Nu}$ ) bond orders. The positions of the reactant glycoside (lower left) and the product (top right) in reaction space are shown. In a pure, stepwise  $D_N + A_N$  ( $S_N1$ ) mechanism, a discrete oxocarbenium ion intermediate is formed by dissociation of the leaving group (top left) before the nucleophile approaches in a separate step. A concerted synchronous  $A_N D_N$  ( $S_N2$ ) mechanism would follow the dashed diagonal line, with approach of the nucleophile precisely equal to loss of the bond order to the leaving group. A dissociative  $A_N D_N$  mechanism would pass through a transition state closer to the top left corner. Each point on the graph represents a trial TS structure generated by the structure interpolation method for which KIEs are calculated.

accurate, partly because of inherent limitations in the computational models, but mostly because solvents and enzymes change transition states. If calculated and experimental KIEs cannot be made to match, there is nothing more that can be done using electronic structure methods. Frequency calculations on quantum mechanical models are valid only at stationary points, i.e. energetic minima or saddle points; vibrational frequencies calculated for arbitrary non-optimized structures, or ones optimized with constraints, have no physical meaning.

Computational models that combine a high level quantum mechanical model of the reaction site surrounded by a layer of lower level semi-empirical or molecular mechanical atoms in the surrounding solvent or enzyme environment will one day make electronic structure calculations of transition states in the condensed phase routine, but these are still some distance in the future. At present, if KIEs calculated from electronic structure models do not match the experimental KIEs, it is necessary to use BOVA to find the transition state.



**Fig. 4** Match of calculated to experimental KIEs in reaction space for the diphtheria toxin-catalyzed hydrolysis of  $\text{NAD}^+$  (see Ref. 17): (bottom right panel) contour plot of calculated  $1\text{-}^{15}\text{N}$  KIEs throughout reaction space; (bottom middle) expansion of the dissociative section of reaction space for  $1\text{-}^{15}\text{N}$  KIEs. The shading shows the areas in each reaction space plot where the calculated KIEs match the experimental KIEs exactly (dark gray) or within the 95% confidence interval (light gray). The open circle shows the location of the experimentally determined transition state in reaction space.

#### *Bond order vibrational analysis (BOVA) and structure interpolation*

Using BOVA, one may calculate KIEs for any pair of reactant and TS structures. There is no requirement to use structures that are stationary points according to electronic structure calculations. One creates a vibrational model that treats the reactant and TS molecules as perfect harmonic oscillators with atoms (point masses) connected together with bonds (massless springs) with defined force constants. If the vibrational model and the structure of the reactant are accurate, then the TS model that gives calculated KIEs matching the experimental ones is considered the experimental transition state.

The *vibrational model* is (1) the set of internal coordinates controlling molecular vibrations, i.e. a list of bond stretches and different kinds of bends (bond angle, out-of-plane, linear, and torsional); (2) the force constants associated with each internal coordinate; and (3) coupling constants between internal coordinates to generate the reaction coordinate. KIEs are calculated from vibrational frequencies, which are in turn calculated using the inputted structures and the vibrational model. Vibrational models have been discussed in greater detail elsewhere.<sup>24,43,56,66</sup> The programs available for BOVA are BEBOVIB<sup>24,25</sup> and VIBIE.<sup>67,68</sup>

*Structure interpolation.* In the past, TS structures for BOVA analysis were generated by the “*ad hoc*” method whereby one searches for the transition state by adjusting the TS structure in an iterative process until the calculated KIEs match the experimental ones. Structural parameters expected to contribute to the KIEs are adjusted and the KIEs recalculated. This approach may not find the best or only solution, and may include a solution that is chemically unreasonable. Enzyme-

produced effects may not be recognized since it is not clear what the expected KIEs are. Also, the modeling process is extremely time consuming. In order to address the limitations of the *ad hoc* method, the structure interpolation approach to BOVA was developed.<sup>43,69</sup> An algorithm describes the structure of a molecule as a function of its position in reaction space (Fig. 3) and generates trial TS structures throughout reaction space. The interpolation method relies on electronic structure calculations, X-ray crystallographic structures and other experimental evidence. In the interpolation algorithm, all geometrical parameters are varied simultaneously in a systematic way. Using BOVA, predicted KIEs are then calculated for each isotopic label for every trial TS structure. The predicted KIEs are plotted as a contour diagram for each isotopic label (Fig. 4, bottom right) and the areas where the calculated and experimental KIEs match are plotted for each isotopic label. Ideally, there will be one unique point in reaction space where the predicted and experimental KIEs for every isotopic label match each other. This is the transition state.

This approach has a number of advantages over the *ad hoc* approach, including both greater speed and greater accuracy. A further advantage of the structure interpolation approach, especially with a unified model (see below), is that a model is created of how structure, and therefore KIEs, change throughout reaction space. Any deviation from that model, such as might be caused by an enzyme, will be recognized by the deviation from the model.

*Unified models.* If experimental KIEs are available for several related reactions, it is possible to construct a “unified model” of the reaction to give the highest possible accuracy TS structures.<sup>43</sup> A unified model differs from any other TS analysis only in that a single vibrational model and structure interpolation model is used to determine transition states for several different reactions of a given type. For example, the transition states of four hydrolytic and two adenosine 5'-diphosphate (ADP)-ribosylation reactions of oxidized nicotinamide adenine dinucleotide (NAD<sup>+</sup>) were determined using a unified model. The fact that this model worked for all these different reactions lent support to the correctness of each step in the process.

*Differences between modeling approaches.* One consistent difference between transition states determined by the *ad hoc* and structure interpolation methods is that the residual leaving group bond order is lower in TS structures determined by structure interpolation. This is a result of the fact that with structure interpolation, the structure of the leaving group ring is varied throughout reaction space along with the ribosyl ring. The increase in bond orders within the ring in response to the loss of bond order in the *N*-glycosidic bond is more accurately reflected. It therefore takes a greater extent of bond breakage to the leaving group to result in the same loosening of the vibrational environment of the departing atom. The practical upshot is that a TS structure is obtained using structure interpolation that has lower bond order to the leaving group ( $n_{\text{LG}}$ ) and higher bond order to the nucleophile ( $n_{\text{Nu}}$ ). The transition state for cholera toxin-catalyzed NAD<sup>+</sup> hydrolysis was reported to have  $n_{\text{LG}} = 0.09$ , and  $n_{\text{Nu}} = 0.005$  by *ad hoc* TS modeling,<sup>70</sup> but  $n_{\text{LG}} = 0.02$ , and  $n_{\text{Nu}} = 0.02$  using structure interpolation that accounts for changes in the nicotinamide ring.<sup>17</sup>



Similarly, inosine hydrolysis catalyzed by inosine–uridine-specific nucleoside hydrolase (IU-NH) was modeled by *ad hoc* methods with  $n_{LG} = 0.19$  and  $n_{Nu} = 0.005$ ,<sup>71</sup> but has been reanalyzed recently using structure interpolation, which gives a TS structure with  $n_{LG} = 0.05$  and  $n_{Nu} = 0.06$  (unpublished results). It is worth emphasizing that these are small changes in structure, reflecting refinement of KIE interpretation over the years.

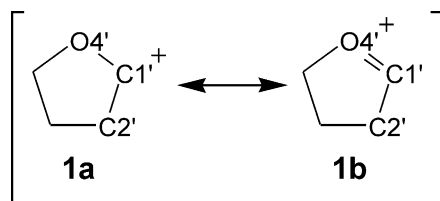
Because the process of TS analysis by BOVA has evolved between early studies cited in this chapter and more recent ones, the amount of detail available for different TS structures varies, which will be reflected in the discussion of some of these studies.

### 3 TS analysis: results and recent developments

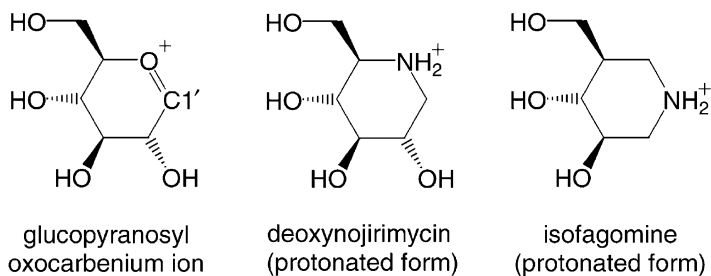
#### THE NATURE OF THE OXOCARBENIUM ION

Whatever the exact mechanism of a particular glycoside hydrolysis or transfer reaction, nucleophilic substitution at the glycosidic bond involves the sugar becoming either an oxocarbenium ion intermediate or passing through a transition state that is highly oxocarbenium ion-like. Catalytic strategies that stabilize a discrete oxocarbenium ion will also likely be effective for an oxocarbenium ion-like  $A_ND_N$  transition state. For this reason, we will discuss interactions as stabilizing an oxocarbenium ion, even when it is known that a particular reaction has an  $A_ND_N$  mechanism and does not form a discrete intermediate.

Understanding catalytic mechanisms and designing inhibitors requires an understanding of the structure and charge distribution of the oxocarbenium ion. The resonance structures of an oxocarbenium ion imply a molecule that is somewhere between a carbocation (**1a**) and an oxonium ion (**1b**).



Information on the nature of the oxocarbenium ion from a variety of experimental and computational approaches has indicated that the oxonium-like resonance form **1b** predominates.<sup>72–77</sup> Evidence emerging from TS analysis supports this model. In TS structures derived from both *ad hoc*<sup>27,28,70,71,78–81</sup> and structure interpolation techniques,<sup>17,47,69</sup> and supported by electronic structure calculations, essentially all the loss in bond order upon leaving group departure is compensated by increases in the C1'–O4' and C1'–C2' bond orders. In  $\text{NAD}^+$  hydrolysis reactions, the total bond



**Fig. 5** Structures of the presumed oxocarbenium ion of glucose and the protonated forms of deoxynojirimycin and isofagomine, potent inhibitors of many  $\beta$ -glycosidases.

order to C1' ( $\sum n_{C1'}$ ) was higher in the transition state than in the reactant; the loss of bond order to the leaving group was compensated by an even larger increase in the bond orders between C1' and the other ribosyl ring atoms C2', O4' and H1'.

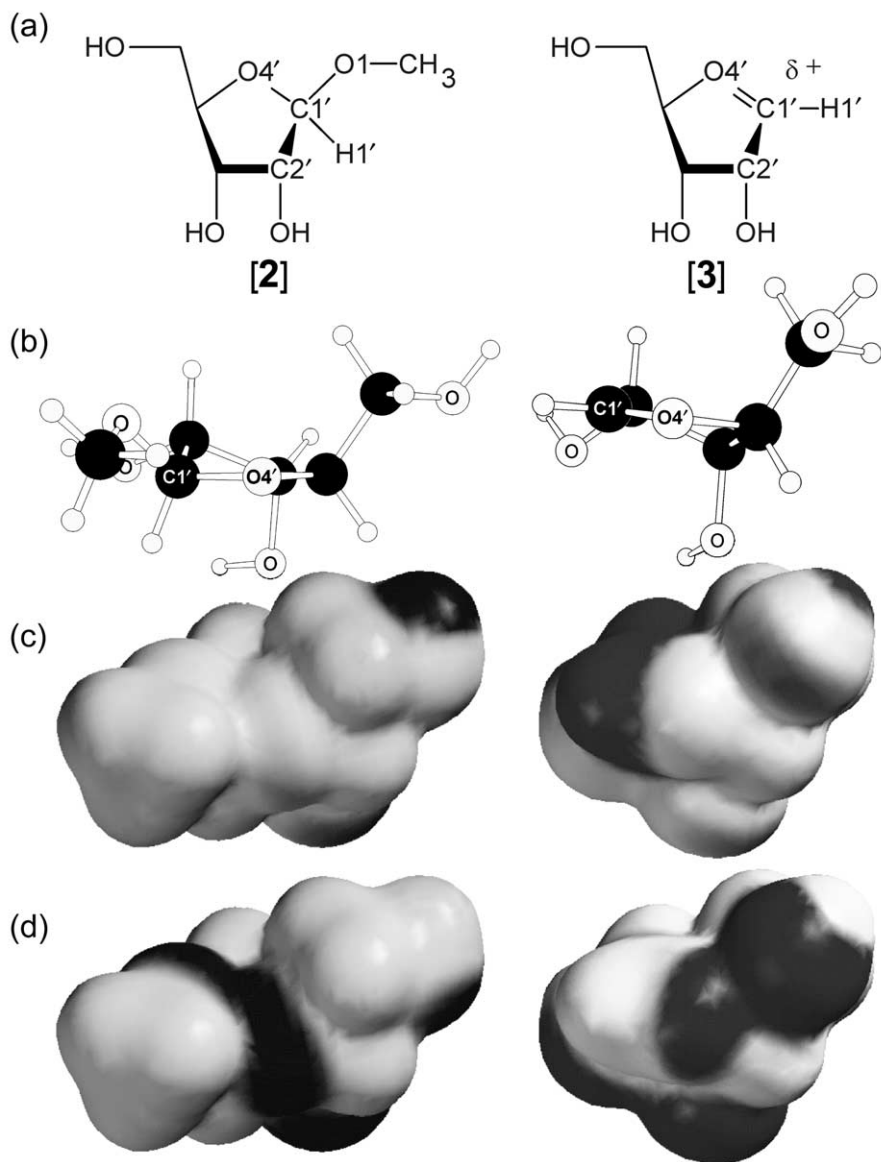
There is evidence that at least some enzymes specifically stabilize the oxocarbenium ion portion of the TS molecule to promote catalysis.<sup>82</sup> The question of how enzymes may stabilize the oxocarbenium ion has generally focused on the change in charge distribution and sometimes on the positive charge that is presumed to accumulate on the ring oxygen. The fact that iminosugar compounds such as deoxynojirimycin (Fig. 5) are effective glycosidase inhibitors<sup>31,83–93</sup> would tend to support this view. There are several lines of evidence, however, that point to other interactions. Electronic structure calculations indicate that the ring oxygen of the oxocarbenium ion is not positively charged, and experimental evidence supports this conclusion. Electronic structure calculations indicate that the ring oxygen in a glycoside bears significant negative charge,  $-0.33$  in **2** (Fig. 6a, Table 1). When the glycosidic bond is broken and an oxocarbenium ion formed,  $\pi$ -bonding develops between C1' and O4'. The charge on O4' increases more than any other atom in the molecule, but only becomes  $-0.03$  in the oxocarbenium ion. Assigning charges to

**Table 1** Selected atomic charges and bond orders in compounds **2** and **3** (see also Fig. 6)

Atom	Charge [ $q(e^-)$ ] <sup>a</sup>		Bond	Pauling bond order ( $n_{ij}$ ) <sup>b</sup>	
	<b>2</b>	<b>3</b>		<b>2</b>	<b>3</b>
C1'	0.04	0.22	C1'–O4'	0.97	1.72
O4'	$-0.33$	$-0.03$	C1'–C2'	1.00	1.09
H1'	0.14	0.26	C1'–H1'	0.95	0.99
O1'	$-0.29$	–	C1'–O1	1.06	–

<sup>a</sup>Mulliken atomic charges on atoms in model compounds.

<sup>b</sup> $n_{ij} = e^{(r_1 - r_{ij})/0.3}$ , where  $r_{ij}$  is the bond length between atoms  $i$  and  $j$ , and  $r_1$  is the bond length for a single bond.<sup>24,56</sup> Single bond lengths ( $r_1$ ): C–H = 1.09 Å, C–C = 1.526 Å, C–O = 1.41 Å.



**Fig. 6** Changes in charge distribution on forming an oxocarbenium ion. (a) Model compounds for glycoside **[2]** and oxocarbenium ion **[3]**. (b) Stick models of **[2]** and **[3]**. (c) Areas of positive electrostatic potential (electron deficient) are shown in gray shading. (d) Areas of negative electrostatic potential (electron rich) are shown in gray shading. Because **2** is neutral and **3** is positively charged, the electrostatic potentials are plotted on different scales, with the shading showing electrostatic potential relative to the average for each molecule. Optimizations were performed using a hybrid DFT method with Becke's exchange

functional<sup>220</sup> and Perdew and Wang's correlation functional,<sup>221</sup> with the 6-31 + G\*\* basis set (RB3PW91/6-31 + G\*\*) using Gaussian-98.<sup>222</sup> The isodensity surface is plotted at 0.002 e/bohr<sup>3</sup>.

atoms in molecules is somewhat arbitrary; however, different methods give essentially the same result, as do calculations of electrostatic potential (Fig. 6d). The exact results for these calculations will depend on the identity of the oxocarbenium ion and its environment. The important result is that the ring oxygen does not accumulate significant positive charge in the oxocarbenium ion. This conclusion is supported by previous calculations at the semi-empirical level.<sup>73,75</sup> This implies that an enzyme active site with a negative charge located adjacent to the ring oxygen in the oxocarbenium ion would not be catalytically effective.

In a recent study, Withers and coworkers concluded that the reactivity of *O*-glycopyranosides is well explained by a Kirkwood–Westheimer model of field effects with all of the charge generated in the oxocarbenium ion being transferred to the ring oxygen.<sup>77</sup> Their analysis is consistent with the model of oxocarbenium ion structure discussed above because the Kirkwood–Westheimer model requires that the charge at the ring oxygen increases; it does not necessarily require that the charge becomes positive.

The computational results are supported by four lines of experimental evidence.

- (1) Aza-sugar inhibitors such as isofagomine, where the nitrogen atom is situated in a position analogous to the anomeric carbon, are extremely potent inhibitors of  $\beta$ -glycosidases, and often better inhibitors than the iminosugar inhibitors like deoxynojirimycin where the nitrogen atom is located at a position analogous to the ring oxygen.<sup>94–99</sup>
- (2) The pH versus  $K_i$  profiles of iminosugar inhibitors indicate that in at least some cases it is the neutral, unprotonated form that binds the enzyme, while in other cases it is the protonated form.<sup>84,100</sup> Some enzymes that bind the protonated form also bind with similar inhibition constants to compounds methylated at the ring nitrogen and therefore bearing a permanent positive charge. This demonstrates that there is not a tight, direct interaction between the enzyme and a positively charged amino group.
- (3) The X-ray crystallographic structures of enzymes complexed with iminosugar inhibitors do not show strong interactions between the ring nitrogen and groups on the enzyme.<sup>26,101,102</sup> As the inhibitors are nearly isosteric with the substrate molecules, this can be taken as an argument against stabilization of the oxocarbenium ion through contacts with the ring oxygen.
- (4) Further evidence comes from a model of the DTA·TS complex for NAD<sup>+</sup> hydrolysis based on the X-ray crystal structure of DTA·NAD<sup>+</sup>.<sup>17,103</sup> In the complex, the positive charge that would accumulate on the anomeric carbon at the transition state was located directly adjacent to the carboxylate of a glutamate residue that is completely conserved in the bacterial toxin sequences.

The nearest possible protein contact to the ring oxygen was with the hydroxyl group of Tyr65, with an oxygen–oxygen distance of 3.1 Å. There were no negative charges located near the ring oxygen. The same features were observed in the docking of the TS structure of pertussis toxin-catalyzed ADP-ribosylation of protein G<sub>iα1</sub> with the enzyme.<sup>47</sup> Thus, the structures of enzyme·TS models also support the idea that positive charge accumulates on the anomeric carbon rather than on the ring oxygen in an oxocarbenium ion.

Taken together, the evidence above suggests that the oxocarbenium ion intermediate or oxocarbenium ion-like transition state has significant C=O double bond character from charge delocalization/resonance stabilization, but that the positive charge accumulates on the anomeric carbon, C1', in spite of the fact that the oxygen atom is formally trivalent. Because of extensive  $\pi$ -bonding stabilization from the ring oxygen, the positive charge on C1' is much less than it would be in an unstabilized carbocation.

*Intermediate lifetime.* The lifetime of the enzyme·oxocarbenium ion complex in D<sub>N</sub> \* A<sub>N</sub> mechanisms cannot be determined by KIE studies. It must exist for at least a few bond vibrations (*ca.* 10<sup>-12</sup> s), but there is no upper limit on its lifetime aside from *k*<sub>cat</sub>.

#### NON-CHEMICAL STEPS

It is crucial in performing TS analysis to know exactly which step of the reaction the experimental KIEs reflect. Using isotope-trapping experiments, it is possible to demonstrate whether formation of the Michaelis complex, E·S, is kinetically significant, and if necessary, to find conditions where it is not. However, internal steps<sup>#8</sup> can also complicate the interpretation of KIEs. These can include, but are not limited to (1) establishment of equilibria between different enzyme-bound intermediates, (2) isotopically insensitive steps, such as conformational changes in the enzyme or substrate, or (3) substrate channeling.

There are at least four instances where non-chemical steps were manifested in KIEs, although in each case the nature of the non-chemical step was not clear. In the sialyltransfer reaction catalyzed by  $\alpha(2 \rightarrow 6)$  sialyltransferase using cytidine monophosphate glycoside of *N*-acetylneuraminic acid (CMP-NeuAc) as the glycosyl donor (equation 4), Michaelis complex formation was kinetically significant,<sup>104</sup> but even after compensating numerically for this, the KIEs were small and inconsistent with any mechanism with only chemical steps being kinetically significant. Later experiments using an alternate substrate, uridine 5'-monophosphate (UMP)-NeuAc, yielded KIEs consistent with an oxocarbenium ion(-like) transition state.<sup>48</sup> This is consistent with a non-chemical step being kinetically significant in the reaction with CMP-NeuAc. A related result is that there

<sup>#8</sup> An internal step is any step that occurs between formation of the Michael complex, E·S, and dissociation of the enzyme·product complex, E·P.



was large and therefore changes were easily observed. The decrease in  $1'/^3\text{H}$  KIE at temperatures  $< 20^\circ\text{C}$  or  $\text{pH} < 7.5$  was interpreted as indicating that some isotopically insensitive step had become at least partially irreversible. For example, if a conformational step after the chemical step became slower under non-optimal conditions, then the lifetime of the enzyme·nicotinamide·ADP-ribosyl- $\text{G}_{i\alpha 1}$  complex might become long enough for some of the complex to undergo the reverse reaction to enzyme· $\text{NAD}^+$ · $\text{G}_{i\alpha 1}$ . In this case, enzyme·nicotinamide·ADP-ribosyl- $\text{G}_{i\alpha 1}$  would partition both backward and forward, and the chemical step would be only partially irreversible. It is equally possible that the kinetically significant isotopically insensitive step occurred before the chemical one.

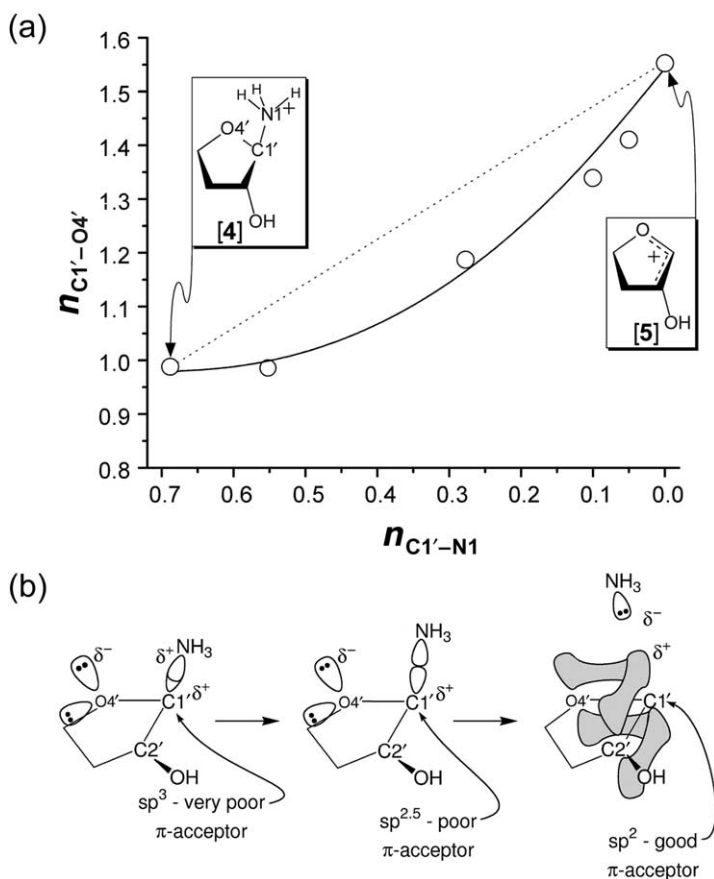
In the depurination of RNA catalyzed by ricin toxin A-chain (RTA), the reaction mechanism involved formation of equilibrium population of an oxocarbenium ion intermediate followed by an isotopically insensitive irreversible step (Fig. 7).<sup>46</sup> The experimental KIEs were most consistent with the calculated EIEs for oxocarbenium ion formation. This is what would be expected for a mechanism involving freely reversible oxocarbenium ion formation followed by an isotopically insensitive step.

In the yeast  $\alpha$ -glucosidase-catalyzed hydrolysis of 4-nitrophenyl- $\alpha$ -D-glucopyranoside,<sup>49</sup> the primary leaving group  $^{18}\text{O}$  KIE was unity, 1.001, and the  $\alpha$ -secondary  $^2\text{H}$  KIE was small, 1.01. However, the  $\alpha$ - and  $\beta$ -secondary KIEs for hydrolysis of  $\alpha$ -D-glucopyranosyl 4-bromoisquinolinium bromide were large, 1.21 and 1.13, respectively. This implied that a partially irreversible conformational change prevented KIEs of the chemical step(s) from being observed for 4-nitrophenyl- $\alpha$ -D-glucopyranoside where the dominant reactant conformation is the  $^4\text{C}_1$  chair. Intrinsic KIEs were determined for  $\alpha$ -D-glucopyranosyl 4-bromoisquinolinium bromide where the reactant conformation is  $^1\text{S}_3$  skew or twist. It was therefore assumed that the skew conformation more closely resembles the transition state, whereas compounds in chair conformations must undergo partially irreversible conformational changes prior to the chemical steps.

#### TRANSITION STATE IMBALANCE

One contribution of TS analysis studies to understanding catalysis has been the observation of TS imbalance effects in the ADP-ribosylation of protein  $\text{G}_{i\alpha 1}$  by pertussis toxin.<sup>47</sup> This observation has previously been discussed only in passing.<sup>43, 69</sup>

In most chemical reactions, several processes must occur between reactants and products. The main processes are the bonds that must be made or broken in the overall reaction. In addition to the main processes, several other processes may occur, including solvation/desolvation, charge delocalization or resonance stabilization. In its most general form, TS imbalance (also known as the Principle of Non-perfect Synchronization)<sup>105,106</sup> simply states that not all these processes occur synchronously.

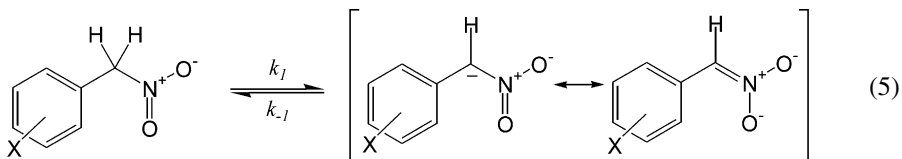


**Fig. 8** TS imbalance effects on C1–N1 bond breakage in an *N*-glycoside analogue. (a) The structure of the model compound (**4**) was fully optimized using a hybrid DFT method, then the C–N bond was held fixed at increasing bond lengths as the rest of the molecule was re-optimized. Compound **5** was optimized in the absence of the leaving group. The Pauling bond order of the C1–O4 bond ( $n_{C1-O4}$ ) in the resulting structures is plotted against the (fixed) Pauling bond order of the C1–N1 bond ( $n_{C1-N1}$ ). The dotted line shows the linear relationship between  $n_{C1-O4}$  and  $n_{C1-N1}$  that would be expected in the absence of TS imbalance. The solid line is the curve fitted to the equation  $\Delta n_{C1-O4} = \chi(n_{C1-N1})^m$ , where the optimal value of the exponent  $m$  was found to be 1.7. Optimizations were performed as in Fig. 6. (b) Molecular orbital rationalization of TS imbalance. See text for details.

An archetypal example of TS imbalance is the nitroalkane anomaly.<sup>107,108</sup> The rate ( $k_1$ ) of deprotonation of aryl nitroalkanes is more sensitive to substituents on the aryl ring than the equilibrium constant ( $K_1 = k_{-1}/k_1$ ), as reflected in an unusually large value of the Brønsted parameter,  $\alpha_{CH}$  (equation 5). In addition,  $\beta > 1.0$  for  $k_1$  and  $\beta < 0$  for  $k_{-1}$ . These data have been interpreted as showing that



while there is strong charge delocalization in the product arylnitronate anion, charge delocalization is not well developed at the transition state even though the main process, C–H bond breakage, is almost complete. The nitroalkane anomaly represents a common form of TS imbalance where, when there is an increase in charge delocalization or resonance stabilization between the reactants and products, it is less advanced at the transition state relative to the main processes than in the products.<sup>#9</sup> The converse is also true; charge localization or loss of resonance stabilization tends to be more advanced in the transition state relative to the main processes than in the products.



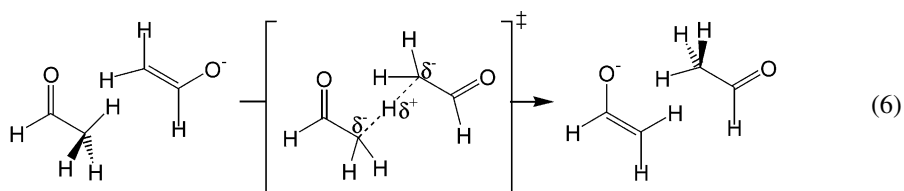
TS imbalance has been studied in detail in contexts such as proton transfer,<sup>105,106,109,111</sup> but was unexpected (by us) in glycoside chemistry. However, the experimental KIEs for ADP-ribosylation of protein  $G_{i\alpha 1}$  by pertussis toxin could not be successfully interpreted using the structure interpolation approach while assuming that variation of the ribosyl ring structure was fully synchronous with the main processes, namely breaking the leaving group bond and forming the nucleophile bond.

Electronic structure calculations on a model (**4**) were used to investigate TS imbalance effects on oxocarbenium ion (**5**) formation, where the main process is breaking the C–N bond (Fig. 8). In these calculations, the structure of **4** was fully optimized, then the length of the C1–N1 bond was fixed at increasing values and the rest of the molecule re-optimized. The extent of charge delocalization/resonance stabilization was followed by plotting the Pauling bond order between C1 and O4,  $n_{C1-O4}$ , as a function of the fixed bond order between C1 and N1,  $n_{C1-N1}$ . This was the bond that underwent the largest change between **4** ( $n_{C1-O4} = 0.99$ ) and **5** ( $n_{C1-O4} = 1.55$ ). The increase in  $n_{C1-O4}$  lagged behind the decrease in  $n_{C1-N1}$ . This was expected by analogy to the nitroalkane anomaly, where resonance stabilization lags the main process.

According to Kresge's model,<sup>107</sup> the lag in resonance stabilization can be modeled as  $\Delta n_{C1-O4} = \chi(\Delta n_{C1-N1})^m$ , where  $m = 2$  and  $\chi$  is some proportionality constant. Application of this equation to proton transfers in aqueous solution suggests values of  $m$  between 2 and 3.<sup>105</sup> In the current study, the best fit was obtained with  $m = 1.7$ . Calculations were performed on oxocarbenium ion

<sup>#9</sup> The language used to describe TS imbalance (e.g., “lag in charge delocalization”, or “resonance stabilization developing late”) has tended to imply a kinetic effect, namely that certain processes such as charge delocalization occur too slowly to keep up with the main processes. As shown by Bernasconi and Wenzel<sup>109,110</sup> and in the results described here, it is a thermodynamic effect. In structures where resonance stabilization “lags” the main processes, these are the most thermodynamically favorable extents of resonance stabilization.

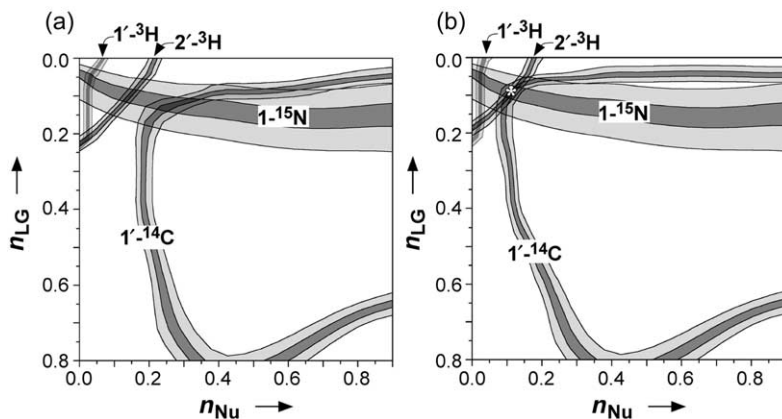
formation with a variety of leaving groups and substituents, and TS imbalance was observed in every system examined, with the extent of TS imbalance depending on the identity of the leaving group and cation being formed (data not shown). TS imbalance was previously studied computationally for the carbon-to-carbon proton transfer between acetaldehyde and its enolate anion.<sup>109,110</sup> Using atomic charge rather than bond order to measure the extent of TS imbalance, values of  $m = 1.1-2.3$  were observed. It was suggested TS imbalance arises, at least in part, as a result of positively charged protons helping to stabilize and localize the negative charge on the carbon atoms (equation 6). The fact that TS imbalance was also observed in oxocarbenium ion formation, where such an effect could not be operative, implies that the structural manifestations of TS imbalance are universal phenomena whenever there is rehybridization of atoms and changes delocalization/resonance stabilization.<sup>#10</sup>



Although the physical basis of TS imbalance is not well understood, one intuitive explanation of the current case is that in **4** the ring oxygen is a good  $\pi$ -bond donor because of its lone pair electrons but C1 is a very poor  $\pi$ -bond acceptor because it is maintained in an  $sp^3$ -hybridized state by its bond to N1. There is not a concomitant increase in  $n_{C1-O4}$  as the C1–N1 bond is broken because C1 remains a poor  $\pi$ -bond acceptor in the continued presence of the C1–N1 bond. It is only as the C1–N1 bond becomes almost completely broken that C1 becomes a good  $\pi$ -bond acceptor and  $n_{C1-O4}$  increases sharply (Fig. 8).

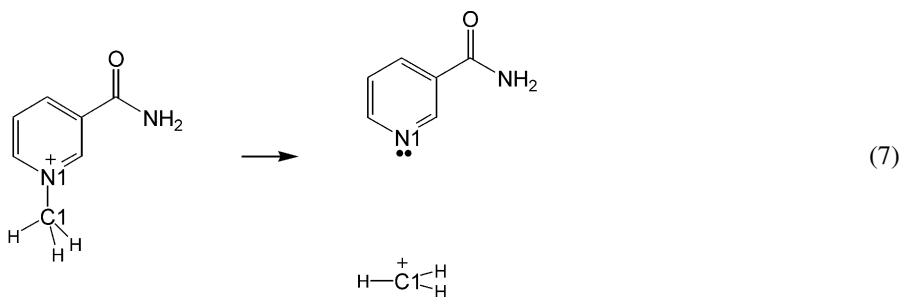
This explanation is complementary with the “fraction of a fraction” explanation advanced by Kresge,<sup>107</sup> which says that development of resonance stabilization will, at most, be proportional to the loss of C1'–N1 bond order. However, the rehybridization of C1' from tetrahedral to planar is not complete, resulting in only partial resonance stabilization due to poorer electronic overlap. Thus, resonance stabilization is only a fraction of the fraction of C1'–N1 bond breakage. These explanations are also consistent with the idea that TS imbalance is correlated with changes in atom hybridization, which is in turn consistent with the results of calculations on the dissociation of methyl nicotinamide (equation 7). The sum of total bond orders to N1 ( $\sum n_{N1}$ ) was a linear function of the main process, i.e. loss of the N1–C1 bond, as was the sum of N1–C bond orders within the ring (data not shown). The essential difference between this and the oxocarbenium ion example is

<sup>#10</sup> There is some question whether the unusual reactivity properties manifested in the nitroalkane anomaly would occur in the gas phase,<sup>108</sup> which is a separate issue.



**Fig. 9** Evidence for TS imbalance in the ADP-ribosylation of protein  $G_{i\alpha 1}$ . The shading shows the areas in reaction space where the calculated KIEs match the experimental KIEs exactly (dark gray) or within the standard deviation (light gray) for the indicated isotopic label. The asterisk indicates the experimentally determined transition state. Isotopic labels are as shown in Fig. 4. The results are shown for calculations done using the structure interpolation approach (a) without TS imbalance and (b) with TS imbalance. This figure is based on Fig. 4 of Ref. 47 with minor modifications of the vibrational model.

that there is no change in hybridization on the nitrogen atom N1; it is  $sp^2$ -hybridized in both the reactant and product structures.



As mentioned above, it was necessary to include TS imbalance effects in the TS analysis of the ADP-ribosylation of protein  $G_{i\alpha 1}$ . Once they were included, the calculated and experimental KIEs at  $1\text{-}^{15}\text{N}$ ,  $1'\text{-}^{14}\text{C}$ , and  $2'\text{-}^3\text{H}$  matched very well (Fig. 9), though the match of  $1'\text{-}^3\text{H}$  was poor in both the cases (see Section 4). The differences between the structure interpolation models that included or neglected TS imbalance were small, with differences in bond length of  $\Delta r_{\text{C1}'\text{-O4}'} = -0.028 \text{ \AA}$ , and  $\Delta r_{\text{C1}'\text{-C2}'} = -0.012 \text{ \AA}$ ,  $\Delta r_{\text{C1}'\text{-H1}'} = 0.006 \text{ \AA}$ . That changes this small could be detected illustrates an important property of using unified models in structure interpolation, namely that they can detect deviations from a model with great

sensitivity. It was possible to detect TS imbalance only because of the deviation from the unified model that had been successful in the TS analysis of four  $\text{NAD}^+$  hydrolysis reactions. It was not detected using the *ad hoc* method.<sup>81</sup> Secondly, the smallness of these differences show that differences in structure can be determined more sensitively than the absolute structure. TS structures are not accurate to within 0.01 Å because they are based on reference structures derived from crystal structures and calculations, both of which have  $>0.01$  Å errors in atom position. However, deviations from the unified model developed for  $\text{NAD}^+$  reactions were detected with great sensitivity.

What is the significance of TS imbalance to the reactivity of glycosides? Probably little. Bernasconi has suggested that resonance stabilization is associated with barriers to intrinsic reaction rates.<sup>105</sup> This can be rationalized in terms of  $\pi$ -bonding electrons being present in the path of the incoming nucleophile, increasing the barrier to nucleophilic attack. It has been shown that there is a significant intrinsic barrier to nucleophilic addition to some carbon cations,<sup>112</sup> and that the extent of resonance stabilization correlates with a reduction of intrinsic rates; however, Richard has shown that the intrinsic barriers for nucleophilic attack on oxocarbenium ions are much smaller than other types of cations.<sup>113</sup> This implies that the barrier to the highly favorable addition of thiolate to a ribooxocarbenium ion will be negligible. The greatest significance of the observation of TS imbalance may be to illustrate the accuracy needed in both KIE measurements and interpretation to derive all the available mechanistic detail for reactions.

#### SECONDARY KIEs

A secondary KIE is any KIE on an atom not involved in the bond making or breaking steps of a reaction. Secondary KIEs are designated in terms of the number of bonds separating the isotopic label from the site where chemistry occurs; thus, in aldoses, the  $1'$ - $^3\text{H}$  KIE is an  $\alpha$ -secondary KIE, the  $2'$ - $^3\text{H}$  KIE is a  $\beta$ -secondary KIE. Because secondary KIEs are generally smaller in magnitude than primary KIEs, it is most commonly hydron<sup>#11</sup> KIEs that are measured. However, secondary  $^{13}\text{C}$ ,  $^{14}\text{C}$ ,  $^{15}\text{N}$ , and  $^{18}\text{O}$  KIEs have been measured, and are large in some cases.<sup>17,50,54,69</sup>

Binding isotope effects on forming a Michaelis complex can be significant,<sup>15,114,115</sup> which could lead to the question of whether KIEs can be interpreted in terms of transition states if there are isotope effects on forming the enzyme-substrate complex. Isotope effects on a given step contribute to the observable KIEs only if that step is kinetically significant. For KIEs on  $k_{\text{cat}}/K_{\text{M}}$ , only

<sup>#11</sup> An unspecified isotope of hydrogen,  $^1\text{H}$ ,  $^2\text{H}$ , or  $^3\text{H}$ .

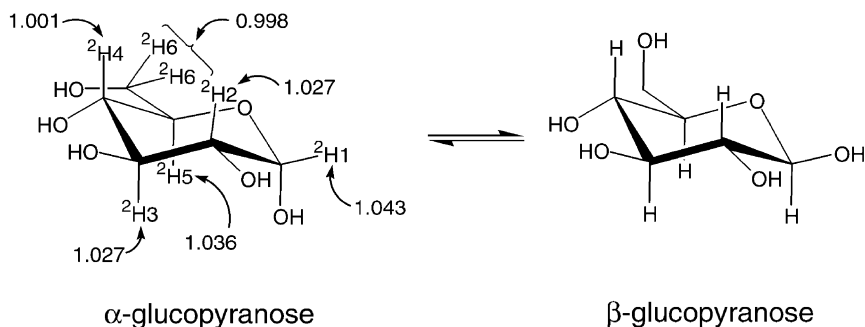
the irreversible step(s) contribute to the observable KIEs, whereas for KIEs on  $k_{\text{cat}}$  (or  $V_{\text{max}}$ ) only the rate-limiting step(s) are relevant.<sup>#12</sup>

### *$\alpha$ -Secondary hydron KIEs*

Early on,  $\alpha$ -secondary hydron KIEs were used to diagnose the mechanisms of glycosidic reactions, and there are many reactions for which that was the only KIE measured.  $^2\text{H}$  KIEs on the order of 1.08–1.17 were almost invariably observed. Instances of small KIEs can now likely be attributed to kinetically significant substrate binding (commitment to catalysis). Large  $\alpha$ -secondary hydron KIEs are a sign of either a highly dissociative  $A_{\text{N}}D_{\text{N}}$  or a  $D_{\text{N}} * A_{\text{N}}$  mechanism because the rehybridization of the anomeric carbon toward  $\text{sp}^2$  and the decreased steric crowding around  $\text{C1}'$  gives increased freedom in the out-of-plane bending modes of  $\text{H1}'$ .<sup>116,117</sup> In a synchronous  $A_{\text{N}}D_{\text{N}}$  mechanism, an inverse KIE at  $\text{H1}'$  would be expected.<sup>118</sup>  $\alpha$ -Secondary hydron KIEs have been studied in detail both experimentally and theoretically,<sup>116,118–122</sup> and a great deal of that knowledge has been summarized by Matsson and Westaway.<sup>117</sup> Until recently, there was debate about what determines the magnitude of  $\alpha$ -secondary hydron KIEs. It has become clear that while there is an inverse contribution from the shortening of the  $\text{C1}'\text{--H1}'$  bond length in an oxocarbenium ion(-like) transition state, this contribution is similar in different transition states and the factor that determines the size of the KIE in a given reaction is the out-of-plane bending modes. These can vary from inverse to large and normal, depending on the TS structure.

Beyond these general trends, however, the detailed interpretation of  $\alpha$ -secondary hydron KIEs in glycosidic reactions has proven problematic. As a specific example, the  $1'/\text{-}^3\text{H}$  KIEs for pertussis toxin-catalyzed reactions were  $1.21 \pm 0.01$  for  $\text{NAD}^+$  hydrolysis,<sup>80</sup> and  $1.20 \pm 0.01$  for the ADP-ribosylation of protein  $\text{G}_{\text{ia1}}$ .<sup>47</sup> The experimental  $1'/\text{-}^3\text{H}$  KIEs were within experimental error of each other in spite of the fact that the transition states were different, with the ADP-ribosylation transition state being more synchronous than the hydrolysis reaction ( $n_{\text{LG}}$  and  $n_{\text{Nu}}$  were 0.05 and 0.001 for hydrolysis, and 0.11 and 0.09 for ADP-ribosylation, respectively). Based on the BOVA vibrational model used in modeling  $\text{NAD}^+$  transition states, the  $1'/\text{-}^3\text{H}$  KIE for the ADP-ribosylation was predicted to be 1.055, which is in general

<sup>#12</sup> This can be rationalized as follows. Consider an enzymatic reaction that displays ideal Michaelis–Menten kinetics, i.e. equilibrium formation of a Michaelis complex, followed by an irreversible chemical step to form products. Further assume that Michaelis complex formation involves one specific enzyme-substrate contact that causes a  $^2\text{H}$  EIE. If that contact persists unchanged in the transition state, then there is no further isotope effect on the chemical step and the observable KIE will be equal to the EIE. In other words, if the specific enzyme-substrate contact is the same in the transition state as in the Michaelis complex, this will be reflected in the observable KIE for that label being equal to the EIE of Michaelis complex formation. If, on the other hand, the specific enzyme-substrate contact is removed in the transition state, then there will be an isotope effect on the chemical step that is opposite and equal in magnitude to the EIE on Michaelis complex formation. The observable KIE will be unity, accurately reflecting the lack of the specific enzyme-substrate contact at the transition state.



**Fig. 10** EIEs on the anomeric equilibrium of  $\alpha$ - and  $\beta$ -glucopyranose. The reported standard errors for all measurements were  $\pm 0.003$  to  $\pm 0.005$ . The EIE at H6 was for the dideutero compound.

agreement with previous computational studies.<sup>116,118</sup> Other experimental  $1'$ - $^3\text{H}$  KIEs have proven similarly difficult to interpret (unpublished data).

One possible complicating factor in understanding these  $\alpha$ -secondary hydron KIEs is that hydron KIEs in general are relatively sensitive to non-covalent and remote interactions. As reviewed by Wade,<sup>123</sup> non-covalent hydron KIEs have been demonstrated in a wide variety of contexts, including isotope effects on affinity/dissociation constants, chromatographic behavior, even smell. Lewis and Schramm recently demonstrated  $^2\text{H}$  EIEs on the anomeric equilibrium between  $\alpha$ - and  $\beta$ -D-glucose in solution (Fig. 10).<sup>124</sup> Binding KIEs or EIEs have been measured for a number of enzyme-substrate interactions, including PNP·adenosine,<sup>125</sup> lactate dehydrogenase·NAD<sup>+</sup>,<sup>126</sup> lactate dehydrogenase·NADH·oxamate,<sup>15</sup> and phosphoenolpyruvate carboxylase·phosphoenolpyruvate.<sup>115</sup> Shifts in peak positions in isotope-edited vibrational spectra of enzyme-ligand complexes provide further evidence of changes in the vibrational environments of atoms upon binding enzymes (e.g., see Refs. 127–131). Isotope effects are vibrational effects, and so observing vibrational frequency shifts strongly implies that there are binding EIEs.<sup>#13</sup> Given the fact that stabilization of the oxocarbenium ion would likely occur through interactions near the anomeric carbon (see above), it would be expected that there would be contributions to the  $1'$ - $^3\text{H}$  KIE from direct enzyme·TS contacts.

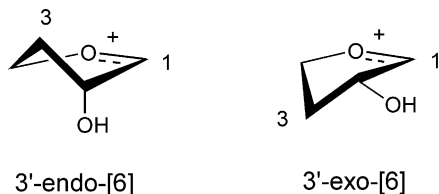
### *$\beta$ -Secondary hydron KIEs and hyperconjugation*

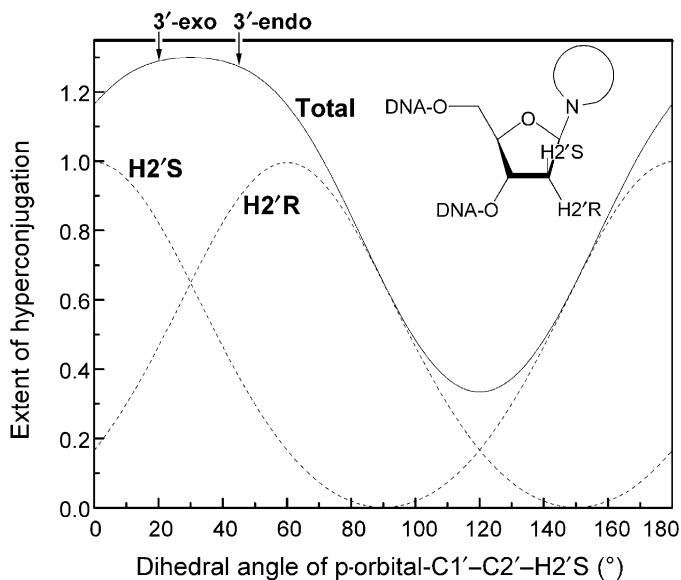
While detailed interpretation of  $\alpha$ -secondary hydron KIEs has been problematic,  $\beta$ -secondary ( $2'$ - $^3\text{H}$ ) KIEs have proven useful in both diagnosing the oxocarbenium ion character of glycosidic reaction transition states, and providing information on the ring conformation.

<sup>#13</sup> An isotope effect reflects the sum of changes in all the bond stretching and bending forces experienced by an atom, so it is not possible to determine an isotope effect from the shift of a single peak in a vibrational spectrum.

*Strong hyperconjugation is common.* In pentofuranosyl oxocarbenium ions, the combination of strong double-bonding character in the C1'–O4' bond and the 5-membered ring constrains the ring to have two energetically favorable envelope conformations, 3'-endo (<sup>3</sup>E) or 3'-exo (E<sub>3</sub>) (e.g., 3'-endo-**6** or 3'-exo-**6**). In the 3'-exo conformation, the C2'–H2' bond is nearly eclipsed with the developing empty p-orbital on C1', with a dihedral angle of 10°. This allows hyperconjugation, with  $\pi$ -bonding between C1' and C2', and a concomitant loss of bond order in the C2'–H2'  $\sigma$ -bond. In the 3'-endo conformer, this dihedral angle increases to 52°. Because of the strong angular dependence of hyperconjugation, this results in a much smaller extent of hyperconjugation.<sup>117,132</sup> Thus, a large  $\beta$ -secondary hydron KIE in riboside reactions implies both a highly oxocarbenium ion-like structure and a 3'-exo ring conformation. In the vast majority of riboside reactions examined, the  $\beta$ -secondary hydron KIE has been large, >1.1 for <sup>3</sup>H, >1.065 for <sup>2</sup>H, indicating that a majority of reactions pass through the transition state in a 3'-exo conformation.

*A 3'-endo conformation with RTA.* To date, the sole exception is RTA-catalyzed RNA hydrolysis, where 2'-<sup>3</sup>H KIE = 1.012<sup>46</sup> (see Section 4). RNA depurination by RTA appears to be unique among the reactions investigated so far, in that the  $\beta$ -secondary <sup>3</sup>H KIE was small, 1.012  $\pm$  0.005.<sup>46</sup> As the other experimental KIEs for this reaction indicated a discrete oxocarbenium ion intermediate, the small 2'-<sup>3</sup>H KIE was interpreted as indicating a 3'-endo conformation. This is supported by two lines of evidence. Calculated 2-<sup>3</sup>H KIEs for compound **6** were 1.18 for the 3'-exo conformer, and 0.994 for the 3'-endo conformer. The latter KIE is close to the experimental one. In NMR<sup>133</sup> and X-ray<sup>134</sup> RNA stem-loop structures, the ribose ring conformation in the reactive adenosine residue was either 3'-endo or an unusual 2'-exo conformation. Conversion of the 3'-endo/2'-exo reactant to a 3'-endo oxocarbenium ion could be accomplished without significant adjustment of the RNA backbone, while conversion to a 3'-exo oxocarbenium ion would have required large changes. Thus, the unusual 3'-endo conformation in the oxocarbenium ion intermediate appears to have been imposed on the tertiary structure of the RNA backbone. It is also possible that other external factors, such as enzyme hydrogen bonding to the 2'-hydroxyl could have enforced a 3'-endo conformation. The fact that this is the only known case of a ribooxocarbenium ion in a 3'-endo conformation and that it appears to be in response to external factors (*viz.* the RNA backbone structure) underscores the preference for the 3'-exo conformation in unconstrained structures.



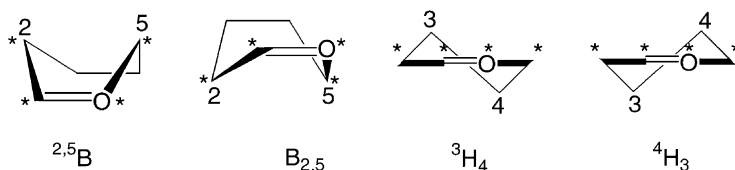


**Fig. 11** Hyperconjugative stabilization of the oxocarbenium ion of 2-deoxy sugars. Using the empirically derived angular dependence of hyperconjugation, where hyperconjugation  $\propto \exp(\cos^2 \theta)$ , and  $\theta$  is the dihedral angle defined by p-orbital-C1'-C2'-H2'S,<sup>132</sup> the total amount of hyperconjugative stabilization is plotted as a function of the angle  $\theta$ .

*2-Deoxy sugars.* Maximal hyperconjugation is achieved for 2-hydroxy sugars with the C2-H2 bond eclipsed with the developing p-orbital. In 2-deoxy sugars, both C2-H2 bonds are capable of hyperconjugation, and maximum total hyperconjugation is achieved when both C2-H2 bonds are at a dihedral angle of  $\approx 30^\circ$  to the C1' p-orbital (Fig. 11). Stereospecific  $2'$ - $^3\text{H}$  KIEs for hydrolysis of the *N*-glycosidic bond of deoxyuridine in DNA by uracil DNA glycosylase (UDG) were large and equal to each other within experimental error:  $2'S$ - $^2\text{H}$  KIE =  $1.10 \pm 0.01$ ,  $2'R$ - $^2\text{H}$  KIE =  $1.11 \pm 0.01$ .<sup>135</sup> Stereospecific KIEs for the RTA-catalyzed depurination of a DNA substrate were also large and similar to each other,  $2'S$ - $^3\text{H}$  KIE =  $1.117 \pm 0.002$ ,  $2'R$ - $^3\text{H}$  KIE =  $1.146 \pm 0.008$ .<sup>58</sup> Using the Swain-Schaad<sup>136</sup> relationship to convert these to  $^2\text{H}$  KIEs gives  $2'S$ - $^2\text{H}$  KIE = 1.08,  $2'R$ - $^2\text{H}$  KIE = 1.10, similar to the UDG reaction. Dideutero  $\beta$ -secondary  $^2\text{H}$  KIEs for reactions involving CMP-NeuAc and its derivatives were 1.218–1.28.<sup>48,54</sup> To achieve such large KIEs, it is necessary that both individual  $^2\text{H}$  KIEs be large, 1.10–1.13, assuming they are equal. This implies that there is a strong hyperconjugative stabilization of the oxocarbenium ion(-like) structures for these reactions.

While the large  $\beta$ -secondary KIEs do indicate hyperconjugation in 2-deoxy sugars, they are not helpful in determining the ring conformation of an oxocarbenium ion. In the optimized structures of deoxy-ribooxocarbenium ion





**Fig. 12** Conformations for a glycopyranosyl oxocarbenium ion. Hydroxyl groups have been omitted for clarity. The coplanar atoms are indicated with asterisks.

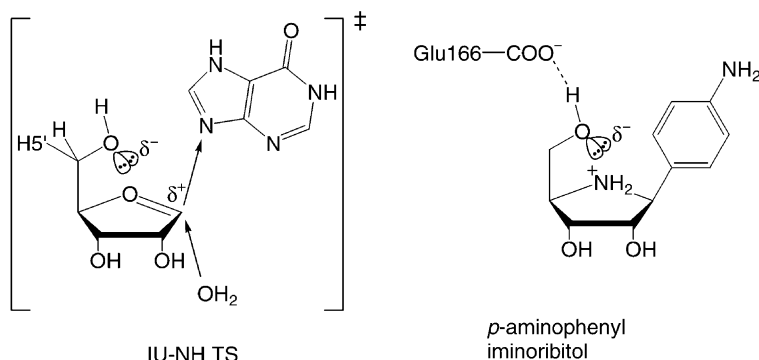
model compounds, the 3'-exo and 3'-endo conformers would both have strong hyperconjugative stabilization and similar  $\beta$ -secondary KIEs for each 2'-hydron.<sup>58</sup>

*Hexopyranosides.* In hexopyranosides, the 6-membered rings lend more conformational variability than pentofuranosides. Four possible ring conformations exist that can accommodate the requisite four coplanar atoms of an oxocarbenium ion (Fig. 12).

For glucopyranosides the B<sub>2,5</sub> boat conformation would have the hydron nearly perpendicular to the incipient cation p-orbital of the anomeric carbon, resulting in no hyperconjugation and possibly an inverse inductive KIE. In the <sup>2,5</sup>B boat, and <sup>3</sup>H<sub>4</sub> and <sup>4</sup>H<sub>3</sub> half-chair conformations, the C2–H2 bond would be almost eclipsed with the incipient p-orbital, leading to large  $\beta$ -secondary KIEs. However, the <sup>3</sup>H<sub>4</sub> conformation is sterically unfavorable for a glucopyranosyl oxocarbenium ion. The  $\beta$ -secondary <sup>2</sup>H KIE values for the yeast  $\alpha$ -glucosidase-catalyzed hydrolysis of  $\alpha$ -D-glucopyranosyl 4-bromoisoquinolinium bromide,<sup>49</sup>  $\alpha$ -D-glucopyranosyl pyridinium bromide<sup>137</sup> and  $\alpha$ -D-glucopyranosyl isoquinolinium bromide<sup>137</sup> were 1.13, 1.12 and 1.11, respectively (see Section 4). These are similar in magnitude to (deoxy)-ribonucleoside reactions, indicating that significant hyperconjugation occurs at the transition state of both groups of reactions. As with pentofuranoses,  $\beta$ -secondary KIEs help determine the hexopyranose ring conformation. Because of the greater conformational flexibility of pyranosides there are two conformations which would allow for strong hyperconjugation: <sup>2,5</sup>B and <sup>4</sup>H<sub>3</sub>. The preponderance of transition states exhibiting hyperconjugative stabilization emphasizes the importance of this effect in stabilizing an oxocarbenium ion(-like) transition state.

### Remote secondary hydron KIEs

Large hydron KIEs have been observed in enzymatic reactions at sites far removed from where chemistry is occurring. In enzymatic hydrolysis and transfer reactions of *N*-ribosides, it has become a common pattern to observe an inverse 4'-<sup>3</sup>H KIE and a normal 5'-<sup>3</sup>H KIE. These KIEs are not intrinsic to the reaction as the KIEs at these positions are negligible in the non-enzymatic reactions.<sup>69,138,139</sup> Examples of such enzymatic KIEs include inosine hydrolysis by IU-NH from *Crithidia fasciculata*, where 4'-<sup>3</sup>H KIE = 0.992, 5'-<sup>3</sup>H KIE = 1.051<sup>71</sup> and NAD<sup>+</sup> hydrolysis by diphtheria toxin A-chain (DTA), where 4'-<sup>3</sup>H KIE = 0.990, 5'-<sup>3</sup>H KIE = 1.032.<sup>17</sup>



**Fig. 13** Proposed TS structure for IU-NH versus crystal structure of inhibitor cocrystallized bound at the active site of IU-NH.

In the IU-NH reaction, several explanations of the large, normal  $5' \text{-}^3\text{H}$  KIE were considered, including the possibility of the  $5'$ -hydroxymethyl group adopting a conformation where the hydroxyl group is positioned above the ribosyl ring, located where it can stabilize the positive charge on the oxocarbenium ion-like transition state through electrostatic interactions (Fig. 13). This model was supported by the determination of the X-ray structure of IU-NH cocrystallized with a transition state analogue that had the  $5'$ -hydroxymethyl group in exactly the proposed position.<sup>101</sup> Based on the cocrystal structure of IU-NH·*p*-aminophenyl iminoribitol (pAPIR), the large  $5' \text{-}^3\text{H}$  KIE may be attributed to the effects of the strong hydrogen bond with the carboxylate residue of Glu166 as well as distortion of the  $\angle\text{C4}'\text{-C5}'\text{-O5}'$  bond angle due to electrostatic interactions between the lone pair electrons of  $\text{O5}'$  and the electron deficient oxocarbenium ion. This bond angle distortion leads to decreases in the bond-bending force constants for  $\angle\text{O5}'\text{-C5}'\text{-H5}'$ ,  $\angle\text{C4}'\text{-C5}'\text{-H5}'$  and  $\angle\text{H5}'\text{-C5}'\text{-H5}'$ , which in turn leads to normal KIEs.

In  $\text{NAD}^+$  hydrolysis, the extended conformation of  $\text{NAD}^+$  in the active site cleft precludes the enzymatic  $5' \text{-}^3\text{H}$  KIE arising from the same factors. However, model calculations showed that increasing or decreasing the  $\angle\text{C4}'\text{-C5}'\text{-O5}'$  bond angle by  $15^\circ$  from optimal would give a calculated  $5' \text{-}^3\text{H}$  KIE that matched the experimental KIE, while protonation of the adjacent phosphate residue gave a calculated  $5' \text{-}^3\text{H}$  KIE of 1.049. Thus, the observed  $5' \text{-}^3\text{H}$  KIE may arise from some combination of geometric distortion and/or protonation or strong hydrogen bonding with the proximal phosphate residue.

Bruner and Horenstein observed a very large inverse  $\zeta$ -secondary  $^3\text{H}$  KIE = 0.944 in a reaction catalyzed by  $\alpha(2 \rightarrow 6)$  sialyltransferase (equation 4).<sup>48</sup> This result demonstrates that, unlike non-enzymatic reactions, there is not necessarily any distance dependence on secondary KIEs in enzymatic reactions; enzymes commonly use binding interactions remote from the reaction site to promote catalysis.

Although it is not always possible to assign the specific sources of remote hydron KIEs, the observation of remote KIEs that are significantly different from the non-

enzymatic reactions is a sign that the enzyme is using binding energy at remote sites to promote catalysis.

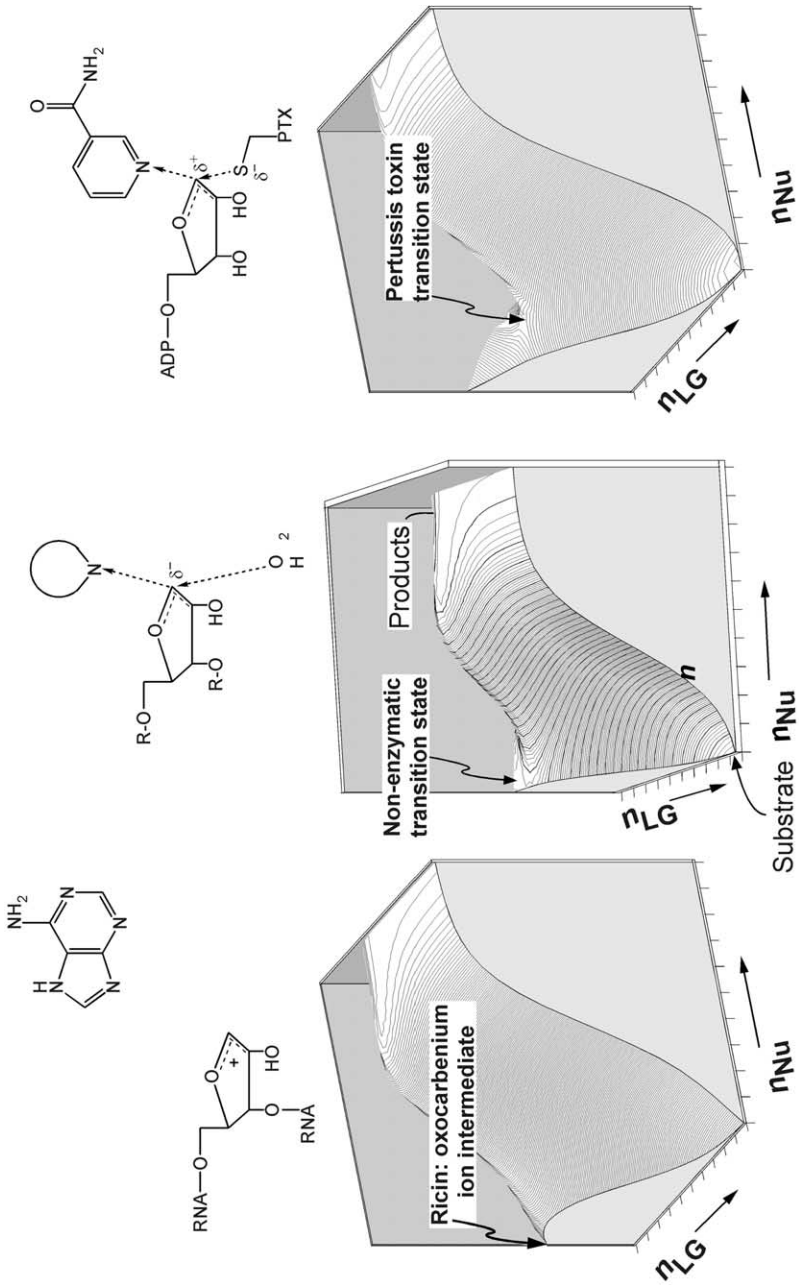
#### CATALYTIC STRATEGIES

##### *Opposite catalytic strategies?*

One striking observation about the reactions catalyzed by RTA and pertussis toxin is that the enzymes appear to use “opposite” catalytic strategies. The analogous non-enzymatic reactions, hydrolysis of adenosine 5'-monophosphate (AMP)<sup>78</sup> and  $\text{NAD}^+$ ,<sup>69</sup> both have highly dissociative  $\text{A}_\text{N}\text{D}_\text{N}$  mechanisms with oxocarbenium ion-like transition states. In the ADP-ribosylation of protein  $\text{G}_{i\alpha 1}$  by pertussis toxin, the  $\text{A}_\text{N}\text{D}_\text{N}$  mechanism is more synchronous, with more nucleophile participation and lower oxocarbenium ion character than the non-enzymatic reaction.<sup>#14</sup> In contrast, the RTA-catalyzed depurination of RNA<sup>46</sup> and DNA<sup>58</sup> substrates proceeds through stepwise  $\text{D}_\text{N} * \text{A}_\text{N}$  mechanisms where the enzyme stabilizes an oxocarbenium ion to the point that it becomes a discrete intermediate. This is illustrated with a hypothetical free energy surface for each reaction (Fig. 14).

A consideration of the evolutionary pressures acting on each enzyme may provide a rationale for why different strategies may be effective. The role of pertussis toxin *in vivo* is to ADP-ribosylate protein  $\text{G}_{i\alpha 1}$ . There is no evolutionary advantage to pertussis toxin hydrolyzing  $\text{NAD}^+$ , as the cellular pool of  $\text{NAD}^+$  is too large for a single enzyme molecule to damage a cell by depleting  $\text{NAD}^+$ . However, a single toxin molecule can ADP-ribosylate enough protein  $\text{G}_{i\alpha 1}$  in a cell to cause a physiological effect. As such, there is evolutionary advantage for the enzyme to bind  $\text{NAD}^+$  but not cause any reaction until protein  $\text{G}_{i\alpha 1}$  has bound to the enzyme- $\text{NAD}^+$  complex. Pertussis toxin uses binding energy from interaction with the second substrate, protein  $\text{G}_{i\alpha 1}$ , to increase the nucleophile participation at the transition state. In the case of RTA, its role is to depurinate and thereby inactivate 28S ribosomal RNA, which is needed for protein biosynthesis. The identity of the incoming nucleophile is unimportant; however, it is convenient that a good nucleophile, water, is present at a concentration of 55 M. It is therefore an evolutionarily effective strategy for RTA to catalyze the formation of a highly reactive oxocarbenium ion. As a ribooxocarbenium ion is too reactive to have a finite lifetime in solution, an enzyme-bound oxocarbenium ion will likely also be highly reactive, undergoing nucleophilic attack as soon as a water molecule diffuses into position. For RTA there is no evolutionary advantage to being selective about the nucleophile; therefore forming a highly reactive oxocarbenium ion is evolutionarily effective. It has been estimated that a single molecule of RTA can kill a cell.

<sup>#14</sup> The ADP-ribosyl transfer reaction has a sulfur nucleophile, as compared with water in the non-enzymatic reaction. Given the very weak dependence on nucleophile ability<sup>140,141</sup> of this reaction, the non-enzymatic transition state with a sulfur nucleophile would be expected to be similar to that with water.



**Fig. 14** Hypothetical free energy surfaces for the glycoside hydrolysis and transfer reactions, as inferred from TS analysis. Compared to the highly dissociative  $A_N D_N$  transition state for the non-enzymatic reaction (middle), RTA (left) and pertussis toxin (right) appear to use opposite catalytic strategies in that they increase and decrease, respectively, the amount of oxocarbenium ion character in the ribosyl ring at the transition state.

Evolutionary pressures have constrained pertussis toxin to a mechanism with significant nucleophile participation while RTA has evolved a catalytic strategy with an oxocarbenium ion intermediate that reacts quickly with nearby water molecules. By this logic, other ADP-ribosylating toxins, such as cholera and diphtheria toxins, would be expected to proceed through relatively synchronous transition states. Nucleoside hydrolases (enzymes that hydrolyze nucleosides to ribose and a purine or pyrimidine base) could use mechanisms with oxocarbenium ion intermediates, though the transition states characterized to date have been  $A_N D_N$  (see below).

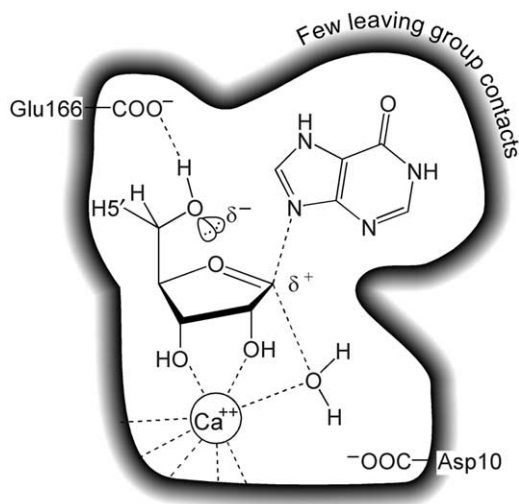
It is striking that the only enzymes characterized to date that form an oxocarbenium ion intermediate, RTA and UDG (see below), are enzymes that act on nucleic acids and which have extended binding sites encompassing several nucleotide residues. It is possible that only these enzymes can form enough enzyme·substrate contacts through their extended binding sites to pay for the energetic cost of forming highly reactive oxocarbenium ion intermediates.

Arguments that invoke evolutionary forces are distinct, of course, from questions of how different catalytic strategies are effected through specific enzyme·substrate interactions. Because very detailed pictures of transition states have not previously been available, these kinds of questions are only now beginning to be addressed.

### *Catalytic strategies from crystal structures*

The combination of protein crystallography and TS analysis has provided important insight into enzyme function not available from either technique in isolation. One especially important lesson is that enzyme structures change dramatically when binding good TS analogue inhibitors. This has led to a virtuous cycle of TS analysis and TS analogue design leading to good inhibitors, which when cocrystallized with their target enzymes lead to further insights into enzyme·TS interactions, and can then lead to further rounds of inhibitor design.

The structures discussed in this section are IU-NH, PNP, the DNA repair enzyme UDG, and DTA, an ADP-ribosylating toxin. These reactions have substantially different catalytic requirements and the enzyme mechanisms reflect this. Purine leaving groups can be activated for departure by protonation, as seen with PNP. Pyrimidines cannot be activated by protonation, but can leave as anions. UDG specifically stabilizes the uracil anion, promoting its departure. The nicotinamide ring of  $NAD^+$  is cationic, but becomes neutral upon departure, so stabilizing positive or negative charges will not be useful in this case. IU-NH, a non-specific



**Fig. 15** A schematic showing the essential features of transition state stabilization by IU-NH, based on the cocrystal structure of an IU-NH·TS analogue complex. The 3'-exo ribosyl ring conformation allows simultaneous favorable interactions between the lone pair electrons of the 5'-hydroxyl oxygen and the positive charge on the oxocarbenium ion-like ribosyl ring, while also forming a bidendate interaction with the active site  $\text{Ca}^{2+}$  ion.  $\text{Ca}^{2+}$  binds and orients the substrate, as well as helping to activate the nucleophile water. Asp10 acts as a general base to deprotonate the nucleophile after the transition state. There are few direct interactions with the leaving group, consistent with the experimental evidence that IU-NH operates primarily through interactions with the ribosyl ring.

nucleoside hydrolase, appears to function primarily through stabilization of the oxocarbenium ion-like portion of the transition state, lessening its dependence on leaving group activation.

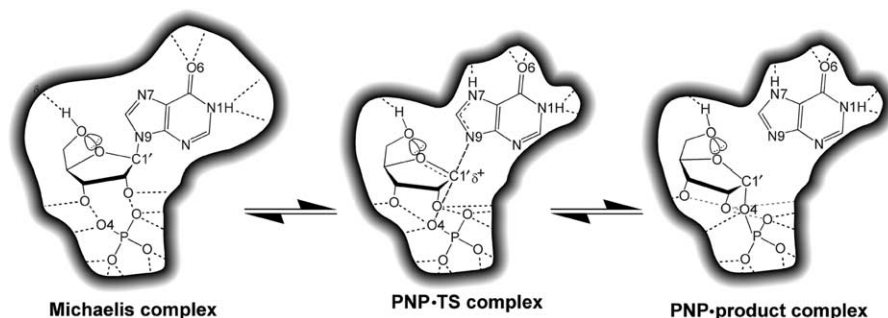
PNP, IU-NH and UDG were cocrystallized with inhibitors, while DTA was cocrystallized with a substrate,  $\text{NAD}^+$ . The structures of unliganded enzymes have been only minimally useful because without a substrate or strong inhibitor molecule bound, it is difficult to know what enzyme·TS contacts are likely to be present. This problem arises partly because of the large number of possible interactions between enzyme and substrate, and is compounded by the fact that the structures of enzyme active sites change upon substrate or inhibitor binding. With IU-NH, side chain motions of greater than 10 Å were observed upon binding a strong inhibitor.

*IU-nucleoside hydrolase (IU-NH)*. The experimental TS structure for IU-NH-catalyzed inosine hydrolysis was used as the basis for designing TS analogue inhibitors, one of which was cocrystallized with the enzyme.<sup>101</sup> IU-NH is relatively non-specific, hydrolyzing all the naturally occurring purine and pyrimidine nucleosides with good efficiency. Given the lack of specificity for the leaving group and the differing catalytic requirements of purine and pyrimidine leaving groups, it might be expected that IU-NH operates primarily through oxocarbenium ion stabilization and/or nucleophile activation. In support of this view is the fact that

IU-NH efficiently hydrolyses *p*-nitrophenyl- $\beta$ -D-ribofuranoside,<sup>82</sup> unlike PNP and other nucleoside hydrolases tested. Also, it is inhibited by a wide variety of iminosugar inhibitors, with little specificity for parts of the inhibitor corresponding to the substrate's leaving group.<sup>142</sup> This is consistent with the small number of contacts in the crystal structure between the enzyme and "leaving group" atoms in the inhibitor. It would appear that the catalytic activity of IU-NH arises predominantly through interactions in the ribosyl ring, a view that is supported by the fact that 2'-, 3'-, and 5'-deoxynucleosides are poor substrates and deoxy-iminoribitols are similarly poor inhibitors. This view of the catalytic mechanism (Fig. 15) is supported by features of the NH-IU·pAPIR complex. The inhibitor pAPIR was bound in a 3'-exo conformation, the conformation predicted by TS analysis,<sup>71</sup> but which is uncommon in crystal structures of ribosides.<sup>143</sup> The carboxylate moiety of Glu166 would stabilize an oxocarbenium ion by hydrogen bonding to the 5'-hydroxyl group, orienting it such that the lone pair electrons of oxygen can electrostatically stabilize the positive charge on the ribosyl ring at the transition state. A Ca<sup>2+</sup> ion bound in the active site was observed in the cocrystal structure that had been assigned as K<sup>+</sup> in the unliganded enzyme. Ca<sup>2+</sup> was subsequently shown to be required for activity. The Ca<sup>2+</sup> had an octahedral coordination sphere with ligands supplied by acidic side chains, and the 2'- and 3'-hydroxyl groups of the inhibitor provided a bidentate ligand. A strong interaction of Ca<sup>2+</sup> with the 2'-hydroxyl could lead to strong polarization of the C2'-O2' bond, or even deprotonation of the O2'H through a catalytic base. The polarized bond or oxyanion would help inductively stabilize the oxocarbenium ion. A water molecule is the last calcium ligand and is ideally located to act as the nucleophile. It is believed that Ca<sup>2+</sup> helps to activate the nucleophilic water and facilitate its deprotonation, with Asp10 acting as a general base. Thus Ca<sup>2+</sup> is proposed to have a role in substrate binding and orientation as well as nucleophile activation and/or possibly interaction with the 2'-hydroxyl.

*Purine nucleoside phosphorylase (PNP)*. In contrast to IU-NH, PNP appears to use extensive contacts with the purine ring to promote catalysis and relatively few contacts with the ribosyl ring. The crystal structure of PNP has been determined in a complex with an iminosugar inhibitor,<sup>26</sup> immucillin H, which was developed based on TS analyses of PNP-catalyzed hydrolysis<sup>27</sup> and arsenolysis<sup>28</sup> reactions. TS analysis revealed that the enzyme catalyzes a dissociative A<sub>N</sub>D<sub>N</sub> mechanism. The crystal structure was compared with the structures determined by Ealick and coworkers<sup>30</sup> of PNP in a Michaelis complex analogue, PNP·inosine·sulfate, and a product complex, PNP· $\alpha$ -D-ribose-1-phosphate·hypoxanthine.

There were numerous enzyme·ligand contacts with the purine ring and the phosphate (or sulfate), but relatively few with the oxocarbenium ion (Fig. 16). The picture that emerges from the PNP structures is a mechanism whereby the leaving group purine and the nucleophile phosphate are tightly bound and relatively immobile, being fixed by many enzyme·ligand contacts. The electrophile ribosyl ring, which makes fewer contacts with the enzyme, moves from the immobile leaving group to the immobile nucleophile – an electrophile migration.

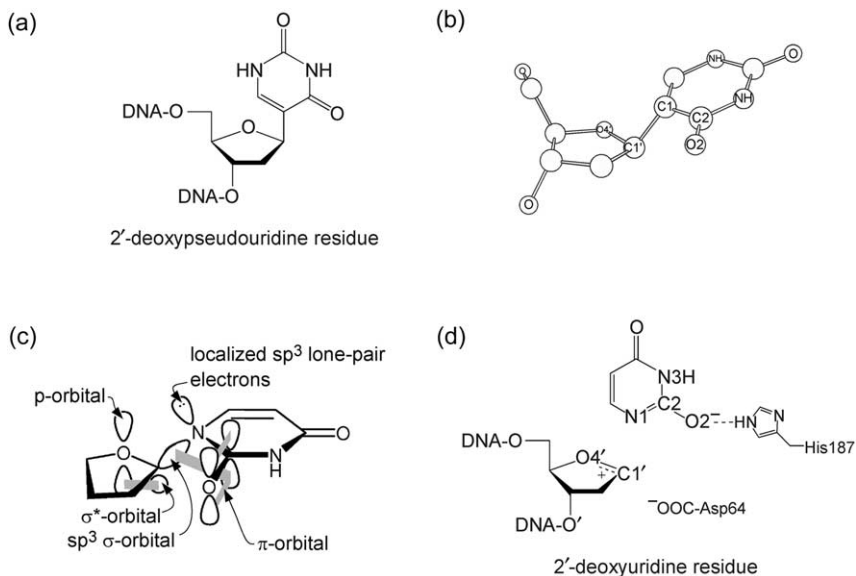


**Fig. 16** A schematic mechanism of PNP-catalyzed inosine phosphorolysis showing electrophile migration. This mechanism is based on cocrystal structures of PNP and TS analyses of inosine hydrolysis and arsenolysis. A large number of direct and water-mediated enzyme-substrate contacts hold the leaving group hypoxanthine and the nucleophile phosphate almost immobile while the ribosyl ring (the electrophile), because of the small number of contacts with the enzyme, is able to migrate from leaving group to nucleophile.

The distance of electrophilic migration can be estimated from the distances between the purine ring and phosphate or sulfate in the substrate analogue (5.6 Å) or product (5.2 Å) complexes, as well as the PNP-immucillin H-phosphate complex (4.8 Å). These distances are less than the 6 Å that is estimated to be the minimum amount of space needed for a discrete oxocarbenium ion intermediate to develop.<sup>26</sup>

Of the three direct contacts between the ribosyl ring and PNP residues, two are hydrogen bonds to the 2'- and 3'-hydroxyls that likely do not contribute directly to stabilization of an oxocarbenium ion. The hydrogen bond between the His257 side chain and the 5'-hydroxyl is the only direct contact that would stabilize the oxocarbenium ion, by orienting the lone pair electrons on O5' to allow electrostatic stabilization of the positive charge. The other apparent factor in stabilizing the oxocarbenium ion is the negatively charged phosphate anion located directly beneath the ribosyl ring. The combination of the lone pair electrons of O5' and the phosphate anion creates an electron-rich "sandwich" to stabilize an oxocarbenium ion. Phosphate makes a modest contribution to oxocarbenium ion stabilization, with  $k_{\text{cat}}$  being only 100-fold higher for phosphorolysis than hydrolysis.<sup>31</sup> This relatively modest oxocarbenium ion stabilization is further illustrated by the fact that *p*-nitrophenyl- $\beta$ -D-ribofuranoside is a very poor substrate for phosphorolysis.<sup>82</sup> A major driving force for catalysis, then, appears to be stabilization of the purine ring leaving group. The crystal structure of PNP-immucillin H showed direct hydrogen-bonding interactions with N7, O6 and N1H of the purine ring analogue, as well as protein-mediated water contacts that appear to be the source of the proton at N7. Protonation at N7 helps to make the hypoxanthine ring in the substrate a better leaving group by making the otherwise anionic leaving group neutral. Catalysis through leaving group stabilization is further supported by the extremely tight binding of product hypoxanthine, with  $K_d = 1.3$  pM.





**Fig. 17** (a) Pseudouridine, (b) Pseudouridine residue from UDG-inhibitor cocrystal structure, PDB entry: 1EMH. (c) Orbital interactions arising from the proposed coupled anomeric/ $\sigma^*$ - $\pi_{Arom}$  interactions.<sup>147</sup> The localized lone pair electrons on N1 are a consequence of the proposed interactions, but not explicitly discussed in the original proposal. (d) The ion pair intermediate formed in the  $D_N * A_N$  mechanism proposed for UDG.

*Uracil DNA glycosylase (UDG)*. UDG catalyzes the first step in the removal of uridine residues from DNA. These arise from spontaneous deamination of cytidine residues or misincorporation of UTP into DNA. TS analysis supported a stepwise  $D_N * A_N$  mechanism.<sup>135</sup> UDG stabilizes the anionic pyrimidine leaving group, as evidenced by the fact that it lowers the  $pK_a$  of N1 by 3.4 units relative to solution.<sup>144, 145</sup> There is a carboxylate side chain, Asp64, that is located adjacent to the  $\alpha$ -face of the ribosyl ring. It is proposed that this stabilizes an oxocarbenium ion electrostatically as well as assisting nucleophilic attack by water, either through orienting it or by acting as a general base. Recent computational results<sup>146</sup> provide additional support for the experimental evidence of a  $D_N * A_N$  mechanism.

Another interesting feature of the active site is evident in the structure of UDG cocrystallized with a pseudouridine-containing oligo-DNA inhibitor (Fig. 17).<sup>147</sup> The pseudouridine residue is distorted about C1' in the cocrystal structure, toward a trigonal geometry, as opposed to the planar geometry seen in other pseudouridine structures. It was proposed that this distortion represents ground state destabilization that promotes catalysis through coupled anomeric and  $\sigma^*$ - $\pi_{Arom}$ <sup>148</sup> stereoelectronic effects (Fig. 17c). In this proposed mechanism, the anomeric effect (interaction of the empty p-orbital of the ribosyl ring oxygen with the  $\sigma^*$ -orbital of C1') leads to weakening of the *N*-glycosidic bond and strengthening of the C1'-O4' bond. Coupled with this effect, the observed distortion around N1 is proposed to facilitate

**Table 2** Effects of distortion by UDG

Bond	Expected change in bond length <sup>a</sup>	Pseudouridine bond lengths (Å)		Change as expected?	Bond	2'-Deoxyuridine bond lengths (Å)		Change as expected?
		Distorted <sup>b</sup>	Undistorted <sup>c</sup>			Distorted <sup>d</sup>	Optimized <sup>e</sup>	
C1'-C1	Increase	1.55	1.52 ± 0.01	Yes	C1'-N1	1.53	1.48	Yes
C1'-O4'	Decrease	1.42	1.41 ± 0.01	— <sup>f</sup>	C1'-O4'	1.43	1.41	No
C1-C2	Increase	1.39	1.43 ± 0.01	No	N1-C2	1.42	1.39	Yes
C2-O2	Decrease	1.22	1.23 ± 0.01	— <sup>f</sup>	C2-O2	1.22	1.22	No

<sup>a</sup>Expected changes in bond lengths due to coupled anomeric/ $\sigma$ - $\pi_{\text{Atom}}$  effects relative to undistorted pseudouridine.

<sup>b</sup>Bond lengths from X-ray crystallographic structure, Protein Databank (PDB) entry 1EMH.

<sup>c</sup>Average of bond lengths in four pseudouridine residues from PDB entries 1EHZ and 1EVV.

<sup>d</sup>Distorted 2'-deoxyuridine had hydrogen atoms fully optimized and all bond lengths optimized, but with heavy atom bond angles constrained to match the distorted pseudouridine from the PDB entry 1EMH.

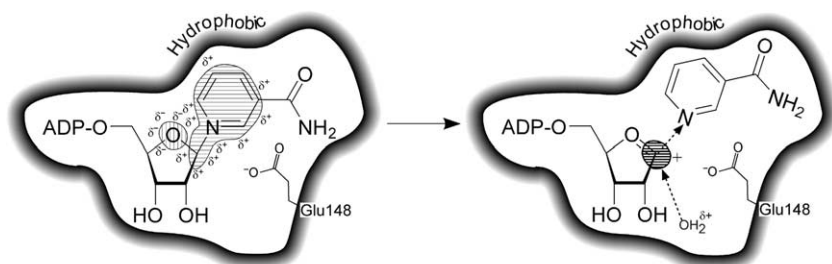
<sup>e</sup>Fully optimized 2'-deoxyuridine. Optimization was as in Fig. 6.

<sup>f</sup>Change in bond lengths is too small to be measured.

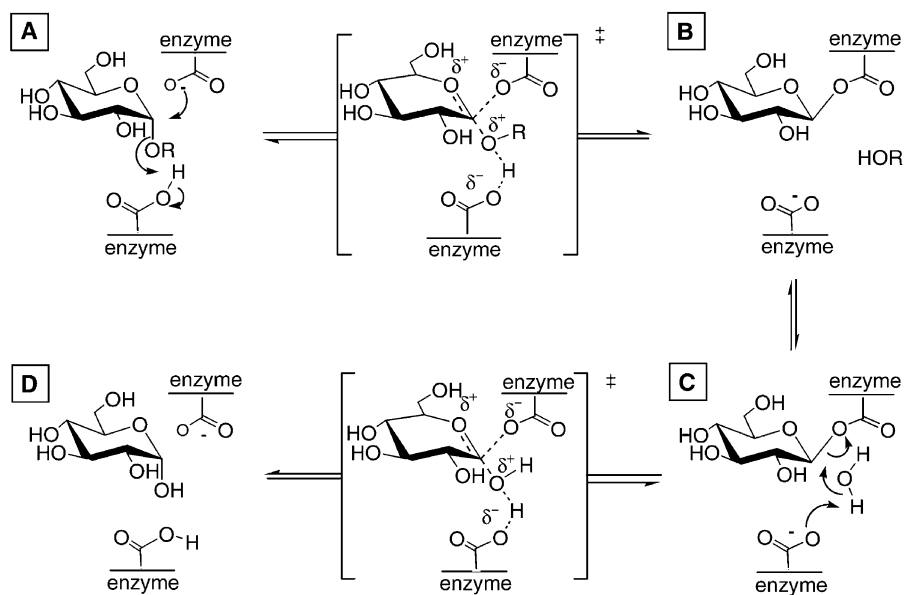
an interaction between the  $\sigma$ -molecular orbital of the C1'–N1  $\sigma$ -bond and  $\pi$ -electrons from the uridine ring (illustrated with the  $\pi$ -orbital of C2–O2). One consequence of this proposed mechanism, however, is that the aromatic delocalization of lone pair electrons from N1 must be lost because there cannot be simultaneous interaction of the ring  $\pi$ -electrons with both the  $\sigma$ -orbital and the lone pair electrons of N1. While this explanation may be reasonable *a priori*, the distorted structure of pseudouridine did not display changes in bond lengths relative to four undistorted pseudouridine residues that would support the proposed coupled anomeric/ $\sigma$ – $\pi_{\text{Arom}}$  interactions (Table 2).<sup>149,150</sup> Comparing four bond lengths between distorted and undistorted pseudouridine residues, the C1–C1' bond length increased as expected, but the other bond lengths either did not change significantly or changed opposite to the direction expected. To determine if these putative stereoelectronic effects were operative in uridine rather than pseudouridine, electronic structure optimizations were performed on uridine, and uridine distorted to have the same bond angles as the distorted pseudouridine residue. As might be expected, the C1'–N1' bond in the distorted structure was longer, but other bond length changes were inconsistent with coupled anomeric/ $\sigma$ – $\pi_{\text{Arom}}$  effects. Thus, while the observed distortion of pseudouridine may indicate a ground state destabilization strategy by UDG, the evidence does not support coupled stereoelectronic effects. However, distortion about N1 would likely aid cleavage of the *N*-glycosidic bond through the conventional orbital interpretation, where the lone pair electrons of N1 remain conjugated with the aromatic  $\pi$ -electrons, and the sp<sup>2</sup>-hybridized  $\sigma$ -bond to C1' is cleaved.

The importance of His187 in stabilizing the uracil anion in the transition state or intermediate has been demonstrated by NMR and Raman spectroscopy, which showed a 34 cm<sup>-1</sup> decrease in the C2–O2 bond stretch frequency in the enzyme·substrate complex, in agreement with the presence of a strong hydrogen bond to stabilize a uracil anion.<sup>144,145,151</sup> There was little change in the uracil ring vibrational modes, which is evidence against extensive ring distortion.

*Diphtheria toxin A-chain (DTA)*. Several crystal structures of diphtheria toxin are available,<sup>152–156</sup> including the cocrystal structure with substrate NAD<sup>+</sup> bound in the active site.<sup>103</sup> Only minor side chain adjustments were necessary to accommodate the TS structure in place of NAD<sup>+</sup>. The salient features of the DTA·TS interactions include a very deep, form-fitting hydrophobic pocket in which the nicotinamide ring binds. The low dielectric environment of this pocket would lower the energy difference between the reactant and transition state by increasing the energy of the positively charged nicotinamide ring relative to the neutral form at the transition state, a case of ground state destabilization. The side chain of Glu148, has been shown by photoaffinity labeling<sup>157</sup> and mutagenesis<sup>158</sup> to be crucial for catalysis, and this glutamate side chain is conserved in all bacterial ADP-ribosylating toxin sequences. It is located directly adjacent to where positive charge accumulates at the anomeric carbon of the ribosyl ring in the transition state, where it could stabilize the formation of the oxocarbenium ion-like transition state (Fig. 18). It may also be involved in nucleophile orientation and/or activation in hydrolysis or ADP-ribosylation of elongation factor 2.



**Fig. 18** A schematic of DTA·NAD<sup>+</sup> interactions in the hydrolysis reaction. Left: in the Michaelis complex, the positive charge due to the quaternary nitrogen is delocalized throughout the nicotinamide ring and somewhat into the ribosyl ring. The ring oxygen possesses a large negative electrostatic potential. Right: at the transition state for NAD<sup>+</sup> hydrolysis, the large extent of C–N bond breakage renders the nicotinamide neutral and hydrophobic. It can now interact more favorably with the surrounding hydrophobic residues. The positive charge has now been localized on the ribosyl ring. It is stabilized by the invariant glutamate residue which is directly adjacent to the site where the positive charge accumulates at the transition state. This glutamate may also have a role in orienting and/or polarizing the water nucleophile.



**Fig. 19** Double displacement mechanism for a retaining  $\alpha$ -glucosidase, A  $\rightarrow$  B glycosylation, C  $\rightarrow$  D deglycosylation.

## 4 Specific reactions

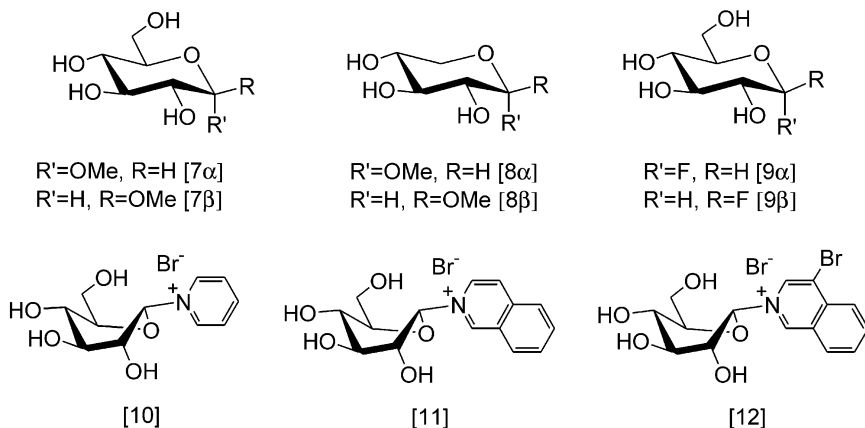
### GLUCOSIDE AND XYLOSIDE HYDROLYSIS AND GLUCOSIDASES

Glycosyl transferases and *O*-glycosidases modify glycoproteins and are important for polysaccharide catabolism. Inhibitors of these enzymes are potential drugs in the treatment of cancer, viral infection and diabetes. There are two mechanistic classes of glycosidases, retaining and inverting.<sup>4,159,160</sup>

Retaining glycosidases operate via a double displacement mechanism (Fig. 19), although the identity of the intermediate formed is the subject of some controversy. Mechanistic studies have attempted to address the nature of the intermediate, whether a full-fledged oxocarbenium ion is formed, or a covalent glycosyl–enzyme intermediate. To this end, mechanistic insight on the ring conformation at the transition state and the degree of nucleophilic assistance can be established from these studies.

#### *Non-enzymatic hydrolysis*

KIEs were measured for the acid-catalyzed hydrolysis of methyl  $\alpha$ - (**7 $\alpha$** ) and  $\beta$ -D-glucopyranoside (**7 $\beta$** ),<sup>50</sup> and methyl  $\alpha$ - (**8 $\alpha$** ) and  $\beta$ -D-xylopyranoside (**8 $\beta$** ),<sup>161</sup> the spontaneous hydrolysis of  $\alpha$ - (**9 $\alpha$** ) and  $\beta$ -D-glucopyranosyl fluoride (**9 $\beta$** )<sup>162</sup> and the spontaneous hydrolysis of  $\alpha$ -D-glucopyranosyl 4-bromoisoquinolinium bromide (**12**).<sup>137</sup> TS analyses of enzymatic hydrolyses have been completed on fluoro  $\alpha$ -D-glucopyranoside (**9 $\alpha$** ),<sup>163</sup>  $\alpha$ -D-glucopyranosyl pyridinium bromide (**10**),<sup>137</sup> and  $\alpha$ -D-glucopyranosyl isoquinolinium bromide (**11**).<sup>137</sup>



*O*-Glucopyranosides and xylopyranosides. Bennet and Sinnott studied acid-catalyzed hydrolysis of methyl  $\alpha$ - and  $\beta$ -D-glucopyranosides, **7 $\alpha$**  and **7 $\beta$** , using a family of KIEs to determine transition state information on glycoside hydrolysis

**Table 3** Experimental KIEs for spontaneous and acid-catalyzed hydrolysis of glucopyranosides

Compound	KIE				
	$\alpha$ -Secondary $^2\text{H}$	$\beta$ -Secondary $^2\text{H}$	Primary $^{13}\text{C}$	Leaving group primary $^{18}\text{O}$ (or $^{15}\text{N}$ )	Ring $^{18}\text{O}$
<b>7<math>\alpha^a</math></b>	1.137 $\pm$ 0.007	1.073 $\pm$ 0.003	1.007 $\pm$ 0.001	1.026 $\pm$ 0.001	0.996 $\pm$ 0.001
<b>7<math>\beta^a</math></b>	1.089 $\pm$ 0.006	1.045 $\pm$ 0.004	1.011 $\pm$ 0.002	1.024 $\pm$ 0.001	0.991 $\pm$ 0.002
<b>8<math>\alpha^b</math></b>	1.128 $\pm$ 0.004	1.088 $\pm$ 0.008	1.006 $\pm$ 0.001	1.023 $\pm$ 0.002	0.983 $\pm$ 0.001
<b>8<math>\beta^b</math></b>	1.098 $\pm$ 0.005	1.042 $\pm$ 0.004	1.006 $\pm$ 0.003	1.023 $\pm$ 0.003	0.978 $\pm$ 0.001
<b>9<math>\alpha^c</math></b>	1.142 $\pm$ 0.008	1.065 $\pm$ 0.008	1.032 $\pm$ 0.003	–	0.984 $\pm$ 0.005
<b>9<math>\beta^{c,d}</math></b>	1.078 $\pm$ 0.001	1.027 $\pm$ 0.007	1.016 $\pm$ 0.002	–	0.985 $\pm$ 0.005
<b>12<math>^e</math></b>	1.188 $\pm$ 0.009	1.094 $\pm$ 0.010	1.005 $\pm$ 0.002	1.015 $\pm$ 0.004 ( $^{15}\text{N}$ )	–

All kinetic runs were completed at 80°C unless stated otherwise.

<sup>a</sup>From Ref. 50.

<sup>b</sup>From Ref. 161.

<sup>c</sup>From Ref. 162.

<sup>d</sup>Data collected at 50°C and corrected to 80°C assuming  $T \times \ln(\text{KIE}) = \text{constant}$ .

<sup>e</sup>From Ref. 137.

(Table 3).<sup>50</sup> Based on the small primary  $^{13}\text{C}$  KIEs for both anomers, the authors concluded that the acid-catalyzed hydrolyses occurred via a  $\text{D}_\text{N} + \text{A}_\text{N}$  mechanism. The leaving group  $^{18}\text{O}$  KIEs suggested that the C–O bond to the aglycon was largely broken at the transition state, and the large  $\alpha$ -secondary  $^2\text{H}$  KIE was consistent with formation of an oxocarbenium ion. The  $\beta$ -secondary  $^2\text{H}$  and ring  $^{18}\text{O}$  KIEs were used to determine the dihedral angle of the hydron at C2 and the incipient p-orbital at C1. These angles were used in combination with molecular mechanics to determine the ring conformation at the transition state. The large  $\beta$ -secondary  $^2\text{H}$  for the  $\alpha$ -anomer was consistent with a flattened ring. The  $\beta$ -anomer conformation was more chair-like, i.e. more similar to the reactant state. One of the major conclusions was that their results were not consistent with the antiperiplanar lone pair hypothesis.<sup>164</sup> The authors concluded that methyl  $\alpha$ -glucopyranoside was hydrolyzed through a skewed or boat conformation, whereas the  $\beta$ -anomer reacted through a chair or chair-like conformation. The antiperiplanar lone pair hypothesis would predict the opposite.

Not surprisingly, most of the KIEs for the acid-catalyzed hydrolysis of the methyl xylopyranosides **8 $\alpha$**  and **8 $\beta$**  (Table 3) were similar to those for the corresponding glucopyranosides **7 $\alpha$**  and **7 $\beta$** . There are differences, however, in the ring  $^{18}\text{O}$  KIEs. The larger inverse KIEs for the xylopyranosides indicated more resonance stabilization of the incipient oxocarbenium ion. Another difference was in the  $\beta$ -secondary  $^2\text{H}$  KIEs of the  $\alpha$ -anomer, where the larger value for the xylose derivative suggested a TS with greater hyperconjugation, more closely resembling a  $^4\text{H}_3$  half-chair or  $^{2,5}\text{B}$  boat conformation as expected for a compound without the sterically encumbering C5 hydroxymethyl group. The more inverse ring  $^{18}\text{O}$  KIE and larger  $\beta$ -secondary KIEs suggest greater charge delocalization and resonance stabilization in xylopyranosides than glucopyranosides.

*N-Glucopyranosides.* KIEs for non-enzymatic reactions are useful as a reference for comparison with enzymatic KIEs. Owing to the low rates for the uncatalyzed hydrolysis of **10** and **11** ( $t_{1/2} \approx 33$  h for **10** at  $80^\circ\text{C}$ ), TS analysis for the spontaneous hydrolysis of **12** was conducted (Table 3) for comparison with the yeast  $\alpha$ -glucosidase-catalyzed reaction on all three compounds.<sup>137</sup> The small primary anomeric  $^{13}\text{C}$  KIE was consistent with a  $\text{D}_\text{N} + \text{A}_\text{N}$  mechanism. The  $\beta$ -secondary  $^2\text{H}$  KIE for **12** was larger than that for **7 $\alpha$** , indicating stronger hyperconjugation. The leaving group primary  $^{15}\text{N}$  KIE of 1.015 suggested significant C–N bond cleavage.<sup>#15</sup>

*Glucopyranosyl fluorides.* The larger primary  $^{13}\text{C}$  KIEs for **9 $\alpha$**  and **9 $\beta$**  (Table 3) are consistent with an  $\text{A}_\text{N}\text{D}_\text{N}$  mechanism.<sup>162</sup> The authors used BOVA and the previously solved TS structure for the enzyme-catalyzed hydrolysis of **9 $\alpha$** <sup>163</sup> as a

<sup>#15</sup> The theoretical maximum KIE for breaking a C–N bond was previously calculated to be 1.044.<sup>165</sup> This calculation, however, neglects the fact that bond orders within the leaving group ring increase to compensate for the loss of the *N*-glycosidic bond, lowering the  $^{15}\text{N}$  KIE. The limits of  $^{15}\text{N}$  KIEs for nicotinamide and adenine departure have been calculated previously to be 1.034 and 1.024, respectively.<sup>17,58</sup> It would be necessary to calculate the maximum possible value for an isoquinolinium bromide leaving group to determine the extent of bond breakage that a  $^{15}\text{N}$  KIE of 1.015 represents.

starting point to solve the TS structure for the non-enzymatic hydrolysis. The experimental transition states had a  ${}^4C_1$  chair conformation, rather than a boat, half-chair or skew conformation as described in the studies by Bennet and Sinnott<sup>50</sup> and Huang *et al.*<sup>137</sup> Overall, the KIEs for the  $\beta$ -anomer (**9 $\beta$** ) were similar to those for the methyl glucoside (**7 $\beta$** ). The major difference was the larger primary anomeric  ${}^{13}C$  KIE for **9 $\beta$** , implying an  $A_ND_N$  mechanism. It will take quantitative analysis of the experimental KIEs to make a definite choice between a bimolecular or stepwise mechanism.

Taken together, these four studies indicate that non-enzymatic hydrolysis of  $\alpha$ -glucopyranosides with neutral leaving groups occurs via  $D_N + A_N$  type mechanisms, whereas  $\alpha$ -glucopyranosides with anionic leaving groups operate via  $A_ND_N$  mechanisms. The  $\alpha$ -secondary  ${}^2H$  KIE value measured for the spontaneous hydrolysis of compound **12** is larger than that reported for the acid-catalyzed hydrolysis of methyl  $\alpha$ -D-glucopyranoside.<sup>50</sup> The  $A_ND_N$  reaction of  $\alpha$ -D-glucopyranosyl fluoride (**9 $\alpha$** ) with azide ion gave an  $\alpha$ -secondary  ${}^2H$  KIE value of 1.154 (corrected to 80°C).<sup>162</sup> Although these values were suggestive of dissociative reactions, the fact that the value for **9 $\alpha$**  lies between those for methyl  $\alpha$ -D-glucopyranoside (**7 $\alpha$** ) and compound **12** is further evidence that  $\alpha$ -secondary  ${}^2H$  KIEs cannot be used to differentiate between  $D_N + A_N$  and  $A_ND_N$  reactions at acetal centers.<sup>50,51</sup>

### *Enzymatic hydrolysis*

KIEs on  $V_{max}$  were investigated for the yeast  $\alpha$ -glucosidase-catalyzed hydrolysis of 4-nitrophenyl- $\alpha$ -D-glucopyranoside and compounds **10–12** (Table 4).<sup>49,137</sup> It was determined that 4-nitrophenyl- $\alpha$ -D-glucopyranoside had a partially rate-limiting conformational change, whereas for the pyridinium type compounds **10** and **12**, only chemical steps were rate-limiting. This difference was attributed to the fact that 4-nitrophenyl- $\alpha$ -D-glucopyranoside exists in a  ${}^4C_1$  conformation which must undergo a conformational change to a skew or twist conformation before the chemical steps, unlike **10** and **12** which have skewed conformations in solution and require only small conformational changes before chemistry can occur. In a related study, large primary  ${}^{13}C$  KIEs for the yeast  $\alpha$ -glucosidase-catalyzed hydrolysis of **10** and **11** (Table 4) demonstrated that both reactions occurred via  $A_ND_N$  mechanisms with a small degree of nucleophilic assistance. These results are consistent with the double displacement mechanism proposed for retaining glycosidases<sup>4,159,160</sup> and *trans*-sialidase. These results are in contrast to the sugar beet  $\alpha$ -glucosidase-catalyzed hydrolysis of the  $\alpha$ -D-glucopyranosyl fluoride (**9 $\alpha$** ) where the primary  ${}^{13}C$  KIE was 1.007,<sup>162</sup> more consistent with a  $D_N * A_N$  mechanism.<sup>163</sup>

The  $\beta$ -secondary  ${}^2H$  KIEs for yeast  $\alpha$ -glucosidase-catalyzed hydrolysis of **10** and **11** are suggestive of substantial overlap of a C–H(D) bond with the p-orbital at the transition state, consistent with the glycosyl ring approaching a  ${}^{2,5}B$  boat conformation. Hosie and Sinnott had reported a similar value for the  $\beta$ -secondary  ${}^2H$  KIE on **10** as well as a large value for **12**.<sup>49</sup>



**Table 4** Experimental KIEs on  $k_{\text{cat}}$  or  $k_{\text{cat}}/K_{\text{M}}$  for the enzymatic hydrolysis of glucopyranosides

Compound	KIE				
	Type	$\alpha$ -Secondary $^2\text{H}$	$\beta$ -Secondary $^2\text{H}$	Primary $^{13}\text{C}$	Leaving group primary $^{15}\text{N}$
<b>9</b> <sup>a</sup>	$k_{\text{cat}}/K_{\text{M}}$	1.103 $\pm$ 0.009	1.027 <sup>b</sup>	1.007 <sup>c</sup>	–
<b>10</b> <sup>d</sup>	$k_{\text{cat}}$	–	1.115 $\pm$ 0.006	1.028 $\pm$ 0.006	1.019 $\pm$ 0.007
<b>11</b> <sup>d</sup>	$k_{\text{cat}}$	–	1.106 $\pm$ 0.009	1.027 $\pm$ 0.005	0.985 $\pm$ 0.005
<b>12</b> <sup>e</sup>	$k_{\text{cat}}$	1.21 $\pm$ 0.03	1.13 $\pm$ 0.02	–	–

<sup>a</sup>From Ref. 163.<sup>b</sup>From  $^2\text{H}$  KIEs calculated from  $^3\text{H}$  KIEs based on the Swain–Schaad relationship.<sup>c</sup>From  $^{13}\text{C}$  KIE calculated from  $^{14}\text{C}$  KIE based on the Swain–Schaad relationship.<sup>57</sup><sup>d</sup>From Ref. 137.<sup>e</sup>From Ref. 49.

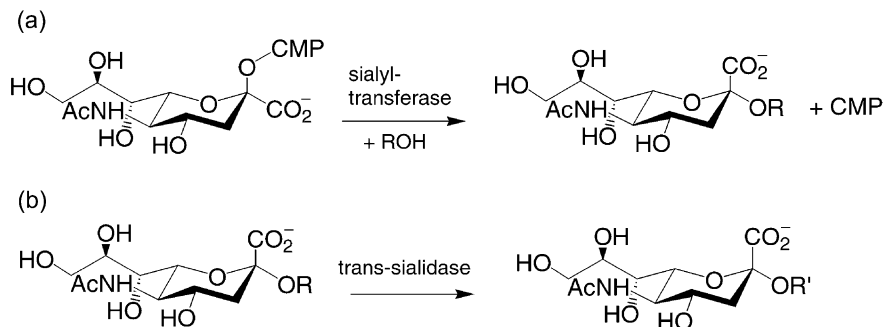
The primary  $^{15}\text{N}$  KIEs for the spontaneous hydrolysis of **12** (1.018, corrected to 25°C) and the yeast  $\alpha$ -glucosidase-catalyzed hydrolysis of **10** (1.019) suggested transition states with partial C–N bond cleavage. Similar results were found in a study by Scheuring and Schramm on pertussis toxin-catalyzed hydrolysis of  $\text{NAD}^+$ .<sup>80</sup> Based on the family of KIEs (primary  $^{15}\text{N}$  KIE value of 1.021), semi-empirical calculations and BOVA, these authors concluded that the reaction transition state had partial C–N bond breakage with a weak nucleophilic component from the incoming water molecule.

The most notable feature of the KIEs for yeast  $\alpha$ -glucosidase-catalyzed hydrolysis of **11** was the inverse primary  $^{15}\text{N}$  KIE of 0.985. No other primary  $^{15}\text{N}$  KIE for glycoside hydrolysis measured to date has been inverse. The  $\beta$ -secondary  $^2\text{H}$  KIE for **11** was large, indicating an oxocarbenium ion-like transition state, while the primary  $^{13}\text{C}$  was too large for a stepwise mechanism. Thus, the sugar ring KIEs indicated an  $\text{A}_\text{N}\text{D}_\text{N}$  mechanism, inconsistent with the inverse primary  $^{15}\text{N}$  KIE. Any loss of C–N bond order in forming an  $\text{A}_\text{N}\text{D}_\text{N}$  transition state should create a looser vibrational environment for the leaving group nitrogen and therefore a normal KIE. Protonation of  $^{15}\text{N}$  isoquinoline gives an inverse EIE of  $(1/1.0216 \pm 0.0005) = 0.979$ .<sup>137</sup> Protonation of the (aromatic) ring nitrogen before or during C–N bond breakage would give an inverse contribution to the KIE, but this does not seem chemically reasonable. The source of the inverse  $^{15}\text{N}$  KIE is not yet understood. Lower than expected primary  $^{15}\text{N}$  KIEs have been observed for PNP- and RTA-catalyzed reactions, although never an inverse KIE.

These studies indicate that for enzyme-catalyzed reactions, **9** $\alpha$  (with an anionic leaving group) reacts via a  $\text{D}_\text{N} * \text{A}_\text{N}$  mechanism, whereas  $\alpha$ -glucopyranosides with neutral leaving groups (**10** and **11**) operate via  $\text{A}_\text{N}\text{D}_\text{N}$  mechanisms. These results are opposite to what was found for the spontaneous hydrolysis reactions. The enzymatic reactions could also indicate differences in the enzyme mechanism, regardless of the leaving group.

#### SIALIDASES AND SIALYLTRANSFERASES

There is considerable interest in sialyltransferase reactions because of their importance in carbohydrate–protein interactions, such as selectin-sialyl Lewis X, which are important for inflammation and metastasis.<sup>166–169</sup> Sialyltransferases catalyze the transfer of *N*-acetylneuraminic acid from cytidine monophosphate (CMP) to an acceptor hydroxyl group of a glycoprotein, glycolipid or oligosaccharide with inversion of anomeric (C2) configuration (Fig. 20a). *Trans*-sialidases catalyze the transfer of  $\alpha$ -D-*N*-acetylneuraminic acid from host glycoconjugates to acceptors on the parasitic cell surface with retention of anomeric configuration (Fig. 20b).<sup>170</sup> Sialylation camouflages the parasites, allowing them to evade the host immune system. Inhibitors of *trans*-sialidases may be useful for treating parasitic infections.<sup>171</sup>

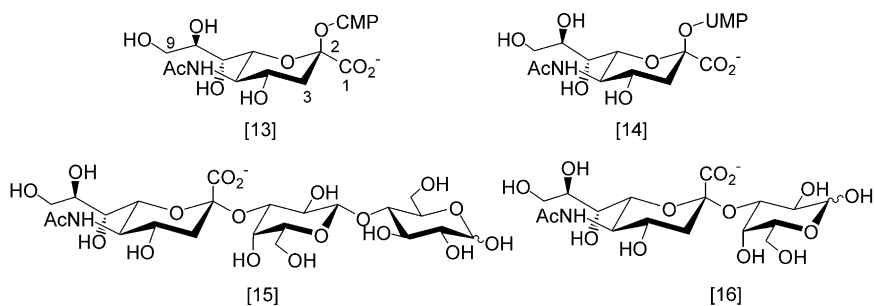


**Fig. 20** (a) Inverting reaction catalyzed by a sialyltransferase. (b) Retaining reaction catalyzed by a *trans*-sialidase.

Sialidases such as the influenza neuraminidase are retaining enzymes that catalyze the hydrolysis of  $\alpha$ -D-*N*-acetylneuraminic acids from oligosaccharides or glycolipids and glycoproteins. Inhibitors of these enzymes are of great interest since it has been shown that neuraminidase activity can correlate with virulence.<sup>4</sup>

#### *Acid-catalyzed hydrolysis*

Horenstein and Bruner performed TS analysis on the acid-catalyzed solvolysis of CMP- $\beta$ -D-*N*-acetylneuraminidine **13** (Table 5).



For the acid-catalyzed solvolysis reaction, the large  $\beta$ -secondary  $^2\text{H}$  and small anomeric primary  $^{13}\text{C}$  KIEs were suggestive of a late transition state that is dissociative in nature. Taken into account with methanolysis data, it was determined that the reaction occurs via a  $\text{D}_\text{N} + \text{A}_\text{N}$  mechanism with the formation of an oxocarbenium ion intermediate with finite lifetime, stabilized electrostatically by the carboxylate ion at C1. This allowed for capture by solvent from

**Table 5** Competitive experimental KIEs for sialoside solvolysis and on  $k_{\text{cat}}/K_{\text{M}}$  for enzyme-catalyzed transfer

KIE	<b>13</b>		<b>14</b>	<b>15</b>		<b>16</b>	
	Solvolysis <sup>a</sup>	Transfer <sup>b,c</sup>	Transfer <sup>d,e</sup>	Solvolysis <sup>e</sup>	Transfer <sup>e</sup>	Solvolysis <sup>e</sup>	Transfer <sup>e,e</sup>
$\beta$ -Secondary <sup>2</sup> H	1.276 ± 0.008	1.044 ± 0.007	1.218 ± 0.010 <sup>d</sup>	1.113 ± 0.012	1.053 ± 0.010	–	1.060 ± 0.008
$\alpha$ -Secondary <sup>14</sup> C	1.013 ± 0.004 <sup>c</sup>	0.998 ± 0.004	–	–	–	–	–
Primary carbon	1.030 ± 0.005 ( <sup>14</sup> C)	1.000 ± 0.004 ( <sup>14</sup> C)	1.028 ± 0.010 ( <sup>14</sup> C)	1.016 ± 0.011 ( <sup>13</sup> C)	1.021 ± 0.014 ( <sup>13</sup> C)	1.015 ± 0.008 ( <sup>13</sup> C)	1.032 ± 0.008 ( <sup>13</sup> C)
Remote <sup>3</sup> H	1.002 ± 0.010	0.984 ± 0.007	0.944 ± 0.010	–	–	–	–

<sup>a</sup>From Ref. 54.<sup>b</sup>From Ref. 104.<sup>c</sup>KIEs corrected for commitment to catalysis.<sup>d</sup>From Ref. 48.<sup>e</sup>From Ref. 170.

either face of the oxocarbenium ion.<sup>54</sup> This is in contrast to the acid-catalyzed solvolysis KIEs for the sialyl-lactose compound (**15**) and the sialyl-galactose compound (**16**) (Table 5),<sup>170</sup> which had large primary <sup>13</sup>C KIEs, suggestive of A<sub>N</sub>D<sub>N</sub> mechanisms.

### Enzymatic transfer

The transfer reaction catalyzed by rat liver  $\alpha(2 \rightarrow 6)$  sialyltransferase using **13** and *N*-acetylglucosamine as the substrates displayed kinetically significant substrate binding.<sup>104</sup> Even after the observed KIEs for **13** were corrected, they were still too low for any mechanism involving only chemical steps, suggesting that a non-chemical step was kinetically significant (Table 5).

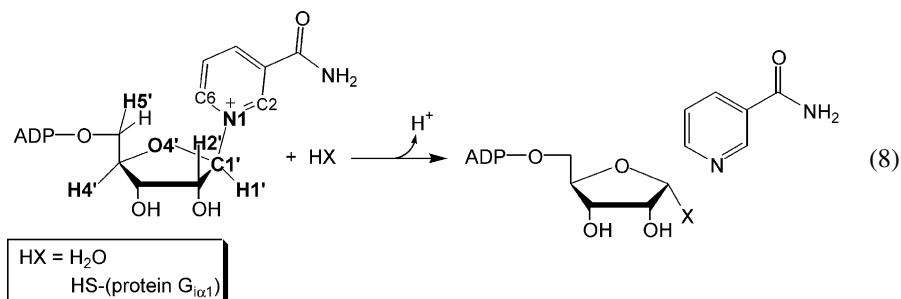
TS analysis was performed using the UMP analogue, **14**, and *N*-acetylglucosamine as substrates. Compound **14** was a less efficient substrate, resulting in an increased barrier for the chemical step and allowing intrinsic KIEs to be determined. The  $\beta$ -secondary <sup>2</sup>H KIE for **14** was similar to the solvolysis reaction of **13**, and 4.5-fold larger than that for enzymatic transfer with **13**.<sup>48</sup> The anomeric primary <sup>13</sup>C KIE for **14** was also similar to that determined for the solvolysis reaction of **13**. Taken together, the KIEs for the enzyme-catalyzed reaction indicate a stepwise reaction, following a D<sub>N</sub> \* A<sub>N</sub> mechanism. A large inverse KIE at H9 was found for **14**, as discussed in Section 3.

Using a *trans*-sialidase from *Trypanosoma cruzi*, TS analysis was performed on the transfer of *N*-acetylneuraminic acid from the tri- and disaccharides **15** and **16**, respectively, to lactose.<sup>170</sup> Small  $\beta$ -secondary dideuterium KIEs and large anomeric primary <sup>13</sup>C KIEs were observed for both compounds (Table 5). The large primary effects were believed to indicate an A<sub>N</sub>D<sub>N</sub> mechanism and could be evidence for a covalent enzyme-intermediate. The low  $\beta$ -secondary effects relative to solvolysis were rationalized by the authors to indicate differences in TS charge development rather than being a consequence of sugar ring conformation change.

### BACTERIAL ADP-RIBOSYLATING TOXINS AND NON-ENZYMATIC NAD<sup>+</sup> HYDROLYSIS

Certain bacteria exert toxic effects on their hosts through the action of ADP-ribosylation reactions where the nicotinamide ring of NAD<sup>+</sup> is displaced and ADP-ribose is attached to some host cell protein (equation 8). DTA ADP-ribosylates diphthamide, a post-translationally modified residue on elongation factor 2, which is required for protein biosynthesis. Blocking protein biosynthesis causes cell death. Cholera and pertussis toxins ADP-ribosylate cellular G-proteins at specific Arg and Cys residues, respectively. In the absence of the physiological targets, all three enzymes will slowly hydrolyze NAD<sup>+</sup> to ADP-ribose and nicotinamide. TS analysis has been performed on NAD<sup>+</sup> hydrolysis catalyzed by cholera toxin,<sup>70</sup> DTA,<sup>17</sup> and

pertussis toxin,<sup>80</sup> as well as the spontaneous hydrolysis.<sup>69</sup>



*TS analysis of NAD<sup>+</sup> hydrolysis.* The hydrolysis reactions of NAD<sup>+</sup> all proceeded through highly dissociative A<sub>N</sub>D<sub>N</sub> transition states. The transition state for the pH-independent solvolytic hydrolysis of NAD<sup>+</sup> had  $n_{LG} = 0.02$  and  $n_{Nu} = 0.005$ . Assignment of the non-enzymatic mechanism as A<sub>N</sub>D<sub>N</sub> was based on a variety of experimental evidence in addition to the experimental KIEs. The large negative Brønsted coefficient,  $\beta_{LG} = -0.9$ , for non-enzymatic NAD<sup>+</sup> hydrolysis<sup>172</sup> was consistent with either a highly asynchronous A<sub>N</sub>D<sub>N</sub> mechanism, or a D<sub>N</sub>\*A<sub>N</sub> mechanism with formation of a discrete oxocarbenium ion intermediate. In the analysis of Jencks,<sup>173,174</sup> the rate-limiting step, and therefore the TS structure, depends on the stability of the oxocarbenium ion. If the oxocarbenium ion is stable enough to have a finite existence in solution, then a D<sub>N</sub>\*A<sub>N</sub> mechanism is possible. Chemical evidence in the literature rules this out for NAD<sup>+</sup> hydrolysis. If an oxocarbenium ion were formed, the product distribution would be expected to be sensitive to nucleophile strength, and a mixture of inversion and retention of configuration at the anomeric carbon would be expected. In NAD<sup>+</sup> reactions, the product distribution depends on the molar ratios of methanol and water rather than their nucleophilicities,<sup>141</sup> and the methanolysis product is predominantly the  $\alpha$ -anomer (22:1,  $\alpha$ : $\beta$ ),<sup>175</sup> indicating that A<sub>N</sub>D<sub>N</sub> predominates. In addition, the 330-fold decrease in the rate of hydrolysis of a riboside analogue with a bulky substituent that prevents “backside solvation”<sup>176</sup> is further evidence for pre-association of the nucleophile and against a D<sub>N</sub>\*A<sub>N</sub> mechanism. Finally, attempts to match the experimental KIEs using BOVA to a D<sub>N</sub>\*A<sub>N</sub> mechanism with either leaving group departure or nucleophile approach as the first irreversible step did not yield reasonable candidate TS structures.

The TS structures initially reported for the cholera and pertussis toxin-catalyzed hydrolysis reactions had leaving group bond orders,  $n_{LG}$ , of 0.09 and 0.1, respectively, and very low nucleophile bond orders,  $n_{Nu}$ , of 0.005 and 0.001. It was later shown using structure interpolation that it is necessary to account for increases in the N1–C2 and N1–C6 bond orders in the nicotinamide ring that partially compensate for the loss of C1'–N1 bond order. After accounting for changes in the nicotinamide ring structure, the TS structures were essentially the same as for DTA, which had  $n_{LG} = 0.02$  and  $n_{Nu} = 0.03$ . It should be emphasized

that these changes are small and reflect a refinement of KIE interpretation methods. The enzymatic hydrolysis reactions form highly dissociative  $A_N D_N$  transition states very similar to the non-enzymatic reaction. The increase in nucleophile bond order at the transition state relative to the non-enzymatic reaction may be a consequence of the invariant glutamic acid residue in the active sites that may help to orient and/or activate the water nucleophile. The experimental TS structure was docked with the DTA structure (see Section 3).

*TS analysis of ADP-ribosylation by pertussis toxin.* TS analyses have been performed on the ADP-ribosylation of a model peptide<sup>81</sup> and protein  $G_{i\alpha 1}$ <sup>47</sup> by pertussis toxin. The KIEs for these reactions were identical within experimental error, meaning that the transition states were identical even though the specificity constant,  $k_{cat}/K_M$ , with protein  $G_{i\alpha 1}$  was 800-fold higher than with the peptide. The ADP-ribosylation reactions were significantly more synchronous,  $n_{LG} = 0.11$ ,  $n_{Nu} = 0.09$ , than the hydrolysis reactions. This indicated that the enzyme uses binding energy to increase the nucleophile participation at the transition state. The fact that the transition states were the same for the peptide and the protein substrates implies that all the structural determinants needed to define the structure of the transition state are present in the 20-mer peptide substrate. The additional enzyme-substrate interactions with protein  $G_{i\alpha 1}$  as the second substrate, which are necessarily remote from the site of catalysis, increase the catalytic efficiency 800-fold without changing the transition state. The ADP-ribosylation of protein  $G_{i\alpha 1}$  was performed using catalytic amounts of  $\beta$ - and  $\gamma$ -subunits, which formed an  $\alpha\beta\gamma$ -trimer. Thus, the experimental KIEs were measured for the TS complex of pertussis toxin $\cdot$ NAD<sup>+</sup> $\cdot$ G $_{\alpha\beta\gamma}$ , a pentamolecular complex with a combined molecular mass of 100 kDa, possibly the most complex system examined to date by TS analysis. In spite of the size and complexity of the system, it was possible to measure accurately KIEs that reflected the chemical steps of the reaction.

Considering that a thiolate anion is  $10^7$ – $10^9$ -fold more nucleophilic than a neutral thiol,<sup>177,178</sup> the nucleophile in this reaction will be the thiolate anion of Cys351 of protein  $G_{i\alpha 1}$ . The inverse SDKIE of 0.65 was originally cited as evidence for a pre-equilibrium deprotonation of Cys351.<sup>47</sup> However, it is not greatly different from the SDKIEs measured for the enzymatic hydrolysis reactions, i.e. 0.73 for pertussis toxin, 0.82 for cholera toxin. SDKIEs of this magnitude can arise from simple viscosity effects.<sup>179</sup> Given the  $pK_a = 8.37$  of an unperturbed cysteine residue in solution, at physiological pH 7.4 a significant fraction would be deprotonated and nucleophilic.

As with DTA, the experimental transition state was docked with the X-ray crystallographic structure of pertussis toxin, along with a model of the reactive peptide from protein  $G_{i\alpha 1}$ .<sup>180</sup> As in DTA, there is a carboxylate residue, Glu129, located directly adjacent to the incipient positive charge in the oxocarbenium ion-like transition state. His35, which has been shown to be important to catalysis and has been proposed to act as a general base to activate the nucleophile,<sup>181</sup> is located near the pyrophosphate of NAD<sup>+</sup> and not in a position to act as a general base. His35 is structurally homologous to His21 of DTA, which also interacts with the

pyrophosphate group, and His44 of cholera toxin, which had also been advanced as a candidate general base.<sup>70</sup>

TS analysis studies, combined with structure and enzyme kinetic studies, have suggested some solutions to Cordes' dilemma,<sup>182</sup> which was originally stated in relation to  $\text{NAD}^+$  glycohydrolase reactions. To rephrase the dilemma: (1) because the leaving group nicotinamide is cationic, general acid catalysis cannot be important; (2) because there is little nucleophile participation at the transition state, general base activation of the nucleophile cannot be important; (3) because both the reactant and transition state are positively charged, electrostatic stabilization is unlikely to be important, and therefore; (4) catalysis by distortion may be a resolution to this dilemma. Points (1) and (2) are true; however, point (4) was undermined by the lack of obvious distortion in the  $\text{DTA}\cdot\text{NAD}^+$  complex.<sup>103</sup> As discussed above, the distribution of positive charge changes dramatically between reactant and the transition state, making it possible for enzymes to stabilize positive charge in a different location in the transition state than in the reactant. Also, hydrophobic interactions with the nicotinamide ring will tend to stabilize the transition state (and products) over the reactant  $\text{NAD}^+$ , which bears significant positive charge delocalized around the nicotinamide ring. Finally, ADP-ribosylating toxins use binding energy from the protein substrates to stabilize transition states through as-yet unknown mechanisms, as evidenced by the 800-fold increase in  $k_{\text{cat}}/K_{\text{M}}$  between the peptide substrate of pertussis toxin and protein  $\text{G}_{i\alpha 1}$ .

#### NUCLEOSIDE AND AMP HYDROLASES

##### *IU-nucleoside hydrolase (IU-NH)*

IU-NH is among the most thoroughly characterized *N*-glycosidases. In addition to kinetic characterization<sup>82,183</sup> and TS analysis,<sup>16,71</sup> the electrostatic potential surfaces of substrate, transition state and products have been analyzed and used as a template for inhibitor design.<sup>184</sup> Inhibitors have been synthesized and characterized.<sup>100,142,185-188</sup> The crystal structure of IU-NH has been determined in the unliganded form<sup>189,190</sup> and as a cocrystal with a potent inhibitor.<sup>101</sup> In addition to kinetic characterization of inhibitors, theoretical studies were used to rationalize and then predict the inhibitory activity of different compounds.<sup>191-194</sup>

The experimental KIEs<sup>71</sup> were qualitatively similar to other hydrolysis reactions. The primary leaving group  $9\text{-}^{15}\text{N}$  KIE =  $1.026 \pm 0.004$  indicated extensive  $\text{C1}'\text{-N9}$  bond breakage at the transition state. The  $\alpha$ - and  $\beta$ -secondary  $^3\text{H}$  KIEs indicated an oxocarbenium ion-like transition state,  $1'\text{-}^3\text{H}$  KIE =  $1.150 \pm 0.006$ ,  $2'\text{-}^3\text{H}$  KIE =  $1.161 \pm 0.003$ , while the primary carbon KIE was too large for a stepwise mechanism,  $1'\text{-}^{14}\text{C}$  KIE =  $1.044 \pm 0.004$ . The large remote  $\delta$ -secondary  $^3\text{H}$  KIE,  $5'\text{-}^3\text{H}$  KIE =  $1.051 \pm 0.003$ , was interpreted as being due to an enzyme-induced conformation of the  $\text{C5}'$  hydroxymethyl group that can help stabilize the oxocarbenium ion-like  $\text{A}_{\text{N}}\text{D}_{\text{N}}$  transition state (see Section 3).

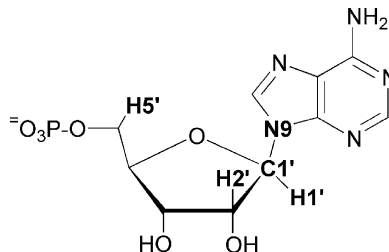


**Table 6** Competitive experimental KIEs for AMP hydrolysis

Isotopic label <sup>a</sup>	Acid catalyzed	AMP nucleosidase <sup>b</sup>		Mutant AMP nucleosidase <sup>c</sup>	
		No ATP	0.5 mM ATP	No ATP	0.5 mM ATP
1'- <sup>14</sup> C	1.044 ± 0.003	1.035 ± 0.002	1.032 ± 0.002	1.041 ± 0.006	1.041 ± 0.003
9- <sup>15</sup> N	1.030 ± 0.002	1.030 ± 0.003	1.025 ± 0.002	1.034 ± 0.002	1.021 ± 0.002
1'- <sup>3</sup> H	1.216 ± 0.004	1.069 ± 0.003	1.047 ± 0.002		
2'- <sup>2</sup> H	1.077 ± 0.002	1.061 ± 0.002	1.043 ± 0.002		
5'- <sup>3</sup> H	1.006 ± 0.002	1.007 ± 0.003	1.006 ± 0.002		

KIEs are on  $k_{\text{cat}}/K_M$  for enzymatic reactions.

<sup>a</sup>



<sup>b</sup>From Ref. 139.

<sup>c</sup>From Ref. 79.

TS analysis revealed a dissociative  $A_N D_N$  transition state with relatively high residual bond order to the leaving group adenine,  $n_{LG} = 0.19$ , and very weak bond order to the water nucleophile,  $n_{Nu} = 0.005$ . However, a reassessment of the experimental KIEs using the structure interpolation approach has indicated a more “balanced” transition state, with  $n_{LG} = 0.05$ , and  $n_{Nu} = 0.06$  (unpublished results; see also Section 2). As discussed above, IU-NH appears to operate primarily through stabilization of the ribosyl portion of the oxocarbenium ion-like transition state, involving little interaction with the leaving group.

### *AMP nucleosidase and acid-catalyzed AMP hydrolysis*

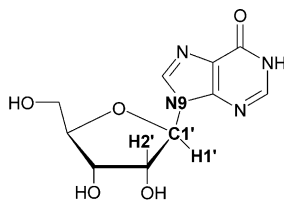
The experimental KIEs for acid-catalyzed AMP hydrolysis indicate an  $A_N D_N$  mechanism. The 9- $^{15}\text{N}$  KIE = 1.030 is less than the semi-classical limit of 1.044<sup>61, 165</sup> because the increase in bond orders within the adenine ring compensate for the loss of the C1'–N9 bond. Protonation at N7 in the acid-catalyzed reaction makes the incipient anionic leaving group neutral, and helps to transfer  $\pi$ -bonding electrons into the bonds with N9.

The AMP nucleosidase reaction was studied by TS analysis with and without adenosine 5'-triphosphate (ATP) as an allosteric activator (Table 6).<sup>78,79,139,195</sup> An allosteric activator activates the enzyme by binding at a location remote from the catalytic site. The presence of 0.5 mM ATP increases  $k_{cat}$  by 200-fold with minimal effect on  $K_M$ . The KIEs for hydrolysis by AMP nucleosidase are similar to those for the non-enzymatic reaction, implying a similar mechanism. In the presence of the allosteric activator ATP, most of the experimental KIEs decreased in magnitude. This could be taken as a sign of non-chemical kinetically significant steps; however, the KIEs would be expected to decrease by the same proportion if that was true. In fact, the secondary hydron KIEs decrease more than the heavy atom KIEs, and the remote 5'- $^3\text{H}$  KIE did not decrease. The lower 9- $^{15}\text{N}$  KIE in the presence of ATP implies a lower extent of C1'–N9 bond breakage at the transition state, i.e. the enzyme stabilizes the leaving group more strongly and thereby achieves the transition state earlier in the C–N bond breakage.

A mutant enzyme was isolated and characterized kinetically.<sup>79</sup> This mutant was not sequenced; it is simply referred to as a  $V_{max}$  mutant because the value of  $k_{cat}$  was decreased by 50-fold while there was little change in other kinetic parameters, including  $K_M$ , activation by ATP, and inhibition by formycin 5'-phosphate. The larger 9- $^{15}\text{N}$  KIE = 1.034 with the unactivated mutant enzyme may be explained either by an even greater extent of C–N bond breakage at the transition state, or a lack of protonation at N7. Allosteric activation by ATP still increased by the same extent, 200-fold, and still caused a decrease in the 9- $^{15}\text{N}$  KIE. In this case, it may indicate protonation at N7 and/or a smaller extent of C–N bond breakage at the transition state.

**Table 7** Experimental KIEs on  $k_{\text{cat}}/K_M$  for PNP-catalyzed reactions with inosine

Isotopic label <sup>a</sup>	Experimental KIE	
	Steady state arsenolysis <sup>b</sup>	Pre-steady state hydrolysis <sup>c</sup>
1'- <sup>14</sup> C	1.026 ± 0.006	1.045 ± 0.005
9- <sup>15</sup> N	1.010 ± 0.005	1.000 ± 0.005
1'- <sup>3</sup> H	1.141 ± 0.004	1.151 ± 0.004
2'- <sup>3</sup> H	1.152 ± 0.003	1.145 ± 0.003

<sup>a</sup><sup>b</sup>From Ref. 28. Experimental KIEs were corrected for commitment to catalysis,  $C_f = 0.19$ .<sup>c</sup>From Ref. 27.

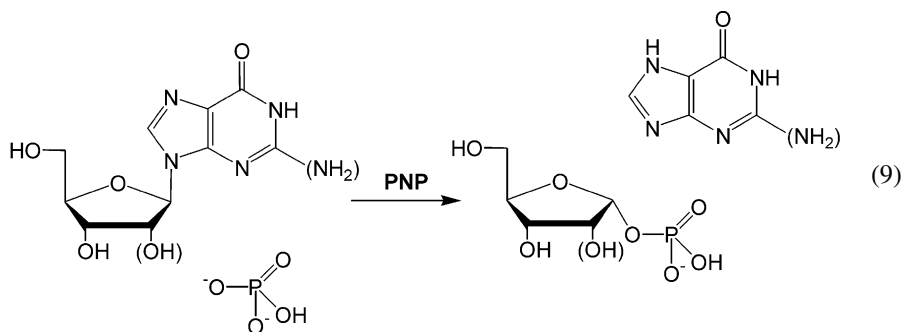
## PHOSPHORYLASE AND PYROPHOSPHORYLASE REACTIONS

*Purine nucleoside phosphorylase (PNP)*

Bovine PNP is involved in the mammalian purine salvage pathway, catalyzing phosphorolysis of inosine, guanosine or their 2'-deoxy analogues (equation 9). It is a trimeric enzyme with three identical subunits. It displays third-of-sites activity, with only one subunit active at any time.<sup>31</sup> KIEs were measured for phosphorolysis of inosine by bovine spleen PNP.<sup>28</sup> The 1'-<sup>3</sup>H KIE =  $1.047 \pm 0.002$  for the overall reaction was equal to the previously measured binding KIE =  $1.047 \pm 0.02$  for formation of the Michaelis complex, PNP·phosphate·inosine.<sup>125</sup> This, along with primary 1'-<sup>14</sup>C KIE =  $1.000 \pm 0.001$  for the overall reaction, indicated non-chemical kinetically significant steps. The commitment to catalysis (ratio of  $k_3/k_2$  in Fig. 2) for phosphorolysis of inosine was later determined to be 2.1.<sup>27</sup>

TS analysis was performed for two PNP-catalyzed reactions, arsenolysis of inosine using arsenate as a phosphate analogue, and a pre-steady state TS analysis of PNP-catalyzed inosine hydrolysis. The ribosyl ring KIEs (Table 7) were typical of those observed previously for other reactions of *N*-ribosides, indicating an  $A_N D_N$  mechanism for hydrolysis and either an  $A_N D_N$  or  $D_N * A_N$  for arsenolysis. The

primary  $^{15}\text{N}$  KIEs, however, are unusually low.



*TS analysis of inosine arsenolysis.* TS analysis was performed on the arsenolysis of inosine under steady state conditions. The primary,  $1'^{14}\text{C}$  KIE was near the lower limit (1.025–1.029) calculated for an  $\text{A}_\text{N}\text{D}_\text{N}$  mechanism with adenosine<sup>58</sup> and could indicate either an  $\text{A}_\text{N}\text{D}_\text{N}$  or  $\text{D}_\text{N} * \text{A}_\text{N}$  mechanism. The large  $\alpha$ - and  $\beta$ -secondary  $^3\text{H}$  KIEs indicated a transition state with high oxocarbenium ion character. Analysis of X-ray crystal structures of PNP demonstrates that there is not enough space in the enzyme active site between the leaving group purine and the phosphate nucleophile to allow formation of a stable oxocarbenium ion (see Section 3). Thus, the most likely mechanism for arsenolysis is an extremely dissociative  $\text{A}_\text{N}\text{D}_\text{N}$  mechanism. The primary,  $9\text{-}^{15}\text{N}$  KIE = 1.010 was lower than expected, as discussed below.

*TS analysis of inosine hydrolysis.* Experimental KIEs were determined for inosine hydrolysis under pre-steady state conditions because of the exceptionally slow dissociation of hypoxanthine (estimated  $K_\text{d} = 1.3$  pM), which is rate-limiting under steady state conditions. Hypoxanthine binds to the other two PNP subunits with much lower affinity. KIEs in the ribosyl ring were typical of an  $\text{A}_\text{N}\text{D}_\text{N}$  mechanism. When the reaction was run in 20% methanol, the product ratio was 85:15 1-methylribose:ribose. This is close to the ratio expected based on the relative nucleophilicities of MeOH and water, indicating that there is significant participation of the nucleophile in the reaction coordinate. As with the arsenolysis, the primary,  $9\text{-}^{15}\text{N}$  KIE of 1.000 was anomalous. These KIEs were initially rationalized as indicating an internal equilibrium formation of ribose and hypoxanthine; however, this is inconsistent with what is now known about the observable KIEs for stepwise reactions.<sup>58</sup>

*Mechanism, and the source of unusual KIEs.* The primary  $9\text{-}^{15}\text{N}$  KIEs for the PNP-catalyzed reactions were anomalously low compared both to calculations and other experimental leaving group primary  $^{15}\text{N}$  KIEs. The expected KIE for complete *N*-glycoside bond breakage would be  $> 1.026$ , the KIE for inosine hydrolysis by IU-NH. Anomalously low  $9\text{-}^{15}\text{N}$  KIEs may arise from the strong enzyme-leaving group interactions observed in cocrystal structures of PNP with substrate, product, and inhibitor complexes. For many reactions discussed in this chapter, the primary KIEs could be modeled by BOVA or quantum mechanical analyses and were apparently

“unperturbed”. In the case of PNP, it is possible that strong leaving group activation by the enzyme affects the vibrational environment of N9, making it more vibrationally constrained. This could occur through interactions observed in the X-ray crystal structures, including protonation at N7 and hydrogen bond donation through the exocyclic oxygen. These would tend to reduce the KIE at N9. If this were occurring, it might be expected that the anomaly would be correlated with the tightness of hypoxanthine binding. The affinity of PNP for hypoxanthine has been estimated under steady state conditions in the presence ( $K_d = 1.7 \mu\text{M}$ ) and absence ( $K_d = 1.3 \text{ pM}$ ) of ribose-1-phosphate. The  $K_d$  of PNP with hypoxanthine in the presence of ribose-1-arsenate is not known, but pre-steady state experiments showed that there was a burst of hypoxanthine formation in the arsenolysis reaction, followed by a 10-fold slower steady state rate, with  $k_{\text{cat}} = 2 \text{ s}^{-1}$ . If rate-limiting hypoxanthine dissociation and diffusion-limited binding of hypoxanthine are assumed, then a value of  $K_d = 5 \text{ nM}$  is estimated. Thus, the size of the anomaly in the  $9\text{-}^{15}\text{N}$  KIE (1.010 for arsenolysis, 1.000 for hydrolysis) correlates with tightness of the enzyme interaction with hypoxanthine ( $K_d = 5 \text{ nM}$  and  $1.3 \text{ pM}$ , respectively).

A mechanism for arsenolysis involving a highly dissociative  $A_N D_N$  transition state, with an anomalously low  $9\text{-}^{15}\text{N}$  KIE arising from enzyme activation of the leaving group is consistent with the pre-steady state and steady state kinetic experiments, with the crystal structures, and with the arsenolysis KIEs. In this model, the reaction proceeds through electrophile migration, where there are many enzyme interactions with the leaving group and nucleophile, but few with the ribosyl ring.

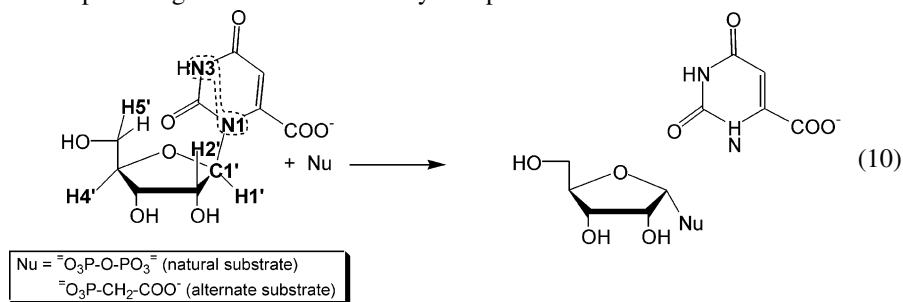
A variant on electrophile migration is suggested for the hydrolysis reaction, based on several lines of evidence: (1) PNP can form exceptionally tight interactions with hypoxanthine ( $K_d = 1.3 \text{ pM}$ ); (2) there are many contacts with the phosphate nucleophile in the crystal structures which orient and activate anionic phosphate through its negatively charged oxygen atoms and increase the reaction rate 100-fold; (3) these contacts would not activate water or methanol nucleophiles, which are much smaller and neutral; (4) the paucity of enzyme-ribosyl contacts argues against strong stabilization of the oxocarbenium ion; and (5) the larger  $1'\text{-}^{14}\text{C}$  KIE = 1.045 for inosine hydrolysis indicates a more synchronous  $A_N D_N$  transition state than arsenolysis, and therefore a smaller distance between leaving group and nucleophile atoms.

Thus, the water (or methanol) nucleophile is poorly situated and chemically incompatible with the nucleophile activation normally catalyzed by PNP, so nucleophilic attack will not be enzyme activated. Nonetheless, the large amount of 1-methylribose formed by PNP indicates that nucleophile participation is important. Taken together, this evidence suggests a mechanism where strong PNP-hypoxanthine binding activates the leaving group toward nucleophilic displacement and creates a vibrationally constrained environment for N9. This activated *N*-glycosidic bond is susceptible to attack from solvent water or methanol, which is not activated by the enzyme. The mechanism is dissociative  $A_N D_N$ , though more synchronous than the arsenolysis reaction.

### Phosphoribosyl transfer reactions

Experimental KIEs have been determined by two groups for the orotate phosphoribosyltransferase (OPRTase)-catalyzed reaction (equation 10)<sup>196,197</sup> and several other phosphoribosyltransferases.<sup>197</sup> Unfortunately, in the latter study, the primary,  $1'-^{14}\text{C}$  KIEs were measured using  $5'-^3\text{H}$  as a remote label, with the assumption that there was no KIE at  $\text{H}5'$ . It is now known that this is generally not true, and is specifically not true in the case of OPRTase, where  $5'-^3\text{H}$  KIE =  $1.028 \pm 0.008$ . KIEs were measured for OPRTase using pyrophosphate, the normal nucleophile, and phosphonoacetic acid, an alternate substrate. Phosphonoacetic acid was used because KIEs measured using pyrophosphate were very small, suggesting non-chemical kinetically significant steps. The ribosyl ring KIEs for OPRTase indicated a dissociative  $\text{A}_\text{N}\text{D}_\text{N}$  transition state. The secondary  $^3\text{H}$  KIEs suggested an oxocarbenium ion-like transition state, with  $1'-^3\text{H}$  KIE =  $1.200 \pm 0.007$  and  $2'-^3\text{H}$  KIE =  $1.140 \pm 0.007$ , while the primary,  $1'-^{14}\text{C}$  KIE =  $1.040 \pm 0.004$  was too large for a  $\text{D}_\text{N} * \text{A}_\text{N}$  mechanism. Interpretation of the primary  $^{15}\text{N}$  KIE was complicated by the fact that the substrate was labeled at two positions, N1 and N3. The  $1,3-^{15}\text{N}$  KIE =  $1.006 \pm 0.005$  was smaller than expected for a dissociative  $\text{A}_\text{N}\text{D}_\text{N}$  mechanism. It was possible to rationalize the observed  $1,3-^{15}\text{N}$  KIE by invoking strong interactions with the orotate ring leading to an inverse KIE at N3. As with PNP, the structure of the transition state was modelled by docking the substrate at the active site cleft of OPRTase determined by X-ray crystallographic analysis<sup>198,199</sup> shows many interactions between the enzyme and the leaving group orotate ring, and between the enzyme and the pyrophosphate nucleophile, but few direct contacts with the ribosyl ring. One may postulate that, as with PNP, the enzyme operates through an electrophile migration mechanism that proceeds through a highly dissociative  $\text{A}_\text{N}\text{D}_\text{N}$  transition state.

The crystal structure of hypoxanthine phosphoribosyltransferase has been solved in a ternary complex of the enzyme with the substrate 5-phosphoribosyl 1-pyrophosphate (PRPP) and an analogue of hypoxanthine with a carbon atom in place of N9.<sup>200</sup> As with PNP and OPRTase, these structures showed many contacts with the leaving group and nucleophile, but few with the ribosyl ring. Again, an electrophile migration mechanism may be operative here.



## DNA AND RNA

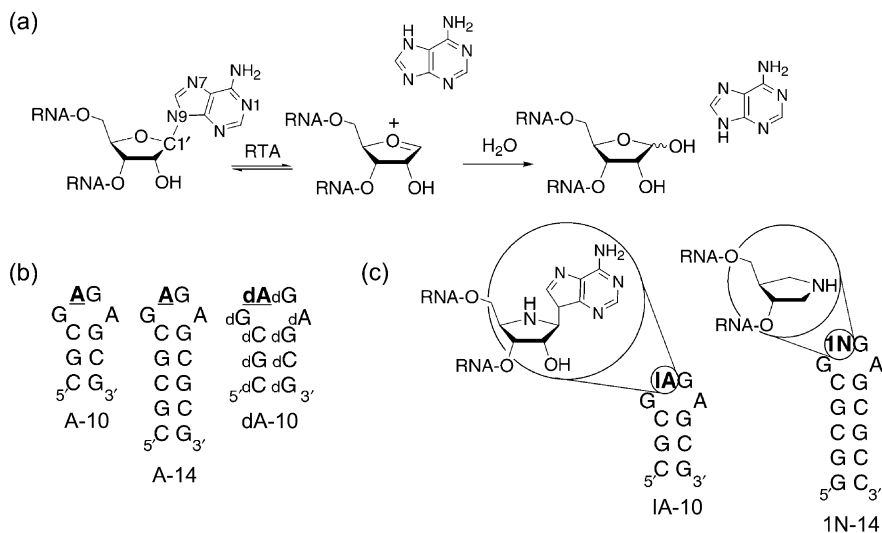
*Uracil DNA glycosylase (UDG)*

UDG removes uridine residues from DNA. These arise from spontaneous deamination of cytidine residues, and from misincorporation of UTP into DNA. A wide variety of experimental approaches has been used to study UDG, including the TS analysis reported by Werner and Stivers<sup>135,144,145,151,201–203</sup> (see also Section 3).

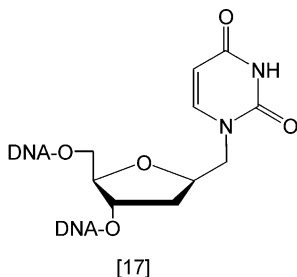
UDG has been shown to exhibit diffusion-limited binding with good substrates;<sup>203</sup> however, selection of a single-stranded trinucleotide substrate avoided kinetically significant substrate association. Experimental KIEs were determined using a novel dual-label technique whereby a non-radioactive isotopic label of interest, e.g.  $1'-^{13}\text{C}$  (Fig. 17d), was placed in the ribosyl ring and a radiolabel,  $2-^{14}\text{C}$ , was placed in the uracil ring to act as a reporter on the label of interest. A tritium label in the uracil ring,  $5-^3\text{H}$ , was used as a reporter on the light isotope at the position of interest,  $1'-^{12}\text{C}$  in this example. Isotope ratios, and hence KIEs, were measured by using ion exchange chromatography to isolate the uracil product from the DNA substrate after reaction.

The experimental  $1'-^{13}\text{C}$  KIE was  $1.010 \pm 0.009$  and the  $1'-^2\text{H}$  KIE was  $1.20 \pm 0.02$ . The  $\beta$ -secondary  $^2\text{H}$  KIEs were large and nearly equal,  $2'S-^2\text{H}$  KIE =  $1.10 \pm 0.01$ ,  $2'R-^2\text{H}$  KIE =  $1.11 \pm 0.01$ , indicative both of high oxocarbenium ion character and of strong hyperconjugation. The authors compared the experimental  $1'-^{13}\text{C}$  and  $1'-^3\text{H}$  KIEs with all available primary and  $\alpha$ -secondary KIEs for similar glycolysis and glycosyl transfer reactions. They concluded that the  $1'-^{13}\text{C}$  and  $1'-^2\text{H}$  KIEs, taken together, likely support a  $\text{D}_\text{N} * \text{A}_\text{N}$  mechanism, although a highly dissociative  $\text{A}_\text{N}\text{D}_\text{N}$  mechanism is also possible. The large secondary  $^2\text{H}$  KIE is indicative of an oxocarbenium ion(-like) structure, as is the small  $1'-^{13}\text{C}$  KIE. The reported standard deviation for the  $1'-^{13}\text{C}$  KIE is somewhat large, 0.009; however, using the reported standard deviation and the number of independent determinations, 14, it is possible to estimate the 95% confidence interval as 0.005. The  $1'-^{13}\text{C}$  is near the calculated values for  $\text{D}_\text{N} * \text{A}_\text{N}$  hydrolysis of adenosine, 1.008–1.009, but it is not unambiguously smaller than the calculated lower limit of 1.013–1.015<sup>#16</sup> for an  $\text{A}_\text{N}\text{D}_\text{N}$  transition state.<sup>58</sup> The inhibition of UDG by DNA containing a  $2'$ -deoxyuridine analogue with a methylene bridge between the deoxyribosyl and uracil moieties (**17**) provides some support for a discrete ion pair intermediate, though  $K_\text{d}$  for the inhibitor (160 nM) was not compared with the corresponding equilibrium dissociation constant,  $K_\text{s}$ , for the analogous substrate DNA.<sup>204</sup> The methylene bridge between the rings would be expected to be too long to mimic an  $\text{A}_\text{N}\text{D}_\text{N}$  transition state, but could mimic an oxocarbenium/uracil ion pair.

<sup>#16</sup> It is possible to estimate a  $^{13}\text{C}$  KIE from a  $^{14}\text{C}$  KIE using the approximate relationship  $^{14}\text{C}$  KIE = ( $^{13}\text{C}$  KIE)<sup>1.89,61</sup>. The reported estimate of  $1'-^{14}\text{C}$  KIE for  $\text{D}_\text{N} * \text{A}_\text{N}$  mechanisms was 1.015–1.018, and the lower limits for an  $\text{A}_\text{N}\text{D}_\text{N}$  mechanism were 1.025–1.029.



**Fig. 21** (a) Depurination reaction catalyzed by RTA. Stem-loop DNA oligonucleotides are also substrates. (b) Substrate oligonucleotides, with reactive (deoxy-)adenosine residue in bold. (c) Inhibitors of RTA.



TS analysis, in conjunction with complementary experimental approaches, has shown that UDG catalyzes uridine hydrolysis through an oxocarbenium ion(-like) transition state with strong leaving group activation through stabilization of the uracil anion. The relative energetic importance of oxocarbenium ion stabilization is not known, but it has been noted that there is an acidic residue, Asp64, located near the  $\alpha$ -face of the oxocarbenium ion, where it may act to stabilize the positive charge electrostatically, and may also assist the water nucleophile by orienting it, and possibly acting as a general base.

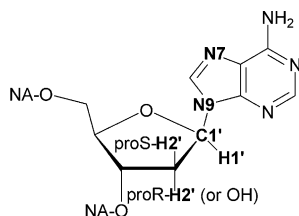
#### *Ricin toxin A-chain (RTA)*

*General.* Ricin is a cytotoxic protein from castor beans.<sup>205</sup> The catalytic domain, RTA, catalyzes the hydrolytic depurination of a single adenosine residue, A4324, of 28S rat ribosomal RNA.<sup>206,207</sup> This single depurination stops protein biosynthesis



**Table 8** Experimental and calculated KIEs on  $k_{\text{cat}}/K_M$  for ricin-catalyzed depurinations

Isotopic label <sup>a</sup>	RNA hydrolysis (A-10) <sup>b</sup>		DNA depurination (dA-10) <sup>c</sup>	
	Experimental KIE	Calculated EIE <sup>d</sup>	Experimental KIE	Calculated KIE <sup>e</sup>
1'- <sup>14</sup> C	0.993 ± 0.004	1.007	1.015 ± 0.001	1.018
9- <sup>15</sup> N	1.016 ± 0.005	1.024	1.023 ± 0.004	1.024
7- <sup>15</sup> N	0.981 ± 0.008	0.985	–	–
1'- <sup>3</sup> H	1.163 ± 0.009	1.288	1.187 ± 0.008	1.368
2'- <sup>3</sup> H or 2'σ- <sup>3</sup> H	1.012 ± 0.005	0.994	1.117 ± 0.002	1.140
2'R- <sup>3</sup> H	–	–	1.146 ± 0.008	1.535 <sup>f</sup>

<sup>a</sup><sup>b</sup>From Ref. 46.<sup>c</sup>From Ref. 58.<sup>d</sup>EIEs for conversion of reactant to oxocarbenium ion plus adenine (see text).<sup>e</sup>Calculated KIEs for  $D_N * A_N^\ddagger$  mechanism (i.e.  $k_4 \gg k_5$ ). The calculated KIEs for a  $D_N^\ddagger * A_N$  mechanism (i.e.  $k_4 \ll k_5$ ), which are similar, were also reported.<sup>58</sup><sup>f</sup>This extremely large KIE is probably an artefact of the computational methods used.

and causes cell death. With a reported  $k_{\text{cat}} = 1777 \text{ min}^{-1}$  on intact ribosomes, a single RTA molecule is sufficient to kill a cell. The minimal substrate of RTA is an RNA or DNA oligonucleotide with a stem of at least three base pairs, and a GAGA stem-loop structure<sup>208–210</sup> (Fig. 21a). RTA has poor activity against small stem-loop substrates at physiological pH, but  $k_{\text{cat}}$  increases at low pH to  $4 \text{ min}^{-1}$  for substrate A-10, and  $214 \text{ min}^{-1}$  for A-14 at pH 4.1, within an order of magnitude of  $k_{\text{cat}}$  against ribosomes.

KIEs were determined for a stem-loop RNA substrate A-10<sup>46</sup> and an analogous DNA substrate, dA-10<sup>58</sup> (Table 8). In both these cases, hydrolysis reaction proceeded through a stepwise  $D_N * A_N$  mechanism. Isotope-trapping experiments showed that substrate binding was not kinetically significant; however, the experimental KIEs with A-10 as substrate were inconsistent with any mechanism where only chemical steps were kinetically significant, implying equilibrium formation of an RTA·oxocarbenium ion·adenine complex, followed by an isotopically insensitive step. In contrast, the KIEs for dA-10 were consistent with a  $D_N * A_N$  mechanism.

*TS analysis of a DNA substrate.* The experimental KIEs for dA-10, in particular the small primary 1'-<sup>14</sup>C KIE =  $1.015 \pm 0.001$ , were not consistent with an  $A_N D_N$

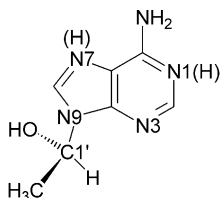
mechanism. This is smaller than the calculated minimum KIE for an  $A_N D_N$  mechanism, 1.025 when calculated by BOVA, and 1.029 by electronic structure methods. The large primary  $^{15}\text{N}$  KIE indicated a large extent of C–N bond breakage at the transition state, and the  $\alpha$ - and  $\beta$ -secondary  $^3\text{H}$  KIEs were also large, indicating high oxocarbenium ion character. Taken together, these KIEs supported a  $D_N * A_N$  mechanism.

The observable KIEs (see Section 3) were calculated using *ab initio* electronic structure methods for model compounds of the RTA-catalyzed depurination of dA-10 (Table 8). The calculated KIEs for the two mechanistic extremes,  $k_4 \gg k_5$  or  $k_5 \gg k_4$ , were very similar to each other and it was not possible to distinguish between these two possibilities from the experimental KIEs.

*TS analysis of an RNA substrate.* Interpretation of the KIEs for A-10 hydrolysis was not straightforward. It was possible to make the following mechanistic deductions only because the KIEs for the DNA reaction were consistent with a  $D_N * A_N$  mechanism with only chemical steps being kinetically significant. Having the DNA reaction as a benchmark made it possible to interpret the unusual KIEs for the RNA reaction. The experimental KIEs were not consistent with a mechanism where only chemical steps were kinetically significant, and isotope-trapping measurements of commitment to catalysis demonstrated that substrate binding was not kinetically significant. Instead, the KIEs indicated an oxocarbenium ion intermediate in equilibrium with reactant RNA, and with the first irreversible step being isotopically insensitive, occurring after oxocarbenium ion formation (Fig. 7). The primary,  $1'^{14}\text{C}$  KIE of  $0.993 \pm 0.004$ , was even lower than for dA-10 and inconsistent with a  $D_N * A_N$  mechanism. The primary  $9\text{-}^{15}\text{N}$  KIE of  $1.016 \pm 0.005$  was less than expected for complete C–N bond breakage, 1.024, but still indicated a large amount of bond breakage. The  $\alpha$ -secondary KIE indicated significant oxocarbenium ion character. These experimental KIEs, in particular the primary  $^{14}\text{C}$  KIE, were the most consistent with the EIEs of forming an oxocarbenium ion. The observable KIEs will be equal to the calculated EIEs of oxocarbenium ion formation if the next step in the reaction,  $k_5$ , is the first irreversible one, and it is isotopically insensitive, i.e.  $\alpha_5 = 1$ . In other words, if  $k_4 \gg k_5$  and  $\alpha_5 = 1$ , then  $\text{KIE}_{\text{observable}} = \text{EIE}_{\text{oxocarbenium}} = (\alpha_1 \alpha_3) / (\alpha_2 \alpha_4)$ . The nature of the isotopically insensitive step  $k_5$  is not known, but could be, e.g. a protein conformational change or diffusion of water into position to perform nucleophilic attack on the oxocarbenium ion. In either case, an isotopic label on the substrate molecule would have no effect on the rate of this step. As seen in Fig. 7, the next step is nucleophilic attack by water. Because the first irreversible step has already been passed, this step is not kinetically significant for  $k_{\text{cat}}/K_M$  and will not be reflected in the observable KIEs.

*Leaving group activation.* There is evidence that RTA activates the adenine leaving group for departure by protonation. The large inverse  $7\text{-}^{15}\text{N}$  KIE was evidence that N7 is protonated in the RTA·oxocarbenium ion·adenine complex. The pH profile of RTA activity against A-10 gave evidence for protonation of N1. The  $\text{pK}_a$  value for N1 of a non-base-paired adenine is near 4.<sup>211</sup> The  $k_{\text{cat}}/K_M$  versus pH

profile of RTA-catalyzed hydrolysis of A-10 is bell-shaped, with maximal activity around pH 4. Activity decreases as pH increases, with a pH-dependence consistent with two groups with  $pK_a = 4.0$ .<sup>212</sup> The pH profile of RTA with 28S RNA in intact ribosomes has not been reported, but must be different from A-10 because the two ionizations in the descending limb would imply a  $10^7$ -fold decrease in  $k_{cat}/K_M$  at the physiological pH of 7.4. The pH profile of A-10 hydrolysis is consistent with N1 of the susceptible adenine being one of the groups with  $pK_a = 4.0$ . This is close to the unperturbed  $pK_a$  of an adenine base, suggesting that RTA is contributing little energy to protonate the substrate at N1. In contrast, it was proposed that the N1 atom of A4234 in ribosomes is protonated by the enzyme to promote catalysis at physiological pH. Thus, the enzyme uses binding energy from interaction with 28S RNA that is unavailable in interactions with A-10 RNA to promote protonation of N1. The energetic importance of protonation at both N1 and N7 was demonstrated by calculating the energetics of C1'–N9 bond dissociation in the model compound (**18**).<sup>46</sup> The bond dissociation energy was approximately 5.5 kcal/mol for N1H,N7H-**18**, as opposed to 68 and 55 kcal/mol, for N1H-**18** and N7H-**18**, respectively.



[18]

*Importance of 2'-hydroxyl group.* The importance of the 2'-hydroxyl group to catalysis can be examined via the kinetic constants for RNA versus DNA substrates, A-10 versus dA-10. The value of  $k_{cat}/K_M$  for A-10 was 5.7-fold higher than dA-10. Adenosine undergoes acid-catalyzed hydrolysis 650-fold slower than 2'-deoxyadenosine,<sup>213</sup> similar to the difference in rates of acid-catalyzed hydrolysis between other 2-hydroxy- and 2-deoxy-*N*- and *O*-glycosides<sup>2</sup> as well as uncatalyzed *O*-glycoside hydrolysis.<sup>214</sup> Given the structural similarity between the highly oxocarbenium ion-like  $A_N D_N$  transition states and the corresponding oxocarbenium ions for 2-hydroxy and 2-deoxy sugars, this difference in reaction rates provides an estimate of the free energy differences between 2-hydroxy- and 2-deoxy-oxocarbenium ions. The combination of a 5.7-fold higher value of  $k_{cat}/K_M$  with the 650-fold lower reactivity means that RTA accelerates the reaction of A-10 by 3700-fold relative the expectation based on its intrinsic reactivity. This means that the enzyme achieves 4.8 kcal/mol of stabilization of the transition state of the RNA reaction from the presence of the 2'-hydroxyl groups. Because every nucleotide residue of A-10 contains a 2'-hydroxyl, it is not possible to attribute this increase in  $k_{cat}/K_M$  to a single group. However, Orita *et al.*<sup>215</sup> reported that a stem-loop RNA substrate with a 2'-deoxyadenosine (dA) residue only at the susceptible position,

GdAGA, of the molecule had 26-fold higher “activity” than the all-RNA analogue. This report does not make it clear whether “activity” corresponds to  $k_{\text{cat}}$  or  $k_{\text{cat}}/K_{\text{M}}$ , and reactions were performed at pH 7.4, so direct comparison with the kinetic constants of A-10 and dA-10 are difficult. Nonetheless, the effect of an A to dA substitution at the susceptible position was between the 650-fold increase expected based on reactivity and the 5.7-fold decrease between A-10 and dA-10 implying contributions from the 2'-hydroxyls both at the susceptible position and at other positions. The 4.8 kcal/mol of stabilization achieved by the enzyme, compared to the 3.8 kcal/mol intrinsically higher activation energy for RNA hydrolysis, implies that more than enough energy is derived from enzymatic interactions with the 2-hydroxyl groups to stabilize the inherently less stable 2-hydroxy-ribooxocarbenium ion.

*Inhibitor design.* The results of recent inhibitor design studies<sup>216</sup> have provided support for the proposed  $D_{\text{N}} * A_{\text{N}}$  mechanism. In this study, an iminosugar inhibitor, IA-10 (Fig. 21c), gave only modest inhibition of RTA,  $K_{\text{i}} = 0.6 \mu\text{M}$ , as did an inhibitor without the purine ring analogue, 1N-14,  $K_{\text{i}} = 0.5 \mu\text{M}$ . However, 50-fold stronger inhibition was observed with 1N-14 in the presence of adenine, which allowed formation of an RTA·1N-14·adenine complex with  $K_{\text{i}} = 0.012 \mu\text{M}$ . Tight binding was expected for the combination of 1N-14 and adenine by analogy to the RTA·oxocarbenium ion·adenine complex, where the distance between the oxocarbenium ion and adenine may be too large to be bridged by the C–C bond in IA-10. More potent inhibition may be possible by combining features of 1N-14 and adenine with a covalent linkage to reduce the entropy loss that must be compensated in forming a ternary complex.<sup>217,218</sup>

## 5 Conclusions and future directions

In this chapter, we have attempted to provide a summary of the use of TS analysis in understanding glycoside chemistry, as well as an overview of recent developments in the field. TS analysis is only one tool in any comprehensive analysis of reactivity and catalysis, but an extremely powerful tool.

### THE IMMEDIATE FUTURE

The immediate future is relatively clear. Continued advances in instrumental techniques, particularly in mass spectrometry and NMR, will make it possible to measure increasingly accurate and precise KIEs on increasingly small amounts of material. At the same time, continued growth in computational power and in the methods of KIE interpretation will make TS analysis an increasingly powerful tool. Currently, one major drawback is that it is too time consuming at present for application in the pharmaceutical industry. TS analysis will have to become much faster to see wide application outside of academia.

## CRUCIAL QUESTIONS

It has become abundantly clear that glycoside hydrolyses and transfers are on the borderline between highly dissociative  $A_N D_N$  transition states and  $D_N * A_N$  stepwise mechanisms. In both cases, the sugar ring takes on cationic character which can be exploited by enzymes to promote catalysis and by chemists to design inhibitors. What other questions can TS analysis address in the study of glycoside chemistry?

- (1) *Conformation of the sugar ring.* Glycosidases and glycosyl transferases can enforce particular sugar ring conformations and there can be strong conformational effects on glycoside reactivity, such as those mediated through the anomeric effect and hyperconjugation. TS analysis can provide information on sugar ring conformations through secondary hydron KIEs. In addition, knowledge of sugar ring conformation can provide indirect information on the direction of the backbone chain in oligosaccharide or oligonucleotide substrates.
- (2) *Oxocarbenium ion stabilization.* Even though all glycoside reactions appear to proceed through oxocarbenium ion(-like) transition states or intermediates, not all enzymes interact strongly with the sugar part of the substrate. This point will not easily be addressed solely with KIE studies, but it is an important issue in catalysis.
- (3) *Leaving group activation.* Related to point 2, those enzymes that do not interact strongly with the sugar ring must achieve catalysis through interactions with the leaving group and nucleophile. In order to clarify the role of leaving group activation, remote KIEs have been measured, such as 7- $^{15}\text{N}$  KIEs in purines. Further study is needed to understand the mechanisms of leaving group activation.
- (4) *Concerted ( $A_N D_N$ ) versus stepwise ( $D_N * A_N$ ) mechanisms.* If an enzyme uses an  $A_N D_N$  mechanism, then the position of the leaving group relative to the glycosyl ring is well defined in the TS structure. However, if a discrete oxocarbenium ion intermediate is formed, then it is possible that the leaving group has moved a large distance and/or has rotated relative to the glycosyl ring in this intermediate. This will have implications for inhibitor design, where compounds with extra atoms inserted between the sugar ring analogue and the leaving group analogue may be effective.<sup>204,219</sup>
- (5) *Enzyme-substrate interactions.* While TS analysis can provide a detailed TS structure, and it is possible to dock that structure into an enzyme active site, it is not possible to determine by inspection or computation the energetics of individual enzyme-substrate contacts. An added complication is the fact that active sites generally change structure upon binding to the transition state and throughout the catalytic cycle. Further experimental studies, in combination with computational analyses of enzyme-substrate interactions are needed to understand the energetics of catalysis.

As the power of TS analysis increases, the questions that can be posed will evolve, becoming more subtle and more powerful.

## Acknowledgments

The authors thank Professor Vern Schramm for his long-term and continuing support, and for helpful discussions. We also thank Drs Andy Bennet and Jim Stivers for sharing their results before publication. The writing of this chapter was supported by the Canadian Institutes of Health Research (CIHR) and the Natural Sciences and Engineering Research Council (NSERC).

## References

1. BeMiller, J.N. (1967). *Adv. Carbohydr. Chem. Biochem.* **22**, 25
2. Capon, B. (1969). *Chem. Rev.* **69**, 407
3. Cordes, E.H. and Bull, H.G. (1974). *Chem. Rev.* **74**, 581
4. Sinnott, M.L. (1990). *Chem. Rev.* **90**, 1171
5. Zechel, D.L. and Withers, S.G. (2000). *Acc. Chem. Res.* **33**, 11
6. Rowe, P.M. (1999). *Lancet* **354**, 402
7. Dwek, R.A. (1996). *Chem. Rev.* **96**, 683
8. Robyt, J.F. (1998). *Essentials of Carbohydrate Chemistry*. Springer, New York
9. Hecht, S.M. (1999). *Bioorganic Chemistry: Carbohydrates*. Oxford University Press, New York
10. Warshel, A. (1978). *Proc. Natl Acad. Sci. USA* **75**, 5250
11. Weiss, P.M. (1991). *Enzyme Mechanism from Isotope Effects*. Cook, P.F. (ed.), p. 291. CRC Press, Boca Raton, FL
12. Parkin, D.W. (1991). *Enzyme Mechanism from Isotope Effects*. Cook, P.F. (ed.), p. 269. CRC Press, Boca Raton, FL
13. Rosenberg, S. and Kirsch, J.F. (1979). *Anal. Chem.* **51**, 1375
14. Bahnson, B.J. and Anderson, V.E. (1991). *Biochemistry* **30**, 5894
15. Gawlita, E., Paneth, P. and Anderson, V.E. (1995). *Biochemistry* **34**, 6050
16. Kline, P.C., Rezaee, M. and Lee, T.A. (1999). *Anal. Biochem.* **275**, 6
17. Berti, P.J., Blanke, S.R. and Schramm, V.L. (1997). *J. Am. Chem. Soc.* **119**, 12079
18. Matsson, O., Axelsson, S., Hussenius, A. and Ryberg, P. (1999). *Acta Chem. Scand.* **53**, 670
19. Xue, H., Wu, X. and Huskey, W.P. (1996). *J. Am. Chem. Soc.* **118**, 5804
20. Zhou, X.Z. and Toney, M.D. (1998). *J. Am. Chem. Soc.* **120**, 13282
21. Rosenberg, S. and Kirsch, J.F. (1979). *Anal. Chem.* **51**, 1379
22. Singleton, D.A. and Thomas, A.A. (1995). *J. Am. Chem. Soc.* **117**, 9357
23. Singleton, D.A., Merrigan, S.R., Kim, B.J., Beak, P., Phillips, L.M. and Lee, J.K. (2000). *J. Am. Chem. Soc.* **122**, 3296
24. Sims, L.B. and Lewis, D.E. (1984). *Isotope Effects: Recent Developments in Theory and Experiment*, Buncel, E. and Leeds, C.C. (eds), vol. **6**, p. 161. Elsevier, New York
25. Sims, L. B.; Burton, G. W.; Lewis, D. E. (1997). BEBOVIB-IV, QCPE No. 337. Quantum Chemistry Program Exchange, Department of Chemistry, University of Indiana, Bloomington, IN

26. Fedorov, A., Shi, W., Kicska, G., Fedorov, E., Tyler, P.C., Furneaux, R.H., Hanson, J.C., Gainsford, G.J., Larese, J.Z., Schramm, V.L. and Almo, S.C. (2001). *Biochemistry* **40**, 853
27. Kline, P.C. and Schramm, V.L. (1995). *Biochemistry* **34**, 1153
28. Kline, P.C. and Schramm, V.L. (1993). *Biochemistry* **32**, 13212
29. Wang, F., Miles, R.W., Kicska, G., Nieves, E., Schramm, V.L. and Angeletti, R.H. (2000). *Protein Sci.* **9**, 1660
30. Mao, C., Cook, W.J., Zhou, M., Federov, A.A., Almo, S.C. and Ealick, S.E. (1998). *Biochemistry* **37**, 7135
31. Kline, P.C. and Schramm, V.L. (1992). *Biochemistry* **31**, 5964
32. Miles, R.W., Tyler, P.C., Furneaux, R.H., Bagdassarian, C.K. and Schramm, V.L. (1998). *Biochemistry* **37**, 8615
33. Kicska, G.A., Long, L., Horig, H., Fairchild, C., Tyler, P.C., Furneaux, R.H., Schramm, V.L. and Kaufman, H.L. (2001). *Proc. Natl Acad. Sci. USA* **98**, 4593
34. Pauling, L. (1946). *Chem. Eng. News* **24**, 1375
35. Fersht, A.R. (1985). *Enzyme Structure and Mechanism*. W.H. Freeman, New York
36. Radzicka, A. and Wolfenden, R. (1995). *Science* **267**, 90
37. Levy, S.B. (1998). *Sci. Am.* **278**, 46
38. Guthrie, R.D. and Jencks, W.P. (1989). *Acc. Chem. Res.* **22**, 343
39. Commission on Physical Organic Chemistry (1989). *Pure Appl. Chem.* **61**, 23
40. Commission on Physical Organic Chemistry (1989). *Pure Appl. Chem.* **61**, 57
41. Gutfreund, H. and Sturtevant, J.M. (1956). *Biochem. J.* **63**, 656
42. Cleland, W.W. (1982). *Methods Enzymol.* **87**, 625
43. Berti, P.J. (1999). *Methods Enzymol.* **308**, 355
44. Rose, I.W. (1980). *Methods Enzymol.* **64**, 47
45. Northrop, D.B. (1981). *Annu. Rev. Biochem.* **50**, 103
46. Chen, X.-Y., Berti, P.J. and Schramm, V.L. (2000). *J. Am. Chem. Soc.* **122**, 1609
47. Scheuring, J., Berti, P.J. and Schramm, V.L. (1998). *Biochemistry* **37**, 2748
48. Bruner, M. and Horenstein, B.A. (2000). *Biochemistry* **39**, 2261
49. Hosie, L. and Sinnott, M.L. (1985). *Biochem. J.* **226**, 437
50. Bennet, A.J. and Sinnott, M.L. (1986). *J. Am. Chem. Soc.* **108**, 7287
51. Huang, X., Surry, C., Hiebert, T. and Bennet, A.J. (1995). *J. Am. Chem. Soc.* **117**, 10614
52. Zhu, J. and Bennet, A.J. (1998). *J. Am. Chem. Soc.* **120**, 3887
53. Zhu, J. and Bennet, A.J. (2000). *J. Org. Chem.* **65**, 4423
54. Horenstein, B.A. and Bruner, M. (1996). *J. Am. Chem. Soc.* **118**, 10371
55. Horenstein, B.A. and Bruner, M. (1998). *J. Am. Chem. Soc.* **120**, 1357
56. Johnston, H.S. (1966). *Gas Phase Reaction Rate Theory*. Ronald Press, New York
57. Melander, L. and Saunders, W.H., Jr. (1980). *Reaction Rates of Isotopic Molecules*. Wiley, New York
58. Chen, X.-Y., Berti, P.J. and Schramm, V.L. (2000). *J. Am. Chem. Soc.* **122**, 6527
59. Houk, K.N., Gustafson, S.M. and Black, K.A. (1992). *J. Am. Chem. Soc.* **114**, 8565
60. Wilkie, J. and Williams, I.H. (1995). *J. Chem. Soc., Perkin Trans. 2* 1559
61. Huskey, W.P. (1991). *Enzyme Mechanism from Isotope Effects*, Cook, P.F. (ed.), p. 37. CRC Press, Boca Raton, FL
62. Suhnel, J. and Schowen, R.L. (1991). *Enzyme Mechanism from Isotope Effects*, Cook, P.F. (ed.), p. 3. CRC Press, Boca Raton, FL
63. Glad, S.S. and Jensen, F. (1996). *J. Phys. Chem.* **100**, 16892
64. Scott, A.P. and Radom, L. (1996). *J. Phys. Chem.* **100**, 16502
65. Wong, M.W. (1996). *Chem. Phys. Lett.* **256**, 391
66. Burton, G.W., Sims, L.B., Wilson, J.C. and Fry, A. (1977). *J. Am. Chem. Soc.* **99**, 3371
67. Huskey, W.P. (1996). *J. Am. Chem. Soc.* **118**, 1663
68. Casamassina, T.E. and Huskey, W.P. (1993). *J. Am. Chem. Soc.* **115**, 14

69. Berti, P.J. and Schramm, V.L. (1997). *J. Am. Chem. Soc.* **119**, 12069
70. Rising, K.A. and Schramm, V.L. (1997). *J. Am. Chem. Soc.* **119**, 27
71. Horenstein, B.A., Parkin, D.W., Estupinan, B. and Schramm, V.L. (1991). *Biochemistry* **30**, 10788
72. Andrews, C.W., Bowen, J.P. and Fraser-Reid, B. (1989). *J. Chem. Soc., Chem. Commun.* 1913
73. Winkler, D.A. and Holan, G. (1989). *J. Med. Chem.* **32**, 2084
74. Andrews, C.W., Fraser-Reid, B. and Bowen, J.P. (1991). *J. Am. Chem. Soc.* **113**, 8293
75. Kajimoto, T., Liu, K.K.C., Pederson, R.L., Zhong, Z., Ichikawa, Y., Porco, J.A., Jr. and Wong, C.-H. (1991). *J. Med. Chem.* **113**, 6187
76. Smith, B.J. (1997). *J. Am. Chem. Soc.* **119**, 2699
77. Namchuk, M.N., McCarter, J.D., Becalski, A., Andrews, T. and Withers, S.G. (2000). *J. Am. Chem. Soc.* **122**, 1270
78. Mentch, F., Parkin, D.W. and Schramm, V.L. (1987). *Biochemistry* **26**, 921
79. Parkin, D.W., Mentch, F., Banks, G.A., Horenstein, B.A. and Schramm, V.L. (1991). *Biochemistry* **30**, 4586
80. Scheuring, J. and Schramm, V.L. (1997). *Biochemistry* **36**, 4526
81. Scheuring, J. and Schramm, V.L. (1997). *Biochemistry* **36**, 8215
82. Mazzella, L.J., Parkin, D.W., Tyler, P.C., Furneaux, R.H. and Schramm, V.L. (1996). *J. Am. Chem. Soc.* **118**, 2111
83. Inouye, S., Tsuruoka, T., Ito, T. and Niida, T. (1968). *Tetrahedron* **23**, 2125
84. Legler, G. (1990). *Adv. Carbohydr. Chem. Biochem.* **48**, 319
85. Jeong, J.H., Murray, B.W., Takayama, S. and Wong, C.-H. (1996). *J. Am. Chem. Soc.* **118**, 4227
86. Hoos, R., Huixin, J., Vasella, A. and Weiss, P. (1996). *Helv. Chim. Acta* **79**, 1757
87. Yagi, M., Kouno, T., Aoyagi, Y. and Murai, H. (1976). *Nippon Nokei Kagaku Kaishi* **50**, 571
88. Legler, G. and Julich, E. (1984). *Carbohydr. Res.* **128**, 61
89. Evans, S.V., Fellows, L.E., Shing, T.K.M. and Fleet, G.W.J. (1985). *Phytochemistry* **24**, 1953
90. Legler, G. and Pohl, S. (1986). *Carbohydr. Res.* **155**, 119
91. Winchester, B., Barker, C., Baines, S., Jacob, G.S., Namgoong, S.K. and Fleet, G. (1990). *Biochem. J.* **265**, 277
92. Cenci di Bello, I., Dorling, P., Fellows, L. and Winchester, B. (1984). *FEBS Lett.* **176**, 61
93. Hughes, A.B. and Rudge, A.J. (1994). *Nat. Prod. Rep.* 135
94. Jespersen, T.M., Dong, W., Sierks, M.R., Skrydstrup, T., Lundt, I. and Bols, M. (1994). *Angew. Chem. Int. Ed. Engl.* **33**, 1778
95. Ichikawa, Y. and Igarashi, Y. (1995). *Tetrahedron Lett.* **36**, 4585
96. Igarashi, Y., Ichikawa, M. and Ichikawa, Y. (1996). *Tetrahedron Lett.* **37**, 2707
97. Bols, M., Hazell, R.G. and Thomsen, I.B. (1997). *Chem. Eur. J.* **3**, 940
98. Bols, M. (1998). *Acc. Chem. Res.* **31**, 1
99. Liu, H., Liang, X., Shoel, H., Bülow, A. and Bols, M. (2001). *J. Am. Chem. Soc.* **123**, 5116
100. Parkin, D.W. and Schramm, V.L. (1995). *Biochemistry* **34**, 13961
101. Degano, M., Almo, S.C., Sacchettini, J.C. and Schramm, V.L. (1998). *Biochemistry* **37**, 6277
102. Shi, W., Li, C.M., Tyler, P.C., Furneaux, R.H., Cahill, S.M., Girvin, M.E., Grubmeyer, C., Schramm, V.L. and Almo, S.C. (1999). *Biochemistry* **38**, 9872
103. Bell, C.E. and Eisenberg, D. (1996). *Biochemistry* **35**, 1137
104. Bruner, M. and Horenstein, B.A. (1998). *Biochemistry* **37**, 289
105. Bernasconi, C.F. (1992). *Adv. Phys. Org. Chem.* **27**, 119



106. Bernasconi, C.F. (1992). *Acc. Chem. Res.* **25**, 9
107. Kresge, A.J. (1974). *Can. J. Chem.* **52**, 1897
108. Yamataka, H., Mustanir, and Mishima, M. (1999). *J. Am. Chem. Soc.* **121**, 10223
109. Bernasconi, C.F. and Wenzel, P.J. (1994). *J. Am. Chem. Soc.* **116**, 5405
110. Bernasconi, C.F. and Wenzel, P.J. (1996). *J. Am. Chem. Soc.* **118**, 10494
111. Bernasconi, C.F. (1985). *Tetrahedron* **41**, 3219
112. Richard, J.P. (1995). *Tetrahedron* **51**, 1535
113. Richard, J.P., Williams, K.B. and Amyes, T.L. (1999). *J. Am. Chem. Soc.* **121**, 8403
114. Rakowski, K. and Paneth, P. (1996). *J. Mol. Struct.* **378**, 35
115. Gawlita, E., Caldwell, W.S., Oleary, M.H., Paneth, P. and Anderson, V.E. (1995). *Biochemistry* **34**, 2577
116. Poirier, R.A., Wang, Y. and Westaway, K.C. (1994). *J. Am. Chem. Soc.* **116**, 2526
117. Matsson, O. and Westaway, K.C. (1998). *Adv. Phys. Org. Chem.* **31**, 143
118. Glad, S.S. and Jensen, F. (1997). *J. Am. Chem. Soc.* **119**, 227
119. Westaway, K.C. (1975). *Tetrahedron Lett.* **48**, 4229
120. Westaway, K.C., VanPham, T. and Fang, Y.R. (1997). *J. Am. Chem. Soc.* **119**, 3670
121. Barnes, J.A. and Williams, I.H. (1993). *J. Chem. Soc., Chem. Commun.* 1286
122. Koerner, T., Westaway, K.C., Poirier, R.A. and Wang, Y. (2000). *Can. J. Chem.* **78**, 1067
123. Wade, D. (1999). *Chem. Biol. Interact.* **117**, 191
124. Lewis, B.E. and Schramm, V.L. (2001). *J. Am. Chem. Soc.* **123**, 1327
125. Stein, R.L., Romero, R., Bull, H.G. and Cordes, E.H. (1978). *J. Am. Chem. Soc.* **100**, 6249
126. LaReau, R.D., Wan, W. and Anderson, V.E. (1989). *Biochemistry* **28**, 3619
127. Gawlita, E., Lantz, M., Paneth, P., Bell, A.F., Tonge, P.J. and Anderson, V.E. (2000). *J. Am. Chem. Soc.* **122**, 11660
128. D'Ordine, R.L., Bahnson, B.J., Tonge, P.J., Carey, P.R. and Anderson, V.E. (1994). *Biochemistry* **33**, 14733
129. Bell, A.F., Wu, J., Feng, Y. and Tonge, P.J. (2001). *Biochemistry* **40**, 1725
130. Cheng, H., Sukal, S., Deng, H., Leyh, T.S. and Callender, R. (2001). *Biochemistry* **40**, 4035
131. Deng, H., Wang, J.H., Callender, R.H., Grammer, J.C. and Yount, R.G. (1998). *Biochemistry* **37**, 10972
132. Sunko, D.E., Szele, I. and Hehre, W.J. (1977). *J. Am. Chem. Soc.* **99**, 5000
133. Jucker, F.M., Heus, H.A., Yip, P.F., Moors, E.H. and Pardi, A. (1996). *J. Mol. Biol.* **264**, 968
134. Correll, C.C., Munishkin, A., Chan, Y.L., Ren, Z., Wool, I.G. and Steitz, T.A. (1998). *Proc. Natl Acad. Sci. USA* **95**, 13436
135. Werner, R.M. and Stivers, J.T. (2000). *Biochemistry* **39**, 14054
136. Stern, M.J. and Vogel, P.C. (1971). *J. Am. Chem. Soc.* **93**, 4664
137. Huang, X.C., Tanaka, K.S.E. and Bennet, A.J. (1997). *J. Am. Chem. Soc.* **119**, 11147
138. Parkin, D.W., Leung, H.B. and Schramm, V.L. (1984). *J. Biol. Chem.* **259**, 9411
139. Parkin, D.W. and Schramm, V.L. (1987). *Biochemistry* **26**, 913
140. Tarnus, C., Muller, H.M. and Schuber, F. (1988). *Bioorg. Chem.* **16**, 38
141. Johnson, R.W., Marschner, T.M. and Oppenheimer, N.J. (1988). *J. Am. Chem. Soc.* **110**, 2257
142. Miles, R.W., Tyler, P.C., Evans, G.B., Furneaux, R.H., Parkin, D.W. and Schramm, V.L. (1999). *Biochemistry* **38**, 13147
143. Moodie, S.L. and Thornton, J.M. (1993). *Nucleic Acids Res.* **21**, 1369
144. Drohat, A.C. and Stivers, J.T. (2000). *Biochemistry* **39**, 11865
145. Drohat, A.C. and Stivers, J.T. (2000). *J. Am. Chem. Soc.* **122**, 1840
146. Dinner, A.R., Blackburn, G.M. and Karplus, M. (2001). *Nature* **413**, 752

147. Parikh, S.S., Walcher, G., Jones, G.D., Slupphaug, G., Krokan, H.E., Blackburn, G.M. and Tainer, J.A. (2000). *Proc. Natl Acad. Sci. USA* **97**, 5083
148. Dunathan, H.C. (1966). *Proc. Natl Acad. Sci. USA* **55**, 712
149. Shi, H. and Moore, P.B. (2000). *RNA* **6**, 1091
150. Jovine, L., Djordjevic, S. and Rhodes, D. (2000). *J. Mol. Biol.* **301**, 401
151. Dong, J., Drohat, A.C., Stivers, J.T., Pankiewicz, K.W. and Carey, P.R. (2000). *Biochemistry* **39**, 13241
152. Bennett, M.J., Choe, S. and Eisenberg, D. (1994). *Protein Sci.* **3**, 1444
153. Weiss, M.S., Blanke, S.R., Collier, R.J. and Eisenberg, D. (1995). *Biochemistry* **34**, 773
154. Bennett, M.J. and Eisenberg, D. (1994). *Protein Sci.* **3**, 1464
155. Bell, C.E. and Eisenberg, D. (1997). *Biochemistry* **36**, 481
156. Choe, S., Bennett, M.J., Fujii, G., Curmi, P.M., Kantardjieff, K.A., Collier, R.J. and Eisenberg, D. (1992). *Nature* **357**, 216
157. Oppenheimer, N.J. and Bodley, J.W. (1981). *J. Biol. Chem.* **256**, 8579
158. Wilson, B.A., Reich, K.A., Weinstein, B.R. and Collier, R.J. (1990). *Biochemistry* **29**, 8643
159. Koshland, D.E., Jr. (1953). *Biol. Rev.* **28**, 416
160. Davies, G., Sinnott, M.L. and Withers, S.G. (1997). *Comprehensive Biological Catalysis*. Sinnott, M. (ed.), p. 120. Academic Press, London
161. Indurugalla, D. and Bennet, A.J. (2001). *J. Am. Chem. Soc.* **123**, 10889
162. Zhang, Y., Bommuswamy, J. and Sinnott, M.L. (1994). *J. Am. Chem. Soc.* **116**, 7557
163. Tanaka, Y., Tao, W., Blanchard, J.S. and Hehre, E.J. (1994). *J. Biol. Chem.* **269**, 32306
164. Deslongchamps, P. (1993). *Pure Appl. Chem.* **65**, 1161
165. Streitwieser, A., Jr., Jagow, R.H., Fahey, R.C. and Suzuki, S. (1958). *J. Am. Chem. Soc.* **80**, 2326
166. Wong, C.-H., Halcomb, R.L., Ichikawa, Y. and Kajimoto, T. (1995). *Angew. Chem. Int. Ed. Engl.* **34**, 412
167. Wong, C.-H., Halcomb, R.L., Ichikawa, Y. and Kajimoto, T. (1995). *Angew. Chem. Int. Ed. Engl.* **34**, 521
168. Simanek, E.E., McGarvey, G.J., Jablonowski, J.A. and Wong, C.-H. (1998). *Chem. Rev.* **98**, 833
169. Sears, P. and Wong, C.-H. (1999). *Angew. Chem. Int. Ed. Engl.* **38**, 2300
170. Yang, J., Schenkman, S. and Horenstein, B.A. (2000). *Biochemistry* **39**, 5902
171. Schenkman, S., Eichinger, D., Pereira, M.E.A. and Nussenzweig, V. (1994). *Annu. Rev. Microbiol.* **48**, 499
172. Tarnus, C. and Schuber, F. (1987). *Bioorg. Chem.* **15**, 31
173. Jencks, W.P. (1981). *Chem. Soc. Rev.* **10**, 345
174. Jencks, W.P. (1980). *Acc. Chem. Res.* **13**, 161
175. Oppenheimer, N.J. and Tashma, R. (1992). *Biochemistry* **31**, 2195
176. Cherian, X.M., Van Arman, S.A. and Czarnick, A.W. (1990). *J. Am. Chem. Soc.* **112**, 4490
177. Ritchie, C.D. (1986). *Can. J. Chem.* **64**, 2239
178. Roberts, D.D., Lewis, S.D., Ballou, D.P., Olson, S.T. and Shafer, J.A. (1986). *Biochemistry* **25**, 5595
179. Karsten, W.E., Lai, C.-J. and Cook, P.F. (1995). *J. Am. Chem. Soc.* **117**, 5914
180. Stein, P.E., Boodhoo, A., Armstrong, G.D., Cockle, S.A., Klein, M.H. and Read, R.J. (1994). *Structure* **2**, 45
181. Antoine, R. and Loch, C. (1994). *J. Biol. Chem.* **269**, 6450
182. Bull, H.G., Ferraz, J.P., Cordes, E.H., Ribbi, A. and Apitz-Castro, R. (1978). *J. Biol. Chem.* **253**, 5186
183. Parkin, D.W., Horenstein, B.A., Abdulah, D.R., Estupinan, B. and Schramm, V.L. (1991). *J. Biol. Chem.* **266**, 20658

184. Horenstein, B.A. and Schramm, V.L. (1993). *Biochemistry* **32**, 7089
185. Horenstein, B.A. and Schramm, V.L. (1993). *Biochemistry* **32**, 9917
186. Horenstein, B.A., Zabinski, R.F. and Schramm, V.L. (1993). *Tetrahedron Lett.* **34**, 7213
187. Boutellier, M., Horenstein, B.A., Semenyaka, A., Schramm, V.L. and Ganem, B. (1994). *Biochemistry* **33**, 3994
188. Deng, H., Chan, A.W.-Y., Bagdassarian, C.K., Estupinan, B., Ganem, B., Callender, R.H. and Schramm, V.L. (1996). *Biochemistry* **35**, 6037
189. Gopaul, D.N., Meyer, S.L., Degano, M., Sacchettini, J.C. and Schramm, V.L. (1996). *Biochemistry* **35**, 5963
190. Degano, M., Gopaul, D.N., Scapin, G., Schramm, V.L. and Sacchettini, J.C. (1996). *Biochemistry* **35**, 5971
191. Bagdassarian, C.K., Schramm, V.L. and Schwartz, S.D. (1996). *J. Am. Chem. Soc.* **118**, 8825
192. Braunheim, B.B. and Schwartz, S.D. (1999). *Methods Enzymol.* **308**, 398
193. Braunheim, B.B. and Schwartz, S.D. (2000). *J. Theor. Biol.* **206**, 27
194. Braunheim, B.B., Miles, R.W., Schramm, V.L. and Schwartz, S.D. (1999). *Biochemistry* **38**, 16076
195. Parkin, D.W. and Schramm, V.L. (1984). *J. Biol. Chem.* **259**, 9418
196. Tao, W., Grubmeyer, C. and Blanchard, J.S. (1996). *Biochemistry* **35**, 14
197. Goitein, R.K., Chelsky, D. and Parsons, S.M. (1978). *J. Biol. Chem.* **253**, 2963
198. Scapin, G., Grubmeyer, C. and Sacchettini, J.C. (1994). *Biochemistry* **33**, 1287
199. Scapin, G., Ozturk, D.H., Grubmeyer, C. and Sacchettini, J.C. (1995). *Biochemistry* **34**, 10744
200. Focia, P.J., Craig, S.P., III and Eakin, A.E. (1998). *Biochemistry* **37**, 17120
201. Werner, R.M., Jiang, Y.L., Gordley, R.G., Jagadeesh, G.J., Ladner, J.E., Xiao, G., Tordova, M., Gilliland, G.L. and Stivers, J.T. (2000). *Biochemistry* **39**, 12585
202. Stivers, J.T. (1998). *Nucleic Acids Res.* **26**, 3837
203. Stivers, J.T., Pankiewicz, K.W. and Watanabe, K.A. (1999). *Biochemistry* **38**, 952
204. Sekino, Y., Bruner, S.D. and Verdine, G.L. (2000). *J. Biol. Chem.* **275**, 36506
205. Olsnes, S. and Pihl, A. (1982). *Molecular Action of Toxins and Viruses*, Cohen, P. and van Heyningeneds, S. (eds), p. 51. Elsevier Biomedical, New York
206. Endo, Y. and Tsurugi, K. (1987). *J. Biol. Chem.* **262**, 8128
207. Endo, Y. and Tsurugi, K. (1988). *J. Biol. Chem.* **263**, 8735
208. Gluck, A., Endo, Y. and Wool, I.G. (1992). *J. Mol. Biol.* **226**, 411
209. Endo, Y., Gluck, A. and Wool, I.G. (1991). *J. Mol. Biol.* **221**, 193
210. Orłowski, M., Orłowski, R., Chang, J.C., Wilk, E. and Lesser, M. (1984). *Mol. Cell. Biochem.* **64**, 155
211. Saenger, W. (1984). *Principles of Nucleic Acid Structure*. Springer, New York
212. Chen, X.Y., Link, T.M. and Schramm, V.L. (1998). *Biochemistry* **37**, 11605
213. Venner, H. (1964). *Z. Physiol. Chem.* **339**, 14
214. Wolfenden, R., Lu, X. and Young, G. (1998). *J. Am. Chem. Soc.* **120**, 6814
215. Orita, M., Nishikawa, F., Kohno, T., Senda, T., Mitsui, Y., Yaeta, E., Kazunari, T. and Nishikawa, S. (1996). *Nucleic Acids Res.* **24**, 611
216. Tanaka, K.S.E., Chen, X.-Y., Ichikawa, Y., Tyler, P.C., Furneaux, R.H. and Schramm, V.L. (2001). *Biochemistry* **40**, 6845
217. Kati, W.M. and Wolfenden, R. (1989). *Science* **243**, 1591
218. Wolfenden, R. (1999). *Bioorg. Med. Chem.* **7**, 647
219. Deng, L., Scharer, O.D. and Verdine, G.L. (1997). *J. Am. Chem. Soc.* **119**, 7865
220. Becke, A.D. (1988). *Phys. Rev. A* **38**, 3098
221. Perdew, J.P. and Wang, Y. (1992). *Phys. Rev. B* **45**, 13244
222. Frisch, M. J.; Trucks, G. W.; Schlegel, H. B.; Scuseria, G. E.; Robb, M. A.; Cheeseman, J. R.; Zakrzewski, V. G.; Montgomery, J. A.; Stratmann, R. E.; Burant, J. C.; Dapprich,

S.; Millam, J. M.; Daniels, A. D.; Kudin, K. N.; Strain, M. C.; Farkas, O.; Tomasi, J.; Barone, V.; Cossi, M.; Cammi, R.; Mennucci, B.; Pomelli, C.; Adamo, C.; Clifford, S.; Ochterski, J.; Petersson, G. A.; Ayala, P. Y.; Cui, Q.; Morokuma, K.; Malick, D. K.; Rabuck, A. D.; Raghavachari, K.; Foresman, J. B.; Cioslowski, J.; Ortiz, J. V.; Stefanov, B. B.; Liu, G.; Liashenko, A.; Piskorz, P.; Komaromi, I.; Gomperts, R.; Martin, R. L.; Fox, D. J.; Keith, T.; Al-Laham, M. A.; Peng, C. Y.; Nanayakkara, A.; Gonzalez, C.; Challacombe, M.; Gill, P. M. W.; Johnson, B. G.; Chen, W.; Wong, M. W.; Andres, J. L.; Head-Gordon, M.; Replogle, E. S. and Pople, J. A. (1998). Gaussian-98, Gaussian, Inc., Pittsburgh, PA, 1998